

AD-753 441

FLUID DYNAMICS OF AIRCRAFT STALLING

Advisory Group for Aerospace Research and  
Development  
Paris, France

November 1972

DISTRIBUTED BY:

**NTIS**

National Technical Information Service  
U. S. DEPARTMENT OF COMMERCE  
5285 Port Royal Road, Springfield Va. 22151

AD753441

# AGARD

ADVISORY GROUP FOR AEROSPACE RESEARCH & DEVELOPMENT

7 RUE ANCELLE 92200 NEUILLY SUR SEINE FRANCE

AGARD CONFERENCE PROCEEDINGS No. 102

on

## Fluid Dynamics of Aircraft Stalling

*aps*

NORTH ATLANTIC TREATY ORGANIZATION



Reproduced by  
NATIONAL TECHNICAL  
INFORMATION SERVICE

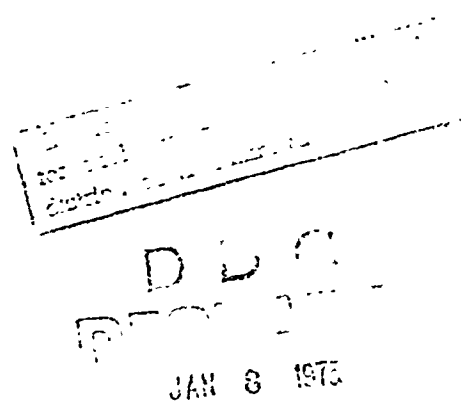
U.S. Department of Commerce  
Springfield, VA 22151

DISTRIBUTION AND AVAILABILITY  
ON BACK COVER

304

**NORTH ATLANTIC TREATY ORGANIZATION**  
**ADVISORY GROUP FOR AEROSPACE RESEARCH AND DEVELOPMENT**  
**(ORGANISATION DU TRAITÉ DE L'ATLANTIQUE NORD)**

**AGARD Conference Proceedings No.102**  
**FLUID DYNAMICS OF AIRCRAFT STALLING**



Copies of papers presented at the Fluid Dynamics Panel Specialists' Meeting,  
held in Lisbon, Portugal 25-28 April 1972.

## THE MISSION OF AGARD

The mission of AGARD is to bring together the leading personalities of the NATO nations in the fields of science and technology relating to aerospace for the following purposes:

- Exchanging of scientific and technical information;
- Continuously stimulating advances in the aerospace sciences relevant to strengthening the common defence posture;
- Improving the co-operation among member nations in aerospace research and development;
- Providing scientific and technical advice and assistance to the North Atlantic Military Committee in the field of aerospace research and development;
- Rendering scientific and technical assistance, as requested, to other NATO bodies and to member nations in connection with research and development problems in the aerospace field.
- Providing assistance to member nations for the purpose of increasing their scientific and technical potential;
- Recommending effective ways for the member nations to use their research and development capabilities for the common benefit of the NATO community.

The highest authority within AGARD is the National Delegates Board consisting of officially appointed senior representatives from each Member Nation. The mission of AGARD is carried out through the Panels which are composed of experts appointed by the National Delegates, the Consultant and Exchange Program and the Aerospace Applications Studies Program. The results of AGARD work are reported to the Member Nations and the NATO Authorities through the AGARD series of publications of which this is one.

Participation in AGARD activities is by invitation only and is normally limited to citizens of the NATO nations.

The material in this publication has been reproduced directly from copy supplied by AGARD or the author.

Published November 1972

533.6.013.64



Printed by Technical Editing and Reproduction Ltd  
Harford House, 7-9 Charlotte St London W1P 1HD



## **AGARD FLUID DYNAMICS PANEL OFFICERS**

**CHAIRMAN:** Professor Dr I. C. Novati  
INSTITUTO DI SCIENZE, Naples, Italy

**DEPUTY CHAIRMAN:** Professor Dr D. Küchemann  
Royal Aircraft Establishment, Farnborough, Hants, UK

## **PROGRAMME COMMITTEE MEMBERS**

Dr J. Seddon (Chairman)  
Mr P. P. Antonatos  
Dr F. J. Hindelang  
Mr L'Ing de l'Armement C. J. Lievens  
Dr R. C. Pankhurst  
Dr Ing U. Sacerdote  
Mr R. J. Templin

## **PANEL EXECUTIVE**

Dr L. H. Townend

## **FOREWORD**

This Meeting was intended to provide a collaborative up-dating of research information on the aerodynamics of the stall at both low and high speeds; to discuss this information in relation to practical problems of designing and operating combat aircraft and transport aircraft; to identify gaps in the knowledge and understanding of the problems involved, and make recommendations for future research in the fluid dynamics field. The meeting comprised twenty two papers, for three of which there were prepared discussions.

Recent work on the mechanics of flow separation was presented. A major subject area was that of the high lift performance and stalling behaviour of three-dimensional wings, including the influence of sweepback, the behaviour of high lift devices and the techniques and methods evolved for wind tunnel research. Flight development experience on recent combat and transport aircraft was described, and some papers concerned post-stall behaviour and the important problem of high speed buffet in relation to the manoeuvring of combat aircraft.

Host to the Fluid Dynamics Panel and all participants in the Meeting was the Portuguese National Delegate to AGARD, Brig. General Eng. Aero. J. de Sousa Oliviera. The Panel wishes to express its thanks for this invitation to hold the Meeting in Lisbon, and for the provision of the necessary facilities and personnel which made the Meeting possible.

# CONTENTS

	Page
AGARD FLUID DYNAMICS PANEL OFFICERS, PROGRAMME COMMITTEE AND FOREWORD	iii
TECHNICAL EXPLANATION OF NOTATION AND ABBREVIATIONS by R.C.Pankhurst	vi
	Reference
<u>SESSION I – REVIEW OF THE FIELD</u>	
<u>INVITED PAPER:</u> ROLE OF FLUID DYNAMICS IN AIRCRAFT STALL AND POST STALL GYRATIONS by G.J.Hancock	1
PREPARED COMMENT by T.C.Muse	1-14
<u>SESSION II – BASIC FLUID DYNAMICS</u>	
SOME RESEARCH ON TWO DIMENSIONAL LAMINAR SEPARATION BUBBLES by E.Dobbinga, J.L. van Ingen and J.W.Kooi	2
RECHERCHES THEORIQUES ET EXPERIMENTALES SUR LES DECOLLEMENTS LIES A UNE DEFORMATION LOCALE DE SURFACE par S.Burnel, G.B.Diep, P.Gougat et B.Prunet-Foch	3
<u>SESSION III – BASIC FLUID DYNAMICS AND TECHNIQUES</u>	
PREVISION DU DECOCHAGE D'UN PROFIL D'AILE EN ECOULEMENT INCOMPRESSIBLE par M.Vincent de Paul	5
PARAMETRIC STUDIES OF SEPARATING TURBULENT BOUNDARY LAYER FLOWS by A.Wortman and W.J.Franks	6
DESIGN OF AIRFOILS WITH HIGH LIFT AT LOW AND MEDIUM SUBSONIC MACH NUMBERS by F.X.Wortmann	7
COMMENT ON THE METHODS DEVELOPED AT THE NLR FOR CONDUCTING TWO-DIMENSIONAL RESEARCH ON HIGH-LIFT DEVICES by O. de Vries	8
CORRECTION DE BLOCAGE DANS LES ESSAIS EN SOUFFLERIE – EFFETS DES DECOLLEMENTS par J.-C Vayssaire	9
<u>SESSION IV – THEORY AND EXPERIMENT ON WINGS</u>	
AERODYNAMICS OF HIGH-LIFT AIRFOIL SYSTEMS by A.M.O.Smith	10
PREPARED COMMENT by D.Küchemann	10-25
THE LOW-SPEED STALLING OF WINGS WITH HIGH LIFT DEVICES by D.N.Foster	11
A SIMPLIFIED MATHEMATICAL MODEL FOR THE ANALYSIS OF MULTI-ELEMENT AIRFOILS NEAR STALL by I.C.Bhateley and R.C.Bradley	12

**THE EFFECT OF LEADING-EDGE GEOMETRY ON HIGH-SPEED STALLING**

by C.F.Moss, A.B.Haines and R.Jordan

5

**SESSION V - THEORY AND EXPERIMENT ON WINGS**

**A PRACTICAL LOOK AT THE STALL AND HIGH LIFT OPERATION OF EXTERNALLY BLOWN FLAP STOL TRANSPORT CONFIGURATIONS**

by D.J.Moorhouse

16

**THE FLIGHT MECHANICS PROBLEM**

**AERODYNAMIC DESIGN AND FLIGHT TEST OF US NAVY AIRCRAFT AT HIGH ANGLES OF ATTACK**

by W.R.Burris and J.T.Lawrence

25

**PREPARED COMMENT\***

by Ph. Poisson-Quinton

25-10

**SESSION VI - FLIGHT EXPERIENCE AND ASSOCIATED WORK**

**FLIGHT DEVELOPMENT OF THE STALLING CHARACTERISTICS OF A MILITARY TRAINER AIRCRAFT**

by W.D.Horsfield and G.P.Wilson

17

**STALL/POST-STALL CHARACTERISTICS OF THE F.111 AIRCRAFT**

by C.A.Anderson.

18

**POST/STALL AERODYNAMICS OF THE "HARRIER" GR1**

by C.L.Bore

19

**AERODYNAMICS OF WING STALL OF THE FOKKER F.28**

by Tj.Schuringa

20

**PREDICTING THE LOW-SPEED STALL CHARACTERISTICS OF THE BOEING 747**

by J.K.Wimpress

21

**SESSION VII - FLIGHT EXPERIENCE AND ASSOCIATED WORK**

**ON AIRFLOW SEPARATION AND BUFFET ONSET DURING FIGHTER AIRCRAFT MANEUVERING**

by P.J.Butkewicz

22

**THE DYNAMIC ANALYSIS OF BUFFETING AND RELATED PHENOMENA**

by J.G.Jones

23

**MANEUVER AND BUFFET CHARACTERISTICS OF FIGHTER AIRCRAFT**

by E.J.Ray, L.W.McKinney and J.G.Carmichael

24

**APPENDICES**

**Appendix A - DISCUSSION OF PAPERS**

Compiled by Madame J.Genet.

**Appendix B - ROUND TABLE DISCUSSION**

Summarised by R.C.Pankhurst

**Appendix C - A SELECTION OF AGARD PUBLICATIONS IN RECENT YEARS**

# TECHNICAL EVALUATION REPORT

by

Dr R.C.Pankhurst  
Aircraft Establishment, Teddington, U.K.

## 1. BACKGROUND, FORM AND SCOPE OF THE MEETING

Aircraft stalling characteristics at take-off and landing have always been of vital concern to aircraft design. Nowadays, however, the importance of high-incidence characteristics is no longer restricted to low speeds, since fighter aircraft engage in high-incidence manoeuvres at high Mach numbers, and high-speed transport aircraft reach high-incidence conditions in cruise when they encounter a gust. Further, novel considerations have arisen from the practical application of high-lift devices to current projects for aircraft with reduced landing and take-off runs: renewed impetus has been given to the study of multi-element wings, for example, and indeed it is only very recently that their fluid-dynamic processes have been studied in depth. Whilst inertial properties and pilot handling play essential parts in determining stalling and post-stall behaviour, aerodynamics fills the key role in the task of ensuring the success of any new project; and it is certainly to the aerodynamicist that the designer is likely to turn first for remedial modifications to a design that falls short of its target specification.

This meeting was therefore concerned with the aerodynamics of the aircraft stall at both low speeds and high, with particular reference to the design and operation of combat and transport aircraft, including buffet penetration and post-stall behaviour. Major subject areas concerned flight experience, flight testing, wind-tunnel measurements and theoretical prediction methods, including the effects of three-dimensional flow, the influence of sweepback and the design and performance of high-lift devices. Consideration of special types of V/STOL aircraft were excluded, however, apart from occasional excursions such as the paper<sup>16</sup> on transport aircraft with externally blown flaps.

Although flight aspects were discussed as well as fluid dynamics per se, this was not a joint meeting with the Flight Mechanics Panel; still less was it allowed to become consecutive sessions devoted to the two topics. The framework that the Programme Committee had constructed for the meeting consisted of three papers, each followed by prepared comment from an invited speaker and then by other papers and discussion in the area concerned, devoted respectively to the general role of fluid dynamics in the overall context of aircraft stalling and post-stall behaviour<sup>1</sup>, the aerodynamics of high-lift aerofoils fitted with slats, slots and flaps<sup>10</sup>, and design considerations and flight test procedures for aircraft at high angles of incidence<sup>25</sup>. This framework made it possible to set fluid dynamics aspects and flight experience side by side so as to help determine the directions that might most profitably be taken by further work.

The achievements and shortcomings of the meeting are assessed in Section 2 of this report, and Conclusions are drawn in Section 7. Section 3 describes briefly the broad technical perspective of the subject, whilst Sections 4 to 6 are concerned with detail. A list of the papers presented follows Section 7.

## 2. ASSESSMENT OF ACHIEVEMENTS AND SHORTCOMINGS

The juxtaposition of the sessions on flight behaviour, on practical aerodynamics and on basic fluid dynamics must certainly have impressed several important considerations on those concerned with the fundamentals of the subject, particularly the great importance of always relating the study of fluid mechanical processes to aircraft flight behaviour. This applies perhaps particularly to the recognition of successive stages that can be passed through from the conditions of cruising flight at low angles of incidence to those obtaining at and beyond the point of departure from controlled flight. Striking examples for two aircraft were included in Paper 25. One of these formed the basis of the illustrative sketch shown in Figure 1 of this evaluation report. All the stages are distinguishable in terms of differences in flight behaviour (cf Section 6.1). Increased appreciation of these successive flight regimes, together with the ability to correlate them closely with their corresponding flow patterns, would help those engaged in aerodynamics research to increase the relevance of their work, particularly as some of the contributions on basic aspects seemed rather far from making an impact on practical problems of aircraft design and operation.

Several of the papers on applied research described important advances and presented valuable results (including some definitive data) on realistic geometrical configurations, and most of the papers on flight experience were of interest in their own right as well as in respect of the fluid dynamic processes underlying the observed flight behaviour.

The Round Table Discussion at the close of the meeting, however, proved to be rather less productive than had been hoped, at least as far as the emergence of clear-cut directives for future work was concerned. For this reason, the conclusions drawn in Section 7 are necessarily the personal interpretation of the author of this Technical Evaluation Report. They are, however, believed to represent fairly the consensus of opinion as far as this was expressed at the meeting.

### 3. THE BROAD TECHNICAL PERSPECTIVE

The continuing need for spin/stall research, and for exhaustive wind-tunnel investigations prior to flight test development, has been underlined by aircraft accident statistics<sup>1a</sup> in terms of loss of life and capital investment, for both civil and military aeroplanes. The vast number of small propeller-driven aircraft constitutes a significant proportion of the total field.

Early during the course of the meeting it became clear that, in the absence of generally agreed usage, such terms as 'stalling', 'flow separation' and 'buffet onset' need to be defined whenever they are introduced. On the other hand, there is little ambiguity in the terms used to describe phenomena that mark the ultimate bound of the term 'departure' to denote loss of control, characterised by divergent uncommanded aircraft motion of large amplitude (such as pitch up, nose slice or snap roll). Also early in the meeting, a large number of problem areas and research requirements were indicated in general terms<sup>1</sup>, particularly the following: further depth-studies of multiple-element wings, including the complex interaction that occurs between the wake shed by an upstream element, the flow through the gap between successive elements, and the newly developing boundary layer on the downstream element; the prediction of wing characteristics in separated flow, and beyond maximum lift, and not just the incidence at which separation occurs; the role of Reynolds number in separated-flow conditions; dynamic effects due to rate of change of incidence; study of the downwash field in the presence of slats and flaps after flow breakdown has occurred, with special reference to conditions at the tailplane; ground effect, and slipstream effects, in separated-flow conditions; wind-tunnel methods for studying and predicting buffet onset and growth; and tunnel interference and constraint effects in separated-flow conditions. A number of these problem areas and research requirements were brought into focus later in the meeting.

Subsequent sections of this Report discuss in turn basic fluid dynamics and wind-tunnel techniques (Section 4), the aerodynamics of high-lift wings (Section 5), and flight experience (Section 6). An attempt is made to draw broad conclusions from the meeting in Section 7.

### 4. BASIC FLUID DYNAMICS, AND WIND-TUNNEL TECHNIQUES

A common feature of many flow patterns at the stall is the occurrence of laminar separation followed by re-attachment (usually after transition in the free shear layer and at least with the flow at reattachment highly disturbed<sup>3</sup>); subsequent separation then takes place towards the trailing edge. Valuable studies (such as those of Papers 2 and 3) have been made in two-dimensional flow. They need to be extended to higher Reynolds numbers, however, and to include detailed examination of conditions at re-attachment and of the subsequent development of the flow downstream. The effects of stream turbulence also warrant study: practical engineering applications include the cascade rows of turbomachinery as well as aircraft wings at high incidence.

In the theoretical treatment, the use of the boundary-layer equations in the presence of separation (see also Paper 5) can only be justified as an engineering approximation, since they are parabolic in form whereas the velocity field in regions of flow separation need to be described by equations that are elliptic. As Prof Domingos pointed out, since the boundary-layer equations are themselves a simplification of elliptic equations, the whole field can be described in these terms; alternatively the region of attached flow can be described by the boundary-layer approximation and the separated region by elliptic equations, the whole problem being solved by iteration.

More data are needed on the transport properties of turbulent boundary-layers<sup>6</sup>, together with further improved mathematical models. This applies especially to three-dimensional flow, and here further complications arise from structural requirements imposed by engineering considerations (such as flap support brackets).

Whilst three-dimensional effects dominate the development of the stall on a wing of finite aspect ratio, valuable pointers can still be obtained from two-dimensional aerofoil characteristics<sup>1,7,8</sup>, at least when the stall is of the trailing-edge type<sup>11</sup>. Boundary-layer control applied to the wind-tunnel wall makes possible a closer approach to two-dimensional flow in high-lift conditions,<sup>8</sup> at the same time it is well known that quite small degrees of spanwise flow can produce marked departures from how the boundary layer and overall flow pattern would have developed in truly two-dimensional conditions.

More work needs to be done on tunnel interference, particularly very close to  $M = 1$ , on support interference and on proper model-scale representation of the engine. Reassuring evidence of the validity of available separated-flow blockage corrections has been obtained<sup>9</sup>.

### 5. AERODYNAMICS OF HIGH-LIFT WINGS

The paper by A.M.O. Smith<sup>10</sup> represents a considerable advance in our understanding of the flow mechanisms of slats, slots and flaps. The use of so-called 'canonical' pressure distributions leads to important practical conclusions about the occurrence of separation and means for preventing separation and attaining high lift, such as 'dumping the flow' at high trailing-edge velocities. The paper also distinguishes four further features in the flow mechanism of multiple-element aerofoils, namely (a) slat circulation (which reduces the velocity peak on the main part of the

aerofoil), (b) circulation effect (increase in lift on a forward element because of the upwash induced at its trailing edge by the element next downstream), (c) off-the-surface pressure recovery (a more effective method than for a boundary layer on the surface), and (d) fresh-boundary-layer effect (leading to a greater ability to surmount adverse pressure gradients further aft). There is also <sup>10a</sup> an adverse inviscid-flow effect due to the non-uniform stream to which a flap is exposed because of the wake shed by the main aerofoil immediately upstream, although its magnitude remains to be determined. Of the areas needing further study, perhaps the most important to aeroplane design are the development of inverse methods (i.e. design procedures) for multiple-element aerofoils and extensions to three-dimensional flow, for which different compressibility factors are needed for the several terms involved: a single 'overall' factor is unlikely to suffice. Meanwhile a simplified mathematical model for two-dimensional aerofoils with short separation bubbles has also been described<sup>12</sup> and is being developed further. Elsewhere methods are also being developed for calculating flows with shock waves, in both two-dimensional and three-dimensional conditions.

In complex practical situations with wings of finite aspect ratio at high incidence with high-lift devices deployed, however, wind-tunnel testing will still be needed, both for final checks and for obtaining exploratory data so as to effect economics in the subsequent development phase. One of the conclusions of Paper 11, for instance, was that wakes shed by slat brackets on the upper surface of a swept wing could trigger flow separation and thus change the stall pattern and the maximum lift coefficient. In model-scale testing at reduced Reynolds numbers it is essential to reproduce the type of flow pattern of the full-scale prototype: this requires fore-knowledge or sure prediction of what the full-scale flow pattern would be, and may involve the use of transition-tripping devices of unacceptably large size. Again, the effect of changes in Mach number depends on the type of stalling pattern, and can thus vary from one Reynolds number to another. Such observations point the need for a wind-tunnel in which Reynolds number and Mach number can be varied independently: basing an aircraft design on the results of tests in existing low-speed tunnels may easily prevent its full-scale potential from being fully realised.

The differing requirements of wing design at high speeds and low, and the need to retain good aerodynamic characteristics throughout the speed range, suggests the desirability of a nose shape that can be varied continuously. A promising practical means of doing so is provided by the variable-aerofoil mechanism developed at the Royal Aircraft Establishment (RAE) and described in Paper 13, which presents studies of various types of change in leading-edge geometry and stresses the need for further research in both two-dimensional and three-dimensional conditions and for developing improved leading-edge devices to operate in the highly complex flow patterns that arise at high Mach numbers and high angles of incidence.

Paper 16 constituted an excursion into the special area of externally blown flaps, and at the same time provided a bridge between wing aerodynamics and flight experience. Salient points were (a) the distinction between the maximum attainable lift and that actually usable in order to ensure acceptable stalling characteristics, (b) the possibility of unacceptable attitudes in the case of a STOL aircraft with externally blown flaps (because of the very low stalling incidence), (c) the importance of adequate lateral control in order to cope with the large rolling moment that arises if an engine fails on one wing of an aircraft with externally flaps, and (d) the insufficiency of applying traditional stall margin criteria to STOL aircraft, for which a load-factor margin is suggested in place of the usual speed criterion.

In the case of powered-lift aircraft there is a dearth of flight experience at speeds below the power-off stall. Flight limitations in this condition will have to be thoroughly investigated, and the aircraft characteristics required need to be specified.

## 6. FLIGHT EXPERIENCE AND ASSOCIATED INVESTIGATIONS

### 6.1. Required scope of investigation.

Flight testing at high angles of incidence must certainly cover the range of flight conditions from buffet onset to departure from controlled flight\*. It should cover also post stall gyrations, spinning and spin recovery, although the greater emphasis should normally be placed on the usable incidence range up to stall/departure and on stall/spin avoidance and prevention. The importance of wind-tunnel and theoretical studies of fluid mechanical processes in relation to aircraft flight dynamics is emphasised in Paper 1, whilst Paper 25 indicates the wide variety of wind-tunnel facilities that need to be employed in order to define the aerodynamics of an aircraft in terms of successive stages of flight dynamical behaviour (cf Fig 1).

In the high-incidence flight test procedures followed by the US Navy<sup>25</sup>, buffet onset is defined to occur when oscillations in normal acceleration at the centre of gravity of the aircraft reach 10.05g. The observations are usually made during a wind-up turn manoeuvre but the band-width of the acceleration signal is not specified. The buffet onset can be calculated on an empirical basis, predicted from wind-tunnel measurements or measured in flight, but the subsequent build-up of buffet intensity of value and importance as a warning of impending stall or departure can be estimated only roughly. There is a need to develop methods for delaying buffet onset and for ensuring that buffet

\* Departure is characterised by divergent uncommanded aircraft motion of large amplitude, such as pitch-up, nose slice or snap roll - it is a post-stall phenomenon although on modern fighter aircraft it occurs at nearly the same incidence as the stall. Post stall gyrations are uncontrollable oscillations following departure and preceding spinning. By way of illustration, the stalling sequence for a particular aircraft is depicted in Figure 1, based on Figure 3 of Paper 25.

intensity builds up in a satisfactory manner while still maintaining a high degree of manoeuvrability: buffet of sufficient intensity impairs tracking ability and weapon effectiveness, to a different extent from one weapon to another. Whilst maximum lift may be estimated from wind-tunnel tests, buffeting may become unacceptable at a lower angle of incidence that is difficult to predict.

The angle of incidence at departure has been shown to correlate well with the dynamic directional-stability parameter defined by the equation

$$C_{n_{\beta dyn}} = C_{n_{\beta}} - (I_z/I_x)C_{l_{\beta}} \sin \alpha$$

where  $C_{n_{\beta}}$  denotes the static directional-stability derivative,  $I_z$  and  $I_x$  are moments of inertia, and  $C_{l_{\beta}}$  the rolling-moment derivative. More research is needed, however, to establish whether or not there may be further parameters of importance.

There is a great need for improved criteria relating to manoeuvring characteristics at high speeds, and for extended test-facility capability: adequate low-speed tunnel installations need to be developed<sup>22a</sup> for testing at extreme angles of incidence and sideslip, such as variable-density tunnels with advanced instrumentation for 6-component measurements of dynamic characteristics up to 90 deg. and with the propulsion system adequately simulated. Provision should also be made for ground-effect investigations, and possibly also for gust simulation. For transonic testing a large pressurised tunnel is essential in order to provide a wide range of Reynolds number and to cover all the flight conditions. In comparisons between wind-tunnel and flight-test results there is a need both for increased measurement accuracy and for improved methods of analysis, whilst the use of the wind-tunnel to check analytical prediction methods that are currently being developed for stalled and post-stall conditions should be preceded by investigations to confirm the validity of the wind-tunnel techniques in these conditions: stalling accidents can only be prevented by extensive wind-tunnel testing combined with analysis in depth. It would be valuable to conduct systematic tests on a control model in a range of wind-tunnels, so as to validate testing techniques and establish reliable wall corrections.

## 6.2. Buffet, buffeting and wing rock<sup>22, 24, 23</sup>

The intense buffeting that arises from extensive flow separation causes severe deterioration of aircraft handling qualities and tracking ability, and thus severely degrades combat potential. In high-speed manoeuvres, the use of flaps and slats can delay flow separation and the subsequent loss of combat capability<sup>22</sup>. Predictions of initial flow separation from wind-tunnel results are then found to be poor, however. Further work is needed on buffet data correlation, on the relationship between heavy buffet and loss of dynamic stability, and on the optimisation of flap/slat operating schedules in manoeuvring flight.

As alternative to leading-edge slats or Kruger flaps as a means of postponing the stall, use can be made of a sharp-edged 'manoeuvre strake'<sup>24</sup>. This device is a highly swept fillet at the wing-fuselage junction, and provides vortex lift up to high angles of incidence, with little weight penalty. Tests on a particular wing configuration showed that, although buffet began at a low lift coefficient, buffet intensity did not exhibit a subsequent rise. No limitation in usable lift appeared to be imposed by buffet induced by vortex bursting. The drag, although increased slightly at low lift, was reduced substantially at high lift, on the other hand, in another series of tests the lift increase and drag reduction due to a manoeuvre strake were diminished when leading-edge flaps were deflected.

The dynamic analysis of buffeting, and the prediction of aircraft behaviour beyond buffet onset, are important to civil transport aircraft when they encounter gusts, as well as to combat aircraft manoeuvring at transonic speeds. Wing structural buffeting (predominantly in the wing bending mode) and wing rocking (a rigid-body mode) can be described mathematically<sup>23</sup> either by a forced-vibration approach based on the fluctuating part of measured aerodynamic forces or by a non-linear flutter-type approach based on mean aerodynamic forces and using equations that represent a limit cycle instead of containing time explicitly. The linear forced-vibration method is generally considered appropriate to the study of wing structural buffeting, although its range of applicability needs to be established. In general there is a closed-loop interaction between wing motion and aerodynamic forces, and the choice between forced-vibration and limit-cycle models can be made on the basis of an experiment in which the power spectra of pressure or load fluctuations for a fixed wing are compared with those for a wing that is forced to oscillate sinusoidally. In the case of wing rocking, further investigations are needed in order to establish which characteristics can be deduced from wind-tunnel tests on rigid models. Buffeting can be predicted from tests of fixed wings, provided wing motion produces a purely additive pressure field.

## 6.3. Stall warning, stalling behaviour and post-stall characteristics

In order to meet the requirements of stall warning through buffet onset or stick shake, of nose-down pitching at the stall (without excessive wing drop), and of maintaining lateral, directional and pitch control up to and beyond the stall, it is often necessary to introduce aircraft modifications at the prototype flight testing stage.

On the BAC Jet Provost Mark 5 (military trainer) and Strikemaster 167, for instance<sup>17</sup>, the nose drop at the stall was initially not sufficiently pronounced for training purposes, and the maximum lift was too low: modifications had to be devised that increased the maximum lift and improved the nose dropping characteristics without loss of stall warning (provided by airframe buffeting due to impingement of the wing wake on the tailplane). Again, wind-tunnel and flight tests determined the modifications needed to ensure high maximum lift combined with nose-down pitching moment at the stall for the Fokker F-28 short-haul aeroplane<sup>20</sup>. Similarly based investigations were also made to ensure good high-incidence handling characteristics (freedom from wing drop, from pitch up and from wing rock) for the Hawker Siddeley Harrier<sup>19</sup>; a method for buffet prediction was also devised.

The economic importance of predicting stalling speed accurately for aircraft such as the Boeing 747 is exemplified by a loss of 38 per cent in payload (or 55 per cent in potential profit) that corresponds to a 5 per cent error in the determination of stalling speed<sup>21</sup> when the aircraft is designed so as to be able to land with full payload in exactly the field length available. For this aeroplane it was found that tunnel tests at a Reynolds number of  $1 \times 10^6$ , together with check tests at  $7.5 \times 10^6$  and a good deal of engineering judgement based on experience, did enable satisfactory estimates of stalling speed to be made for the full-scale Reynolds number of  $40 \times 10^6$ . It should be noted, however, that the extrapolations were able to make use of factors derived from previous Boeing aircraft of largely similar basic design: in general, a detailed understanding of the aerodynamics would need to be obtained.

From investigations made to establish the stalling and post-stalling characteristics of the Convair F-111 aircraft<sup>18</sup> it was concluded that wind-tunnel static and dynamic derivative data for use in flight-simulator studies need to be obtained at high Reynolds numbers and full-scale Mach numbers. Results from instrumented, radio-controlled dropped-model measurements of the overall aerodynamic coefficients help to improve the data obtained from a wind-tunnel and provide information on departure characteristics, post stall behaviour and spin susceptibility; because of Mach number and Reynolds number limitations, however, full-scale flight test data also are required. As regards full-scale flight tests, it was concluded that emphasis should be placed on stall/post stall recovery procedures and on spin susceptibility. Prior tests using a model in free flight in a wind tunnel serve to indicate conditions for yaw divergence and thus provide a valuable basis for determining the maximum angles of incidence to be used at full scale, but the vertical (spin) tunnel is regarded as having only limited value. Analytical prediction methods are expected to be used increasingly.

## 7. CONCLUSIONS

The broad conclusions to be drawn from the meeting may be summarised as follows:

- (a) Accident statistics, the operating economics of civil aeroplanes, and the effect of buffet on the tracking ability, weapon effectiveness and combat potential of military aircraft, combine to emphasise the vital importance of the aerodynamics of the stall to both military and civil aircraft at take-off and landing, to military aircraft in high-speed manoeuvres, and to civil aircraft on encountering gusts during cruise.
- (b) Besides ensuring that buffet onset does not occur at unacceptably low angles of incidence, the aircraft designer must also ensure that the subsequent build-up of buffet intensity with increase of lift coefficient takes place in a manner that is conducive to satisfactory aircraft handling characteristics.
- (c) Several novel considerations will be involved in certain aspects of the stalling of special types of VTOL and STOL aircraft such as those with externally blown flaps. For the most part, however, such configurations lay outside the scope of the meeting.
- (d) A great deal of work is currently in progress on the basic fluid dynamics of stalling phenomena. It tends, however, to be pre-occupied with considerations of boundary-layer separation: not enough attention is being paid to reattachment and the subsequent development of the flow downstream.
- (e) The effects of stream turbulence on stalling characteristics warrant investigation because of their importance to turbomachinery cascades.
- (f) Highly significant advances have been made recently concerning the mechanism of flow over multiple-element aerofoils (i.e. aerofoils with slats, slots and flaps) in two-dimensional, incompressible flow conditions. There is great scope for the extension of this work to wings of finite aspect ratio in compressible flow, the development of inverse methods (i.e. design procedures), inclusion of the effects of partial separation, detailed study of wakes in pressure gradients, and investigations of the complex interactions that take place between the flow leaving one element and that developing on the next.
- (g) Wind-tunnel techniques need to be improved in respect of constraint corrections near  $M = 1$ , model support interference, engine-flow simulation, and testing at extreme angles of incidence and sideslip (including dynamic characteristics).



- (h) Wind-tunnel capability must provide for both an adequate range of Reynolds number and the variation of Reynolds number and Mach number independently.
- (i) To base the design of future aircraft on results obtained at low Reynolds number, and failure to improve upon existing tunnel techniques, could easily prevent the full potential of new projects from being realised.
- (j) Consideration should be given to the possibility of testing a control model in various wind-tunnels in order to validate wind-tunnel techniques and establish reliable wall constraint corrections.
- (k) Improved methods are needed for predicting the rate of increase of buffet intensity with lift coefficient.
- (l) Before embarking on expensive and crucial flight-testing programmes, adequate and exhaustive wind-tunnel investigations must be made over the whole incidence range, and the results analysed thoroughly.
- (m) Flight tests at high incidence must extend up to or beyond the conditions of departure from controlled flight, greater emphasis being normally placed on the usable incidence range (up to stall/departure), and on stall/spin avoidance and prevention, than on post-stall gyrations, spinning and spin recovery.
- (n) Improved methods of analysis are needed for the adequate comparison of wind-tunnel and flight test results.

## REFERENCES

1. G.J. Hancock                      Role of fluid dynamics in aircraft stall and post-stall gyrations  
(invited paper)
- 1a. T.C. Muse                        Prepared comment on Paper 1
2. E. Dobbinga                      Some research on two-dimensional laminar separation bubbles  
et al.
3. S. Burnel                         Recherches théoriques et expérimentales sur les décollements liés à une déformation  
et al.                                  locale de surface
4. (Paper withdrawn)
5. M. Vincent de Paul              Prévision du décrochage d'un profil d'aile en écoulement subcritique
6. A. Wortman                      Parametric studies of separating turbulent boundary layer flows  
W.J. Franks
7. F.X. Wortmann                  Design of aerofoils with high lift at low and medium subsonic Mach numbers
8. O de Vries                        Comments on the methods developed at the NLR for conducting two-dimensional  
research on high-lift aerofoils
9. J-C Vayssaire                    Corrections de blocage dans les essais en souffleries – effects dus aux décollements
10. A.M.O. Smith                    Aerodynamics of high-lift aerofoil systems
- 10a. D. Küchemann                Prepared comment on Paper 10
11. D.N. Foster                      The low-speed stalling of wings with high lift devices
12. I.C. Bhateley                    A simplified mathematical model for the analysis of multi-element airfoils near stall  
R.G. Bradley
13. G.F. Moss                        The effect of leading-edge geometry on high-speed stalling  
et al.

14. Paper incorporated into No 13
15. Paper withdrawn
16. D.J. Moorhouse      A practical look at the stall and high lift operation of externally blown flat STOL transport configurations
17. W.D. Horsfield      Flight development of the stalling characteristics of a military trainer aircraft  
G.P. Wilson
18. J.E. Goode      Stall and post-stall characteristics of the F-111 aircraft
19. C.L. Bore      Post-stall aerodynamics of the Harrier
20. T. Schuringa      Aerodynamics of wing stall of the Fokker F-28
21. J.K. Wimpess      Predicting the low-speed stall characteristics of the Boeing 747
22. P.J. Butkewicz      On airflow separation and buffet onset during fighter aircraft maneuvering
23. J.G. Jones      The dynamic analysis of buffeting and related phenomena
24. E.J. Ray      Manoeuvre and buffet characteristics of fighter aircraft  
et al.
25. W.R. Burris      Aerodynamic design and flight test of US Navy aircraft at high angles of attack  
J.T. Lawrence
- 25a. Ph. Poisson-Quinton      Prepared comment on Paper 25

# ROLE OF FLUID DYNAMICS IN AIRCRAFT STALL AND POSTSTALL BEHAVIOUR

by G.J. Hancock

Dept. of Aeronautical Engineering, Queen Mary College (University of London)

## SUMMARY

Stall of an aircraft is defined as a limiting condition for normal flight operation; airworthiness requirements for stall and post stall behaviour are briefly reviewed.

The distinct dynamic and aerodynamic contributions to a stall manoeuvre and post stall gyration are described; the pilot's influence is assessed, and some implications on airframe design are outlined.

The various aerodynamic aspects are then described in further detail; the present state of knowledge of flow separation on wings, the control of flow separation and the role of model experiments are reviewed.

## 1. INTRODUCTION

Throughout the history of prototype flight testing, accidents arising from a stall situation have been, unfortunately, a recurring theme. Within the last decade a sequence of accidents and incidents on some high  $\Gamma$  tail plane configurations has been caused by the deep stall phenomenon. Current prototypes are not immune; an Aerospatiale Corvette has recently crashed, due, it is thought, to a lack of control in a stall. Fighter military type aircraft have been lost because of unexpected difficulties in the handling characteristics in the stalled regime and in the mode of spin recovery.

In commercial airline operation, however, because of the thoroughness of the prototype flight test programme, the stringency of the registration authorities, and the evolution of an empirical set of safety factors, it is thought that a satisfactory level of safety in respect of aircraft stall is being achieved; typical quoted figures suggest that the probability of reaching a stall warning is of the order of 1 in  $10^5$ , whereas the probability of occurrence of a (recoverable) stall is of the order of 1 in  $10^6$ .

Large military transport aircraft meet roughly the same requirements as those for civil transport aircraft, and consequently attain about the same level of safety. Smaller fighter type service aircraft are more often involved in accidents arising from post stall gyrations and spin type manoeuvres, both in training and in combat; training accidents occur rather more frequently than those in combat. Such occurrences are due to marginally acceptable handling qualities in the extreme attitude conditions which are called for to meet some of the limits of operational requirements.

The problem of stall is therefore to ensure that an aircraft is recoverable during excursions into the stall regime, whether inadvertent due to atmospheric gusts or intentional in manoeuvring flight, and to ensure that the aircraft cannot under any circumstances exceed the specified limitations and so enter an uncontrollable state. Civil aircraft, for example, are precluded from entering a spin. Fighter military aircraft must be capable of recovery from all of its spin modes.

It is mandatory to demonstrate satisfactory stall and post stall behaviour in flight; the aircraft designer must, therefore, ensure that the safety of the prototype aircraft is not in any way prejudiced. Ideally the aim at the design stage must be to acquire all the pertinent information necessary to predict the behaviour of an aircraft at high angles of attack, sideslip, and rates of roll, throughout the speed range; prototype flight tests should then be made to check out and quantify predicted trends not to investigate unknown conditions.

Attention at this conference is being focused on those fluid dynamic aspects relevant to the problem of the stall behaviour of an aircraft. Onset of flow separation on a main wing in its many slat-flap combinations, the progression of flow breakdown on a main wing, the effect of the separated flow field on the whole aircraft configuration, in particular on the tailplane, the effects of dynamic manoeuvres on the separated flow field characteristics; these are the basic ingredients of the problem. Theoretical prediction methods, incorporating empirical data, for any of the above items are, to say the least, sparse. Results from wind tunnel testing can be totally misleading unless the tunnel Reynolds number is high enough, and even then very small differences between the shape of the model and full scale aircraft can lead to significant differences in flow behaviour at the stall onset. Because of the uncertainty of design data, together with the imperative requirement for safety of the production aircraft, flight tests of the stall behaviour on a prototype aircraft are necessarily extensive, covering a wide range of parameters, time consuming and expensive. Advances in fundamental knowledge of flow separation and in the techniques of the acquisition of reliable data at high angles of attack, and high angles of sideslip, are urgently needed.

In the past when flight tests have indicated areas of inadequacy in meeting any of the airworthiness stall requirements; it has often been possible to rectify the situation with so called 'quick fixes', such as vortex generators, leading edge fences, etc., which are relatively easy to install on the structure; nevertheless finding the optimum position of these 'quick fixes' by a successive series of flight tests can be anything but 'quick'. Nowadays inadequacies are appearing in the behaviour of some prototype aircraft in stalled flight which the traditional 'quick' fixes cannot readily alleviate, so although modifications are therefore called for it is not altogether clear in our present state of knowledge what form these modifications should take.

Another factor which adds a further dimension of difficulty concerns the wide range of size and shape of contemporary configurations: the T-tail configuration with its ill defined stall; the highly swept configuration whose flow separation does not in itself introduce any handling problems but whose minimum speed conditions then become ill defined so one potentially hazardous condition is replaced by another;

the variable sweep aircraft often with significant aeroelastic effects; the V/STOL aircraft where power and aerodynamics are inextricably tied up together. Empirical know-how and experience built up on one type of configuration cannot be readily extrapolated to another type.

It should be emphasized that allowable stall behaviour cannot be quantified, requirements to be met are phrased in terms of 'satisfactory' recoveries obtained with the normal use of the controls. Such criteria are subjective rather than objective, qualitative rather than quantitative; it is the pilot from the Air Registration Board who pronounces the final verdict. The question arises of how far this attitude should be reflected in the type and quality of aerodynamic detail, an answer could possibly lead to an indication on the direction of future research.

Since this note is intended to be introductory to the overall conference proceedings the aim is to discuss some preliminary aspects of the flight mechanics of stall manoeuvres and then to assess the content of the various fluid mechanic problems; the state-of-the-art of the fundamental prediction methods are outlined and testing techniques are discussed.

Most of this material presented here is extracted from Ref. 1; however, one or two more recent developments are noted.

## 2. SOME FLIGHT MECHANICS ASPECTS OF AIRCRAFT STALL

First it is advisable to attempt to clarify some of the concepts and phraseology used in the field of aircraft stall.

Aircraft stall is a limiting condition of normal flight when the pilot experiences a noticeable change in the orthodox handling characteristics of the aircraft. Some changes in the elevator angle can lead to rapid manoeuvres, about either or, both, the longitudinal and lateral axes. Sometimes the opposite occurs, the handling characteristics become vague; moderate changes in the elevator angle induce little change in aircraft attitude.

Identification of the stall is the most important aspect of any flight test programme. Two series of tests are called for in the civil aircraft airworthiness requirements, namely, a slow approach to the stall (the speed of the aircraft is reduced by about 1 knot per second) and a dynamic stall (essentially obtained by the rapid application of an up elevator). In a slow approach to the stall the speed is gradually reduced until the airplane commences a large rolling or pitching motion, subsequent recovery is deemed satisfactory if the aircraft returns to a pre-stall condition using, if required, the elevator control. All aircraft configurations must be tested with and without the extension of slats and flaps, various C.G. positions, undercarriage up and down, asymmetric power, etc.

The classical ideal of a natural nose down motion of the aircraft at the stall onset is no longer mandatory. As long as there is a clear indication that the stall has been reached and that there is sufficient elevator power to restore the aircraft to its pre-stall state without the pilot feeling that he has lost control then the stall characteristics are said to be satisfactory. Much depends, however, on the pilot's skill and experience; the timing of the recovery initiation and the rate of application of the recovery elevator are left to the pilot's discretion and so significant differences in the stall recovery manoeuvre can be experienced on the same aircraft. Large overshoot conditions can occur in the recovery manoeuvre especially following the dynamic stall; angles of  $15^\circ$  above the angle of the onset of stall are frequent; in extreme cases the maximum incidence can be much higher, the D.E. Buffalo actually went up to  $45^\circ$  in one stall test.

For those aircraft which do not possess a natural large motion at the onset of the stall it is mandatory in the U.K. that an artificial stall identification system be installed. This system usually takes the form of a stick pusher device which automatically pushes the elevator down when the aircraft reaches a specified incidence (which depends on the rate of increase of incidence) thus pitching the aircraft nose down; the aircraft is not allowed to stall.

Once the stall has been identified it is mandatory to provide stall warning at a few degrees below the incidence at which onset of stall occurs. Ideally stall warning should take the form of mild buffetting with the intensity of buffetting increasing up to the stall. Effectiveness of all control surfaces should be maintained. Unfortunately such an ideal is rarely attained so artificial stall warning has to be given to the pilot. Stall warning devices usually takes the form of a stick knocker or shaker, actuated via an incidence vane on the side of the fuselage.

As already implied many aircraft in the early flight development stages demonstrate unsatisfactory stall characteristics, for example; too rapid a nose drop at the stall, too rapid a pitch up, sluggish stall recovery, insufficient control effectiveness even in the pre-stall state, intense buffetting, uncontrollable wing drop; wing rock, loss of directional stability leading to lateral limit cycle oscillations, all have been experienced at one time or another. Prevention of these phenomena is the basic aim of the designer, although, in practice remedying them once they have appeared seems to be the more usual occurrence.

It has to be emphasized that aircraft stall is concerned with the flight behaviour of an aircraft involving either the longitudinal or lateral degrees of freedom, although more often a complex coupling of the longitudinal and lateral motions results. Fluid mechanics is only one factor which contributes to aircraft stall. Other equally important factors concern the inertial characteristics of the aircraft, and the piloting technique involved in the sequence and mode of operation of the controls during recovery.

A knowledge of the fluid mechanics of flow separation, flow breakdown, and its progression, cannot by itself indicate whether a stall behaviour will, or will not be acceptable. On the other hand any deficiencies in a stall behaviour have to be rectified by fluid mechanic means.

Stall and the post stall motion prior to initiation of the recovery by the pilot involves the interaction of the various aerodynamic forces and moments. Assuming for now that lateral control is maintained, the longitudinal motion above the stall depends on the changes in overall lift, drag, and pitching moment with incidence. As incidence gradually increases loss of  $C_L$  above  $C_{L_{max}}$  causes the aircraft to fall, tending to increase both the glide path angle and incidence. A large increase in drag at the stall decreases the forward speed, causing the glide path angle to increase. But as the aircraft comes out of trim a nose down pitching moment should be induced which leads to decrease incidence. In the first few seconds following the onset of the stall the effects of the changes in lift and moment dominate; the effect of the changes in drag builds up relatively slowly; drag therefore becomes significant in the more sluggish recovery. What happens depends on the balance of these various effects. The influence of the inertial characteristics is apparent. A nose down pitching moment on a large aircraft will induce a sluggish response which when associated with lift changes and large increase of drag can delay and possibly imperil recovery. According to Wimpenny (2) the small BMD 125 executive jet and the far larger BMD Trident have similar lift and pitching moment coefficients at the onset of the stall but the nose down motion of the BMD 125 is rated as excellent while the Trident is regarded as far more sluggish.

One point to note is that it is usual for stall tests to be performed without any reference of the incidence to the pilot (the argument of whether or not an indication of the incidence should be installed as a standard piece of equipment is a continuing debate). A pilot's impression of the longitudinal stall manoeuvre is deduced primarily from the pitch response characteristics. It is the orientation of the aircraft in space to which the pilot responds; thus an increase in incidence coupled with an increase in glide path angle could leave the aircraft at the same pitch angle and so the pilot would be unaware of the changes taking place apart from the loss in height. One pilot reported satisfactory stall behaviour on a C-141 aircraft when his aircraft pitched nose down in the recovery even though the aircraft trimmed out several degrees above the stall angle of incidence. Again in the deep stall incidents the rate of increase of glide path angle matched the rate of increase of incidence with little change of pitch attitude, thus a pilot had little foreboding of the disastrous rates of change taking place, when the pilot realized his position the controls were ineffective.

Having established that the basic ingredients of the aircraft stall manoeuvre are aerodynamics, inertial characteristics and pilot handling, it is possible to proceed to the discussion of the role of aerodynamics in aircraft stall.

As a preliminary step it is worth distinguishing between some of the terms and expressions used in this particular field. As stated earlier aircraft stall is recognized by the behaviour and handling qualities of an aircraft in flight as it reaches a limiting incidence condition, the stall recovery manoeuvre involves flight in the post stall regime, referred to as a post stall gyration. Aerodynamicists, however, are more familiar with flow separation and flow breakdown, rather than with aircraft stall. But even within the aerodynamicists' domain it is necessary these days to differentiate between flow separation and flow breakdown. On an aircraft with highly swept wings for example flow separation can occur in an organized manner, forming a leading edge vortex, but flow breakdown would not have occurred; although the incremental changes in lift, drag, and pitching moment would be non-linear the aircraft would not necessarily be regarded as stalled; it is possible however, that unless the leading edge vortices were 'fired' by a fence, or a notch, their tendency to wander over the span of the wing could lead to some difficulty in lateral control. Perhaps aerodynamicists could be more careful in their use of the phrases flow separation and flow breakdown. In general there is the sequence, flow separation is followed by flow breakdown, both are essential preconditions for the onset of aircraft stall.

It might be agreed that whereas it is appropriate to refer to aircraft stall, it is misleading to refer to wing stall. Wings experience flow separation and/or flow breakdown but stall implies a much wider notation of the aircraft as a whole. The aerodynamics in aircraft stall embraces the aerodynamic flow environment about the entire aircraft, flow breakdown on the wing affects directly the downstream conditions around the tailplane and rear mounted engines. Pitching moment characteristics depend on the mutual interference effects between main wing and tail plane. In discussing aircraft stall the complete aircraft must be considered; the wing and tailplane combination for the symmetric stall motions and wing, fuselage, fin, tail plane for the asymmetric stall motions. Furthermore, it is important to appreciate that the aerodynamics of aircraft stall are concerned not only with the aerodynamics in the pre-stall phase but more especially in the post stall gyrations in the recovery manoeuvres.

The role of buffetting illustrates to some extent the distinction between aircraft stall and flow breakdown, for buffetting can be a pre-stall warning even though buffetting can only arise from flow breakdown. Buffetting is not necessarily accompanied by the large pitching or rolling motion which heralds the stall, neither is the control effectiveness significantly impaired. Again it is necessary to distinguish between buffet and buffetting; buffet is the random aerodynamic phenomena associated with flow breakdown whereas buffetting concerns the response of the elastic airframe to buffet, whether or not there is a feed back from the responding structure as the buffet phenomena itself is not really known. Intensity of buffet is related to the intensity of buffetting only through the inertial and structural characteristics of the aircraft; if for example intensive buffet occurs around a nodal line on a wing buffetting will be small, on the other hand minor buffet around a antinode could lead to significant buffetting. Pilot assessment of intensity of buffetting depends critically on the location of the cockpit in relation to the structural mode excited by buffetting.

Returning now to the problem of aircraft stall, some overall design principles can be formulated (even if they cannot always be implemented). Onset of flow breakdown on the wing should be localised initially and then spread progressively with increase in incidence. A sudden complete flow breakdown gives too little warning possibly leading to a violent manoeuvre, especially for a lighter aircraft. Breakdown in the wing tip region need not lead to a significant loss of lift but wing drop would be likely, associated with loss of aileron effectiveness. Inboard breakdown would lead to loss of lift and possibly inducing large downwash effects on the tailplanes. Thus flow breakdown about mid-span is called for, possibly moving inboard gradually rather than outboard. One design parameter to vary the location of the initial flow breakdown and its subsequent progression is washout i.e. a decrease of twist toward the wing tips; performance could be reduced for example by the modification to the induced drag characteristics, so a compromise has to be made.

A recent paper on this aspect for non-swept wings in Ref.3. A low tailplane is preferable to a high tailplane; on increasing incidence a low tailplane moves away from the separated wake behind the main wing thus increasing the tailplane stabilising effectiveness whereas a high tailplane moves gradually into the wing wake thus losing its stabilising effectiveness; the elevator effectiveness behaves in a corresponding manner.

In general terms the main problems of aerodynamics in aircraft stall can be listed.

- 1) at low speeds: the onset of flow separation and the onset of flow breakdown on the main wings, both in their clean configuration and with their various slat-flap extensions; the progression of the regions of flow breakdown with incidence up to high incidences; the sensitivity of this progression to lateral disturbances the factors which control this progression; devices to control the progression; flow separation and breakdown from the front fuselage at high angles of incidence; the flow field behind the main wing; the tailplane characteristics when the tailplane is either immersed in, or situated near the separated wing wake; the effects of large lateral motions; the overall forces and moments up to high angles of incidence ( $90^\circ$  for military aircraft) and sideslip; effectiveness of elevator, aileron, rudder at all angles of incidence and sideslip;
- 2) at high speeds: the additional complications of the development of the shock formations; the containment of shock induced separation and buffet; the utilisation of available  $C_L$  for manoeuvrability.
3. STATE-OF-THE-ART REVIEW OF FLOW BREAKDOWN

A broad brief survey of the problems associated with flow separation and breakdown is now outlined. It is not intended to be a comprehensive survey, a fuller account is given in Ref.1; the aim is to highlight some of the more important problems where research is needed.

### 3.1. TWO DIMENSIONAL AEROFOIL CHARACTERISTICS

From a fundamental point of view it is necessary to start with two dimensional aerofoil sectional characteristics.

At low speeds flow breakdown on a two dimensional aerofoil can take the form of a leading edge 'bubble' burst or a trailing edge boundary layer separation. Significant advances have been made in the understanding and structure of leading edge laminar boundary layer separation 'bubbles' but as far as the author is aware although many useful empirical formulae have been developed the theoretical prediction of the breakdown of a 'bubble' on an actual airfoil to predict  $C_{L,max}$  has not yet been obtained. The trailing edge boundary layer separation phenomena is also unresolved. Some success has been obtained in the prediction of the pressure distribution assuming a position of separation by Jacob<sup>(2)</sup> for example as shown in Fig.1; it is not clear how far this approach has been followed up.

The flow field behind a two dimensional aerofoil once the flow has separated (e.g. wake characteristics, entrainment effects, general downwash characteristics) has not received sufficient attention. Silverstein and Katzoff<sup>(3)</sup> looked at downwash fields, mainly for attached flow, although some discussion on an empirical level was given to the flow separation case.

When slats and flaps are introduced the optimum synthesis of slat-wing-flap combination to give maximum lift seems to be when the boundary layer is on the point of separation all along the aerofoil upper surface. Flow breakdown in such a case leads to a drastic and sudden lift loss. At the present time it is not possible to calculate the incidence for the onset of flow separation, mainly because of the interaction of the flows between the slots and the wakes from the upstream surfaces. More emphasis should be given to the characteristics of slat-wing-flap arrangements well above  $C_{L,max}$ .

No studies either theoretical or experimental of the separated flow field behind a slat-wing-flap arrangement are known to the author. It is possible that once this flow field has separated it behaves in much the same way as that behind a single aerofoil with the same values of  $C_L$ ,  $C_D$  and  $C_M$ , however this suggestion needs to be checked.

In all of the above phenomena, as indeed throughout this whole field of flow separation and breakdown the effects of Reynolds number is of paramount importance. In a wind tunnel only results from model tests at sufficiently high Reynolds number will be indicative of the type of flow separation and breakdown of the full scale section. What is not so clear is that once flow separation has occurred, how long does Reynolds number remain a fundamental parameter in the subsequent variation of  $C_L$ ,  $C_D$ ,  $C_M$ , wake characteristics, downwash field etc? Presumably once flow breakdown takes place near the leading edge both Reynolds number and sectional profile shape become less significant.

A difficulty in wind tunnel testing when measuring two dimensional characteristics is the maintenance of two dimensional conditions once the flow has broken down. Considerable differences in static hysteresis effects in  $C_L$  above  $C_{L,max}$  are noticeable in the literature on the same aerofoils, the reason is due presumably to differing three dimensional separation patterns in various wind tunnels.

Stall by definition involves a dynamic manoeuvre and so the effect of the rate of increase of incidence on the development of flow breakdown and the rate of decrease of incidence on the flow reattachment needs to be assessed. There has been considerable work on two dimensional aerofoils oscillating about mean high incidences in relation to the performance of helicopter rotor blades. As shown in Fig.2 there is an increase in  $C_{L,max}$  due to the rate of increase in incidence above the static  $C_{L,max}$  but the loss in  $C_L$  can be considerably increased.

In this era of V/STOL configurations, of blown flaps and wings in slipstreams, the effect of mean flow shear is important. A significant and continuing contribution is being made at the Cornell Aero. Laboratory; Ref.4 is the latest publication.

The effect of mean flow shear on two dimensional aerofoil characteristics has been measured. Large effects have been observed in appreciable shears. Theoretical methods have been successful in predicting pressure distributions at incidences below flow separation. Some care is needed when comparing results from different sources since there is a degree of arbitrariness in the definition of the reference dynamic pressure. Significant effects on the flow breakdown characteristics have also been observed.

Increasing the free stream Mach number introduces further modifications. The angle of incidence at which a trailing edge separation occurs decreases with free stream Mach number. The angle at which a leading edge 'bubble' bursts is little affected by Mach number, but a critical stage is reached when the 'bubble' is suppressed by the local flow becoming supersonic, flow separation then depends on the subsequent shock-boundary layer interaction. Considerable emphasis is being given in present day research to the problem of delaying the drag rise Mach number, by appropriate design the aerofoil profile is shaped to give shock free, or weak shock, flow conditions at a cruise condition. At higher incidences than the cruise incidence shocks induce first boundary layer separation and then buffet, which is often intense, the values of  $C_L$  at which these effects occur is usually below  $C_{L_{max}}$ . The main design problem is to restrain the intensity of buffet so that the higher values of  $C_L$  can be utilized for increased manoeuvrability. These aspects are to be covered by other contributions to this conference proceedings so other topics are passed on to.

### 3.2. FINITE WING CHARACTERISTICS

Attention is now turned to finite wings at low speeds. The first question is how far one can apply the scanty knowledge of two dimensional aerofoil sectional characteristics to the more practical three dimensional problem. For a non-swept wing of moderate to high aspect ratio, constant chord, constant section, and zero twist the maximum local  $C_L$  will be reached in symmetric flow in the wing centre regions and so the flow separation and breakdown will occur in the inboard regions. With spanwise taper there is a shift outboard of the maximum sectional lift coefficient, accompanied by a decrease in sectional Reynolds number; both of these effects tend to move the onset of flow separation outboard. Without or little used to control the position of flow separation. Calculation of the position of the onset of flow separation on a non-swept wing, determining in this case,  $C_{L_{max}}$  based on a lifting line model, using sectional characteristics, is described in Ref. 3. But this study does not go beyond the stage of the onset of separation to discuss the rate of progression of the flow separation to determine  $C_L$  above  $C_{L_{max}}$ .

Progression of flow breakdown poses an interesting problem. Onset of flow separation depends on the intensity of the boundary layer to remain attached to the wing surface. Once the flow has separated then, as in the two dimensional case, there is an interaction between the pressure distribution as induced by the separated flow and the effect of that pressure distribution on the boundary layer characteristics which influence the separation characteristics, the final result is a complex balance of these two effects. In three dimensions it is the lateral progression which is of primary interest. As far as the overall field of flow is concerned if there is part span separation then there exists a region of separated flow adjacent to a region of attached flow. And because of the discontinuity in lift between the two regions trailing vorticity between the two regions is created. The overall effect of the downwash velocities induced by the part span trailing vorticity is to decrease the effective incidence of the sections in the attached flow region (thus decreasing the tendency of the flow to separate in that region) while at the same time increasing the effective incidence of the sections in the separated flow region (thus more firmly establishing the flow separation there). It has been experienced that on a clean wing (slats, flaps up; no stall control devices) at flow separation the initial progression of flow breakdown is rapid over a significant area of the wing surface and that it stabilises at a far slower rate of progression with further increase of incidence. Whether or not lifting line methods using sectional data with flow separation could be extended to assess the lateral progression on non-swept wings is not known; lifting line theory would incorporate the influences of the separated and non-separated flow regions as described above.

An important implication of the above argument is that the main region of flow breakdown will be stabilized and localised to the region where flow separation is initiated. Reynolds number can have a most important effect here for it is possible that the position where flow breakdown starts is sensitive to Reynolds number; results of flow separation and progression of flow breakdown at one Reynolds number could then be totally different from the results at another Reynolds number.

When the wing is swept the sectional characteristics lose their significance in the process of flow separation. Usually flow separation begins in the wing tip regions first because of the thicker boundary layers (which are created by the outboard flow in the overall three dimensional boundary layer), and secondly because of the increased streamwise pressure gradients in the tip regions compared with the decreased pressure gradients in the centre regions. Once the flow separation is initiated, the initial progression is usually fairly rapid and again this stabilizes for an incidence range, in a similar manner as that described above.

The surface flow pattern when the flow has separated depends mainly on the wing sweep; for low sweep (less than  $45^\circ$ ) the surface streamlines show a large 'swirl' pattern whereas at high angles of sweep (above  $55^\circ$ ) the separation pattern shows a 'herring bone' pattern. (Fig.3).

Of these two patterns the 'herring-bone' pattern is the more understandable, since it is associated with the organised rolled-up leading edge vortex which has been so thoroughly investigated in relation to the flow about slender wings. But the large 'swirl' pattern on a wing with moderate sweep is more difficult to interpret; in this case there appears to be reverse flow in the tip region induced by vorticity shed from the leading edge region but what happens in the intermediate region between the separated and attached flow regions is not clear. More work is required on the flow characteristics in the region of flow breakdown to establish the distribution of vorticity and flow characteristics above the wing surface. A further complication is that surface flow patterns can be misleading since there are rapid changes in flow directions away from the surface. Apart from the classic paper by Küchemann(?) in 1953 there appears to be little subsequent thought given to these qualitative aspects.



As far as is known accumulation of design data for swept wings has not been actively pursued; tests with washout angles, sweep, sectional variations etc. would be required to form a basis of an empirical theory for the prediction flow separation breakdown and progression.

Control of the progression of the stall on a swept wing is often obtained by judicious application of devices such as fences, vortex generators, notches, leading edge droop etc.,. Such ingenuity has gone into the successful development of many of these devices but the aerodynamic behaviour of many of these devices is still not fully understood. For example, fences at the leading edge usually induce a vortex at high incidence on their inboard surface, this vortex essentially cuts off the inboard boundary layer from the outboard boundary layer. Some basic work on fences, at low Reynolds number, has been done by Das<sup>(6)</sup> and by Weber and Lawford<sup>(5)</sup>. But the subtleties of fence: length, height, amount of wrap round the leading edge, the form of the contour etc., are still unresolved. Vortex generators, at least for control of flow separation from shock boundary layer interactions have been fully discussed by Fearney<sup>(16)</sup>. One of the more ingenious devices is the "vortilon" developed at Douglas Aircraft Co. for the D.C.9.; the vortilon is essentially an undersurface leading edge bump which at high incidence creates a vortex over the upper surface; this vortex not only controls the wing upper surface boundary layer but also induces a favourable downwash field at the tailplane for an overall nose down moment.

On commercial aircraft stall control devices are mostly necessary in conjunction with the high lift flap and slat system, optimum positioning has to be obtained by the time consuming process of trial and error mainly in flight. Reynolds number effects are again most important, tests in tunnels at unrepresentative Reynolds numbers can be misleading. This statement is also applicable in proving the high lift system itself.

As already mentioned another class of problem concerns a wing in a slipstream for application to many S.W.L. configurations. Slipstream effects on finite wings have been investigated throughout the past fifty years with some measure of success and understanding, but the limiting case of flow separation and breakdown under such conditions has not received as much attention. Some useful measurements have been made, for example by Breckman<sup>(11)</sup>, but the interaction between the regions outside the slipstream and the regions inside the slipstream when flow separation occurs is extremely complicated. A large number of investigations on particular S.W.L. type configurations have been tested but as far as is known no attempt has been made to extract and synthesis any of the fundamental background information.

### 3.3 DOWNWASH FIELDS AND TAIL EFFECTIVENESS

Flow breakdown on the main wing, together with the progression of the flow breakdown, forms a large wake which affects the effectiveness of the tail plane. Since aircraft stall involves the aircraft as a whole this flow environment about the tailplane is of paramount importance. Both the dynamic pressure field within the separated region and the downwash field about the tailplane need to be known.

A large number of tests have been made on tailplane effectiveness itself for a wide range of wing-tailplane combinations. Optimum arrangements have been empirically derived and design guides have been drawn up. Direct investigations of the flow fields themselves however are few and far between. The deep stall phenomena was an incentive to investigate some of these flow fields in specific cases, for example on the Javelin; and it was only by looking in some detail at the flow field inside the completely separated wake that the tailplane design on the DC9 was finalised.

At Q.M.C. some preliminary experiments have been made of the flow fields behind swept wings with part span separation. A typical set of results as shown in Fig.4. Experimental results are shown for the flow field behind a swept wing (aspect ratio 4.0, angle of sweep  $22\frac{1}{2}^\circ$ ) at low speeds in the neighbourhood of a tailplane when part span flow separation exists over the outer 50% of the wing surface. Fig.4.1 shows the total head loss; there appears to be two regions of loss of head, one is associated with the tip vortex which still retains its identity and an inboard region around  $3s/4$ ; longitudinal velocity measurements show large decreases in streamwise velocity in these regions of head loss. Fig. 4.2 shows the downwash field; large changes in downwash appear around the tip vortex and the downwash pattern inboard of the tip about  $3s/4$  suggests a vorticity field in the same sense as the tip vortex. Fig 4.3 shows the sidewash field; there appears to be a lack of symmetry in sidewash flow above and below the wake, more sidewash is present in the lower regions of the wake, inboard of the tip vortex, than in the upper regions of the wake. Finally Fig.4.4. gives a qualitative guide to the vorticity field as derived from the measurement of the downwash and sidewash velocities; there is a large concentration of vorticity, as expected, around the tip vortex and there is another concentration inboard about  $3s/4$  which ties in with the total head measurements; little vorticity appears in the upper wake between these two regions of concentrated vorticity, it should be noticed that there is a region of negative vorticity inboard of  $s/2$  in the lower wake region, this could possibly be interpreted as the image vorticity shed from the trailing edge of the wing induced by the part span vorticity.

Very little fundamental information seems to be available on the downwash and flow fields behind wings with slats and flaps extended, when the flow has separated. It is not known what is the influence of the slats and flaps on the downwash field.

Again the effect of slipstream on the downwash field especially in the stall condition is another major area where more insight and information is urgently required. Difficulties have arisen in this respect on at least one contemporary aircraft a considerable amount of time was required to develop a satisfactory solution.

### 3.4. MISCELLANEOUS TOPICS

A number of important areas remain which are briefly catalogued.

1) Ground effects are extremely important especially in the modifications of the downwash and in the flow field about the tailplane; little information seems to be available on the ground effect when the flow has separated about the main wing.



2) Although flow breakdown progression is an important aspect of stall development, flow breakdown regression is an important aspect of stall recovery; this aspect of flow behaviour does not appear to be mentioned in the literature.

3) Dynamic effects on the progression of flow separation on finite wings is yet another area in which information is scarce.

4) Most fundamental studies on flow separation tend to be purely symmetric, some consideration should be given to the effects of lateral asymmetry.

5) It is most important to realize that interests in the fluid dynamic problems of aircraft stall do not cease when the flow has broken down over a region of the wing surface, investigations up to extremely high incidences are often necessary.

#### 4. EXPERIMENTAL TESTING

It is accepted that the main design tool, because of the intrinsic difficulty of stall prediction, has to be the wind tunnel. It is assumed for now that the separate testing of the wing, wing & fuselage, tailplane etc., are essentially completed and that the overall stall characteristics on a complete model are under investigation. For reliable results the wind tunnel must be capable of generating sufficiently high Reynolds numbers to represent full scale behaviour; attempts to simulate high Reynolds effects by transition trips or reliance on high levels of turbulence in the wind tunnel stream are suspect. The question remains what is sufficiently high? The answer often depends on which aspect of the problem is under consideration. As far as the pattern of flow separation on the main wing is concerned comparison between tunnel and flight showed that for BAC 1-11 configurations a tunnel Reynolds number of  $1.10^6$  (based on mean chord) was sufficient whereas for a Trident configuration it was necessary to reach  $4.10^6$ . However, the incidences when flow separation occurred were about  $2^{\circ}$ - $3^{\circ}$  higher in flight than the tunnel so the measured values of  $C_L$  and  $C_D$  would be in error at high incidence although the qualitative behaviour above the stall should have been obtained.

Although an obvious observation, geometrical similarity between a model and full scale is essential, the fine detail is important in flow separation studies. Engine nacelle and pylon contours; fairings between fuselage and wings, and between wings and nacelles; undercarriage details etc., all need to be correctly reproduced. Wind tunnel models are constructed in the B. & D. stage of the aircraft design and it is important to ensure that all of the subsequent design modifications to the prototypes are also incorporated into the wind tunnel model of the complete aircraft. It is pertinent to query whether adequate wind tunnel testing is undertaken for stall investigations, covering the full range of parameters which need to be investigated.

Another problem which then arises is the correction for wall interference effects. Blockage effects are large and so corrections, in particular to measured rolling, yawing, and pitching moments are obscure. Blockage effects can also modify the downstream flow characteristics behind a wing with flow separation leading to errors in measured tail effectiveness.

One point which requires more thought and debate concerns the type of wind tunnel testing which should be undertaken even when sufficiently high Reynolds number can be attained. Static tests on a six component balance can be made over the complete range of incidences and sideslip angles. Since stall manoeuvres involve dynamic motions it is necessary to consider first whether dynamic tests are necessary and if so what kind of tests should be undertaken. In a sense both of these questions are interrelated for the complexity of the development of an experimental rig has to be balanced against the urgency of the results. Dynamic oscillation rigs for either longitudinal or lateral aerodynamic derivatives are difficult to engineer, elimination of cross coupling effects is often a long and arduous process. Even so when operational these rigs are purely sinusoidal with a limited angle of incidence, or sideslip, amplitude. Such results may be directly applicable to the problems of wing rock and limit cycle lateral oscillations. But in general a difficulty arises in the utilization of oscillatory derivatives to a stall manoeuvre which is non-linear and non-oscillatory, and involves large changes in incidence and sideslip. Effects of frequency on the stiffness would indicate an order of magnitude of the dynamic effects to be applied, to the static measured derivatives. Usually, however the unsteady effects are more pronounced on the damping derivatives, then the difficulty in application appears.

Some consideration needs to be given to whether or not special rigs should be developed for wind tunnel stall tests. One suggestion for longitudinal manoeuvres is shown in Fig. 5. With a hydraulic servo-actuator a large scale incidence motion can be initiated and the instantaneous loads and moments measured. A similar arrangement could be set up for the sideslip - yaw combination. Here again the specific problem of sting interference can be significant if the flow about the rear fuselage-fin-tailplane is modified by the presence of the rear mounted sting.

Measurement of the levels of buffet, and buffeting, in wind tunnels and the interpretation of these results for the application to full scale aircraft is a major field of research. Trailing edge pressure divergence seems to be established as a general technique for the indication of onset of buffet and subsequent buffet intensity.

As an intermediate stage between wind tunnel testing and prototype flight testing consideration is also being given to the possibility of using free flight models to check out the predicted behaviour in potentially hazardous stall areas from earlier wind tunnel measurements. Such techniques are already being used for the investigations of spin recovery of models of fighter type aircraft dropped from helicopter. Models for the purpose of stall investigations with their associated guidance, control and telemetry systems would be necessarily complex and expensive; however, it is hoped that this aspect offsets some of the hazards in flight on the full scale aircraft. One disadvantage of the free flight experiments model is, the relatively low Reynolds number of the model in flight; since Reynolds number is so important it is imperative that the flow behaviour on the model represent full scale conditions otherwise the interpretation of the results could possibly be dangerous.

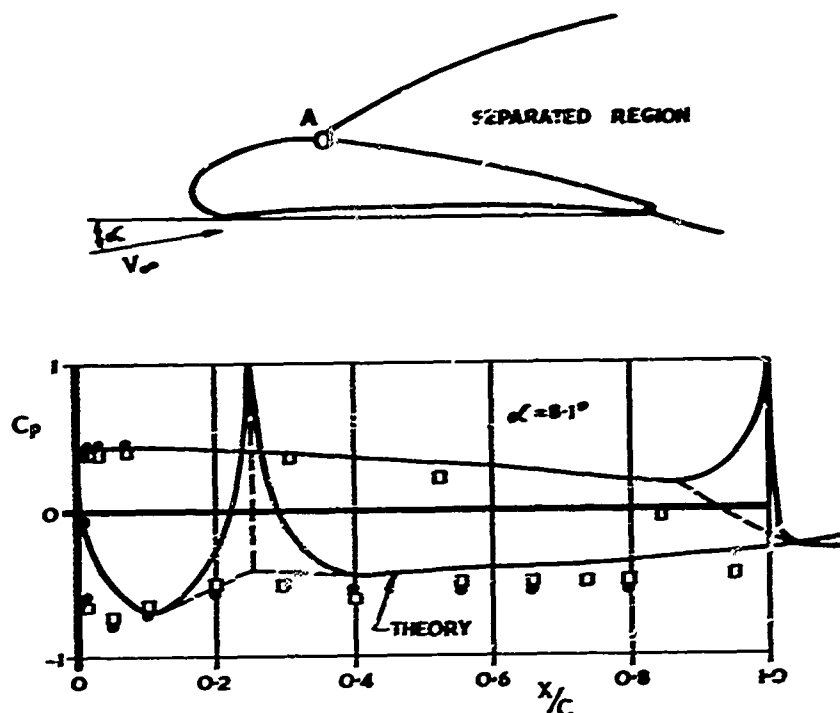
## CONCLUDING REMARKS

In this introductory note an attempt has been made to relate the fluid dynamic problems associated with flow separation, flow breakdown, progression of flow breakdown, and the overall wake field to the problem of aircraft stall, which is essentially a flight mechanics phenomena, in which the pilot plays an influential role.

Unless the research aerodynamicist appreciates exactly what are the fluid dynamic problems, and realizes the context in which fluid dynamic information is used he is in danger of digression from the main problems; it is hoped that these notes help to keep him on the right lines.

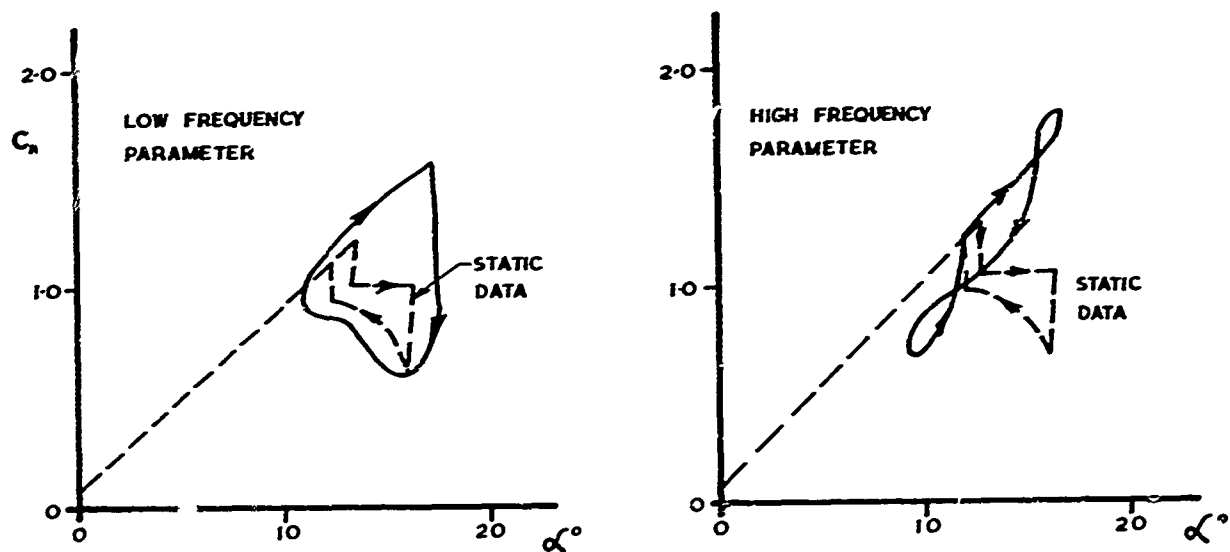
## REFERENCES

1. G.J. Hancock Problems of Aircraft Behaviour at High Angles of Attack. AGARDograph 136. 1969
2. J.C. Wimpenny Low Speed Stalling Characteristics. AGARD Report 356 1968.
3. H.A. McVeigh and B. Kisielowski A Design Summary of Stall Characteristics of Straight Wing Aircraft. NASA CR 1546 June 1971.
4. E. Jacob Berechnung der Potentialströmung um Profile mit Anströmung. Ingenieur-Archiv Vol 32 1963
5. A. Silverstein and S. Katzoff Design Charts for Predicting Downwash Angles and Wake Characteristics Behind Plain and Flapped Wings. NACA Report 643 1959.
6. J.R. Ludwig and J.C. Erickson Jr. Airfoils in Two Dimensional Non-uniformly Sheared Slipstreams Jour. Aircraft. November 1971.
7. D. Küchemann Types of Flow on Swept Wings. Jour. Roy. Aero. Soc. Vol. 57 1955.
8. D. Das Untersuchungen über den Einfluss von Grenzschichtsaugen auf die aerodynamischen Eigenschaften von Pfeil- und Delta flügeln. Zeitschrift für Flugwissenschaft Vol. 7 1959.
9. J. Weber and J.A. Lawford The Reflection Effect of Fences at Low Speeds ABC RM 2977. 1956.
10. H.E. Pearcey Shock Induced Separation and its Prevention by Design and Boundary Layer Control. Part II of 'Boundary Layer and Flow Control' edited by G.V. Lachmann Vol. 2 Pergamon Press 1961.
11. M.E. Breckmann. Experimental Investigation of the Aerodynamics of a Wing in a Slipstream. Jour. Aero Sciences Vol 25. May 1958.



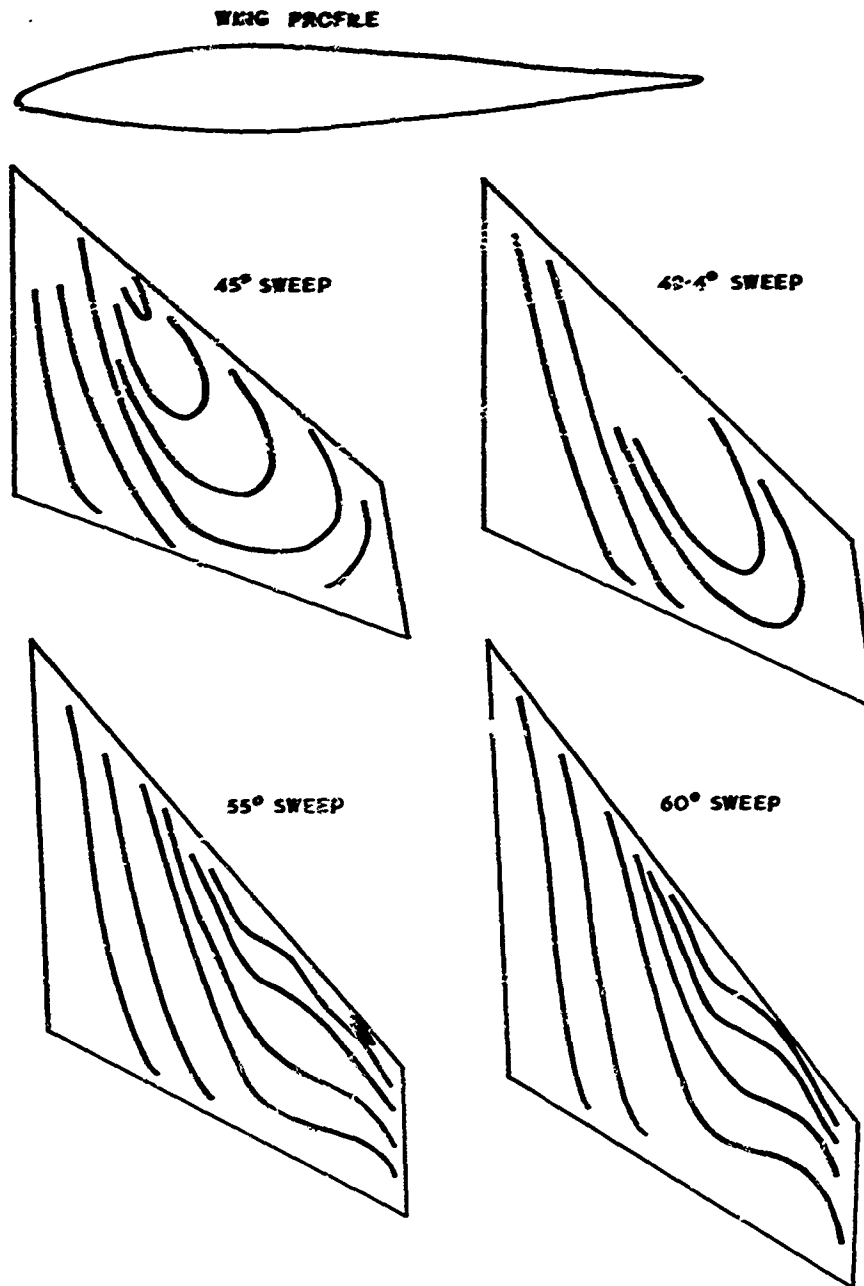
CALCULATION OF SEPARATED FLOW ON AN AIRFOIL (JACOBS)

FIG. 1

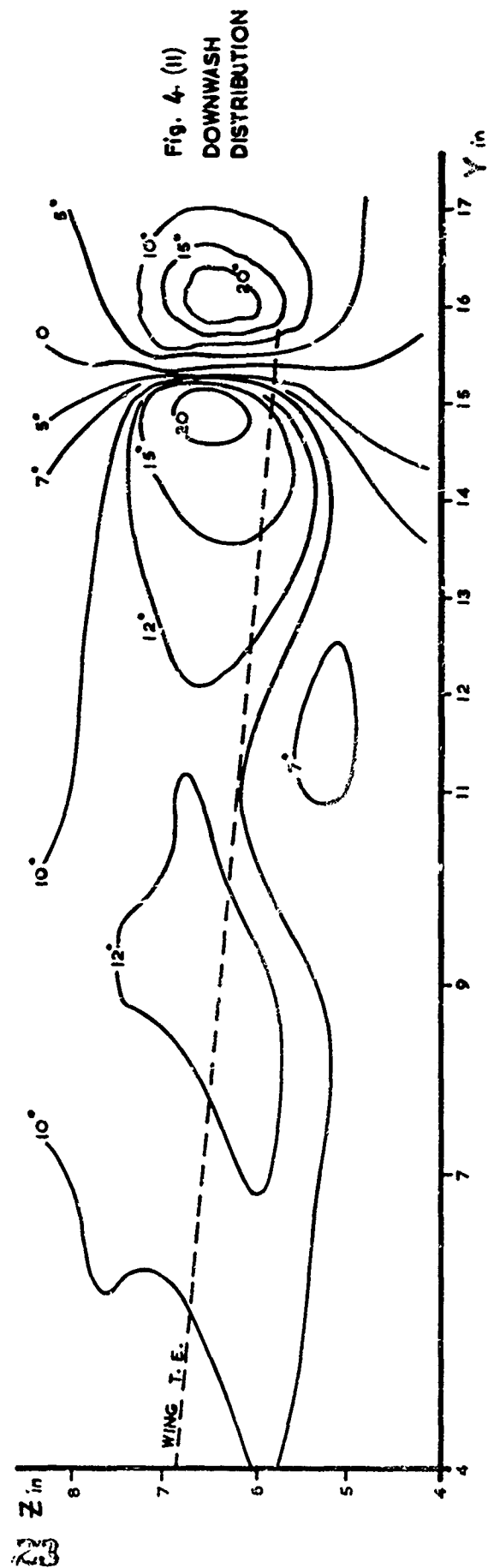
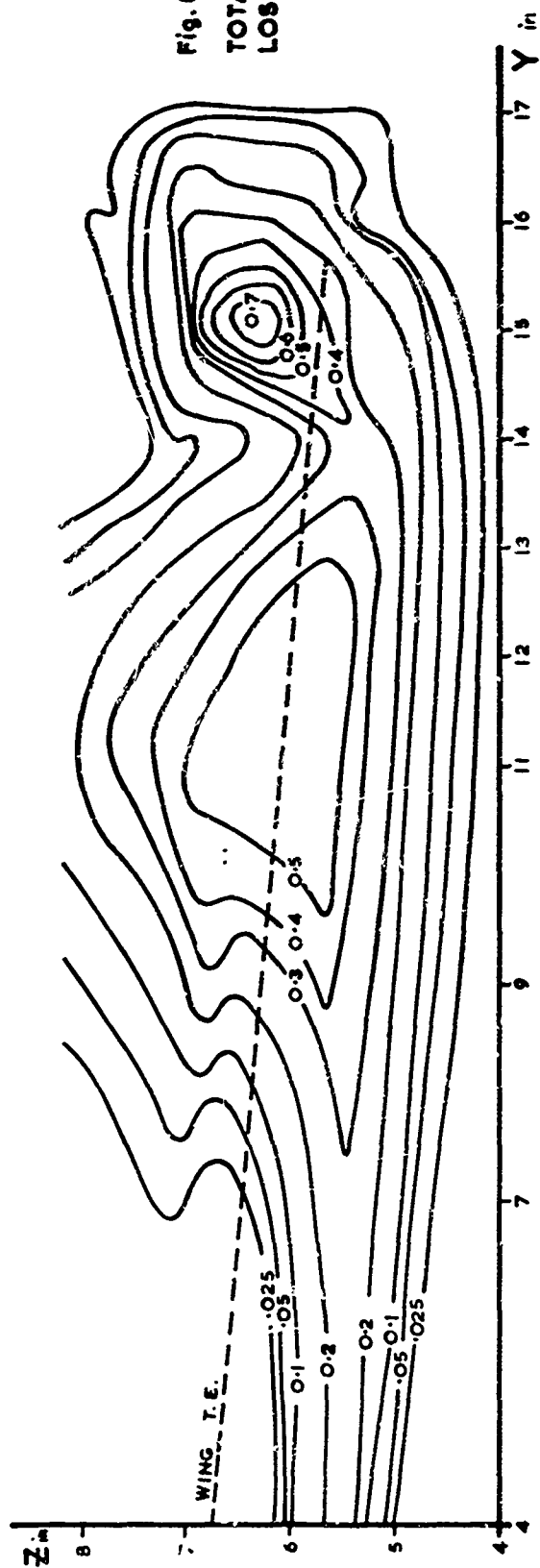


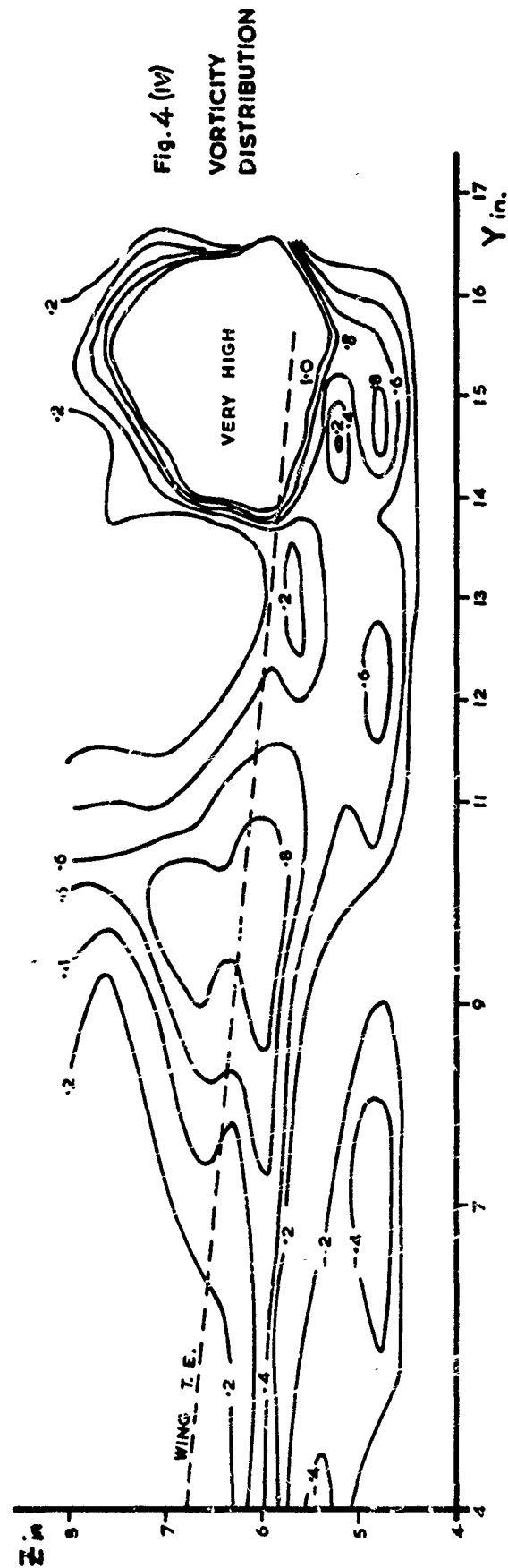
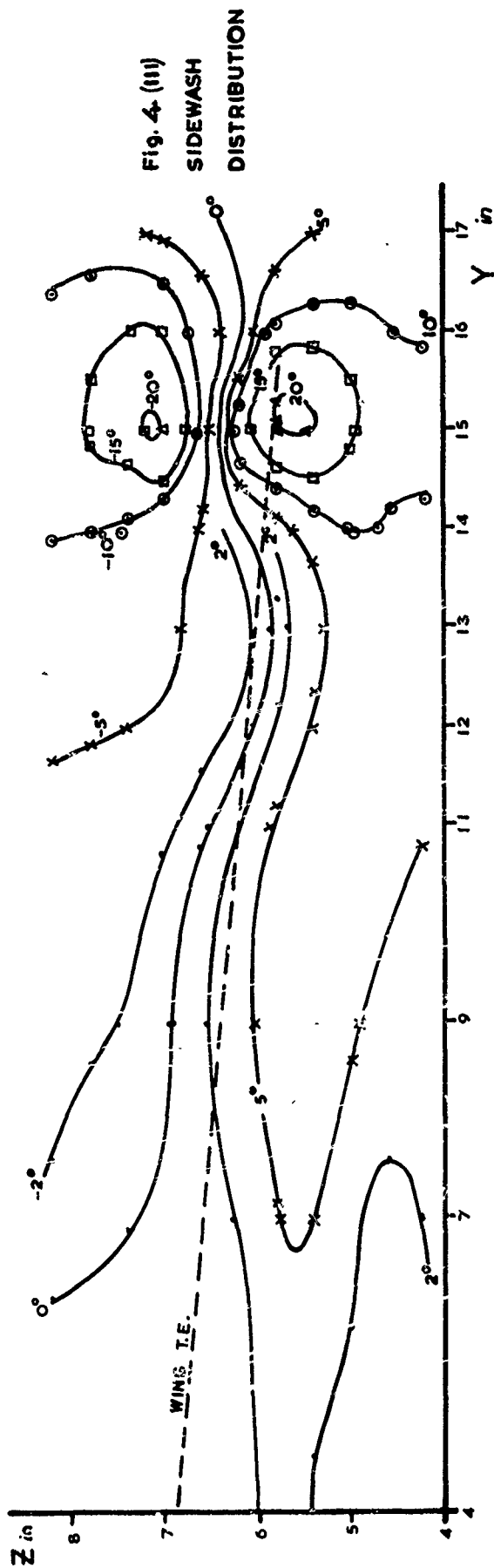
DYNAMIC EFFECTS ON FLOW SEPARATION

FIG 2

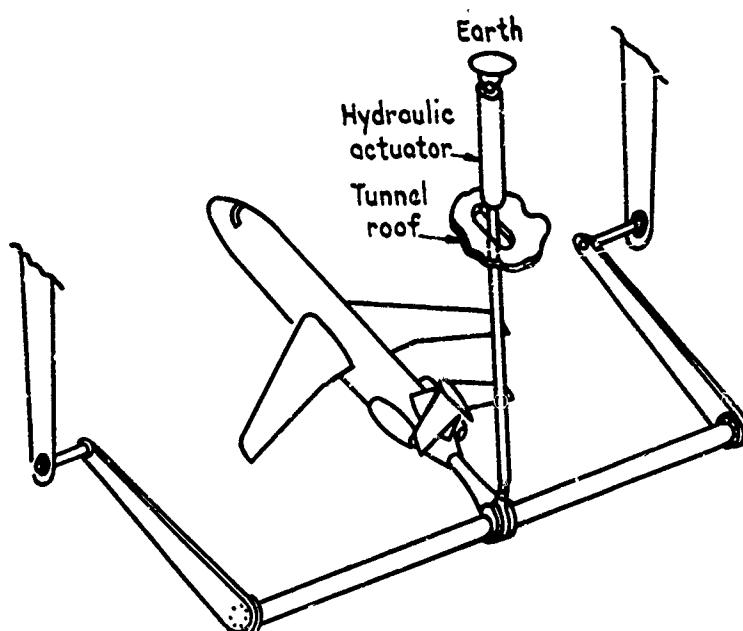


TYPICAL SURFACE FLOW PATTERNS ON SWEEP WINGS  
WITH FLOW SEPARATION  
FIG. 3.

Fig. 4. Flow field behind  $22\frac{1}{2}^\circ$  swept wing



**Fig. 4 Flow field behind  $22\frac{1}{2}^\circ$  swept wing**



## COMMENTS ON PAPER I

prepared by

Thomas C. Muse  
U.S. Dept. of Defense

It is a sincere pleasure to participate with you in this meeting. The subject of aircraft stall is of prime interest to everyone involved in aircraft design since it spans almost every aspect of aeronautical research and development — fluid dynamics, inertias, boundary layers, stability and control, power effects, piloting techniques, Reynolds numbers, practical hardware design, wind-tunnel and flight tests. It is an overview of a wide range of technical challenges that Prof. Hancock has so ably presented to you in his opening paper. He has covered the many and varied aspects of the very complex stalling problem, putting them into the proper overall perspective and expertly identifying the most important factors, but not going into such detail as to detract from the papers on specific subjects to be given by later speakers — an expert and professional job of whetting one's technical appetite.

Prof. Hancock also has properly stressed the importance of good stalling characteristics. Let me take a moment to reinforce his argument for more and better research and development in this area.

Almost two years ago, when examining the U.S. programs for research and development in the spin area, I obtained some rather striking statistics. The data were presented several months ago at a Spin/Stall Symposium† sponsored by the U.S. Air Force at Wright Patterson Air Force Base, Ohio. Some of you are familiar with them. However, they may be new to others, and I think they are so appropriate to the present subject that they warrant repeating.

TABLE I

## U.S. Military Spin Related Aircraft Losses 1966-1970

	<i>Spins</i>	<i>Stalls</i>	<i>Loss of control</i>	<i>Total</i>	<i>Investment aircraft losses (\$ in millions)</i>
Army	-	-	-	18	\$ 1.4
Navy	31	30	-	61	121.6
Air Force	31	44	62	147	244.0
TOTALS	62	74	62	226	\$367.0

Table I gives some statistics on U.S. Military Spin Related Aircraft Losses. An attempt was made to classify these accidents as stall, spin or loss-of-control. The Army accidents have happened at such a low altitude that it is hard to classify them. Accordingly they are listed together. For the five-year period, 1966 through 1970, there was a total of 226 accidents. The investment costs alone of those airplanes have been estimated to be \$367M. Fatalities have not been included. A rule-of-thumb is that military fatalities are about one-half of the number of accidents. That means that out of 226 accidents there would have been over 100 fatalities. It is clear we are paying a very high price for not having good spin/stall characteristics.

Table II shows the total accidents and the spin accidents for the U.S. military. There were slightly over 3000 total accidents for that five year period, 226 of which were classified as spin/stall or about 7% of the total. These data are not precisely accurate because there was a conversion from fiscal year to calendar year without a monthly breakdown.

When the data were initially compiled, the primary interest related to the military situation. However, some data were also collected relating to general aviation. These data are given in Table III and were supplied by the Federal Aviation Agency.

† Stall/Post Stall/Spin Symposium, 15-17 December, 1971. Sponsored by the U.S. Air Force Aeronautical Systems Division — Flight Dynamics Laboratory, Wright Patterson Air Force Base, Ohio



TABLE II

## U.S. Military Relative Spin Accidents 1966-1970†

	Total accidents	Spin/Stall
Army	259	18
Navy	1607†	61
Air Force	1214	147
	<u>3080</u>	<u>226</u>
RATIO	$\frac{226}{3080} = .074 \text{ or } 7\%$	

† Approximate due to conversion from fiscal years to calendar years

TABLE III

## U.S. General Aviation Spin/Stall Accidents 1966-1969

Total Accidents	Deaths	Spin/Stall	Deaths
2335	5271	455	599
RATIO	$\frac{455}{2335} = .195 \text{ or } 20\%$		

There was a total of 2335 accidents in general aviation in a four year period, 1966 through 1969 as the information for 1970 was not available when these numbers were compiled. Of these there was a total of over 5000 deaths, and in the spin/stall area alone there were 455 accidents with almost 600 deaths. These statistics show a ratio of spin/stall accidents to total accidents of about 20%.

Analysis of transport accidents reveals that of the 600 reported from 1962 through 1969 only 7 listed stall as a primary cause. While there is high confidence of achieving good stall characteristics for transports, substantial effort may be required to do so. For instance, data presented at the previously mentioned Spin Symposium indicated hundreds, and sometimes thousands, of instrumented stalls are required before acceptable characteristics are obtained and documented. Clearly the losses due to stall/spin accidents, and the costs of achieving good characteristics in flight are expensive and better methods are required. It would be interesting to see what the costs for a good comprehensive stall research program would be compared to the accident and aircraft development costs.

By far the major effort in the western world is devoted to the stalling of jet-driven aircraft, and Prof. Hancock only briefly mentioned propeller effects. Most people would be happy to be relieved of ever having to consider the propeller slipstream. In fact, in reading the abstracts, I do not recognize any papers on that particular subject. Of about 150,000 aircraft registered and active in the U.S. about 95% are propeller driven. Of these, some 50,000 are 1-3 place, single engine (100 hp or less). It is highly probable that this type of small general aviation aircraft will always be propeller driven so we should make sure we are doing everything possible to enhance their performance and safety.

There is another aspect of the stall situation that should not be overlooked. Achievement of good characteristics should not be limited to the configuration in hand. The current economic facts of life dictate that essentially every military or civil aircraft procured today must serve a rather lengthy life. The U.S. military B-52's, F-4's, C-130's and A-4's were laid down in the 1950's and they still form the bulk of our inventory. During this long life, missions, loadings, inertias, even configurations factors that can have powerful effects on stall characteristics undergo significant changes. Initial good stall characteristics, therefore, like powerplants and airframes, should have "stretch" capabilities.

Prof. Hamrock with his outstanding survey of the field has set the stage for what promises to be an instructive and exciting three days. The objective of achieving successful solutions to the aircraft stall-induced problems promises something for everyone. For the fluid dynamics it has always been a difficult challenge but now new tools such as the modern computer, new laser techniques, high frequency response instrumentation, etc., should assist greatly in understanding the complex flows involved. However, because of the many factors and disciplines that interface in the stalling problem, it appears that this is an area that particularly needs a coordinated research program especially in the maneuvering area. A major contribution of this meeting might be to initiate action to organize such a program.

## SOME RESEARCH ON TWO DIMENSIONAL LAMINAR SEPARATION BUBBLES

P. Dooling, J.L. van Ingen and J.M. Kord

Department of Mechanical Engineering, Delftse Hogeschool van Techniek, Delft, The Netherlands.

## SUMMARY

For the development of a calculation method for the laminar part of separation bubbles in two-dimensional incompressible flow, it was found necessary to gather experimental information on the angle  $\gamma$  at which the separation streamline leaves the wall.

In seven different models in three different low speed windtunnels the angle  $\gamma$  has been determined from mirror photographs taken with a camera which was specially built for this purpose. The flows which were investigated were:

- flow stagnation point boundary layer flow; separation induced by means of a forward facing step.
- a cylinder (diameter 70 mm) with a tail; "natural" separation on the cylindrical nose part.
- a cylinder (diameter 400 mm) with a tail; "natural" separation on the cylindrical nose part.
- a long cylinder with rounded nose, aligned axially with the wind; separation induced by a forward facing step.
- a short flat plate; separation induced by means of auxiliary airfoils.
- the same flat plate as in (e); separation induced by a forward facing step.
- a long flat plate; separation induced by a forward facing step.

The measured angles  $\gamma$  are plotted as a function of the Reynolds number  $\frac{UR}{\nu}$  at separation =  $(Re)_{sep}$ . The investigations cover a range of  $(Re)_{sep}$  from 25 up to about 700. All measured points fall reasonably well on a single curve.

## NOMENCLATURE

- B constant in Eq. (3)
- c reference length, radius of cylinder for confs. (b) and (c)
- h step height
- p static pressure
- $\frac{p}{\rho}$   $\frac{p}{\rho}$
- $\frac{p}{\rho}$   $\frac{p}{\rho}$
- u velocity component parallel to wall in boundary layer
- U velocity component parallel to wall at edge of boundary layer
- $U_{ref}$  reference speed
- $\frac{U}{U_{ref}}$   $\frac{U}{U_{ref}}$
- x distance along the wall
- y distance normal to the wall
- $\gamma$  angle at which the separation streamline leaves the wall (defined in Fig. 5)
- $\delta$   $\int_0^{\delta} u(1-u) dy$ , momentum loss thickness
- $\nu$  coefficient of kinematic viscosity
- $\tau_0$  wall shear stress

Subscript sep denotes conditions at the separation point.

## 1. INTRODUCTION

It is not necessary to stress in this paper the importance of the laminar separation bubble for the subject of aircraft stalling. It is well known that an overriding influence on the stalling behavior is exerted by the type of flow in the separation bubble, that is to say whether or not the separated flow will reattach to the surface after it has become turbulent. Our own interest in the subject is related to the development of a computer program for the design of airfoil sections (Ref. 1,2). We can distinguish three main topics in the investigation of separation bubbles. (Fig. 1)

- 1) the laminar flow leaving the wall,
- 2) transition to turbulent flow in the separated shear layer,
- 3) reattachment or failure to reattach of the turbulent flow.

Topic 3 is discussed by Horton in Ref. 3 where a method is described which enables us to determine whether turbulent reattachment will occur. To apply this method, the position of transition in the separated flow has to be known.

Our own research is mainly concerned with topics 1 and 2. The second topic will be the subject of an investigation which will be started later this year. It is intended to try and extend the second author's transition prediction method for attached flows (Ref. 4,5) to the case of separated flows. In this method the amplification of unstable disturbances in the laminar flow, as calculated by means of linear stability theory, is used to predict transition. A similar method has been developed independently by Smith and Gamberoni (Ref. 6).

The present paper deals with the first topic, the investigation of the separated laminar flow field.

## 2. SOME THEORETICAL CONSIDERATIONS

Calculating the separation point by means of laminar boundary layer theory has been the subject of many investigations; a review of this work may be found in the article by Horne and Stevenson (Ref. 7). When the pressure distribution is prescribed, generally a singularity will occur at separation such that the wall shear stress  $\tau_0$  tends to zero like

$$\tau_0 \sim (x_{sep} - x)^{1/2} \quad (1)$$

This was shown first by Goldstein (Ref. 8); Eq. (1) is confirmed by accurate numerical solutions of the boundary layer equations, such as given by Leigh (Ref. 9) and Terrill (Ref. 10). With these numerical methods it was impossible to calculate through the separation point; in fact the step size for the calculation in  $x$ -direction had to be reduced to very small values when approaching the separation point. It seems that the question has not yet been answered whether the boundary layer equations can describe a separating flow in the true (measured) pressure distribution is used. One might find however that already small deviations from the true pressure distribution could cause the difficulties to arise again. However, it is difficult to determine a priori the pressure distribution which will occur.

Some light is thrown on the real behaviour of the flow in the neighbourhood of the separation point by the work of Legendre (Ref. 11) and Görtler (Ref. 12). By using a Taylor series expansion for the solution of the Navier-Stokes equations around the separation point, they proved that the separation streamline leaves the wall at an angle  $\gamma$  which is given by

$$\tan(\gamma) = -\gamma \frac{\frac{\partial \tau_0}{\partial x}}{\frac{\partial p}{\partial x}} \quad (2)$$

The right-hand side of Eq. (2) has to be evaluated at the separation point. In this equation  $\tau_0$  denotes the wall shear stress;  $x$  is the distance along the wall and  $p$  is the static pressure which (because Eq. (2) is based on the full Navier-Stokes equations) may be a function of  $x$  and  $y$ .

According to Eq. (1) accurate boundary layer calculation methods, when not applied to the actual pressure distribution, tend to lead to  $\frac{\partial \tau_0}{\partial x} = -\infty$  at separation so that Eq. (2) would predict a separation angle  $\gamma$  of  $90^\circ$ ; this is in contradiction with experimental evidence. Therefore, if we want to calculate the separated flow, we have to use one of the following approaches.

1. Investigate whether boundary layer calculations based on the actual pressure distribution lead to a useful result; this would still leave us with the difficulty of providing this pressure distribution.
2. Use the full Navier-Stokes equations in the neighbourhood of the separation point and match the result to those of boundary layer calculations further away.
3. Use some empirical information of a sufficiently general nature so that simple calculation methods might be used for the separated flow.

The third approach was followed in our work. The simple calculation method, which will be outlined in section 4, employs an empirical relation between the separation angle  $\gamma$  and some parameter which can be found from a boundary layer calculation upstream of the separation point. It seems appropriate to choose for this parameter the Reynolds number  $\frac{U_0 x}{\nu}$  at separation, denoted by  $(Re)_p$ . This parameter will not be influenced too much by details of the flow in the direct vicinity of the separation point. Therefore it can be expected that a boundary layer calculation, based on a prescribed pressure distribution, will give  $(Re)_p$  with sufficient accuracy.

To get an idea about the type of relation to be expected between  $(Re)_p$  and  $\gamma$  we will make the following (questionable!) assumption:

- (1) Boundary layer theory remains valid at separation.
- (2) The two-dimensional pressure distribution around a given body at a given angle of attack is independent of the Reynolds number  $Re$ .

These assumptions lead to the following relation

$$\tan(\gamma) = \frac{B}{\left(\frac{U_0^2}{\nu}\right)_{sep}} \quad (3)$$

in which  $B$  is a constant for a given body at a given angle of attack. In view of assumption (2), it follows that the "constant"  $B$  in Eq. (3) may be different for separation bubbles developing on different bodies or on the same body at different angles of attack.

It may be argued that  $B$  should be the same for all bubbles, developing under different two-dimensional pressure distributions, if the following additional assumptions (3) and (4) are made.

- (3) The flow can be described by a one-parameter boundary layer calculation method such as Pohlhausen's.
- (4) The graph of the velocity  $U$  at the edge of the boundary layer as a function of  $x$  has a point of inflexion at separation. (Some evidence in favour of assumption (4) seems to follow from our experiments).

Although the assumptions (1) through (4) may be questionable, it was thought that Eq. (3) might be a good reference frame in which to place our experimental results.

## 3. THE EXPERIMENTAL APPARATUS AND SOME RESULTS

Measurements have been performed on seven different model configurations (a) through (g) in three different low speed windtunnels. These configurations have been indicated schematically in Fig. 2. Some details about the models and experimental techniques have been collected in Table 1. In all cases considered, the shape of the front part of the laminar separation bubble has been determined photographically. From the photographs the angle  $\gamma$  between the dividing streamline and the wall at the separation point could be determined. Examples of flow pictures for configurations (b) and (d) are shown in Fig. 4. The angle  $\gamma$  is defined in Fig. 5.

The flow has been made visible by means of tobacco smoke introduced into the separation bubble. A narrow region around the plane of measurement has been illuminated by means of a small electronic flash with 1/3000 sec flash duration.

In situation (a) the flash was installed inside the tube and the light passed through two diaphragms with narrow slits (5.3 mm wide) and through the transparent (peroxy) front plate of the model.

In the situations (b) through (g) the flash-with-diaphragm was installed outside the tunnel; in these cases long-focus lenses have been used to focus the light in the front part of the separation bubble in a narrow region around the plane of measurement.

Flow pictures have been taken with rather long camera's especially built for the purpose; in fact in all cases the pictures on the film were larger than the original flow phenomena so that rather fine flow details can be distinguished. A schematic drawing of the photographic equipment as used with configuration (g) is shown in Fig. 3.

The main results of the present investigation are shown in Fig. 6 where measured values of  $\tan(\gamma)$  are plotted vs. the corresponding value of the Reynolds number at separation  $(Re)_{sep}$ . In all cases a rather large number of photographs was taken for each flow situation.

With respect to the upper end of the range of  $(Re)_{sep}$  it should be noted that at high Reynolds numbers the boundary layer will become turbulent so that no further separation will occur. Along a flat plate in a stream of low turbulence, transition will occur for  $Re$  between 1000 and 1200. With an adverse pressure gradient transition will occur earlier; hence  $(Re)_{sep} = 1000$  is an upper limit for a flat plate that of Fig. 6. In that figure no points for  $(Re)_{sep} > 720$  have been given because in that region the introduction of a sufficient amount of smoke without disturbing the flow gave severe problems. Moreover the angle  $\gamma$  in that region is so small that good accuracy of the measurements can hardly be expected.

For most of the configurations tested the Reynolds number has been varied by changing the wind speed. In configuration (d) also the length  $x$  over which the boundary layer developed could easily be changed. In fact measurements have been made at  $x = 150$  mm, 550 mm and 950 mm. However, only the results for  $x = 150$  mm have been given in Fig. 6. The results for configuration (d) at  $x = 550$  and 950 mm, which were included in the pre-print of the paper, have been left out now. Already in the pre-print some doubt had been expressed with regard to the validity of these results: "the flow at separation was not very steady and not very two-dimensional around the circumference of the central body". Since then additional detailed measurements have shown that one should read here: "at large values of  $x$  for configuration (d) the flow at separation was not two-dimensional at all".

With respect to the steps used in the experiments, the following remarks can be made. In order to obtain a situation which sufficiently resembles "natural" separation, the step height  $h$  should not be too small; it should be such that the step generates an adverse pressure field which extends over a distance normal to the wall which is larger than the boundary layer thickness. If the step height is chosen too small the angle  $\gamma$  is found to increase. Several series of measurements with different step heights in the configurations (d), (f) and (g) showed that in these cases it was certainly sufficient to make  $h$  equal to three times the boundary layer thickness at separation.

The results shown in Fig. 6 for the configurations (d), (f) and (g) all refer to situations in which the steps were sufficiently high. For configuration (a) the influence of  $h$  has not been measured; the step height used in that case was 4 mm, which, at all speeds was more than the boundary layer thickness at separation. However, in the light of the observations given above  $h$  may have been a little too small at the lowest wind speed. If this is true, the points given in Fig. 6 for the lowest values of  $(Re)_{sep}$  might be somewhat too low.

In general, it can be seen from Fig. 6 that the measurements indicate a reasonably unique relation between  $\gamma$  and  $(Re)_{sep}$ . The value of the "constant"  $B$  in Eq. (3) is about 15 to 20.

Some results of pressure distribution measurements on configuration (c) are shown in Fig. 7 in the form of dimensionless velocity  $\bar{u}$  at the edge of the boundary layer. The values of  $\bar{u}$  have been determined from the measured pressure distribution along the wall by assuming that  $p$  is constant across the boundary layer and applying Bernoulli's theorem outside the boundary layer. The measured distributions show a characteristic flattening especially when the Reynolds number is low. This flattening is reproduced by the calculation method to be described in section 4.

#### 4. APPROXIMATE CALCULATION OF THE LAMINAR FLOWFIELD DOWNSTREAM OF SEPARATION

A calculation method has been developed which can approximately predict the laminar flowfield downstream of separation. This method employs the von Kármán momentum integral relation and the first "compatibility condition" of the boundary layer equations. This condition relates the curvature of the velocity profile at the wall to the streamwise pressure gradient. The following additional assumptions are made.

1. The angle  $\gamma$  can be determined from  $(Re)_{sep}$  by an empirical relation such as Eq. 3.
2. The "separation streamline" as defined in Fig. 5 remains straight over the full length of the laminar part of the bubble.
3. The reverse flow velocity profiles can be represented by the Stewartson second branch solutions of the Falkner-Skan equation.

In view of our experimental results assumption 2 seems to be reasonable. It would not be difficult however to extend the method to curved separation streamlines.

It should be observed that the pressure distribution in the separated region is not given a priori but it follows from the calculations. In other words: the pressure distribution is determined such that the assumed shape of the separation streamline (for instance straight) is compatible with assumption 1 and 3 and with the equations used.

Initial conditions which are required to start the calculation at the separation point are  $\theta$  and  $U$ . These conditions follow from the boundary layer calculation upstream of the separation point.

Details of the calculation method will not be given here but will be published in a later paper by the second author.

Some preliminary results of the method are shown in Fig. 7 where the calculated pressure distribution is compared to results of some measurements on configuration (c).

## 5. REFERENCES

1. Inger, J.L. von: Advanced Computer Technology in Aerodynamics: a program for airfoil section design utilizing computer graphics. VRL Lecture series 16, April 24-25, 1969.
2. Inger, J.L. von: On the design of airfoil sections utilizing computer graphics. *De Ingenieur*, vol. 81, no. 42, 24 October 1969, p. 1 100-1 112.
3. Horton, H.P.: A semi-empirical theory for the growth and bursting of laminar separation bubbles. *A.R.C.-CP 1073*, 1967.
4. Inger, J.L. von: A suggested semi-empirical method for the calculation of the boundary layer transition region. Report VRL-74, Dept. of Aeron. Eng., University of Technology Delft, 1966.
5. Inger, J.L. von: Theoretical and experimental investigations of incompressible laminar boundary layers with and without suction. Report VRL-124, Dept. of Aeron. Eng., University of Technology Delft, 1969.
6. Smith, A.W.C. and Gamberi, R.: Transition, pressure gradient and stability theory. Report 25 2538, Douglas Aircraft Co., 1956.
7. Brown, G.N. and Stewartson, K.: Laminar separation. In: Annual Review of Fluid Mechanics, vol. 2, Palo Alto, Annual Reviews Inc., 1969, p. 45-72.
8. Goldstein, S.: On laminar boundary layer flow near a position of separation. *Quart. J. Math. Appl. Math.*, vol. 1, 1948, p. 43-69.
9. Leigh, D.C.: The laminar boundary layer equations: A method of solution by means of an automatic computer. *Proc. Camb. Phil. Soc.*, 51, 1955, p. 320-332.
10. Terrill, R.W.: Laminar boundary layer flow near separation with and without suction. *Phil. Trans. A 253*, 1960, p. 55-100.
11. Legendre, R.: Développement laminaire régulier. *Comptes Rendus 241*, 1955, p. 1132-1134.
12. Görtzsch, K.: Die Ablösungsbedingung von Grenzschichten. In: Grenzschichtforschung/Boundary Layer research. IUTAM Symposium, Freiburg / Fr. 1957, Springer Verlag 1958, p. 351-367.

## ACKNOWLEDGMENT

The authors wish to thank the technical staff of the low speed aerodynamics laboratory for their able assistance during the preparation and execution of the experimental stages of the work described in the present paper. Especially Mr. Peter Struckman should be mentioned in this respect.

configuration	separation induced by	pressure distribution obtained from	$\delta$ obtained from
(a) plane stagnation point flow on flat nosed airfoil. 400 x 400 = tunnel.	forward facing step	crifices in flat nose	calculation by means of Thwaites-type method using the measured pressure distribution.
(b) 70 = dia.cylinder with tail (to suppress fluctuating wake). 400 x 400 = tunnel.	natural separation on cylindrical nose.	crifices in cylindrical nose; detailed pressure distributions obtained by rotating nose part.	
(c) 400 = dia.cylinder with tail (to suppress fluctuating wake). 1610 x 1250 = tunnel.			
(d) 106 = dia.cylinder with rounded nose; aligned axially in a windtunnel with cross section 300 = $\delta$ ; by moving the central pipe in streamwise direction w.r.t. the tunnel and the measuring apparatus, the length $x$ over which the boundary layer had developed before separation could be varied.	forward facing step (flat disk).	crifices in surface of central pipe.	measured velocity profiles. (total head from traversing flattened total head tube; static pressure from crifice).
(e) flat plate 400 x 400 = tunnel	auxiliary airfoils	crifices in surface of plate.	
(f) flat plate 400 x 400 = tunnel	forward facing step		
(g) flat plate 1610 x 1250 = tunnel			

Table 1: Some details about the experimental apparatus (see also Fig. 2).

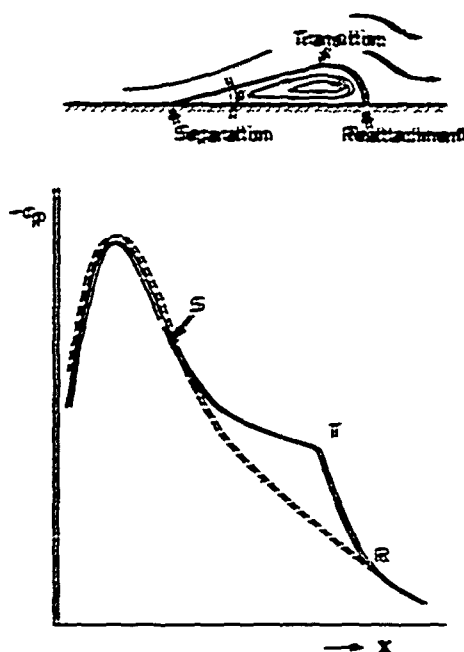
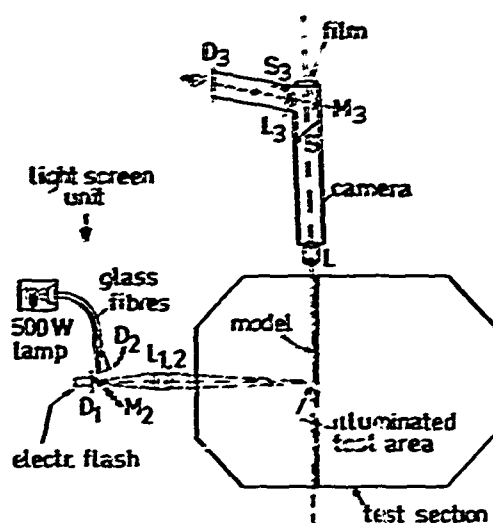
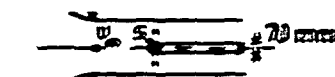
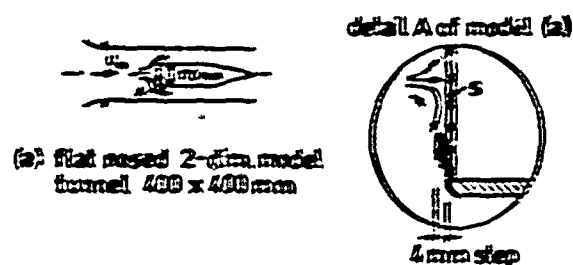


Fig. 1: Schematic diagram of flow field and pressure distribution in a laminar separation bubble.

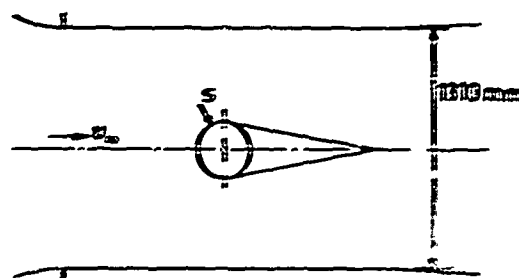


- |   |                             |   |   |
|---|-----------------------------|---|---|
| L | lens                        | 1 | flash illumination                      |
| D | diaphragm with narrow slits | 2 | continuous light                        |
| M | mirror                      | 3 | projection of reference lines in camera |
| S | shutter                     |   |   |

Fig. 3: Schematic diagram of photographic equipment used with configuration (g).



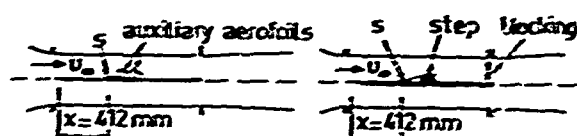
(b) cylinder:  $\phi 70$  mm, length 400 mm  
tunnel 400 x 400 mm



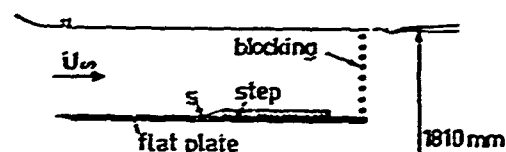
(c) cylinder:  $\phi 400$  mm, length 1250 mm  
tunnel 1250 x 1810 mm



(d) long body  
tunnel  $\phi 300$  mm



(e) flat plate with sharp leading edge, tunnel 400 x 400 mm



(g) flat plate with step, tunnel 1250 x 1810 mm

Fig. 2: The experimental configurations.

(plane of measurement in middle of tunnel, S = laminar separation point).

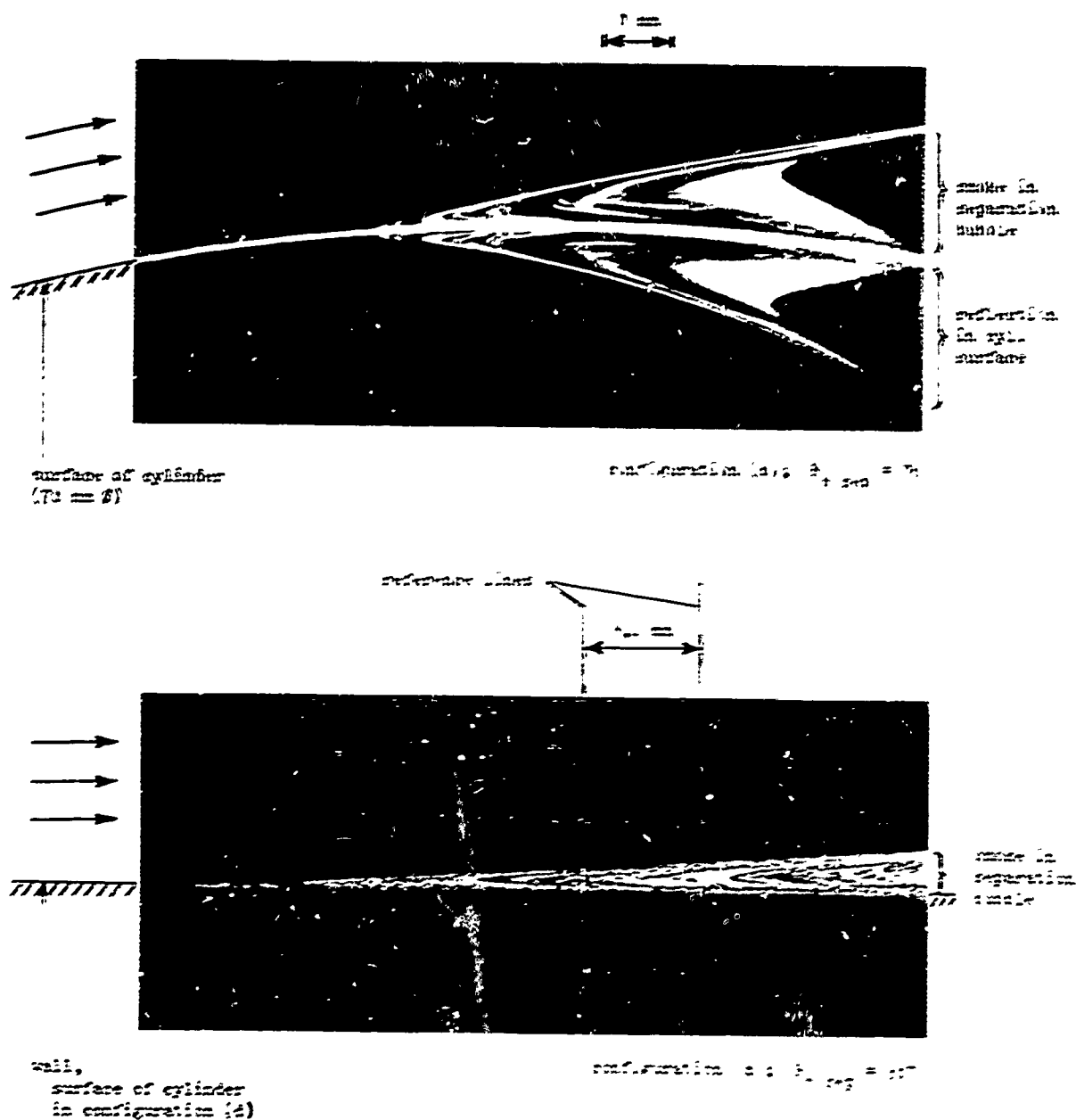


Fig. 1. Examples of flow pictures.

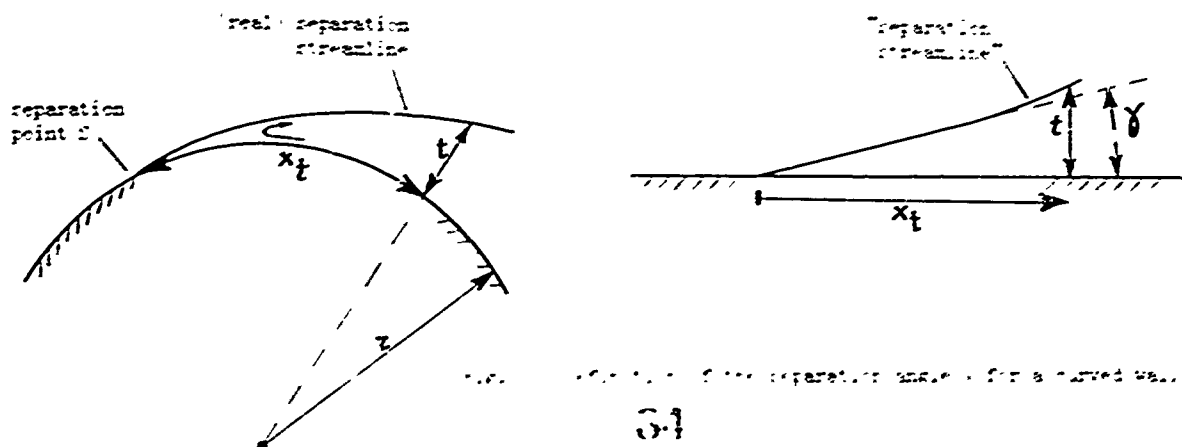


Fig. 2. Flow separation angle  $\gamma$  for a curved wall.



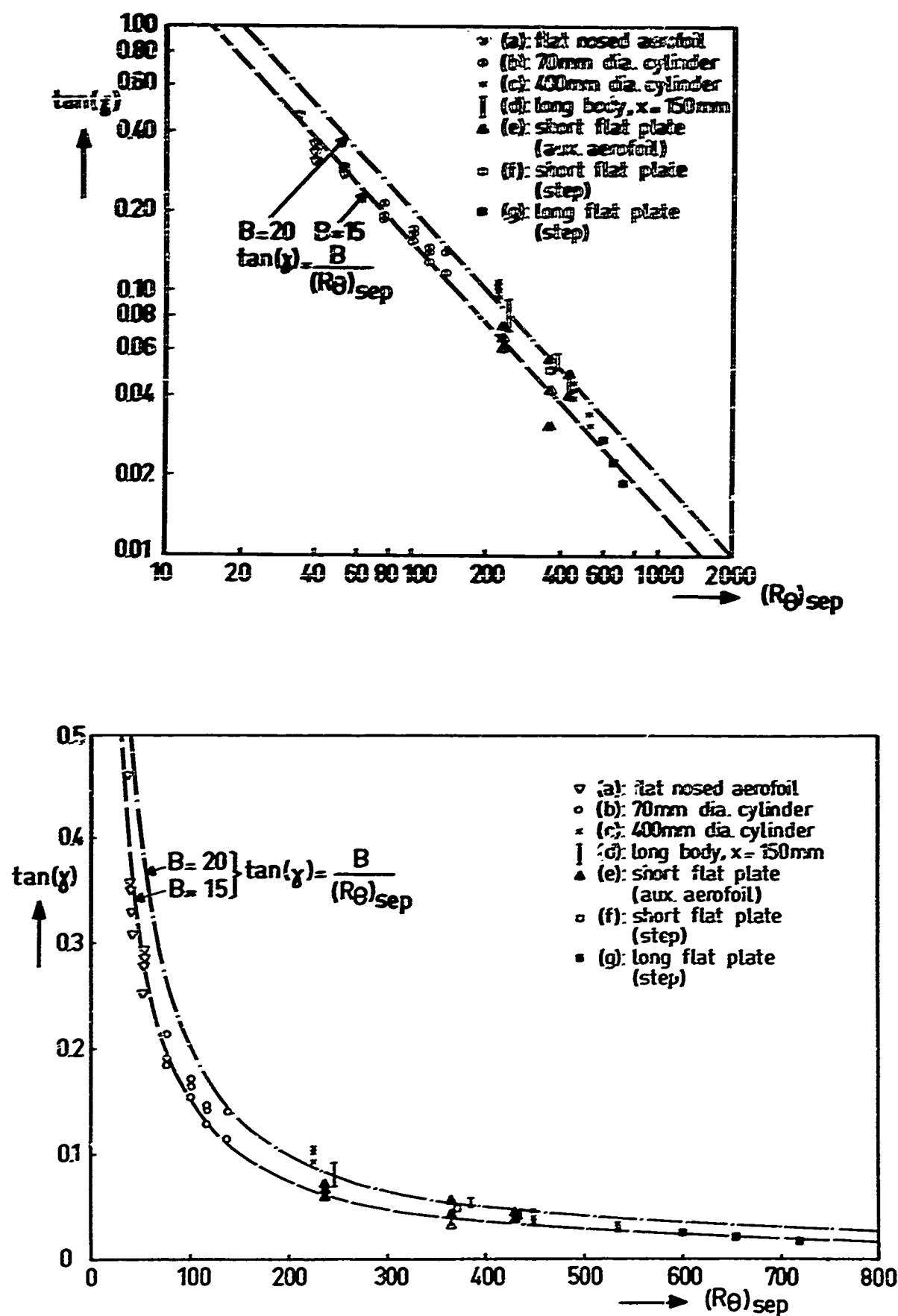


Fig. 6: Separation angle  $\gamma$  as function of the Reynolds number at separation  $(Re)_{sep}$ .

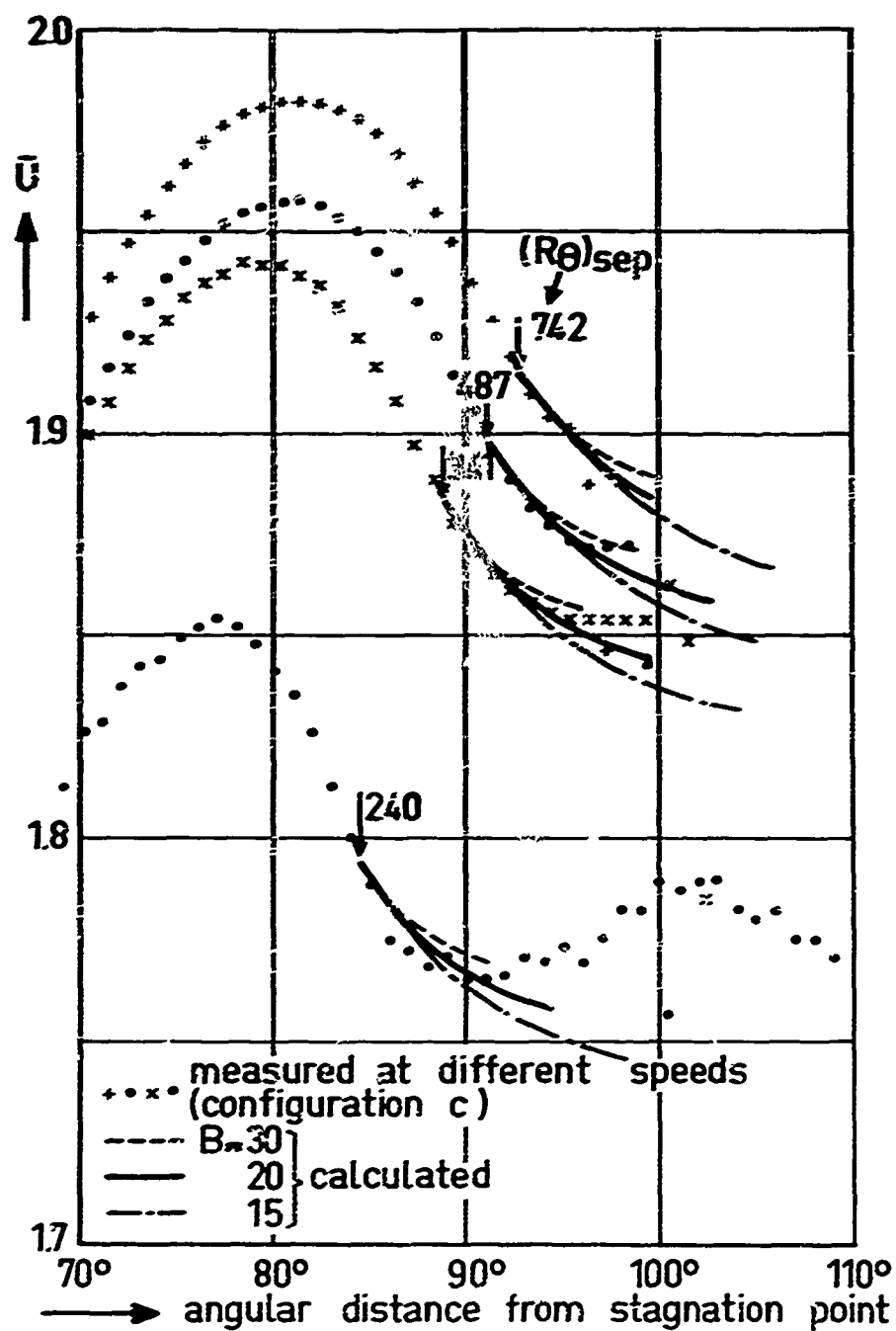


Fig. 7: Some pressure distributions for configuration (c).

# RECHERCHES THEORIQUES ET EXPERIMENTALES SUR LES DECOLLEMENTS LIES A UNE DEFORMATION LOCALE DE SURFACE

S. Burnel , G.B. Diep , P. Gougat , B. Prunet-Foch  
Laboratoire d'Aérodynamique du Centre National de la Recherche Scientifique  
4 ter, route des Gardes, 92-MEUDON (France)

## RESUME

Le problème du décollement laminaire est apparu avec l'étude de la rugosité harmonique de paroi et plus précisément avec l'étude d'une plaque plane à paroi sinusoïdale. Nous présentons ici, dans une première partie, l'étude en écoulement incompressible, de ces décollements.

De tels décollements peuvent être prévus en utilisant différentes méthodes de calcul. Toutes ces méthodes supposent connu le champ de vitesse. Ces décollements ont d'autre part été mis en évidence sur des plaques de différents rapports amplitude sur longueur d'onde. Les profils de vitesse dans la couche limite ont été établis à l'aide d'un anémomètre à fil chaud, les signaux obtenus ayant été aussi analysés en fréquence. La répartition des pressions statiques à la paroi est présentée. Ces mesures confirment la présence d'un décollement prévu par le calcul et qui a de plus été visualisé par fumée.

Dans une deuxième partie, l'étude a été poursuivie sur une plaque déformable. La paroi de la plaque sert de couvercle à une cavité. Le réglage de la pression dans cette cavité permet d'obtenir des déformations en saillie ou en creux. L'exploration des densités spectrales de puissance fournit une mesure de l'amplification spatiale des instabilités naturelles dans la couche limite. La connaissance du champ de vitesse à la frontière de la couche limite permet de relier le développement de ces instabilités au paramètre de Föhlhausen caractéristique du gradient de vitesse extérieure.

## INTRODUCTION

L'étude des décollements se produisant sur une plaque plane à paroi sinusoïdale dans un écoulement incompressible /1/ nous a amenés à nous intéresser principalement à l'influence de la perturbation harmonique sur une couche limite laminaire ; il s'agit alors d'un mécanisme de déclenchement artificiel de la transition tel que peuvent le provoquer des irrégularités de paroi sur des avions à grandes vitesses.

D'autres formes de perturbations auraient pu être aussi envisagées :

- soit un phénomène acoustique créé à l'extérieur de la couche limite dans l'écoulement,
- soit un phénomène produit à l'aide d'un écoulement pulsé,
- soit encore une vibration harmonique de la paroi /2/, vibration qui serait une fonction sinusoïdale du temps, d'une part, et de l'abscisse comptée suivant la direction de l'écoulement, d'autre part.

Les travaux ont été entrepris au laboratoire d'Aérodynamique dans le but de vérifier une théorie, émise par R. Hirsch /3/ permettant de voir comment varie, à l'intérieur d'une couche limite, une perturbation provoquée par des ondulations harmoniques de faible amplitude de la paroi. Une première vérification expérimentale avait été tentée sur une plaque ondulée dont l'ondulation avait  $2.10^{-2}$  m de longueur d'onde et  $0.2.10^{-3}$  m d'amplitude. Bien que les mesures semblent bien correspondre aux prévisions du calcul de R. Hirsch, des doutes sont apparus quant à la présence éventuelle de décollements se produisant à la paroi /4/, /5/. Nous avons alors entrepris l'étude de plaques présentant des ondulations plus importantes, afin de pouvoir grossir les phénomènes et, ainsi, essayer de les mesurer. Par ailleurs, un calcul approché fondé sur la méthode de Karman-Pohlhausen nous avait permis de prévoir l'apparition de décollements sur de telles parois ondulées.

La détection de ces phénomènes qui sont de faibles dimensions, a nécessité la mise en oeuvre de techniques expérimentales différentes : mesures de pressions - anémomètre à fil chaud - analyses en fréquence.

La première partie de cette communication présente les expériences qui ont permis de mettre en évidence la présence de micro-décollements à la surface de parois ondulées. L'analyse en fréquence nous a montré que ceux-ci, même s'ils étaient suivis de recolllements, n'en perturbaient pas moins la couche limite et, par conséquent, pouvaient avoir une influence non négligeable sur les phénomènes de transition.

Dans la deuxième partie, l'étude est étendue à la zone de transition sur une plaque déformable, en saillie ou en creux, l'analyse des densités spectrales de puissance des fluctuations de vitesse permet alors d'étudier l'amplification des instabilités naturelles et en particulier l'influence, sur leur développement, du gradient local de la vitesse extérieure.

## I

### I.1 CONSIDERATIONS ET RAPPELS THEORIQUES

#### I.1.1 Calcul de la distribution des vitesses dans l'écoulement potentiel le long d'une plaque plane à paroi sinusoïdale

L'intégration des équations dynamiques de la couche limite dans le cas d'un écoulement laminaire permanent le long d'un profil ne peut se faire que si l'on connaît les conditions aux limites et, par suite, l'évolution de la vitesse  $U$  à la frontière de la couche limite.

Plusieurs méthodes sont applicables pour déterminer cette évolution :

- soit un calcul direct à l'aide d'un écoulement potentiel complexe /6/,
- soit un calcul de l'expression de la vitesse à l'aide de la théorie des petites perturbations /7/,
- soit une évaluation de cet écoulement potentiel par la méthode de l'analogie rhéoelectrique /8/ ou par une méthode numérique. Ces dernières méthodes présentent le grand intérêt de tenir compte de la présence des parois de la veine et de la forme géométrique du bord d'attaque.

La géométrie des parois des plaques utilisées est telle que les sommets des ondulations sont dans le plan de la partie plane qui suit le bord d'attaque. Nous devons dès lors retrouver la vitesse de l'écoulement libre,  $U_\infty$ , dans les sections situées au droit des sommets des ondulations. L'expression de la distribution des vitesses que l'on obtient à partir de l'une ou l'autre des 2 premières méthodes citées est :

$$(I.1) \quad U/U_{\infty} = \sqrt{\frac{1 + \frac{2\pi a}{\lambda} \cos \frac{2\pi x}{\lambda}}{1 + \frac{2\pi a}{\lambda}}}$$

où  $U$  et  $U_{\infty}$  sont respectivement la vitesse potentielle et la vitesse à l'infini de l'écoulement;  $a$  et  $\lambda$ , l'amplitude et la longueur d'onde de l'ondulation.

Dans ce qui suit, c'est cette expression qui sera retenue comme distribution des vitesses à la frontière de la couche limite.

### I.1.2 Calcul des décollements

#### a) Méthodes intégrales /9,10,11/

Parmi les méthodes de calculs approchés employées pour une telle étude, celle de T. Von Karman et K. Pohlhausen, permet de prévoir de manière simple le cas du décollement.

Nous ne reviendrons pas sur les hypothèses faites pour mener le calcul. L'équation de quantité de mouvement après intégration devient :

$$(I.2) \quad \frac{d(\delta_2^2/v)}{dx} = \frac{F(K)}{U}$$

$$K = \frac{\delta_2^2}{v} \frac{dU}{dx}$$

A partir de la valeur  $\delta_2$  de l'épaisseur de quantité de mouvement à une abscisse de départ, la résolution de ce système peut s'effectuer soit directement par construction graphique, soit en adoptant la simplification de Walz. Nous pouvons aussi reprendre la méthode de Thwaites /12/ qui détermine à partir des expériences, la fonction universelle  $F(K)$  et ramène alors, comme celle de Walz, l'équation (I.2) à une seule quadrature.

#### b) Méthode des différences finies

La méthode qui a été appliquée est connue /13/; connaissant la répartition des vitesses dans la couche limite en deux tranches, nous avons calculé celle de la tranche suivante, ceci en nous bornant dans les dérivées des vitesses, aux termes du deuxième ordre, et en reprenant l'expression de l'écoulement potentiel (I.1).

#### c) Comparaison des deux méthodes

La méthode de Pohlhausen est fondée sur un développement du quatrième degré de l'expression du profil des vitesses. Les expériences ont montré que le point de décollement prédit par cette méthode est trop reculé.

Si l'application de la méthode de Pohlhausen met en évidence la présence d'un décollement, nous pouvons être sûrs qu'il se produit en réalité. Par contre, dans le cas où cette méthode ne révèle pas de décollement, nous ne pouvons en conclure pour autant que celui-ci n'existe pas.

Comme l'avaient déjà constaté d'autres auteurs /9/, le critère de Thwaites rend mieux compte des phénomènes dans le cas de plaques planes à parois présentant des déformations sinusoïdales de très faible amplitude devant la longueur d'onde. La méthode des différences finies fournit d'ailleurs une abscisse de décollement beaucoup plus proche de celle à laquelle aboutit le critère de Thwaites.

## I.2 DISPOSITIFS EXPERIMENTAUX

### I.2.1 Description générale des conditions d'expérience

Les expériences ont été réalisées dans une soufflerie subsonique à circuit ouvert. Cette soufflerie fonctionne en aspiration. La veine de la soufflerie est de section carrée (0,5 m de côté); elle est longue de 1,5 m. Avant le convergent, de rapport 9, sont placés des filtres de dépoussiérage.

La pré-turbulence de la soufflerie a été mesurée; elle est de l'ordre de 0,35 %.

Dans la veine de la soufflerie, nous avons placé différentes plaques, de 1,20 m de long, 0,5 m de large et 0,03 m d'épaisseur. Le bord d'attaque de ces plaques a une forme elliptique d'allongement 10. Trois plaques différentes ont été utilisées :

- une plaque plane lisse  $P_1$ ,
- deux plaques ondulées dont l'ondulation sinusoïdale présentait une longueur d'onde  $\lambda$  de 0,1 m :
  - l'une  $P_2$ , d'amplitude  $a = 0,5 \cdot 10^{-3}$  m soit  $a/\lambda = 1/200$ ,
  - l'autre  $P_3$ , d'amplitude  $a = 0,25 \cdot 10^{-3}$  m soit  $a/\lambda = 1/400$ .

Les ondulations sur ces plaques commencent à 0,195 m du bord d'attaque pour éviter les effets de la sur-vitesse, due au profil elliptique, sur l'écoulement au-dessus des ondulations.

La plaque, ainsi que le porte sonde, sont solidaires d'un châssis isolé des parois de la veine; ceci pour supprimer au maximum les vibrations parasites, vibrations qui auraient pu avoir une grosse influence sur le comportement de la couche limite. Cette dernière a en effet tendance à amplifier beaucoup les basses fréquences /14/.

Le réglage de l'incidence des plaques a été fait de manière à obtenir un gradient longitudinal de vitesse nul. Nous avons constaté par ailleurs que ce réglage d'angle est très sensible, une variation de  $10^\circ$  d'angle entraînant des inégalités appréciables dans les pressions statiques.

### I.2.2 Instruments et méthodes de mesure

Pour mesurer les vitesses moyennes et les fluctuations de vitesse, nous avons utilisé une chafne anémométrique /15/. Nous avons en outre cherché à mettre en évidence le décollement par une analyse en fréquence du signal fourni par le fil chaud. Ce signal peut être caractérisé pour une fonction du temps  $t$  :

$$e(t) = e + e'(t)$$

où  $e$  et  $e'(t)$  sont respectivement les tensions moyennes et les fluctuations.

L'analyse en fréquence se propose de mettre en évidence la décomposition spectrale de puissance de la fonction centrée  $e'(t)$  attachée à ce signal /16/, /17/, /18/. Nous avons employé le processus direct par méthode analogique qui permet d'obtenir, à l'aide d'un analyseur, la densité spectrale en prenant la transformée de Fourier en  $t$  de la fonction  $e'(t)$ .

### 1.3 RESULTATS. MISE EN EVIDENCE DU DECOLLEMENT

#### 1.3.1 Profils de vitesse moyenne

Nous avons effectué sur les différentes plaques une exploration systématique de la couche limite. Des profils de vitesse moyenne et de fluctuations de vitesse ont été relevés pour de nombreuses abscisses.

a) Pour la plaque  $P_2$  : la figure 1 montre que, pour une vitesse de 12,5m/s, nous avons un décollement prononcé dès le premier creux. Il commence légèrement avant le quart de longueur d'onde, il se termine peu après le point le plus bas, c'est-à-dire au moment de la recompression. Le point de décollement est un peu plus avancé que celui qui avait été prévu par le calcul de Pohlhausen, il est plus proche de celui obtenu par le calcul à l'aide de la méthode des différences finies.

Dans le deuxième creux, les profils sont moins déformés ; cela est dû au fait que nous nous trouvons en fin de zone de transition. En effet, la pente à l'origine des profils est plus forte que celle des profils laminaires ; il est par ailleurs aussi possible de constater ce début de transition sur le signal retransmis sur un oscilloscope.

Nous remarquons, en outre que, après la zone de décollement, nous retrouvons des profils de vitesse correspondant au régime laminaire. Ceci nous amène à dire que nous sommes en présence d'un décollement laminaire à recollement laminaire.

Dans le cas d'une vitesse de 25m/s, nous nous sommes bornés à la première ondulation ; l'écoulement immédiatement après se trouve déjà fortement perturbé. Il ne semble pourtant pas que nous soyons là en face d'un décollement laminaire à recollement turbulent ; en effet, le premier profil immédiatement après le recollement n'est pas vraiment turbulent, mais la transition est très avancée par rapport au cas précédent.

b) Pour la plaque  $P_3$  : la figure 2 montre les profils des vitesses moyennes pour une vitesse de l'écoulement égale à 12,5m/s. Nous constatons qu'une très faible perturbation se produit dès la première ondulation, l'écoulement restant néanmoins pratiquement laminaire.

L'importance de ces perturbations augmente au fur et à mesure que l'on se trouve sur des ondulations plus éloignées du bord d'attaque. Néanmoins, à la fin de la troisième ondulation, le signal vu sur l'oscilloscope montre que la zone de transition commence.

Pour une vitesse de 25m/s, la transition est nettement avancée et commence dès le deuxième creux.

#### 1.3.2 Distribution des pressions statiques

Lorsqu'un décollement se produit en un point d'un profil, la pression statique en ce point augmente /19/ et, par conséquent, il est possible de mettre en évidence une zone de décollement en relevant la distribution des pressions statiques à la paroi.

La pression statique  $p$  est directement reliée au coefficient de pression  $C_p$  par :

$$C_p = \frac{p - p_\infty}{\frac{1}{2} \rho U_\infty^2}$$

Sur les différentes plaques, nous avons placé une série de prises de pression statique.

Nous observons bien, sur les courbes de la figure 3, donnant l'évolution du coefficient  $C_p$  le long de la plaque  $P_2$ , que celle-ci est sinusoïdale et présente des "creux" aux abscisses correspondant à la zone de décollement. Sur la plaque  $P_3$ , nous constatons aussi que l'évolution du coefficient  $C_p$  est sinusoïdale. Les "creux" correspondant au décollement n'apparaissent pas nettement, comme dans le cas de la plaque  $P_2$ . La légère dispersion des points est peut-être due à la faible amplitude de la sinusoïde.

#### 1.3.3 Analyse en fréquence

L'analyse en fréquence du signal fourni par le film chaud a été faite de manière systématique dans la couche limite. Dans les zones perturbées, les spectres présentent des pics importants dans des plages de fréquences bien déterminées.

Pour chaque plaque et chaque vitesse, nous avons, en outre, relevé systématiquement l'évolution des pics lorsqu'on faisait varier l'ordonnée du film chaud, son abscisse demeurant constante. L'importance de ces pics augmente quand on éloigne le fil de la plaque ; elle atteint son maximum à une distance de  $0,2 \cdot 10^{-3}$  m environ ; elle diminue ensuite, mais son influence se fait sentir loin encore dans la couche limite. La figure 4 montre, pour la plaque  $P_2$ , un exemple de l'évolution de ce maximum lorsque l'on se déplace suivant l'axe des abscisses, ceci pour les deux vitesses envisagées. L'observation des spectres obtenus montre que nous avons une plage de fréquences privilégiées. Il apparaît que la situation de cette plage sur l'échelle des fréquences est fonction de la vitesse de l'écoulement libre, qu'elle est peu fonction de l'amplitude, et demeure la même dans tous les creux d'une même plaque se trouvant, bien entendu, dans la zone d'écoulement laminaire. On trouve vers 350 Hz pour 12,5m/s et vers 700Hz pour 25m/s.

#### 1.3.4 Mise en évidence du décollement par les fumées

En injectant de la fumée à une abscisse où la couche limite est laminaire, nous la voyons partir très régulièrement depuis le trou. Par contre, si le point d'injection se trouve être au niveau du milieu de la zone de décollement sur la plaque  $P_2$ , nous voyons nettement la fumée sortir du trou, s'étaler en tous sens, remonter un peu l'écoulement pour ensuite être entraînée vers l'aval.

Nous avons essayé de refaire la même expérience sur la plaque  $P_3$  ; le phénomène de remontée de la fumée dans l'écoulement n'est pratiquement pas visible à l'oeil nu.

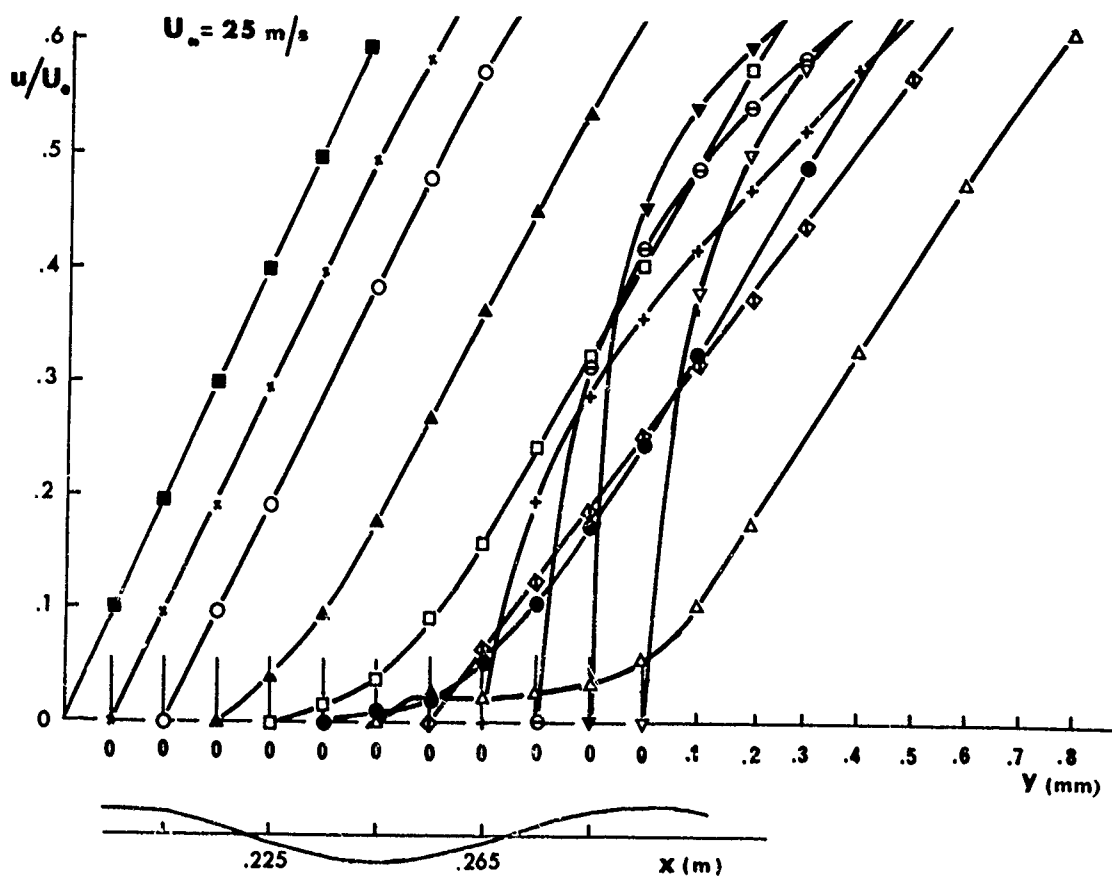
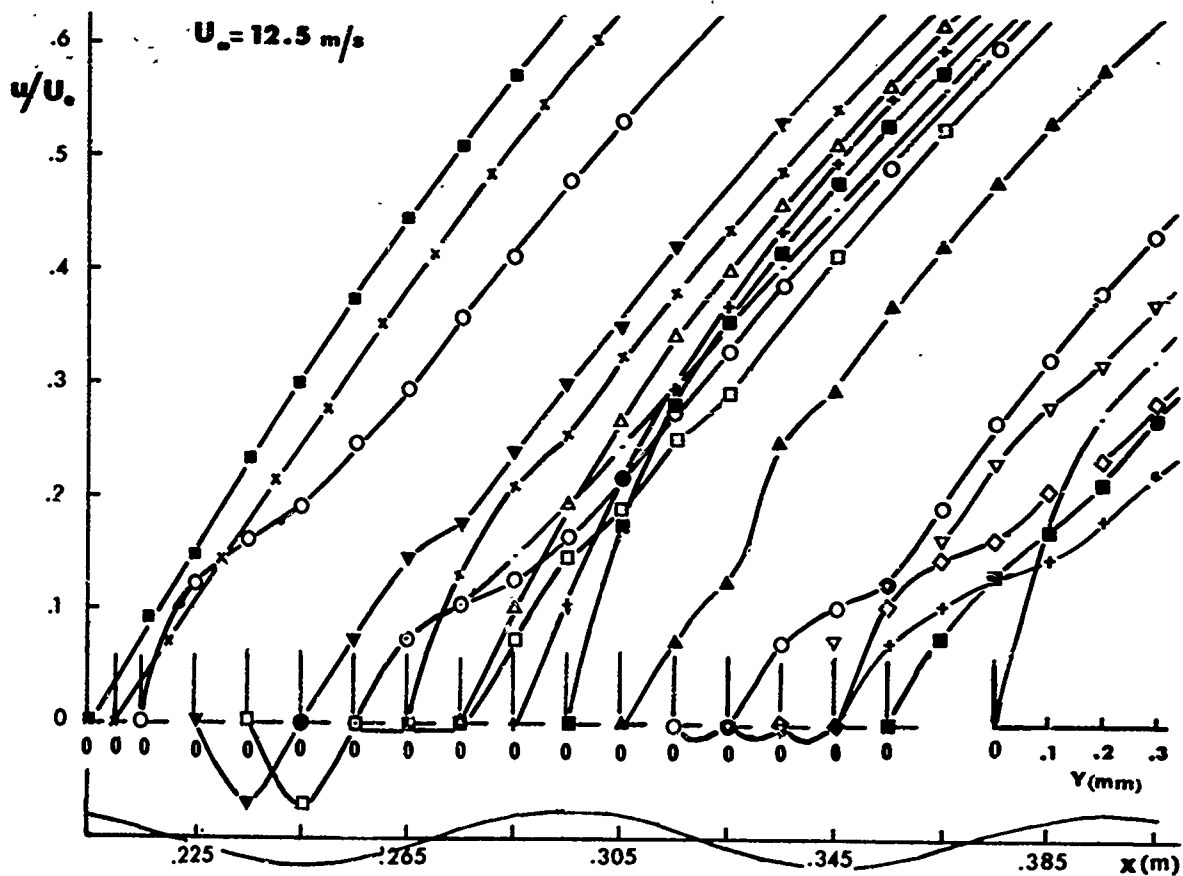


Fig. 1 - Détails des profils de vitesse près de la paroi - Plaque  $P_2$

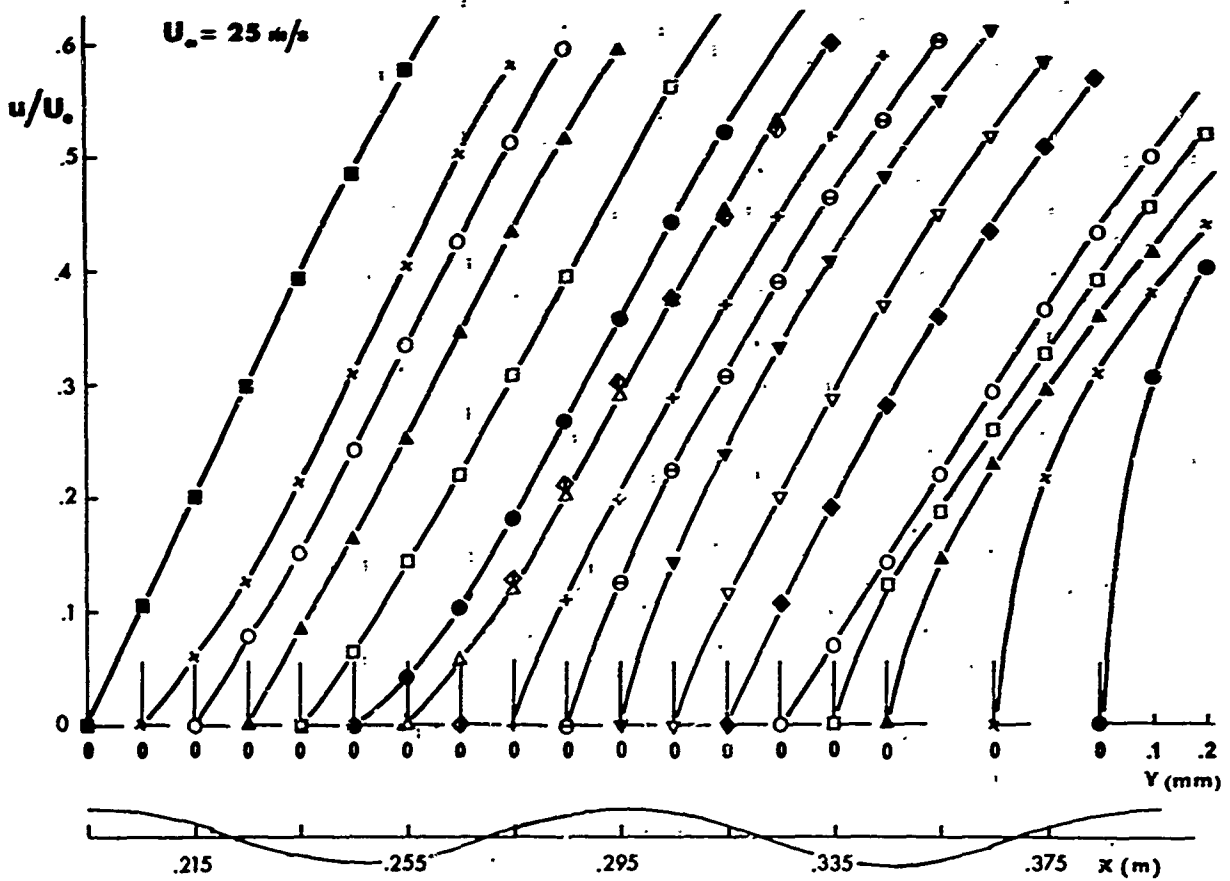
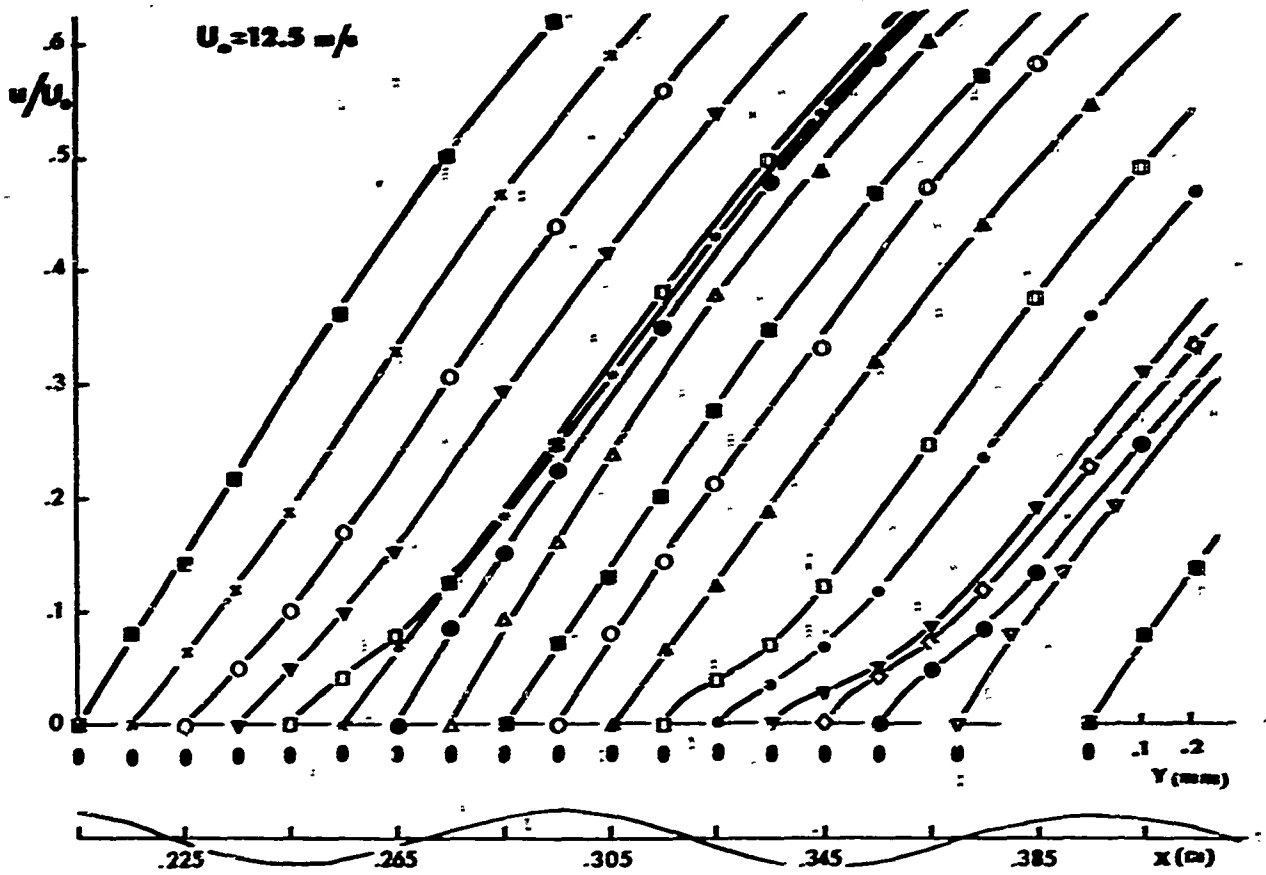


Fig. 2 - Détails des profils de vitesse près de la paroi - Plaque  $P_3$

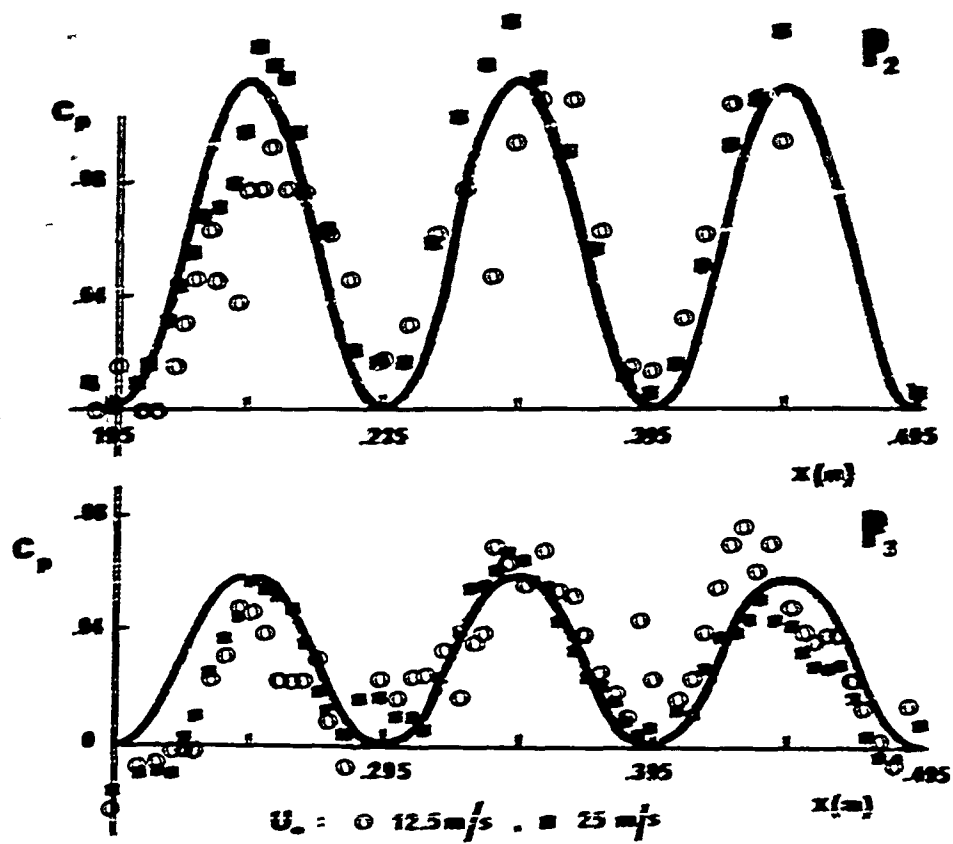


Fig. 3 - Distribution des pressions statiques

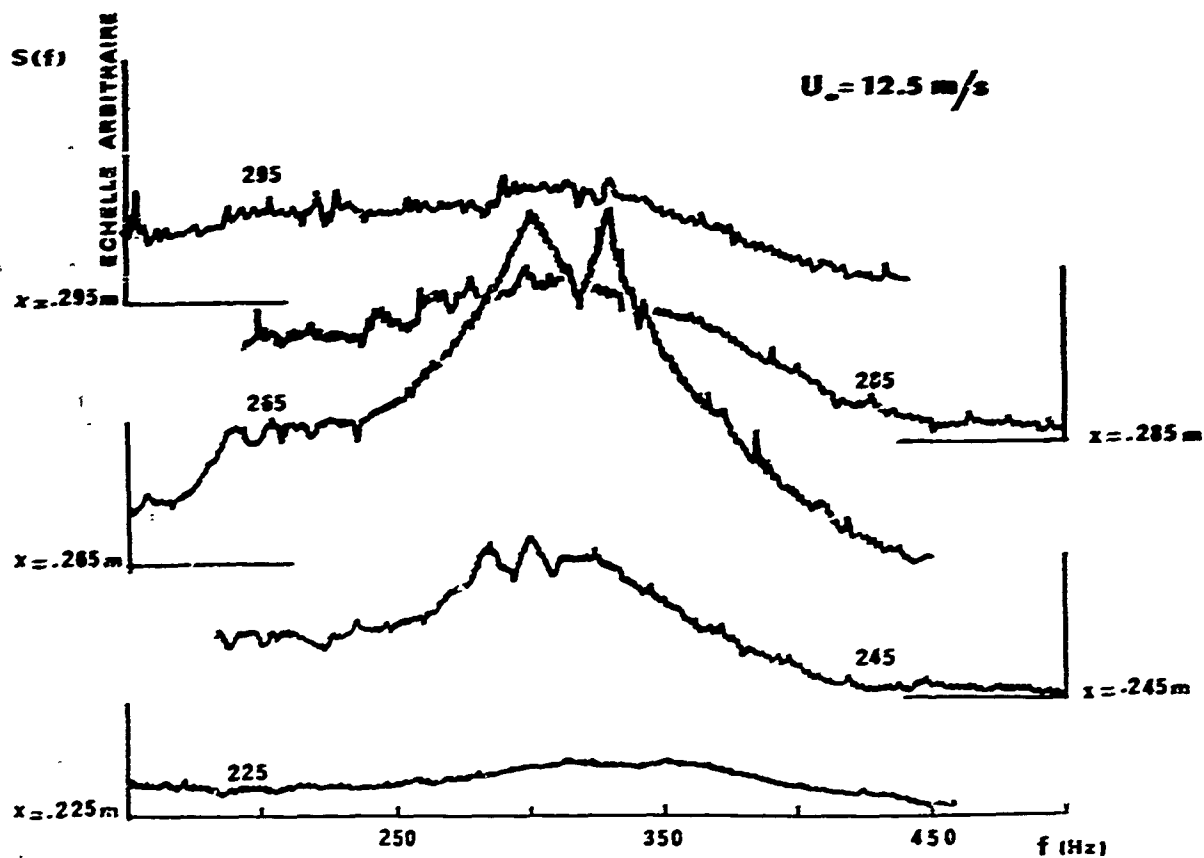


Fig. 4 - Spectres de puissance à  $y = 0,2 \text{ m}$  - Plaque P<sub>2</sub>



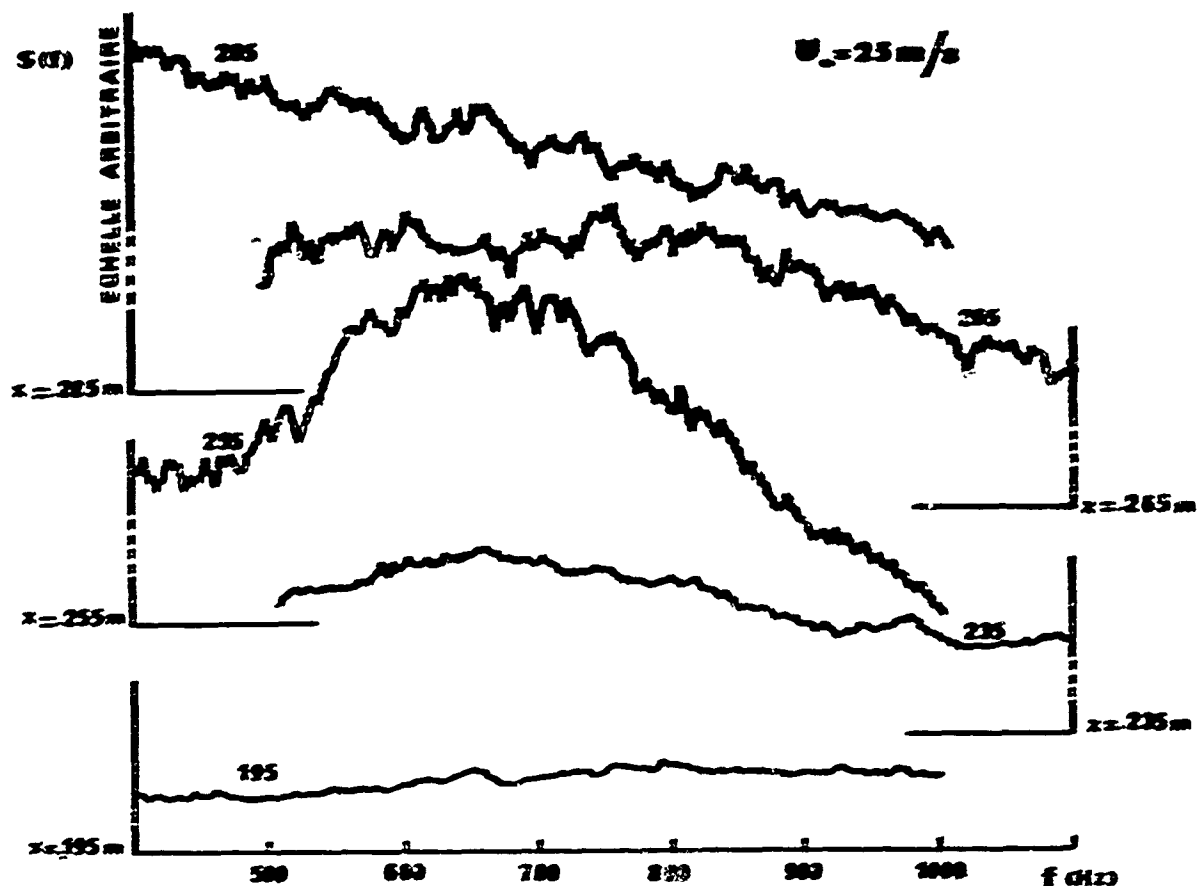


Fig. 4 - Suite

#### 1.4 CONCLUSION

L'application des critères de Pohlhausen et de Thwaites et le calcul par différences finies ont conduit à prévoir un décollement sur la plaque  $P_2$ ; ceci est bien vérifié expérimentalement. Pour la plaque  $P_3$ , par contre, le critère de Pohlhausen mène à des conclusions différentes de celles qui sont données par le critère de Thwaites et le calcul par différences finies. Il ne nous a pas été possible, dans l'état actuel de nos techniques de mesure ou de visualisation, de lever le doute expérimentalement. Si le décollement existe sur cette plaque, il est de si faible dimension que nos moyens d'investigation se révèlent insuffisants. Néanmoins, nous pouvons remarquer que, dans les zones où pourraient se produire ces micro-décollements, les mesures par fil chaud mettent en évidence des déformations de profil de vitesse moyenne analogues à celles constatées dans le cas de la plaque précédente où le décollement existe. Il en est de même en ce qui concerne l'analyse spectrale des fluctuations de vitesse.

## II

Une étude récente a montré l'influence considérable que peut avoir sur la transition une rugosité sinusoïdale de paroi ( $a=0,5$  mm,  $\lambda=100$  mm,  $a/\lambda=0,5/100$ ) [20]. L'étude des micro-décollements a donc été étendue à la zone de transition pour déterminer l'influence du paramètre  $a/\lambda$  sur la position de la transition.

### II.1 DESCRIPTION DE LA PLAQUE

La plaque a été usinée dans le but d'avoir à notre disposition une paroi déformable de manière continue et présentant un excellent raccordement avec le bord d'attaque. L'étude et la réalisation de ces dispositifs sont dues à la Société Lérospatiale (SNIAS).

La plaque (fig. 5) sert de couvercle à un châssis métallique solidaire du bord d'attaque dans lequel trois cavités étanches ont été usinées. Pour chaque cavité, la paroi est déformable sur une longueur de 0,1 m et sur toute l'envergure de la plaque. Sur la face inférieure de la plaque, deux orifices sont prévus pour l'alimentation en pression et un trou central permet la mesure du déplacement ou des éventuelles vibrations de la paroi sans contact mécanique par un capteur à variation de capacité.

Les trois cavités sont indépendantes ce qui confère à l'ensemble une grande souplesse d'utilisation. La déformation en saillie ou en creux d'une ou plusieurs cavités permet de mesurer l'influence d'un gradient local de vitesse ou de la succession de gradients favorable et défavorable.

Nous appellerons  $2a$  l'amplitude de la déformation par analogie avec l'amplitude crête à crête des plaques à rugosité sinusoïdale décrites ci-dessus. Cette amplitude est mesurée au point de déformation maximale. La partie déformable de 1 mm d'épaisseur est encadrée sur les quatre côtés et est soumise à une pression uniforme. Nous avons vérifié que la déformée est approximativement sinusoïdale.

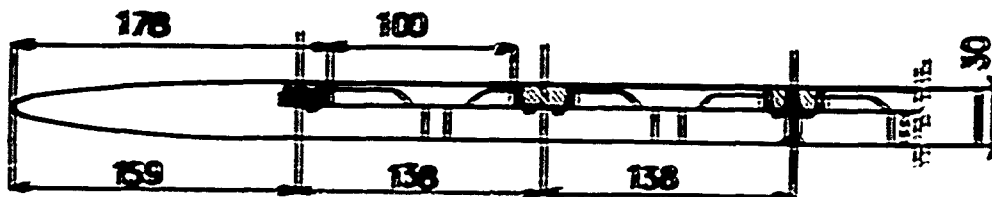


Fig. 5 - Plaque déformable

## II.2 INSTALLATION DE LA PLAQUE EN SUBSONIQUE

Tous savons [23] que le réglage de l'angle d'incidence d'une plaque a un effet important sur la position de la transition : la sensibilité des mesures de transition nécessite un collage de la plaque avec une erreur angulaire inférieure à deux minutes. Nous expliquons là les difficultés rencontrées lors des mesures comparatives de position de transition sur différentes plaques comportant des rugosités similaires. Avec le cône à petit déformable, nous évitons ces difficultés : le bord d'attaque reste inchangé tant en forme qu'en position et incidence quelle que soit l'amplitude de la déformation.

Tout de plus que les modifications de position dans la cavité et les mesures des déformations sont liées en présence de l'écoulement. En particulier, nous pouvons à chaque instant retrouver les résidus de la plaque plane.

Nous avons choisi de coller la plaque en respectant le plus possible le divergent de la veine d'expériences mais aucune correction n'a été faite dans les pentes de la veine pour compenser l'énorme surcharge due au bord d'attaque. Signalons simplement que le raccordement entre le profil elliptique d'allongement 10 et la partie plane a été calculé pour réduire cette surcharge.

Dans ces conditions, pour les différentes déformations, nous pouvons faire de très bonnes comparaisons de positions de la transition tout en sachant qu'il ne s'agit pas d'une mesure absolue car le tour de précession et les phénomènes acoustiques et vibratoires liés à la soufflerie entrent en jeu.

Les résultats que nous fournissons ci-dessous sont relatifs à des déformations de la première cavité pour une vitesse de l'écoulement libre de 16 m/s.

## II.3 MESURES

Tous les résultats que nous présentons sont tirés du traitement des tensions analogiques instantanées fournies par la chaîne d'enregistrement à fil chaud.

En plus de l'exploitation des mesures des vitesses moyennes et des niveaux de fluctuations, nous avons voulu connaître la gamme de fréquence de ces fluctuations, ce qui nous a conduits à faire en chaque point de l'écoulement les mesures des densités spectrales de puissance des signaux instantanés.

Ce nombre considérable d'analyses spectrales a été obtenu à l'aide d'un analyseur en temps réel dont l'incertitude réside dans la compression de temps associée à la mesure d'acquisition de données.

L'appareil prélève des échantillons du signal à analyser et les insère dans une mémoire en respectant leur ordre chronologique d'arrivée. La mémoire est explorée à un rythme synchronisé au rythme d'acquisition mais beaucoup plus rapide. Les échantillons du signal ainsi comprimés sont appliqués à un filtre interférométrique à largeur de bande d'analyse constante.

Les échantillons filtrés sont détectés et présentés en sortie, soit sous forme analogique pour l'étude du spectre instantané, soit sous forme digitale en vue d'une sommation dans un intégrateur numérique qui délivre la densité de spectre de puissance avec toute la précision statistique désirée.

## II.4 RESULTATS

### II.4.1 Profil des vitesses moyennes

La réponse de l'anémomètre à fil chaud n'est pas linéaire en fonction de la vitesse. En fait, nous n'exploitons les relevés des vitesses moyennes que pour la connaissance du point moyen de fonctionnement autour duquel il faut linéariser la relation tension-vitesse.

### II.4.2 Profil des niveaux de fluctuations

Soit à la paroi, la quantité  $\sqrt{u'^2}/U$  passe par un maximum avant de tendre asymptotiquement vers la turbulence de l'écoulement libre. Notons que cette mesure de la valeur efficace des fluctuations englobe toutes les fluctuations quelle que soit leur fréquence.

### II.4.3 Evolution des instabilités

En régime laminaire, à l'aval immédiat du bord d'attaque, le spectre des fluctuations n'est constitué que de basses fréquences. A partir d'un nombre de Reynolds critique, il apparaît des instabilités dans le signal instantané. Cela se traduit par une gamme de fréquences privilégiées sur l'analyse spectrale. Ces ondes instables ont des fréquences qui coïncident avec les fréquences instables de Tollmien-Schlichting mais il s'agit de bouffées en trains d'ondes intermittents et non d'ondes progressives entretenues.

La mesure de l'énergie contenue dans ces bouffées caractérise le développement des instabilités.

### III.5 LOCALISATION GLOBALE DE LA TRANSITION

En chaque section, nous obtenons en fonction de l'abscisse le profil des taux de fluctuations longitudinales de vitesse (Fig. 6). Une caractérisation complète de la transition consistant à présenter l'évolution de ces profils en fonction de l'abscisse. Pour simplifier la représentation et la rendre à deux dimensions, nous exprimons le fait que chacun de ces profils présente un maximum en  $y/\delta$ . Nous sommes ainsi arrivés à caractériser la transition par l'évolution, en fonction de l'abscisse, du niveau maximal de fluctuation rencontré dans chaque section.

Les résultats sont présentés sur la figure 7. La courbe relative à la plaque plane montre que le taux maximal de fluctuations reste faible en régime laminaire ( $< 5\%$ ) passe par un maximum en zone de transition pour tendre vers une limite ( $10\%$ ) en régime turbulent établi. Sur cette même figure, nous avons porté les courbes relatives à deux amplitudes de déformation ( $a/\lambda = +0,5/100$  et  $a/\lambda = -0,5/100$ ). L'allure des courbes est conservée mais l'existence d'un maximum sur chacune de ces courbes peut être noté pour définir convenablement une "abscisse de début de transition". En présence d'une perturbation de petit, la transition vers l'état de ce maximum caractérise l'avance de la transition. Notons qu'une déformation sinusoidale forte ( $a/\lambda = 0,5/100$ ) favorise à l'avant l'apparition du maximum entre le bord d'attaque et la plaque plane soumise de  $30\%$  l'abscisse de ce "début de transition".

Nous avons, par ailleurs, constaté que l'évolution du phénomène, bien d'être linéaire en fonction de l'amplitude, est tout au moins monotone. D'autre part, les modifications apportées par la déformation,

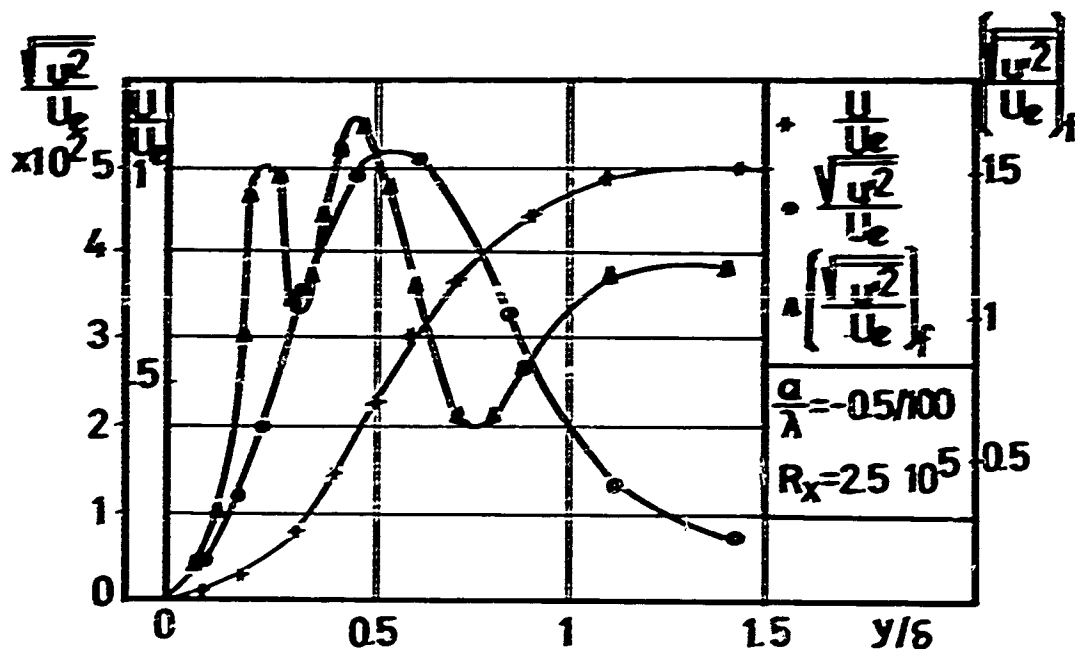


Fig. 6 - Profils caractéristiques

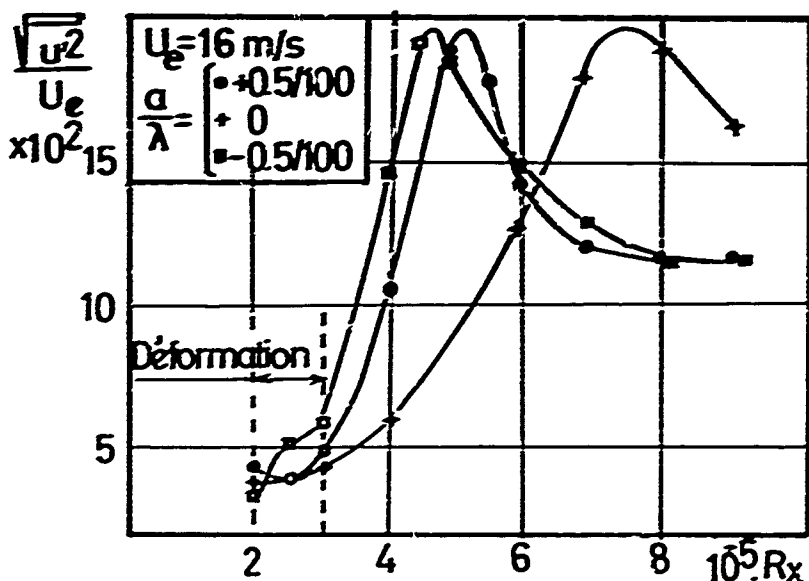


Fig. 7 - Localisation de la transition

sans être significatives semblent être du même ordre de grandeur, surtout qu'il s'agit d'une base  $(a > 0)$  ou d'un creux  $(a < 0)$ .

### III.6 MESURE DES AMPLIFICATIONS DES INSTABILITÉS

Le cas cité au paragraphe III.5 nécessite en fait une méditation approfondie du phénomène de déclenchement de la transition. L'interprétation des analyses spectrales fournit une mesure de l'énergie contenue dans les instabilités.

Sur la figure 6 nous avons porté en fonction de  $x/\delta$  l'évolution de la valeur efficace de la fluctuation longitudinale de vitesse pour une fréquence donnée (celle des instabilités). Cette courbe présente deux sections : l'une située à  $x/\delta = 0,20$ , l'autre à  $x/\delta = 0,40$ . Le premier section correspond à l'existence d'un point d'inflection sur le profil des vitesses moyennes (critère d'instabilité), le second section est en accord avec les résultats théoriques de Jamnison [22] et nous avons retenu ce niveau comme caractéristique de l'état d'amplification des instabilités pour une section donnée.

Sur la figure 8, nous avons porté les courbes d'amplification correspondant à la plaque plane et à deux déformations.

La courbe relative à la plaque plane est régulière. Par contre, les courbes relatives aux déformations positive et négative présentent chacune une très nette cassure. Ainsi, non seulement

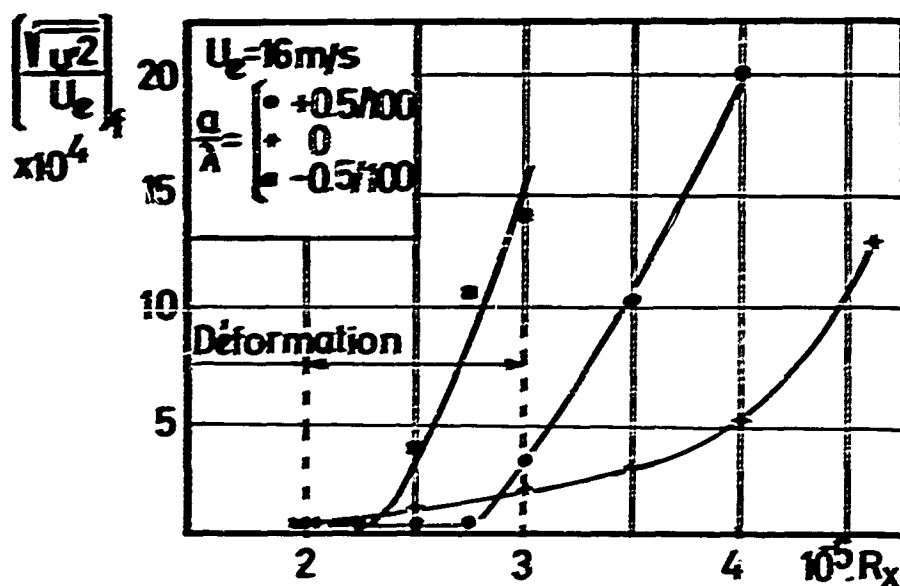


Fig. 8 - Amplification des instabilités

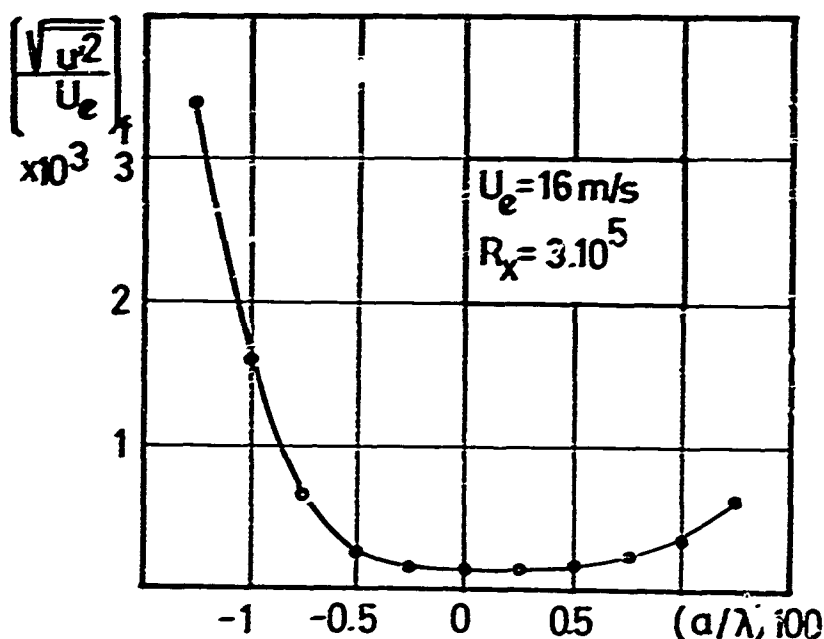


Fig. 9 - Niveau d'instabilité à l'aval de la déformation

L'amplification n'a pas lieu de la même manière suivant qu'il y a ou non déformation mais, de plus, le signe de la déformation entraîne une localisation différente de la boucle amplification.

Nous pouvons rattacher ceci à la constatation faite au paragraphe III.5 et relative à la dissymétrie de la position de la transition suivant le signe de la déformation. L'amplification de ce phénomène se trouve dans la localisation des gradients locaux attachés à la déformation :

- s'il s'agit d'une déformation en creux ( $\alpha/\lambda = -0,5/100$ ) le gradient négatif (défavorable) apparaît dès le début de la déformation et l'amplification des fréquences instables se fait très tôt,

- s'il s'agit d'une déformation en sautoir ( $\alpha/\lambda = +0,5/100$ ) la déformation conduit d'abord un gradient positif (favorable) et la couche limite est stabilisée. Ce n'est qu'en fin de déformation que le gradient défavorable apparaît et déclenche l'amplification.

Nous avons voulu avoir une confirmation de cette interprétation pour d'autres amplitudes de déformation. Sur la figure 9 nous avons porté en fonction de l'amplitude de la déformation le niveau des fréquences accrétées à l'aval immédiat de la déformation. Cette courbe met à nouveau en évidence la dissymétrie citée ci-dessus. Notons, d'autre part, que l'amplitude de la déformation a une influence minime sur l'amplification /23/.

## II.7 CONCLUSIONS

Ces mesures confirment l'effet important de faibles amplitudes de déformation de paroi sur la position de la transition. Une étude détaillée de la densité de spectre de puissance des fluctuations de vitesse permet de mieux comprendre la naissance de la transition. En particulier par la mesure de l'amplification des instabilités, nous avons pu corréler les résultats avec l'existence de gradients locaux de vitesse existante. Suivant la localisation respective des gradients favorable et défavorable le développement des instabilités se fait de manière très différente.

Enfin, quand l'amplitude de la déformation augmente, c'est-à-dire pour une probabilité croissante d'existence de micro-déformations l'amplification des instabilités et la position du milieu de transition semblent évoluer sans présenter de discontinuité.

## BIBLIOGRAPHIE

- /1/ G.B. DIEP, P. GUGAT, T.S. DUONG et B. PRINCE-FOCH : Etude des décollements, en écoulement isovolume, se produisant sur une plaque plane à paroi sinusoïdale. Rapport du Laboratoire d'Aérodynamique du CRS 70-1 (février 1970)
- /2/ E.L. BELEN : Some recent contributions to the study of transition and turbulent boundary layers. NACA TN-1146 (avril 1947)
- /3/ R. HIRSH : Couches limites perturbées par des ondulations harmoniques de la paroi (rapport). Document privé non publié
- /4/ A.K. GITA et E.L. WILLO-CHRISTENSEN : An experimental investigation of air flow over a wavy plate. Massachusetts Institute of Technology, Aerodynamic and Structures Research Laboratory (août 1956)
- /5/ T. BUCKE BENJAMIN : Shearing flow over a wavy boundary. J.F.M., 6, p. 161 (1959)
- /6/ L.M. MILNE-THOMSON : Theoretical Hydrodynamics. Macmillan and Company Limited, p. 461 (1960)
- /7/ L. SEIGNE : Mechanics of Fluids. Mac Graw Hill Book Company, p. 456 (1962)
- /8/ M.L. MILNE-THOMSON : Sur les théories et les méthodes de calcul relatives aux lignes et surfaces portantes. Cours de l'ENSA
- /9/ R. MICHEL : Couches limites, frottement et transfert de chaleur. Cours d'Aérodynamique de l'ENSA, fasc. 2 (1953)
- /10/ E.A. PRINCE : Introduction à l'étude de la couche limite. Gauthier-Villars (1955)
- /11/ E. SCHLICHTING : Boundary-layer Theory. Mac Graw Hill Book Company, 6ème éd. (1968)
- /12/ B. TEJGAARD : Incompressible Aerodynamics. Oxford, Clarendon Press (1960)
- /13/ A.W. QUICK et K. SCHNEIDER : Verhalten der laminaren Grenzschicht bei periodisch schwankendem Druckverlauf. Math. Nachr. 8, 217-238 (1953)
- /14/ L.S. KOVASKAY, H. KOMODA et B.R. VASUDEVA : Detailed flow field in transition. Proceedings of the 1962 Heat transfer and Fluid Mechanics Institute, Stanford University Press (1962)
- /15/ J.O. HINZE : Turbulence. Mac Graw Hill Book Company (1959)
- /16/ G.B. DIEP, T.S. DUONG, P. GUGAT et B. PRINCE-FOCH : Analyse spectrale des fluctuations d'une couche limite. Rapport du laboratoire d'Aérodynamique du CRS 69-2 (juin 1969)
- /17/ J. STERN : Méthodes pratiques d'études des fonctions aléatoires. Dunod (1967)
- /18/ J.S. BENNETT : Measurements and analysis of random data. John Wiley and Sons (1967)
- /19/ G.B. GULLOUGH et D.E. CAULT : Examples of three representative types of airfoil-section stall at low speed. NACA TN-2502 (septembre 1951)
- /20/ T.S. DUONG : Contributions à l'étude comparative de la transition sur plaque plane et ondulée. Thèse de Docteur-Ingénieur. Faculté des Sciences de Paris (1er juin 1970)
- /21/ T.S. DUONG, P. GUGAT, G. LENGELLE : Etude de la transition sur une plaque plane à paroi sinusoïdale en écoulement incompressible. C.R. Acad. Sci. Paris, 271, A, 175 (20 juillet 1970)
- /22/ R. JORDINSON : Numerical integration of the Orr Sommerfeld equation. J.F.M., 43, 4 (1970)
- /23/ S. BURNEL et P. GUGAT : Influence d'un gradient local de pression sur le développement des fréquences instables dans la couche limite laminaire. Rapport du laboratoire d'Aérodynamique du CRS 71-5 (oct 1971)

(O.N.E.R.A.)

92 - COMPTES - RENDUS

1954

RECHERCHES SUR LE DÉTACHEMENT D'UNE COUCHE LIMITÉ EN ÉCOULEMENT INCOMPRESSIBLE

A simple calculation method is proposed to calculate the small separation zones ("small bubbles") which are formed near the leading edge of an airfoil at incidence. This calculation permits to know the details of the separation process and to predict the maximum lift that may be obtained at least within a certain Reynolds number range.

RÉSUMÉ

Une méthode de calcul, très simple, est proposée pour calculer les zones décollées de très faible dimension ("bulles courtes") qui apparaissent dans la région du bord d'attaque des profils d'ailes en incidence. Ce calcul a permis de préciser les processus du détachement et de prévoir la portance maximale qui peut être obtenue, tout au moins dans un certain domaine de nombre de Reynolds.

NOTATIONS

$A_n$  fonction égale à  $D_n + C_n (\epsilon_p(z))$  (Annexe I)

$b$  paramètre définissant le profil de vitesse  $b = \frac{K_0}{\delta_2^2}$

$C$  courbe du profil

$C_F$  coefficient de frottement à la paroi  $C_F = \frac{\tau_0}{\frac{1}{2} \rho U^2}$

$C_n$  terme complémentaire  $(\epsilon_p(z))$  Annexe I

$C_z$  coefficient de portance

$$D_n = -\frac{b+1}{2\delta_2^2} \int_0^{\delta_2} \left(\frac{u}{U}\right)^n \frac{\partial \delta_2}{\partial y} dy$$

$E_n$  fonction définie dans l'Annexe II (§ 3)

$H$  paramètre de forme classique  $H = \frac{\delta_2^*}{\delta_2}$

$H_2$  paramètre de forme  $H_2 = \frac{\delta_2}{\delta_2^*}$  ( $H_0 = -H$ ,  $H_1 = 0$ ;  $H_2 = 1$ )

$i$  incidence

$$\ell_1 = x_T - x_S$$

$$\ell_2 = x_A - x_T$$

$n$  numéro de l'équation intégrale utilisée (Annexe I)

$p$  pression

$q_0$  pression cinétique de référence

$r$  rayon de courbure

$R_x$  nombre de Reynolds pour la longueur  $x$   $R_x = \frac{U_0 x}{\nu}$

$u, v$  composantes de la vitesse dans la couche limite

$u', v'$  fluctuations des composantes de la vitesse

$$(\overline{u'v'}, \overline{u'^2}) : \text{moyennes dans le temps de } u'v' \text{ et } u'^2 ;$$

$U$  vitesse à l'extérieur de la couche limite

$$\bar{U} = \frac{U}{U_T}$$

$x, y$  coordonnées intrinsèques d'un point

$y_0$  cote de la ligne de courant  $\psi = 0$

$\alpha_n$  constante :  $\alpha_1 = 3$   $\alpha_\infty = 1$  (eq. 1)

$\beta_n$  constante  $\beta_1 = 0,41$   $\beta_\infty = 0,577$  (eq. 2)

$\gamma_n$  constante  $\gamma_1 = 0,0187$   $\gamma_\infty = 0,1$  (eq. 3)

$\delta$	épaisseur de la couche limite
$\delta^*$	épaisseur de déplacement
$\delta_m = \int_0^{\delta} \left[ \frac{u}{U} - \left( \frac{u}{U} \right)^2 \right] dy$	
$\mu$	viscosité
$\rho$	masse volumique
$\tau$	frottement
$\psi$	fonction de courant

### NOTES

- $e$  : quantité prise sur la courbure ( $y = \delta$ ) de la couche limite  
 $R$  : quantité intégrée se rapportant à l'équation d'ordre  $n$   
 $P$  : quantité prise à la paroi  
 $S, P, T, Q$  : quantité prise respectivement aux points S, P, T, Q

### ABBREVIATIONS

- R.A. - bord d'attaque  
 R.F. - bord de fuite  
 S - point de décollement  
 P - point de recollement  
 T - point de transition  
 Q - fin du plateau de vitesse, début de la recompression

## 1) INTRODUCTION

Le décrochage peut être défini comme l'ensemble des phénomènes liés aux décollements de la couche limite qui ont pour effet de limiter et de diminuer plus ou moins brutalement la portance d'un aile.

Sur les profils d'ailes, trois types principaux de décrochage ont été mis en évidence aux vitesses subsoniques [ref 1] :

- 1 - décrochage des "ailes minces", où un décollement de la couche limite laminaire près du bord d'attaque, la zone décollée ("bulbe long") s'étend progressivement jusqu'en delà du bord de fuite lorsque l'incidence croît.
- 2 - décrochage de bord d'attaque associé à "l'écèlement" d'une petite zone décollée ("bulbe court") et caractérisé par une diminution très brutale de la portance.
- 3 - décrochage de bord de fuite, dans lequel le point de décollement de la couche limite se déplace du bord de fuite vers le bord d'attaque quand l'incidence croît; il est caractérisé en général par une baisse progressive de portance.

Pour prévoir le type de décrochage en fonction du nombre de Reynolds, des corrélations ont été trouvées, basées en général sur des considérations géométriques des profils [ref 2 et 3]. Mais ces corrélations établies à partir d'essais sur des profils NACA classiques, ne conviennent plus lorsqu'on les applique à des profils nouveaux. Sur la figure 1 sont reportés les  $C_{L_{max}}$  obtenus pour des profils d'ailes symétriques qui ne diffèrent que par la région du R.A. [ref 4] ; on peut voir que, aux faibles nombres de Reynolds, le profil "B" décroche suivant le premier type et le profil "A" suivant le deuxième alors que les critères prédiraient l'inverse.

Les tentatives pour essayer de prévoir le décrochage par le calcul n'ont fait l'objet que de publications peu nombreuses parmi lesquelles on peut citer la méthode simple, semi-empirique, proposée par le Queen Mary College pour le calcul des "bulbes courts" [ref 5]. Un schéma analogue dans ces grandes lignes à celui proposé par le Queen Mary College sera présenté dans la première partie de cette note ; les hypothèses faites y sont discutées et les résultats obtenus seront confrontés à l'expérience.

Ils seront utilisés dans la deuxième partie, pour la discussion des problèmes de décrochage de profils d'aile.

## 2) Calcul des zones décolées - Les bulbes courts -

### 2.1 - Calcul simplifié d'une zone décolée en écoulement incompressible lorsqu'on connaît la loi de vitesse à l'extérieur de la couche limite $U(x)$ :

Pour calculer une zone décolée par une méthode intégrale, on la décompose en régions (voir pl.2) dans lesquelles on suppose que les profils de vitesse peuvent être représentés par une famille de profils dépendant d'un paramètre (par exemple  $b = \frac{y}{\delta}$  ou  $y_0$  désigne la cote de la ligne de courant  $\psi = 0$  par rapport à la paroi (fig.2) :  $\frac{u}{U} = f(b, \frac{y}{\delta_n})$  (voir annexe II).

La zone décolée sera complètement déterminée si l'on sait calculer, en fonction de  $x$ , la valeur du paramètre  $b$  et une grandeur caractéristique  $\delta_n$ . Deux équations intégrales sont donc nécessaires. Nous utiliserons les équations d'énergie cinétique (correspondant à  $n = 1$  dans l'Annexe I) et d'entrainement ( $n = \infty$ ) qui se présentent sous une même forme très simple :

$$(1) \quad \frac{1}{U^{2n}} \frac{dU^{2n} \delta_{n+2}}{dx} = D_n$$

$$n=1 \quad \alpha_n = \alpha_1 = 3 \quad \delta_{n+2} - \delta_3 = \int_0^x \left[ \frac{u}{U} - \left( \frac{u}{U} \right)^3 \right] dy$$

$$D_n = D_1 \quad \text{fonction de dissipation définie dans l'annexe I et calculée dans l'annexe II}$$

$$n=\infty \quad \alpha_n = \alpha_\infty = 1 \quad \delta_{n+2} - \delta_\infty = \delta - \delta^* = \int_0^x \frac{u}{U} dy$$

$$D_n = D_\infty \quad \text{fonction d'entrainement (voir annexes I et II).}$$

#### 2.1.1 - Calcul de $\delta_{n+2}$ (détails des calculs dans l'annexe III).

a) en laminaire : on trouve

$$(2) \quad \left( \frac{U}{U_S} \right)^{2\alpha_n} \left[ \frac{\delta_{n+2}}{(\delta_{n+2})_S} \right]^2 = 1 + 2 \beta_n \frac{1}{\delta_{25} R_{\delta_{25}}} \int_{x_S}^x \left( \frac{U}{U_S} \right)^{2\alpha_n-1} dx$$

où l'indice  $S$  indique la valeur d'une grandeur prise au point de décollement  $S$  ; et où

$$R_{\delta_{25}} = \frac{U_S \delta_{25}}{\nu}$$

Les quantités  $\beta_n$  sont des constantes :  $\beta_1 \approx 0,41 \quad \beta_\infty \approx 0,677$

b) en écoulement turbulent :

$$(3) \quad \left( \frac{U}{U_T} \right)^{\alpha_n} \frac{\delta_{n+2}}{(\delta_{n+2})_T} = 1 + \gamma_n \frac{1}{(\delta_{n+2})_T} \int_{x_T}^x \left( \frac{U}{U_T} \right)^{\alpha_n} dx$$

où l'indice  $T$  désigne la valeur d'une grandeur au point de transition  $T$ .

$$\gamma_1 \approx 0,0187 \quad \gamma_\infty \approx 0,1$$

#### 2.1.2 - Calcul de $b$

Le rapport des 2 équations (2) en laminaire ou (3) en turbulent donne (en posant  $\delta_{n+2} = H_{n+2} \delta_2$ , étant l'épaisseur de quantité de mouvement)

$$\frac{H_3}{H_{35}} \frac{H_{\infty 5}}{H_{\infty}} = g(U, \delta_{25})$$

$H_3$  et  $H_{\infty}$  ne dépendent que du paramètre  $b$  ; connaissant  $U$  et  $\delta_{25}$  on peut alors théoriquement en déduire  $b$  ; le problème est alors complètement résolu. Mais les rapports  $H_{n+2}$  varient très peu (Annexe II fig.a.4 et a5).

Aussi de faibles erreurs soit sur  $g(U, \delta_{25})$ , soit sur les profils de vitesse utilisés, risquent d'introduire des erreurs importantes sur  $b$ . On ne pourra donc déterminer avec précision, à l'aide de ces 2 équations, ni le paramètre  $b$  ni par conséquent  $\delta_2$  dans la zone décolée (sauf au recollement où  $b = 0$ ), mais uniquement  $\delta_3$  et  $\delta_\infty$ .

## 2.2 - Etude des "bulbes courts"

Nous appellerons "bulbes courts" des zones décolées, provoquées par un décollement laminaire et d'assez petite dimension pour n'apporter que des modifications très locales à la distribution de vitesse en fluide parfait. L'évolution de  $U(\infty)$  au droit de ces zones n'est pas connue ; aussi serons-nous amenés à la déterminer en première approximation en faisant certaines hypothèses basées sur des considérations expérimentales.



### 2.2.1 - Schématisation (planche 2)

On supposera que la présence du bulbe n'a d'influence sur la distribution des vitesses que dans la zone ST.

- la position du point de décollement S et la valeur de  $\delta_{25}$  seront donc déterminées par un calcul de couche limite laminaire à partir de la distribution de vitesse en fluide parfait.

- Expérimentalement on trouve que l'on peut distinguer deux zones entre S et R :

- zone ST : après une légère recompression  $U$  reste sensiblement constant. La forme de l'évolution des vitesses est variable. En général  $\Delta U = U_S - U_T > 0$ ; on considérera que  $\frac{\Delta U}{U_S}$  est faible, de l'ordre de 0,05. On suppose que l'écoulement est laminaire jusqu'en T (cf [ref 5]) et que la transition se produit en ce point.

- zone TR : au cours de cette recompression en régime turbulent, l'évolution de  $U(x)$  est sensiblement linéaire (sauf au voisinage de T et R).

- la planche 3 montre des exemples de distributions de vitesses (calculées à partir des pressions relevées à la paroi). Dans le cas III l'augmentation de vitesse en amont de T met en défaut le schéma proposé ; elle est sans doute due au fait que la transition commence bien avant T. Dans des conditions proches du décrochage les répartitions de vitesses observées sont généralement du type I.

### 2.2.2 - Etude de la partie ST supposée laminaire

a) Calcul de  $(\delta_{n+2})_T$ .

A partir de (2) on trouve (Annexe III)

$$(4) \quad \left[ \frac{(\delta_{n+2})_T}{(\delta_{n+2})_S} \right]^2 = 1 + 2 \alpha_n \frac{\Delta U}{U_S} + \beta_n \frac{l_1}{\delta_{25} R \delta_{25}} \left( 1 + k \frac{\Delta U}{U_S} \right)$$

où  $l_1 = x_T - x_S$

et où  $k$  est une constante comprise entre 1 et  $\frac{2\alpha_{n+1}}{2}$ , qui définit la distribution de vitesse entre S et T

b) Détermination de  $l_1$

Il n'est pas encore possible à l'heure actuelle de prévoir la transition par une voie purement théorique. Aussi déterminerons-nous  $l_1$ , qui définit un "point de transition" à partir de corrélations expérimentales. La première corrélation est due à Von Doenhoff [ref 6] qui a proposé la relation  $\frac{U l_1}{\nu} = 5 \cdot 10^4$ .

. Horton [ref 5] après avoir examiné un grand nombre de cas, propose une valeur différente de la constante :  $\frac{U l_1}{\nu} = 4 \cdot 10^4$ . Les points de Horton sont reportés, avec quelques points ONERA sur la figure 4 en ordonnée réduite  $\frac{l_1}{\delta_{25} R \delta_{25}}$ .

On constate qu'aux faibles valeurs de  $R \delta_{25}$ , les points expérimentaux sont voisins de la courbe  $\frac{U l_1}{\nu} = 3 \cdot 10^4$  alors que pour des valeurs plus élevées de  $R \delta_{25}$  ils se rapprochent de  $\frac{U l_1}{\nu} = 5 \cdot 10^4$ .

Nous prendrons pour nos calculs une courbe passant mieux par les points expérimentaux (Fig.4).

Ceux-ci semblent converger vers un point où  $l_1 = 0$  pour  $700 < R \delta_{25} < 1000$ ; la transition se ferait alors juste au point de décollement laminaire et il n'y aurait plus de bulbe. L'existence d'une telle valeur limite de  $R \delta_{25}$  est en accord avec certains critères de transition hors des zones décollées ( $R \delta^* = 3000$ , critère de Grattree [ref 7]); par contre d'autres critères comme ceux de Michel ou de Granville ne mettent pas en évidence une telle valeur limite.

### 2.2.3 - Détermination du point de recollement (R) et des caractéristiques de la couche limite en ce point

Posons  $\frac{U_R}{U_T} = \bar{U}_R$  ; en supposant pour l'intégration  $U(x)$  linéaire entre T et R, les équations (3) deviennent :

$$(6) \quad \bar{U}_R^{\alpha_n} \frac{(\delta_{n+2})_R}{(\delta_{n+2})_T} = 1 + \frac{\delta_n}{\alpha_{n+1}} \frac{l_2}{(\delta_{n+2})_T} \frac{1 - \bar{U}_R^{\alpha_{n+1}}}{1 - \bar{U}_R}$$

où  $l_2 = x_R - x_T$

Nous supposons qu'à la transition les quantités  $\delta_{n+2}$  pour  $n=1$  et  $n=\infty$ , restent continues;  $(\delta_{n+2})_T$  sera alors donné par (4) et  $(H_{n+2})_R$  étant connu ( $b=0$ ), (6) fournit 2 relations pour déterminer les 3 inconnues  $\delta_{2R} = \frac{(\delta_{n+2})_R}{(H_{n+2})_R}$ ,  $\bar{U}_R$  et  $l_2$

L'élimination de  $\delta_{2R}$  fournit une relation  $\bar{U}_R(l_2)$ ; la position du point de recollement  $R$  sera ensuite obtenue comme intersection de la courbe  $(l_2)$   $\bar{U}_R(l_2)$  et de la courbe des vitesses calculées en fluide parfait. On trouve

$$(7) \frac{l_2}{1-\bar{U}_R} = \left[ \frac{\delta_{\infty T}}{H_{\infty R}} - \frac{\delta_{2T}}{H_{2R}} \frac{1}{\bar{U}_R^2} \right] / \left[ \frac{\delta_1}{4H_{2R}} \frac{1-\bar{U}_R^4}{\bar{U}_R^2} - \frac{\delta_{\infty}}{2H_{\infty R}} (1-\bar{U}_R^2) \right]$$

$\delta_{2R}$  est ensuite calculé par (6)

$$(H_{2R} \simeq 1,52; H_{\infty R} \simeq 4,1)$$

#### 2.2.4. - Comparaison avec la méthode de la [ref 5] et avec l'expérience.

a) Méthode de la [ref 5] : Horton utilise l'équation de Karman (correspondant dans l'annexe I à  $n=0$  avec  $C_0=0$ ) et l'équation de l'énergie cinétique ( $n=1$  avec  $C_1=0$ ).

L'équation de Karman appliquée entre S et T, en supposant  $U=U_\infty$  et le coefficient de frottement  $C_F \simeq 0$ , entraîne que  $\delta_{2T} = \delta_{2S}$ .

Le calcul de  $\delta_{2R}$  et de la position de  $R$  est fait à partir de la relation  $\frac{\delta_{2R}}{\bar{U}_R} \left( \frac{dU}{dx} \right)_R = \lambda_R$  (obtenue par combinaison linéaire des 2 équations) et de la relation (6) écrite pour  $n=1$  en supposant  $H_{2T} = H_{2R}$ . La valeur de  $\lambda_R$  théorique est voisine de -0,006, alors que la valeur moyenne trouvée expérimentalement est de -0,0082. Cet écart provient essentiellement des approximations faites dans les équations ( $C_0=0$ ) et du fait qu'expérimentalement on n'obtient pas  $\lambda_R = \frac{\delta_{2R}}{\bar{U}_R} \left( \frac{dU}{dx} \right)_R$  mais une grandeur  $\Lambda_R = \frac{\delta_{2R}}{\bar{U}_R} \frac{\bar{U}_R - U_T}{l_2}$ . Avec cette expression on obtient la relation cherchée entre  $\bar{U}_R$  et  $l_2$  qui s'écrit :

$$(8) \frac{l_2}{\delta_{2T}} = \frac{1-\bar{U}_R}{\left( \Lambda_R + \frac{D_{1R}}{4H_{2R}} \right) \bar{U}_R^4 - \frac{D_{1R}}{4H_{2R}}}$$

b) comparaison avec l'expérience :

La figure 5a représente la distribution de vitesses obtenue expérimentalement sur un profil d'aile, dans des conditions d'essais précédant d'assez peu le décrochage, et la distribution de vitesse théorique en l'absence de bulbe. Celle-ci a été reportée en coordonnées réduites  $\left( \bar{U} = \frac{U}{U_\infty} \right)$  en fonction de  $\bar{X} = \frac{x - x_{ST}}{\delta_{2T} H_{2R}}$  sur la figure 6a où sont tracées également les courbes  $(l_2)$  déduites des équations (7) et (8). Cette dernière courbe (méthode de [ref 5]) ne coupe pas la courbe des vitesses, ce qui signifierait qu'il y a eu décrochage. Notre méthode par contre prévoit un recollement. Le calcul de la couche limite à l'aval du bulbe a été effectué à partir de la valeur de  $\delta_2$  ainsi trouvée en R. Les résultats fig. 6b sont en bon accord avec ceux des sondes de couche limite.

On notera que les valeurs de  $\delta_2$  qu'on obtiendrait en négligeant la présence du bulbe et en supposant que la transition s'opère en S, sont par contre, très inférieures aux valeurs expérimentales.

#### 2.2.5. - La méthode proposée permet donc d'obtenir le point de recollement et la valeur de $\delta_2$ en ce point.

Etant donné que les perturbations que cette zone décollée entraîne sur les vitesses sont très faibles, il est de peu d'intérêt de faire le calcul complet (calcul de b) qui permettrait d'avoir une 2ème approximation de la loi de vitesse (mais qui nécessiterait de faire le couplage fluide parfait-fluide visqueux, qui est très compliqué en subsonique).

La nécessité d'utiliser une relation empirique pour déterminer la transition dans le bulbe constitue un point faible de la méthode.

### 3 - APPLICATION A LA PREVISION DU DECROCHAGE

#### 3.1 - Détermination du nombre de Reynolds $\mathcal{R}_L$ au dessous duquel un "bulbe court" ne peut plus exister.

a) - Lorsque le nombre de Reynolds varie, toutes les autres conditions étant fixées par ailleurs, il peut arriver que la courbe  $(l_2)$  (eq (7)) devienne tangente à la courbe des vitesses en fluide parfait (Fig. 7a). Cette condition de tangence fixe alors le nombre de Reynolds limite  $\mathcal{R}_L$ .

- en fait ceci se produit rarement avec la courbe  $(l_2)$  déduit de (7) (mais très souvent par contre si l'on utilise l'équation (8)). On trouve un point de recollement (Fig. 7b) mais la longueur  $l_2$  de la recompression turbulente et par conséquent  $\delta_{2R}$ , augmente rapidement (Fig. 8).

Expérimentalement on a constaté qu'un bulbe court ne pouvait plus exister lorsque la recompression devenait trop importante.

Crabtree [ref 8] indique une valeur limite de 0,35 pour  $\tau = \frac{P_R - P_S}{P_S}$  (soit  $\frac{U_R}{U_S} = 0,805$ ).

b) divers processus amenant à la disparition de ce bulbe court peuvent être imaginés :

- à cause de l'accroissement important de  $\delta_2$  un décollement turbulent se produit un peu en aval du point de recollement R, dans une région où les gradients de vitesse sont encore très élevés.

- la zone décollée devient trop étendue et la distribution de vitesse sur le profil va subir des modifications par rapport à la distribution en fluide parfait, modifications qui vont devenir de plus en plus importantes au fur et à mesure que l'incidence augmente et que la zone décollée s'étend. La distribution de pression dans cette zone comprend toujours une partie sensiblement isobare suivie d'une recompression, mais l'intensité de celle-ci diminue c'est-à-dire que  $U_R/U_S$  augmente. Le début de la recompression Q ne peut plus être confondu avec le point de transition T : en effet  $\delta_2$  augmente,  $\delta_2/(\delta n_2)Q$  diminue (puisque  $U_R$

augmente, cf pl.6) donc  $(\delta n_2)_Q$  doit croître plus rapidement que ne l'indique l'équation (4) ce qui ne peut être réalisé que s'il existe une partie turbulente dans la région isobare (on a alors  $\frac{(\delta n_2)_Q}{(\delta n_2)_T} = 1 + \delta n \frac{\delta_2}{(\delta n_2)_T}$ )

où  $\delta_2 = x_Q - x_T$  )

La zone décollée est alors habituellement appelée "bulbe long".

### 3.2 - Décrochages de bord d'attaque : détermination du $C_z$ max.

#### Comparaison avec l'expérience

#### 3.2.1. - Détermination du $C_z$ max.

Pour un profil d'aile, lorsque le décrochage a pour origine la région du bord d'attaque, on constate expérimentalement 2 évolutions différentes de la portance en fonction de l'incidence suivant le nombre de Reynolds :

- diminution progressive de la portance par rapport à la valeur qu'elle aurait s'il n'y avait pas de décollement (pl.1 : profil "E").
- baisse brutale de la portance à partir d'une certaine incidence. (Pl.1 : profil "A")

Dans ce dernier cas, on pourra considérer que le  $C_z$  max. à un nombre de Reynolds  $R_c$  correspond à la distribution de vitesse pour laquelle  $R_c = R$ . Ceci suppose que, à  $C_z$  fixé, les répartitions de vitesse expérimentales et en fluide parfait sont confondues ; c'est assez bien vérifié pour la majorité des profils tant qu'il n'y a pas de décollement dans la région du B.F.

#### 3.2.2 - Application du critère de Crabtree ( $\frac{U_R}{U_S} = 0,805$ )

La figure 9 présente les  $C_z$  max. obtenus en soufflerie sur un profil (ONERA "D") en fonction de  $R_c$ . Les  $C_z$  max. calculés à partir du critère de Crabtree sont en assez bon accord avec l'expérience dans le domaine de  $R_c$  où l'augmentation de  $C_z$  max. est très rapide.

Les nombres de Reynolds plus faibles correspondent au 1er type d'évolution de la portance évoqué au § 3.2.1.. Le  $C_z$  max. varie alors très peu avec  $R_c$  ; on constate qu'il est atteint lorsque la zone décollée occupe environ 60% de la corde du profil.

Pour des nombres de Reynolds plus élevés un décrochage brutal se produit alors que la recompression est inférieure à la limite trouvée par Crabtree, et que l'accroissement de  $\delta_2$  est modéré.

#### 3.2.2. - Calcul du nombre de Reynolds où apparaît un décollement turbulent dans la région du B.A.

Les calculs de couche limite turbulente à partir du point de recollement, donnent des valeurs de  $R_c$  à  $C_z$  donné proches des résultats expérimentaux dans le domaine  $1 < C_z \text{ max.} < 1,6$ . Ces calculs sont très sensibles à de faibles variations de  $\delta_2 R$  par exemple ; expérimentalement cette sensibilité se retrouve bien comme le montre la comparaison d'essais dans deux souffleries différentes. Pour  $C_z < 1$ , on n'a pas mis en évidence de décollement turbulent (pour  $R_c > 0,6 \cdot 10^6$ ). Le décrochage doit correspondre au 2ème processus décrit au § 3.1b.

Pour  $C_z > 1,25$ , les gradients de vitesse sont suffisamment élevés à l'aval du bulbe court pour provoquer un décollement turbulent bien que la valeur de  $\delta_2 R$  soit modérée. Au delà de  $C_z = 1,6$  environ les calculs ne prévoient plus un décollement turbulent dans la région du B.A. Ceci est conforme aux essais effectués par la technique du bord d'attaque agrandi, qui permet d'obtenir, sur la partie avant tronquée du profil, réalisée à grande échelle, la configuration d'écoulement du profil complet [ref 9]. Le comportement du bord d'attaque est ainsi étudié indépendamment de celui du bord de fuite.

Ces essais réalisés à des nombres de Reynolds  $R_c$  (calculés sur la corde du profil équivalent) supérieurs à  $2,8 \cdot 10^6$ , n'ont mis en évidence aucun décrochage bien que des pics de survitesse très importants (correspondant à des  $C_z$  sur profil complet supérieurs à 2) aient été atteints.

La limitation de la portance est alors due aux décollements turbulents prenant naissance dans la région de bord de fuite.

Pour de nombreux profils ces décollements turbulents dans la région du B.F. apparaissent à des nombres de Reynolds plus élevés que les décollements turbulents de B.A. Les calculs précédents donnent alors une valeur trop forte du  $C_z$  max.

### 3.3 - Décrochages de bord de fuite -

Ce type de décrochage est dû au décollement de la couche limite turbulente dans la région du B.F où les gradients de vitesse sont en général très modérés mais où la couche limite est épaisse. Cette modification de l'écoulement au B.F va entraîner une diminution de la circulation par rapport à sa valeur en l'absence de décollement. La perte de portance sera plus ou moins rapide suivant que la position du décollement sera plus ou moins sensible à une variation d'incidence ou de nombre de Reynolds.

Il sera intéressant de calculer pour une incidence donnée, le nombre de Reynolds auquel apparaît ce décollement, mais le  $C_L$  calculé ne sera égal au  $C_{Lmax}$  à ce nombre de Reynolds que si le coefficient de déplacement du décollement  $\frac{\Delta x_s}{\Delta x_c}$  ou  $\frac{\Delta x_s}{\Delta R_c}$  est élevé.

En fait ce calcul est assez difficile car dans la région du B.F les gradients de vitesses diffèrent sensiblement de ceux calculés en fluide parfait à même  $C_L$ ; il faut donc tenir compte du couplage fluide parfait-fluide visqueux. On pourra avoir recours à des méthodes simplifiées comme celle de la référence [10].

Le calcul complet avec zone décollée dans la région du B.F n'a pu encore être effectué actuellement à notre connaissance.

### 4 - CONCLUSION :

Une méthode simple a été proposée pour calculer la position du point de recollement, et les caractéristiques de la couche limite en ce point, des zones décollées de très faible dimension ("bulbe court") provoquées par le décollement de la couche limite laminaire dans la région du bord d'attaque des profils d'aile en incidence. Ce calcul a permis de préciser les processus du décrochage en courant plan et de prévoir la portance maximale, tout au moins dans une certaine gamme de nombre de Reynolds  $R_c$ . Trois courbes limites ont été mises en évidence dans le plan  $(C_L, R_c)$  :

- (1) limite d'existence du "bulbe court" (caractérisée, par exemple, par une valeur maximale de la recompression),
- (2) apparition des décollements turbulents dans la région du B.A en aval du point de recollement,
- (3) apparition des décollements turbulents dans la région du B.F.

Pour des nombres de Reynolds compris entre deux valeurs limites  $R_1$  et  $R_2$ , qui dépendent du profil considéré, ces courbes permettent de prévoir correctement la valeur du  $C_{Lmax}$ . Par contre, la courbe (1) au-dessous de  $R_1$ , et la courbe (3) au-dessus de  $R_2$  donnent une évaluation du  $C_{Lmax}$  trop faible; la connaissance de ces courbes limites est cependant importante pour la prévision de l'apparition du buffeting.

### ANNEXE I

#### Discussion des équations utilisées pour la zone visqueuse

Considérons les équations intégrales obtenues en multipliant par  $U^n$  la première équation de Navier-Stokes (appliquée à l'écoulement moyen en turbulent) et en intégrant suivant  $y$  de 0 à  $\delta$  (où  $y = \delta$  définit la frontière de la couche limite sur laquelle  $u = U$ ) en tenant compte de l'équation de continuité.

On obtient :

$$(a1) \quad \frac{1}{\rho_e U^{n+2}} \frac{d}{dx} \left( \rho_e U^{n+2} \delta_{n+2} \right) - (n+1) \frac{\delta_n}{U} \frac{dU}{dx} = A_n$$

$$\text{ou} \quad \delta_n = \int_0^\delta \frac{\rho}{\rho_e} \frac{u}{U} - \frac{\rho}{\rho_e} \left( \frac{u}{U} \right)^n dy$$

$$A_n = D_n + C_n$$

$$D_n = - \frac{(n+1)}{\rho_e U^2} \int_0^\delta \left( \frac{u}{U} \right)^n \frac{\partial \tau}{\partial y} dy$$

$$\text{avec} \quad \tau = \mu \frac{\partial u}{\partial y} - \rho \overline{u'v'}$$

$$C_n = \frac{(n+1)}{\rho_e U^2} \int_0^\delta \left( \frac{u}{U} \right)^n \frac{\partial}{\partial x} \left[ \rho - \rho_e + \rho \overline{u'^2} - \mu \frac{\partial u}{\partial x} - \frac{\mu}{3} \left( \frac{\partial u}{\partial x} + \frac{\partial v}{\partial y} \right) \right] dy$$

Ce terme complémentaire  $C_n$ , difficile à déterminer est en général négligé. Nous allons examiner son importance suivant l'équation (a1) utilisée.

On retrouve pour

- $n = 0$  l'équation de Karman
- $n = 1$  l'équation de l'énergie cinétique
- $n = \infty$  l'équation d'entraînement

$$\frac{1}{\rho U} \frac{d \rho U \delta}{dx} = A_{\infty} \quad (\delta_{\infty} = \delta - \delta^*)$$

Solons qu'une autre expression de l'entraînement est obtenue directement par intégration de l'équation de continuité :

$$\frac{1}{\rho U} \frac{d \rho U \delta}{dx} = \frac{d \delta}{dx} - \left( \frac{v}{u} \right) \gamma = \delta$$

Cette équation qui donne la direction de la vitesse en  $\gamma = \delta$  est en général utilisée pour le couplage fluide parfait-fluide visqueux.

### 1) Importance des gradients de pression normaux

- a) La planche (a1) présente des relevés de pressions statiques effectués à l'ONERA en écoulement turbulent, dans la zone décollée à l'arrière d'une marche [ref 11]. Dans la région de recompression le terme  $\frac{\partial(P-P_e)}{\partial x}$  représente environ 15% de  $\frac{dP_e}{dx}$ , tout au moins près de la paroi.

Ce pourcentage diminue vers l'extérieur.

- En laminaire ce terme peut être important également. On peut s'en rendre compte indirectement à partir d'un exemple simple calculé en résolvant les équations de Navier-Stokes [ref 12]. On constate (pl. a8) en effet que dans la partie où  $U = c \frac{\delta}{2}$  l'épaisseur de quantité de mouvement  $\delta^2$  croît de façon non négligeable ce qui est contraire à l'évolution prévue par l'équation de Karman qui s'écrit

$$\frac{d \delta^2}{dx} = \frac{C_F}{2} \frac{\delta^2}{\delta} \quad \text{si l'on néglige } C_0 \text{ qui se réduit pratiquement, dans l'exemple considéré, à la contribution de } \frac{\partial(P-P_e)}{\partial x}$$

### b) Influence sur les équations :

- pour  $n$  grand : l'influence de ce terme  $\frac{\partial(P-P_e)}{\partial x}$  sera très faible. En effet le produit

$\left( \frac{u}{U} \right)^n \frac{\partial(P-P_e)}{\partial x}$  reste très petit lorsque  $\gamma$  varie de 0 à  $\delta$  ;  $\left( \frac{u}{U} \right)^n$  est pratiquement nul sauf au voisinage de  $\gamma = \delta$ , valeur pour laquelle on a précisément  $\frac{\partial(P-P_e)}{\partial x} = 0$ . Par conséquent le terme

$$\left| \frac{n+1}{\rho U^2} \int_0^\delta \left( \frac{u}{U} \right)^n \frac{\partial(P-P_e)}{\partial x} dy \right| \text{ est très inférieur à } \left| \frac{n+1}{\rho U^2} \delta n \frac{dP_e}{dx} \right| = \left| (n+1) \delta n \frac{dU}{dx} \right|$$

et il sera légitime de le négliger devant le premier membre de l'équation (a1).

- pour  $n$  faible, par contre, et particulièrement pour  $n=0$  (équation de Karman) une telle simplification n'est plus justifiée. Mais la prise en compte du terme en  $\frac{\partial(P-P_e)}{\partial x}$  est difficile.

### 2) Importance des fluctuations de vitesse en écoulement turbulent :

La planche a2 présente des mesures de  $\overline{u'^2}$  faites dans un "bulbe court" [ref 13]. Dans la

recompression  $\frac{\partial \overline{u'^2}}{\partial x}$  représente environ 10% de  $\frac{dP_e}{dx}$ . Son influence sur les équations est donc du même ordre de grandeur que celle de  $\frac{\partial(P-P_e)}{\partial x}$ .

### 3) Influence de $\frac{\partial^2 \mu}{\partial x^2}$

En incompressible  $\frac{\partial \mu}{\partial x} + \frac{\partial v}{\partial y} = 0$  et on peut introduire le terme  $\frac{\partial^2 \mu}{\partial x^2} = - \frac{\partial^2 v}{\partial y \partial x}$  dans Dn.

Cela revient à considérer au lieu de  $\tau$ , la fonction  $\tau' = \tau - \mu \frac{\partial v}{\partial x} = \mu \left( \frac{\partial u}{\partial y} - \frac{\partial v}{\partial x} \right) - \rho \overline{u'v'}$

On pourra en général négliger  $\mu \frac{\partial v}{\partial x}$  devant  $\tau$  surtout en écoulement turbulent, sauf éventuellement au voisinage de  $\gamma = \delta$  où  $\frac{\partial \mu}{\partial y}$  et  $\rho \overline{u'v'}$  deviennent très faibles.

Il en résulte que le terme en  $\mu \frac{\partial v}{\partial x}$  pourra avoir une certaine importance pour la fonction d'entraînement  $A_{\infty}$  qui dépend essentiellement du comportement de  $\tau'$  au voisinage de  $\gamma = \delta$ . Cela sera vrai surtout en laminaire, dans le cas de très fortes variations du gradient de vitesse extérieur (au voisinage de S, R ou Q dans une zone décollée (n1.2)).

4) En conclusion, le terme complémentaire  $G_n$  détermine rapidement lorsque  $n$  croît et son importance relative par rapport aux autres termes de l'équation (a1) devient quasiment nulle lorsque  $n$  augmente indéfiniment. Les meilleurs résultats devraient donc être obtenus par utilisation de l'équation d'entassement ( $n=\infty$ ) à condition toutefois que l'on connaisse avec suffisamment de précision l'évolution de  $\tau$  au voisinage de  $y=\delta$ . Par contre des réserves doivent être faites quant à l'utilisation de l'équation de Laman.

Le choix que nous avons fait (équations  $n=1$  et  $n=\infty$ ) résulte de ces considérations, mais aussi (pour  $n=1$  notamment) de la forme de ces équations, qui permet une intégration très facile.

## ANNEXE III

### Évaluation des coefficients de forme $H_n$ et des fonctions $D_n$

On détermine  $H_n = \frac{\delta_n}{\delta^2}$  et  $D_n$  en général en faisant des hypothèses sur les profils de vitesse et sur le frottement.

1) On recherche souvent à représenter les profils de vitesse par une famille dépendant d'un paramètre en fonction duquel les quantités intégrales peuvent être exprimées.

a) en laminaire incompressible : nous utiliserons, comme il est fait généralement dans les méthodes intégrales appliquées aux zones décollées, les profils de Stewartson [ref 14]. Étant donné leur origine (qui suppose  $U \propto x^m$ ) on peut penser qu'ils représenteront mal les zones isobares. Les expériences numériques comme celle de [ref 12] devraient permettre de trouver des familles de profils mieux adaptées.

b) en turbulent incompressible : l'évolution de  $u$  au voisinage immédiat de la paroi est extrêmement rapide, et l'on peut considérer, pour le calcul des quantités intégrales, que l'on a un profil de vitesse avec une vitesse  $u_p$  à la paroi non nulle. Des mesures faites à l'ONERA [ref 11] ont montré que dans la zone de recompression d'un décollement à l'aval d'une marche, les profils de vitesse se regroupent de façon satisfaisante sous la forme  $\frac{U-u}{U-u_p} = \frac{\rho}{\tau} (\gamma/\delta)^2$  (fig a3).

Nous avons pris pour les calculs la forme d'Abraevitch  $\frac{U-u}{U-u_p} = \left[1 - (\gamma/\delta)^{3/2}\right]^2$

2) Hypothèses sur le frottement apparent  $\tau = -\rho \overline{u'v'}$ . On le relie soit à la turbulence, soit le plus souvent, au champ de vitesses moyennes. Dans ce cas deux hypothèses sont en général utilisées dans les méthodes intégrales

a)  $-\overline{u'v'} = l^2 \left| \frac{\partial u}{\partial y} \right| \frac{\partial u}{\partial y}$  avec  $l(\gamma)$  longueur de mélange

b)  $-\overline{u'v'} = E \frac{\partial u}{\partial y}$  avec  $E = K U \delta_2$ ,  $K$  étant sensiblement constant, de l'ordre de 0,06.

Nous prendrons cette dernière hypothèse pour le calcul des quantités  $D_n$  lorsque  $n$  n'est pas trop élevé ; en effet, dans ce cas, l'imprécision sur  $\tau$ , en raison de l'intégration sur toute l'épaisseur de la couche limite n'entraînera pas de grosses erreurs. Il n'en est pas de même pour le calcul de  $D_\infty$  qui dépend uniquement du comportement de  $\tau$  en  $y=\delta$  (on peut démontrer en effet, en supposant que  $\tau=0$  en  $y=\delta$ , que  $D_\infty = -\frac{1}{\rho U} \left( \frac{\partial \tau}{\partial y} \right)_{y=\delta}$ , résultat qui a été obtenu directement dans la référence [15] en écrivant l'équation de quantité de mouvement locale en  $y=\delta$ ).

3) Evolution de  $H_n$  et  $D_n$  (en écoulement incompressible)

a) Les figures a4 et a5 présentent l'évolution de  $H_n$  en fonction de  $b = \frac{\gamma_b}{\delta^2}$  pris comme paramètre de la famille de profils utilisée, pour diverses valeurs de  $n$ .

b) Calcul des  $D_n$

- en laminaire :  $\tau = \mu \frac{\partial u}{\partial y}$  et  $D_n$  peut s'écrire sous la forme  $D_n = \frac{\gamma^n}{U \delta^2}$  En (b)

avec  $E_n(b) = -(n+1) \int_0^{\delta/\delta_2} \left( \frac{u}{U} \right)^n \frac{\partial^2 u/\partial y^2}{\partial(\gamma/\delta_2)^2} d\gamma/\delta_2$

Les fonctions  $H_{n+2}$  et  $E_n$  qui seront utilisées par la suite sont tracées sur la figure a5 pour  $n=1$  et  $n=\infty$

- en turbulent : avec  $\tau = \rho E \frac{\partial u}{\partial y}$  ( $E = K U \delta_2$ ) les fonctions  $D_n$  s'écrivent sous la forme  $D_n = K E_n(b)$ ; elles ne dépendent plus de  $\delta_2$  mais uniquement du paramètre  $b$ . La fonction  $D_1$  est tracée sur la figure a7.

### Calcul des grandeurs intégrales $\delta_{n+2}$

1) en écoulement laminaire :

a) les équations (1) s'écrivent

$$\frac{1}{U^n} \frac{dU^n \delta_{n+2}}{dx} = \frac{V}{U \delta_2} E_n(b) \quad (\text{voir annexe III})$$

En multipliant les 2 membres par  $U^{2n} \delta_{n+2}$  et en intégrant à partir du point de décollement  $S$  il vient :

$$\left(\frac{U}{U_S}\right)^{2n} \left[ \frac{\delta_{n+2}}{(\delta_{n+2})_S} \right]^2 = 1 + \frac{2V}{U_S (\delta_{n+2})_S^2} \int_S^x H_{n+2} E_n \left( \frac{U}{U_S} \right)^{2n-1} dx$$

$$= \int_S^x H_{n+2} E_n \left( \frac{U}{U_S} \right)^{2n-1} dx = (H_{n+2} E_n)_{x=x_i} \int_{x_i}^x \left( \frac{U}{U_S} \right)^{2n-1} dx$$

où  $(H_{n+2} E_n)_{x=x_i}$  est la valeur de  $H_{n+2} E_n$  pour une abscisse  $x_i$  intermédiaire entre  $x_S$  et  $x$ .

Ces fonctions sont tracées sur la figure 35, elles varient très peu, aussi prendra-t-on

$$(H_{n+2} E_n)_{x=x_i} = (H_{n+2} E_n)_S$$

On obtient alors les équations (2) avec  $\beta_n = \frac{(H_{n+2} E_n)_S}{(H_{n+2})_S^2}$

Le planche (36) montre les résultats obtenus par ces équations dans un cas simple où le calcul par les équations de Karier-Stokes a pu être effectué [ref 12]. On vérifie que les valeurs trouvées pour  $\delta_0/\delta_{0S}$  et  $\delta_0/\delta_{0S}$  au point de recollement où  $b=0$ , sont identiques et on constate qu'elles coïncident bien avec la valeur en ce point de  $\delta_2/\delta_{2S}$  déterminée dans la [ref 12].

b) Ces équations (2) appliquées à la partie SE du bulbe aboutissent aux équations (4) lorsqu'on ne garde que les termes du 1er ordre en  $\frac{\Delta U}{U_S}$ . La constante  $k$  qui apparaît dans la formule est comprise entre 1 et  $\frac{2n+1}{2}$ . Ces valeurs extrêmes correspondent à des bornes inférieure et supérieure de l'expression :

$\left(\frac{U}{U_S}\right)^{2n} \int_{x_6}^x \left(\frac{U}{U_S}\right)^{2n-1} dx$ , obtenues en utilisant pour l'intégration les lois de vitesse suivantes :

$$2) \text{ en écoulement turbulent : } \begin{cases} k=1 & \frac{U}{U_S} = 1 - \frac{\Delta U}{U_S} \quad (\text{avec } \frac{\Delta U}{U_S} = C \frac{b}{x}) \\ k=\frac{2n+1}{2} & \frac{U}{U_S} = 1 - \frac{x-x_S}{L_1} \frac{\Delta U}{U_S} \end{cases}$$

L'équation (1) s'écrit  $\frac{1}{U^n} \frac{dU^n \delta_{n+2}}{dx} = D_n(b)$

En l'intégrant à partir d'un point de transition  $T$  il vient :

$$\left(\frac{U}{U_T}\right)^{n} \frac{\delta_{n+2}}{(\delta_{n+2})_T} = 1 + \frac{(D_n)_{x=x_j}}{(\delta_{n+2})_T} \int_{x_T}^x \left(\frac{U}{U_T}\right)^{n} dx$$

où  $(D_n)_{x=x_j}$  est la valeur de  $D_n$  pour une abscisse  $x_j$  intermédiaire entre  $x_T$  et  $x$ . L'évolution de  $D_n$  est moins bien connue qu'en laminaire du fait de l'incertitude sur  $\tau$ .

- on voit sur la figure a7 que, au moins jusque vers  $b = 0,6$ ,  $D_1$  varie peu. On prendra donc

$$(D_1)_{x=x_j} = D_{1S} = \gamma_1 = 0,0187$$

- Le calcul de  $D_\infty$  est très imprécis (Annexe II § 2). D'après les analyses de sondages de bulbes courts présentées dans la référence 5, la valeur de l'entraînement déduite de l'expression  $\frac{1}{U} \frac{dU \delta_\infty}{dx}$  varie dans la zone de recompression entre 0,09 et 0,12

On prendra  $(D_\infty)_{x=x_j} = \gamma_\infty = 0,1$

# REFERENCES

- [1] - No GUNDEL, G.T. - GUNT D.3  
Examples of three representative types of airfoil section stall at low speed.  
NACA, TN 2512, (1953).
- [2] - GUNT D.3  
A correlation of low speed airfoil section stalling characteristics with Reynolds Number and airfoil geometry.  
NACA, TN 3963, (1957).
- [3] - VENTRE  
Influence des décollements du bord d'attaque sur les caractéristiques aérodynamiques de voilures.  
4<sup>e</sup> colloque AEROS - Lille 1967.
- [4] - E. VENTRE de PAUL - A. VENTRE  
Recherches sur les profils d'ailes en écoulement subsonique écoulé.  
Colloque AEROS, Toulouse, (Nov. 1967).  
"Aérodynamique et Astronautique" N° 12, (Nov. 1967).
- [5] - HUBBARD H.P.  
A semi empirical theory for the growth and bursting of laminar separation bubbles.  
NACA CP n° 1473.
- [6] - Van DIEREN A.2  
A preliminary investigation of boundary layer transition along a flat plate with adverse pressure gradient.  
NACA, TN 632, (1956).
- [7] - GILBERT L.F.  
Prediction of natural transition in the boundary layer on an airfoil  
J. Roy Soc. 62 (7), 1956, p.265.
- [8] - GILBERT L.F.  
The formation of regions of separated flow on wing surfaces  
NACA R et E 5122, (1955).
- [9] - BRICE, E.  
Recherches sur les profils dans la soufflerie subsonique à courant plan SIO Toulouse.  
Colloque AEROS, (Nov. 1969), (GERSA TP 756).
- [10] - ROGELL, B.J.  
The calculation of the pressure distribution of a thick cambered airfoil at subsonic speed including the effect of the boundary layer.  
NACA Aero Rep. 1236, (1957).
- [11] - E. SIBRY - J. MIRANDE  
Documents non publiés
- [12] - BRIDY W.R.  
A numerical study of laminar separation bubbles using the Navier Stokes equations.  
J. Fluid Mech., (1971) vol 47, part 4, p.713-736.
- [13] - WOODWARD D.S.  
An investigation of the parameters controlling the behaviour of laminar separation bubbles.  
RAE TECH. REPO AERO 1003, (1967).
- [14] - STEWARTSON K.  
Further solutions of the Falkner-Skan equations  
Proceeding of the Cambridge Philosophical society, vol 50, part 3, (Juillet 1954).
- [15] - R. MICHEL, C. QUENARD, R. DURANT  
Hypothesis on the mixing length and application to the calculation of the turbulent boundary layers.  
AFOSR-IFP Stanford 1968 - Conference on turbulent boundary layer prediction, Vol.1.  
(voir aussi H.T. OZGARA n° 154, (1969)).



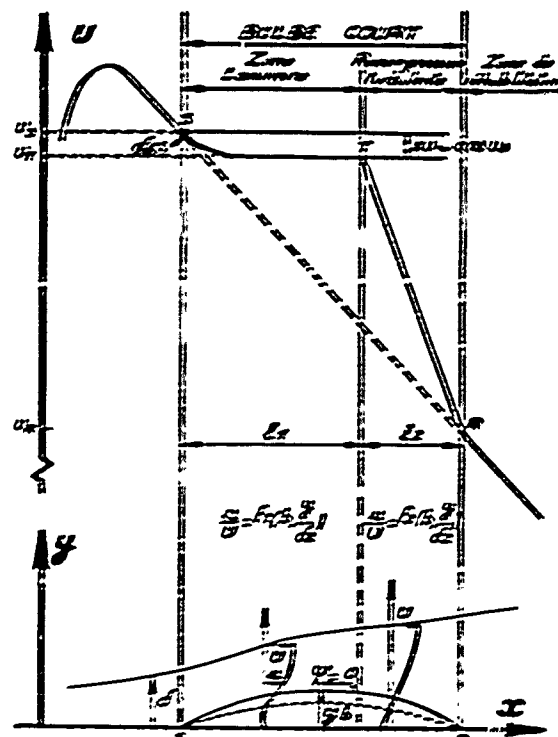
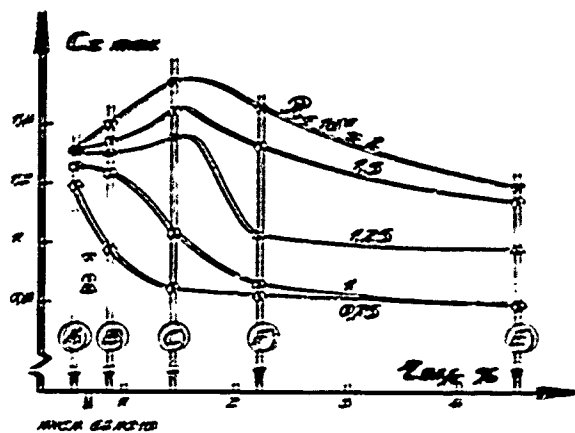


Fig 1 - Courbe d'une famille de profils d'écoulement. Répartition du type de décollement par la corrélation de [réf.2].

Fig 2 - Schématisation d'un bulbe court.

Fig 3 - Différentes formes de distribution de pression à la paroi dans un bulbe court.

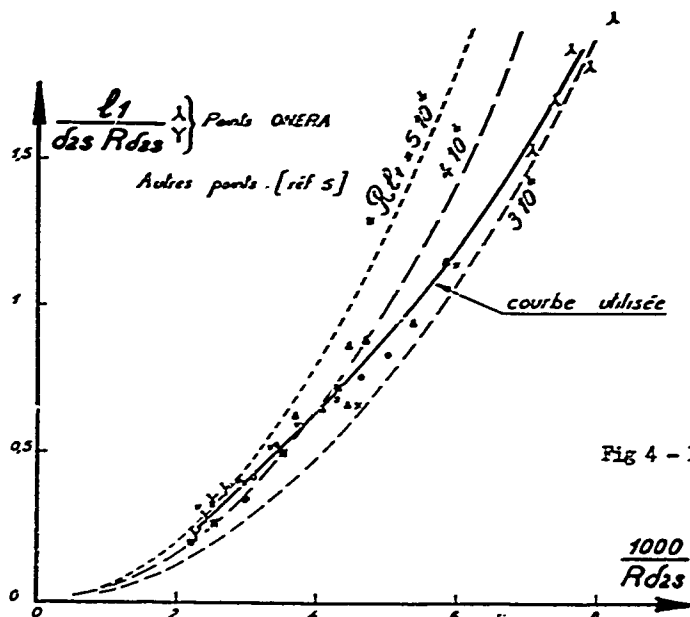
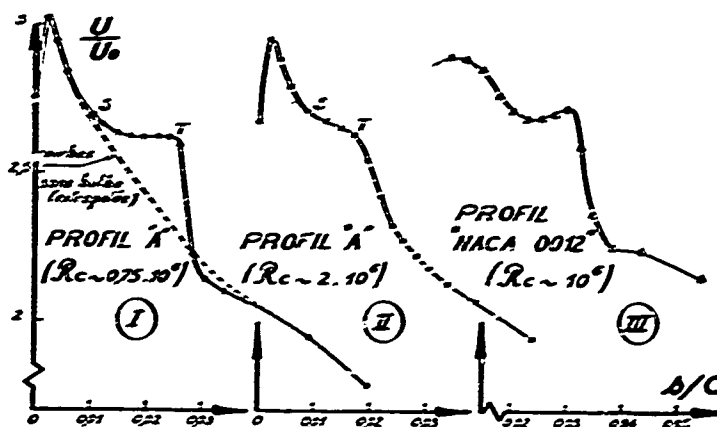


Fig 4 - Longueur de la partie laminaire.

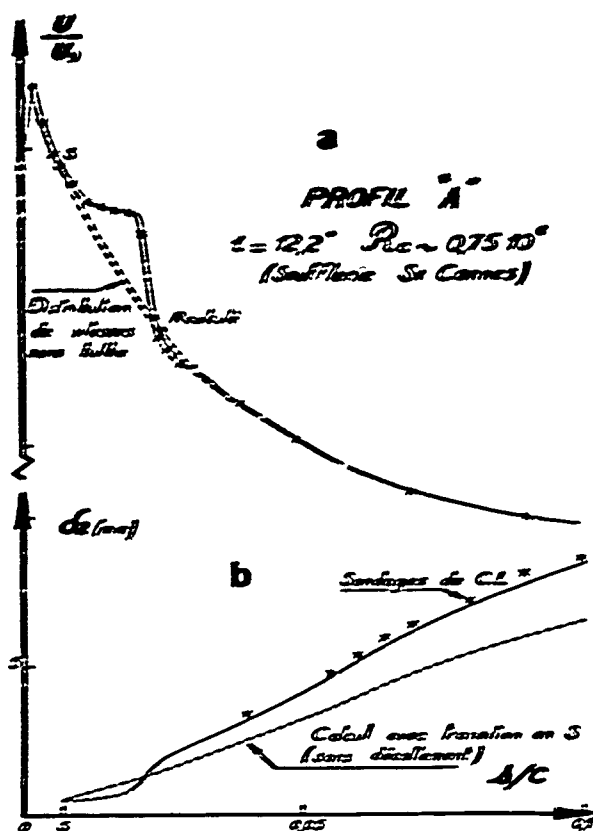


Fig 5 - Valeurs de  $\delta_2$  calculées et expérimentales juste à l'aval d'un bulbe ouvert

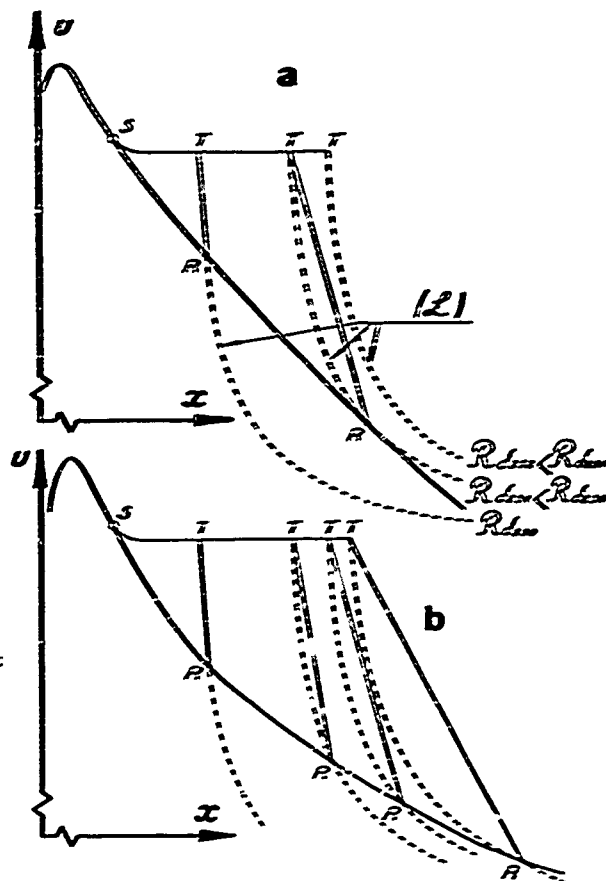


Fig 7 - Evolution du point de recollement quand  $R_{\text{bas}}$  varie.

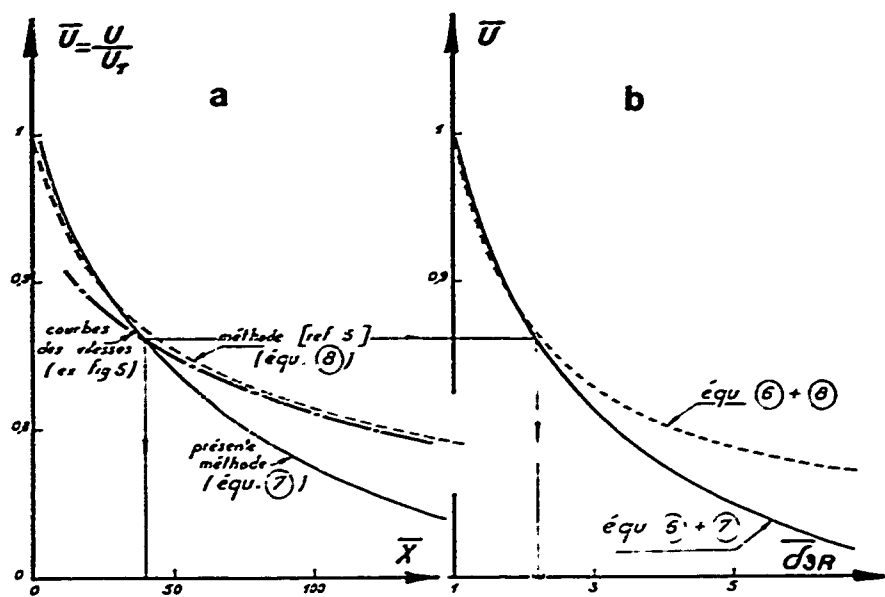
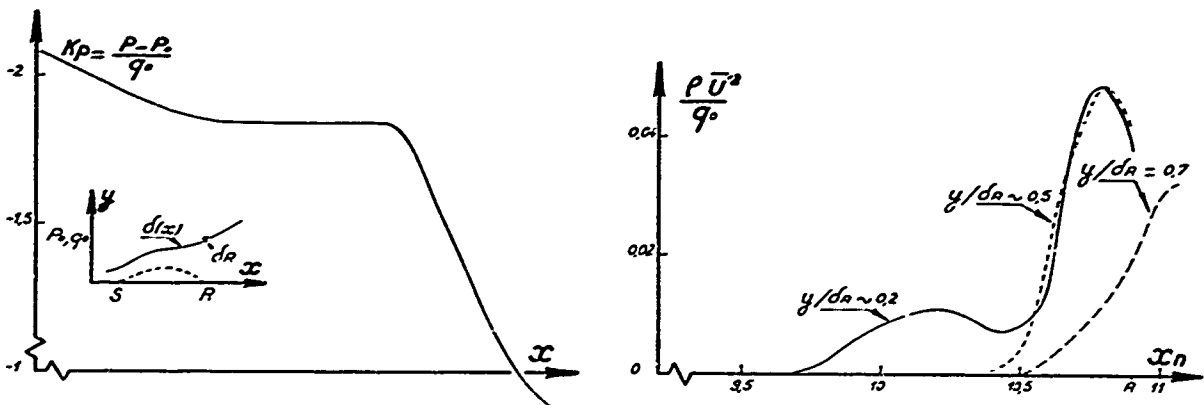
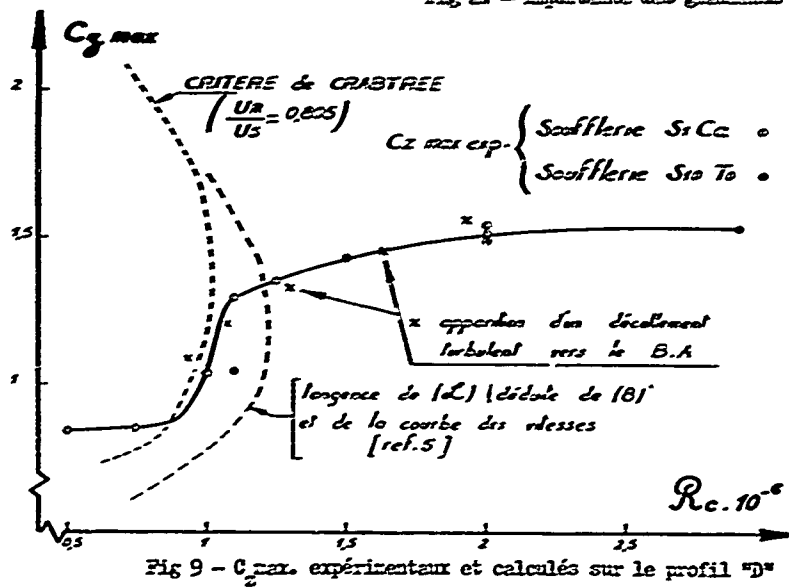
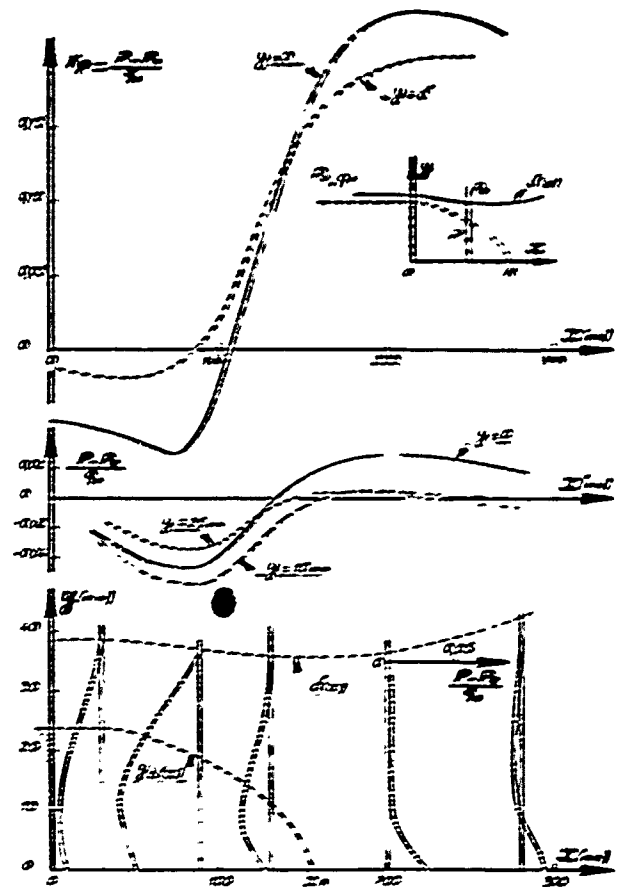
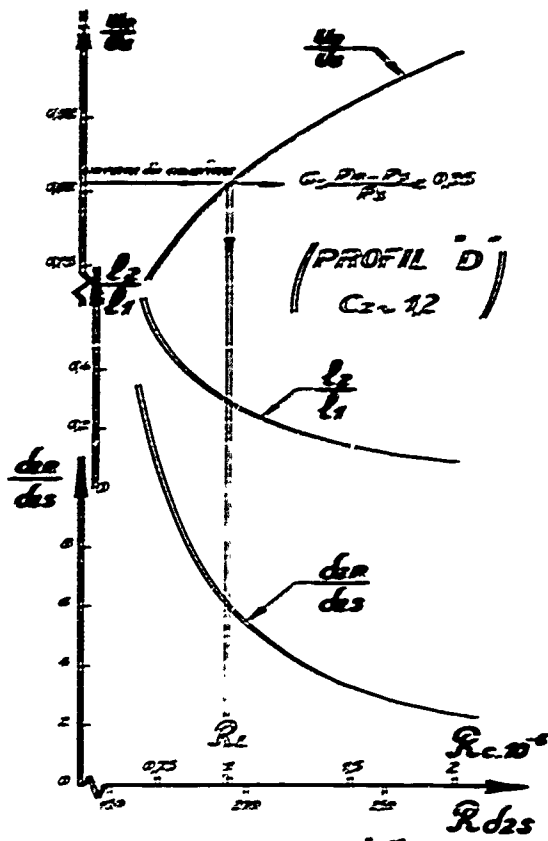


Fig 6 - lois  $\bar{X}(\bar{U})$  et  $\delta_3(\bar{U})$  pour la recompression turbulente



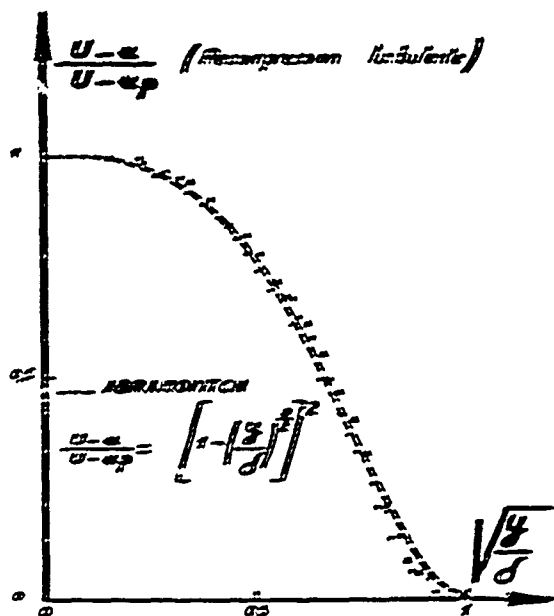


Fig. 45 - Regroupement des profils de vitesse dans la zone de recompression laminar [réf. 11]

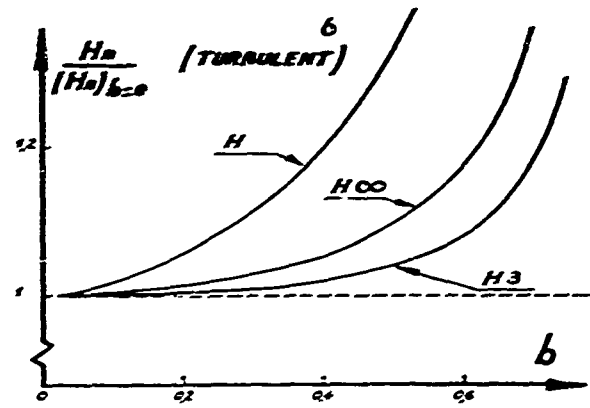
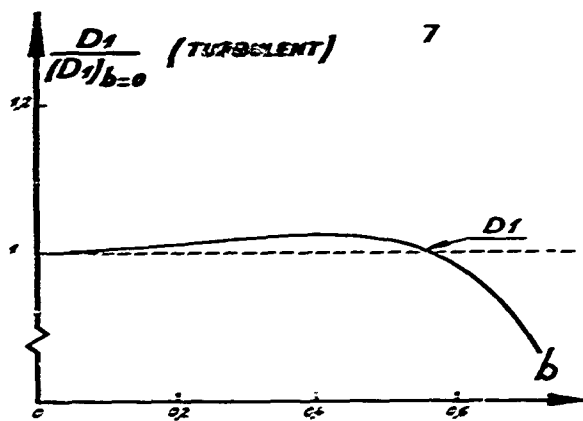
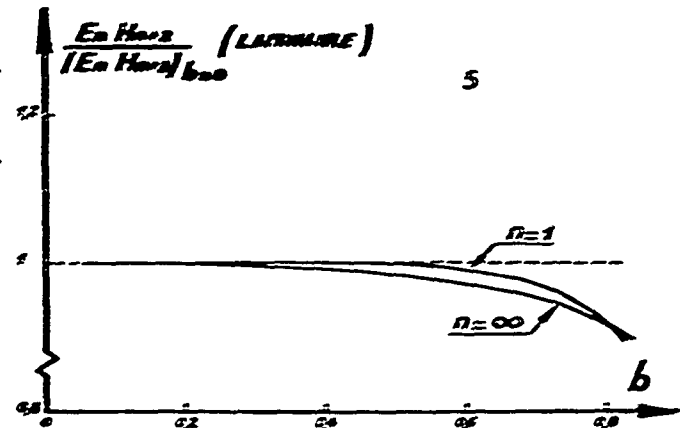
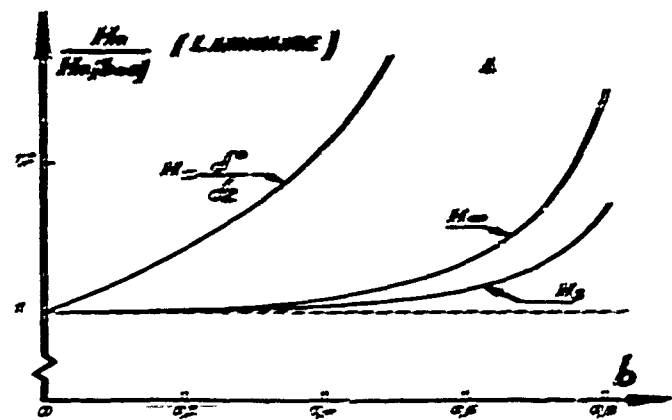


Fig. 4-5-6-7 - Evolution de  $H_n$  et  $D_n$  dans une zone décollée

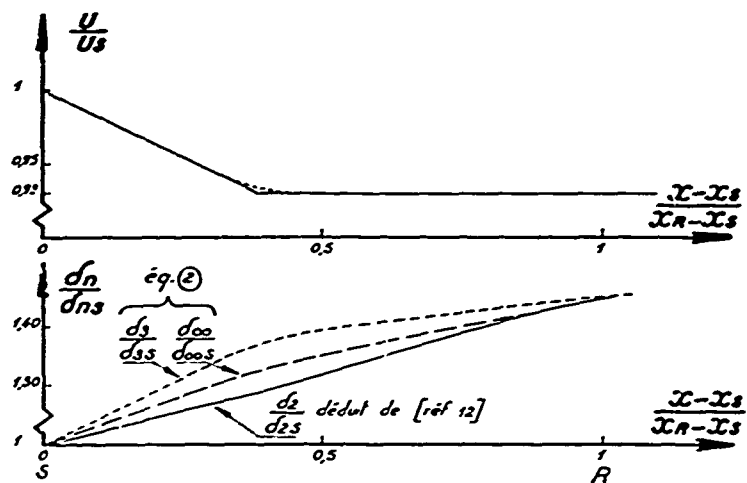


Fig. 48 - Calcul de  $\delta_n$  dans un cas simple de zone décollée laminaire [réf. 12].

## PARAMETRIC STUDIES OF SEPARATING TURBULENT BOUNDARY LAYER FLOWS

Andrzej Wortman\* and W.J. Franks\*\*

Northrup Corporation, Aircraft Division  
2403 West Broadway  
Burbank, California 91520, U.S.A.

A new technique for the exact solutions of laminar or turbulent two- or three-dimensional boundary layer flows has been developed (Reference 1). The technique differs from previous approaches in the use of functional analysis to obtain exact semi-analytical solutions in a small fraction of the computer time normally required for such computations. The main advantage of the semi-analytical aspect of the technique is that the functional forms of the relations in the governing differential equations are retained and the use of the computer is relegated to the performance of simple quadratures and fluid properties evaluations. Thus, the study of the various turbulent viscosity models is simply a matter of programming the model into the subroutine where such calculations are performed (typically, such a description consists of a few FORTRAN statements).

A wide range of eddy viscosity relations can therefore be studied in a few parametric runs. A typical three-dimensional calculation at a point on a body requires 3 seconds of IBM 360/65 computer time, so that extensive parametric studies can be performed quickly and economically.

## LIST OF SYMBOLS

$A_{ij}$ = Coefficients in Equation 1	$\hat{a}$ = Crossflow parameter, Equation 12
$C = \rho u_f(\rho u)_e$	$\beta = \frac{d \ln u_{1,e}^2}{d \ln \xi}$
$E_1 = \frac{u_{1,e}^2}{2H_e}$	$\delta_e$ = Cone half angle
$f_1$ = Stream function $\psi_1 = u_1 / u_{1,e}$	$\delta^*$ = Displacement thickness
$\xi = H/H_e$	$\epsilon$ = Eddy viscosity
$H$ = Total enthalpy	$\eta = \frac{u_{1,e}}{\sqrt{2\xi}} \int_0^\eta \rho dy$
$H_1$ = Nonsimilar terms in Equation 1	$\delta$ = Momentum thickness
$L$ = Chord length	$\mu$ = Dynamic viscosity
$M$ = Mach number	$\nu$ = Kinematic viscosity
$p$ = Pressure	$\xi = \int_0^{x_1} \rho_e \mu_e u_{1,e} dx_1$
$Pr$ = Prandtl number	$\rho$ = Density
$R = \rho_e / \rho$	$\tau$ = Shear stress
$Re_L$ = Reynolds number based on $L$	
$u_1$ = Velocity in direction 1	
$x_1$ = Coordinate in direction 1	

## Subscripts

$e$ = Edge of boundary layer
$i$ = Direction, 1 principal; 2 transverse; 3 normal
$s$ = Surface
$\infty$ = Freestream

Primes denote differentiation with respect to  $\eta$

\*Engineering Specialist, Aerodynamics Research Group. Presently on leave. U.S.A. National Academy of Sciences Exchange Scientist with the Polish Academy of Sciences, I.P.P.T. - Z.M.C. : G., Ul. Swietokrzyska 21, Warszawa, Poland.

\*\*Engineering Specialist, Propulsion Systems Group.

## 1. INTRODUCTION

The present level of understanding of turbulent boundary layer flow phenomena necessitates the development and utilization of simple flow models which rely heavily on experimental data. Most of the models proposed thus far are adjusted to perform satisfactorily in fairly simple flow situations which are often of minor engineering significance. On the other hand, turbulent viscosity models intended for use in more interesting situations usually have a limited range of validity whose extension to general turbulent flow problems represents a major engineering challenge. Development of generally valid, reliable eddy viscosity models requires extensive experimentation with turbulent shear flows with the aim of matching the widest possible range of measured data. Unfortunately, test data are quite sparse and the current computing techniques are ill-suited to such comprehensive parametric studies.

The methods of calculation used in turbulent boundary layer research are usually specialized to perform certain specific tasks and are consequently too expensive and cumbersome for efficient, comprehensive investigations of turbulent viscosity models. A brief outline of some of these methods will be given here to indicate how even the best calculational procedures are normally so highly specialized that they lack the versatility which is considered necessary to the development of engineering techniques. Among the oldest are the integral methods which with the present fast, large computers indicate a certain lack of mathematical sophistication since they employ generally unjustified profile approximations and attempt to bury the details of the flow in integral quantities characterizing the boundary layer. Quite popular are "shooting" techniques which endeavor to treat the two-point boundary value problem of boundary layer flow as an initial value problem in which the derivatives of the functions at the inner boundary are guessed repeatedly until integrations out to the outer boundary yield acceptably close approximations of the outer boundary conditions. Computing costs for this technique are exorbitant for variable fluid properties two-dimensional flows, and quite unacceptable for general compressible three-dimensional flows. Purely numerical schemes which cast the governing differential equation in finite difference form and march along the surface have achieved considerable success, but they are expensive to use because of the necessity of taking small steps along the surface and are usually rather difficult to run in more interesting flow problems. Also, the basic computing scheme is closely tied to the fluid physical and transport properties models whose changes require extensive reprogramming and program redevelopment.

The method employed to obtain the results displayed here was developed in Reference 1, where it was applied to a wide range of laminar, two- and three-dimensional homogeneous and two-component flows. By employing a semi-analytical approach which retains the functional form of the basic relations in the formal analytical integrations of the differential equations, finite differencing is avoided and the computer is used for function evaluation, data storage and quadratures in the final stages of the calculation. The solution is exact in that arbitrarily high order of accuracy can be obtained and the functional approach offers a high degree of versatility together with efficient, economical computations.

The potential of the method is exhibited in parametric studies of turbulent viscosity models in separating two-dimensional flows and the effects of crossflow in three-dimensional separating flows. A sample laminar flow airfoil calculation is included to show a possible application as an engineering tool if a reliable turbulent viscosity model could be developed. Advantage is taken of this method to investigate the influence of the principal parameters quickly and economically. In contrast to the usual turbulent flow studies, which concentrate on a limited number of specific calculations, the attitude taken here is that physical insight and understanding can be most readily obtained from illustrations of the influence of parameters such as the Mach number, wall cooling, suction, turbulent viscosity models and the three-dimensional aspects of the flow. Our position here is that of a user rather than a developer of turbulent flow models, and our study is aimed at development of an engineering understanding of influence for the common parameters so that boundary layer flows on aircraft surfaces can be calculated reliably. Heretofore it has not been possible to separate clearly the influence of parameters used in turbulence models from idiosyncrasies of the computational schemes in which they are incorporated.

## 2. GOVERNING EQUATIONS

Three-dimensional boundary layer flow equations are well known so that only their final form will be shown here. With the use of the usual lower order Reynolds time-averaging process, the laminar and turbulent equations assume identical functional forms, thus permitting the use of a single solution procedure. A form convenient for computations is given by Chan<sup>2</sup> who transforms the basic equations to balance the purely self-similar terms by the nonsimilar terms which contain all the derivatives along the surface of the stream and enthalpy functions together with all their transformed normal derivatives, i.e.,

$$(Cf_1'')' - (A_{11}f_1' - A_{12}f_2')f_1'' - A_{13}(R - f_1'f_2') - A_{14}(R - f_1'^2) - A_{15}(R - f_2'^2) = H_1 \quad (1a)$$

$$(Cf_2'')' - (A_{11}f_1' - A_{12}f_2')f_2'' - A_{23}(R - f_1'f_2') - A_{24}(R - f_2'^2) - A_{25}(R - f_1'^2) = H_2 \quad (1b)$$

$$\left(\frac{C}{Pr}g\right)' - (A_{11}f_1' - A_{12}f_2')g' - \left[C(1 - Pr^{-1})(E_1f_1'^2 + E_2f_2'^2)\right]' = H_3 \quad (1c)$$

The boundary conditions are:

$$\eta = 0 \quad f_1 = f_1(0); \quad f_1' = 0; \quad g = g_s \quad i = 1, 2 \quad (2a)$$

$$\eta \rightarrow \infty \quad f_1 \rightarrow 1.0; \quad g \rightarrow 1.0 \quad i = 1, 2 \quad (2b)$$

The coefficients  $A_{ij}$  and the nonsimilar terms  $H_i$  are functions of surface geometry and flow conditions. Thus, for instance, the simplest Falkner-Skan type flows are characterized by  $A_{11} = 1.0$ ,  $A_{14} = \beta$  the pressure gradient parameter, and  $A_{ij} = 0 = H_i$  for all other  $i$  and  $j$ .

### 3. METHOD OF SOLUTION

The basic method employing generalized operators of functional analysis was developed in Reference 1, where it was analyzed and applied to a wide range of two- and three-dimensional problems. A brief outline of the basic approach is given here and a specific example of two-dimensional incompressible flow is in the Appendix to show the details of the application of the scheme. Three-dimensional, compressible calculations proceed in an entirely analogous manner but are too unwieldy for inclusion here. In operator form Equation 1 may be expressed as

$$\dot{\psi} + F \cdot \psi = G \quad (3)$$

where

$$\psi = \left( Cf_1'', Cf_2'', \frac{C}{Pr} g \right), \text{ a column vector} \quad (4a)$$

$F$  = a diagonal matrix with the elements

$$\left[ C^{-1} (A_{11} f_1 + A_{12} f_2), C^{-1} (A_{11} f_1 + A_{12} f_2), Pr C^{-1} (A_{11} f_1 + A_{12} f_2) \right] \quad (4b)$$

$$G = \text{a column vector consisting of all the remaining terms.} \quad (4c)$$

Integrating formally

$$\psi = \psi(0) \cdot \phi^{-1} + \phi^{-1} \int_0^\eta \phi \cdot F d\bar{\eta} \quad (5)$$

with

$$\phi = \exp \left( \int_0^\eta F d\bar{\eta} \right) \quad (6)$$

The constant of integration  $\psi(0)$  is obtained from the boundary conditions which are brought in through an integration of Equation 5 over the whole interval  $[0, \infty]$ . In operator form:

$$\psi = P(\psi) \quad (7)$$

where  $P$  is a nonlinear operator which itself is a function of  $\psi$ . In the form of Equation 7 the problem is ready for an attempt at an iteration scheme of the type:

$$\psi_{i+1} = P(\psi_i) \quad i = 0, 1, \dots \quad (8)$$

Convergence of the iteration was discussed in Reference 1 where it was shown that, in general, simple iteration schemes diverge for the more interesting boundary layer flows, and means for ensuring convergence had to be devised. Restriction of the range of the operator  $P$  which in most cases could be achieved by means of simple weighted averaging of successive approximations was adequate for rapid convergence to an answer of arbitrarily high order of accuracy for most engineering problems.

The present approach computes the highest order derivatives normal to the surface in terms of the integrals of the functions themselves so that the usual finite differencing problems are avoided entirely. Wall shear stresses and heat transfer are computed with integrals over the whole domain and their values are quite insensitive to the method of integration or the integration step size. Finite differences appear in the calculations of  $H_1$  but these are relatively unimportant since by the fundamental boundary layer assumption the derivatives along the surface are an order of magnitude smaller than those normal to it. In contrast to the stability requirements of the finite difference techniques, there are no mathematical limitations on the step size along the surface so that flow regions with relatively mild variations may be spanned rapidly and economically. It should be noted that the present method differs significantly from the Hartree-Womersley scheme in that the derivatives along the surface are updated at each iteration rather than trailing one step behind. Thus a much more rapid diffusion of profile distribution information is achieved.

The method is essentially analytical because the basic equations are integrated formally so that the parameters  $C$ ,  $Pr$  and  $R$  appear explicitly until the final quadratures are performed. By placing  $C$ ,  $Pr$  and  $R$  in separate subroutines, parametric studies of models of laminar and turbulent fluid properties variations are performed with only a few card changes in the program. The computations are not in any way tied to any particular  $C$ ,  $Pr$  and  $R$  relations so that the method is well suited to analytical "experimental" research. Comprehensive parametric studies in References 3, 4 and 5 are typical of such research efforts.

The validity and accuracy of the technique were established in the cited reference, which showed that 4-decimal-place accuracy could be achieved in most cases with 150 trapezoidal integration steps across the boundary layer. Fewer integration steps are needed with, for instance, Simpson's rule, and the results are insensitive to gross overestimates of boundary layer thickness because of the exponential form of the integrating factor  $\phi$  which drives the highest order derivatives to zero in the outer regions of the boundary layer. A boundary layer thickness overestimate of a factor of 2 left the results virtually unaffected. In nonsimilar calculations the transformed normal coordinates are scaled by the transformed coordinates along the surface so that in the transformed plane where the computations are performed boundary layer thickness varies slowly with the actual body coordinates. Computer core storage is 108K when running the full equations with turbulent flow on an infinite yawed wing. A complete computation at a station on a body requires about 3 seconds of IBM 360.65 time so that calculation of a boundary layer on a typical profile requires about 1 minute of computer time.

Accuracy of the present separating flow calculations was checked by comparison with Reference 6, which in turn checked with the results of Rogers<sup>7</sup>, who claimed 6-decimal-place accuracy for his results. The sample comparisons in Table 1 are for self-similar boundary layers with  $C \equiv 1.0 \equiv Pr$ .

TABLE 1. COMPARISON WITH ROGERS FOR  $f(0) = 0$ ,  $C \equiv 1.0 \equiv Pr$ 

No. of Steps	Step Size	Reference 6			Rogers <sup>7</sup>	
		$g_0$	$-\beta$	$g_0'$	$-\beta$	$g_0'$
250	.036	0.2	.30862	.22601	.30862	.22601
200	.036	0.2	.30865	.22602		
150	.080	0.6	.24756	.12509	.24757	.12510

The present program using Simpson's rule with between 70 and 120 integration steps checked the above results satisfactorily, and thus its accuracy is considered to be good to at least 3 decimal places.

#### 4. RESULTS

This section summarizes the results of parametric studies of two- and three-dimensional separating turbulent flows. In the first part, the number of flow field parameters is minimized by considering self-similar flows and comparing the predicted separation pressure gradients for three fairly representative eddy viscosity models. Three-dimensional flow effects are studied in the following section employing a turbulent viscosity model modified to account for the crossflow velocity gradients. Finally, because of the obvious lack of a reliable turbulent viscosity model, prediction of separation on airfoils is found to be, at the present time, impractical, and a laminar flow calculation for a NACA 0012 airfoil is displayed to show that such calculations represent routine preliminary design type of applications of the present computing technique.

##### Two-Dimensional Separating Flows

Self-similar flows are characterized by a few parameters, thus enhancing the display of the characteristics of various eddy viscosity models investigated parametrically. The turbulent viscosity models considered here are fairly representative of the current thinking in the field and are selected here without any intent to advocate or criticize any particular relation but simply because of ready availability in the literature. In the models of Ng, Patankar and Spalding<sup>8</sup> and Cebeci and Smith<sup>9</sup>, use is made of essentially the classical Prandtl mixing length model with damping,

$$\epsilon \propto x_3^2 \cdot \left| \frac{\partial u_1}{\partial x_3} \right| \cdot \left[ 1 - \exp \left( - \frac{x_3}{26\nu} \sqrt{\frac{\tau}{\rho}} \right) \right]^2 \quad (9)$$

This is the model, except for some changes in the constants, used in Reference 8, but Reference 9 attempts to account for the effects of pressure gradient by modifying the friction velocity relation

$$(\tau/\rho)^{1/2} \approx \left( \tau_s + \left( \frac{dp}{dx_1} \right) x_3 \right)^{1/2} \quad (10)$$

On the other hand, Alber<sup>10</sup> follows the suggestion of Lees and avoids the problem of  $\epsilon \rightarrow 0$  as  $\tau \rightarrow 0$  by choosing

$$\epsilon \propto x_3 u_{1,e} \left[ 1 - \exp \left( - x_3 \sqrt{\frac{dp}{dx_1} \cdot x_3 / 26\nu} \right) \right] \quad (11)$$

Near separation the basic relation (Equation 9) is not expected to be valid since not only the velocity gradient but also the damping term tend to disappear, and thus  $\epsilon$  virtually disappears in an extended region near the wall. This situation is not acceptable on physical grounds, so that the model of Reference 8 should not be expected to be applicable and is included here mainly for comparison. The model of Reference 9 attempts to remedy the situation somewhat by not permitting the damping term to vanish at separation. The model of Lees, as adopted by Alber, is quite different as it assumes a different variation of  $\epsilon$  with the normal coordinate and  $\epsilon$  does not vanish as the velocity gradient disappears.

Although the above models were not developed specifically to account for the effects of suction, this effect was included in the parametric study since it is frequently employed in engineering systems to delay or prevent separation. The three turbulent viscosity models were selected for the study to indicate the differences between two models developed specifically for highly retarded or separating flows (References 9 and 10) and to compare the predicted separation pressure gradient with that computed using a well-known eddy viscosity model (Reference 8).

For all the compressible flow calculations, the frequently employed Howarth-Dorodnitsyn type of transformation (e.g., Mager<sup>11</sup>, Spence<sup>12</sup>) is followed and all the lengths in the describing relations are trans-

formed into  $\eta \propto \int_0^y \rho dx_3$  with  $\rho$  being the local density and  $x_3$  the coordinate normal to the surface. The new

Mach number data do not include this somewhat speculative assumption, and thus the models are compared in their original form.

The predicted separation pressure gradients  $\beta = \ln u_{1,e}^2 / \ln x$  for incompressible flow are shown in Figure 1 for three viscosity models and a range of suction rates. The models of References 8 and 9 agree for the lower and intermediate suction rates, but disagree strongly for the high values of  $f_s$ . For no suction the model of Alber predicts a 50 percent greater separation pressure gradient than the other two models. In Figure 2 we show the complete lack of agreement among the models on the separation profile shape factor  $H = \delta^*/\theta$ . Again, however, the models of References 8 and 9 agree for no suction but differ strongly from



the model of Reference 10. The results tend to indicate that, for no suction at least, the modification of the damping term by Reference 9 is not worthwhile for the prediction of separation pressure gradient. It may be of interest to note that an incompressible laminar boundary layer is known to separate at  $\beta \approx -0.2$ , so that the predicted results of all the models appear unrealistically low.

Unlike the other two eddy viscosity models, the relation of Reference 10 was developed specifically for separating flows, and was therefore used in a brief study of Mach number and wall cooling effects (Figure 3). It should be noted that the essentially incompressible eddy viscosity model of Reference 10 predicts an opposite influence of wall cooling from that normally observed experimentally. Since the accuracy of the calculations and the method of solution are clearly established, some of the anomalies observed in the computed data must be due to the assumptions of the eddy viscosity model and its dependence on the compressibility effects. The scarcity of basic experimental data on suction retarded compressible flows renders any calculated results somewhat speculative and points out the need for studies such as this one to expose the characteristics of various turbulent viscosity models in a wide range of engineering situations.

### Three-Dimensional Flow Effects

Three-dimensional flow effects were investigated briefly to determine the sensitivity of the predicted separation pressure gradient results to small amounts of crossflow. A very simple shape with a decelerating pressure gradient in the flow direction and outflow normal to it was considered. Such a flow field approximates that found on a three-dimensional Oswatitsch spike or an axisymmetric compression spike at a slight angle of attack. The strength of the crossflow is characterized by a parameter  $\hat{\alpha}$  which is a function of the Mach number and geometry and is defined in terms of the crossflow velocity  $u_{2,e}$ , cone angle  $\delta_c$ , and the most windward velocity  $u_{1,e}$  as:

$$\hat{\alpha} = \frac{2 \partial^2 u_{2,e} / \partial x_2^2}{3 u_{1,e} \sin \delta_c} \quad (12)$$

Two-dimensional viscosity relations when applied to three-dimensional separating flows tend to give anomalous results of questionable engineering utility. After some experimentation with various forms it was found that reasonable results could be obtained when the crossflow effects were introduced in the form

$f'' = \left( f_1''^2 + (A_{12} f_2'')^2 \right)^{1/2}$  where  $f_1''$ ,  $f_2''$  are the nondimensional velocity gradients on the longitudinal and transverse directions, respectively. The resulting expression was used in the turbulent viscosity relation proposed by Reference 8 and longitudinal pressure gradients required to cause separation were computed for  $E = 0, 0.5$  (Mach numbers 0 and  $\sqrt{5}$ ), three suction rates ( $f_1 = 0, 1.0, 2.0$ ) and crossflow parameters up to 0.5. Some of the calculated results are summarized in Table 2 and shown in Figure 4.

TABLE 2. SEPARATION PRESSURE GRADIENT  $\beta$ ,  $E = 0$ ,  $f_s = 0$

$\hat{\alpha} = 0$	0.1	0.3	0.5
$-\beta = 0.2$	0.28	0.4	0.51

The extreme sensitivity of the results to small crossflow is readily appreciated when it is pointed out that a cone in Mach 1.5 flow generates a value of crossflow parameter  $\hat{\alpha}$  of 0.12 at only 1 degree angle of attack. These data indicate that semiempirically derived separation criteria should be carefully examined to determine the extent of influence of three-dimensional flow.

### Airfoil Calculations

Predictably, the general lack of agreement among the turbulent models appears in turbulent airfoil calculations, and therefore the demonstration of the use of the computing technique is limited to calculations of laminar flow over a NACA 0012 airfoil at  $M_\infty = 0.4$ ,  $g_s = 0.9$ , and chord Reynolds number of 100,000 with pressure distribution taken from Reference 13. The variation of the displacement thickness, shear stress, and the pressure gradient parameter with the chordwise coordinate is shown in Figure 5. Complete compressible three-dimensional relations were actually calculated but the crossflow terms were then annihilated by setting all the crossflow  $A_{ij}$ 's equal to zero. Calculations were made at  $1/30$  chord intervals and the whole computation including the isentropic expansions needed for coordinate transformations, required 0.57 minute of IBM 360/65 time. No attempt was made to accelerate calculations which proceeded automatically from the basic inputs of geometry and flow conditions. The point of separation could have been approached more closely but this refinement was not deemed worthwhile because of the doubtful validity of nonsimilar boundary layer equations near separation.

The rate of increase of the displacement thickness rises rapidly as separation ( $\tau_s \rightarrow 0$ ) is approached. It should be noted that with a fairly flat  $\beta$  curve such as exhibited here a 40 percent change in predicted separation pressure gradient  $\beta$  results in a shift of predicted point of separation from  $x_1/L = 0.5$  to 0.4. Such differences are well within the kind of prediction of the turbulent models considered here, so at the present time predictions of separation do not appear to be fruitful. The need for the development of reliable turbulent viscosity models is thus quite apparent.

## 5. CONCLUSIONS

Our results indicate that at least three of the currently employed turbulent viscosity models fail to agree on the predicted two-dimensional flow separation pressure gradient. More importantly, we have exhibited the extreme sensitivity of the results to crossflow effects. Current efforts being analyzed are aimed at exhibiting the effects of Mach number, pressure distribution and sweep on the separation on typical transonic wings. On the basis of the computed results, it is concluded that turbulent viscosity models must be approached with some degree of caution when a wide range of parameters is considered, and that purely two-dimensional calculations are frequently of doubtful value in the analysis of typical aircraft flow problems.

## REFERENCES

1. Wortman, A., Mass Transfer in Self-Similar Laminar Boundary Layer Flows. Doctoral dissertation, UCLA (1969).
2. Chan, Y. Y., A Note on a Similarity Transformation for Three-Dimensional Compressible Laminar Boundary Layer Equations, National Res. Council of Canada, Aero. Report LR-469 (1967).
3. Wortman, A., and Mills, A. F., Highly Accelerated Compressible Laminar Boundary Layer Flows with Mass Transfer, ASME Journal of Heat Transfer, Vol. 93, Ser. C, No. 3, pp 281-289 (1971). Also presented at the ASME Space Technology and Heat Transfer Conference, Los Angeles, June 1970.
4. Wortman, A., Boundary Layer Flow at Three-Dimensional Stagnation Points in High-Speed Air Streams, presented at the AIAA Third Fluid and Plasma Dynamics Conference, Los Angeles, June 1970.
5. Wortman, A. and Mills, A. F., Two-Dimensional Stagnation Point Flows of Binary Gas Mixtures, accepted for publication in the International Journal of Heat and Mass Transfer.
6. Wortman, A., and Mills, A. F., Separating Self-Similar Laminar Boundary-Layers, accepted for publication in the AIAA Journal.
7. Rogers, D. F., Reverse Flow Solutions for Compressible Laminar Boundary-Layer Equations, the Physics of Fluids, Vol. 12, No. 3, pp 517-523, March 1969.
8. Ng, K. H., Patankar, S. V., and Spalding, D. B., The Hydrodynamic Turbulent Boundary Layer on a Smooth Wall, Calculated by a Finite Difference Method, Proceedings: Computation of Turbulent Boundary Layers - 1968 AFOSR-IFP-Stanford Conference.
9. Cebeci, T., Smith, A. M. O., A Finite-Difference Solution of the Incompressible Turbulent Boundary-Layer Equations by an Eddy Viscosity Concept, Proceedings: Computation of Turbulent Boundary Layers - 1968 AFOSR-IFP-Stanford Conference.
10. Alber, I. E., Similar Solutions for a Family of Separated Turbulent Boundary Layers. AIAA Paper No. 71-203, presented at the AIAA Ninth Aerosciences Meeting, New York (1971).
11. Mager, A., Transformation of the Compressible Turbulent Boundary Layer, Journal of the Aeronautical Sciences, 25, pp 305-311 (1958).
12. Spence, D. A., Distributions of Velocity, Enthalpy and Shear Stress in the Compressible Turbulent Boundary Layer in a Flat Plate, RAE (Farnborough) Report No. Aero. 2631 (1959).
13. Sears, W. R. (editor), General Theory of High-Speed Aerodynamics, Vol. 6, High-Speed Aerodynamics and Jet Propulsion, Princeton University Press, Princeton, New Jersey (1954), pp 88-91.

## APPENDIX

Here we consider the details of application of the present method in the case of simple two-dimensional, incompressible, nonsimilar flow with  $C \equiv 1.0$ . This particularly simple example is chosen for clarity since extensions to more general three-dimensional compressible flows follow immediately from the discussion in the paper. The governing equation is:

$$f''' + f f'' = -\beta(1 - f'^2) + H \quad (A-1a)$$

with

$$\eta = 0 \quad f = f_0 \quad f' = 0 \quad (A-1b)$$

$$\eta \rightarrow \infty \quad f' \rightarrow 1.0 \quad (A-1c)$$

and

$$H = 2\xi \left( f' \frac{\partial f'}{\partial \xi} - f'' \frac{\partial f}{\partial \xi} \right) \quad (A-2)$$

Integrating formally with

$$\phi = \exp \left( \int_0^\eta f d\bar{\eta} \right)$$

$$f'' = \phi^{-1} \left( f_0'' - \beta \int_0^\eta (1 - f'^2) \phi d\bar{\eta} + \int_0^\eta H \phi d\bar{\eta} \right) \quad (A-3)$$

Shear stress at the surface,  $f_0''$ , is evaluated in the next integration, which brings in the boundary conditions

$$f_0'' = \frac{1 + \int_0^\infty \beta \phi^{-1} \int_0^\eta (1 - f'^2) \phi d\bar{\eta} d\eta + \int_0^\infty \phi^{-1} \int_0^\eta H \phi d\bar{\eta} d\eta}{\int_0^\infty \phi^{-1} d\bar{\eta}} \quad (A-4)$$

and

$$f' = \int_0^\eta f'' d\bar{\eta} \quad f = \int_0^\eta f' d\bar{\eta} + f_0 \quad (A-5)$$

The computation proceeds as follows:

A. First point on the body

1. Set  $\xi = 0$
2. Start with arbitrary  $f f' f''$ . Linear, constant and exponential decay are quite adequate.
3. Compute the first approximation for  $f''$  using Equation A-3
4. Set  $f_1'' = (f_0'' + w f_1'') / (1 + w)$ . Usually,  $w = 1$  suffices.
5. Compute  $f', f$  using Equation A-5
6. Repeat steps 3-5 until satisfactory convergence is attained.

A typical example of such an iteration is shown in Figure 6 for the case of a cylindrical stagnation point compressible flow. The variation of viscosity with enthalpy is  $\mu \propto h^{s_1}$ ,  $h$  being static enthalpy.

B. Second point on the body

1. Compute  $\xi$ . Set  $H \equiv 0$
2. Compute  $f''$  using existing profiles (from the first point)
3. Set  $f_1'' = (f_0'' + w f_1'') / (1 + w)$
4. Compute  $f_1', f_1$
5. Compute  $H$  using simple differences
6. Repeat steps 2-5 using profiles computed in the preceding iteration.

From the third point and onwards  $H$  may be computed using 3 point difference formulae, but this refinement becomes worthwhile only in cases of significantly rapid longitudinal variation of the flow. Note that  $\Delta \xi$  is determined externally to the calculation and reflects the judgment of the user regarding an adequate description of the flow and geometry.

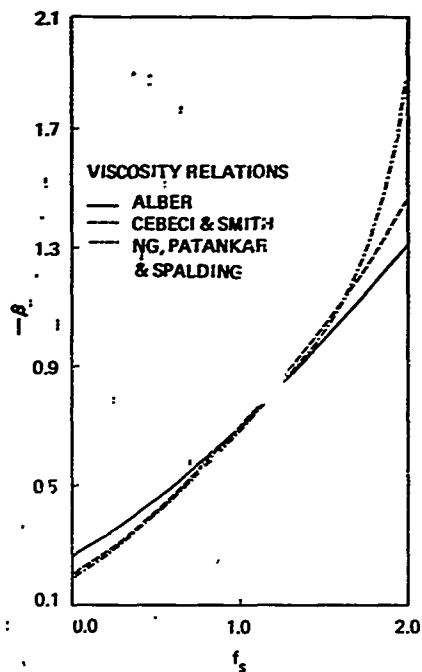


FIGURE 1. PREDICTION OF THE SEPARATION VELOCITY GRADIENT,  $E = 0.0$ ,  $g_s = 1.0$

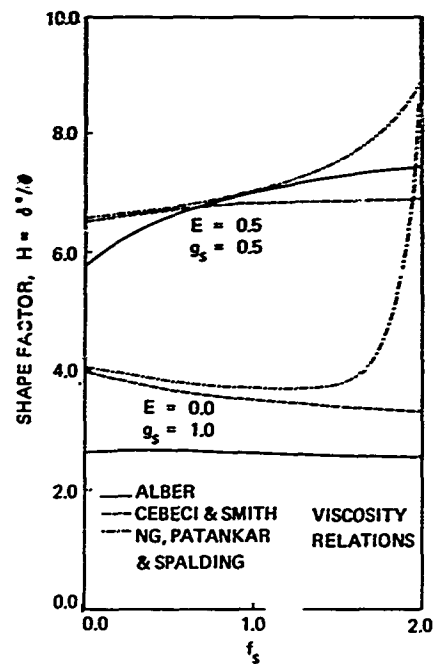


FIGURE 2. PREDICTION OF THE SHAPE FACTOR

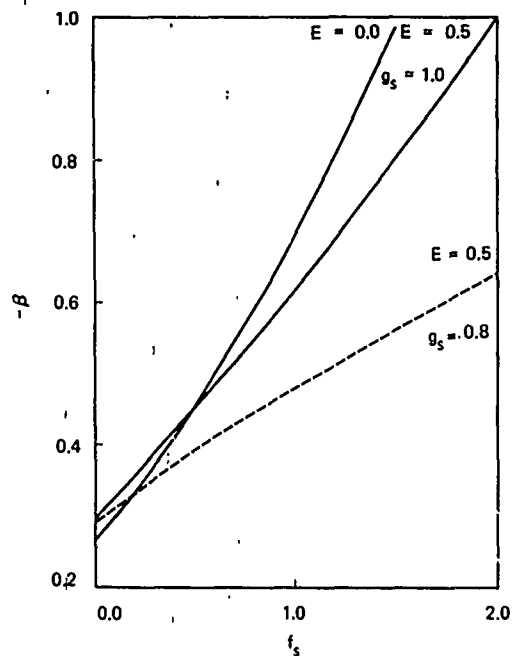


FIGURE 3. EFFECT OF SUCTION ON  $\beta$

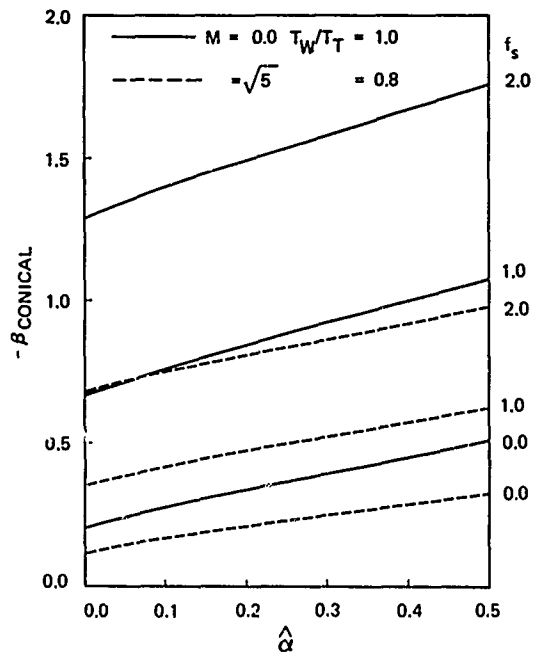


FIGURE 4. TURBULENT SEPARATION WITH CROSSFLOW - III-D VISCOSITY

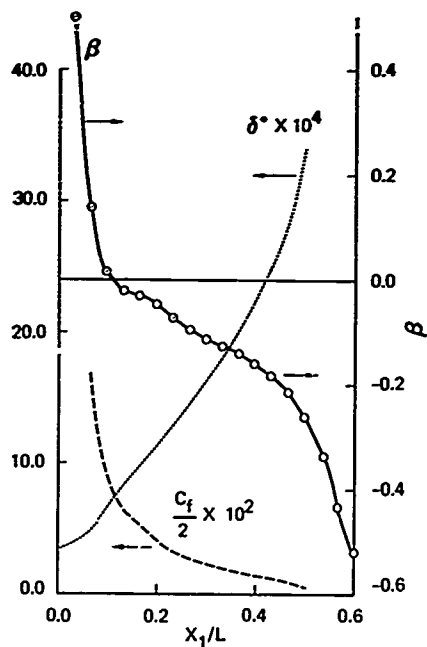


FIGURE 5. NACA 0012 AIRFOIL BOUNDARY LAYER  
CALCULATION,  $M_\infty = 0.4$ ,  $Re_L = 10^5$ ,  $g_s = 0.9$

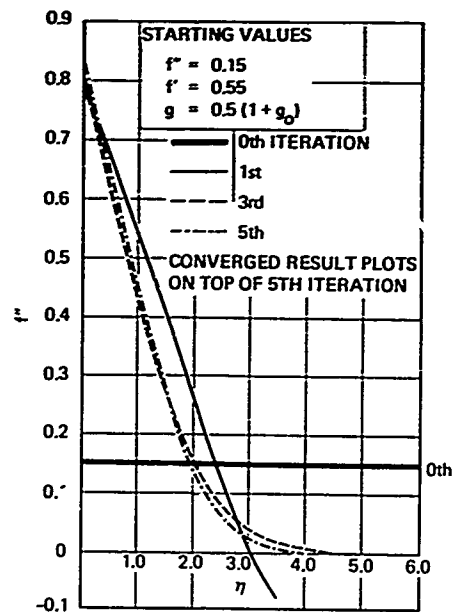


FIGURE 6. RATE OF CONVERGENCE  
OF ITERATION.  
 $E = 0$ ,  $\beta = 0.5$ ,  $Pr = 0.7$ ,  $s_1 = 0.745$ ,  $g_0 = 0.802$ .

# DESIGN OF AIRFOILS WITH HIGH LIFT AT LOW AND MEDIUM SUBSONIC MACHNUMBERS

by

F.I. Wortmann

Institut für Aerodynamik und Gasdynamik der Universität Stuttgart

## Summary

The highlift capabilities of airfoils are restricted by the boundary layer separation on the upper airfoil surface. Therefore it is obviously desirable to design airfoils with pressure distributions which shift the onset of separation to higher angles of attack. In doing this the topside nose region becomes more and more important, not only with respect to the maximum lift but also for post-stall behaviour. Fortunately the nose region, especially with cambered airfoils, is to some extent free for modifications which do not necessarily injury the airfoil drag qualities at low incidences i.e. at high speeds.

As long as the Machnumber stays below, say, .2 the design task on the one hand strives for lower velocity peaks at the nose insofar as this is compatible with the high speed requirements, and on the other hand for reduced velocity gradients behind the peak in the first 4-10% of the chord to produce turbulence without a pronounced laminar separation bubble. In other words, one aims for more favorable initial conditions for the turbulent boundary layer while at the same time avoiding the critical bursting of the separation bubble.

At higher Machnumbers and high angles of attack local supersonic fields will soon develop which are usually terminated by a shock. The best boundary layer control in this case is to avoid the shock by an appropriate design of the airfoil nose for a given angle of attack and Machnumber. The resulting form of the airfoil nose for shockless flow turns out to be quite near to the optimum form produced by the first design task, which takes into account only boundary layer considerations. Therefore it can be expected that an airfoil designed for high lift at a certain Machnumber say .5, will have excellent high lift values not only at this but also at lower Machnumbers, down to the incompressible case.

The common feature of these airfoils is a slight second peak in the curvature at 4 - 10% of the chord. The effectivity of this "hump" to increase the  $C_{L \max}$  will be shown by experimental results.

## 1. Introduction

The maximum lift of an airfoil and its stall behaviour are important qualities of any airfoil. They are strongly influenced by details of the boundary layer development and obviously any airfoil through its form and pressure distribution exerts some sort of boundary layer control.

It is now an interesting question to see what can be gained with respect to the maximum lift if the form of the airfoil is designed to produce the desired boundary layer control for a specific value of the Reynolds- and Machnumbers.

Since the underlying concepts are by no means new it is the purpose of this paper to illustrate the expected improvements by some experimental results.

## 2. High lift at low Machnumbers

At higher angles of attack all airfoils develop a small "laminar" separation bubble on the upper side near the leading edge, even at high Reynoldsnnumbers. This separation has a strong and well-known influence on the maximum lift. The most striking feature of this tiny bubble is the ability to break up and burst into a big separated region. For thin airfoils this happens early, and due to the relatively low incidences the separated turbulent layer will soon reattach.

With increasing incidences the lift and the bubble grow until the reattachment line reaches the trailing edge. The maximum lift is moderate and the "thin airfoil" stall is steady.

With airfoils of medium thickness the length of the laminar separation bubble will be reduced with increasing incidences and reaches the break up condition only at high angles of attack.

A steady transition is now impossible. The bursting of the bubble causes completely separated flow and a sudden and significant loss of lift. This characterizes the leading edge stall.

With thicker airfoils the separation of the turbulent boundary layer in front of the trailing edge prevails and the stall will be reached before the laminar separation bubble at the nose becomes critical. The trailing edge stall may be more or less steady depending on how fast the separation point of the turbulent boundary layer moves forward. Even in this case the tiny laminar separation bubble has its effect; due to the large pressure differences and the type of pressure distributions associated with high angles of attack, the turbulent boundary layer becomes more and more sensitive to the initial conditions and without doubt the laminar separation bubble at the nose has a strong and detrimental influence on the turbulent boundary layer [1].

Thus it may be interesting to design airfoils with little or no laminar separation and to see if it is possible to increase the maximum lift or to change the type of stall. With respect to the laminar boundary layer this means locally reduced pressure gradients in the nose region and a shift of the separation point behind the transition point.

The chord length necessary to provoke the transition shortens with increasing Reynoldsnumber. On the other hand, speaking in terms of airfoil design it is easier to change the pressure gradients over a short rather than an extended chord length. Therefore the full benefits of this old concept [2] can be expected rather at higher Reynoldsnumber, say above  $6 \cdot 10^6$ .

In the following two symmetrical airfoils, the NACA 0009 and 0012, have been chosen to demonstrate the value of a nose modification.

Figure 1 and 2 show the form, the potential velocity at  $\alpha = 14^\circ$  and the curvature of these airfoils and their modifications. The windtunnel tests were restricted to a Machnumber of .2 and a Reynoldsnumber of  $3 \cdot 10^6$  to avoid any sonic velocities to within a fair margin.

Figure 3 shows the laminar separation bubbles of the 0012 and the FX 71-120 airfoil at  $14^\circ$  and  $16,6^\circ$  respectively, i.e. nearly one degree below  $C_{L \max}$ .\*)

Despite the longer laminar flow of the modified airfoils with adverse pressure gradients, the Reynoldsnumber is not high enough to avoid the separation bubble completely. It may be argued however that in this case the height of the separation bubble, and therefore the initial thickness of the turbulent boundary layer, is far less than with the 0012 airfoil.

Figures 4 and 5 give the lift and drag value of both the NACA airfoils and their modifications, and Figure 6 the  $C_{L \max}$  values as function of the Reynoldsnumber.\*)

The modified airfoils exhibit a gain in  $C_{L \max}$  of 15 - 20% and increase the associated angle of attack by 2 or 3 degrees.

In both cases the stall of the modified airfoils has been changed to a trailing edge stall. The steep loss of lift beyond the stall could probably be moderated if the modifications were extended over the rear part of the airfoils. There is, however, at low incidences a drag penalty of 5 to 15% for the smooth airfoils due to the earlier transition on the modified versions. If the transition were enforced by some roughness at nearly 5% - 7% of the chord, the drag penalty would diminish. The coordinates of the modified airfoils are given in Table I.

It may be mentioned that symmetrical airfoils are in some sense the hardest example with which to demonstrate the effectivity of a bubble control. For cambered airfoils there exists a greater degree of freedom to "hide" the modifications into the nose camber, and to avoid the drag penalty even with smooth airfoils.

### 3. High lift at medium Machnumbers

The high lift which an airfoil may attain at low Machnumbers will always decline when the Machnumber increases and the velocity peaks near the leading edge form a local supersonic field which is usually terminated by a more or less pronounced shock. The shock interference in turn hits a boundary layer, which in any case is already exhausted by the large pressure differences at high incidences.

It is thus not too surprising to find a pronounced depression in the envelope of the maximum lift curves in the Machnumber range between .3 and .55 [4]. This Machnumber range is of relevance especially to the helicopter rotor, which needs a high lift on the retreating blade to balance the disk loading in forward flight.

\*1

In these tests the tunnel speed accelerated in 30 sec from zero to  $Re = 3 \times 10^6$ . Therefore in details the oil streak pattern needs some cautious interpretation.

\*) All measurements were done by Dipl.-Phys. D. Althaus in the laminar wind tunnel of the institute [3].

In order to retain the high lift in the low to medium Machnumber range, it will be mandatory to design the upper nose region of the airfoil for a specifically chosen Machnumber and a certain high angle of attack. Similarly to the incompressible case, one must first reduce the velocity peaks by thickness and camber distribution as far as is compatible with the high speed requirements. The second design principle strives for an isentropic recompression in the supersonic field to reduce the strength of the terminating shock [5]. The recompression which may be achieved on the basis of the "peaky" concept or an analysis of the expansion and compression waves inside the supersonic field ensures at the same time that the residual shock in off-design conditions never interferes with a laminar boundary layer.

In a previous paper [6] the author has shown that at high incidences the pressure at the crest has a strong relationship to the point at which the maximum lift eventually recovers with increasing Machnumbers, and reaches a second maximum.

This pressure must be sufficiently low (or in other words the speed in the crest region must be higher than usual) to be of any value for Machnumbers between .3 and .55. Figure 7 gives an example of an airfoil designed for an improved maximum lift at  $M_{\infty} = .5$ . Disregarding the chord position the nose form, the incompressible potential velocity and the curvature distribution resemble the features which are typical for the airfoils in the first part of this paper. Figure 8 illustrates the expansion and compression waves in the supersonic field of this airfoil for  $\alpha = 9.8^\circ$ , at two Machnumbers near .5. The necessary compressible potential velocity distributions were calculated on the basis of the NLR formula [7].

In Figure 9 and 10 experimental results are evaluated<sup>\*)</sup>. Figure 9 shows for a constant angle of attack of  $11^\circ$  the development of the local Machnumber on the upper nose region of the FX 69-H-098 airfoil. The extremely high peaks of local Machnumbers right at the nose indicate clearly the favorable effects of a partly isentropic recompression. This is again demonstrated in Figure 10, where the overall maximum lift is given as a function of the Machnumber.

Since this paper concentrates on  $C_L \max$ , however one should not lose sight of the complete problem, which includes the high speed properties of the airfoil. The high velocities in the 10% chord region, which yield the typical curvature distribution of Figure 7 are compatible with the low pitching moments desirable for any rotor blade.

It may be fair to state the drag divergence at high Machnumbers and low incidences compares well with other airfoils, at least for the airfoil presented here.

With respect to helicopter airfoils it would certainly be necessary to apply the concept of local supersonic flow with isentropic recompression not only to the high lift case of an airfoil but to its low lift properties as well. This challenging problem would seem to be solvable, and windtunnel tests are under way to prove the potential advantages of such airfoils, optimized for two differing conditions.

#### 4. Conclusion

It has been shown by experimental results that the maximum lift of a symmetrical airfoil at low Machnumbers can be increased by some 15 to 20% if the airfoil nose is slightly modified and designed to yield lower velocity peaks and less pronounced laminar separation bubbles.

A similar improvement for the maximum lift at medium Machnumbers is possible if the upper nose region of the airfoil is designed to produce a "peaky" configuration at a certain Machnumber and high angle of attack. In both cases the airfoil exhibits as a common feature a high curvature or even a slight second peak in the curvature distribution between 4 to 10% of the chord.

#### References

- [1] F.X. Wortmann  
"Experimentelle Untersuchungen an neuen Laminarprofilen für Segelflugzeuge und Hubschrauber"  
Zeitschrift f. Flugwiss. 5 (1957) S. 228-243
- [2] F.X. Wortmann  
"Progress in the design of Low Drag Airfoils"  
"Boundary Layer and Flow Control" Pergamon Press London 1961, p. 748-770

<sup>\*)</sup> These tests were done in the UAC-windtunnel (Hartford, Connecticut, USA) and were part of a research program of the Bell Helicopter Co., Fort Worth, Texas. I am grateful to this company for the permission to publish these data.



- [3] P.I. Wortmann und D. Althaus  
 "Der laminarwindkanal des Instituts für Aero- und Gasdynamik der TH Stuttgart"  
 Zeitschrift f. Flugwiss. 12 (1954) S. 129-134
- [4] L.R. Wootton  
 The Effect of Compressibility on the Maximum Lift Coefficient of Airfoils  
 at Subsonic Airspeeds  
 J.R.Aer.Soc. 71 (1967), p. 476
- [5] H.E. Pearcey, J. Osborne  
 "Some Problems and Features of Transonic Aerodynamics"  
 7. Congress of ICAS (1970), Rom
- [6] P.I. Wortmann, J.M. Drees  
 Design of Airfoils for Rotors  
 CAL/AVLABS Symposium 1969, Cornell Aeron. Lab. Buffalo
- [7] Th. B. Labrujere, W. Loefer, J.W. Slooff  
 "An approximate Method for the Determination of the Pressure Distribution  
 on Wings in the lower Critical Speed Range"  
 AGARD CP Nr. 35 (1968) Paris.

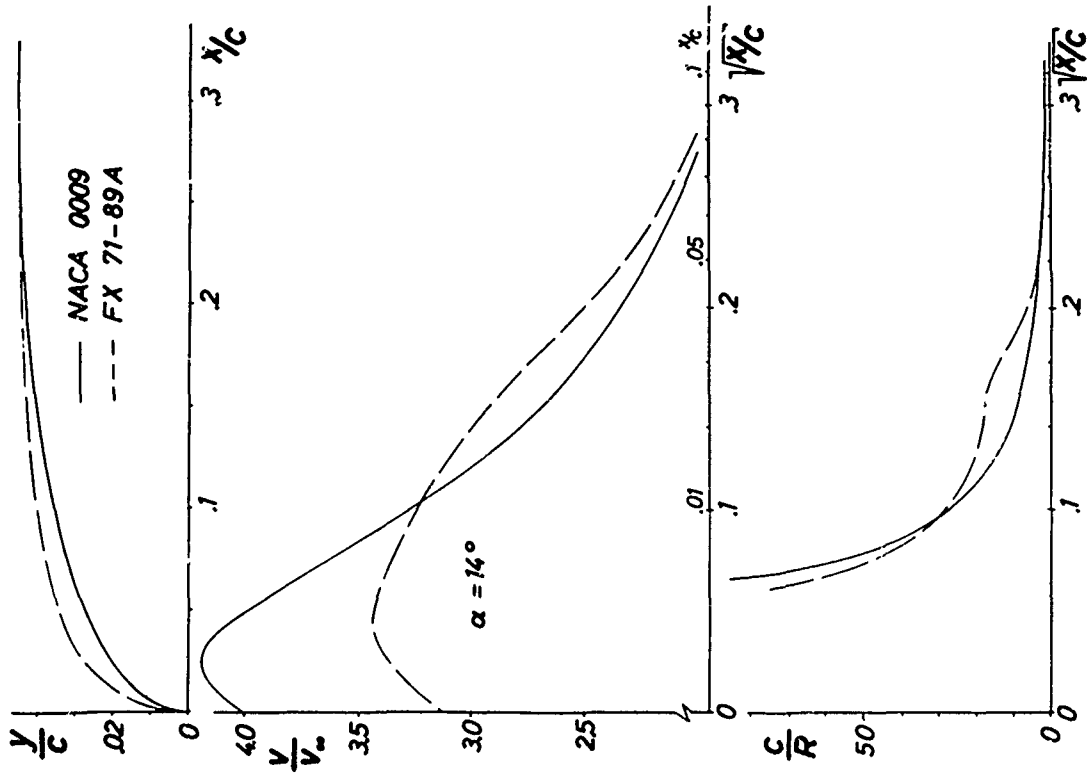


Fig. 1 Form of airfoil nose, inviscid velocity distribution at  $\alpha = 14^\circ$  and curvature distribution for the NACA 0009 and the FX 71-89A.

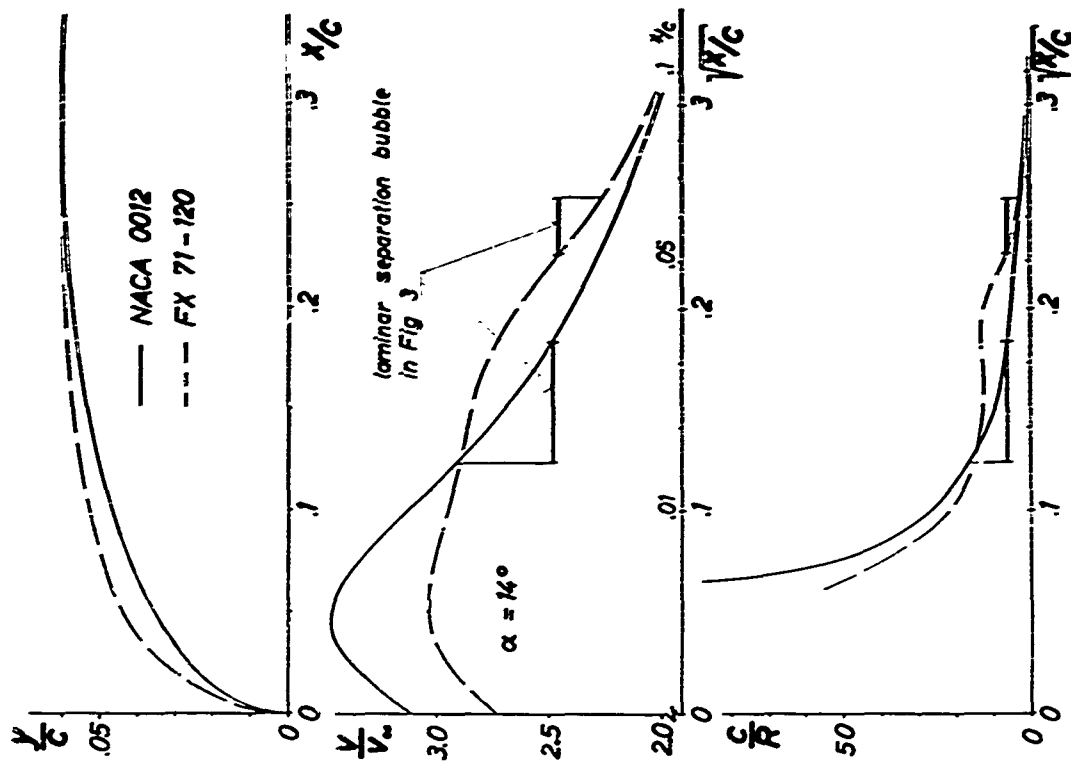


Fig. 2 Form of airfoil nose, inviscid velocity distribution at  $\alpha = 14^\circ$  and curvature distribution for the NACA 0012 and the FX 71-120

Table I

Airfoil coordinates given in per cent  
of airfoil chord

FX 71-120 FX 71-029A

No.	x/c	y/c	y/c
4	.03433	.00693	.00033
6	.07347	.00344	.00257
8	.08544	.00555	.00487
10	.09157	.01037	.00769
12	.07582	.01493	.01107
13	.05355	.01745	.01295
14	.02951	.02011	.01491
15	.00430	.02293	.01701
16	.77779	.02580	.01912
17	.74073	.02879	.02133
18	.72114	.03179	.02356
19	.66117	.03476	.02576
20	.61072	.03771	.02794
21	.62941	.04053	.03005
22	.55753	.04331	.03209
23	.52520	.04595	.03406
24	.53271	.04830	.03580
25	.51071	.05072	.03763
26	.46732	.05275	.03915
27	.43474	.05400	.04057
28	.40243	.05627	.04179
29	.37653	.05760	.04280
30	.33920	.05662	.04359
31	.30860	.05937	.04416
32	.27880	.05963	.04456
33	.25000	.05993	.04467
34	.22221	.05960	.04460
35	.19562	.05931	.04435
36	.17033	.05833	.04376
37	.14603	.05700	.04291
38	.12473	.05531	.04171
39	.11332	.05323	.04037
40	.09427	.05072	.03965
41	.06699	.04786	.03646
42	.05150	.04443	.03411
43	.03800	.04069	.03113
44	.02653	.03480	.02818
45	.01704	.02312	.02341
46	.00961	.02110	.01904
47	.00420	.01400	.01220
48	.00107	.00714	.00630

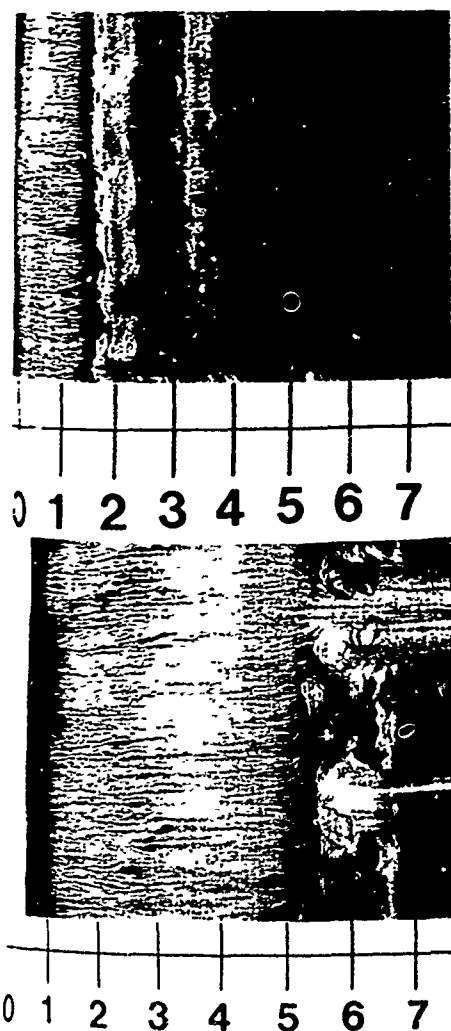


Fig.3 Oil film pattern of the NACA 0012 at  $\alpha = 14^\circ$  (upper part) and of the FX 71-120 at  $\alpha = 16.6^\circ$  (lower part). indicating the laminar separation bubble. Scale in per cent of airfoil chord.

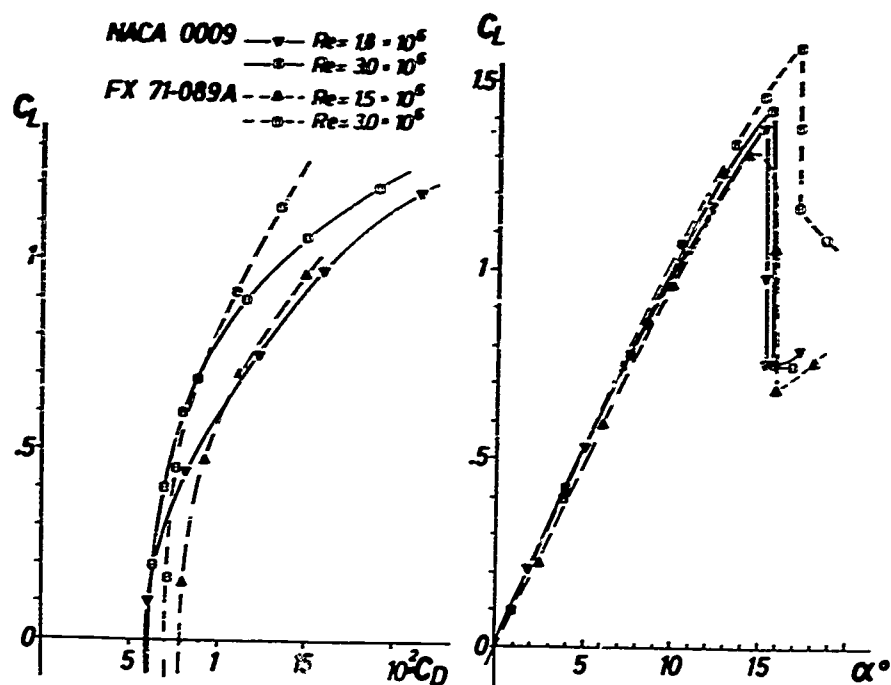


Fig.4: Experimental aerodynamic characteristics of the NACA 0009 and FX 71-089A for Reynoldsnumbers between  $1.5 \cdot 10^6$  and  $3 \cdot 10^6$ .

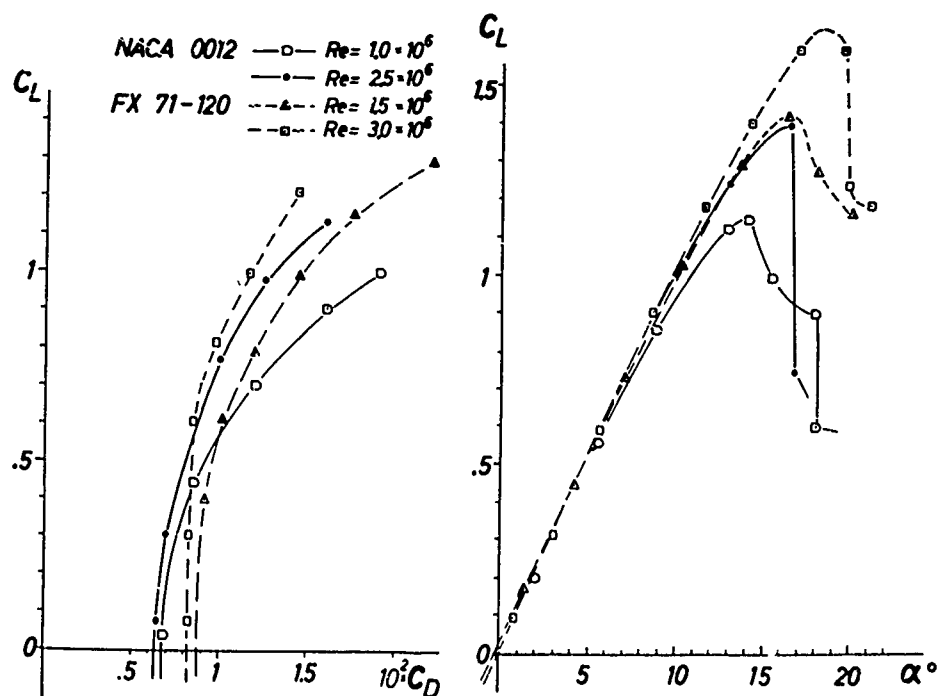


Fig.5: Experimental aerodynamic characteristics of the NACA 0012 and FX 71-120 for Reynoldsnumbers between  $1 \cdot 10^6$  and  $3 \cdot 10^6$ .

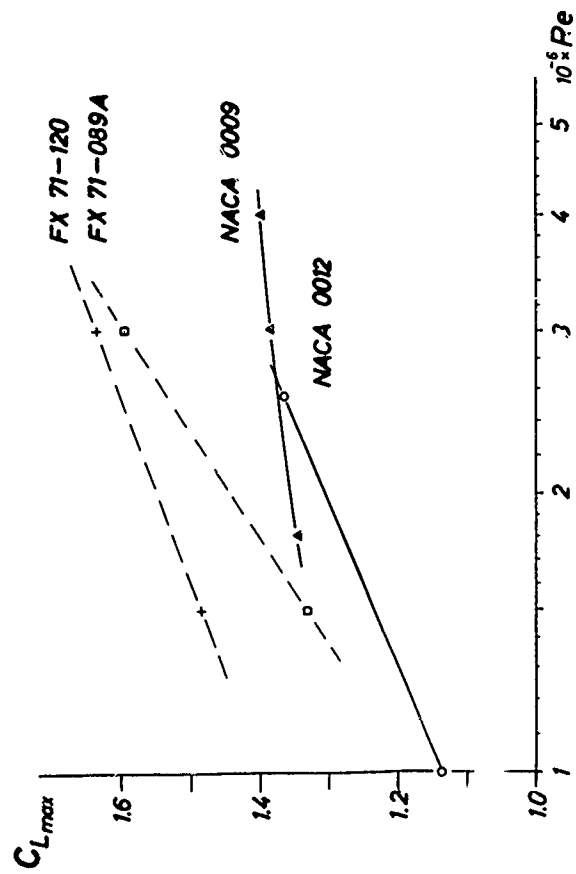


Fig. 6: Variation of maximum lift coefficient with Reynolds number for two NACA airfoils and their modifications.

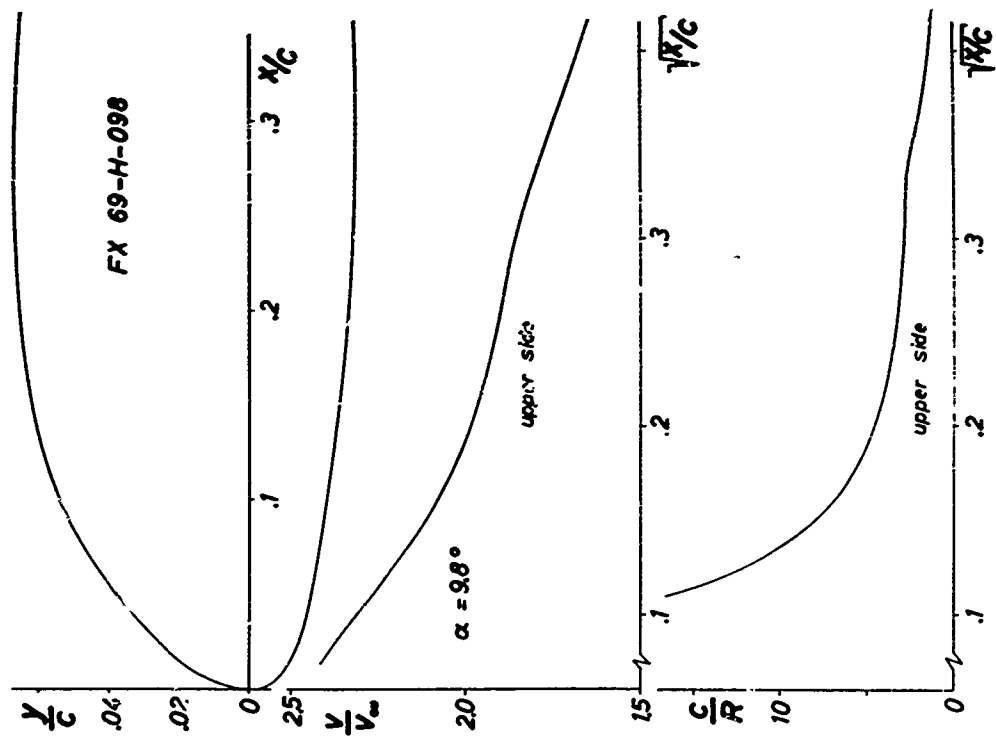


Fig. 7: Form of airfoil nose, inviscid and incompressible velocity distribution at  $\alpha = 9.8^\circ$  and curvature distribution on the upper side of FX 69-H-098.

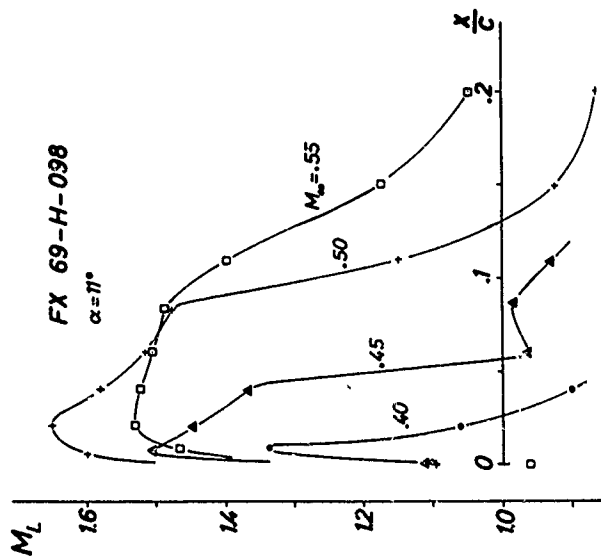


Fig. 9: Variation of local Mach numbers in the upper nose region of FX 69-H-098 at  $\alpha = 11^\circ$  for free stream Mach numbers between .4 to .55. UAC-windtunnel.

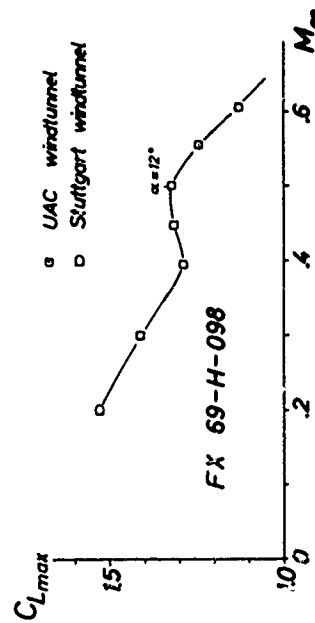


Fig.10: Variation of maximum lift coefficient at low and medium free stream Mach number for the FX 69-H-098.

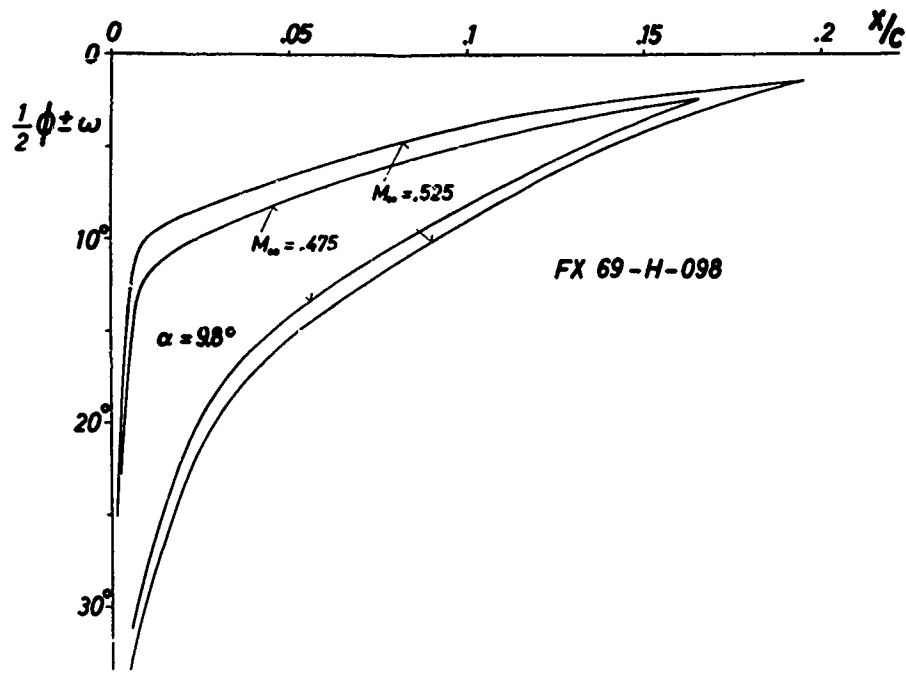


Fig.8: Wave cancellation analysis for FX 69-H-098 at  $\alpha = 9.8^\circ$  and two Mach numbers.

COMMENTS ON THE METHODS DEVELOPED AT NLR FOR CONDUCTING  
TWO-DIMENSIONAL RESEARCH ON HIGH-LIFT DEVICES.

by

O. de Vries

National Aerospace Laboratory NLR,  
Amsterdam, The Netherlands.

SUMMARY

Research on high-lift devices has been carried out at NLR along the following lines.

An experimental approach consisting of pressure measurements at the mid-span section of a two-dimensional wing (chord about 0.6 m, span 2 m), with boundary layer control at the tunnel wall-wing junctions by blowing slots. Premature flow separation can be avoided and the maximum lift can be determined reliably.

This testing technique is already applied on a routine basis to wing sections with both leading and trailing edge high-lift devices.

A theoretical approach consisting of potential flow calculations by means of a singularity method with a source distribution on the contour. This is applied with a limited number of contour points on the aerofoils (essentially the co-ordinates of the pressure measuring stations at the model). The calculations were compared with experimental results. The agreement is reasonable.

RÉSUMÉ

La recherche sur volets hypersustentateurs est exécutée au NLR suivant deux voies

La première voie consiste à mesurer des pressions sur la section à demi envergure d'une aile en courant plan (la corde environ de 0.6 m, envergure 2 m), avec contrôle de la couche limite par soufflage tout près des jonctions entre l'aile et les parois. On peut empêcher le décollement prématuré de l'écoulement et la portance maximale est obtenue avec assez de certitude. Cette méthode expérimentale en courant plan est déjà appliquée comme une méthode de routine aux profils munis de volets hypersustentateurs à bord de fuite comme à bord d'attaque.

La seconde voie consiste à calculer l'écoulement potentiel au moyen de la méthode des singularités. Cette méthode est appliquée avec un nombre limité de points sur le contour des profils (essentiellement les coordonnées des points de mesure sur la maquette). Les résultats calculés sont comparés avec les résultats expérimentaux. La correspondance est assez bonne.

## 1. INTRODUCTION.

At NLR, the research in connection with the development of high-lift devices, mainly involves two-dimensional wind tunnel investigations, using pressure plotting models, because of the relative simplicity of test set-up and model construction.

In trying to carry out these investigations as good as possible, two major problems emerged:

- An experimental difficulty, caused by the premature flow separation at the tunnel wall-wing junctions, which made the determination of the true two-dimensional maximum lift unreliable.
- A theoretical difficulty, in the sense that potential flow calculations were required to guide the two-dimensional wind tunnel tests.

This resulted in two more or less separate lines of research, viz.:

- The development of a system to control the boundary layer on the wind tunnel walls at the wing-wall junctions.
- The development of a computer programme, based on a singularity method (Ref.3), for the calculation of the potential flow around a composite aerofoil. The results of the calculations have been compared with experiments. (Ref.4)

## 2. THE BOUNDARY LAYER CONTROL SYSTEM FOR THE WIND TUNNEL WALLS.

### 2.1 Description of the problem.

With the advent of still more efficient high-lift devices, one becomes increasingly concerned about the determination in the wind tunnel of the two-dimensional coefficients and especially the two-dimensional maximum lift. The difficulties arise from the boundary layer on the tunnel wall, mixing with the boundary layer on the wing at the wing-wall junctions. The main problem is, to prevent the premature flow separation at the wing-wall junctions. A secondary problem (and up till now still unsolved) is to avoid a possible trailing vorticity, if no flow separation at the wing-wall junction occurs.

Near the stalling angle, premature flow separation occurs at both ends of the model, due to the boundary layer on the tunnel walls. The main effects are:

- The flow loses its two-dimensional character and the model behaves more or less like a three-dimensional wing. The measured coefficients (e.g. at the mid-span section) deviate from the true two-dimensional coefficients.
- The true two-dimensional maximum lift cannot be obtained, because of the rapid increase of the flow separation at the ends of the model by increasing the angle of attack (see Ref.1).

Below the stalling angle, there may be some secondary effect from trailing vorticity in the tunnel wall boundary layer, originating from the wall-wing junctions. This trailing vorticity may induce a small downwash, causing a small deviation from the true two-dimensional flow.

### 2.2 Blowing versus suction.

Boundary layer control at the wing-wall junctions by blowing or by suction, is used by a number of investigators. Wispress and Swihart (Ref.5) applied blowing slots and were probably the first to use boundary layer control at the wing-wall junctions in two-dimensional testing. Foster and Lawford (Ref.6) applied suction, whereas Mavriplis (Ref.7) used blowing slots again.

NLR has chosen wall blowing instead of suction for the tunnel wall boundary layer control, because:

- The auxiliary system for suction had a limited capacity, whereas the blowing system had ample capacity (pressure vessel of the supersonic blow-down tunnel).
- Preliminary tests had shown the feasibility of blowing (see Ref.1).
- Blowing was considered to be most easily adaptable to different model configurations

In our opinion, however, both blowing and suction can lead to satisfactory two-dimensional test results.

### 2.3 The test set-up.

The development of the blowing system in the tunnel walls (Ref.2) was carried out in the low speed tunnel of NLR (LST 3x2), with a two-dimensional model, provided with a double slotted flap (see Fig.1). The basic (flap up) chord is 0.60 m and the span about 2 m. The model was clamped between the upper and lower turntables of the test-section. It has two sections with pressure measuring holes, viz. at the mid-span section and close to the upper tunnel wall (0.08 m from the wall). The surface pressures at the two sections were measured and integrated numerically to sectional force and moment coefficients.

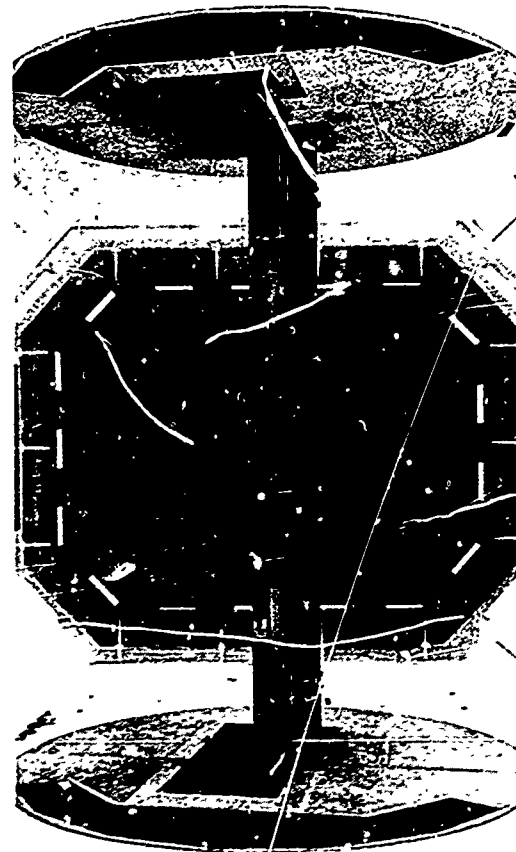


Fig.1 The standard test set-up for two-dimensional pressure measurements with blowing slots at the tunnel walls for boundary layer control at the wing-wall junctions.



The upper and lower turntables were provided with three blowing slots each (see fig.2). The position of the blowing slots could be varied and also the blowing ratio  $\lambda$  (i.e. the ratio of the dynamic head in the blowing nozzle and the free-stream dynamic head). During incidence variation, the position of the blowing slots relative to the model remained fixed. Only the flap blowing slot had to be moved, when the flap setting was changed.

The two-dimensional character of the flow can be inferred from:

- The equality of the integrated forces and moment coefficients at the wall and mid-span section.
- Flow visualization with tufts on the model surface; absence of premature flow separation.

#### 2.4 Results of the blowing tests.

Figure 3 shows the influence of the blowing ratio  $\lambda$  on the lift at  $\alpha = 0$  and the maximum lift for the mid-span and the wall sections. The figure also shows this influence for the case, that the flap blowing slot is inoperative.

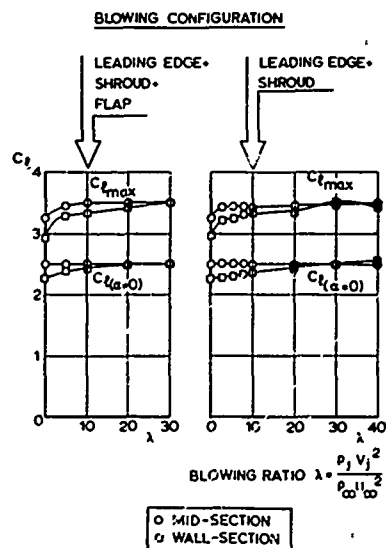


Fig.3 Influence of the blowing ratio and the blowing slot configuration on the lift for mid-span and the wall section. All slots have the same blowing ratio  $\lambda$ , when operative.

blowing at the tunnel wall does not lead to an over-estimation of the maximum lift at the mid-span section

- Neglecting small fluctuations of the coefficients of the wall section, that are almost within the experimental accuracy, figure 3 shows, that flap blowing is not necessary to obtain satisfactory results. Blowing at the leading edge and the shroud is sufficient. This simplifies the experimental set-up for routine measurements, because the blowing slots need not be moved, when the flap setting is changed.

Figure 4 gives the influence of leading edge and shroud blowing on the lift curves of the mid-span and the wall sections. The increase in maximum lift and the improvement in the two-dimensional character of the spanwise lift distribution is clearly shown.

Although definite improvements were obtained, the experimental criteria of this investigation for the assessment of the two-dimensional character of the flow, are too rough to discern the weak effects of the possible trailing vorticity in the tunnel wall boundary layer, originating from the wing-wall junctions. Therefore, slight deviations in angle of attack (and possibly in lift slope) from the true two-dimensional values can still be expected.

Recently, this testing technique with wall blowing was applied on a routine basis to wing sections with trailing and also leading edge high-lift devices. In this case, two fixed blowing slots have also given satisfactory results. One slot was positioned at the shroud of the flap and the other at a small distance in front of the leading edge slot. No blowing slot was needed at the leading edge of the main wing in this case.

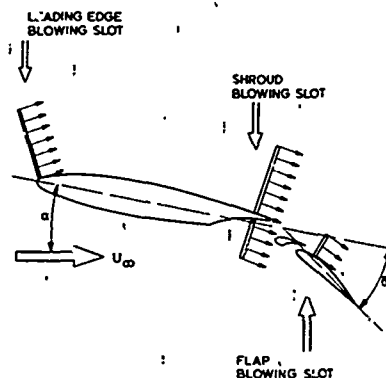


Fig.2 The blowing slot arrangement in the turntables of the tunnel wall.

The following conclusions can be drawn from figure 3:

- By increasing the blowing ratio  $\lambda$ , the coefficients of the wall and the mid-span section will differ less and become equal at values of  $\lambda$  of about 30. At these values of  $\lambda$ , the spanwise lift distribution is two-dimensional.
- The lift at  $\alpha = 0$  at the mid-span section is hardly affected by wall blowing. Therefore, this quantity is not affected by the boundary layer at the wall, when wall blowing is not applied.
- The maximum lift increases with increasing  $\lambda$  at both the wall and the mid-span section. Without any control of the tunnel wall boundary layer at the wing-wall junctions, the measured maximum lift at the mid-span section is definitely lower than the true two-dimensional maximum lift.
- The wall blowing ratio is not critical. Excessive

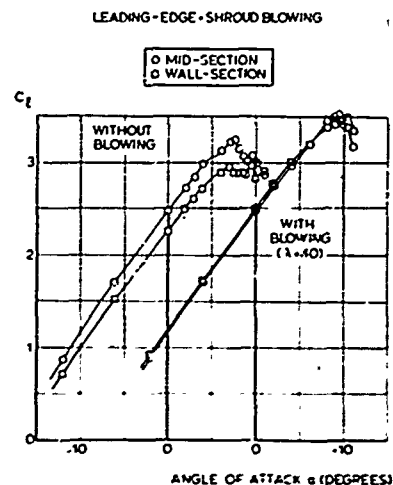


Fig.4 Influence of leading edge and shroud blowing on the lift curves of mid-span and wall section.

### 3. POTENTIAL FLOW CALCULATIONS AROUND A COMPOSITE AEROFOIL.

#### 3.1 General remarks.

With a singularity method (Ref.3) it is possible to obtain the potential flow pressure distribution around a two-dimensional wing with high-lift devices. A number of investigators have already shown the feasibility of calculating the potential flow around composite aerofoils, e.g. Giesing (Ref.9), Foster (Refs. 6 and 7) and Mavriplis (Ref.8).

The development of high-lift devices can be aided by potential flow calculations in the following ways:

- Interpretation of wind tunnel test results. Discrepancies between calculation and experiment may be used to discover local separations and other specific viscous effects. E.g. the interaction between main wing and flap can be analysed somewhat further, see the investigation of Foster (Ref.7).
- Modification of a configuration already tested in the wind tunnel. It seems feasible to decide, whether the proposed modification of the shape has the expected effect.
- It is possible to estimate the load on a two-dimensional model in an early stage, especially on the small elements like the vane of a double slotted flap or the slat.
- Selection by calculation of the most promising configuration out of a number of proposed high-lift systems. This makes the input of empirical data necessary in judging the calculated pressure distributions (suction peaks, pressure gradients etc., cf. Mavriplis, Ref.8).

Developing high-lift devices by mere calculation would require a combined boundary layer and potential flow calculation, with reliable predictions of transition and separation points. Moreover, it would be necessary to calculate the mixing of the wake of a leading aerofoil with the boundary layer of a trailing one. An adequate method does not exist at NLR at the moment.

#### 3.2 Short description of the calculations.

The singularity method used, consists of a source distribution on the contour and a vortex distribution on the mean line. For further details see the references 3 and 4.

The method was applied to three different configurations (for which experimental data were available), viz. to a single slotted flap, a double slotted flap and a double slotted flap combined with a leading edge slat.

In order to find out if, for routine purposes, the sometimes trouble-some interpolation of contour data can be avoided, the co-ordinates of the pressure measuring holes in the corresponding models are taken as the contour points in the calculations. These co-ordinates were readily available. As a consequence of this choice, only a limited number of contour points is used in the calculations, compared with the number required for the exact solution. However, the pressure distribution obtained in this way, has the same characteristics as the potential flow pressure distribution, which is sufficient, taking into account the limited applicability of the results.

#### 3.3 Comparison with experiment.

Figure 5 compares the calculated pressure distribution with the experimental one around a single slotted flap. Notwithstanding the limited number of contour points, the agreement is reasonable and the general character of the pressure distribution is not changed by increasing the number of contour points on the main wing from 44 to 66.

The discrepancies on the shroud lower surface and the flap upper surface are due to a separation bubble on the shroud lower surface, which modifies the flow through the flap slot and induces a local suction peak on the flap upper surface. This could be concluded from some additional calculations on a modified shroud shape, imitating the "free streamline" of the separation bubble and is an example of the use of potential flow calculations in interpreting wind tunnel test results.

The calculated and experimental pressure distribution around a double slotted flap is shown in figure 6 and the pressure distribution around a double slotted flap combined with a leading edge slat is shown in figure 7.

Relatively small elements, such as the vane and the slat, are magnified in the chordwise direction, to obtain greater clarity.

In these two cases, the overall agreement is also good. Some small irregularities in the calculated pressure distribution are due to an irregular distribution of the contour points, however, they do not affect the general character of the pressure distribution. The difference between calculation and experiment in the pressure distribution on the slat lower surfaces, due to flow separation, is revealed in figure 7.

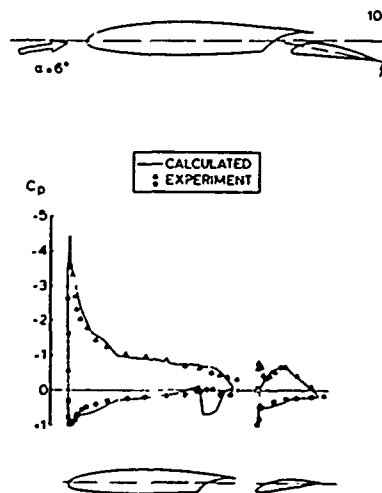
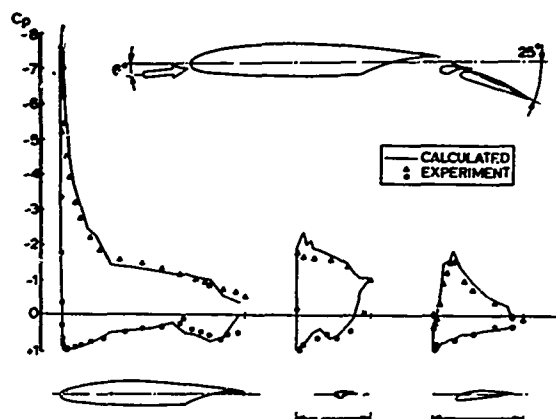
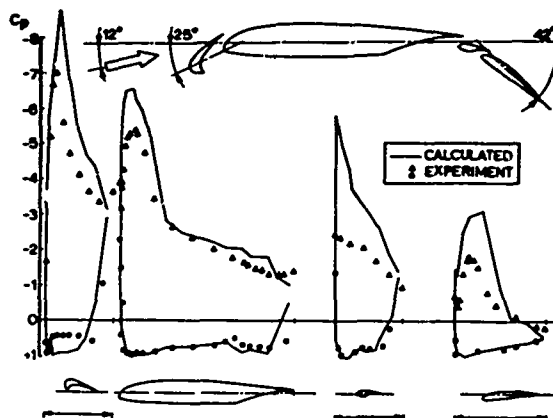


Fig.5 Comparison between the calculated and experimental pressure distribution around a single slotted flap.



**Fig.6** Comparison between the calculated and experimental pressure distribution around a double slotted flap.



**Fig.7** Comparison between the calculated and experimental pressure distribution around a double slotted flap combined with a leading edge slat.

The calculated and experimental lift curves for three configurations are given in figure 8. The corresponding pitching moment curves (referenced to the  $\frac{1}{4}$ -chord point of the basic chord) are given in figure 9. Considering that no boundary layer effects are taken into account, the discrepancy between calculation and experiment is smaller than would be expected. This is caused by the small number of contour points used in the calculations. If a better approximation to the potential flow lift is required, it is necessary to increase the number of contour points.

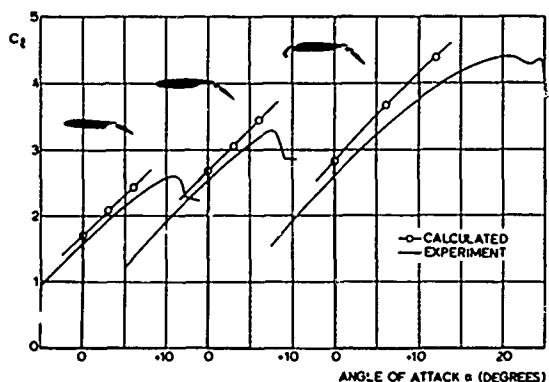


**Fig.8** The calculated and experimental lift curves for the single slotted flap with  $\delta_f = 25^\circ$ , the double slotted flap with  $\delta_f = 40^\circ$  and the double slotted flap with  $\delta_f = 42^\circ$  combined with a slat, deflected  $25^\circ$ .

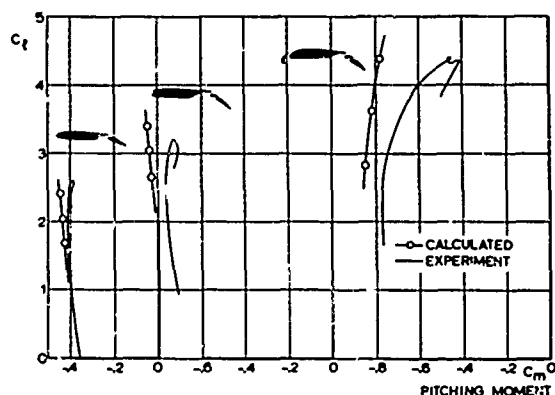


**Fig.9** The calculated and experimental pitching moment curves for the single slotted flap with  $\delta_f = 25^\circ$ , the double slotted flap with  $\delta_f = 40^\circ$  and the double slotted flap with  $\delta_f = 42^\circ$  combined with a slat, deflected  $25^\circ$ .

The calculated and experimental tangential force and normal force of the double slotted flap are compared in figure 10. The deflection of the vane varies with the flap deflection. At vane deflection zero, the vane is retracted onto the flap, forming a single slotted flap. The coefficients are referred to the basic wing chord instead of the flap chord. The agreement between theory and experiment is reasonable, although the discrepancy for the tangential force is large, indicating strong viscous effects.

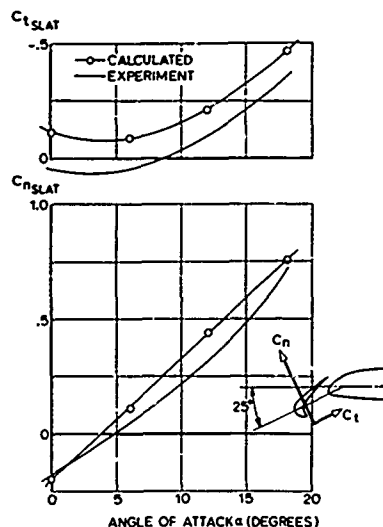


**Fig.10** The calculated and experimental load on the double slotted flap at an angle of attack  $\alpha = 6^\circ$ .

**Note:** The coefficients  $c_n$  and  $c_t$  are referred to the basic wing chord instead of the flap chord.

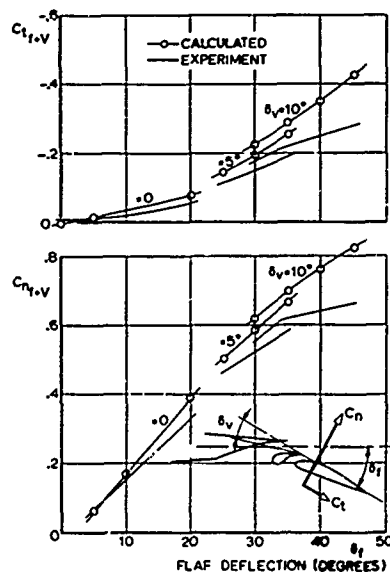


**Fig.11** The calculated and experimental load, on a slat deflected  $25^\circ$ . The trailing edge flap is deflected  $\delta_f = 18^\circ$ .

A similar comparison is made in figure 11 for the slat. Due to the large flow separation on the slat lower surface, there is a large discrepancy between the calculated and experimental tangential force. The normal force shows a good agreement. The conclusion can be drawn, that the potential flow calculations give a reasonable estimate of the loads on small elements, such as slats or flaps.

#### 4. CONCLUDING REMARKS.

In order to obtain a good approximation of the true two-dimensional flow in wind tunnel tests, it is sufficient to apply tunnel wall boundary layer control at the tunnel wall-wing junctions by a relatively simple system of compressed air blowing slots. Acceptable results are obtained by using two blowing slots, viz. at the leading edge of the main wing and at the shroud. After this investigation, the experience accumulated in large series of measurements on two-dimensional models equipped with trailing and leading edge high-lift devices has shown that the blowing system could be easily adapted to the various model configurations.

Potential flow pressure distributions can be used to aid the interpretation of wind tunnel test results, to modify a configuration already tested in the wind tunnel and to estimate the loads on the elements of a composite aerofoil, e.g. for model construction purposes.

The singularity method developed at NLR, offers the possibility to use the calculations on a routine basis. Even with a limited number of contour points, the calculated pressure distribution gives a fair approximation of the potential flow distribution.

#### REFERENCES.

- 1 Van Den Berg, B. Some notes on two-dimensional high-lift tests in wind tunnels. AGARD Lecture Series No.43, Lecture No.5, February 1971.
- 2 De Vos, D.M. Low speed wind tunnel measurements on two-dimensional flapped wing model using wall boundary layer control at the wing-wall junctions. NLR TR 70050 U (to be published).
- 3 Labrujere, Th.E. Loeve, W. Slooff, J.W. An approximate method for the calculation of the pressure distribution on wing-body combinations at subcritical speeds. AGARD Conference Proceedings No.71, Paper No.11, September 1970.
- 4 Labrujere, Th.E. Schipholt, G.J. De Vries, O. Evaluation of a method for the calculation of the pressure distribution on two-dimensional wing-flap configurations in subsonic flow. NLR TR (to be published).
- 5 Wimpers, J.K. Swihart, J.H. Influence of aerodynamic research on the performance of supersonic air-planes. J. of Aircraft, Vol.1, No.2, 1964.

- 6 Foster, D.N.  
Lawford, J.A. Experimental attempts to obtain uniform loading over two-dimensional high-lift wings.  
R.A.E. TR 68283 ; 1968.
- 7 Foster, D.N. The flow around wing sections with high-lift devices.  
R.A.E. Tech. Memo Aero 1269, November 1970.
- 8 Mavriplis, F. Aerodynamic research on high-lift systems.  
AGARD Lecture Series No. 43, Paper No. 15,  
February 1971.
- 9 Giesing, J.P. Potential flow about two-dimensional airfoils.  
Douglas Aircraft Co. Rept. No. LB31946,  
December 1966.

## CORRECTION DE BLOCAGE DANS LES ESSAIS

## EN SOUFFLERIE

## EFFETS DES DECOLLEMENTS

par

Jean-Ch. Vayssaire (\*)

Avions Marcel Dassault - Bréguet - Aviation

92 - Saint-Cloud

FRANCE

## RESUME

Les corrections de blocage, puis les corrections fonctions du coefficient de portance  $C_z$  doivent être appliquées aux résultats d'essais obtenus à partir de mesures effectuées sur les maquettes d'avions placées en soufflerie. Elles corrigent en grandeur et direction la vitesse "infini amont" et restituent ainsi aux coefficients aérodynamiques influencés par les parois des valeurs sensiblement égales à celles que l'on obtiendrait en plaçant le modèle dans un écoulement fluide illimité.

On analyse les termes correctifs de blocage qui modifient la pression cinétique de référence. Pour les maquettes non motorisées, ils sont au nombre de trois. Ils correspondent au volume de la maquette, à son sillage et à ses décollements. Chacun d'eux se présente sous une forme utilisable en régime incompressible, 2 dim, 3 dim, maquette complète, demi-maquette et en subsonique.

Les décollements sur l'aile apparaissent généralement aux grandes incidences. Les corrections appropriées résultent des travaux de Maskell développés dans le cas d'un écoulement incompressible dans une veine de soufflerie à parois guidées. Elles doivent être utilisées dès que la polaire expérimentale n'est plus confondue avec la polaire parabolique théorique. A iso- $C_z$ , elles sont fonctions de la différence des coefficients de traînée des deux polaires. Elles dépendent donc de l'allongement et de l'incidence des modèles. Elles permettent de regrouper les caractéristiques aérodynamiques de maquettes semblables de tailles différentes essayées dans plusieurs souffleries, en particulier dans le domaine du  $C_z$  maximum.

On étend ces corrections d'une part à des veines d'expériences comportant divers types de parois et d'autre part au subsonique.

Enfin on compare des résultats de souffleries ainsi corrigés avec des résultats d'essais en vol.

## SUMMARY

Blockage corrections, then corrections dependent on the lift coefficient  $C_l$ , must be applied to wind tunnel test measurements made on aircraft models. They correct the velocity "to infinity upstream", thus restoring to the wall affected aerodynamic coefficients, values which are fairly equivalent to those obtainable by placing the model in an unlimited fluid stream.

The corrective blockage terms which modify the reference kinetic pressure are analyzed. There are three of them in the case of non-powered models. They correspond to the model volume, wake and separations. Each of them assumes a form which is usable in incompressible, compressible, two-dimension and three-dimension flows, on whole or half-models.

Separation corrections result from the extension of Maskell's work. They appear at incidences for which the experimental polar does not coincide any longer with the theoretical parabolic polar. When the lift coefficients are identical, these corrections are functions of the difference between the drag coefficients of the two polars. Therefore, they depend on the model aspect ratio and incidence. They make it possible to derive the aerodynamic characteristics of similar models of different sizes tested in several wind tunnels, particularly within the  $C_{l_{max}}$  range.

(\*) Direction Générale Technique - Département Aérodynamique.

## NOTATIONS

Am	- Aire d'un profil dans le plan zx
B	- Epaisseur du sillage (au maître-couple du bulbe)
C	- Section de la veine de la soufflerie (voir tableau 1)
Cp	- Coefficient de pression
Cx	- Coefficient de traînée
Cxd	- Coefficient de traînée de décollements
Cz	- Coefficient de portance
Cz max	- Valeur maximum du coefficient de portance
H	- Hauteur de la veine d'essais (voir tableau 1)
M	- Nombre de Mach
S	- Surface de référence du modèle
V	- Vitesse du vent dans la direction des x
Vm	- Volume de la maquette
c	- Corde de référence d'un profil
k	- Paramètre de pression
P	- Pression statique
q	- Pression cinétique
u	- Composante dans la direction des x de la vitesse de perturbation
x,y,z	- Coordonnées cartésiennes
$\alpha$	- Incidence
$\beta$	- $\sqrt{1-M_0^2}$
$\varepsilon$	- Rapport des vitesses u/V, facteur de blocage
$\lambda$	- Allongement
$\lambda'$	- Allongement équivalent d'une aile
$\theta$	- Paramètre de blocage de décollements.

Indices

b	- Relatif au culot
c	- Corrigé
M	- Compressible
O	- Infini amont
u	- Non corrigé
1	- Blocage de volume
2	- Blocage de sillage
3	- Blocage de décollements.

## 1 - INTRODUCTION

## 1.1 - Généralités

Dans l'étude en soufflerie du comportement d'une maquette, la présence des parois qui limitent l'écoulement apporte une différence fondamentale avec l'écoulement en fluide illimité.

Les corrections de blocage, puis les corrections fonctions du coefficient de portance Cz rendent homogènes les résultats obtenus sur des maquettes d'un même avion testées dans diverses souffleries. En particulier, aux fortes incidences, lorsque prennent naissance des décollements, les corrections appropriées de blocage permettent le regroupement des résultats autour d'un même Cz maximum. Ces corrections de décollements viennent alors s'ajouter aux corrections de blocage de volume et de blocage de sillage déjà appliquées aux incidences pour lesquelles l'écoulement est potentiel.

On remarquera que l'ensemble de ces corrections ne doit être utilisé que lorsque les résultats bruts ont déjà été corrigés de l'effet des gradients éventuels propres aux veines d'expériences, de celui de l'ascendance du courant d'air, de l'interaction des supports, etc...

Mais, après avoir rendu homogènes les résultats des divers tunnels aérodynamiques, le problème final demeure la comparaison : soufflerie - vol.

## 1.2 - Corrections de blocage

On suppose la maquette non motorisée placée au centre de la veine d'essais. Si l'on désigne par  $q_c$  la pression cinétique corrigée et par  $q_u$  la pression cinétique de référence qui correspond à la vitesse "infini amont" vraie  $V_0$ , il vient, au niveau du modèle, en régime incompressible :

$$q_c \approx q_u \left(1 + 2 \frac{u}{V_0}\right) = q_u (1 + 2\varepsilon) \quad [1]$$

avec :

$$\varepsilon = \varepsilon_1 + \varepsilon_2 + \varepsilon_3 \quad [2]$$

Les définitions de  $\mathcal{E}_1$ , blocage de volume, de  $\mathcal{E}_2$ , blocage de sillage et de  $\mathcal{E}_3$ , blocage de décollements, sont données par le tableau 1. On a encore :

$$\left(\frac{\partial \mathcal{E}}{\partial x}\right)_{x=0} = \left(\frac{\partial \mathcal{E}_1}{\partial x}\right)_0 + \left(\frac{\partial \mathcal{E}_2}{\partial x}\right)_0$$

Alors que le gradient dû au blocage de sillage existe quel que soit le type de parois, le gradient dû au blocage de volume n'apparaît que pour les parois perméables sous l'influence de la viscosité de l'air qui les traverse.

Dans la présente étude, on ne s'intéresse qu'au blocage de décollements,  $\mathcal{E}_3$ , qui de par la nature des hypothèses de calcul, ne comporte pas de gradients. Sa contribution est essentielle dans le pourcentage des corrections appliquées aux résultats obtenus aux incidences élevées et plus spécialement en ce qui concerne les  $C_z$  et le domaine du  $C_z$  maximum.

## 2 - SCHEMA DES ECOULEMENTS DECOLLES

Alors que l'on sait calculer  $\mathcal{E}_1$  et  $\mathcal{E}_2$  à partir de modèles mathématiques, tels que doublets ou sources, et de leurs images, on remarque qu'il n'existe pas de modèles représentatifs des décollements. On doit admettre actuellement le principe de la solution semi-empirique des problèmes techniques, fondée sur la notion d'eau morte (1).

### 2.1 - Plaques planes

Le coefficient  $\mathcal{E}_3$  est établi en analysant physiquement des écoulements décollés derrière des plaques planes exposées normalement au vent (2).

L'écoulement autour et en aval de plaques rectangulaires, de divers allongements, se ramène toujours à celui représenté sur la fig. 1, observé derrière un disque circulaire. Il a une forte tendance à prendre une symétrie axiale. Sa principale caractéristique est la formation d'un bulbe fermé, dit "eau morte", où la ligne  $\psi = 0$  est considérée comme sa limite. A partir du bord extérieur du disque se détache une ligne de courant, frontière, à l'extérieur de laquelle il n'y a pas de pertes de charge totale.

Jusqu'à la moitié de la longueur du bulbe, dont la section droite est maximum en cette abscisse, cette frontière demeure isobare et sa pression statique est égale à la pression de culot  $p_b$ , mesurée sur la face arrière du disque. Au-delà de cette abscisse, il se produit une recompression. Un tel aspect d'écoulement symétrique se retrouve derrière une plaque, en allongement infini (3,4).

Comme  $p_b$ , la longueur du bulbe varie avec l'allongement (tableau 2). Mais cette dimension n'intervient pas dans la suite des calculs.

### 2.2 - Ailes décollées

On observe encore ce type d'écoulement, avec tendance à la symétrie axiale, derrière une aile placée à forte incidence.

Comme le mentionne Hancock (5), les exemples publiés sont peu nombreux. Cependant, on confirme de tels écoulements à partir d'études anémométriques effectuées en aval d'ailes droites avec ou sans volets braqués (6), ou d'ailes en flèche ou delta (7). On peut les schématiser ainsi qu'il est montré sur la figure 2.

Actuellement, le tunnel hydrodynamique de la Direction Aérodynamique de l'O.N.E.R.A. apporte une importante contribution dans le domaine des visualisations.

Les fig. 3a, 3b, 3c, photographies prises dans ce laboratoire, mettent en évidence des écoulements avec bulbe d'eau morte aussi bien localement derrière des volets (8) que globalement en arrière de profils (1, 8).

### 2.3 - Remarques

Les tourbillons d'apex, bien organisés, de la figure 4, qui apparaissent sur une aile delta, par exemple, à faible incidence, sont entièrement différents des décollements avec bulbe d'eau morte (9).

Mais, lorsque l'incidence croît, le tourbillon éclate d'abord en aval du bord de fuite, puis remonte vers le bord d'attaque et sur la figure 5, on retrouve un décollement qui se rapproche de ceux observés sur les figures 2 et 3 (9).



## 3 - THEORIE DE MASKELL (10-11)

En l'absence d'études théoriques sur la connaissance du mécanisme interne des décollements, Maskell s'attache à évaluer leur forme globale et à essayer de reproduire leurs effets extérieurs au voisinage du modèle. Pour cela il reprend le schéma d'écoulement relatif au disque circulaire de la figure 1. Il définit une surface frontière entre le sillage et l'écoulement externe non perturbé. Elle s'étend de la plaque plane jusqu'au plan 2 où la section droite du bulbe est maximum. Sur cette surface, la pression  $p_b$  est constante et égale à la pression de culot de la plaque. La vitesse correspondante est  $k.V_0$  où  $V_0$  désigne la vitesse dans le plan 1 (figure 6) ; Maskell considère alors un tel schéma d'écoulement incompressible placé dans une soufflerie comportant des parois guidées. Le but recherché consiste à obtenir une estimation quantitative de la contrainte de paroi sur le coefficient  $k$  - Autrement dit, connaissant le coefficient  $k$  en soufflerie, il convient de déterminer le coefficient  $k_c$  en écoulement libre.

L'hypothèse essentielle consiste à supposer que la contrainte se traduit uniquement par un accroissement de vitesse par rapport à l'écoulement illimité. On pose ainsi que la distribution de pression  $p$  sur le corps n'est pas influencée par la paroi ( $x$ ).

Donc, le rapport :

$$\frac{P - P_b}{H_0 - P_b}$$

doit être indépendant de la contrainte. Mais :

$$H_0 = P_0 + \frac{\rho}{2} V_0^2 = P_b + \frac{\rho}{2} k^2 V_0^2$$

Un coefficient de pression de culot :

$$C_{Pb} = \frac{P_b - P_0}{q_u} = 1 - k^2$$

étant alors défini, la précédente hypothèse revient à écrire :

$$\frac{P - P_b}{k^2 q_u} = \frac{C_x}{k^2} = \frac{C_x}{1 - C_{Pb}} = \text{Constante}$$

Cette dernière relation a été vérifiée expérimentalement et trouvée égale à 0,837. Elle justifie donc l'hypothèse de départ tout en montrant que  $\partial \epsilon_3 / \partial x = 0$ . Ainsi :

$$\frac{k^2}{k_c^2} = \frac{C_x}{C_{xc}} = \frac{V_0^2}{V_c^2} = \frac{1 - C_{Pb}}{1 - C_{Pbc}}$$

Puis on établit la conservation des quantités de mouvement dans l'écoulement non perturbé à travers la surface de contrôle définie sur la figure 6. Elle est formée des parois guidées de la soufflerie, de la surface du corps et de la surface isobare limitant le sillage effectif ainsi que des plans 1 et 2 normaux au vecteur vitesse  $V_0$ . On considère, dans le plan 1, la section de passage C où la vitesse est  $V_0$  et dans le plan 2, la section C - B où la vitesse est  $V_2$ . Par continuité, avec  $m = B/S$  :

$$V_2 = V_0 \frac{C}{C-B} = V_0 \left(1 - \frac{B}{C}\right)^{-1} = V_0 \left(1 - m \frac{S}{C}\right)^{-1}$$

Négligeant les termes du second ordre, on arrive à :

$$C_x = m \left(k^2 - 1 - m \frac{S}{C}\right),$$

relation qui se vérifie encore expérimentalement.

Si le disque de surface  $S$  est placé en atmosphère illimitée, ou, ce qui revient au même, si l'on fait tendre vers zéro le rapport  $S/C$ , la relation précédente devient :

$$C_{xc} = m_c (k_c^2 - 1)$$

(\*) La répartition des pressions sur un cylindre circulaire est influencée par la présence de parois. Un tel corps, par exemple, n'est donc pas redevable de cette théorie. On utilisera plutôt les formules de corrections de l'effet du blocage données par Glauert dans l'A.R.C. Rand M 1566 - 1933 - pp 56 - 59.

Alors, si l'on pose  $m = mc$ , avec  $C_x/k^2 = \text{Constante}$ ,  
on a :

$$\frac{C_x}{C_{xc}} = \frac{k^2}{k_c^2} = 1 + \frac{C_{xc}}{k_c^2 - 1} \cdot \frac{S}{C} \quad [3a]$$

L'expérience invalide cette relation. On doit faire intervenir la distorsion du sillage, c'est-à-dire, écrire :  $m \neq mc$ . Sous l'effet des parois, le sillage a tendance à se contracter. Une relation auxiliaire est introduite, telle que :

$$\frac{m}{mc} = 1 - f(C_x, C_{xc}, C_{pb}, C_{pbc}) \frac{S}{C}$$

et qui, supportée par quelques expériences, conduit à remplacer, dans le second terme du membre de droite de l'éq. 3a, le coefficient  $C_{xc}$  par le coefficient  $C_x$  mesuré.

Il en résulte les relations fondamentales :

$$\frac{k^2}{k_c^2} = \frac{C_x}{C_{xc}} = 1 + \frac{C_x}{k_c^2 - 1} \cdot \frac{S}{C} \quad [3]$$

$$\frac{1 - C_{pb}}{1 - C_{pbc}} = 1 + \frac{C_x}{k_c^2 - 1} \cdot \frac{S}{C} \quad [4]$$

que l'on peut transcrire en forme usuelle de correction de pression cinétique :

$$\frac{q_c}{q_u} = 1 + \frac{C_x}{k_c^2 - 1} \cdot \frac{S}{C}$$

ou :

$$2\varepsilon_3 = \frac{\Delta q}{q_u} = \theta \frac{S}{C} C_x \quad [5]$$

avec :

$$\theta = \frac{1}{k_c^2 - 1} = - \frac{1}{C_{pbc}}$$

A partir de coefficients de pression de culot mesurés sur la face arrière de plaques planes rectangulaires, placées normales au vent, d'allongement variable de 1 à 20 (2) et d'allongement infini (4), des valeurs de  $\theta$  sont données dans le tableau 2 et placées sur la figure 7.

Toutefois, pour des plaques de même allongement,  $\theta$  peut varier d'une soufflerie à une autre, toutes choses égales par ailleurs (10). Ainsi, pour un allongement égal à un, il a été trouvé soit  $\theta = 2,77$  avec  $C_{pbc} = -0,361$ , soit  $\theta = 2,66$  avec  $C_{pbc} = -0,375$ . Cette différence est vraisemblablement liée à la turbulence du courant d'air dans la veine d'essais.

En allongement infini,  $\theta$  varie avec l'inclinaison de la plaque par rapport à la direction du vent et son évolution en fonction de l'incidence, donnée dans le tableau 3, correspond sensiblement à celle obtenue avec des profils (4).

#### 4 - GENERALISATION

Une double démarche, hardie mais justifiée par l'expérience comme il est montré dans les conclusions, permet de transcrire le résultat dû à l'observation de l'écoulement derrière une plaque plane, fondée sur la notion d'eau morte, en termes de corrections de blocage dû aux décollements sur une aile placée à forte incidence.

La première, basée sur l'analogie entre les écoulements rapportée dans le paragraphe 2, consiste à utiliser l'éq. 5 comme terme correctif de pression cinétique autour d'une aile décollée (10, 11). Alors, pour des allongements compris entre 1 et 10, Maskell propose d'adopter  $\theta = 2,5$  et pour l'allongement infini,  $\theta = 1$ . Reste à définir le coefficient de traînée de décollement,  $C_{xd}$ , qui doit être substitué au coefficient  $C_x$  de l'éq. 5. Ces deux paramètres  $\theta$  et  $C_{xd}$  sont discutés plus loin.

La seconde démarche propose d'additionner le coefficient  $\varepsilon_3$  aux coefficients  $\varepsilon_1$  et  $\varepsilon_2$  comme le montre l'éq. 2 (10, 11, 12). En l'absence de décollements, la correction de pression cinétique apparaît sous sa forme usuelle (12, 13). Cette superposition linéaire, qui évite toute discontinuité dans les calculs, se confirme par le fait que les décollements n'apparaissent

pas généralement d'une façon subite. Ils s'amorcent, par exemple, vers le bord de fuite d'un profil pour remonter vers son bord d'attaque, avec le bulbe d'eau morte (fig. 3a et 3b).

Ce phénomène est aussi vrai en bidimensionnel qu'en tridimensionnel, Mais dans ce dernier cas, de plus, ils s'étendent progressivement à toute l'envergure de l'aile. On doit enfin remarquer que si les coefficients  $\epsilon_1$  et  $\epsilon_2$  sont fonctions de la position de la maquette dans la veine d'essais puisqu'ils sont établis à partir de la théorie des images, le coefficient  $\epsilon_3$  est indépendant de cette position de par la nature même de son calcul (14).

#### 4.1 - Coefficient $\theta$ - Tarage des souffleries

Il peut sembler prudent, à cause de la turbulence, de contrôler la valeur de  $\theta$  pour chaque soufflerie munie de veines à parois guidées. Mais il devient impératif de connaître la valeur de ce paramètre pour tout autre type de parois, comme par exemple, pour des veines rectangulaires semi-guidées.

Pour cela, on place successivement dans la veine d'expériences des plaques planes soit circulaires, soit rectangulaires de même allongement, mais de surfaces  $S$  différentes. Leurs coefficients de traînée  $C_x$  sont mesurés. Par un procédé graphique, il est possible de déterminer la valeur de  $\theta$ , puisque grâce à l'équation 3 :

$$\frac{C_x}{C_{x_c}} = 1 + \frac{C_x}{k_c^2 - 1} \cdot \frac{S}{C} \quad [3]$$

on a :

$$\theta = \frac{1}{C_{x_c}} \cdot \frac{C_x - C_{x_c}}{\Delta S/C \cdot C_x} = \frac{\lg \varphi}{C_{x_c}}$$

où  $C_{x_c}$  désigne la valeur du  $C_x$  obtenu lorsque  $S/C$  tend vers zéro. Autrement dit,  $C_{x_c}$  est la valeur du coefficient de traînée de la plaque de surface  $S$  comme si elle était soumise à un écoulement en atmosphère illimitée.

On peut encore mesurer les coefficients de pression de culot en arrière des plaques et, se rappelant que :

$$\frac{C_x}{k^2} = \text{constante},$$

tracer simplement  $C_{pb}$  en fonction de  $S/C$ . On en déduit pour  $S/C = 0$ , le coefficient :

$$\theta = - \frac{1}{C_{pb_c}}$$

Si les pressions sur la face arrière des plaques sont perturbées, on peut prendre leur valeur moyenne (4). Cependant, dans ce cas, la méthode par les  $C_x$  semble préférable.

Des exemples sont proposés sur les figures 8 et 9. La figure 8 est relative à la soufflerie circulaire guidée n° 1 de l'Institut Aérotechnique de Saint-Cyr (15). On obtient  $\theta = 2,69$ , valeur placée sur la figure 7.

La figure 9 correspond à des tarages effectués dans la veine rectangulaire semi-guidée de la soufflerie Bréguet à Vélizy (16). On a deux valeurs de  $\theta$  à savoir 1,92 et 2,18. On adopte  $\theta = 2$ . Ces points sont également portés sur la figure 7.

#### 4.2 - Définition du coefficient de traînée de décollement $C_{xd}$

Le coefficient de traînée de décollement  $C_{xd}$  est le paramètre le plus important car il définit, en fait, l'allure de la polaire expérimentale. Il apparaît aux incidences pour lesquelles cette polaire n'est plus confondue avec la polaire parabolique théorique, parallèle à la polaire induite. A iso- $C_z$ , le coefficient  $C_{xd}$  n'est autre que la différence des coefficients de traînée de ces deux polaires :

$$C_{xd} = C_{xu} - \left( C_{xu_{c.o}} + \frac{C_{zu}^2}{\pi \lambda^2} \right),$$

où  $\lambda^2$  désigne l'allongement équivalent de l'aile,  $C_{xu}$  et  $C_{zu}$  les coefficients expérimentaux bruts et en supposant que le  $C_x$  minimum correspond au coefficient de portance nulle.

Bien souvent, les corrections de blocage ne sont pas utilisées d'une façon systématique. Celles dues aux décollements ne le sont qu'accessoirement et servent uniquement de contrôle (17). On détermine alors le  $C_{xd}$  graphiquement (10, 11). Dans les cas simples, on trace  $C_{xu}$  expérimental en fonction du  $C_{zu}^2$  (fig. 10). Les points expérimentaux se placent sur la droite de pente  $1/\pi \lambda^2$  puis s'en éloignent dès qu'apparaissent les décollements, d'où, par différence, les valeurs de  $C_{xd}$ .

On peut rapprocher de cette méthode, celle qui, utilisée actuellement en bidimensionnel (18), consiste à calculer la valeur de  $\pi \lambda^2$  en recherchant les coefficients  $C_{xuf}$  et  $C_{zuf}$  qui correspondent sur la polaire expérimentale au point de finesse maximale en supposant qu'à l'incidence correspondante il n'y ait pas de décollements. Pour un profil symétrique, on a :

$$\frac{1}{\pi \lambda^2} = \frac{C_{xuf}}{2 C_{zuf}^2}$$

#### 4.3 - Remarque importante

Depuis 1966, les Avions Marcel Dassault emploient couramment les relations de corrections (1) et (2). Puis, suivant les recommandations de la section Etudes Générales du Service Technique de l'Aéronautique du Gouvernement Français, dès 1968, ce procédé a été étendu à la plupart des souffleries françaises basse-vitesse qui corrigent leurs résultats bruts des effets du blocage (12).

Ces relations ont été nécessairement transformées en programmes machines pour être introduites dans les chaînes de dépouillements des résultats d'essais. Mais, revenant au blocage dû aux décollements, on exprime  $C_{xd}$  sous sa forme la plus générale, comme il est montré sur la fig. 11 :

$$C_{xd} = C_{xu} - \left[ C_{xum} + \frac{(C_{zu} - C_{zum})^2}{\pi \lambda^2} \right]$$

On recherche l'élément de parabole confondu avec la polaire expérimentale sur la plus grande plage de  $C_{zu}$  en utilisant la méthode des moindres carrés. Cette programmation rend aisée et précise la détermination de la valeur de  $\pi \lambda^2$  mais implique de connaître une plage de points expérimentaux limitée par un  $C_{zu}$  supérieur et un  $C_{zu}$  inférieur, bornes de la polaire sans décollements. Ce  $C_{zu}$  inférieur peut être aussi utilisé, par exemple, pour délimiter et rejeter du calcul de  $\pi \lambda^2$  la zone d'apparition d'une poche laminaire sur la polaire de certains profils. La recherche de la valeur de  $\pi \lambda^2$  défini par :

$$\frac{1}{\pi \lambda^2} = \frac{C_{xu} - C_{xum}}{(C_{zu} - C_{zum})^2}$$

est d'autant plus précise que les points expérimentaux sont plus serrés.

On remarque enfin que pour des ailes hypersustentées, et bien que l'avionneur s'intéresse surtout aux incidences élevées, on peut être amené, en soufflerie, à faire quelques points de mesures à des incidences très faibles (fig. 3a) pour délimiter la borne inférieure de la polaire théorique.

Ce procédé s'est révélé satisfaisant et d'un emploi tout à fait général même pour des ailes dont le  $C_z$  max. est de l'ordre de 3 (12).

#### 4.4 - Ecoulement compressible subsonique

L'introduction de la compressibilité est aisée. Grâce à l'utilisation de la règle de Göttert (19,20), avec  $\beta = \sqrt{1 - M_0^2}$  l'éq. 5 devient :

$$\varepsilon_{3M} = \frac{1}{\beta^2} \left[ \frac{\theta}{2} \cdot \frac{\beta S}{\beta^2 C} C_{xd} \right] = \beta^{-3} \frac{\theta}{2} \cdot \frac{S}{C} \cdot C_{xd}$$

$$\varepsilon_{3M} = \beta^{-3} \varepsilon_3$$

En première approximation, on admet que le coefficient  $\theta$  n'est affecté par la compressibilité que par l'intermédiaire de l'allongement qui s'exprime par  $\beta \lambda$ . Ainsi, en tridimensionnel et pour :

$$1 < \beta \lambda < 10,$$

on adopte la relation facile à introduire en machine (22) :

$$\theta = 2,8 - 0,068 \beta \lambda$$

qui, pour  $\beta = \sqrt{1 - M_0^2} = 1$ , se réduit à la relation proposée sur la figure 7 :

$$\theta = 2,8 - 0,068 \lambda$$

La polaire induite n'étant pas modifiée par la compressibilité, la recherche du  $C_{xd}$  se fait comme il a été écrit plus haut en 4.3. La borne supérieure du  $C_{zu}$  à partir de laquelle les deux polaires ne sont plus confondues décroît lorsque le nombre de Mach augmente. On a ainsi une limite à la détermination du  $C_{xd}$ .

Enfin les relations (1) et (2) s'écrivent maintenant :

$$q_c = q_u \left[ 1 + (2 - M_0^2) \varepsilon_M \right]$$

avec

$$\varepsilon_M = \varepsilon_{1M} + \varepsilon_{2M} + \varepsilon_{311}$$

Les facteurs de compressibilité qui affectent  $\epsilon_1$ ,  $\epsilon_2$  et  $\epsilon_3$  sont donnés dans le tableau 1. En outre, intervient une correction sur le nombre de Mach :

$$\Delta M = \epsilon_M (1 + 0,2 M_0^2) M_0$$

qui, à cause de la linéarisation, n'a une signification que lorsqu'elle demeure inférieure à 4 % de  $M_0$ .

## 5 - CONCLUSIONS

### 5.1 - Remarques

En conclusion, on va prouver par des exemples la justesse des idées émises précédemment. On fera également, suivant les méthodes préconisées par l'AGARD, quelques recommandations afin de situer les résultats acquis par rapport à ceux qui demandent encore certaines précisions.

Le support de toute théorie semi-empirique demeure sa vérification expérimentale. C'est pourquoi la démonstration de la validité de la théorie de Maskell et de sa généralisation ne peut être apportée que par l'utilisation intensive des relations de corrections de blocage dû aux décollements qui apparaissent sur des ailes placées dans un écoulement incompressible à des incidences élevées ou même à des incidences modérées dans un écoulement compressible. Leur application aux résultats d'essais bruts obtenus à partir des maquettes d'un même avion, réalisées à différentes échelles, placées dans diverses souffleries, permet le regroupement de leurs caractéristiques aérodynamiques. Pour une même configuration de vol, les résultats corrigés deviennent homogènes. Mais l'effet essentiel des corrections de décollements demeure le regroupement des coefficients de portance autour d'une même valeur et tout spécialement dans le domaine des  $C_z$  max.. Les exemples proposés concernent les Avions Marcel Dassault : MIRAGE III, MIRAGE G, MIRAGE F. De plus, des résultats d'essais en vol viennent confirmer les résultats de souffleries ainsi corrigés, obtenus en tridimensionnel incompressible aussi bien sur maquettes complètes que sur demi-maquettes à la paroi.

En tridimensionnel compressible, les résultats relatifs à des maquettes complètes sont satisfaisants. Mais l'utilisation de ces corrections n'en est encore qu'au stade préliminaire. Il en est de même pour le bidimensionnel quoiqu'encore les résultats obtenus soient déjà plus nombreux.

### 5.2 - Etudes en cours - Bidimensionnel

Une remarque s'impose : il est rare que l'allongement infini soit réalisé et l'allongement équivalent  $\lambda'$  dépend surtout du montage expérimental. Il est souvent de l'ordre de 20 à 30 bien qu'il atteigne des valeurs voisines de 50 comme dans la soufflerie S1 de l'O.N.E.R.A. à Cannes (21), ces valeurs de  $\lambda'$  étant déterminées dans le domaine sans décollements. Le coefficient  $\theta$  semble alors pouvoir être déduit de la fig. 7. Mais  $\theta$  est variable avec l'incidence comme le montre le tableau 3 (4, 10). Ainsi,  $\theta$  est déterminé par une double entrée :

$$\theta_{\lambda=\infty}(\alpha) \text{ et } \theta_{\alpha=90^\circ}(\lambda')$$

On est donc tenté de prendre  $\theta$  légèrement supérieur à 1.

Des essais récents et comparatifs, entrepris à basse vitesse, sur un même profil de corde  $c$  placé dans deux souffleries de hauteurs  $H$  différentes confirment que  $\theta$  doit être compris entre 1 et 1,15, l'influence de l'allongement équivalent étant prépondérante. Ces valeurs de  $\theta$  peuvent être conservées jusqu'à  $M_0 \approx 0,3$ , limite d'utilisation actuelle de la soufflerie S 10 du C.E.A.T. (18).

Pour déterminer et préciser  $\theta$ , dans le cas de profils décollés placés en présence de parois guidées ou perméables à nombres de Mach élevés, on envisage, en se servant de l'éq. 3, d'utiliser d'une part la valeur moyenne de leurs coefficients de pression d'extrados et d'autre part leurs coefficients de traînée. Regrouper autour d'une même valeur les  $C_z$  max d'un profil, mesurés en présence de parois de perméabilités différentes, justifierait cette méthode.

De tels essais sont actuellement en cours dans la soufflerie  $R_1$  Ch de l'ONERA à Chalais Meudon. Mais dès à présent, on doit mentionner que même pour des nombres de Mach de 0,8, on obtient des valeurs de  $\theta$  qui sont en bon accord avec celles du tableau 3. L'allongement équivalent étant très élevé, l'influence de l'effet d'incidence semble importante.

Dans tous les cas, on doit se rappeler le modèle proposé par Maskell et la nature des décollements a été observée en particulier à  $R_1$  Ch par films cinématographiques.

### 5.3 - Etudes en cours - Résultats acquis - tridimensionnel compressible

Pour des nombres de Mach compris entre 0,5 et 0,9 et à incidence variable, un avion de transport muni d'une aile en flèche, d'allongement voisin de 7, a été essayé dans la soufflerie  $\Sigma 4$  de l'Institut Aérotechnique de Saint-Cyr dont la veine carrée se prête à la réalisation de deux configurations :

- veine à quatre parois pleines ;
- veine à parois verticales pleines et à parois horizontales perforées possédant une perméabilité géométrique de 29 %.

Dans les deux cas, le rapport de la surface  $S$  de l'aile à la section  $C$  de la veine est égal à  $1/24$ , et les corrections de blocage de volume  $\epsilon_{1M}$  et de sillage  $\epsilon_{2M}$  sont négligeables ou nulles (22). L'effet des décollements apparaît sur les courbes issues de la veine guidée. L'application des corrections en  $\epsilon_{3M}$  correspondantes du paragraphe 4.4, donne des résultats satisfaisants comme il est prouvé par les exemples de la figure 13.

#### 5.4 - Résultats acquis - Tridimensionnel incompressible

##### Maquettes complètes et demi-maquettes à la paroi

##### 5.4.1 - Ailes delta

La fig. 12 montre des résultats obtenus sur des maquettes d'ailes delta du type de celles dont sont équipés les avions DASSAULT : MIRAGE III et IV. On confirme ainsi les corrections appliquées par Maskell à des ailes delta d'allongement 3 placées à des incidences supérieures à  $15^\circ$  (10, 11). Cependant, il convient de faire une remarque. Revenons à la fig. 12. En fait, pour les incidences inférieures à  $12^\circ$ , les résultats sont redevables des corrections  $\epsilon_1$  et  $\epsilon_2$  uniquement, c'est-à-dire que le tourbillon d'apex, bien organisé, créateur de portance tourbillonnaire, n'est en aucun cas assimilable à un décollement du type d'eau morte. Mais dès que l'incidence atteint et dépasse  $12^\circ$ , la courbe unitaire de portance s'infléchit. Le tourbillon d'apex s'épanouit et on doit alors ajouter le terme correctif  $\epsilon_3$ , dû aux décollements.

##### 5.4.2 - Avion MIRAGE G

On donne quelques exemples d'application des corrections de blocage, en mettant en évidence la part de celle due aux décollements, à des résultats de maquettes et demi-maquettes de l'avion MIRAGE G dans sa configuration ; voilure en flèche modérée, fortement hypersustentée.

Les essais ont été réalisés dans les souffleries du C.E.A.T., à Toulouse, de l'ONERA, à Chalais-Meudon et BREGUET à Vélizy, les courbes correspondantes sont données sur les fig. 14 et 15. On a également porté l'importance des corrections les unes par rapport aux autres.

A partir de fortes incidences, le terme en  $\epsilon_3$  peut être de l'ordre de grandeur de  $\epsilon_1 + \epsilon_2$ , voir même supérieur.

Enfin, on doit noter que dans la soufflerie BREGUET, bien que le coefficient  $\theta$  soit pris égal à 2, la correction  $\epsilon_3$  est très faible et n'intervient qu'à partir d'un  $C_z$  voisin du  $C_z$  max.. Ce résultat est important car il met en évidence la part prépondérante de la poire et du Cxd. De plus, on se appellera que dans cette soufflerie  $\epsilon_1 \approx \epsilon_2 \approx 0$ , de par la nature des parois : veine rectangulaire semi-guidée par plancher et plafond.

##### 5.4.3 - Avion MIRAGE F

La figure 16 donne des résultats obtenus, avant et après corrections, sur des maquettes et demi-maquettes de l'avion MIRAGE F. Son aile, en forte flèche, est fortement sustentée.

Les essais ont été effectués dans les souffleries de l'Institut Aérotechnique de Saint-Cyr, de l'O.N.E.R.A., à Chalais-Meudon, et du C.E.A.T., à Toulouse.

On remarque encore, sur la figure 17, à forte incidence, l'importance des corrections de décollements dans le cas du grand encombrement ou  $S/C \approx 1/5$ .

##### 5.4.4 - Soufflerie - Vol

La figure 18 compare des résultats de souffleries corrigés avec ceux du vol et montre la confiance qu'il est permis d'accorder aux corrections de blocage de décollements superposées à celles de volume et sillage même pour des valeurs élevées de  $S/C$ . L'estimation de  $\epsilon_3$ , grande par rapport à  $\epsilon_1 + \epsilon_2$ , est largement satisfaisante.

Maskell pensait que le support de sa théorie, relative aux écoulements derrière des plaques planes, et transposée aux ailes portantes décollées, ne pouvait provenir que des résultats obtenus après application de la correction de blocage elle-même (10 - p. 15).

Les quelques exemples proposés prouvent la validité de telles hypothèses. On a donc généralisé l'utilisation des corrections de façon à rendre leur emploi systématique dans la technique des essais de souffleries.

## 6 - REFERENCES

- (1) P. Carrière - Confluences d'écoulements - Notions générales sur les problèmes de confluences -  
Revue Française de Mécanique - n° 24 Paris 1967 - pp 7 - 28.
- (2) R. Fail  
J.A. Lawford  
R.C.W. Eyre - Low-speed experiments on the wake characteristics of flat plates normal to an  
air-stream.  
A.R.C. R and M - 3120 London 1957.
- (3) A. Fage  
F.C. Johansen - On the flow of air behind an inclined flat plate of infinite span -  
A.R.C. R and M 1104 - London 1927.
- (4) A. Fage  
F.C. Johansen - The structure of vortex sheets  
A.R.C. R and M 1143 - London 1927.
- (5) G.J. Hancock - Problems of aircraft behaviour at high angles of attack -  
AGARD ograph 136 - 1969.
- (6) Silverstein  
et al. - Downwash and wake behind plain and flapped aerofoils -  
NACA Reports 648-651 - 1939.
- (7) D.A. Kirby  
A. Spence - Low speed - tunnel model tests on the flow structure behind a delta-wing aircraft  
and a 40 deg swept wing aircraft at high incidences -  
A.R.C. R and M 3078 - London 1955.
- (8) H. Werlé  
M. Gallon - Contrôle d'écoulements par jet transversal -  
L'Aéronautique et l'Astronautique - N° 34 - pp 21 - 33 - Paris 1972 - 2.
- (9) H. Werlé - Sur l'éclatement des tourbillons  
O.N.E.R.A. Note technique n° 175 - 1971.
- (10) E.C. Maskell - A theory of the blockage effect on bluff bodies and stalled wings in a closed  
wind-tunnel -  
A.R.C. R and M 3400 London 1963.
- (11) E.C. Maskell - Bluff bodies and high-lift systems -  
AGARD ograph 109 - Chapter VII - 1966.
- (12) J.C. Vayssaire - Nouvelle méthode de calcul de correction des résultats d'essais en soufflerie  
basse-vitesse.  
L'Aéronautique et l'Astronautique n° 15 et 16 - Paris 1969.
- (13) F.W.E. Rogers - Blockage effects in closed or open tunnels -  
AGARD ograph 109 - Chapter V - 1966.
- (14) R.W.F. Gould - Wake blockage corrections in a closed wind tunnel for one or two wall-mounted  
models subject to separated flow.  
A.R.C. R and M 3649 - London 1969
- (15) J. Barbieux - Contribution à l'étude de l'effet de paroi en écoulement plan incompressible -  
Publications Scientifiques et Techniques du Ministère de l'Air n° 304 - Paris 1956.
- (16) Fréguet-  
Aviation - Comparaison d'essais dans trois souffleries. Résultats avec et sans corrections  
de blocage -  
Avion ECAT JAGUAR DT/AC - Soufflerie PT/JZ n° 137/67 - Rapport non publié.
- (17) D. Isaacs - Wind-tunnel measurements of the low speed stalling characteristics of a model of  
the Hawker-Siddeley Trident 1 C -  
A.R.C. R and M 3608 - London 1968.

- (18) L.Taurel - 1ère p - Présentation de la soufflerie S.10 du C.E.A.T.  
 E.Erich 2ème p - Exemples de recherches sur les profils dans la soufflerie S.10 du C.E.A.T.  
 O.N.E.R.A. TP N° 766 - 1969.  
 6ème Colloque d'Aérodynamique Appliquée -  
 A.F.I.T.A.E. Toulouse 1969.
- (19) B.Güthert - Ecoulement plan et spatial dans le domaine subsonique (Généralisation de la règle  
 de Prandtl) - Bericht 127 der Lilienthal Gesellschaft für Luftfahrtforschung -  
 Berlin 1940 - pp. 97 - 101.  
 - Traduction française - S.D.I. n° 3693  
 Ministère de l'Armement - Paris 1946.  
 - Traduction américaine - NACA TM 1105 - 1946.
- (20) B.Güthert - Transonic wind tunnel testing -  
 AGARDograph 49 - 1961 p.97.
- (21) A.de Sievers - Communication privée - 1970.
- (22) I.A.T. - Etude en écoulement transsonique  
 St-Cyr Institut Aérotechnique de Saint-Cyr  
 Rapport 347 4 - 1972.
- (23) J.C.Vayssaire - Essais en soufflerie basse vitesse - Corrections de blocage et de parois sur  
 maquettes du MIRAGE G.  
 Avions Marcel Dassault - Saint-Cloud.  
 Note Aéro n° 770 - 1967.
- (24) J.C.Vayssaire - Essais en soufflerie - Corrections de blocage et de parois sur maquettes du  
 MIRAGE F -  
 Comparaison vol - soufflerie -  
 Avions Marcel Dassault - Saint-Cloud -  
 Note Aéro n° 742 - 1967 -



TABLEAU 1

## Facteurs de correction de blocage

$$\varepsilon = \varepsilon_1 + \varepsilon_2 + \varepsilon_3$$

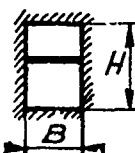
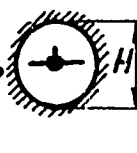
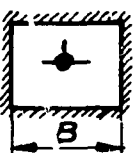

2 Dimensions	$\varepsilon = \Omega_1 \cdot \frac{\pi}{6} \cdot \frac{Am}{H^2} + \Omega_2 / 4 \cdot \frac{c}{H} \cdot Cx_u + \theta / 2 \cdot \frac{c}{H} \cdot Cx_d$						
	Veine	$\Omega_1$	$\Omega_2$	$\theta$			
	Guidée	1	1	1			
	Libre	-0,5	0				
3 Dimensions	$\varepsilon = \Omega_1 \cdot \frac{Vm}{c^{3/2}} + \Omega_2 / 4 \cdot \frac{S}{c} \cdot Cx_u + \theta / 2 \cdot \frac{S}{c} \cdot Cx_d$						
	Veine	$\Omega_1$	$\Omega_2$	$\theta$			
	Guidée	1	1	2,5			
	Libre	-0,25	0				
Facteur de compress. $\beta$		$\varepsilon_{1M} = \beta^{-3} \cdot \varepsilon_1$	$\varepsilon_{2M} = \frac{1+0,4M_o^2}{\beta^2} \cdot \varepsilon_2$	$\varepsilon_{3M} = \beta^{-3} \cdot \varepsilon_3$			
2 dim.		3 dim.		3 dim.		3 dim.	
$C = B.H$		$C = \frac{\pi H^2}{4}$		$C = B.H$		$C < \frac{\pi H^2}{4}$	

TABLEAU 2

$$\theta = f(\lambda) \quad 2 \text{ et } 3 \text{ Dimensions}$$

$\lambda$	1	2	5	10	20	$\infty$
$S/c \%$	1,45	1,45	1,45	1,45	1,45	7,15
$x/\sqrt{S}$	2,96	2,86	2,46	2,26	0,96	
$Cp_{bc}$	-0,360	-0,370	-0,415	-0,470	-0,680	-1,04
$\theta$	2,77	2,70	2,41	2,13	1,47	0,96

TABLEAU 3

$$\theta = f(\alpha^\circ) \quad 2 \text{ Dimensions}$$

	Profils		Plaque plane		Profils	Plaque plane		
$\alpha^\circ$	10	20	30	40	45	50	70	90
$Cp$	-0,70	-0,78	-0,80	-0,92	-0,94	-0,92	-0,91	-1,05
$\theta$	1,43	1,28	1,25	1,08	1,06	1,02	1,10	0,96

Fig 1 Ecoulement derrière un disque  
circulaire de surface S

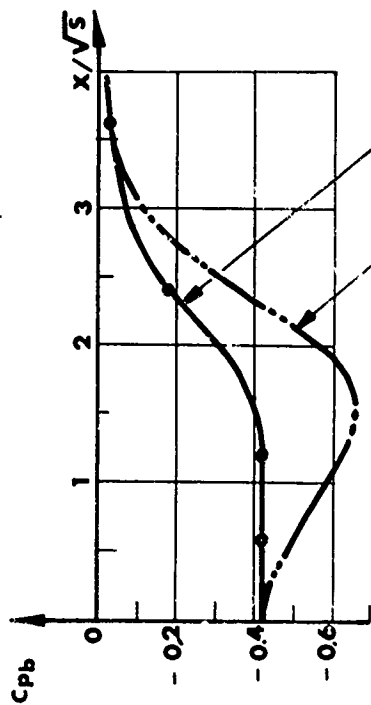
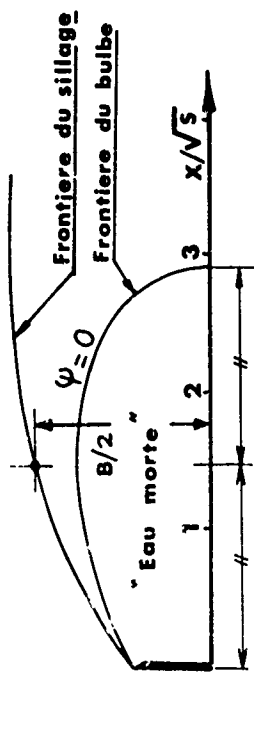
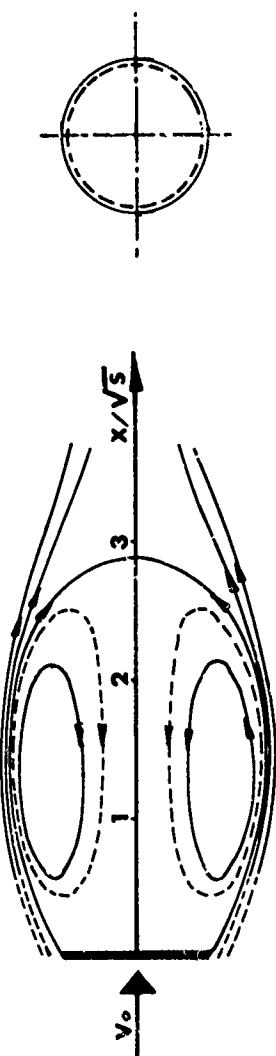


Fig 6 Modele de MASKELL

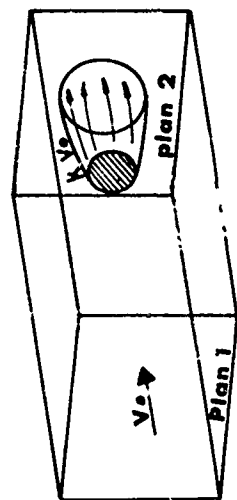
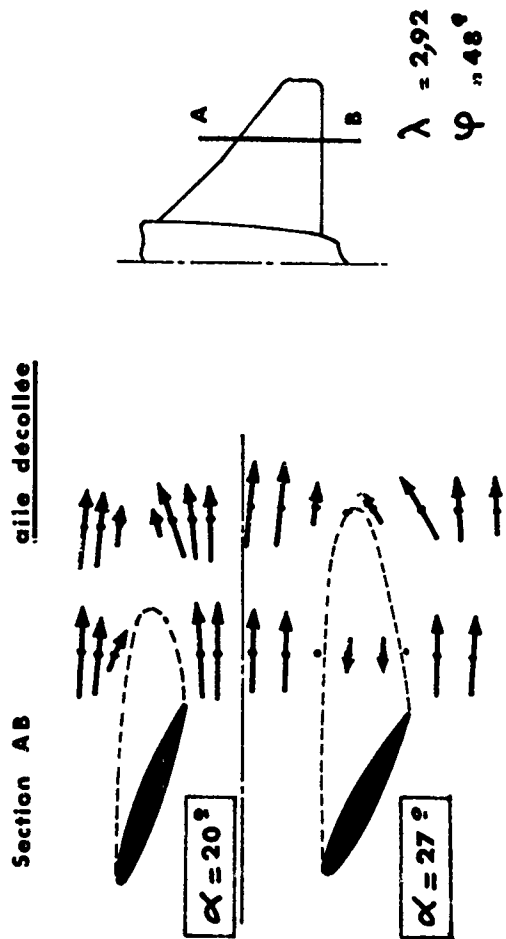


Fig 2 Ecoulement 3 dim derrière une  
aile décollée



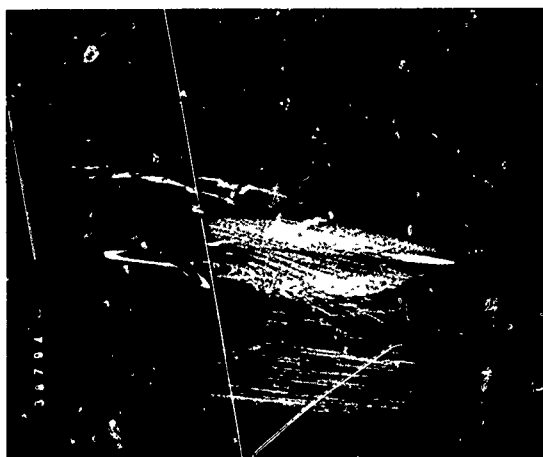
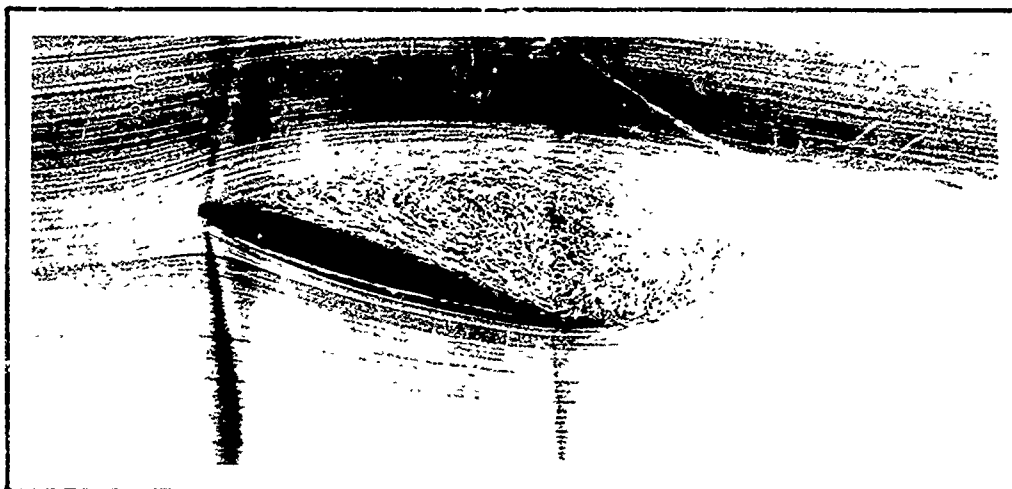


Fig 3a:       $\alpha = 2,5^\circ$   
*Volet braqué à  $25^\circ$*   
*(Décollement local sur le volet)*



Fig 3b:       $\alpha = 10^\circ$   
*Volet braqué à  $25^\circ$*   
*(Décollement sur toute la voilure)*



*Fig 3c: Profil 2 dim.  $\alpha = 15^\circ$*



*Fig 4: Tourbillon d'apex organisé*

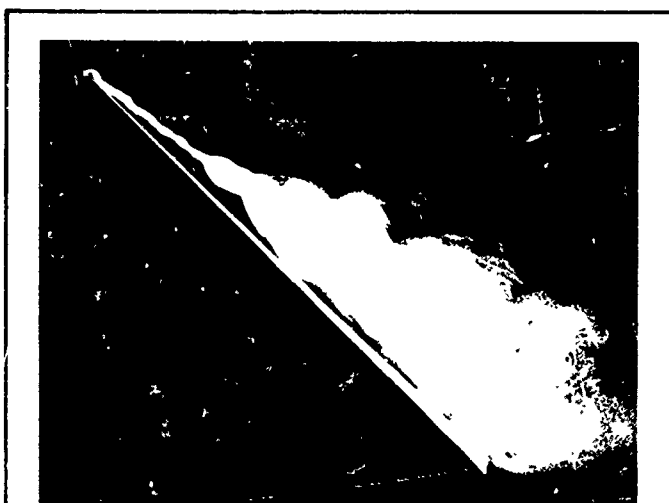


*Fig 5: Tourbillon d'apex éclaté*

*Photos Laboratoire hydrodynamique ONERA*

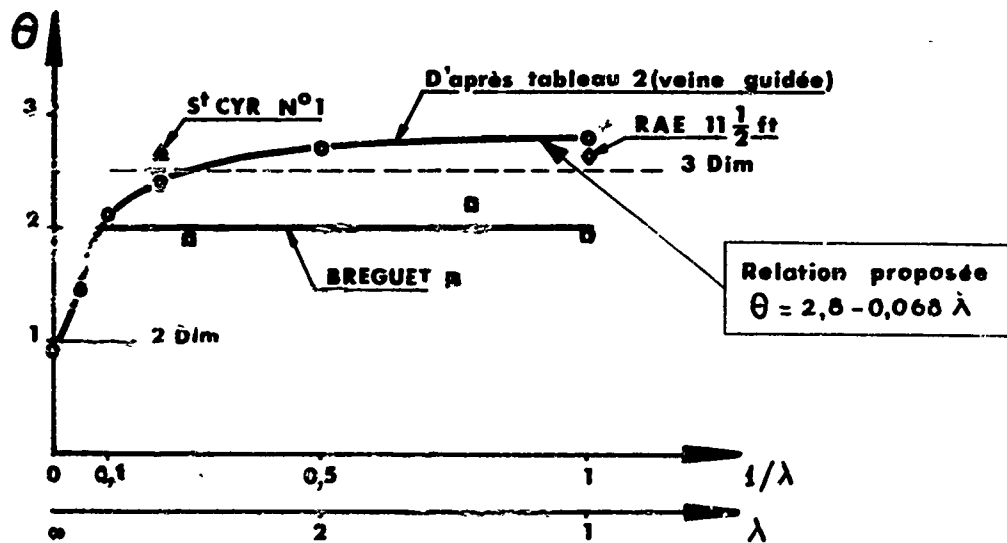
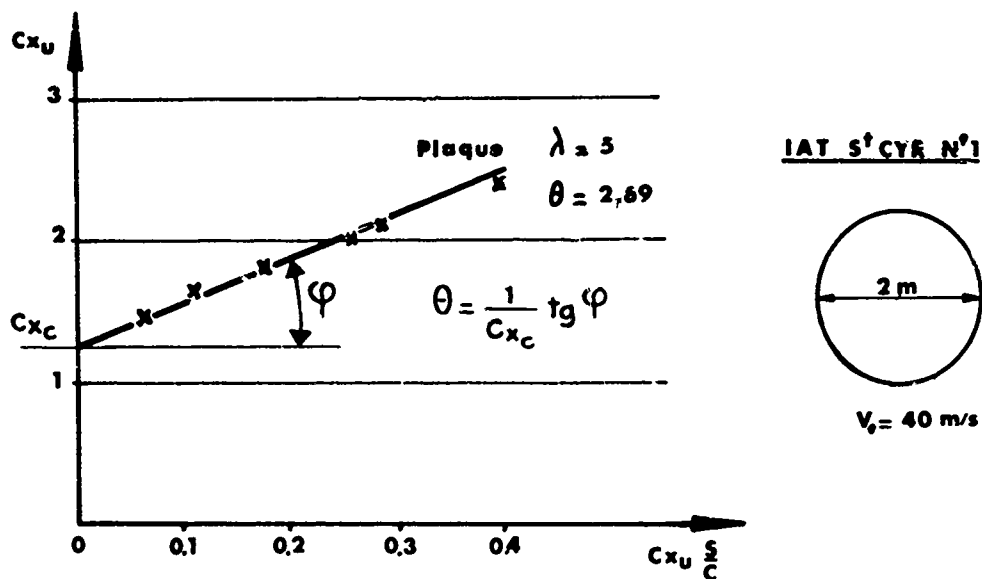
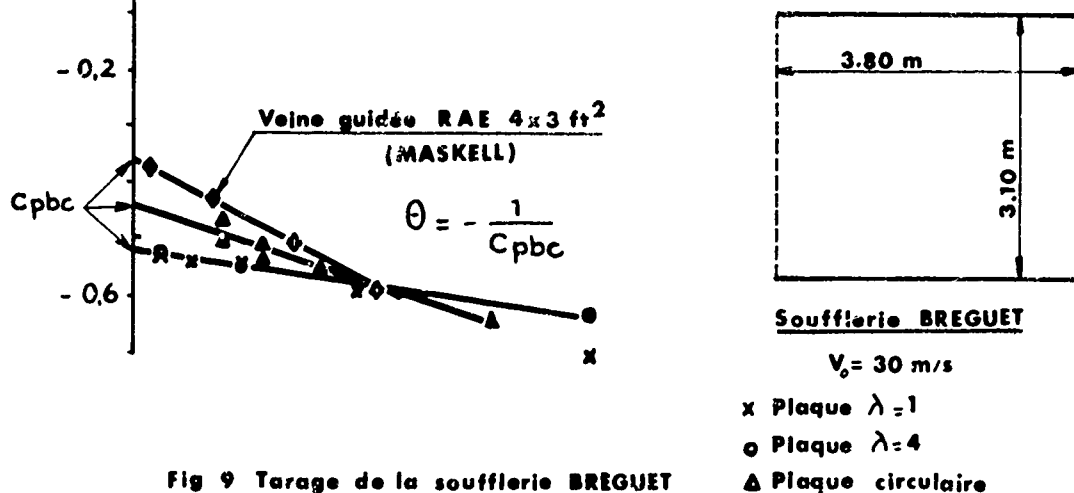
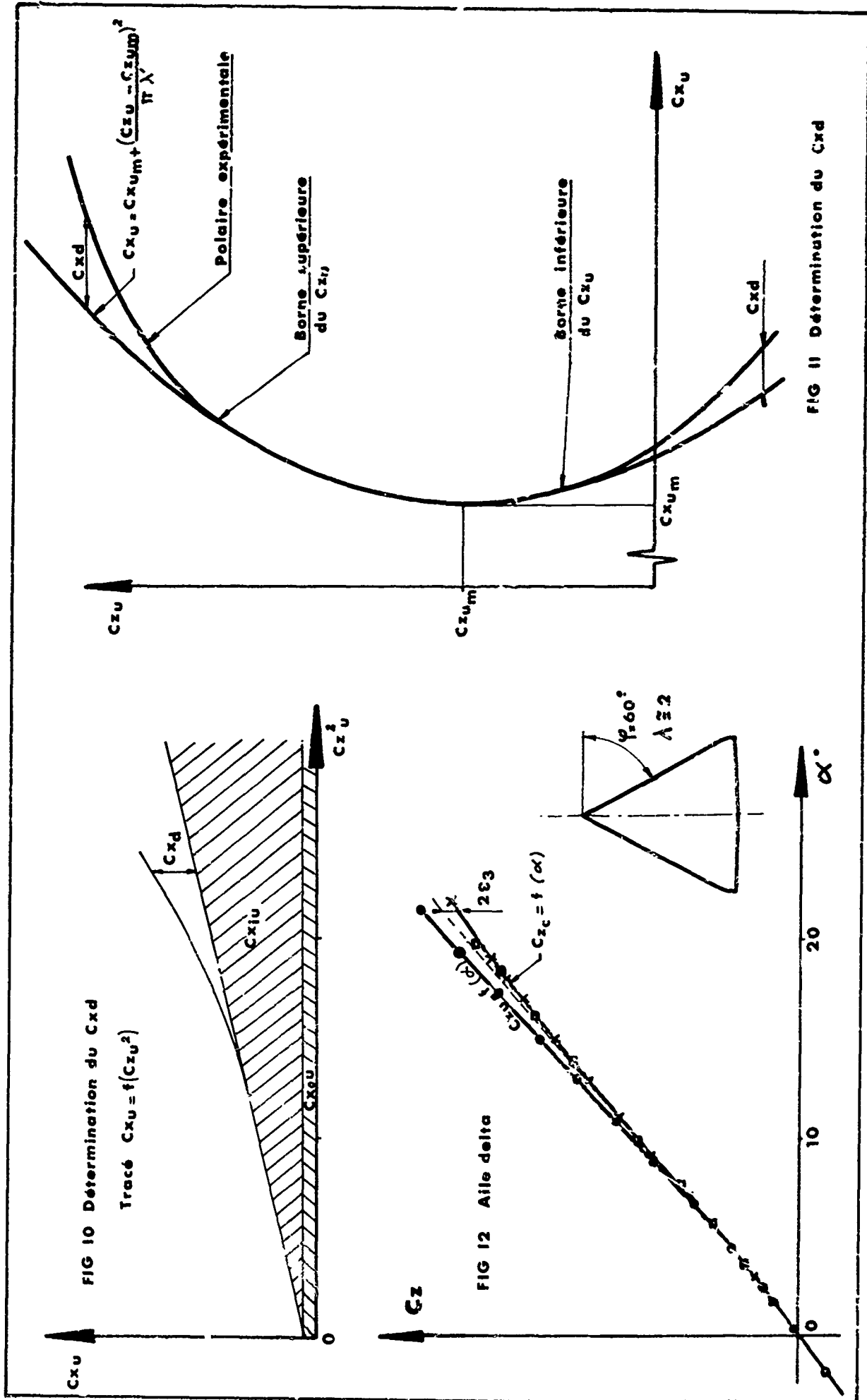
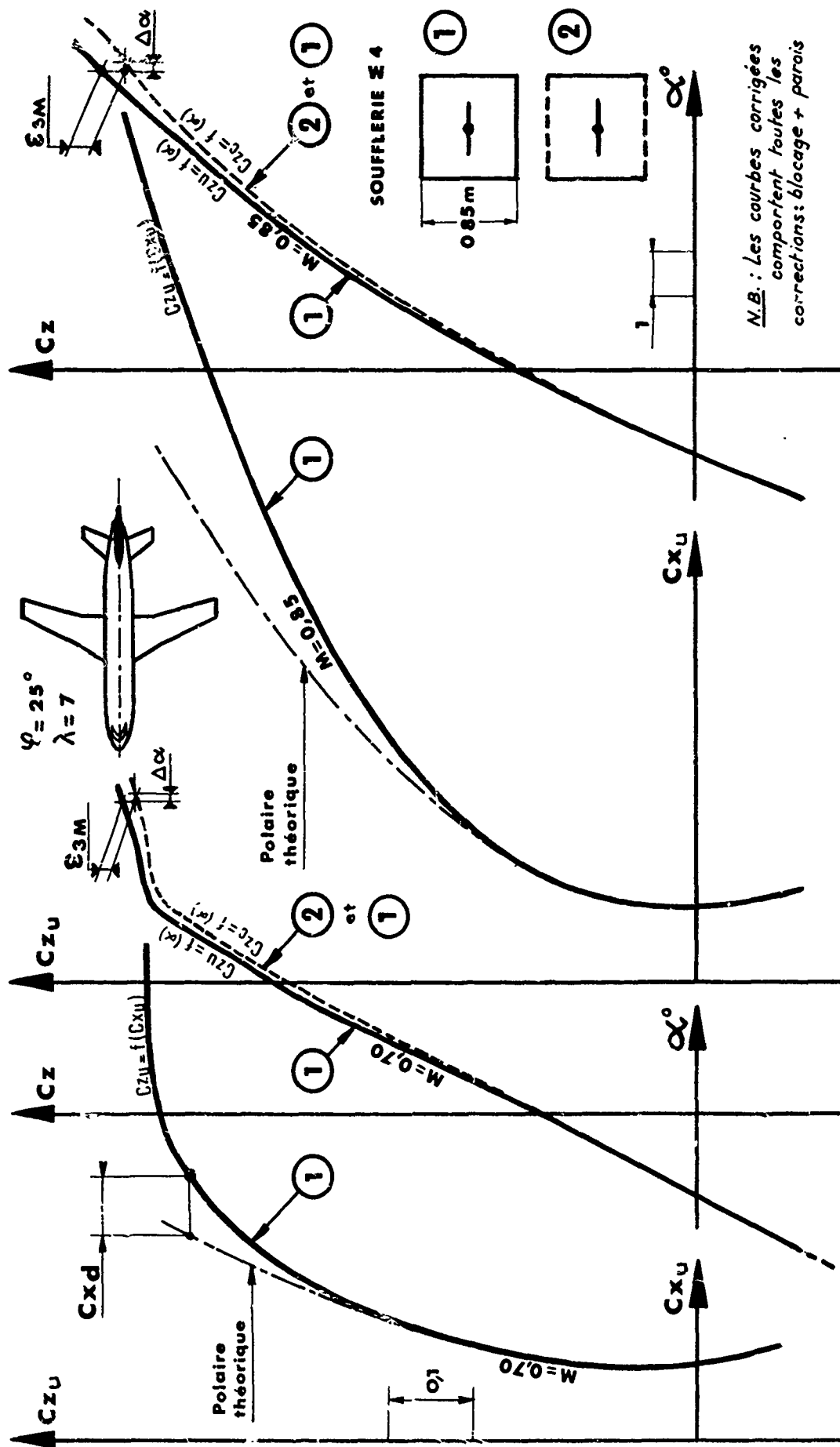
Fig. 7 PARAMETRE  $\theta = f(\lambda)$ Fig 8 Tarage de la soufflerie S<sup>t</sup> CYR N°1

Fig 9 Tarage de la soufflerie BREGUET



# AVION DE TRANSPORT

FIG 13



# MIRAGE G (Hypersustente)

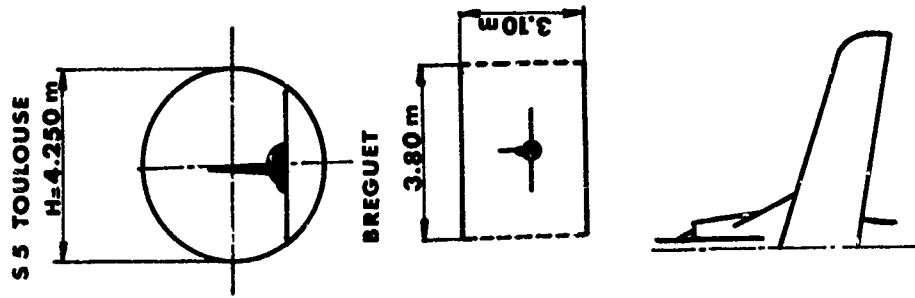
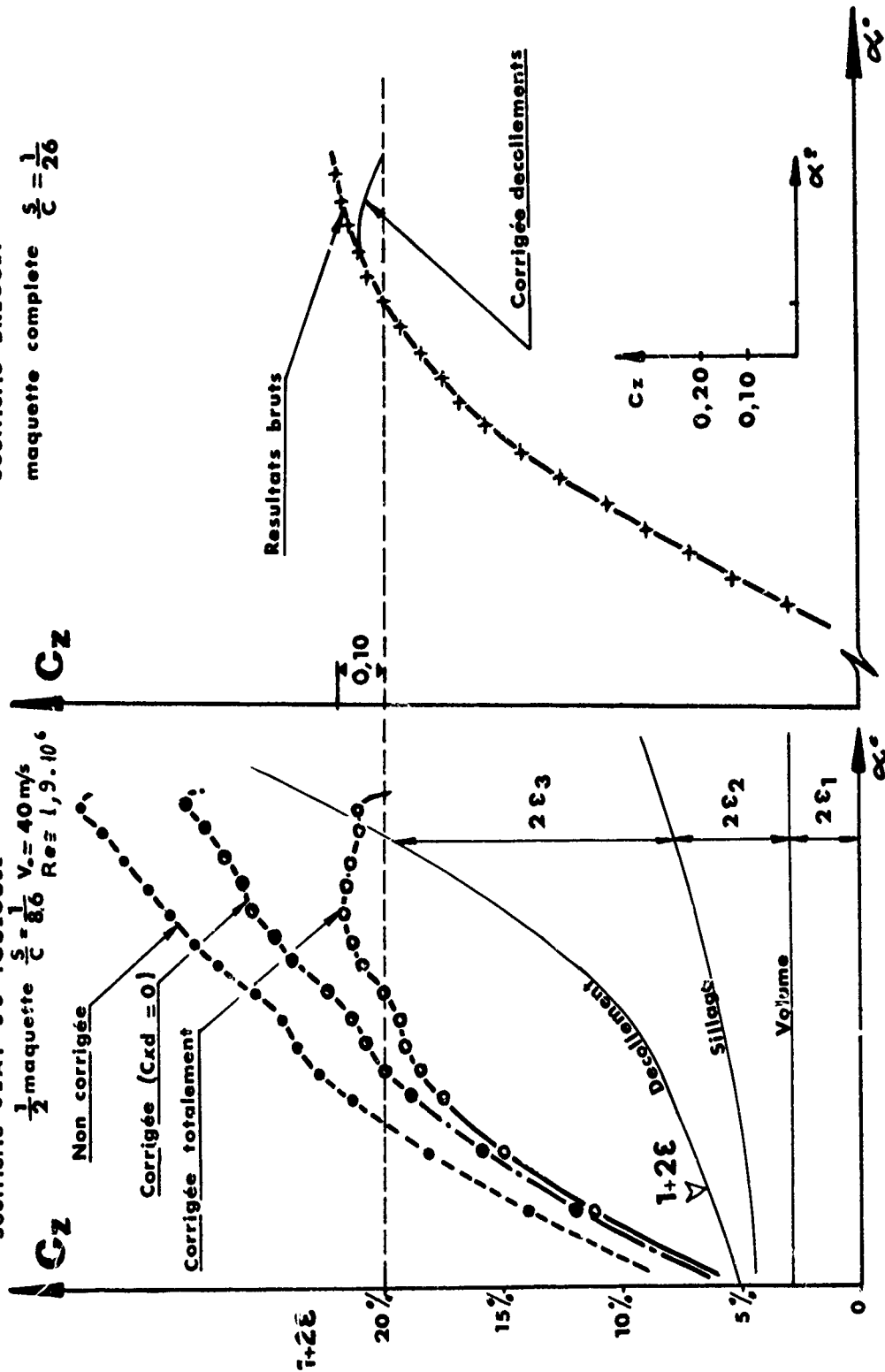
FIG 14

Soufflerie CEAT S5 TOULOUSE

$\frac{1}{2}$  maquette  $\frac{S}{C} = \frac{1}{86}$   $V_{\infty} = 40 \text{ m/s}$   
 $Re \approx 1,9 \cdot 10^6$

Soufflerie BREGUET

maquette complete  $\frac{S}{C} = \frac{1}{26}$

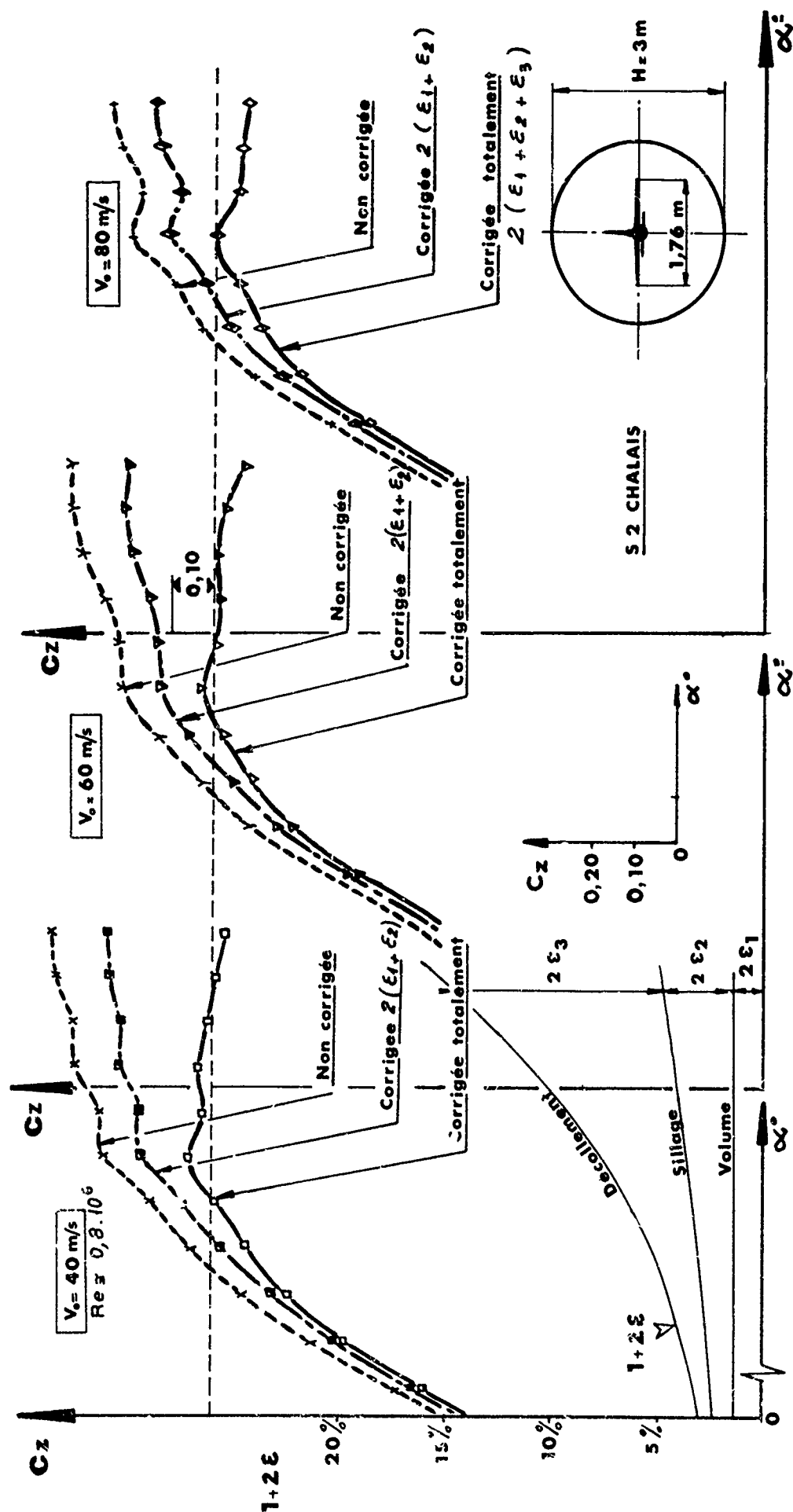




## MIRAGE G

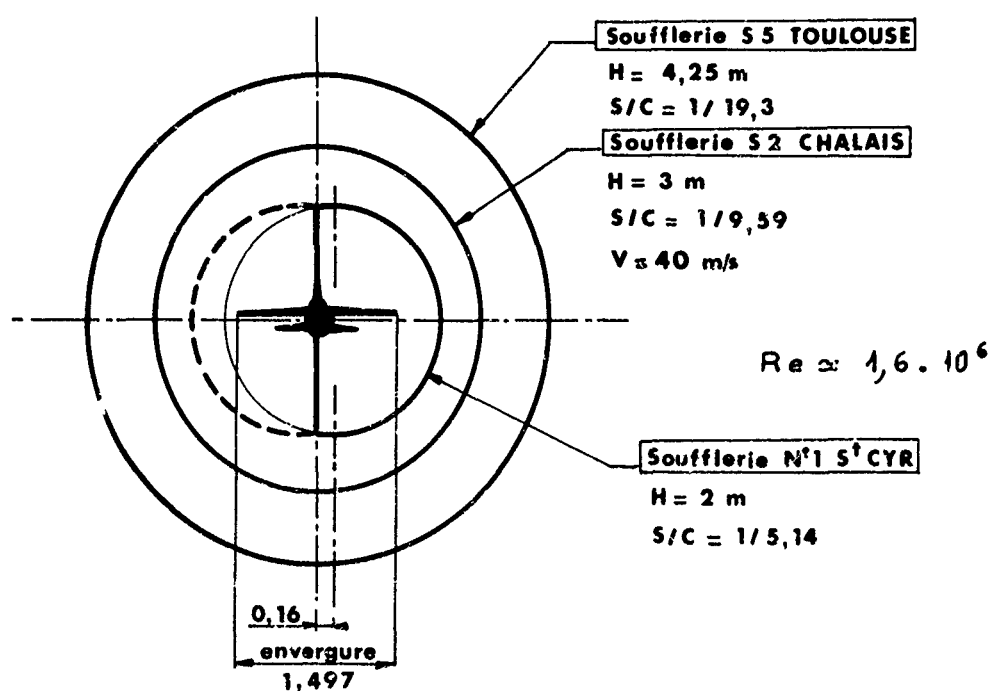
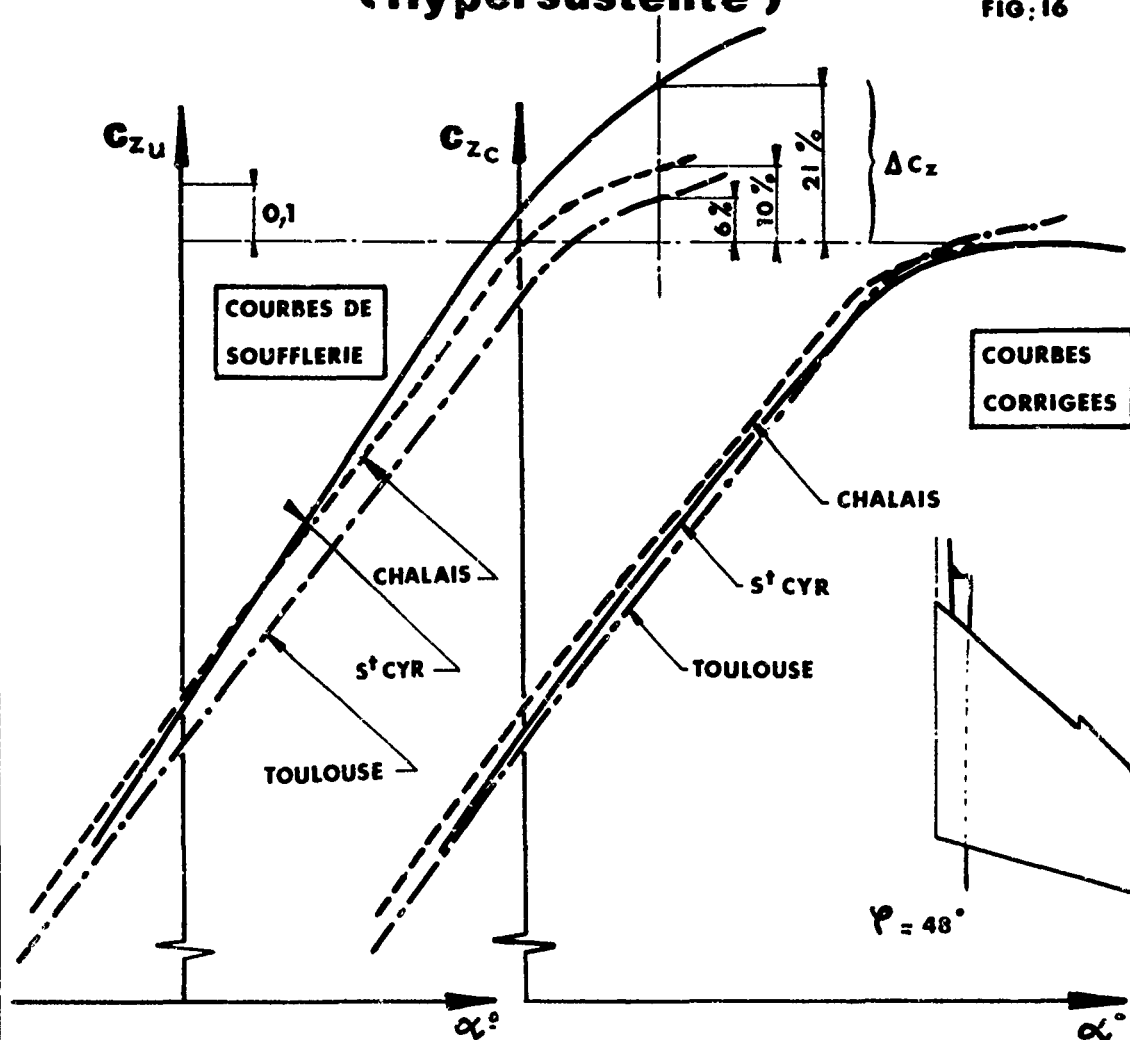
SOUFFLEPIE ONERA S 2 CHALAIS MEUDON  $\frac{S}{C} = \frac{1}{15}$

FIG 15



# MIRAGE F (Hypersustenté)

FIG. 16



$$Re \approx 1,6 \cdot 10^6$$

# MIRAGE F (Hypersustenté)

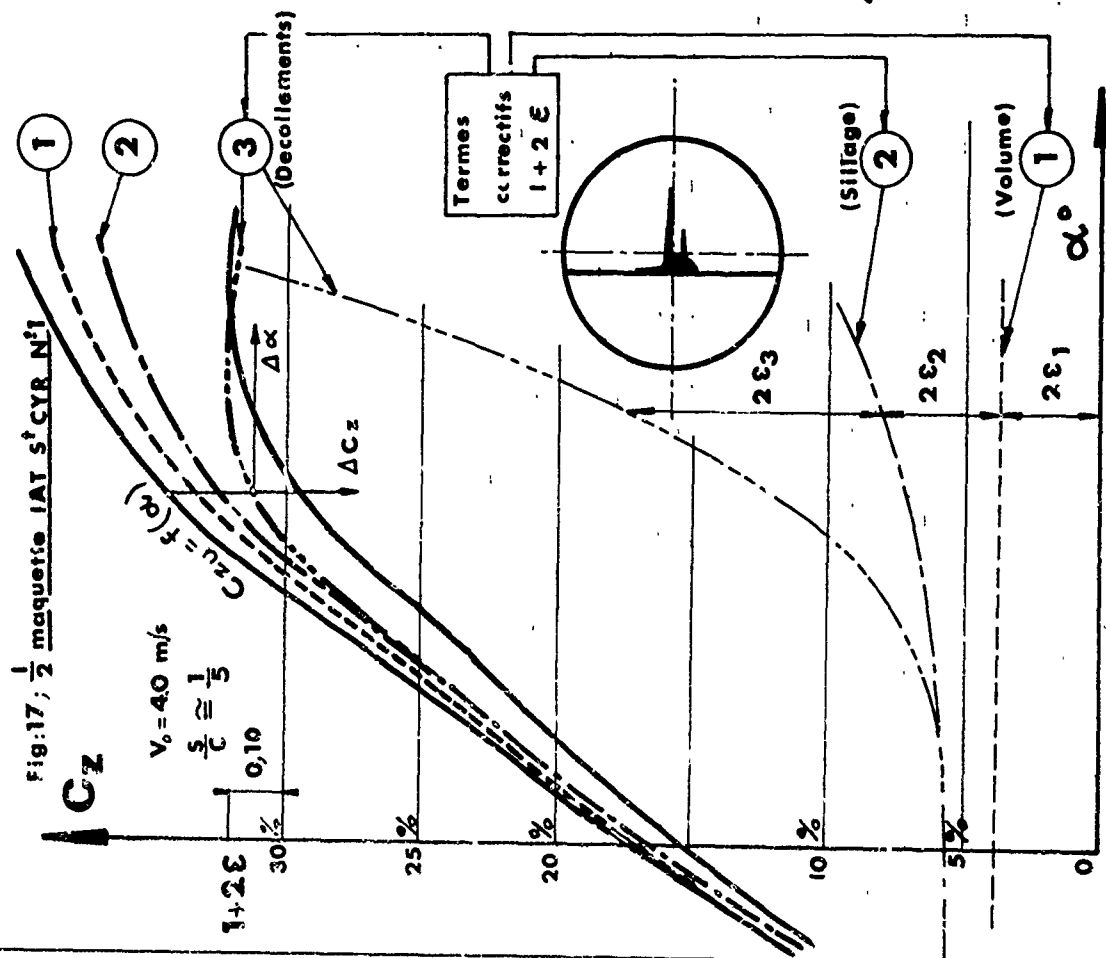
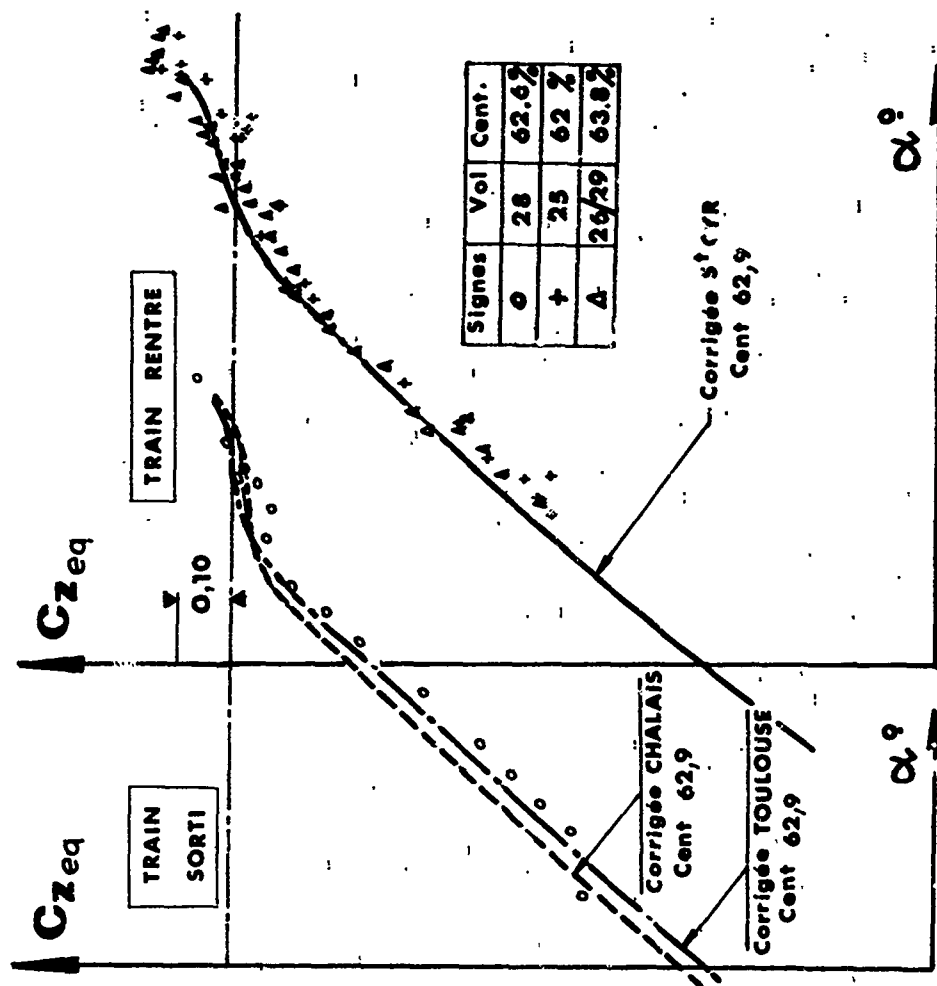


Fig. 18 ; Vols - Souffleries



## AERODYNAMICS OF HIGH-LIFT AIRFOIL SYSTEMS

by

A. M. O. Smith  
Douglas Aircraft Company

## SUMMARY

The purpose of this paper is to clarify and illuminate the aerodynamic processes that occur in flow past unpowered multi-element airfoils in the high-lift attitude. Charts showing permissible pressure recovery for retarded flows are presented. The best possible load carrying pressure distributions are described, as well as airfoils that develop the maximum possible lift in fully attached flow. The processes of interaction between elements of a multi-element airfoil are discussed at some length. It is shown that for a given optimum type of pressure distribution a two-element airfoil can develop more lift than a single element airfoil shaped to develop this same pressure distribution.

## PRINCIPAL NOTATION

a, b,	constants in Stratford's pressure distribution, eq. (6)	q	velocity magnitude
c	chord	$R_c$	chord Reynolds number, $u_\infty c/\nu$
$c_l$	section lift coefficient	$R_l$	length Reynolds number, $u_0 l/\nu$
$C_p$	canonical pressure coefficient, $\frac{p - p_0}{1/2 \rho u_0^2}$ , see Figure 6	$R_0$	length Reynolds number for flat plate flow forward of pressure rise. $R_0 = u_0 x_0/\nu$
$C_p$	conventional pressure coefficient, $\frac{p - p_\infty}{1/2 \rho u_\infty^2}$	S	circumferential distance around an airfoil
$f_1, f_2, f_3$	chord fractions, eq. (16)	u	velocity
l	length of a flat plate, eq. (14)	x	length
M	Mach number	$\alpha$	angle of attack
m	exponent in canonical pressure distributions, see Figure 8	$\beta$	polar angle around a circular cylinder measured from forward stagnation point
$m_2, m_3$	velocity magnification ratios, eq. (16)	$\theta$	momentum thickness of the boundary layer
n	exponent in Stratford's eq. (5)	( ) <sub>0</sub>	conditions at start of pressure rise
p	pressure	( ) <sub>sep</sub>	conditions at separation
$p_0$	pressure at start of pressure recovery, see Figure 6	( ) <sub>e</sub>	conditions at the edge of the boundary layer
$p_\infty$	ambient pressure	( ) <sub>T.E.</sub>	conditions at the trailing edge
		( ) <sub>∞</sub>	reference conditions, far away

## 1. INTRODUCTION

In surveying the literature and knowledge pertaining to the problem of low speed separation as related to the development of high lift the author finds little clear discussion of the fundamentals of the flow processes. Often a paper deals more with "how to" than "why". In some cases wrong thinking is clearly perceived, in other cases correct thinking shows through but the processes are never explicitly discussed, or in all probability the processes have never been considered in detail.

The subject of interest is simple two-dimensional flow, not complicated by laminar bubbles and reattachment, B.L.C., or partial separation. Hence, documents such as that from the AGARD Conference on Separated Flows [1] do not contribute to the problem of interest. Reference [2] is an informative survey of lift augmentation devices and supporting studies. But it too has different interests. The work in it that is closest to the present subject is by McRae entitled Aerodynamics of Mechanical High Lift Systems. Its aerodynamics is sound but it is primarily concerned with general correlations, and it considers too large a variety of devices to get into much detail.

The purpose of this paper then is to clarify and illuminate the underlying aerodynamics of developing high lift. The problem resolves itself into two sub-problems - (1) the aerodynamics of the boundary layer flow and (2) the aerodynamics of the inviscid flow. The boundary layer type of analysis (problem 1) tells us whether and where separation will occur. It amounts to the allowable load problem. The inviscid analysis (problem 2) tells us what can be done to produce pressure distributions more favorable to the avoidance of separation. This amounts to the applied load problem. In particular the effect of slots as on multi-element airfoils is dealt with at some length.

\*Chief Aerodynamics Engineer - Research

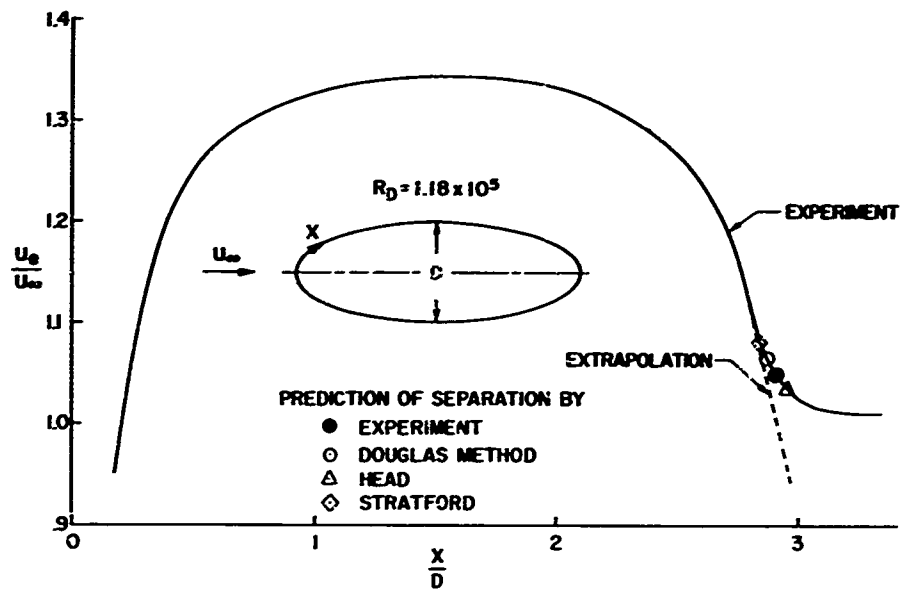


Figure 1. A comparison of predicted separation points with experiment for Schubauer's elliptic cylinder,  $R_D = 1.18 \times 10^5$ .

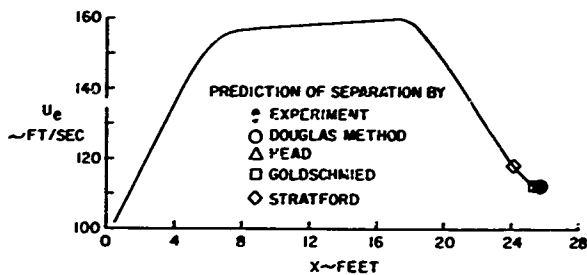


Figure 2. Comparison of predicted separation points with experiment for the airfoil-like body of Schubauer and Klebanoff.

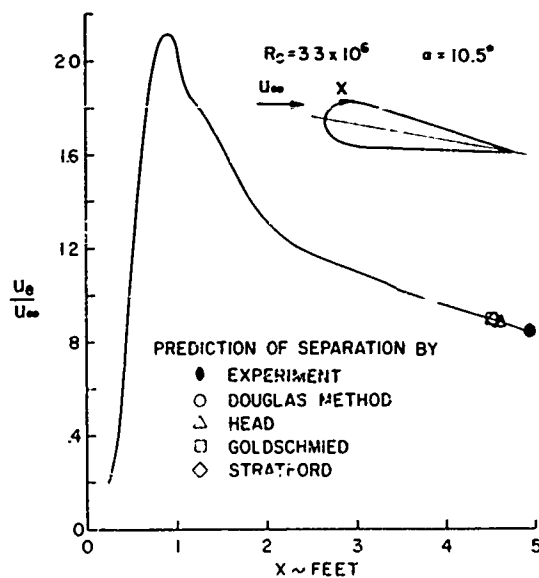


Figure 3. Comparison of predicted separation points with experiment for Newman's airfoil.

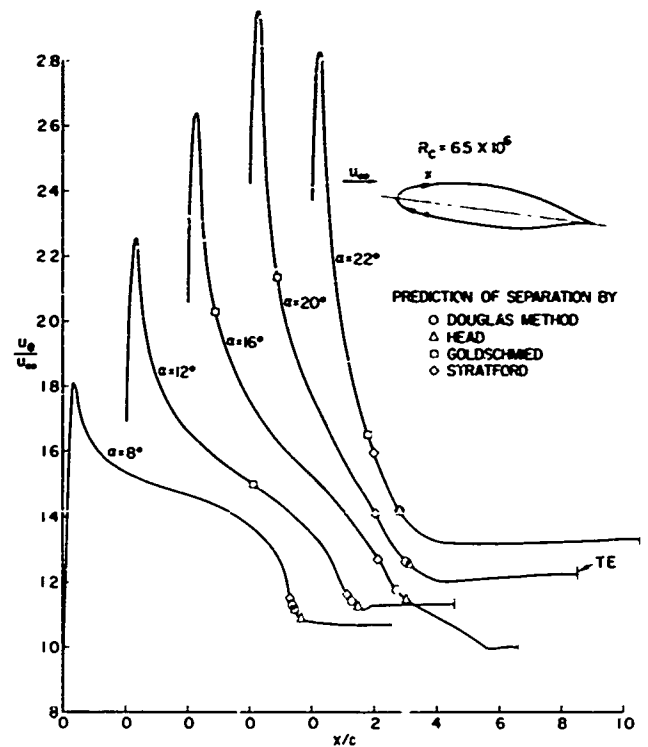


Figure 4. Predicted separation points for the experimental pressure distribution on the NACA 66,2-420 airfoil.

## PART I. THE ABILITY OF BOUNDARY LAYERS TO ENDURE PRESSURE RISE

## 2. THE ABILITY TO PREDICT SEPARATION POINTS

Whether lifting or not, any streamlined body moving through a fluid causes a local speedup of the velocity, followed by a retardation towards the trailing edge, at which point the velocities are not far from those of the ambient environment. At higher angles as lift is increased the local velocities on the suction side increase, so that decelerations near the trailing edge become greater. Finally as angle of attack and lift are still further increased the flow will begin to separate. Therefore accurate prediction of separation points is seen to be a vital step in the analysis of high lift systems. Extensive studies of theoretical separation points have meaning only if the methods of analysis have sufficient accuracy. Hence the first question to be answered is the accuracy of existing methods.

Just such a study is described in [3] which is a condensation of [4]. Four methods of predicting separation were examined and three proved satisfactory for purposes of general engineering analysis. These were Head's method, the Cebeci-Smith method and Stratford's method. Figures 1, 2, 3 and 4, taken from [3], show typical results. Tests carefully locating separation points are scarce, but Figures 1, 2 and 3 do have such information. In Figure 4 separation points must be inferred as the point where the velocity distribution assumes a constant value. In general there is satisfactory agreement between the methods and with experiment. Based on examination of many more cases than shown here the Cebeci-Smith partial differential equation method seems best, but Head's is not far behind. The errors in Stratford's method average several times as great but it still can be considered satisfactory. (It should be noted that the constants used by Stratford have been changed somewhat in order to improve the accuracy, see [3].) Stratford's method has great convenience because it does not require solution of the boundary layer equations. It is slightly conservative in that it usually predicts separation early.

In the studies that follow, calculations have been made by the Cebeci-Smith method. Not only does it seem to be the most accurate but also it is the only one of the three that can account for high Reynolds number and Mach number effects accurately. Figure 5 is a summary of further studies made at Douglas and hitherto unreported. It is concluded that for rear separation (no laminar bubble-reattachment situation) existing boundary layer methods are sufficiently accurate to justify a careful theoretical look at various pressure distributions.

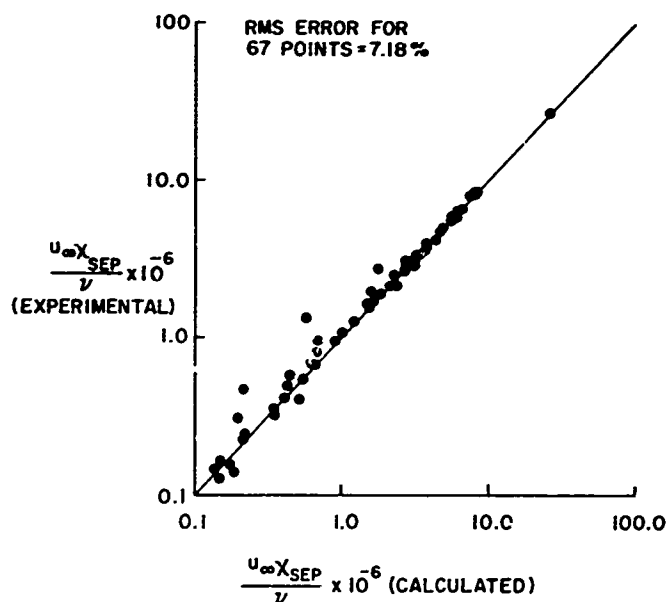


Figure 5. Accuracy of predicting turbulent separation points by the Cebeci-Smith method.

## 3. CANONICAL PRESSURE DISTRIBUTIONS

Normally in airfoil and flap design the engineer looks at a pressure distribution as a whole. Consequently the fundamental character of the flow is obscured by magnitude of  $C_p$  values together with the many other details of the pressure distribution. But we know from basic scaling and similarity laws that boundary-layer results are the same for two pressure distributions if they can be made congruent by proper scaling. In particular, the separation points will be the same except for weak Reynolds number effects. A 1-inch chord airfoil at 200 mph will have very high velocity gradients while a 100-inch chord airfoil of the same shape at 2 mph will have very gentle velocity gradients. Yet the flows are exactly similar. It is the dimensionless shape that counts. Hence the fundamentals of a flow involving adverse gradients can be described by a canonical system. It is illustrated in Figure 6. The essential feature is that velocities are normalized by dividing everywhere by the velocity at the start of deceleration. Then the only remaining parameter is a Reynolds number,  $R_0$ , the momentum thickness at the start of the

pressure rise, is a very convenient one, although an  $R_x$  measure is also suitable. In the system of Figure 6  $\bar{C}_p = +1$  means that all the original velocity head at  $x = 0$  has been converted to pressure head.

If two pressure distributions can be made congruent in the canonical sense an airfoil having a deceleration of  $(u_e/u_\infty)^2$  from 10 to 5 is no more or no less likely to separate than one decelerating from  $(u_e/u_\infty)^2$  of 1.5 to 0.75, or even from 0.10 to 0.05. The canonical plot is the one that is meaningful to boundary-layer analysis. The conventional is the one that is meaningful to lift, critical Mach number, etc.

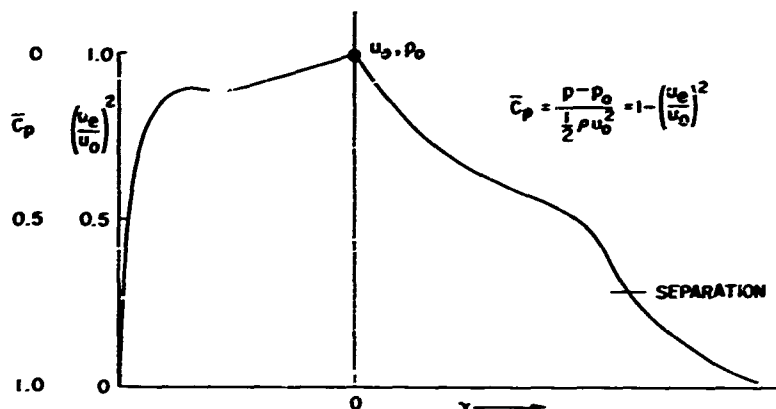


Figure 6. Canonical pressure distributions. The left hand corner might represent the nose of an airfoil. The origin of  $x$  is at the beginning of pressure rise. The pressure distribution can be thought of as that of the upper surface of an airfoil. Separation might occur at some point as noted. In boundary layer analysis  $x$  is properly distance along a surface, although on most airfoils peripheral distance differs little from chordwise distance. Because of the very simple relation between pressure coefficient and velocity ratio, the phrase pressure distribution is applied indiscriminately to either pressure coefficient or velocity ratio plots.

### 3.1 Relation of canonical pressure distribution to the conventional

The canonical pressure distribution is easily related to the conventional airfoil pressure distribution, where the reference velocity and pressure are  $u_\infty$ . It is clearer to work out relations in terms of velocity squared rather than  $C_p$ . The primary relation is very simple. It is

$$\left(\frac{u_e}{u_\infty}\right)^2(x) = \left(\frac{u_e}{u_0}\right)^2(x) \cdot \left(\frac{u_0}{u_\infty}\right)^2 \quad (1)$$

The last term in (1) amounts to a constant. If one starts with a canonical pressure distribution,  $u_0$  or  $u_0/u_\infty$  are not necessarily known, they are just scaling factors. Equation (1) is useful for calculating the canonical distribution from a given airfoil distribution, for then  $(u_e/u_\infty)^2$  and  $(u_0/u_\infty)^2$  are known. The constant  $(u_0/u_\infty)^2$  has a definite value for one important problem. It is the problem of applying to an airfoil a canonical pressure distribution that has separation located somewhere on it as illustrated in Figure 6. Since we do not want separation to occur on the airfoil this separation point must be at the trailing edge. Then from (1) we can write

$$\left(\frac{u_e}{u_\infty}\right)_{\text{sep}}^2 = \left(\frac{u_e}{u_0}\right)_{\text{sep}}^2 \left(\frac{u_0}{u_\infty}\right)^2$$

Solve for  $(u_0/u_\infty)^2$  and substitute in (1)

$$\left(\frac{u_e}{u_\infty}\right)^2(x) = \frac{(u_e/u_\infty)_{\text{sep}}^2}{(u_e/u_0)_{\text{sep}}^2} \left(\frac{u_e}{u_0}\right)^2(x) \quad (2)$$

We know from general airfoil theory that  $(u_e/u_\infty)^2$  at the trailing edge, where separation is assumed to be just avoided, is about 0.8, corresponding to  $C_p = 0.2$ . Then if the canonical pressure distribution separates at  $(u_e/u_0)^2 = 0.4$  the factor is  $0.8 \div 0.4 = 2.0$ . Equation (2) is a true statement no matter where separation is allowed to occur on the airfoil. However in practice airfoils are not deliberately designed to have separation. Therefore since separation is common in canonical distributions as will be seen, the assumption that the corresponding separation point on the airfoil is at the trailing edge is reasonable. Then (2) can be rewritten

$$\left(\frac{u_e}{u_\infty}\right)^2(x) = \frac{(u_e/u_\infty)_{\text{T.E.}}^2}{(u_e/u_0)_{\text{sep}}^2} \left(\frac{u_e}{u_0}\right)^2(x) \quad (3)$$

Equation (3) is easily written in terms of  $C_p$ . Writing

$$c_p = 1 - \left(\frac{u_e}{u_\infty}\right)^2, \quad (c_p)_{T.E.} = 1 - \left(\frac{u_e}{u_\infty}\right)_{T.E.}^2$$

$$\bar{c}_p = 1 - \left(\frac{u_e}{u_0}\right)^2$$

we have, from (3).

$$c_p(x) = 1 - \frac{1 - (c_p)_{T.E.}}{1 - \bar{c}_{p_{sep}}} [1 - \bar{c}_p(x)] \quad (4)$$

Observe from (4) that if  $(c_p)_{T.E.}$  can be reduced (velocity increased)  $c_p(x)$  is increased linearly all over the airfoil and hence  $C_L$  undergoes a like increase. This effect will be discussed later with examples.

### 3.2 Location of separation on several canonical distributions

Our interest is mainly the analysis of several families of pressure distributions, but before presenting results it is useful to discuss limiting flows. In connection with development of his separation criterion Stratford [5] solved for the  $\bar{c}_p$  distribution that developed incipient separation all along a region of pressure rise. Hence it is a solution for the fastest possible pressure rise and so has considerable technical interest. In [6] Stratford experimentally produced one of these flows. Experiment and theory were in good agreement.

For the beginning of the pressure rise his solution is

$$\bar{c}_p = 0.645 \left\{ 0.435 R_0^{1/5} \left[ \left(\frac{x}{x_0}\right)^{1/5} - 1 \right] \right\}^{2/n}, \quad \bar{c}_p \leq \frac{n-2}{n+1} \quad (5)$$

where  $x_0$  is the effective length of turbulent flat plate flow ahead of the beginning of pressure recovery.  $R_0$  is  $u_0 x_0 / \nu$  and  $x$  is distance measured from the start of the entire flow. The quantity  $n$  is an exponent whose value is approximately 6. The equation for the final portion of the flow is

$$\bar{c}_p = 1 - \frac{a}{(x/x_0 + b)^{1/2}}, \quad \bar{c}_p \geq \frac{n-2}{n+1} \quad (6)$$

In (6)  $a$  and  $b$  are constants that permit (6) to match values and slopes with (5) at  $\bar{c}_p = (n-2)/(n+1)$ .

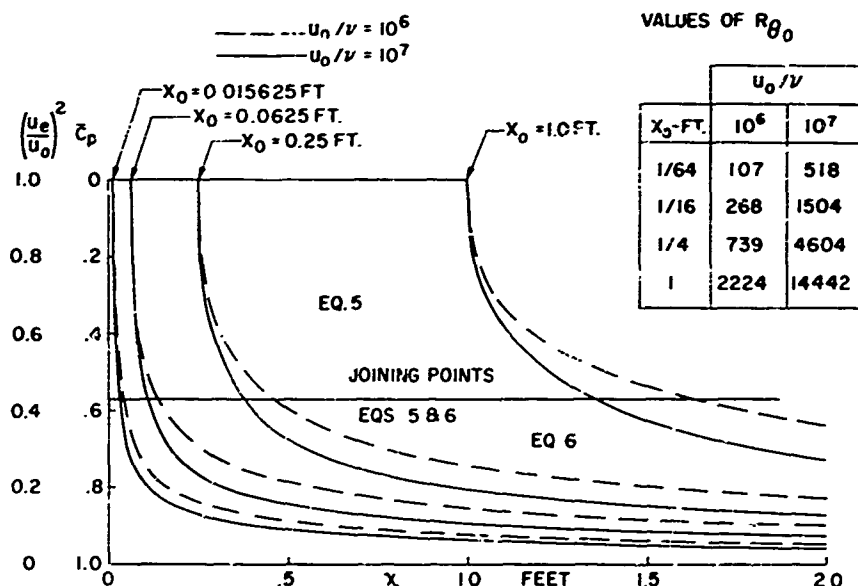


Figure 7. Stratford limiting flows at two values of unit Reynolds number

A family of typical velocity distributions is presented in Figure 7. All flows start at  $x = 0$  and pressure recovery starts at four locations as shown. Two unit Reynolds numbers are considered. The smallest  $x$ -Reynolds number corresponds to  $x_0 = 0.015625$  feet and  $u_0/\nu = 10^6$  per foot or 15,625. The largest is  $10^7$ . The constant velocity roof-top portion is assumed to be turbulent throughout. Stratford presents a method for calculating an effective initial length up to  $x_0$  when the initial flow is partially laminar and of variable pressure. Another way of using the curves is just to match values of  $R_0$  at the start of



pressure rise. The figure includes a table of initial values. Matching  $R_0$  is just as sound as matching  $x_0$  values, and more flexible.

Besides the general character of the curves several features are noteworthy.

1. The initial slope  $d\bar{C}_p/dx$  is infinite, so that small pressure rises can be made in very short, to zero distances.
2. In the initial stages the pressure rise varies as  $x^{1/3}$ .
3. The dominant variable is  $x/x_0$ , see (5). Hence when the  $x_0$  distance is small and the boundary layer is thin, pressure recoveries may be rapid. When the initial run is long and the boundary layer is thick, the allowable average pressure gradient is much lower. Or conversely, thick boundary layers are much more likely to separate than thin.
4. The unit Reynolds number effect is relatively small.
5. One hundred percent of the dynamic pressure can theoretically be recovered, but the distance required is infinite.
6. Aside from error in the theory, the curves of Figure 7 are the shortest possible pressure recoveries having fully attached flow. Nothing better can be done except by B.L.C. They are the "end of the line".

Stratford's flows are the real limits for rapid pressure recovery. They are a very special kind of flow and provide no information about allowable pressure rises for other flows, or about the effect of the shape of the pressure distribution upon the amount of pressure recovery. Accordingly two families of pressure distributions were studied. One is where  $\bar{C}_p$  varies as  $x^m$  and the other where  $\bar{C}_p$  is represented by a family of circles. The results are shown in Figures 8, 9, 10, and 11. In all these figures the region of pressure rise is assigned a length of 1 foot, and unlike Figure 7 all pressure rises start at the same point. Four different lengths of flat plate flow are studied and their origins are noted. To illustrate the use of the charts we shall go through an example. Assume the flow had an effective turbulent rooftop run of 0.25 feet before retardation commences, and that the retardation is to obey the equation  $\bar{C}_p = x^2$ . Then using Figure 8 the flow begins at  $x = -0.25$ , passes  $x = 0$  and velocities follow the  $m = 2$  curve downward. When the flow reaches the line marked 0.25 separation occurs. This point is at about  $x = 0.7$  foot and  $\bar{C}_p = 0.5$ . If the flow had started at  $x = -1.0$  foot and followed the same  $\bar{C}_p = x^2$  line it would have separated earlier, at the line marked 1.0. For convenience feet and  $u_0/\nu$  were used as parameters. These together form Reynolds numbers. If the pressure rise portion were considered to represent 10 feet instead of 1 foot, it is equally applicable, if  $u_0/\nu$  is divided by 10, because then Reynolds numbers are unchanged. Or viewed another way, if the length of the pressure rise is called  $\lambda$ , the abscissa on the charts represents  $x/\lambda$ .

The shortest flat plate run, 0.015625 feet approximates a thin airfoil at an angle of attack. For the flat plate run of 1.0 foot the steps used in the Cebeci-Smith boundary layer method are noted at the bottom of Figure 8. They represent about average spacing. In the region of pressure rise the steps are 0.05 foot. By examination of the plots it is seen that with this step length, for  $m < 1$  the average slope  $d\bar{C}_p/dx$  as computed by finite difference formulas is relatively moderate, whereas initially it should be infinity. This difference may be a source of error in the analysis, however, it is not expected to be great. Boundary layer effects would tend to eliminate any infinite gradient. For the case of the 0.0625 foot run the calculations just aft of the start of pressure rise begin with steps equal to 0.0025 foot, much smaller values.

The charts represent fully turbulent flow along flat plates of the lengths noted. The  $x$ -length as a parameter is a matter of convenience; the more fundamental parameter is  $R_0$  at  $x = 0$ . If  $R_0$  is held at a fixed value corresponding to one of the flat plate runs then the boundary layer calculations still apply closely, no matter by what path the value of  $R_0$  was reached. The value of  $R_0$  might come from an accelerating turbulent flow whose velocity distribution was like that sketched in Figure 6. Or it might contain a good deal of laminar flow, in which case the equivalent plate length would be much greater. Tabulated below are values of  $(R_0)_0$  for the  $M = 0$  flows. The values are also tabulated on the figure immediately under the  $x$ -length values.

$x_0$ Feet	$U_0/\nu = 10^6$	$U_0/\nu = 10^7$
0.015625 (1/64)	107	518
0.0625 (1/16)	268	1504
0.25 (1/4)	739	4604
1.0	2224	14442

Table I. Values of  $R_0$  at the beginning of pressure recovery, for the flows of Figures 8-11,  $M = 0$ .

The separation loci are crossplotted on the  $\bar{C}_p$  curves. A slightly concave pressure distribution provides not only the greatest recovery but also in much shorter distance. This fact is in agreement with Figure 7. Also in agreement with Figures 7 is the fact that higher unit Reynolds number for these plots delays separation. It is interesting that in both Figures 8 and 9 separation did not occur instantly for  $m < 1/3$ , see the figures. In fact for the 0.0625 case at  $u_0/\nu = 10^7$  separation did not occur until  $\bar{C}_p = 0.81$ . Resolution of this disagreement with Stratford's solution is a problem for the future.

In connection with the design of thin airfoils Loftin [7] proposed the criterion that separation occurs when  $\bar{C}_p = 0.88$ . This line is noted on Figure 9. For a thin airfoil with some laminar flow near the nose the effective flat plate run could easily approximate the 0.015625 value. Then for some  $\bar{C}_p$

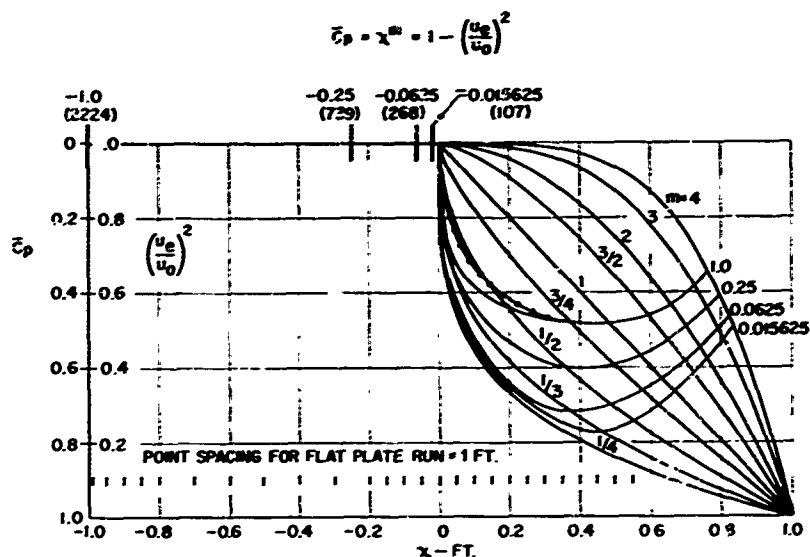


Figure 8. Separation loci for a family of canonical pressure distributions. Point spacing used in the boundary layer calculations for the one-foot rooftop run is noted. The dotted curve for the one-foot rooftop run is the separation locus for  $1 - (u_e/u_0)^2 = x^m$  when  $M = 1.0$ . Except for fractional values of  $m$ , the locus is nearly the same as for  $M = 0$ . Values in parentheses under origins of flow are values of  $R_0$  at  $x = 0$ .  $u_0/\nu = 10^6$ ,  $M_0 = 0$ .

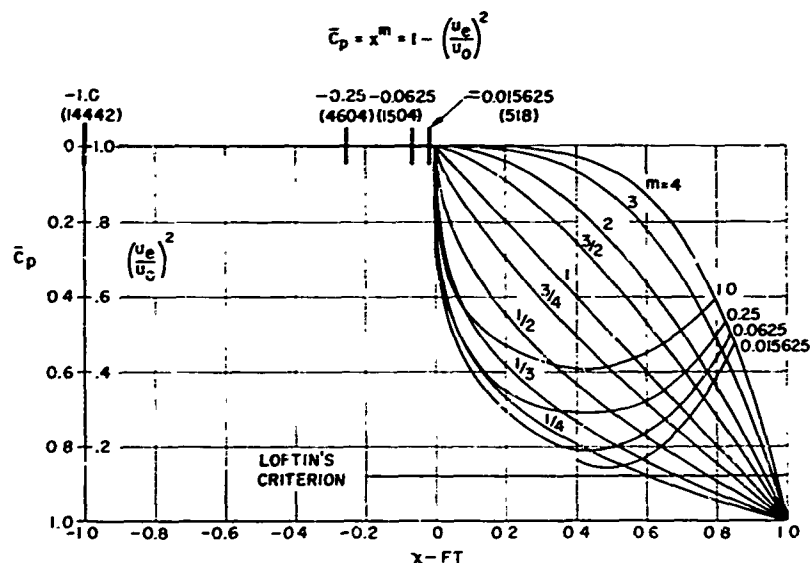


Figure 9. Separation loci for a family of canonical pressure distributions. Loftin's criterion  $\bar{c}_p = 0.88$  is noted.  $u_0/\nu = 10^7$ ,  $M_0 = 0$ .

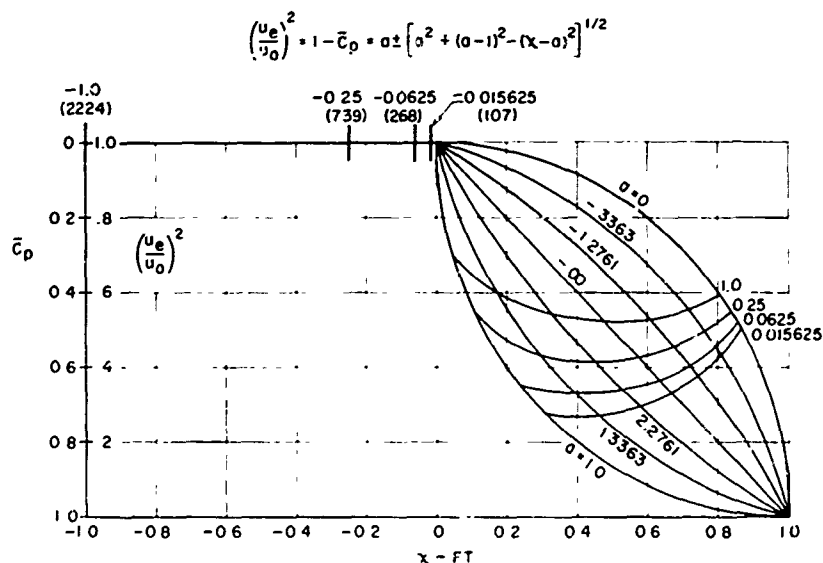


Figure 10. Separation loci for a family of canonical pressure distributions.  $u_0/\nu = 10^6$ ,  $M_0 = 0$ .

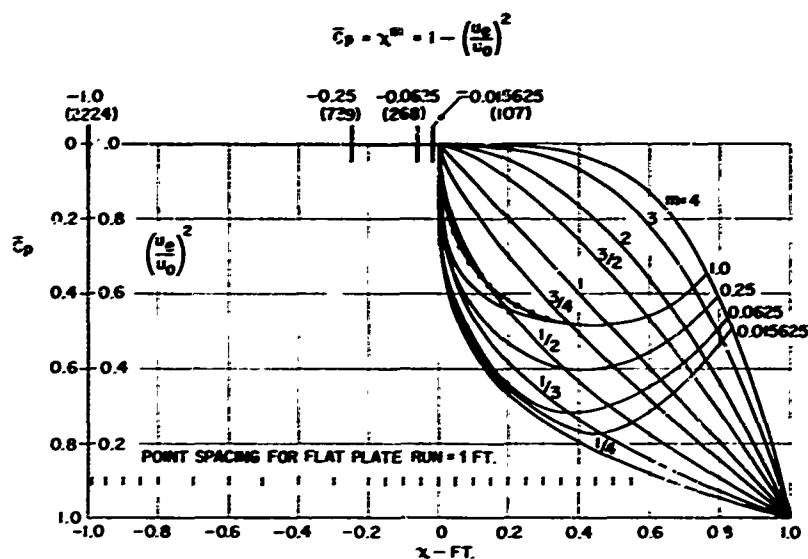


Figure 8. Separation loci for a family of canonical pressure distributions. Point spacing used in the boundary layer calculations for the one-foot rooftop run is noted. The dotted curve for the one-foot rooftop run is the separation locus for  $1 - (u_e/u_0)^2 = x^m$  when  $M = 1.0$ . Except for fractional values of  $m$ , the locus is nearly the same as for  $M = 0$ . Values in parentheses under origins of flow are values of  $R_\theta$  at  $x = 0$ .  $u_0/\nu = 10^6$ ,  $M_0 = 0$ .

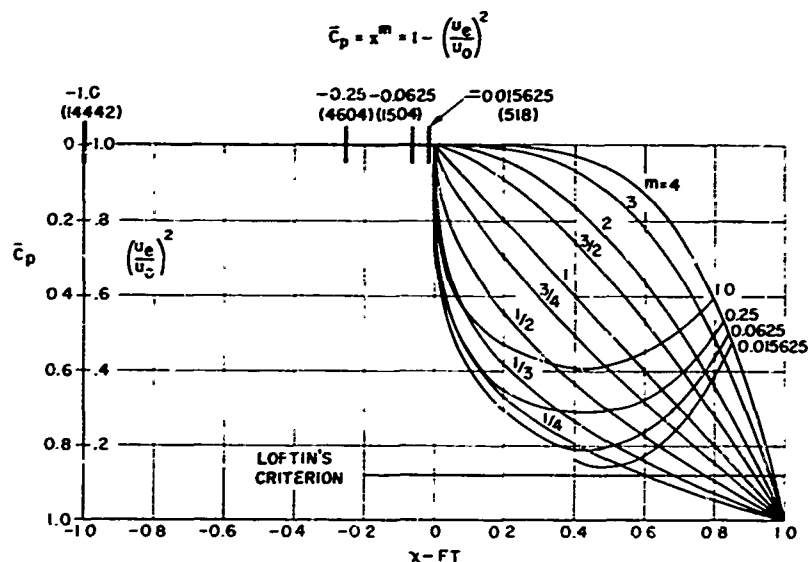


Figure 9. Separation loci for a family of canonical pressure distributions. Loftin's criterion  $\bar{c}_p = 0.88$  is noted.  $u_0/\nu = 10^6$ ,  $M_0 = 0$ .

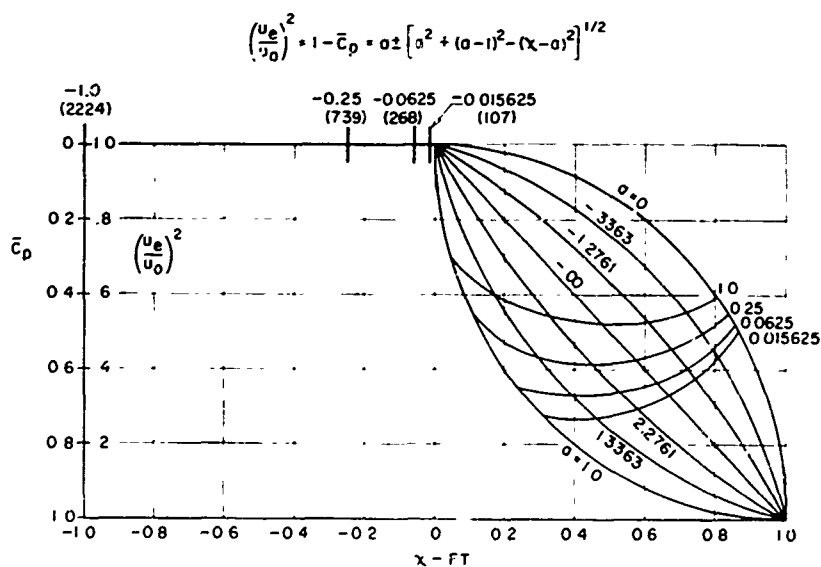


Figure 10. Separation loci for a family of canonical pressure distributions.  $u_0/\nu = 10^6$ ,  $M_0 = 0$ .

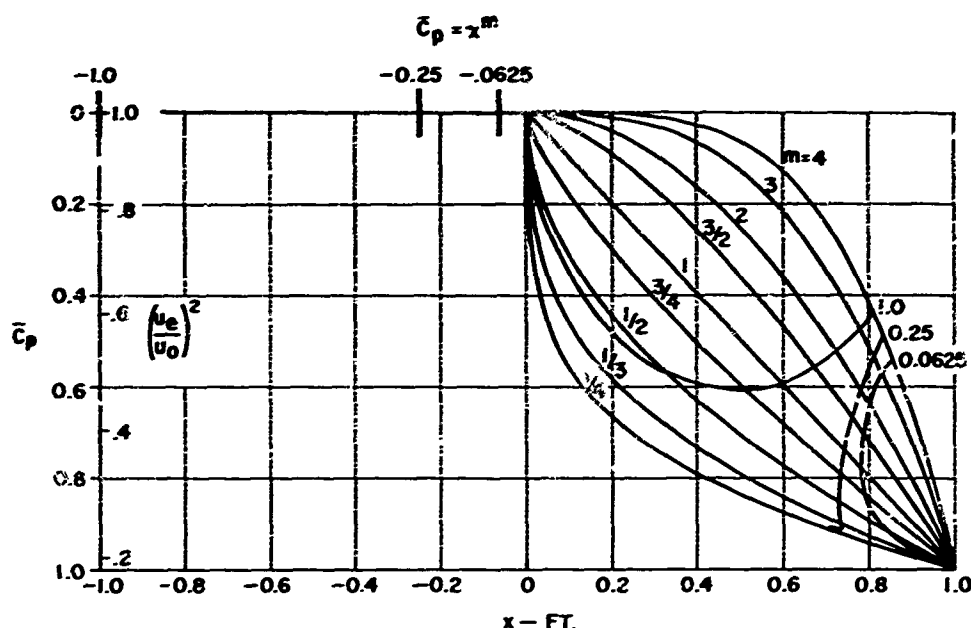


Figure 13. Separation loci for a family of canonical pressure distributions.  $u_0/v = 10^6$ ,  $M_0 = 1.0$ .

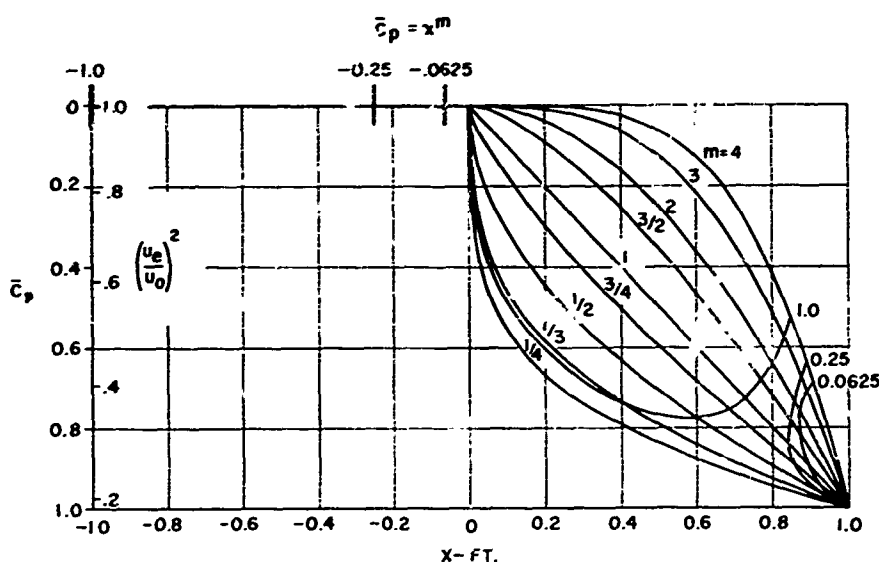


Figure 14. Separation loci for a family of canonical pressure distributions.  $u_0/v = 10^7$ ,  $M_0 = 1.0$ .

$$\bar{c}_p = \frac{2}{\gamma M_0^2} \left\{ \left[ 1 + \frac{\gamma-1}{2} M_0^2 \left( 1 - \frac{u_e^2}{u_0^2} \right) \right]^{\frac{\gamma}{\gamma-1}} - 1 \right\} \quad (7)$$

When this is solved for  $(u_e/u_0)^2$  the  $u_e/u_0$  gradients are noticeably reduced. In fact the curve for  $m = 1/3$  considerably resembles the Stratford curves, Figure 7. The effect is roughly indicated by the  $(u_e/u_0)^2$  scales spotted beside the  $\bar{c}_p$  scales. When  $\bar{c}_p = +1$ ,  $(u_e/u_0)^2 \approx 0.18$  which is far from stagnation.

The alternate treatment is to specify that  $(u_e/u_0)^2 = 1 - x^m$ , independent of Mach number. One case of this sort was studied and the result is shown on Figure 8. Very little effect of Mach number is evident. Hence the answer as to the effect of Mach number depends considerably on what is being held constant.

### 3.3 Maximum suction lift on a single surface

If Stratford limiting pressure distributions like those of Figure 7 are considered it is seen that a short rooftop allows more rapid pressure rise as well as a longer distance for it to occur in. A long roof top for a given chord has very little length for pressure recovery. Inviscid flow constraints specify that the dumping velocity be nearly the same regardless of pressure distribution. If held exactly the same then it is clear that one of these Stratford families contains the maximum area. Being the limiting flow it crudely represents the maximum possible lift on the upper surface of a one piece airfoil. Figure 15 shows a family of such curves constructed for a total chord Reynolds number  $u_\infty c/v$  of  $5 \times 10^6$ . In

Figure 15 the flow is completely turbulent just as in Figure 7. If the rooftop flow were laminar a much longer rooftop run could be had for equal momentum thickness at the start of pressure recovery. This family is shown in Figure 16. For these simplified situations the best possible high lift distribution for fully attached flow is indicated and the best possible lift coefficients for turbulent and laminar rooftop flows are about 1.0 and 2.0 respectively. The great advantage of extensive laminar flow is clearly exhibited; the suction lift is more than doubled. In calculating the  $c_{L_u}$  values of Figures 15 and 16  $C_{p_\infty}$  was assumed to be zero.

These concepts have been applied by R. H. Liebeck [8] [9] to complete airfoils where many more considerations and constraints enter. Furthermore the application has been done in terms of surface distance and circulation instead of projections on a chord plane. Figure 17 shows one of the shapes designed with a laminar rooftop to operate at  $R_C = 5 \times 10^6$ . The lift is quite high and the drag very low. Wind tunnel tests verify this theory very well.

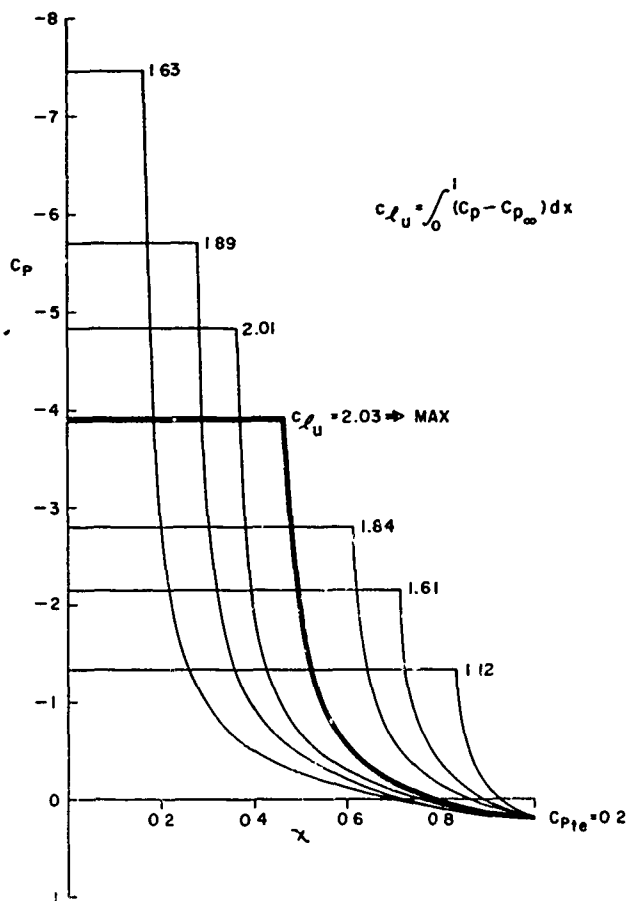


Figure 16. Suction side pressure distributions using Stratford pressure recovery to  $C_p = 0.20$  at trailing edge. Laminar rooftop,  $R_C = 5 \times 10^6$ .

### 3.4 Off-the-surface pressure recovery.

At times the boundary layer may undergo pressure rise in a different fashion. Its final deceleration is in the form of a wake, away from the surface. The wake is shed from an upstream element, for example a slat. Figure 18 shows calculated streamlines for a high lift configuration. On the top side flow leaves a forward element and streams past the following surfaces at a slight distance off the surface. The flow leaving each surface is boundary layer and hence it forms a wake. If a forward surface, say a slot, is sufficiently far out, the

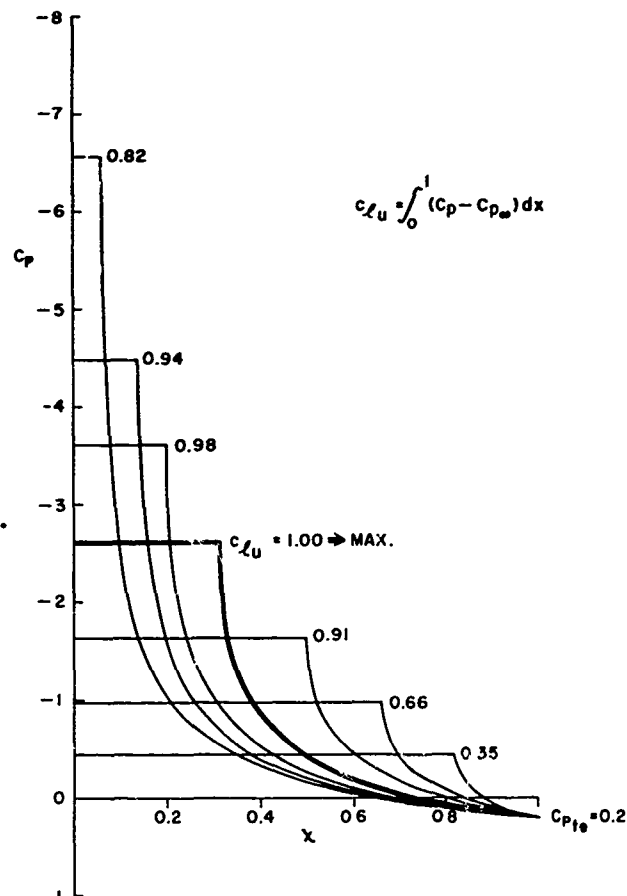


Figure 15. Suction side pressure distributions using Stratford pressure recovery to  $C_p = 0.20$  at trailing edge. Turbulent rooftop,  $R_C = 5 \times 10^6$ .

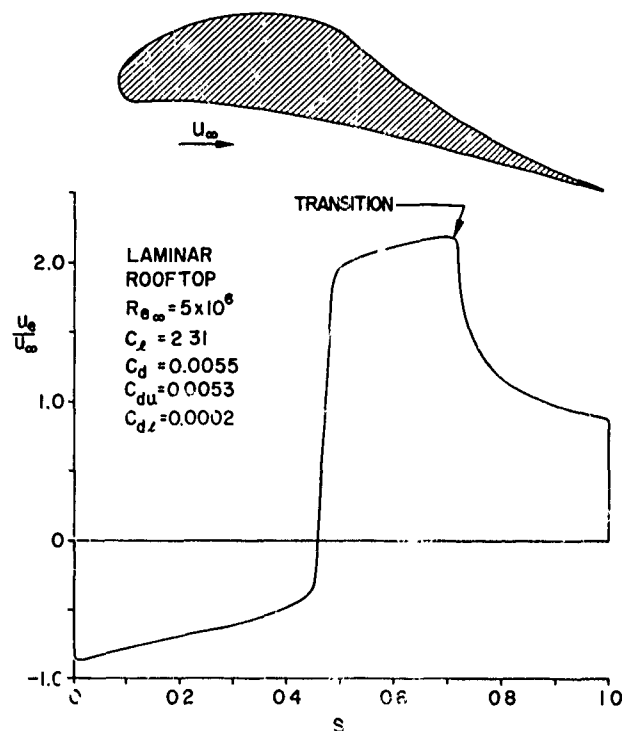


Figure 17. An optimized high lift airfoil that uses a Stratford pressure recovery. Values noted are theoretical.  $s$  is peripheral distance, measured from the trailing edge.

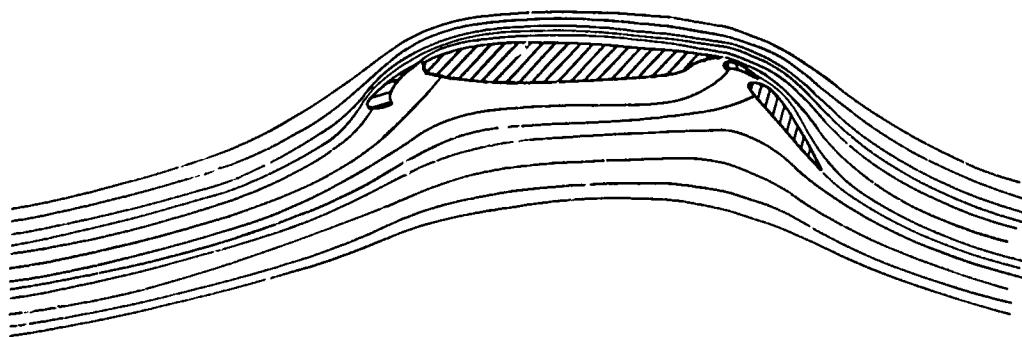


Figure 18. Calculated streamline flow field for airfoil with leading edge slat and double slotted flap

wake is entirely in the main stream, separated by a region of inviscid flow. If closer in, the wake and boundary layer of the main airfoil may merge, giving what is called a confluent boundary layer. These wakes flow into a region of higher pressure. For example in Figure 33 the final  $C_p$  for the slot is about -1.4. The final  $C_p$  at the flap trailing edge is about +0.35. Since the slot wake is never very far from the surface it is reasonable to assume it too must undergo this pressure rise. Can it make it? At times flow reversal can occur off the surface. The possibility is easily demonstrated by considering

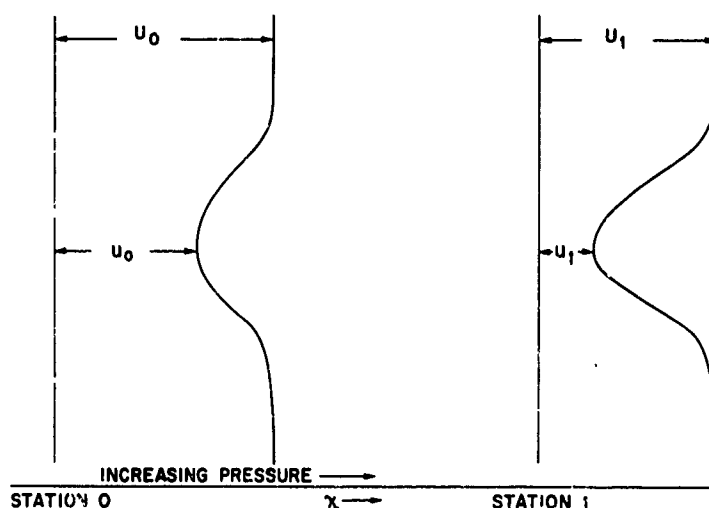


Figure 19. Flow of a wake into a pressure rise

Bernoulli's equation. Consider the situation illustrated in Figure 19. Assume (correctly) that pressures are impressed by the inviscid flow. Bernoulli's equation applies exactly in the inviscid flow. Assume it applies too in the wake along streamlines. In the wake consider a streamline having the initial velocity  $u_0$ . It could be any streamline, but our attention shall be given to the one having the minimum velocity. Write Bernoulli's equations for the two stations, remembering that pressures within the wake are the same as those outside. Then

$$p_0 + \frac{1}{2} \rho U_0^2 = p_1 + \frac{1}{2} \rho U_1^2 \quad (8)$$

$$p_0 + \frac{1}{2} \rho u_0^2 = p_1 + \frac{1}{2} \rho u_1^2 \quad (9)$$

Solve for  $U_1^2$  and  $u_1^2$

$$U_1^2 = \frac{2}{\rho} \left[ p_0 - p_1 + \frac{1}{2} \rho U_0^2 \right]$$

$$u_1^2 = \frac{2}{\rho} \left[ p_0 - p_1 + \frac{1}{2} \rho u_0^2 \right]$$

Their ratio is

$$\left(\frac{u_1}{U_1}\right)^2 = \frac{p_0 - p_1 + \frac{1}{2} \rho U_0^2}{p_0 - p_1 + \frac{1}{2} \rho U_0^2} \quad (10)$$

Now introduce our canonical pressure coefficient  $\bar{C}_p = (p_1 - p_0)/\frac{1}{2} \rho U_0^2$ . After some manipulation (10) becomes

$$\left(\frac{u_1}{U_1}\right)^2 = \frac{\left(\frac{U_0}{U_1}\right)^2 - \bar{C}_p}{1 - \bar{C}_p} \quad (11)$$

If  $(U_0/U_1)^2$  were 1/2 eq.(11) shows that  $(u_1/U_1)^2$  reaches zero when  $\bar{C}_p$  reaches 0.5, so that the velocity defect ratio becomes magnified. Hence the possibility of separation in the stream entirely away from the wall is demonstrated. Here viscosity helps because it tends to assist the slowest parts of the flow.

Newman [10] has considered this problem at some length, with viscosity effects included. Gartshore [11] extends it and attempts to apply it to a problem closely related to ours. He has derived a test for whether the depression in a wake fades away or grows. It is, in our notation

$$\frac{1}{1 - \bar{C}_p} \frac{d\bar{C}_p}{dx} = \frac{1}{1 - \bar{C}_p} \frac{d\bar{C}_p}{dx} > \frac{0.007}{\delta^*} \quad (12)$$

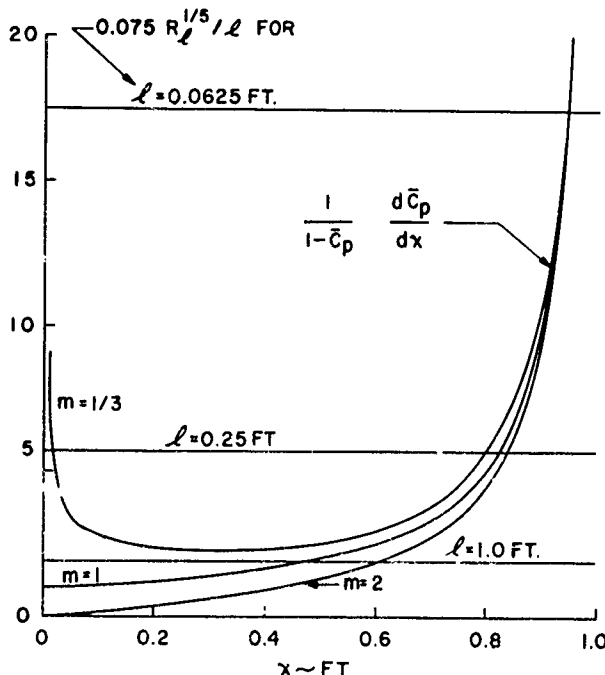
where  $\delta^*$  is the displacement thickness at the beginning of pressure rise. When the left hand side of (12) exceeds  $0.007/\delta^*$  a velocity defect will magnify. Information on this problem is scarce, and the theory is not very well developed and proven. Therefore Gartshore feels justified in representing the derivative by a simple finite difference relation. He writes a quantity  $C$  that measures the magnitude of the inequality in terms of values at Stations 0 and 1, Figure 19. We write it in both conventional and canonical  $\bar{C}_p$  form. In canonical form  $\bar{C}_p$  at station 0 is zero.

$$C = \frac{1}{1 - \bar{C}_{p0}} \frac{\bar{C}_{p1} - \bar{C}_{p0}}{x_1 - x_0} - \frac{0.007}{\delta^*} = \frac{\bar{C}_{p1}}{x_1 - x_0} - \frac{0.007}{\delta^*} \quad (13)$$

The test is illustrated by applying it to the pressure distributions of Figure 9, with  $u_1/v = 10^7$  as in that figure. It is assumed that a flat plate of lengths 1, 0.25 and 0.0625 feet discharges both its boundary layers into the pressure gradients of Figure 9. The trailing edge is at  $x = 0$ , so that the physical setup is quite similar to that of Figure 9. Equation (12) shall be applied. The thickness  $\delta^*$  is conveniently represented by the 1/7 power formula with sufficient accuracy

$$\delta^* = \frac{0.0463 \ell}{R_\ell^{1/5}} \quad (14)$$

When twice this value, to account for both boundary layers, is inserted into (12) we obtain



$$\frac{1}{1 - \bar{C}_p} \frac{d\bar{C}_p}{dx} > \frac{0.075 R_\ell^{1/5}}{\ell} \quad (15)$$

where  $\ell$  is the length of the flat plate and  $R_\ell = \frac{U_0 \ell}{\nu}$ . Figure 20 shows plots of both sides of (15) for some of the flows of Figure 9. When the  $\bar{C}_p$  function passes above the horizontal lines the wake depression supposedly magnifies.

For fractional exponents the flows start out unstable, if the criterion is to be believed. Then for a period the flows may be stable, but finally they always become unstable. The linear distribution ( $m = 1$ ) starts out with a finite value, while with  $m > 1$  the  $\bar{C}_p$  function always begins at zero. Ultimately curves for any  $m$  merge and reach infinity at  $x = 1.0$ , the stagnation point. Referring to (13), this equation could easily miss the infinity occurring near  $x = 0$  for fractional exponents, because of the finite nature of the derivatives.

Figure 20 shows a strong effect of boundary layer thickness as measured by the three lengths of flat plate. The levels of these horizontal lines would lower as the unit Reynolds number is reduced, in fact by the 1/5 power. For the run of length 1 foot the  $m = 1/3$  flow is always unstable, but the two others begin stably. Hence, if to be believed, a wake may be more prone to trouble for the  $m = 1/3$  flow than a

Figure 20. Evaluation of equation (15) for the decelerating flows of Figure 9.  
 $U_0/\nu = 10^7$

boundary layer. However for thinner wakes, as for the 0.25 foot plate which is more the characteristic length for a slot, difficulties are not encountered until  $x = 0.8$ , neglecting the very short region near  $x = 0$  for  $m = 1/3$ . Upon examining Figure 9, for  $l = 0.25$  foot it is found separation occurs first, so that wake type instability is not critical. Even more margin occurs for the  $l = 0.0625$  foot flow.

Gartshore cites experimental evidence that confirms his deductions. It was obtained by examining flow over deflected plain flaps. Without doubt the effect can and has occurred - separation off the surface. But very little has been done on this problem so that validity of relation (12) is in question. Especially in question are some of the derived consequences, such as the initial instability for some fractional values of  $m$ , e.g.,  $m = 1/3, 1/2$ , but which do not separate as boundary layers. The principal purpose in presenting example applications is to get the concept into the open, and at least exhibit in a qualitative way the effect and the interaction between wake thickness and pressure gradient.

In practical applications with their lack of infinite adverse gradients through which a wake must flow, this wake instability problem should rarely be critical, meaning that wakes can endure pressure rises that boundary layers cannot endure. What a multi-element airfoil does then, in effect is to use two methods of pressure recovery, the conventional, i.e. on-the-surface pressure recovery plus - off-the-surface pressure recovery. On a slatted airfoil for instance the history of the flow is: air flows over the slat, reaches a peak velocity and then decelerates in contact with the surface. It leaves the surface and continues to decelerate until trailing edge pressures are reached, after which it gradually accelerates back to free stream conditions. By this off-the-surface deceleration, recovery from very high negative  $C_p$  values can be made in much shorter distance than can be done when all the deceleration is in contact with a surface.

Lockheed [12] has developed a very general method for analyzing flows when the wakes and boundary layers merge. Because of the complicated nature of the flow bold simplifications had to be made, and it too suffers from the lack of detailed experimental data to guide or verify the analysis.

## PART II. DEMANDS ON THE BOUNDARY LAYER AND THEIR CONTROL

### 4. SINGLE ELEMENT AIRFOILS

This subject has been rather automatically covered by the material in Part I. The canonical pressure distributions show general limits to the pressure rises and the set of charts can be used for eyeball checks prior to careful examination of more nearly final designs by detailed boundary layer calculations. If a boundary layer is overloaded, separation will occur. Then some change must be made in a design if it is to be prevented. On a one-piece airfoil there are a number of means, - changed leading edge radius, a flap, or changed camber near the trailing edge, a nose flap, or a change in type of pressure distribution. A pressure rise may be changed from convex to concave, in the direction of Stratford's type. Use of canonical pressure distributions for preliminary scanning is useful.

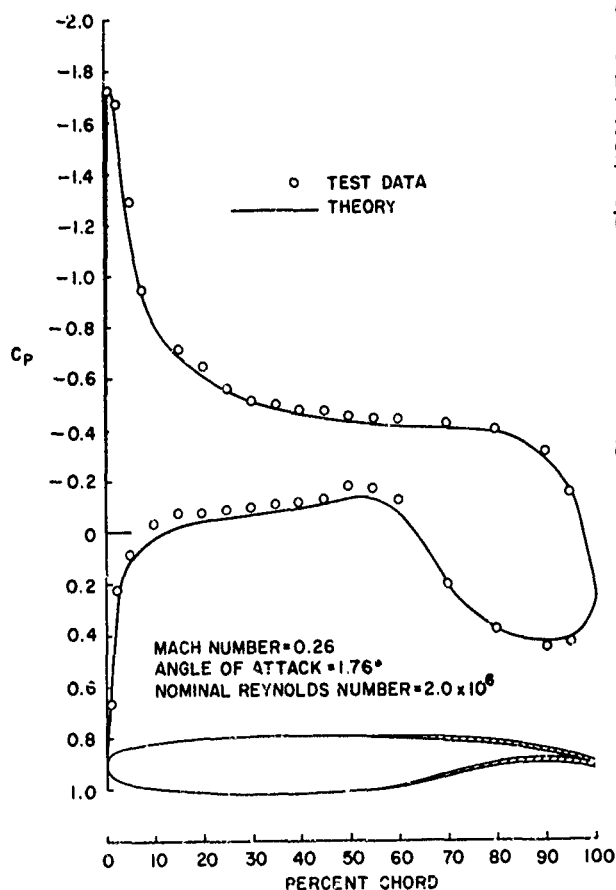


Figure 21. A pressure distribution for a typical aft-loaded airfoil. Pressure distribution is corrected for boundary-layer effects.

Figure 21 shows a conventional pressure distribution. Where is separation most imminent?, near the front on top?, near the rear on top?, or on the bottom? Figure 22 is the canonical form of Figure 21. Upon comparison with the curves of Figures 8 and 9 it would appear that the nose is far from separation. The rear upper surface is marginal, but only behind about 97 percent chord. The lower surface retards to  $C_p$  of about 0.5 in a rather short distance. Figures

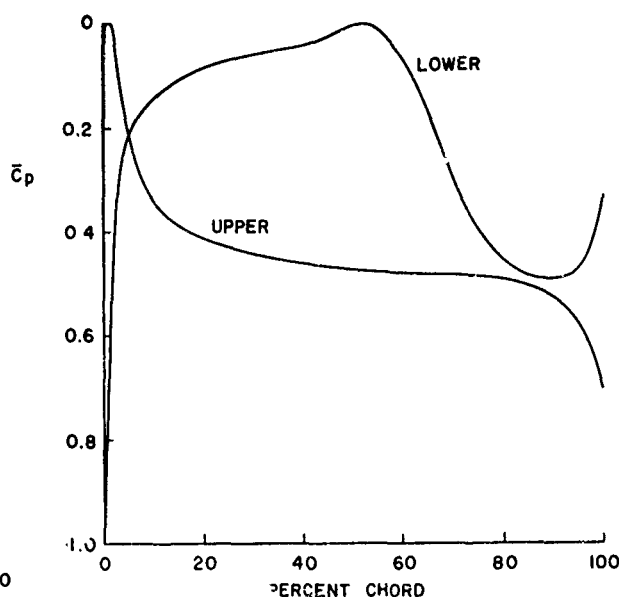


Figure 22. The pressure distribution of Figure 21 in canonical form.



8 and 9 indicate  $C_p$  of about 0.6 could be reached in this distance. Hence there is some margin, but not much. Provided other constraints allow it, the faintly S-shaped pressure distribution aft of 50 percent chord on the bottom could have been improved by replacing it with one that is concave all the way. In problems and approaches like this the advantages of an inverse airfoil method are evident; that is, given a pressure distribution, find the shape.

An interesting problem relating to separation and the most rapid possible pressure rise is: "What is the thickest possible strut that can be made that has no separation on it, and what is its shape?" This problem is being worked on using Stratford's pressure recovery distribution and inverse airfoil methods.

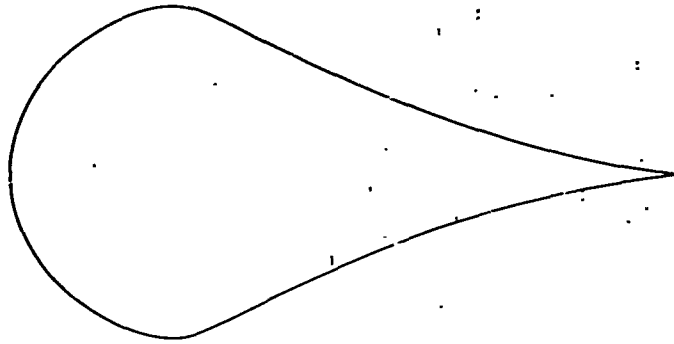


Figure 23. Preliminary form of a very thick strut that uses a Stratford pressure recovery.  $R_c = 5 \times 10^6$ . Accelerating flow is laminar.

Final answers have not been found, but one trial is shown in Figure 23. This shape is about 46 percent thick. Possibly 50 percent can be reached.

#### 5. MULTI-ELEMENT AIRFOILS

There seems to be a great deal of ignorance and confusion about the effect of properly designed gaps inherent in multi-element airfoil systems. The writer has heard the question, "Shouldn't the best single element airfoil always have a higher lift than a multi-element? The multi-element has a number of leaks that amount to short circuiting". Abbott and von Doenhoff [13] merely make the comment, "Slots to permit the passage of high energy air from the lower surface to control the boundary layer on the upper surface are common features of many high lift devices." This statement rather implies that the effect of slots is thought of as a sort of blowing boundary layer control. It really is not because all the inviscid flow has the same total head. Perkins and Hage [14] make the harmless and non-informative statement, "The air flowing through the slot in Figure 2-49 is accelerated and moves toward the rear of the airfoil section before slowing down and separating from the surface". Lindfield in Lachmann [15] has a brief article on the slot effect. The essential features were studied by Lachmann in 1922 by considering a Joukowski airfoil, but his theoretical studies seem to have gradually been forgotten. Furthermore, he considered only half the problem. Lindfield's article is correct as far as it goes but is not very factual. He points out the need for better analytical methods before the slot effect can be well analyzed. A very recent remark is the following taken from a NASA report [12]: "It is well recognized that the usual function of the slot is that of a boundary layer control device permitting highly adverse upper surface pressure gradients to be sustained without incurring severe separation. This stabilizing influence results from the injection of the high energy slot flow into the upper surface boundary layer." It should be clear that there is room for further work. Furthermore, there is not really any boundary layer control at all, as will be shown.

There are five primary effects of gaps, and here we speak of properly designed aerodynamic slots.

##### 1. Slat Effect

The circulation on a forward element (e.g., a slat) runs counter to the circulation on the downstream element and reduces negative pressure peaks on the downstream element.

##### 2. Circulation Effect

In turn the downstream element places the trailing edge of the adjacent upstream element in a region of high velocity that is inclined to the mean camber line at the rear of this forward element. This flow inclination induces appreciably greater circulation on the forward element.

##### 3. Dumping Effect

Because the trailing edge of a forward element is in a region of appreciably higher velocity, the boundary layer flow "dumps" at higher velocity. This higher discharge velocity relieves the pressure rise impressed on the boundary layer, so alleviating separation problems.

#### 4. Off-The-Surface Pressure Recovery

The boundary layer from forward elements is dumped at velocities appreciably higher than free stream. The final deceleration to free stream velocity is done in an efficient way. The deceleration of the wake occurs out of contact with a wall. This is usually more effective than the best possible deceleration in contact with a wall.

#### 5. Fresh Boundary Layer Effect

Each new element starts out with a fresh boundary layer at its leading edge. Thin boundary layers can withstand stronger adverse pressure gradients than thick ones.

These effects will now be explained and discussed in turn at some length. Laminar bubbles, merging boundary layers and the like may complicate the case, but when Reynolds numbers are high and at design conditions such side effects should not be important. Therefore, only conventional boundary layer effects are considered.

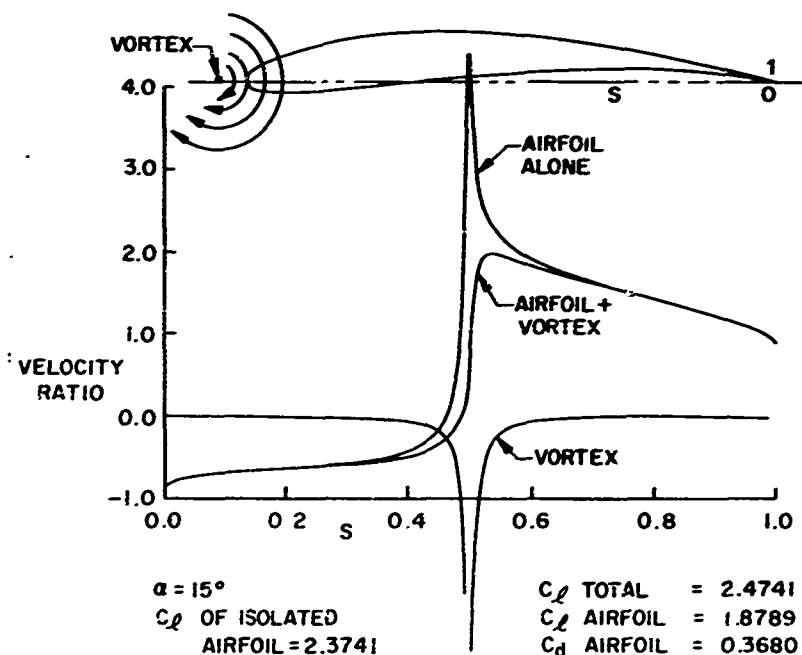


Figure 24. Velocity distributions on an airfoil with and without a vortex located as shown. S is the arc length around the airfoil surface beginning at the trailing edge, measured in a clockwise direction. Total perimeter is unity.

#### 5.1 The Slat Effect

Figure 24 illustrates this effect. A slat that is lifting has circulation in the direction sketched, see upper part of figure. Approximately, then, the slot may be simulated by a vortex. It is evident from the sketch that the velocities induced on the airfoil run counter to those near the nose of the airfoil, especially at high angle of attack. Therefore pressure peaks should be reduced. Liebeck and Smyth [16] have recently studied this effect using a special generalized Joukowski airfoil program with computer graphics. Figure 24 is an example of the work. In the method the vortex could be moved around at will. The best location was typical of that for a best real slat location. The "best" location is not a precise statement; it is the location where the suction peak was largely eliminated and the resulting pressure distribution was regular. At  $\alpha = 15^\circ$  the plain airfoil developed a very strong suction peak as seen. As noted at the bottom of the Figure  $c_L$  for the airfoil alone is 2.37. With a vortex located as shown (its strength is not noted) the pressure peak was eliminated, the airfoil  $c_L$  fell to 1.88 but the total lift including the vortex increased to 2.47. Flow near the rear of the airfoil was almost unaffected. This, then, is the slat effect. The peak nose velocity ratio was reduced from about 4.4 to under 2. Obviously the boundary layer is much better able to negotiate the modified distribution. Note that with vortex operating there is only a very small increase in total lift. This fact is consistent with wind tunnel observations. With slat extended the main effect is to delay the angle of stall, not to shift the angle of zero lift.

There is an interesting and more physical way of considering and explaining the slat effect: consider Figure 24. When the airfoil is at an angle of attack, flow whips around the nose, which has a small radius. High centrifugal forces on the flow are developed. Without auxiliary help, high negative pressures around the nose are needed to balance out the centrifugal force and bring the flow around the sharp turn of the nose. But in Figure 24 the vortex is a turning aid, and a true slat also would be one.

There should be a close correlation between the amount of load taken by the slat and the average  $C_p$  reduction over the nose. This problem would be a good one for farther study. The writer looked at Figure 24, and crudely made the following estimates. Area modulated - 10 percent chord, mean  $C_p$  of airfoil alone for this region = -8. Mean  $C_p$  for same region with vortex present = -2. Net  $C_p$  change = 6. Then the approximate force on vortex =  $c_l = 6 \times 0.10 = 0.6$ . The difference between  $c_{l \text{ total}}$  and  $c_{l \text{ airfoil}}$  is just the lift on the vortex. According to the numbers at the bottom of Figure 24,  $c_l = 0.6$  is indeed the load carried by the vortex. This analysis probably cannot be made quantitative, but it does add to the understanding of the flow processes. In the above analysis the force exerted by the vortex is not just vertical. It has a drag component too. According to Figure 24 its  $c_d$  value is -0.3680, a negative force which causes slats to extend automatically. A more careful estimate would consider this component.

The slat effect on real airfoils is exhibited by Figures 31 and 32. Figure 31 shows three airfoils together, all at the same angle of attack. The pressure distribution of the basic isolated airfoil is shown by the dashed line. Observe the extreme rounding of the peaks that has occurred on the two rear airfoils. This rounding is not due solely to the circulation as in Figure 24. Part of the effect is due to thickness. Because the flow on the two sides of the front airfoil is merging at the trailing edge the flow is retarded, and the nose of the following airfoil is in this retarded field. Another method of considering the interference effect is to consider surface source, sink singularities that can define the airfoil as in the Douglas Munk program. At the rear of the airfoil they are sinks, and hence locally add velocity perturbations that are counter to the main flow field.

Figure 32 shows the effect still further. The peak velocities on the main airfoil have been reduced dramatically by the slat. Later in Section 5.3 it will be shown that the high velocities on the slat itself can be tolerated.

## 5.2 The Circulation Effect

The slat effect has been recognized before, in fact clearly as far back as 1922 by Lachmann [15]. But the circulation effect does not seem to be explicitly recognized. Figure 25 shows the effect in

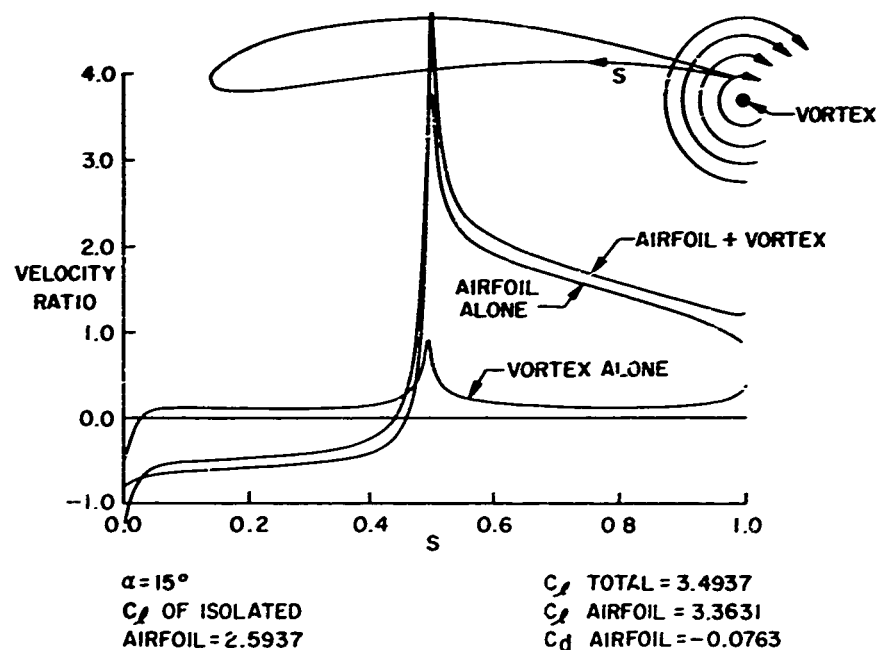


Figure 25. A point vortex used to simulate a slotted flap. Vortex increases  $c_l$  of airfoil at  $\alpha = 15^\circ$  from 2.59 to 3.36.

its simplest form. It comes from the same computer graphic setup as used for Figure 24. Here the vortex is located directly below the trailing edge as sketched. If it represents a slotted flap the sign of the vortex circulation will be as noted. This flow effectively places the trailing edge at a high angle of attack, and if the Kutta condition is still met the circulation must increase. The effect is very little different from deflecting a small plain flap on the isolated airfoil. In that case the onset flow would be approaching the rear of the airfoil at a considerable angle. But in the case of Figure 25 we did not turn the trailing edge; instead we used a device to turn the flow. Figure 25 shows a slightly different airfoil from that of Figure 24, but again at the same angle of attack. The vortex has a drastic effect on circulation, increasing  $c_l$  from 2.59 to 3.49. Also notice that the final upper surface velocity is

increased considerably over values for the isolated airfoil. Because of the additional velocity caused by adding the vortex to the general translational flow, the airfoil discharges boundary layer at the trailing edge into a stream that is locally of higher velocity. This is the "damping effect" about which more will be said later.

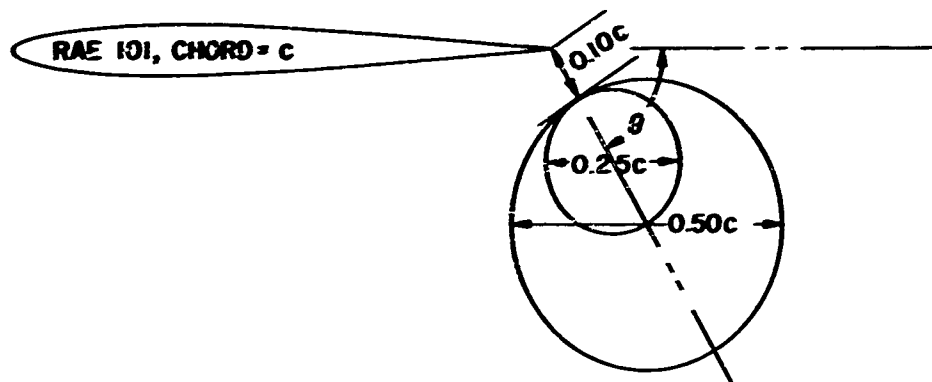


Figure 26. Airfoil - circular cylinder combinations studied to learn effect of obstruction on circulation.

Any method that causes the onset flow to be at greater angle of attack near the trailing edge will increase the circulation. An obstruction properly placed can be a powerful control of the circulation. Figure 26 shows a system studied. Two circular cylinders of different diameters are centered on a ray from the trailing edge as shown. The gap is 0.1 chord. The angle of the ray,  $\theta$ , was varied from  $0^\circ$  to  $90^\circ$ . The lift on the airfoil and on the combination was calculated. For the case where the cylinders

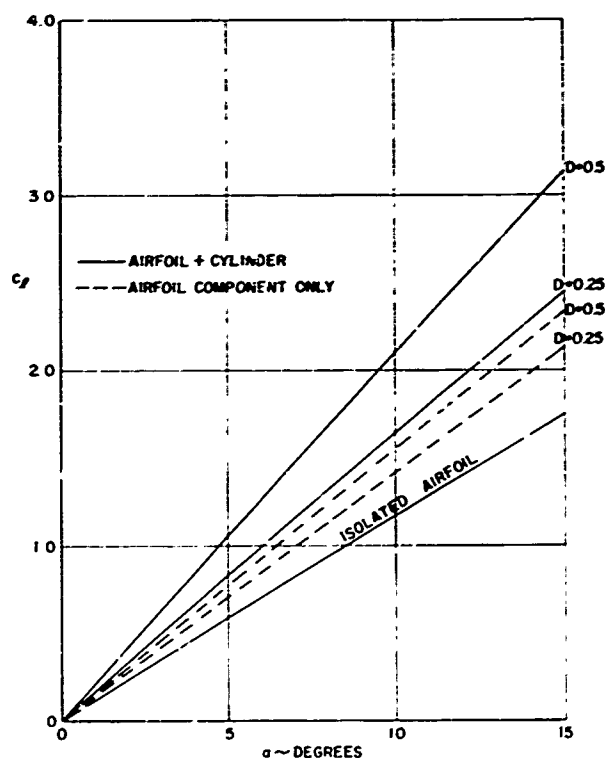


Figure 27.  $C_L$  vs.  $\alpha$  curves for airfoil-cylinder combinations, showing strong effects on circulation.  
 $\theta$  of cylinder (cf Fig. 26) =  $0^\circ$

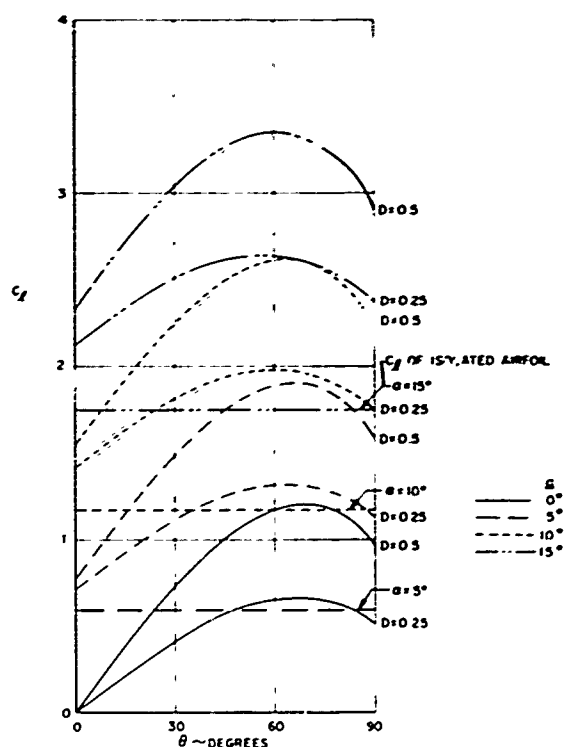


Figure 28. Airfoil - circular cylinder combinations. Effect of  $\alpha$ ,  $\theta$  and diameter on lift coefficients.

are on the chord line ( $\theta = 0^\circ$ ), Figure 27 shows some results. Significant increases in lift are indicated. However, this geometry is far from being the most favorable. Figure 28 shows the effects more completely and also indicates the most favorable position as measured by  $\theta$ , which here is the abscissa, instead of  $\alpha$ . The most effective position for the cylinder is seen to be about  $\theta = 60^\circ$  or  $70^\circ$ . At  $15^\circ$  angle of attack the lift coefficient for the isolated airfoil is  $C_L = 1.75$ . With the 0.50c circular cylinder set at  $\theta = 60^\circ$ ,  $C_L = 3.35$ , nearly double. Hence the effect is very great. Figure 26 is drawn with  $\theta = 60^\circ$ . It appears that this most effective position is similar to the position found most effective for airfoil-slotted flap and slat combinations.

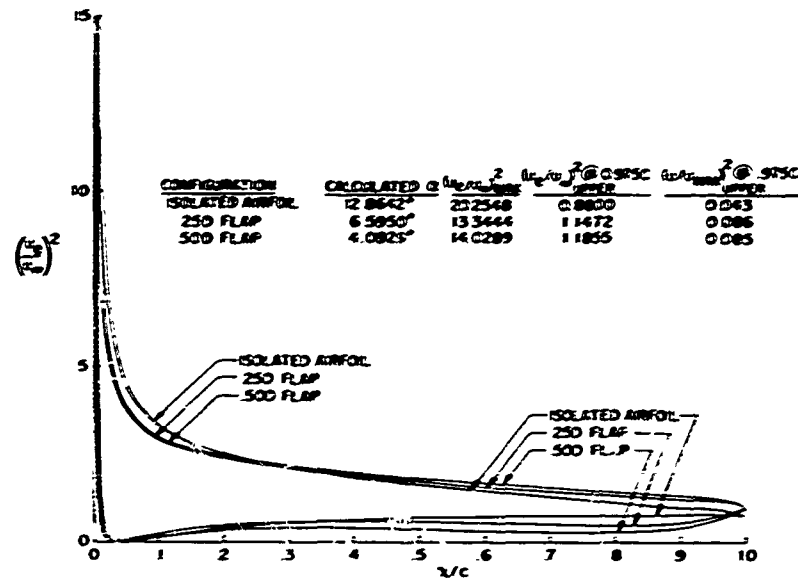


Figure 29. Pressure distributions at  $c_l = 1.5$  for airfoil-cylinder combinations.  $\theta = 60^\circ$

Figure 29 shows pressure distributions for the cases  $\theta = 60^\circ$ , and with  $c_l$  held constant at 1.5. The corresponding  $\alpha$  values are noted in the figure. Peak values of velocity at the nose are considerably reduced by the cylinder. If the pressures were plotted in canonical form the ones with the cylinder would appear considerably more favorable. Velocities at 0.975c are noticeably increased by the cylinders.

The formula for velocity on the surface of an isolated circular cylinder is  $q/u_\infty = 2 \sin \beta$ , where  $\beta$  is angle from the nose. To find the component of flow that is normal to the airfoil multiply by  $\cos \beta$  so that  $(q/u_\infty)_{\text{normal}} = \sin 2\beta$ . The maximum of this value occurs at less than  $\theta = 60^\circ$  but is close enough to indicate that a qualitative understanding of the effect of an obstacle on circulation can be gained by considering the crossflow induced at the trailing edge.

Another aid in thinking about this problem of affecting the circulation is to consider the rear stagnation point in non-lifting flow. Without the circulation component of the complete solution, for combinations such as that of Figure 26, the rear stagnation point will be on the upper surface some distance ahead of the trailing edge. The further it is moved forward by any means, the greater the circulation required to move it to the trailing edge. These two guidelines - crossflow strength and non-lifting stagnation point location are the best that can be proposed as a means for understanding and designing to maximize circulation. There are too many interactions to really isolate factors. Fortunately, accurate multi-element airfoil analysis methods are available, together with much experience. But perhaps factors such as discussed here will help in endeavors to improve design.

The reason augmented circulation is desirable needs discussion. In numerical airfoil methods of the Douglas-Neumann type the complete solution is a linear combination of three fundamental solutions which are shown in Figure 30. Because of the small radius of the leading edge, local velocity ratios in this region are very high indeed for both the  $90^\circ$  and circulation solutions. A positive lifting circulation is shown in Figure 30. It is clear that its disturbance velocities add to those of the  $90^\circ$  solution for positive angles of attack. For an ordinary airfoil, developing more lift requires increasing the angle of attack. But in the process more of the  $90^\circ$  solution enters into the summation. Now if the airfoil nose can be kept at low angle of attack, a gain will be made if circulation can be produced by some means other than pitching. A plain flap does this effectively, because when deflected a considerable cross flow component of the onset velocity exists at the trailing edge. The vortex or an obstacle near the trailing edge has the same effect. To avoid nose peaks the nose should be at a slight negative angle in any real design so that the

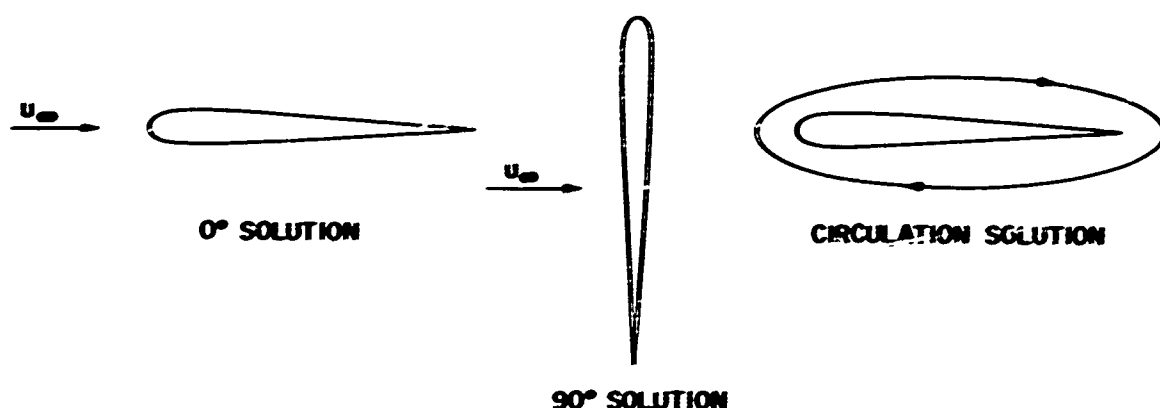


Figure 30. The three fundamental solutions used for calculating flow about a lifting airfoil at angle of attack.

circulation and 90° solutions oppose each other and cancel out, or more properly, the sum of the three solutions essentially cancels out. In short, considering the separation problem, high lift is best obtained by keeping the nose angle of attack low, and inducing circulation by means other than pitching.

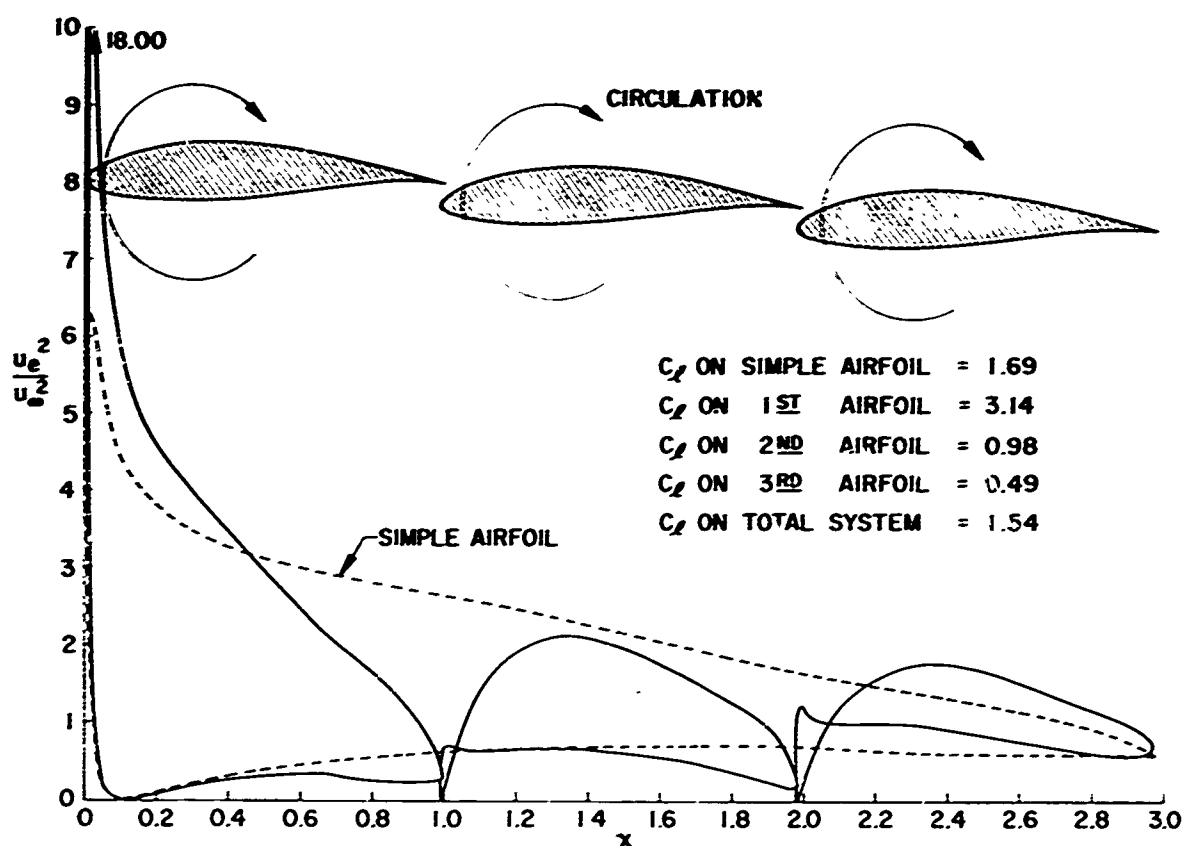


Figure 31. Pressure distribution on three-element airfoil formed from three NACA 632-615 sections, arranged as shown. All are at the same angle of attack, 10°. Shown also is the pressure distribution on the basic simple airfoil at 10° of attack.

Figure 31 further illustrates interaction effects. Three airfoils, all at the same angle of attack were placed together as illustrated. A common angle of attack was selected in order to display better the interference effects. The slot gaps were 1 percent of local chords. The pressure distributions are affected tremendously. In addition to local cross flow effects at the trailing edges there are global effects. On each airfoil circulation is as sketched in the upper part of the figure. The rear airfoils then induce more upwash on the front airfoil and the two front airfoils in turn induce more downwash

on the rear. Hence the front becomes very heavily loaded, the rear very lightly loaded, and the center of pressure moves forward. In the beginning of Section 5 the view was raised that slots amount to a short-circuiting of the lift. That effect apparently can exist when the elements are not properly positioned. Observe the dropoff in pressure near the slots. It is interesting to note that at  $10^\circ$  angle of attack the single element airfoil carries slightly more load than the three-airfoil system.

The same kind of interaction occurs between sails on a sailboat, or even between boats in close proximity. According to Figure 31 if the front airfoil corresponded to a boat in the lead, boats drawing up on the leader, corresponding to the rear airfoils, would have a very difficult time passing the leader because they are augmenting his lift and reducing theirs. Of course the effects are much stronger between sails on the same boat. A jib and a mainsail correspond roughly to a slat-wing combination. A useful and very interesting study of the problem has been made by A. E. Gentry [17]. By using the electrical analogy technique and conducting paper, he greatly clarified this long time puzzle to sailing people.

### 5.3 The Damping Effect

Closely related to the circulation effect is the damping effect. The favorable interference of a downstream element induces cross flow at the trailing edge which enhances the circulation. But the interference also increases velocities in a tangential direction so that the flow from a forward element is discharged into a higher velocity region, thus reducing pressure recovery demands. This is an effect that is quite favorable to the boundary layer. It was anticipated in Figure 12, where it was shown that for the same canonical pressure distribution increased damping velocity would permit significantly increased lift.

Does this effect really exist? The answer is yes indeed. It can be seen in any properly designed multi-element airfoil. It is also clearly shown in Figure 29 and values are tabulated in the right hand columns. The damping velocity is not a precisely defined quantity. It is the effective final velocity on the suction side of the airfoil with boundary layer taken into account. It cannot be at the very trailing edge because there the velocity is always zero, if the flow is inviscid and the trailing edge is finite. Velocities at about 97 percent chord would be a typical place to determine the value. Discharge velocity is probably an equally accurate term; so is recovery velocity. Trailing edge velocity is not. Effective trailing edge velocity would be suitable but it is a cumbersome term.

For the RAE 101 airfoil with the circles, Figure 29, the damping velocity ratios squared for airfoil alone, airfoil plus 0.25c circle and airfoil plus 0.50c circle are 0.88, 1.1472 and 1.1855 respectively, a change of 35 percent. Figure 32 based on Figure 12 of Reference 18 shows the effect for a slat. On the main airfoil the damping velocity squared is about (0.85). On the slat it is about (2.35).

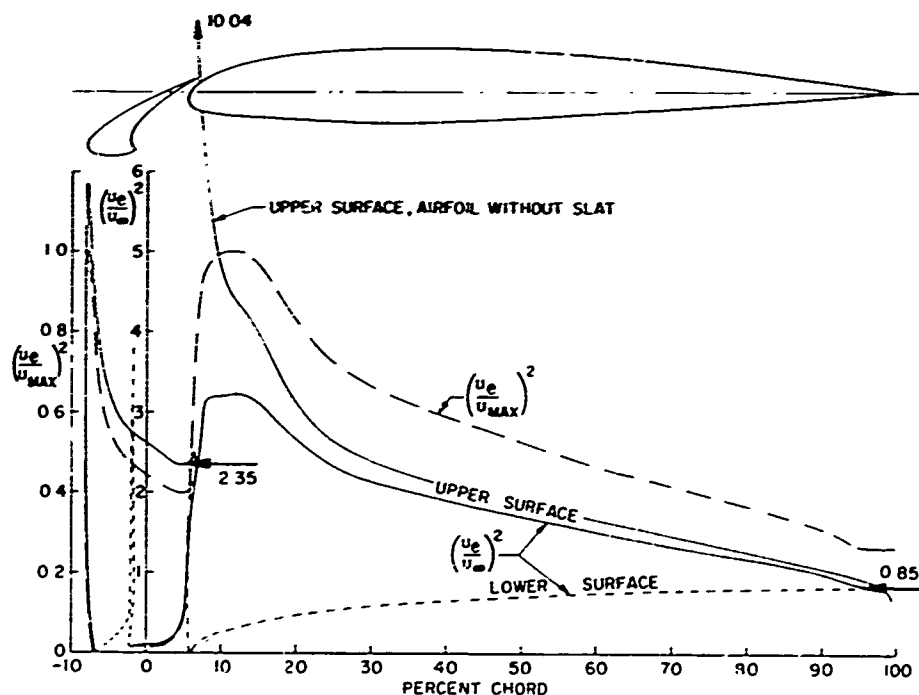


Figure 32. A typical theoretical pressure distribution for a two-element airfoil, corrected for the boundary layer. The damping velocity is denoted by the arrows. Also included is the canonical pressure distribution for the upper surface, as well as pressure distribution for the main airfoil alone. The latter exhibits clearly the favorable effect of a slat.  $\alpha = 13.15^\circ$ ,  $c_l = 1.45$  for 2-element airfoil.

This fact explains why slats can carry such high loads. The reason is shown more clearly by the canonical plot in Figure 32 which shows that the slat has a slightly less severe pressure distribution than the main airfoil, in spite of its very high loading.

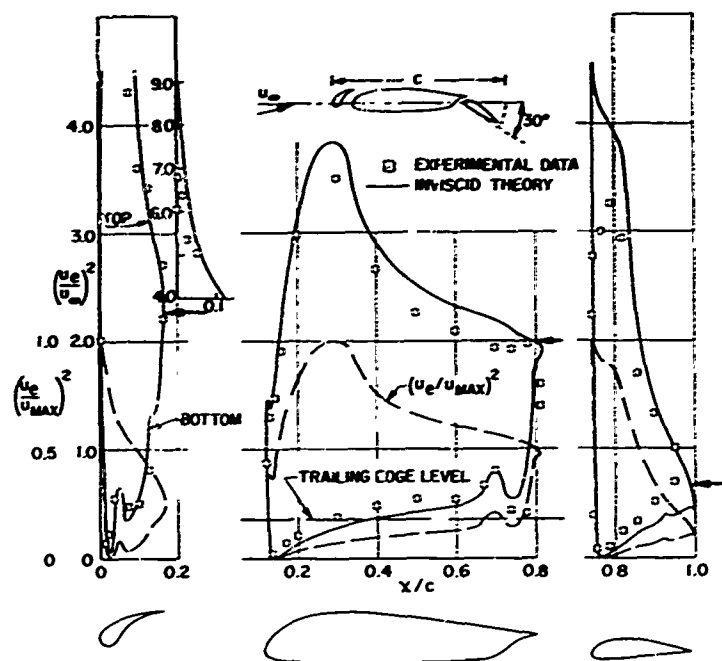


Figure 33. A typical three-element airfoil, showing dumping velocity effect. Arrows denote dumping velocity. NACA 23012 airfoil,  $\alpha = 8^\circ$ . Line marked trailing edge level is trailing edge dumping velocity divided by maximum velocity on main element.

Figure 33 shows a typical three-element airfoil. Again the dumping velocity effect is clearly exhibited. The canonical plots indicate that the main airfoil is less severely loaded than the slat and flap. These results are typical. Any properly designed multi-element airfoil shows the effect.

It is interesting to conjecture about what might be done with this effect if an inverse design method for multi-element airfoils were available, and assuming the complete inviscid airfoil requirements permitted. Start with some desired pressure distribution. An example is shown in Figure 34

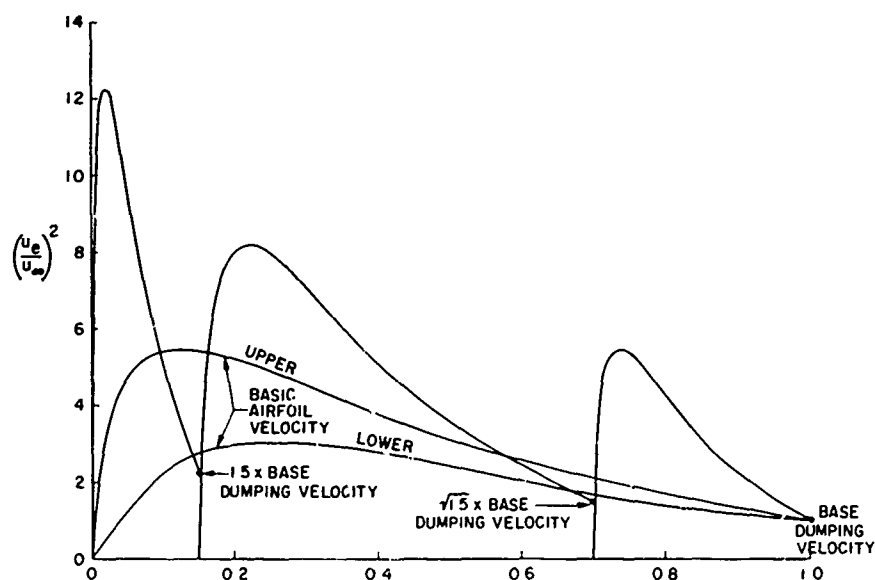


Figure 34. Illustration of compounding of lift by using multi-element airfoils. For illustration the factor  $m$  is  $\sqrt{1.5}$ .



for a hypothetical three-element airfoil. The base airfoil is shown plotted for the full chord length. Then suppose a three-element airfoil was sought that had this same canonical pressure distribution on each of the three elements. Furthermore assume that the rear element induces a damping velocity ratio  $(u/u_\infty)^2$  of 1.5 on the element immediately forward. Because this center element now can have higher circulation it should induce even greater effects on the front element. Assume the induced velocity ratio is the same for each element, (which is a bold assumption) with respect to its own velocities. Then the pressure distribution for the three elements of Figure 34 is as sketched. The load carried is far greater than that of the single element airfoil, yet the four individual canonical pressure distributions are all the same. The effect is readily quantitized. It shall be done only for a three-element airfoil but the analysis is easily generalized. Let

$$\begin{aligned} c &= \text{chord of the ensemble} \\ f_1 c &= \text{chord of rear airfoil, the flap} \\ f_2 c &= \text{chord of second or center airfoil} \\ f_3 c &= \text{chord of front airfoil, the slat.} \end{aligned}$$

Then for three elements  $f_1 + f_2 + f_3 = 1$ . Also let

$$\begin{aligned} \pi_2 &= \text{magnification ratio for velocity at trailing edge of second element due to being in the high velocity field of the nose of the rear element, element 1.} \\ \pi_3 &= \text{magnification ratio for velocity at trailing edge of third element due to being in the high velocity field of the nose of the second element.} \end{aligned}$$

The lift coefficient is  $c_{l1}$  for the given base pressure distribution. Then for the rear element, ignoring pressure-side effects, the suction-side lift is  $f_1 c_{l1}$ . On element 2 the apparent wind speed over the whole element is greater by a factor  $\pi_2$ . Hence for this element the lift is  $f_2 c_{l1} \pi_2^2$ . For the front element the apparent wind speed is increased by a factor  $\pi_3$ . But the center element has already been increased by a factor  $\pi_2$ . Hence on element 3 the lift is  $f_3 (\pi_2 \pi_3)^2 c_{l1}$ . Then the lift of the ensemble is

$$c_l = f_1 c_{l1} + f_2 \pi_2^2 c_{l1} + f_3 (\pi_2 \pi_3)^2 c_{l1}$$

and the ratio is

$$\frac{c_l}{c_{l1}} = f_1 + f_2 \pi_2^2 + f_3 (\pi_2 \pi_3)^2 \quad (16)$$

For the example of Figure 34  $f_1 = .30$ ,  $f_2 = .55$ ,  $f_3 = .15$ . Also  $\pi_2 = \pi_3 = \sqrt{1.5}$ . Then using (16)

$$\begin{aligned} c_l / c_{l1} &= .30 + 1.5 (.55) + 2.25 (.15) \\ &= .30 + .825 + .338 = 1.463 \end{aligned}$$

i.e., a 46 percent gain, with no greater tendency for separation than on the base airfoil. The effect definitely exists, but where real design is considered many more factors enter, so that the complete problem is not nearly this simple. How nearly the above relations could be approximated with real airfoils is a challenging problem for inverse airfoil theory.

#### 5.4 Off-the-Surface Pressure Recovery

This effect has already been discussed in Section 3.4. Without assistance of this effect, boundary layers would often be unable to meet the entire pressure rise requirements. As an example consider Figure 33. On the main element the pressure recovery demands are not great. But the flow from this element moves along slightly off the surface and must pass through pressures nearly as high as at the trailing edge. If it were in contact with the surface, as for a simple flap, it is doubtful that the trailing edge pressure level demands could be met except by off-the-surface pressure recovery. To verify this conclusion compare the canonical plot in Figure 33 with those of Figures 8-11.

#### 5.5 The Fresh-Boundary-Layer Effect

On each element of a properly designed multi-element airfoil the boundary layer starts out fresh. Here it is merely enough to identify and mention this fact, for it is well known that thinner boundary layers can sustain greater pressure gradients. Such measures of separation as Stratford's criterion

$$\bar{c}_p \left( \frac{v}{\frac{d}{dx} \bar{c}_p} \right)^{1/2} = 0.39 (10^{-6} R_0)^{1/10}$$

indicate explicitly by the factor  $x$  the effect of thickness of the boundary layer. Figures 7, 8, 9, 10, 11, 13, and 14 show the effect in more detail. It is clear that breaking up a boundary layer into several thinner boundary layers is favorable to the delay of separation.

## 6. CLOSING REMARKS

By this time it should be clear that a slot does not act like a source of high energy air as in blowing boundary layer control. In the inviscid region it has the same total head as all the rest of the inviscid stream. Indeed it has higher total head than the boundary layers on either side of it, but it is improper to state that the flow through a slot energizes the boundary layer. A boundary layer is always flowing adjacent to an inviscid stream and in an ordinary single element airfoil we never say that the inviscid stream energizes the boundary layer. The principal effects are that the upstream element reduces peak velocities on the downstream element and in reciprocation the downstream element increases the lift on the upstream element - a sort of "you help me and I will help you" situation.

Can a two-element airfoil develop more lift than a single element airfoil? We shall attempt to show that it can. In order to realize the pressure distributions considered, a two-element inverse method would be necessary. Unfortunately that is not available, although Wilkinson's method [19] is a good step in that direction. We assume

1. The lower surface plays only a weak role, so that it is only necessary to consider the suction surface.
2. Reynolds number effects are weak, which they are at large scale. Hence the lift attainable on an airfoil whose chord is unity is no more nor no less than the lift attainable on two of the same airfoils whose chords are  $1/2$ .

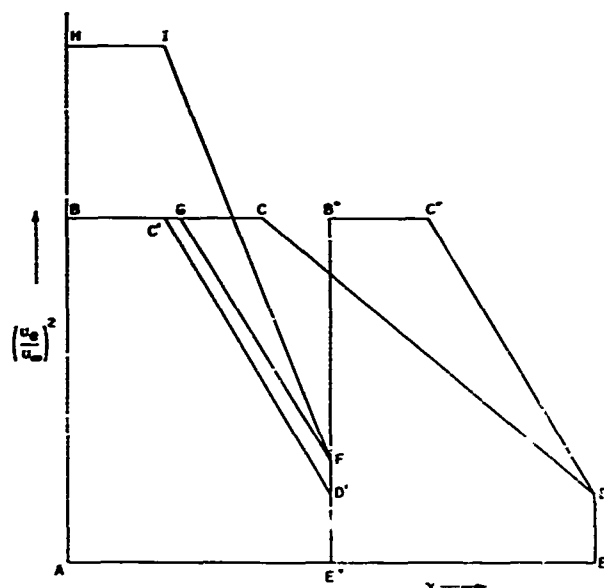


Figure 35. Load diagram for proof that a two-element airfoil can develop more lift than a single element airfoil.

Consider Figure 35. Let  $A B C D E$  be the pressure distribution on the upper side of an airfoil of chord  $A E$ . Assume that this distribution is some kind of optimum. The optimum load distribution is determined by boundary layer considerations. Hence this same load distribution could be applied twice, to two  $1/2$  chord elements as loads  $A B C' D' E'$  and  $E' B'' C'' D E$ . The sum of these two areas equals area  $A B C D E$ . By proper inverse methods shapes needed to develop the two pressure distributions can probably be found, although this point is a weak link in the proof. Now the basic dumping velocity squared is  $E'' D' = E D$ . On any properly designed multi-element airfoil the flow off the trailing edge of a forward element always discharges into a region whose velocity ratio is greater than unity. Hence for the front element the modified dumping velocity ratio squared is  $E'' F$ . Two cases now arise:

Case A - there is a limit to the maximum velocity that can be attained.

Case B - there is no limit to the maximum velocity ratio that can be attained.

Consider Case A first. Perhaps the velocity limit is local Mach number. Because velocity  $E'' F > E'' D'$  the start of pressure rise can be moved back from the point  $C'$  to a point  $G$ . Now area  $A B G F E'' > A B C' D' E'$ , which proves our case. Next consider Case B. If dumping velocity of the forward element is increased from  $E'' D'$  to  $E'' F$  the entire velocity distribution can be scaled by the ratio of the two. We obtain area  $A H I F E''$ . Again, and even more strongly area  $A H I F E'' > A B C' D' E'$ . Q.E.D.

It is not necessary to the proof that the two elements have equal chord. Furthermore by the same arguments three elements could be shown to be better than two. Only if velocity  $D E$  reduced enough to compensate for the increase  $D' F$  would a gain fail to be made. This is highly unlikely, although the ultimate test must be through inverse airfoil theory.

This paper began by stating that much can be learned about maximum lift by using the tools for analysis that are already available. The statement is believed to be confirmed by the work just presented. However, many interesting questions arise, which to answer require new or extended methods of analysis. Some of these are wakes in a pressure gradient, control boundary layers, accurate inverse methods for multi-element airfoils, and flows with partial separation. Remarkable progress on the problem of design and analysis of multi-element airfoils has been made, but much still remains to be done. For fully attached low-speed flow the maximum possible lift coefficient has been found and the necessary shape has been calculated. What is the maximum possible lift coefficient and the necessary shape for a two-element? a three-element? a four-element? a ...-element airfoil?

## 7. REFERENCES

1. Separated Flows, Parts 1 and 2 AGARD Conference Proceedings No. 4, Rhode-Saint-Genese, Belgium, May 1968.
2. Assessment of Lift Augmentation Devices, AGARD Lecture Series No. 43 (AGARD LS-43-71) Rhode-Saint-Genese, Belgium, February 1971.
3. Cebeci, T., Mosinskis, G.J., and Smith, A.M.O.: Calculation of Separation Points in Incompressible Turbulent Flows. J. Aircraft. (To be published.)
4. Cebeci, T., Mosinskis, G.J., and Smith, A.M.O.: Calculation of Viscous Drag and Turbulent Boundary-Layer Separation on Two-Dimensional and Axisymmetric Bodies in Incompressible Flows. Douglas Aircraft Company Report No. MDC-J0973-01, Long Beach, California, November 1970.
5. Stratford, B.S.: The Prediction of Separation of the Turbulent Boundary Layer, J.F.M., Volume 5, January, 1959, pp. 1-16.
6. Stratford, B.S.: An Experimental Flow with Zero Skin Friction throughout Its Region of Pressure Rise. J.F.M. Volume 5, January, 1959, pp. 17-35.
7. Loftin, L.K.Jr., and von Doenhoff, A.E.: Exploratory Investigation at High and Low Subsonic Mach Numbers of Two Experimental 6-Percent-Thick Airfoil Sections Designed to Have High Maximum Lift Coefficients. NACA RM L51F06, 1951.
8. Liebeck, R.H. and Ormsbee, A.I.: Optimization of Airfoils for Maximum Lift. J. Aircraft, Volume 7, No. 5, September-October, 1970, pp. 408-415.
9. Liebeck, R.H., and Smith, A.M.O.: A Class of Airfoils Designed for High Lift Without Separation in Incompressible Flow. Douglas Aircraft Report No. MDC-J1097/01, Long Beach, California, December 1971.
10. Newman, B.G.: Turbulent Jets and Wakes in a Pressure Gradient. In Fluid Mechanics of Internal Flow, G. Sovran, ed. Elsevier Publishing Company, Amsterdam, 1967.
11. Gartshore, I.S.: Predictions of the Blowing Required to Suppress Separation From High-Lift Airfoils. CASI Transactions, Volume 4, No. 1, March 1971, pp. 39-46.
12. Stevens, W.A., Goradia, S.H., and Braden, J.A.: Mathematical Model for Two-Dimensional Multi-Component Airfoils in Viscous Flow. NASA CR-1843, 1971, p. 92.
13. Abbott, I.H., and von Doenhoff, A.E.: Theory of Wing Sections, Dover Publications, New York. 1958, p. 227.
14. Perkins, C.D., and Hage, R. E.: Airplane Performance Stability and Control. John Wiley and Sons. New York, 1954, p. 78.
15. Lachmann, G.V. ed.: Boundary Layer and Flow Control, Volume 1, Pergamon Press, London, 1961, pp. 186-195.
16. Liebeck, R.H., and Smyth, D.N.: A Simple Model for the Theoretical Study of Slat-Airfoil Combinations. AIAA Paper 72-221, 1972.
17. Gentry, A.E.: The Aerodynamics of Sail Interaction. Proc. 3rd AIAA Symposium on the AER/HYDRONAUTICS OF SAILING. Western Periodicals Co., 13000 Raymer Street, North Hollywood, California, 91605.
18. Callaghan, J.G., and Beatty, T.D.: A Theoretical Method for the Analysis and Design of Multi-Element Airfoils. AIAA Paper 72-3, 1972.
19. Wilkinson, D.H.: A Numerical Solution of the Analysis and Design Problems for the Flow Past One or More Aerofoils or Cascades. British R and M, No. 3545, 1968.

# COMMENTS ON PAPER 10

prepared by  
 Prof. Dr D.Küchemann  
 Royal Aircraft Establishment  
 Farnborough, U.K.

and presented by  
 Dr R.C.Pankhurst  
 Royal Aircraft Establishment  
 Teddington, U.K.

Prof. Küchemann has asked me to convey his apologies and great regret at not being able to attend this meeting. He has, however, prepared several comments on Mr A.M.O. Smith's paper which I shall present on his behalf. In doing so, I should like to pay my own tribute to the paper for its depth of understanding, and to the way in which it disposes of several half-truths of long standing, as well as to its great relevance to a subject of vital importance. With Prof. Küchemann I welcome the emphasis placed on the design problem, and the manner in which the paper provides liberation from a heritage of reliance on empirical data and trial-and-error procedures. The approach to the design problem is, moreover, in line with that advocated by Prof. Küchemann himself and followed at the Royal Aircraft Establishment: some of this work is to be described by Mr Foster in the next paper.

Prof. Küchemann's first point concerns possible effects of viscous layers. These are considered in detail in Mr Foster's paper (especially for the case in which boundary layers and wakes do merge after all); but there is also an inviscid-flow effect that occurs when, for example, the wake behind the main aerofoil passes downstream above a flap, even when the wake does not touch the flap. The wake then introduces a nonuniformity into the stream; and in such a stream (inviscid but non-uniform) a body experiences a lift force which, compared to that in a corresponding uniform stream, always tends to be directed towards the region of highest velocity or total pressure. In our case, therefore, the induced force is directed away from the wake. Hence the lift on the flap will be reduced by the presence of the wake from the main aerofoil, even if viscosity is ignored. This effect may well have to be taken into account in a complete design method. Some theoretical background already exists, supported by experimental evidence; for example, the general problem of non-uniform flows has been treated in a paper by Ruden<sup>1</sup>.

Prof. Küchemann's second point concerns three-dimensional effects. These have not been considered in the paper, but the present work should surely be followed up and extended to three-dimensional wings. If one follows Smith's approach and uses the three fundamental solutions for calculating the flow, as shown in Figure 30 of Paper 10, then one must expect that all three of these will be strongly influenced by the effects of the central kink on swept wings and of the wing tips. For a kink section, even the first-order solutions differ significantly in all three cases from those obtained in two-dimensional flows. This means that fundamental differences must be expected and, in particular, that the resulting shapes for given pressure distributions will differ from those that can be calculated now for two-dimensional multiple aerofoils. This presents us with a big problem. Of course, the design principles stated by Smith still stand and should be applicable also to three-dimensional wings.

In the same context, it will probably also be necessary to take compressibility into account, even at these low speeds. This will be especially difficult on three-dimensional wings. We have now found that the ordinary compressibility factors are not good enough in the regions where the three-dimensional kink effects matter. It seems that we shall have to make do with empirical factors. But these must be different for the different terms involved there will be different factors for the first-order and for the second-order terms and also for the two-dimensional terms and the three-dimensional terms. We must therefore have a calculation method where all these different terms can be identified so that the different factors can be established and applied: there is not likely to be a single compressibility factor which one could apply to an overall answer such as that obtained by a panel method. So even if A.M.O. Smith's method could be extended to three-dimensional wings, more work would need to be done to determine the pressures in compressible flow. Perhaps, for instance, A.M.O. Smith's approach might be combined with the RAE Standard Method.

Prof. Küchemann's third point is concerned with the effect of vortices as discussed in connection with Figure 25 of the paper. These effects are quite real and can be demonstrated in practice. For example, the flow field of a line vortex can be produced by rotating a wing about its lateral axis, as Maxwell has shown in 1853. Since then, the properties of rotating wings have been studied by many people (like Riabouchinsky, Joukowski and von Holst) and by Prof. Küchemann himself about 30 years ago. Figure 1 shows measured values of the maximum lift coefficient for a wing with a rotating flap as a function of the ratio of the circumferential velocity of the flap to the velocity of the mainstream. This confirms all the concepts put forward by Smith. The overall lift depends on the position of the flap, and position 2, which was calculated to be on an optimum line, did indeed produce the highest lift.

That the maximum lift coefficient was not higher than about 3.8 was a consequence of flow separation in the junctions with the endplates used in the test and cannot be blamed on the rotating wing. These matters were discussed in a subsequent paper by L. F. Crabtree<sup>2</sup>, and a theory for the flow past a twodimensional aerofoil with rotating flap has been provided by S. Neumark<sup>3</sup>.

Just for completion, and since we are talking about high lift achieved by mechanical means, Dr Küchemann's second figure shows the lift and drag measured on a rotating wing by itself in the second slide. He comments – I suspect somewhat lightheartedly – that if anybody wants a lift coefficient of better than 12 and does not mind a drag coefficient of 10, then this is one way of achieving it!

Altogether, A.M.O. Smith has again given us much to think about, and it is to be hoped that his advice, together with the results described in the next paper will be duly heeded and will lead to better aircraft.

#### REFERENCES

1. Ruden, P.                      Theorie des Tragflügelprofiles in der Nachbarschaft sprunghafter Gesamtdruckänderungen. (Strahl und Windschatten mit Rechteckprofil.) Jb. dtsh. Luftfahrtf 1, 98, 1939.  
Ruden, P. Windkanalmessungen über den Windschatteneinfluss auf Rechtecktragflügen mit symmetrischen Profil. Jb. dtsh. Luftfahrtf 1. 204, 1940.
2. Crabtree, L.F. (with        The Rotating Flap as a High-Lift Device. ARC Current Paper 480, 1957.  
Appendix by Kirby,  
D.A.).
3. Neumark, S.                    Rotating Aerofoils and Flaps. Journ Roy Aeron Soc Vol.67, 47, January 1963.

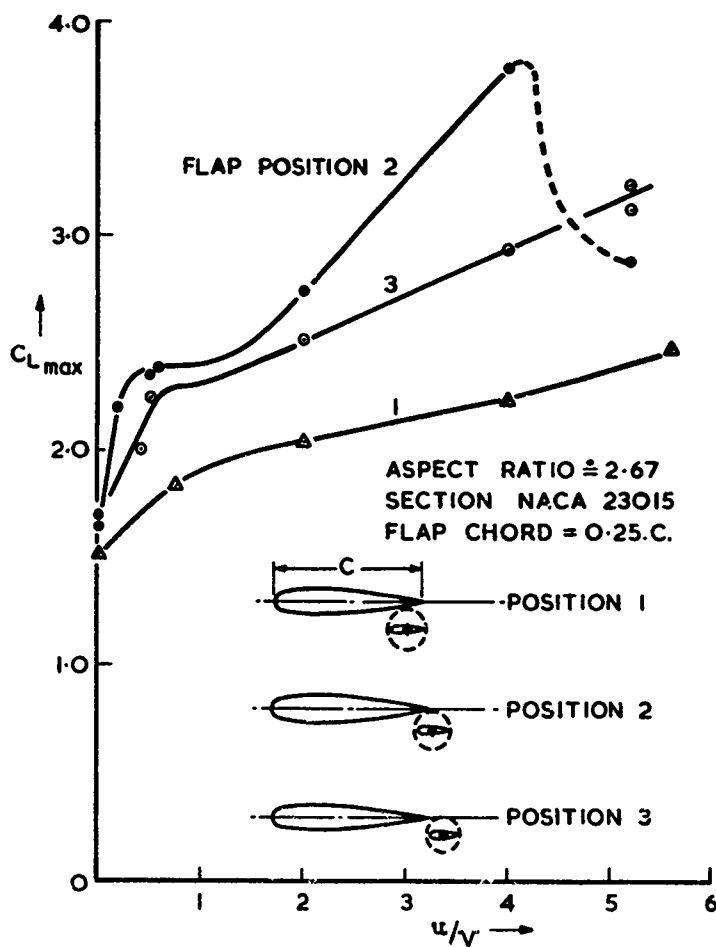


Fig.1 Values of maximum lift for a wing with rotating flat in different positions (Küchemann, 1941)

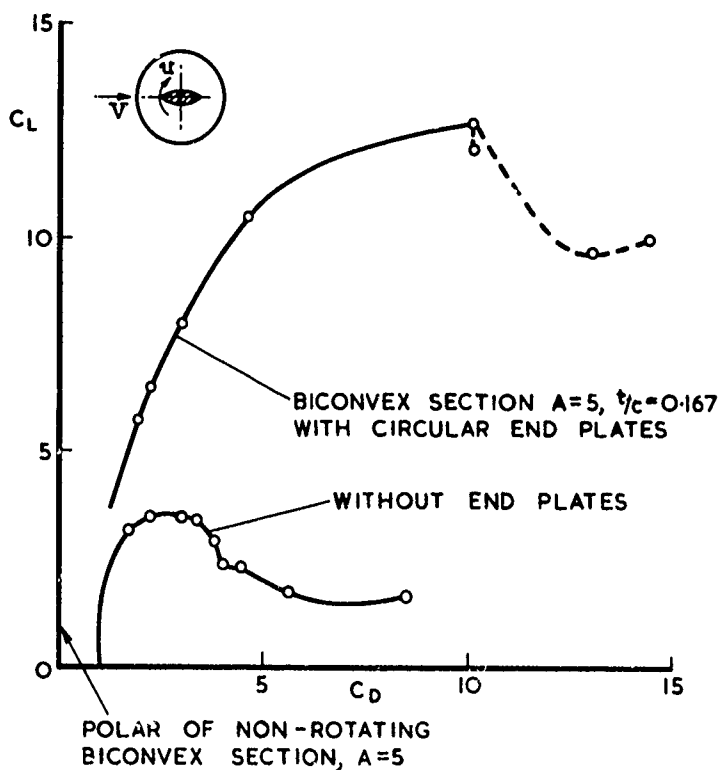


Fig.2 Drag polars for a rotating wing with circular-arc section, with and without end plates (Küchemann, 1942)

## THE LOW-SPEED STALLING OF WINGS WITH HIGH-LIFT DEVICES

by

D. N. Foster

Royal Aircraft Establishment, Farnborough

## SUMMARY

The paper commences by considering the mechanism of the stall of wing sections with high-lift devices such as slats and slotted flaps in twodimensional flow, showing the similarities to the stalling mechanism for single aerofoils, and the differences which arise as a result of the close proximity of the multiple lifting elements of the wing section to each other.

The effect of sweepback is discussed for an infinite sheared wing and for a finite aspect ratio wing without high-lift devices. The effects of practical features such as part-span flaps, and flap and slat support brackets, are then illustrated by reference to flow patterns measured on a swept-back wing.

Further experimental results are considered in order to demonstrate the effect of variation of Reynolds number and Mach number on the development of the stall and on the forces and moments through the stall. These results indicate the need for a facility in which these factors can be varied independently over a wide range. The paper ends with a discussion of the design of such a facility, the RAE 5 metre wind tunnel, and of the design of the models to be tested in it.

## NOTATION

$b$	span of wing	$R_c$	Reynolds number based on mean chord
$c$	chord of wing section	$R_l$	Reynolds number based on local chord, defined normal to mean sweep
$c_o$	chord of wing section with high-lift devices retracted	$s$	distance around contour of wing section, from stagnation point
$\bar{c}$	mean chord of wing	$t$	maximum thickness of wing section
$C_f$	skin friction coefficient	$V_o$	free-stream velocity
$C_L$	lift coefficient	$x$	distance along chord line from leading edge of aerofoil section
$\bar{C}_L$	lift coefficient in equivalent two-dimensional flow	$y$	distance along span from centre line of wing
$C_{Lmax}$	maximum value of lift coefficient	$\alpha$	angle of incidence
$C_m$	pitching moment coefficient	$\bar{\alpha}$	angle of incidence in equivalent two-dimensional flow
$C_p$	pressure coefficient	$\phi$	angle between chord line of slat and chord line of wing
$M$	Mach number		

## 1 INTRODUCTION

The stalling of swept-back wings with high-lift devices can at best be described as imperfectly understood. The lack of methods for predicting the onset and development of the stall; and the inadequacies of existing low-speed wind tunnels have led, on the one hand to the necessity of expensive and time-consuming flight tests in order to achieve acceptable stalling characteristics and, on the other hand to designs which, by showing satisfactory stalling characteristics in a conventional low-speed wind tunnel, do not realise their full potential under full-scale conditions.

Whilst the time at which a useful prediction method will be available is still a matter for speculation, some advances in the understanding of the mechanism of the stall have recently been made. These have resulted from careful experiments in both twodimensional and threedimensional flow, allowing the stalling of a wing section with high-lift devices to be related to the stalling of the plain wing section, and the stalling of a swept-back wing with high-lift devices to be related to the stalling of the plain swept-back wing. The results of these experiments are discussed in this paper and, where possible, mention is made of calculation methods which may ultimately be synthesised to yield the desired prediction method.

A better understanding has also been obtained recently of the performance required of a wind tunnel, if it is to be a satisfactory aid to the development and understanding of acceptable stalling behaviour for swept-back wings with high-lift devices. The design of such a wind tunnel, and the design of the models to be tested in it, are also discussed in this paper.

## 2 THE STALL IN TWODIMENSIONAL FLOW

## 2.1 The single aerofoil

As a basis for the discussion of the mechanism of the stall of wing sections with high-lift devices, the classical classifications of the single aerofoil stall will first be discussed<sup>1</sup>. The stall is characterised by flow separations occurring on the upper surface of the aerofoil, and the three types to be described are illustrated in Fig.1. This shows typical variations of lift coefficient with angle of incidence, together with the upper surface pressure distribution, and the upper surface flow, at a lift coefficient just less than the maximum value.

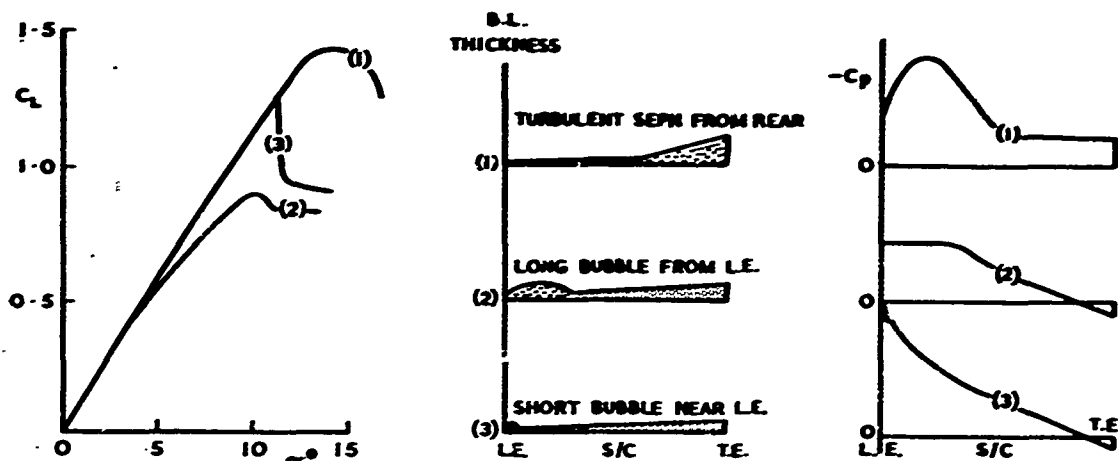


FIG.1 STALLING CHARACTERISTICS OF SINGLE AEROFOILS  
(DIAGRAMMATIC ONLY)

On very thick aerofoil sections, where a rounded suction peak first appears at about 10% chord and with only moderate adverse pressure gradients over the forward part of the chord, the turbulent boundary layer will separate near the trailing edge. As a result of the increasingly adverse pressure gradients the separation point will move forward as the lift coefficient increases. The corresponding curve of lift coefficient against angle of incidence exhibits a rounded maximum, type 1 of Fig.1, this being the rear or trailing-edge stall. When Reynolds number is increased, the maximum lift coefficient may be increased due to thinning of the turbulent boundary layer, without any marked change in the stalling behaviour.

On very thin sections, separation of the laminar boundary layer may occur before transition to a turbulent boundary layer. Transition will then occur in the separated layer and the resulting turbulent layer will re-attach to form a long bubble (say 2% to 3% of the chord, on formation at low angles of incidence). As the angle of incidence is increased, the bubble extends rearwards until it reaches the trailing edge, and then extends beyond the trailing edge. During this process the gradient of the lift curve decreases steadily and a smooth maximum again results, type 2 of Fig.1, this being the long-bubble or thin-aerofoil stall.

For moderately thick aerofoil sections, laminar separation may again occur, but now the turbulent layer re-attaches in a very short distance (less than 1% chord) to form a short bubble. As the angle of incidence increases, the pressure decreases in the bubble, and this is accompanied by increased curvature, which in turn implies a shortening of the bubble. At some critical lift coefficient this bubble bursts by a failure of the turbulent shear layer to re-attach, and the lift curve has a sharp maximum, type 3 of Fig.1, the leading-edge stall.

It has been found<sup>2</sup> that some aerofoil sections of moderate thickness can change their stalling characteristics from a leading-edge stall to a trailing-edge stall with increase of Reynolds number. Further, a range of Reynolds number may exist for which the characteristics of both types of stall (1 and 3) are present, that is, a laminar separation bubble and separation of the turbulent boundary layer ahead of the trailing edge. Under these circumstances the maximum lift coefficient may be defined either by the bursting of the leading-edge bubble, or by the forward movement of the rear separation point, this movement being accelerated by the thickening of the turbulent boundary layer resulting from the existence of the laminar separation bubble. This type of stall is sometimes known as the combined stall.

Jacob<sup>3</sup> has recently considered the trailing-edge stall, and has extended the surface singularity method of Jacob and Riegels<sup>4</sup>, for the calculation of the potential-flow pressure distribution, to include a separated region ahead of the trailing edge. This is simulated by a source distribution on the upper surface of the aerofoil, between an assumed separation point and the trailing edge. A pressure distribution is calculated from the basic unseparated pressure distribution for the given angle of incidence, with allowance for the source distribution, and the development of the boundary layer over the upper surface of the aerofoil is then calculated, to ascertain whether the boundary layer does separate at the assumed position. If this is not so, other separation positions are considered, until the process converges. By repeating the calculation for a range of angles of incidence, a curve of lift coefficient against angle of incidence can be constructed which has a form similar to type 1 of Fig.1, and a maximum lift coefficient can be determined. For an aerofoil such as the NACA 2412, Jacob<sup>3</sup> has obtained very good agreement between the experimental and theoretical variation of the maximum lift coefficient with Reynolds number.

Crabtree<sup>5</sup> has discussed the flow around an aerofoil with either a short or a long bubble, and has shown that a method due to Maskell can provide a good estimate of the pressure distribution over an aerofoil with a long bubble. The contour considered in this method consists of a constant pressure boundary, assumed to extend as far as the maximum thickness, followed by a constant displacement thickness up to the trailing edge. In contrast, Crabtree shows that the short bubble results in only a very small perturbation, in the region of the bubble, to the pressure distribution corresponding to the contour



of the aerofoil. Horton<sup>6</sup>, in his semi-empirical theory for the bursting of short bubbles, has built upon the experimental investigations into the structure and behaviour of laminar separation bubbles at Queen Mary College, London. His calculation procedure assumes that the inviscid velocity distribution applies up to the point of separation of the laminar boundary layer, that the velocity over the laminar part of the bubble is constant, and that the velocity falls nearly linearly between the transition and the re-attachment points. The method predicts a series of values of the position around the aerofoil contour at which re-attachment could occur, and the flow velocity at re-attachment; if none of these values are compatible with the inviscid velocity distribution around the aerofoil, the bubble is assumed to have burst.

In principle, a calculation procedure using Jacob's method to allow for boundary-layer separations near to the trailing edge, and incorporating Horton's method to determine the effect of the laminar separation bubble on the development of the boundary layer, and to indicate if the bubble has burst, should predict the occurrence of a combined stall.

## 2.2 The aerofoil with slotted flap

A typical development of the viscous layers around a wing with a slotted flap is shown in Fig.2. There are two main differences compared with the development of the viscous layers around a single aerofoil section. The first difference lies in the separation bubble which is present on the lower surface of the wing near to the trailing edge. The length of this bubble is to some extent dependent on the shape of the wing lower surface which exists when the flap has been deployed, but even if, as here, an attempt is made to eliminate discontinuities in the surface slope by the addition of a smooth fairing, a bubble still exists. Some small movements of the chordwise position of the leading edge of the bubble have been noted with increase of angle of incidence, but the presence of the bubble does not affect the mechanism of the stall.

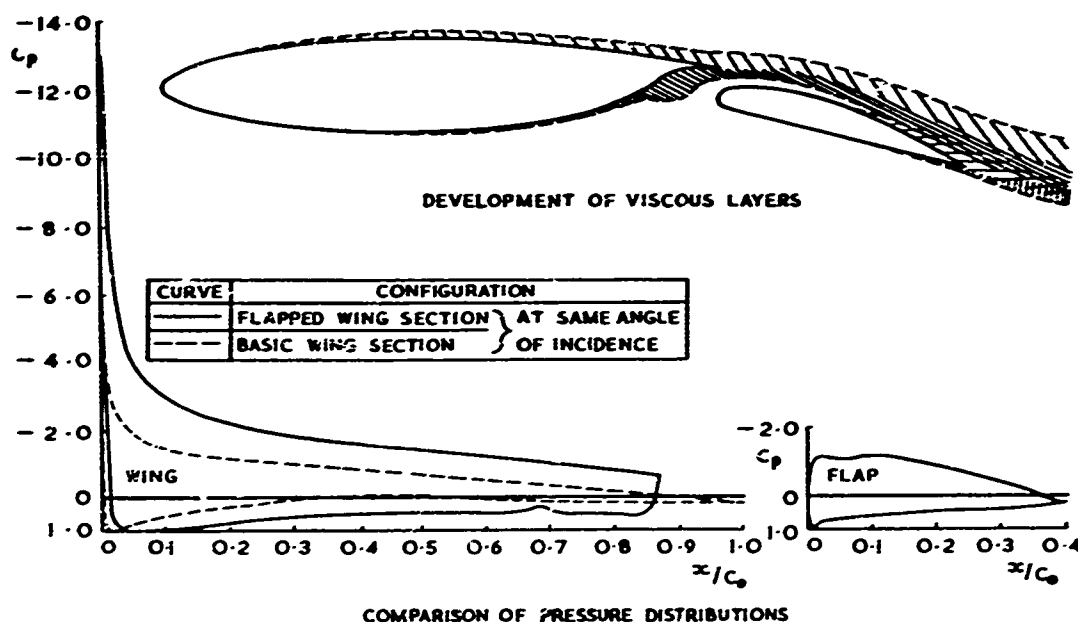


FIG.2 FLOW AROUND WING WITH PLAIN LEADING EDGE  
AND SLOTTED FLAP DEFLECTED  $20^\circ$

The second novel feature of the flow is the mixing of the wake from the wing and the boundary layer on the upper surface of the flap. Experiments<sup>7</sup> have shown that for positions of the flap for which the wing-flap combination yields optimum aerodynamic performance the interference between the wake and the boundary layer is comparatively weak, with the two viscous layers retaining their separate identities almost to the flap trailing edge. Theoretical calculations for the inviscid flow around the wing and flap, using the method of Hess and Smith<sup>8</sup>, suggest that the pressure distribution over the flap varies only slowly with angle of incidence. Under conditions of weak interference from the wake of the wing, the development of the boundary layer on the flap upper surface, and the position of separation of this viscous layer, might therefore also be expected to be almost invariant with angle of incidence.

In general, therefore, the stall does not occur as a result of the effects of the viscous layer above the flap upper surface, but as a result of a breakdown of the flow over the upper surface of the main wing. Since there is a simple boundary layer on this surface, the mechanism of the stall will be identical to one of the mechanisms described above for a single aerofoil. Fig.2 also gives a comparison of the pressure distribution on the main wing and flap with that on the basic section (flap retracted) at the same angle of incidence. The adverse pressure gradient over the rear half of the wing upper surface, when the flap is deflected, is similar to that for the basic section, but the adverse pressure gradient just downstream of the leading edge is much increased. Thus it is to be expected that there will be a tendency for the flapped wing section to exhibit a leading-edge stall even if the basic section has a trailing-edge stall. As for the combined stall of the single aerofoil section considered above, a calculation procedure based on Horton's method<sup>6</sup> for the detection of bubble bursting could, in principle, be used to predict the stall of the wing-flap combination, provided that a suitable method can be devised to allow for the presence of the wing wake, when calculating the pressure distribution over the flap.

### 2.3 The aerofoil with leading-edge slat and slotted flap

Fig. 3 shows the development of the viscous layers for a wing section with a leading-edge slat and slotted flap. As for the wing with a plain leading edge, there is a separation bubble on the lower surface of the wing near to the trailing edge, and weak interference between the combined wake from the slat and main wing and the boundary layer on the flap. In contrast it has been found<sup>9</sup> that for the optimum aerodynamic position of the slat there is extensive mixing between the wake from the slat and the boundary layer on the upper surface of the wing, so that close to the trailing edge of the wing the two layers are almost completely merged. Measured pressure distributions on the slat, main wing and flap are also shown on Fig. 3. Although the wing with a plain leading edge and slotted flap would have stalled at an angle of incidence below that to which the figure corresponds, a comparison of theoretical and experimental pressure distributions at angles of incidence below the stall has enabled an estimate of the pressure distribution for the wing with plain leading edge to be made for this angle of incidence, and the values have been added to Fig. 3. This serves to emphasise the large reduction in the peak suction pressure coefficient resulting from the presence of the slat.

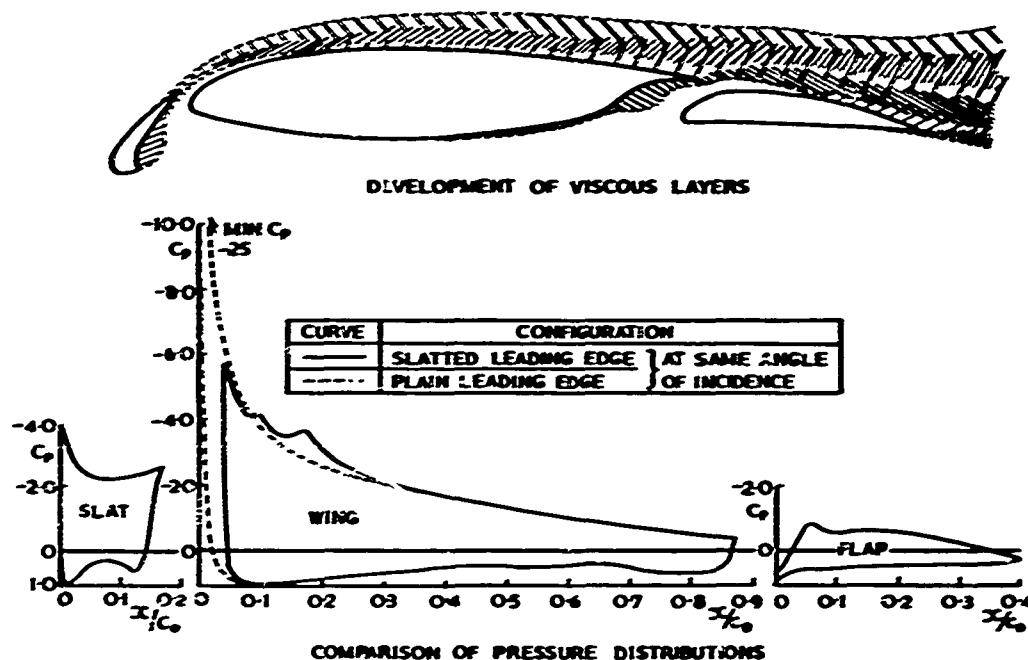


FIG. 3 FLOW AROUND WING WITH SLAT DEFLECTED  $28^\circ$  AND SLOTTED FLAP DEFLECTED  $10^\circ$

A wing with a leading-edge slat may stall either as a result of a breakdown of the flow on the upper surface of the slat or a breakdown of the flow on the upper surface of the main wing. The surface on which the breakdown does occur is determined by the geometric position of the slat relative to the wing, and is most readily illustrated by considering the effect of varying the angle of the slat to the wing chord line. Fig. 4 shows pressure distributions on the slat and leading edge of the wing for three slat angles. It can be seen that for the smallest slat angle the pressure gradients around the leading edge of the wing are very mild, but that there is a very strong adverse pressure gradient on the leading edge of the slat. This suggests that at this slat angle the slat will experience a leading-edge stall. At the highest slat angle the adverse pressure gradients on the slat upper surface are comparatively mild, but there has been an increase in the peak suction pressure coefficient on the main wing. In these circumstances, it is probable that the flow will breakdown on the upper surface of the wing.

There will again be the possibility of either a leading-edge or a trailing-edge stall for the flow on the main wing. The flow around the leading edge which will exist if there is a leading-edge stall will be similar to that for a single aerofoil, as it is unlikely that at the position of laminar separation there will be any mixing of the wing boundary layer and slat wake. However it has been noticed in experiments into the flow over a slotted flap<sup>7</sup> that, even if there is no mixing, the presence of a turbulent wake may induce an early transition of the boundary layer. This could therefore reduce the possibility of a leading-edge stall. The effect of the interaction of the wake from the slat with the wing boundary layer must, however, be included in any consideration of a trailing-edge stall. Fig. 5 shows the values of the skin-friction coefficient on the upper surface of the wing for various slat gaps, as predicted by an extension of an integral method for calculating the simultaneous development of the boundary layer and wake<sup>10</sup>. In this figure the initial characteristics of the slat wake and the pressure distribution on the upper surface of the wing have been held constant, in order to isolate the effect of the interaction. In practice both would vary slightly as the gap changed. It can be seen that when the slat is closest to the wing (smallest gap) the interaction causes the flow to separate from the wing surface (skin friction equals zero) nearly 10% of the chord ahead of the position corresponding to the largest gap, for which there is no interaction as the layers do not merge. This interaction is therefore an additional factor in the consideration of a trailing-edge stall and any calculation method designed to predict the stall of a wing with a leading-edge slat must take account of it.

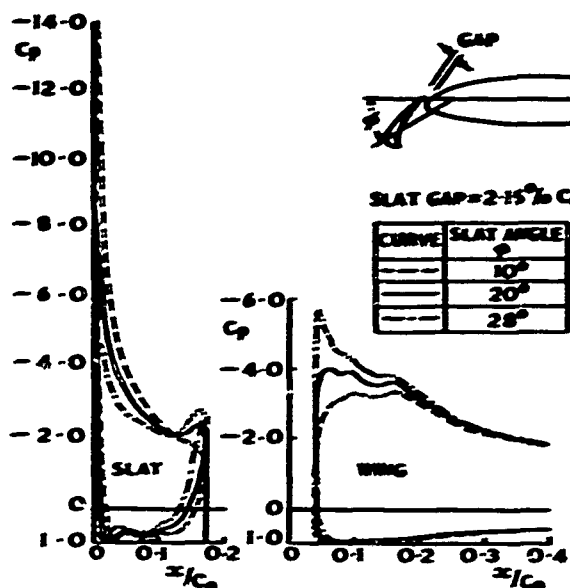


FIG.4 PRESSURE DISTRIBUTIONS OVER SLAT AND LEADING EDGE OF WING FOR VARIOUS SLAT ANGLES

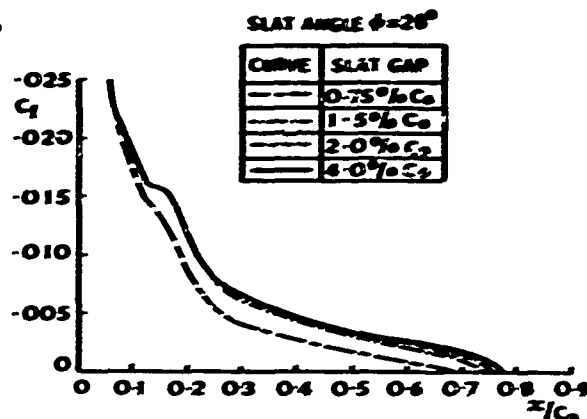


FIG.5 EFFECT ON SKIN FRICTION ON WING OF CHANGE OF WAKE ~ BOUNDARY LAYER INTERACTION DUE TO VARIATION OF SLAT GAP

### 3 THE STALL IN THREE-DIMENSIONAL FLOW

#### 3.1 Effect of sweepback for an infinite sheared wing

Weber has shown<sup>11</sup> that in the inviscid flow around an infinite sheared wing without high-lift devices the value of the peak suction pressure coefficient, and its position around the wing section, is independent of the angle of sweep. However it is noted that this does not imply that the viscous flow is independent of sweep, and this comment applies also to wings with high-lift devices. The character of the boundary layer on the upper surface of the wing will be affected by the transverse pressure gradients, and this may result in the layer separating at a lower lift coefficient for the sheared wing than for two-dimensional flow. It is also possible that the different character of the wake from the slat and of the boundary layer on the wing would increase the severity of the interaction between them, and as Fig.5 shows, result in a forward movement of the position of separation of the viscous layer on the upper surface of the wing. Thus whilst the mechanism of the stall on the sheared wing may not be different to that in two-dimensional flow, the values of the maximum lift coefficient achievable on the sheared wing may be less than is achievable in two-dimensional flow.

#### 3.2 Effect of sweepback for a wing of finite aspect ratio

Measurements have recently been made<sup>12</sup> of the spanwise variation of the chordwise pressure distribution for a swept, tapered half-wing model, with a full-span leading-edge slat and slotted flap, each having a constant deflection across the span. Preliminary analysis of the results suggests that the effects of finite aspect ratio and sweepback are generally similar to those for a wing without high-lift devices and with constant camber-shape across the span. Fig.6 illustrates two of the areas of difference between typical loadings on plane unswept and swept-back wings. The first lies in the shape of the spanwise distribution of lift, as an increase of sweepback tends to be accompanied by a movement of the position of the maximum value towards the wing tip. On this basis alone it might be expected that the origin of the stall would move towards the tip as sweepback is increased. The second area of difference lies in the shape of the chordwise loading, which varies across the span of the swept-back wing, the variation becoming more pronounced as sweepback is increased. The section nearest the tip then has the highest adverse pressure gradient downstream of the leading-edge suction peak, and in terms of the mechanisms of the stall in two-dimensional flow the tip region would then have a tendency towards a leading-edge stall. A further aspect, not illustrated, is that the thickness of the boundary layer at the trailing edge of the swept-back wing tends to rise as the wing tip is approached<sup>13</sup>. These three features combine to produce an increasing tendency towards a stall originating at the wing tip as sweepback is increased.

In the absence of a detailed analysis of the flow over a swept-back wing with high-lift devices, the extensive tests of Woodward and Lean<sup>14</sup> may usefully be employed to illustrate how the pattern of the stall of a wing section on a swept-back wing may differ from that for the same section in two-dimensional flow. Their wing, which is illustrated in Fig.7, was designed using the RAE Standard Method<sup>15</sup> to have identical chordwise pressure distributions at all spanwise stations at a lift coefficient of 0.8. The wing section was chosen so that at the lowest test Reynolds number (based on the chord normal to the mean sweep line at mid semi-span) the section exhibited a leading-edge stall, and at the highest test Reynolds number a trailing-edge stall.

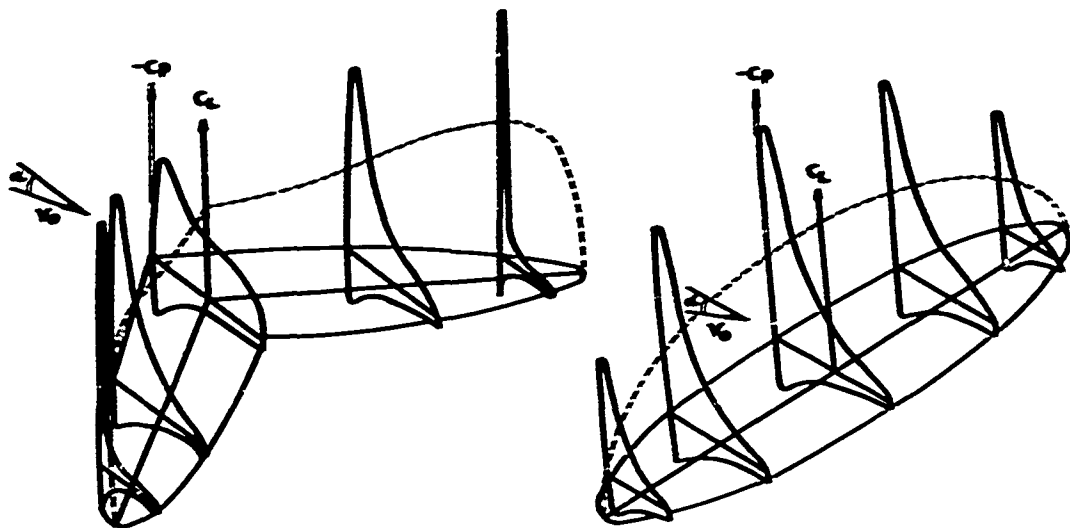


FIG.6 PRESSURE AND LIFT DISTRIBUTIONS DUE TO INCIDENCE ON SWEEP-BACK AND UNSWEEP WINGS

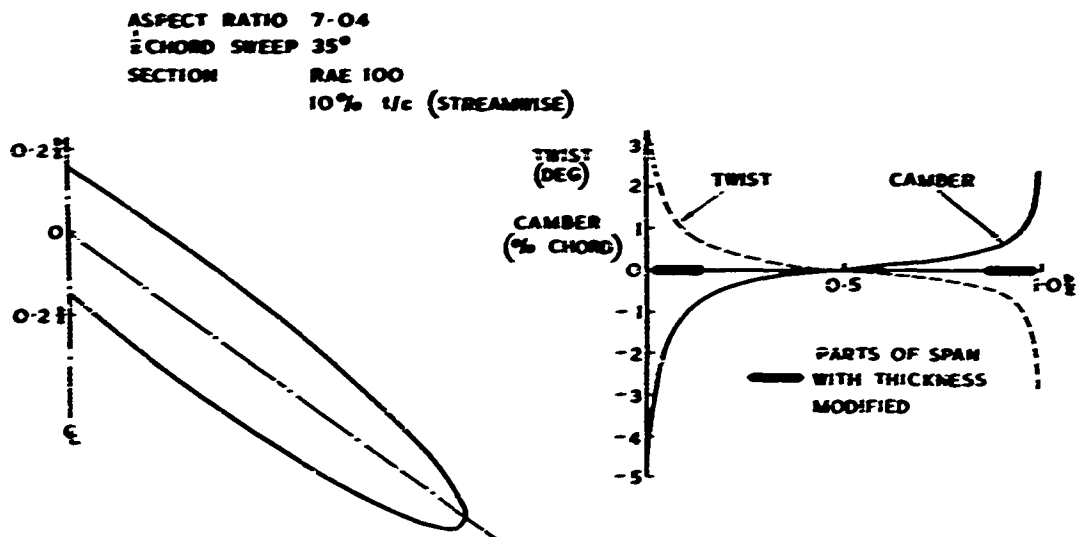


FIG.7 WING DESIGNED FOR UNIFORM PRESSURE DISTRIBUTION AT  $C_L = 0.8$

Detailed chordwise pressure distributions were measured at a large number of spanwise stations and these chordwise pressure distributions were integrated to yield a spanwise distribution of lift. The downwash equation<sup>1</sup> for a lifting surface and its associated trailing vortex sheet, assumed to be planar, was then applied to this spanwise load distribution in order to derive the effective angle of incidence at each spanwise station. Finally the effective angle of incidence and the normal and axial force coefficients were combined to generate quasi-two-dimensional lift coefficients. Values at four spanwise stations are compared in Figs.8a and 8b with results of earlier two-dimensional tests on the same wing section<sup>16</sup>. For the range of Reynolds numbers shown on Fig.8a, the wing section is known to exhibit a trailing-edge stall in two-dimensional flow, and there is generally good agreement between the results for the section on the swept-back wing and in two-dimensional flow, both at and beyond the stall. In contrast, when the Reynolds numbers are such that the wing section has a leading-edge stall in two-dimensional flow (Fig.8b) the post-stall lift coefficients do not bear any resemblance to the behaviour observed in two-dimensional flow. The reason for this behaviour lies in the nature of the stall of the wing at this Reynolds number. Woodward and Lean suggest that as a result of the leading-edge stall a vortex sheet is formed, springing from the leading edge close to the apex of the wing, and crossing the trailing edge at some 70% of the semi-span. The effect of this vortex sheet may be seen by comparing the development of the chordwise pressure distribution at 85% and 40% semi-span, Figs.9 and 10. At 85% semi-span, Fig.9, the pressure distribution just before the stall shows a short bubble and a good trailing-edge pressure recovery; just subsequent to the stall the upper surface pressure distribution is almost constant and has a suction level similar to that in two-dimensional flow. At 40% semi-span, Fig.10, the pre-stall development is similar, but subsequent to the stall the level of the upper surface suction is much higher than would be experienced in two-dimensional flow, due to the presence of the vortex sheet.

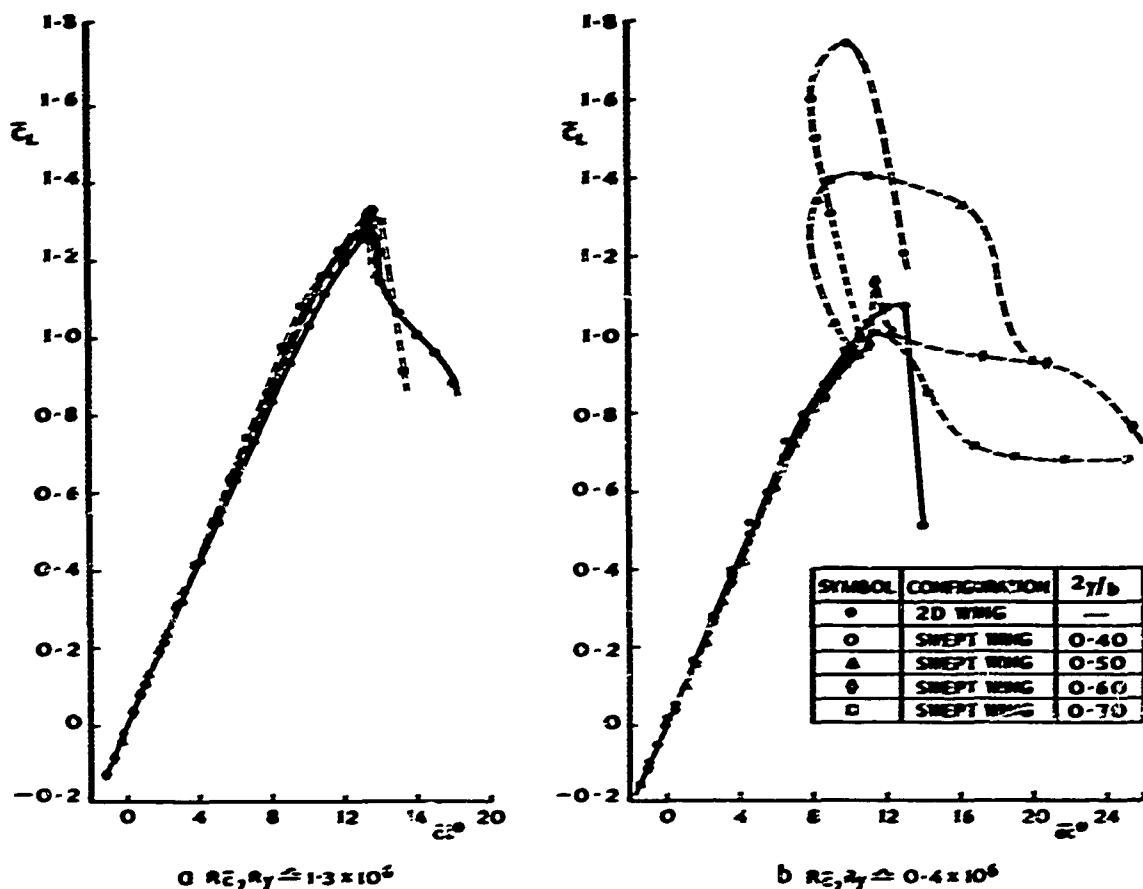


FIG. 8 a & b COMPARISON OF SECTION LIFT CHARACTERISTICS  
OBTAINED FROM TWO-DIMENSIONAL AND THREE-DIMENSIONAL TESTS

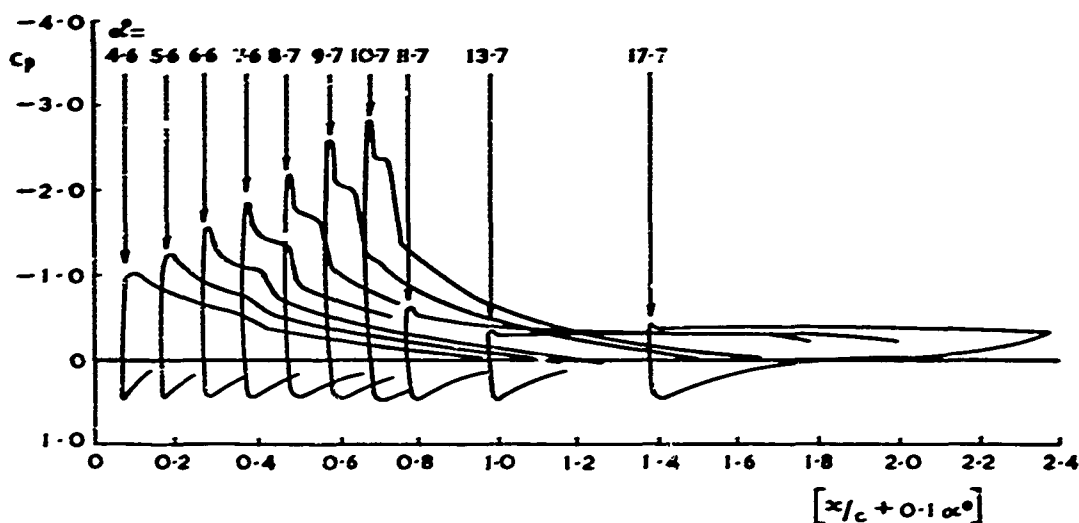


FIG. 9 VARIATION OF CHORDWISE PRESSURE DISTRIBUTION WITH  
INCIDENCE AT 85% SEMISPAN STATION,  $Re = 0.51 \times 10^6$

It can therefore be concluded that, under conditions in which separation bubbles may exist close to the leading edge in the flow just below the stall, there is unlikely to be any connection between the post-stall behaviour of a section on a wing with moderate to high sweepback and that for the section in two-dimensional flow. This situation will occur for a wing with high-lift devices if there is a slat stall, or if the main wing exhibits a leading-edge stall.

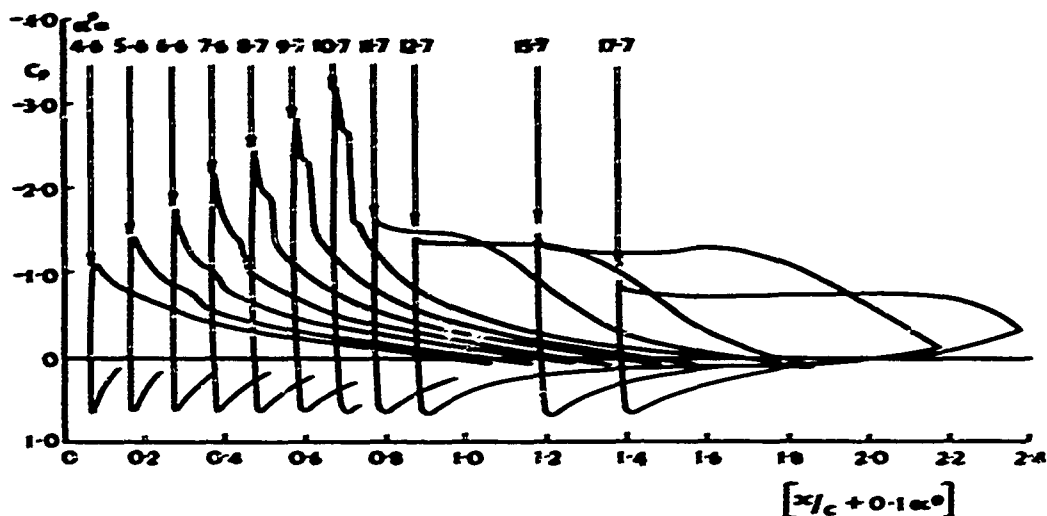


FIG.10 VARIATION OF CHORDWISE PRESSURE DISTRIBUTION WITH  
INCIDENCE AT 40% SEMISPAN STATION,  $Re = 0.51 \times 10^6$

### 3.3 Effect of practical features: part-span flaps and supports for slats and flaps

For the majority of swept-winged aircraft the flap does not span the whole of the wing trailing edge, but terminates at about 75% to 80% of the wing span. The carry-over of lift, from the flapped portion of the wing to the unflapped portion, results in the flow around the wing section just outboard of the flap tip having to sustain a peak suction pressure coefficient with a magnitude approaching that on the flapped wing section, but without the compensation of the suction pressure coefficient at the trailing edge, which accompanies the extension of a slotted flap. Again, the flap and slat must be supported from the main wing. In the case of the slat, the supports must emanate from the region of the leading edge of the wing, and because of the complex changes of flow direction which exist in this region, it is unlikely that the support can be made to lie wholly in the direction of the flow. As a result, wakes are shed from the supports and pass over the upper surface of the wing in close proximity to the wing surface, so that locally the development of the boundary layer on the wing is subjected to a more intense adverse interaction.

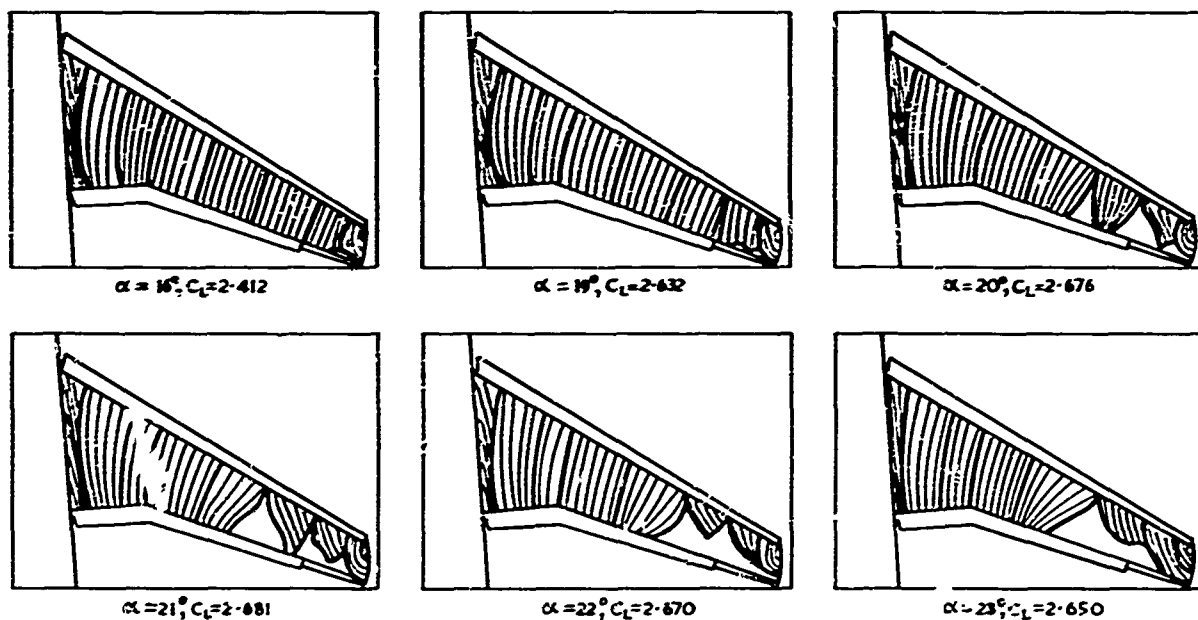


FIG.11 FLOW PATTERNS FOR A SWEEPBACK WING THROUGH THE STALL

The effects of these two practical features are shown in Fig.11, derived from surface-flow patterns obtained by Lovell<sup>17</sup>. At the lowest angle of incidence illustrated, all the support wakes (denoted by the heavy lines), except that from the most outboard slat support, are clearly defined back to the wing trailing edge and do not provoke a separation. There is a small region of separated flow near to the trailing edge on the unflapped portion of the wing and this appears to originate from the wake of the most outboard slat support. This region of separated flow grows slowly as the angle of incidence is

increased, but more marked is the appearance of a second region of separated flow, which results from the adverse effect of the wake of the slat support in line with the outboard tip of the flap on the boundary layer on the highly loaded section just outboard of the flap. As the angle of incidence is further increased another region of separated flow appears, due to the wake from the next slat support; subsequently these regions increase in area and join up. Finally, after the maximum lift coefficient has been reached, the area of separated flow does not appear to increase, but more cross-flow is evident inboard of the separated region.

The stall therefore appears to result from a combination of the effect of the spanwise load distributions on the chordwise pressure distribution carried by wing sections just outboard of the flap tip, and the effect of the interaction of the wake from a slat support with the wing boundary layer. It is possible that, had the supports for the slat been at different spanwise positions, the stall pattern and the maximum lift coefficient would have been markedly different.

#### 4 THE EFFECTS OF REYNOLDS NUMBER AND MACH NUMBER

Wind-tunnel tests on a swept-back wing with high-lift devices at low Reynolds number can suggest a stalling behavior which is quite different to that which would be experienced in flight. This is illustrated in Fig.12, which compares flow-separation boundaries for the Trident 1 aircraft, fitted with a drooped leading edge and double slotted flaps, measured during flight tests at a Reynolds number of about  $15 \text{ to } 20 \times 10^6$ , with boundaries measured on a model of this aircraft in a conventional wind tunnel at a Reynolds number of about  $1 \times 10^6$ , transition-free. In flight, the stall commenced at about 40% of the wing semi-span and spread inboard as the angle of incidence was increased, resulting in a nose-down pitching moment at the stall. In the wind tunnel, on the other hand, as a result of the comparatively thicker boundary layer at the trailing edge of the wing, the stall commenced at about 60% of the wing semi-span and subsequently spread rapidly both inboard and outboard to yield a tip stall, accompanied by severe pitch-up. Tests in a variable-density wind tunnel, on another model of this aircraft<sup>18</sup>, over a range of Reynolds number at constant Mach number, demonstrated the change-over of the stall pattern, as shown by the curves of pitching moment coefficient against angle of incidence shown on Fig.12. Attempts to reproduce the stall pattern corresponding to the flight Reynolds number in the conventional wind tunnel required an extreme form of transition-fitting device<sup>19</sup>.

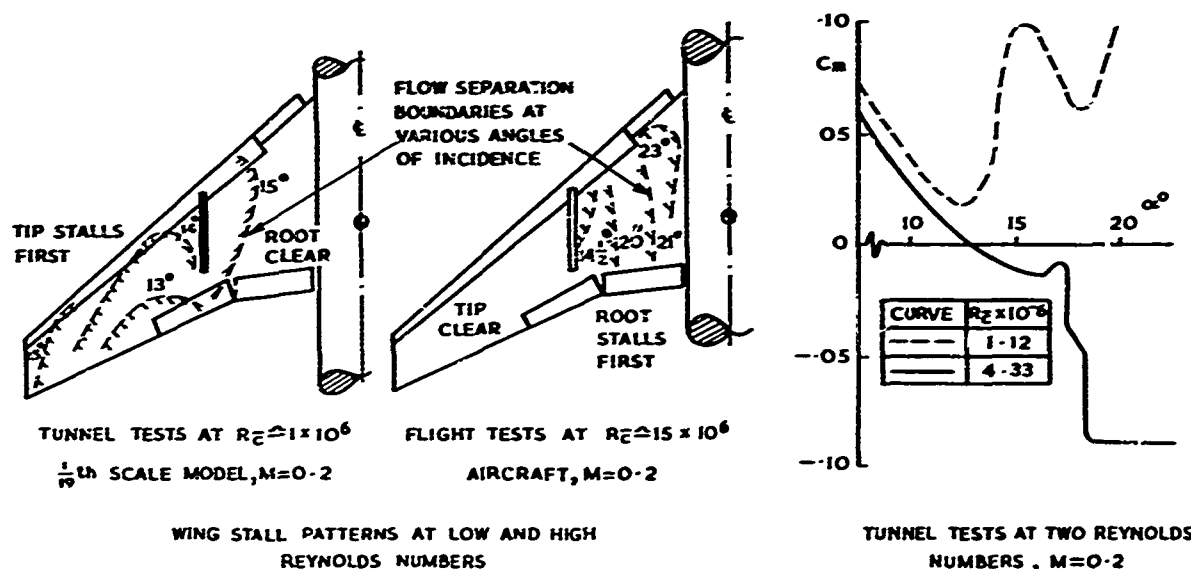


FIG.12 SCALE EFFECT ON THE STALL PATTERN, TRIDENT 1

Fig.13 shows the variation of the maximum lift coefficient with Reynolds number, at various constant values of Mach number corresponding to low-speed flight, resulting from this change in the development of the stall pattern. At the lowest value of the Reynolds number Mach number was found to have no effect on the maximum lift coefficient, but at a higher Reynolds number it has a pronounced effect, the rate of decrease of maximum lift coefficient with Mach number being of a similar magnitude to that measured in flight, as shown by the inset. Theoretically, increase of Mach number will increase the lift coefficient on each section of the wing, but with an accompanying increase in the severity of the adverse pressure gradients. At the lower Reynolds number, when the maximum lift coefficient is defined by a tip stall, it would appear that this theoretical increase of lift due to Mach number is offset by a reduction of the stalling angle of incidence, as a result of the more severe adverse gradients, to yield an almost constant maximum lift coefficient. When the maximum lift coefficient is defined by a root stall, as at the higher Reynolds number, the effect of the increase of the adverse pressure gradient on the trailing-edge separation appears to be greater than the increase of lift due to Mach number, and hence there is a reduction in the value of the maximum lift coefficient.

These results emphasise the need to be able to both test at a high value of the Reynolds number, probably of the order of at least  $5 \times 10^6$ , in order to achieve a representative stall pattern, and to vary Reynolds number and Mach number independently; tests in which changes of Reynolds number were interlinked with changes of Mach number would, if their separate effects were as above, be of no value in any attempt to determine the performance of the wing under full-scale conditions.

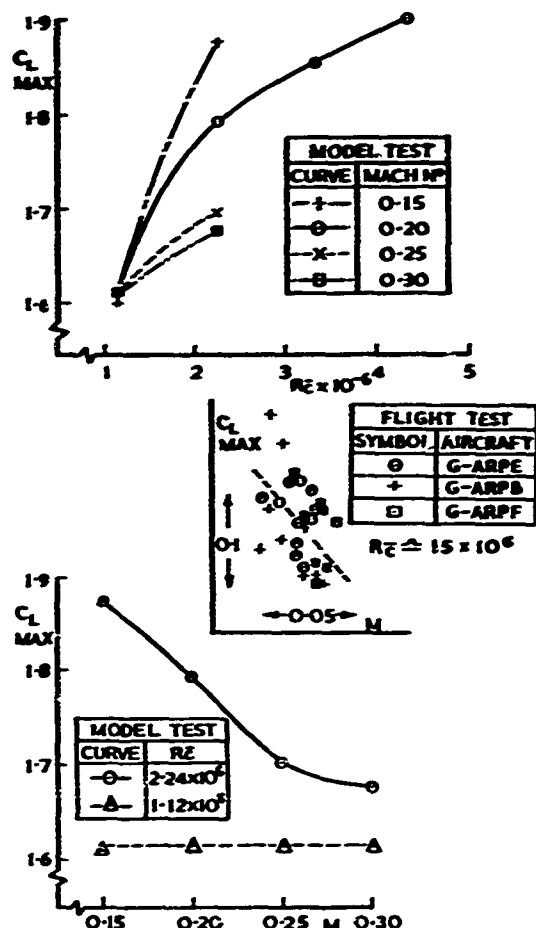


FIG.13 EFFECT OF REYNOLDS NUMBER AND MACH NUMBER ON  $C_{L\text{MAX}}$  FROM MODEL AND FLIGHT TEST

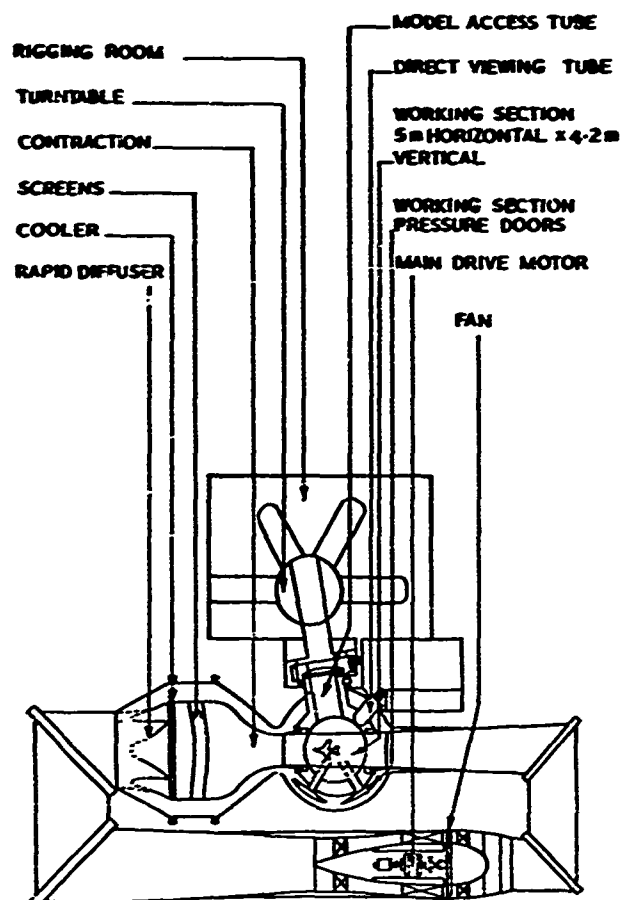


FIG.14 5 METRE WIND TUNNEL

##### 5 THE 5 METRE PRESSURISED LOW-SPEED WIND TUNNEL

A facility in which it will be possible to vary both Reynolds number and Mach number independently, and to achieve a Reynolds number of at least  $6 \times 10^6$  is currently being constructed at RAE Farnborough. This is the 5 metre low-speed wind tunnel<sup>20</sup>, illustrated in Fig.14. During the design of this wind tunnel a range of sizes was considered, and these studies showed conclusively that the cost of the tunnel shell fell rapidly as the size was reduced. In spite of the accompanying increase in pressure required to maintain the same Reynolds number. The present size, with a working section 5 m x 4.2 m, is considered to be the smallest wind tunnel which will satisfy the requirement of a Reynolds number of  $6 \times 10^6$  for a complete model of a typical transport aeroplane, of about 3.5 m span, and for which models with high-lift devices can be built with sufficient accuracy and strength.

The wind tunnel can be pressurised to 3 bars, and has a maximum speed of 107 m/s at 2 bars. As the effect of variation of Reynolds number and Mach number on the flow around the model could to some extent be masked by variation of the uniformity and turbulence in the airstream, care has been taken to ensure good uniformity and low turbulence in the flow. To this end there is only a small change in the sectional shape along the length of the contraction and therefore crossflow should be minimised. Model tests of the rapid diffuser have shown attached flow everywhere, and the elliptic tubes and closely spaced fins of the cooler will act as a small scale honeycomb. Two 1.5q screens in the settling chamber will improve the flow uniformity and give further reductions in the turbulence level, so that in the working section the turbulence intensity should be of the same order as that for the best of the atmospheric wind tunnels at RAE.

The models will be mounted on model carts which essentially form the rear 9.8 m (32 ft) of the working section floor. Two model carts will be provided initially, one carrying a mechanical balance suitable for both full and half models, and the other a sting balance. Other carts and balances may be added later.

Testing of models with high-lift devices often involves repeated measurements with small changes in the configuration of the high-lift devices. In order to effect such changes within a reasonable length of time, special attention has been paid to the problem of entry into the working section. This is enclosed within two concentric spheres, and large pressure doors housed between the spheres can be closed onto the inner sphere, which can then be depressurised to allow access to the model, whilst maintaining pressure in the remainder of the circuit. Additionally, the working section can be rotated to allow the



model carts to be interchanged through the model access tube. The time required to depressurise or repressurise the inner sphere will be of the order of two minutes, and charging of the remainder of the circuit can occur whilst the inner sphere is depressurised so avoiding any further loss of time.

The design of the models themselves, to allow these rapid changes of configurations, presents severe problems. For current models designed for atmospheric wind tunnels, continuous variation of the position of, say, the flap relative to the wing is obtained by a sliding or screw adjustment. Because of the magnitude of the loads involved, such schemes are considered to be unacceptable for models designed for the pressurised wind tunnel. At present, the only method which appears to be acceptable is to have a set of mounting brackets for each desired configuration of the high-lift device. Even this provision of a large number of interchangeable components may be unacceptable for a complete model with a tapered wing, since the physical size of the flap or slat near to its tip may be such as to preclude the possibility of attaching the bracket by any method which will have sufficient strength and yet will allow the bracket to be removed subsequently. It will, of course, be possible to manufacture the slat or flap and its brackets as a unit from one piece of material. Alternative approaches, involving, perhaps, attaching the brackets to the slat or flap by means of welding, are currently being investigated in order to ensure that the models will be made in the most economical manner possible.

## 6 CONCLUSIONS

The results of the experiments in twodimensional flow which have been discussed suggest that there is a close analogy between the mechanism of the stall for a wing, without a leading-edge device, having a slotted flap and the mechanism of the stall for a plain wing section. This analogy may, in some circumstances, be extended to the mechanism of the stall for a wing with a leading-edge slat and slotted flap, but there may exist conditions in which the close proximity of the wake from the slat to the boundary layer on the wing influences the mechanism of the stall in a manner which has no analogy in the stall of the plain wing section.

The experiments on the swept-back wing without high-lift devices have shown that under conditions for which the wing section exhibits a leading-edge stall the post-stall behaviour of the sections on a swept-back wing is dependent on the nature of the threedimensional development of the stall, and this behaviour may have no counterpart in twodimensional flow. Only when conditions are such that the wing section exhibits a trailing-edge stall, and the wing has been designed so that at a lift coefficient very near to the stall the pressure distributions on all wing sections are identical, will the sections on the swept-back wing exhibit a stalling behaviour similar to that in twodimensional flow. Practical features, such as part-span flaps and the support brackets of leading-edge slats, may combine to produce a development of the stall which is specific to the geometric arrangement of these features and to the Reynolds number of the flow. It will then be extremely difficult to obtain a general understanding of the mechanism of the stall of a swept-back wing with high-lift devices from such tests.

Calculation methods are currently being proposed which will enable a prediction to be made of the stall in twodimensional flow and which may ultimately form a basis for a method of predicting the development of the stall in threedimensional flow. Experimentally, increased understanding of the mechanism of the stall will best be achieved by the use of a facility in which the two parameters of the flow which have the greatest influence on the stall - Reynolds number and Mach number - can be varied independently over a wide range, and it has been shown that the 5 metre wind tunnel now being constructed at RAE should fulfil these requirements. When other factors affecting the stall, such as the influence of ground proximity, or the possibility of dynamic effects due to rapid variation of attitude or ground clearance, have to be considered, it will be essential to conduct experiments at representative values of Reynolds number and Mach number, and the 5 metre wind tunnel will again be the best facility for such tests.

## 7 ACKNOWLEDGEMENTS

The author acknowledges permission of Hawker Siddeley Aviation Ltd. to include data from flight tests of the Trident 1 aircraft on Fig.13, and permission of Her Britannic Majesty's Stationery Office to reproduce the paper, which is British Crown Copyright.

## REFERENCES

- 1 B. Thwaites (Editor). Incompressible Aerodynamics. Clarendon Press, Oxford, 1960.
- 2 D.E. Gault. A correlation of low-speed, airfoil-section stalling characteristics with Reynolds number and airfoil geometry. NACA TN 3963, 1957.
- 3 K. Jacob. Theoretische Berechnung von Druckverteilung und Kraftbeiwerten für beliebige Profile bei inkompressibler Strömung mit Ablösung. A.V.A. Bericht 67A62, 1967. Translated as: Theoretical calculations of pressure distribution and force coefficients for any profile in incompressible flow with separation. ARC 31936, 1970.
- 4 K. Jacob, F.W. Riegels. Berechnung der Druckverteilung endlich dicker Profile ohne und mit Klappen und Vorflügeln. Z. Flugwiss. 11, 9, pp.357-367, 1963. Translated as: The calculation of the pressure distribution over aerofoil sections of finite thickness with and without flaps and slats. RAE Library Translation 1011, 1965.
- 5 L.F. Crabtree. Effects of leading-edge separation on thin wings in twodimensional incompressible flow. J. Aero. Sci., 24, pp.597-604, 1957.
- 6 H.P. Horton. A semi-empirical theory for the growth and bursting of laminar separation bubbles. CP 1073, 1967.

## REFERENCES (Contd)

7. D.N. Foster, H.P.A.H. Irwin, B.R. Williams. The twodimensional flow around a slotted flap. R & M 3681, 1971.
8. J.L. Hess, A.M.O. Smith. Calculation of potential flow about arbitrary bodies. Progress in Aeronautical Sciences, Vol.8, 1, 138, Pergamon Press, London, 1967.
9. D.N. Foster. The flow around wing sections with high-lift devices. AIAA Paper 71-96, 1971.
10. H.P.A.H. Irwin. A calculation method for the twodimensional turbulent flow over a slotted flap. RAE Technical Report (in preparation).
11. J. Weber. An estimate of the suction peak on infinite sheared wings. J. Roy. Aero. Soc., 63, pp.476-477, 1959
12. D.S. Woodward. Measurements of the flow around a swept wing with high-lift devices. RAE Technical Report (in preparation).
13. G.G. Brebner, L.A. Wyatt. Boundary layer measurements at low speed on two wings of 45° and 55° sweep. CP 554, 1961.
14. D.S. Woodward, D.E. Lean. The lift and stalling characteristics of a 35° swept-back wing designed to have identical chordwise pressure distributions at all spanwise stations when near maximum lift. RAE Technical Report 71050, 1971.
15. Anon. Method for predicting the pressure distribution on swept wings with subsonic attached flow. Roy. Aero. Soc. Transonic Data Memorandum 6312, 1963.
16. D.S. Woodward. The twodimensional characteristics of a 12.2% thick RAE 100 aerofoil section. R & M 3648, 1971.
17. D.A. Lovell. A wind-tunnel investigation of the effects of flap span, wing planform and a body on the high-lift performance of a 28° swept wing. RAE Technical Report (in preparation).
18. D. Isaacs. Wind tunnel measurements of the low speed stalling characteristics of a model of the Hawker-Siddeley Trident 1C. RAE Technical Report 68108, 1968.
19. G.F. Moss. Some examples of RAE investigations of transition fixing effects on sweptback wings. Lecture given at Euromech 14 Colloquium, 'Boundary layer transition', Stockholm, 1969.
20. J.Y.G. Evans, A. Spence. Development of wind tunnels at the RAE. RAE Technical Report 71040, 1971.

# A SIMPLIFIED MATHEMATICAL MODEL FOR THE ANALYSIS OF MULTI-ELEMENT AIRFOILS NEAR STALL<sup>1</sup>

by

I. C. Bhateley<sup>2</sup> and R. G. Bradley<sup>3</sup>

General Dynamics, Convair Aerospace Division, Fort Worth, Texas, USA

## SUMMARY

Potential-flow analysis methods, based on distributed-singularity models, are adequate for the prediction of aerodynamic characteristics for 2-D multiple-airfoil systems where viscous effects are negligible. However, for analysis and design of high-lift systems where viscous effects dominate, potential-flow methods are not adequate. In order that these viscous effects may be accounted for, a method has been formulated by which a solution is obtained through analysis of an equivalent airfoil system in potential flow. The mathematical model for the equivalent system consists of a linearly varying vorticity distribution over the surface of each airfoil element and a source distribution embedded inside each airfoil element to simulate the separated wake. The boundary-layer displacement thickness is superimposed on the airfoil contour to form an equivalent airfoil surface for each element. The flow downstream of a separation point is allowed to develop as a "free streamline" flow with no surface boundary conditions. The mathematical model is evaluated for cases where the location of the separation point is specified from experimental data. The predicted chordwise pressure distributions are shown to correlate well with experimental data for several multiple airfoils (including leading-edge slats and trailing-edge slotted flaps) for angles of attack near stall. Currently, this model is being incorporated into an iterative procedure to predict the complete aerodynamic characteristics, including stall.

## 1. INTRODUCTION

Analytical methods for computing the aerodynamic performance of high-lift systems near stall must be capable of treating cases where viscous effects dominate the flow phenomena. Potential-flow analysis methods, based on distributed-singularity models, have been successfully employed for the prediction of aerodynamic force and moment coefficients and chordwise pressure distributions for multi-element airfoil systems for conditions where viscous effects are small (References 1-4). But the potential-flow methods alone are not sufficient for analysis of high-lift systems where significant viscous effects are encountered, as in the case of large incidence and/or large deflections of slats and flaps.

Of course, no closed-form solution exists for viscous flow over multiple-element airfoil systems at the present time, although finite-difference techniques for solving the Navier-Stokes equations seem to hold some promise for the future. An approximate method for taking viscous effects into account for an arbitrary airfoil system is through an inviscid analysis of an equivalent airfoil system defined from viscous considerations. Jacob (Reference 5) has developed such a method for single-element airfoils that shows very good correlation with experimental data, including the prediction of  $C_{l_{max}}$ . Various researchers (References 6 and 7), including the authors, are currently engaged in developing a technique for the solution of multi-component airfoil systems. To a large degree, the success of the method hinges on the definition of the equivalent system used in the inviscid analysis. The evolution of a simple mathematical model to define the equivalent system is the main subject of this paper.

## 2. VISCOUS SOLUTION CONCEPT

The Convair Aerospace Division of General Dynamics has been actively engaged in the development of a multi-element airfoil analysis and design capability for several years. Consequently, several analytical techniques have been developed that are applicable to the design and analysis of high-lift systems. Some of these techniques are discussed in detail in the following sections. Guidance to the development of the analytical methods has been drawn from numerous 2-D wind-tunnel tests on various high-lift configurations.

<sup>1</sup>This work was accomplished under General Dynamics' Independent Research and Development program. Continued work is being sponsored by the U.S. Air Force Flight Dynamics Laboratory (FXM).

<sup>2</sup>Senior Aerodynamics Engineer

<sup>3</sup>Design Specialist

A potential-flow analysis method was first developed for multi-element airfoil systems. The method was found to be extremely useful but suffered from two restrictions. First, it did not give accurate pressure predictions for airfoils with blunt bases and, second, it was not satisfactory for flow conditions where viscous effects were significant as a result of either large deflections of individual elements or large incidence of the onset flow. The method was first extended to allow analysis of airfoil systems with blunt bases. Then, a technique that accounts for viscous effects was sought.

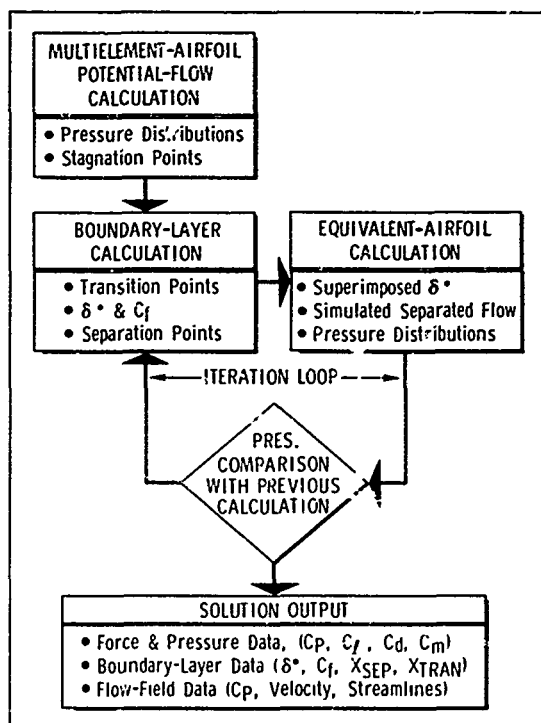


Figure 1. Multi-Element Airfoil Analysis Procedure

The resulting extension to the basic method (currently under development) permits the analysis of multi-element airfoils in viscous flow. The method is based on obtaining a viscous solution for a given high-lift system through the analysis of an equivalent system in potential flow. The iterative cycle is depicted diagrammatically in Figure 1. The first step in the procedure is to calculate the inviscid, potential-flow pressure distributions. The computed pressure distributions are then used to determine laminar and turbulent displacement thickness, transition location, separation points, and laminar-flow bubbles through the use of boundary-layer prediction methods. From these boundary-layer characteristics, an equivalent-airfoil system is next defined. The equivalent system is then analyzed in inviscid, potential flow. The resulting pressure distributions are compared with the previously calculated pressure distributions and, if the maximum difference is not within specified limits, the iterative cycle may be continued by calculating new boundary-layer characteristics from the latest pressure distribution. When convergence is obtained, the final pressure distributions are integrated to give forces and moments.

The present paper is not intended to deal with all the details of the complete iterative method, elements of which are still under development. Rather, emphasis is placed on the mathematical modeling of the equivalent-airfoil system and on the validity of the model for simulating the viscous flow near stall. The mathematical model is verified by comparing pressure calculations for the equivalent system, where the separation points have been estimated from experimental data, with experimental pressure distributions.

### 3. POTENTIAL-FLOW SOLUTIONS

A method based on a distributed-singularity model has been developed for the analysis of arbitrary two-dimensional airfoils in potential flow. Sharp or finite-thickness trailing-edge conditions can be treated within the basic framework of the method. Details of the method are sketched in the following subsections.

#### 3.1 Sharp-Trailing-Edge Airfoils

The potential flow about an arbitrary body can be exactly simulated by a vortex sheet of continuously varying vortex strength lying on the surface. The strength of this vortex sheet is determined by requiring the body contour to form a closed streamline. In the present method, it is assumed that this

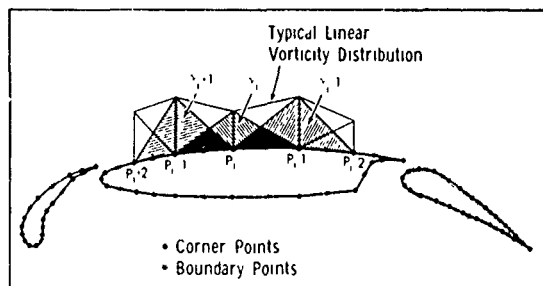


Figure 2. Distributed-Singularity Model - Sharp Trailing Edge

continuous vortex sheet can be approximated by a vortex sheet formed by a connected series of straight-line segments along each of which the vortex strength is permitted to vary linearly. This model is shown schematically in Figure 2. The condition that the body form a closed streamline is relaxed to a condition that the flow be parallel to the surface at a finite number of points, designated as boundary points in this discussion, located at the mid-points of the straight-line segments of the vortex sheet. The extremities of the straight-line segments of the vortex sheet lie on the body surface and are referred to as corner points. If the

vortex density at the corner points is determined, then the assumed vortex sheet is completely specified. It must be emphasized that the points should be so placed that the inscribed-polygon vortex sheet comes as close to the actual airfoil as possible.

The vorticity distribution of the vortex sheet can be defined in terms of the unknown values of vortex density  $\gamma$  at the corner points. Figure 2 also shows a typical distribution of the values of  $\gamma_i$  over the surface of one of the elements. The linear distribution of  $\gamma_i$  over the  $i$ th segment can be considered as the sum of two triangular distributions of  $\gamma_i$  and  $\gamma_{i+1}$  over the  $i$ th segment, as shown in Figure 2. Another way of looking at the same problem is to assume that the influence of  $\gamma_i$  is spread over the adjacent  $(i-1)$ th and  $i$ th segments, except at the first and the last corner points.

The velocity induced by the vortex of unknown strength  $\gamma_i$  at any boundary point can be found as a linear function of  $\gamma_i$  by integrating two triangular distributions of  $\gamma_i$  over the  $(i-1)$ th and the  $i$ th segments by use of Biot-Savart's law. Special treatment is necessary when the boundary point lies in either the  $i$ th or  $(i-1)$ th segment. The velocity induced at the  $k$ th boundary point due to  $\gamma_i$  can be expressed as a linear function of  $\gamma_i$  as

$$u_{k,i} = p_{k,i} \gamma_i \quad \text{and} \quad v_{k,i} = q_{k,i} \gamma_i \quad (1)$$

Then the sum of the velocity induced at the  $k$ th boundary point due to the complete vorticity distribution and the freestream velocity is given by

$$u_k = \sum_{i=1}^N p_{k,i} \gamma_i + U_\infty \cos \alpha \quad \text{and} \quad v_k = \sum_{i=1}^N q_{k,i} \gamma_i + U_\infty \sin \alpha \quad (2)$$

where  $N$  is the total number of corner points or unknown  $\gamma$ s,  $U_\infty$  is the freestream velocity, and  $\alpha$  is the angle of attack. The condition of zero velocity in the normal direction has to be satisfied at each boundary point; thus, the equation is written

$$\sum_{i=1}^N (p_{k,i} \sin \theta_k - q_{k,i} \cos \theta_k) \gamma_i = U (\cos \alpha \sin \theta_k - \sin \alpha \cos \theta_k) \quad (3)$$

where  $\theta_k$  is the slope of the tangent at the  $k$ th boundary point. Let

$$a_{k,i} = p_{k,i} \sin \theta_k - q_{k,i} \cos \theta_k \quad (4)$$

and

$$b_k = U (\cos \alpha \sin \theta_k - \sin \alpha \cos \theta_k) \quad (5)$$

Then Equation (3) can be written as

$$\sum_{i=1}^N a_{k,i} \gamma_i = b_k \quad (6)$$

Here,  $a_{k,i}$  is referred to as the influence coefficient of the  $i$ th vortex at the  $k$ th boundary point. An equation of this type can be generated for each boundary point.

It is apparent in Figure 2 that there is one less boundary point than the number of corner points for each airfoil part. In order to obtain a square system of equations an additional equation has to be generated for each airfoil. The Kutta condition is used to generate this equation, the simplest form of which is the requirement that the net vorticity at the trailing edge be zero. Another form, used in the present program, is to specify a pseudo-boundary point very close to the trailing edge and to force the flow to take a direction which is the average of the lower- and upper-surface slopes at that point. When this latter form is used, another equation of the type discussed above results.

Equation (6) generated for each boundary point coupled with the Kutta condition equation for each element can be written in matrix form as

$$[A][\gamma] = [B] \quad (7)$$

and can be readily solved for  $\gamma$ s by the use of a digital computer. The velocities induced at each boundary point by the vortex sheet can then be readily found from Equations (2). However, to determine the total velocity at any boundary point in the tangential direction requires that the velocity contributed by the local vortex-sheet density also be considered. The local vorticity density contributes a velocity in the tangential direction whose magnitude is equal to  $1/2(d\gamma/dl)$  on the top surface and  $-1/2(d\gamma/dl)$  on the lower

surface. Addition of this velocity to the induced-velocity components already determined yields the total velocity  $u_t$  at each boundary point. Finally, the local pressures are calculated by use of the incompressible relationship

$$C_p = 1 - \left( \frac{u_t}{U_\infty} \right)^2 \quad (8)$$

The pressure distributions can be corrected for compressibility effects by the Karman-Tsien Rule and numerically integrated to give force and moment coefficients.

Typical results obtained by the potential-flow analysis method are shown in Figures 3 and 4 for an NACA 23012 airfoil with single-slotted flap and leading-edge slat. Experimental pressure distributions (Reference 8) are also shown on the plots. For a flap

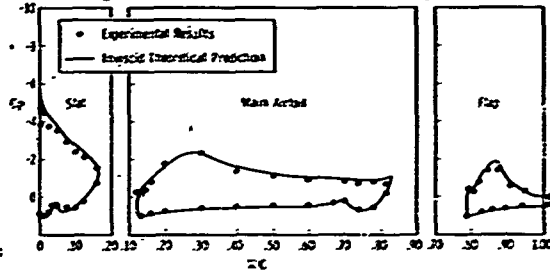


Figure 3. Potential-Flow Results - Slat and Flap Deflected  $20^\circ$ ,  $\alpha = 8^\circ$

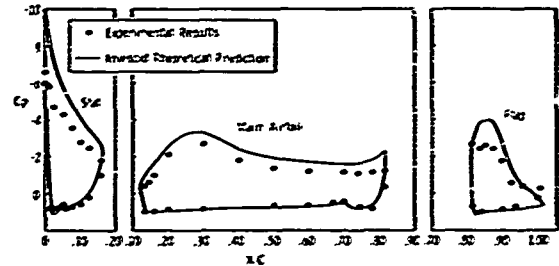


Figure 4. Potential-Flow Results - Slat and Flap Deflected  $40^\circ$ ,  $\alpha = 8^\circ$

deflection of 20 degrees, viscous effects are small and good agreement is exhibited between experimental and theoretical pressure distributions (Figure 3). However, when the flap deflection is increased to 40 degrees, the viscous effects become significant. Experimental pressure distributions indicate flow separation at the flap trailing edge; thus, agreement between experimental and theoretical pressure distributions is only fair, as shown in Figure 4. It is to be noted that flow separation on the flap not only reduces the load carried by the flap but also reduces the load carried by the main airfoil and slat because of a decrease in the total flow circulation.

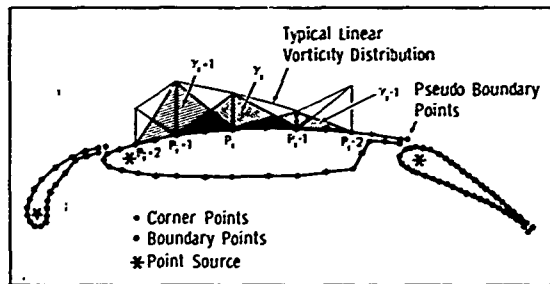


Figure 5. Distributed-Singularity Model - Finite-Thickness Trailing Edges

### 3.2 Finite-Thickness Trailing-Edge Airfoils

The potential-flow method described in the previous section has been extended to permit the analysis of airfoils with finite-thickness trailing edges. The mathematical model used in the extended program is illustrated in Figure 5, which shows the model to be quite similar to that used for sharp trailing-edge airfoil analysis, except that (1) the vortex sheet defining the airfoil describes an open-sided polygon instead of a closed polygon, and (2) a concentrated source singularity of unknown strength is embedded within the contour of each body.

The velocity at any boundary point 'k' can be expressed as

$$u_k = \sum_{i=1}^N p_{k,i} \gamma_i + \sum_{j=1}^M r_{k,j} m_j + U_\infty \cos \alpha \quad \text{and} \quad v_k = \sum_{i=1}^N q_{k,i} \gamma_i + \sum_{j=1}^M s_{k,j} m_j + U_\infty \sin \alpha \quad (9)$$

where  $p_{k,i}$ ,  $q_{k,i}$ ,  $N$ ,  $U_\infty$ , and  $\alpha$  are the same as defined earlier,  $r_{k,j}$  and  $s_{k,j}$  represent the components of velocity induced at the 'k'th boundary point by a unit source embedded in the jth airfoil element,  $M$  is the total number of airfoil elements, and  $m_j$  is the unknown source strength.

If the vortex and source singularities are lumped together, these equations reduce to

$$u_k = \sum_{i=1}^{N+M} g_{k,i} S_i + U_\infty \cos \alpha \quad \text{and} \quad v_k = \sum_{i=1}^{N+M} h_{k,i} S_i + U_\infty \sin \alpha \quad (10)$$

where

$$S_i = \gamma_i \quad \text{for } 1 \leq i \leq N \quad \text{and} \quad S_i = m_{i-N} \quad \text{for } N+1 \leq i \leq N+M \quad (11)$$

and

$$\left. \begin{aligned} g_{k,i} &= p_{k,i} \\ h_{k,i} &= q_{k,i} \end{aligned} \right\} \quad \text{for } 1 \leq i \leq N \quad \text{and} \quad \left. \begin{aligned} g_{k,i} &= r_{k,i-N} \\ h_{k,i} &= s_{k,i-N} \end{aligned} \right\} \quad \text{for } N+1 \leq i \leq N+M \quad (12)$$

Satisfying the condition of tangential flow at each boundary point gives the following linear equation in the unknown singularity strengths:

$$\sum_{i=1}^{N+M} c_{k,i} s_i = q_k \quad (13)$$

where  $c_{k,i}$  again is referred to as the influence coefficients of the  $i$ th singularity at the  $k$ th boundary point.

For each airfoil part there are now two less boundary points than the number of unknown singularity strengths (one more due to the unknown source). In order that a square system of equations be obtained, two additional equations have to be generated for each airfoil element. This is done by specifying two pseudo boundary points, one each located on the upper and lower surfaces just downstream of the trailing edge of each airfoil part as shown in Figure 5. The condition of continued flow tangential to the last surface element is satisfied at these pseudo boundary points. The resulting system of equations can be written in matrix form as

$$[A][S] = [B] \quad (14)$$

These equations can be readily solved for the vorticity and source strengths from which velocities, pressure, and forces can be calculated in a manner similar to the analysis for zero-thickness trailing-edge systems.

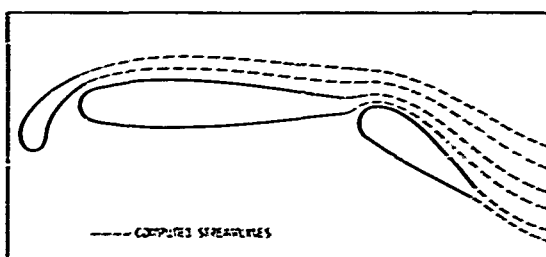


Figure 6. Wake Boundaries - Finite-Thickness Trailing-Edge Analysis

This model for the finite-thickness airfoil defined above has an additional feature in that wake boundaries are simulated by the outflow generated by the source located within each airfoil. It is pointed out that the internal viscous wake condition, i.e., the velocity defect in the wake, is not simulated through this analysis but, perhaps, could be approximated by imposing velocity conditions at certain points in the wake. The typical streamline traces, shown in Figure 6, depict the wake boundaries simulated by the method.

The blunt-trailing-edge airfoil approach has been evaluated by comparison of computed results with experimental data for a modified NACA 64A210 section. Results for both the sharp-trailing-edge airfoil and the modified airfoil with a filled trailing edge are shown in Figures 7 and 8. Lift and pitching-moment coefficients are shown in Figure 7, where the theory is seen to predict the incremental effects of trailing-edge blunting very well. The pressure distributions computed for  $\alpha = 4.07^\circ$  are seen to be in good agreement with data in Figure 8.

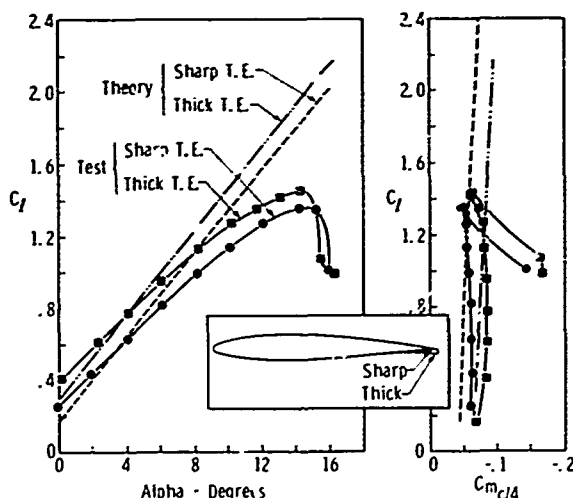


Figure 7. Force Data for Sharp and Blunt Trailing-Edge Airfoil

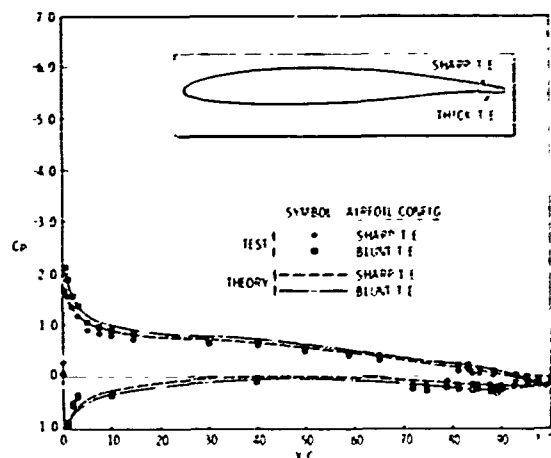


Figure 8. Pressure Distributions for Sharp and Blunt Trailing-Edge Airfoil,  $\alpha = 4.07$  Degrees

#### 4. EQUIVALENT AIRFOIL SYSTEM

The definition of the equivalent-airfoil geometry that simulates the viscous phenomena constitutes a critical step in the iterative solution cycle. Two distinct cases

occur, depending on whether boundary-layer separation occurs or not. The mathematical model for each case is described below in some detail.

The initial step in each case consists of calculating the boundary-layer characteristics on the basis of the predicted potential-flow pressure distributions. Particularly stringent requirements are placed on the methods used to compute the boundary layer, since laminar and turbulent calculations are necessary with transition determined analytically. Accurate prediction of incipient separation for both laminar and turbulent flow is required.

#### 4.1 Attached-Flow Case

Boundary-layer characteristics over any element are computed by the Cebeci and Smith (Reference 9) finite-difference method for solving the differential equations of boundary-layer flow. The calculation is initiated at the airfoil stagnation point located from the potential-flow solution. Turbulent flow is computed by making use of the eddy-viscosity concept.

The location of boundary-layer transition is computed by the method developed by Ward (Reference 10), which is applicable to high Reynolds number. The method relates the transition location to the momentum-thickness Reynolds number. In some cases a laminar separation bubble occurs before transition. In this instance, the short-bubble criterion of Gaster (Reference 11) is employed to determine whether or not the bubble has burst. If the bubble has not burst, the assumption is made that transition occurs at that point and the boundary-layer calculations are continued. When a burst bubble is indicated, laminar separation is assumed to have occurred with no reattachment. The above treatment does not allow for the formation of a long reattached bubble, as has sometimes been observed on very thin airfoils. Thus, only very short bubbles are assumed, with immediate transition at reattachment. This simplified model is adequate in many practical cases.

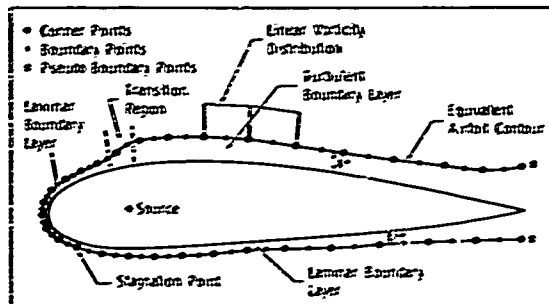


Figure 9. Equivalent-Airfoil Model - Attached Flow

The equivalent-airfoil surface is defined for the case when no boundary-layer separation occurs by superimposing the computed boundary-layer displacement thickness normal to the airfoil contour. A schematic diagram is shown in Figure 9. Since the displacement thickness is not zero at the trailing edge, the resulting equivalent body is analogous to an airfoil with a finite-thickness trailing edge. Thus, the blunt-trailing-edge potential-flow method described in the previous section is directly applicable.

In the analysis of the resulting equivalent multi-element airfoil system, the complex mixing phenomena associated with the interaction of the viscous wake shed from a forward element with the slot efflux and boundary layer developing on the following element has not been considered. This confluent-boundary-layer problem has been considered by Goradia, as reported in Reference 6. The precise impact of the mixing process on the airfoil-system pressure distribution is not known. Thus, in the interest of simplicity, the effect has been omitted in the present model.

#### 4.2 Separated-Flow Case

The next step is to define the mathematical model for those airfoil elements where boundary-layer separation is indicated. The boundary-layer calculation methods described above predict the separation point but, of course, do not carry out calculations past the separation point. Therefore, no values for an equivalent displaced surface are readily available past the separation point.

One approach is to allow the separation streamline to remain a free boundary and fix its position by specifying a constant pressure condition along the streamline from the separation point to the airfoil trailing-edge location. Experimental data tend to support such a constant-pressure separated-wake condition. Jacob (Reference 5) approximated this condition for a single-element airfoil by assuming equal pressures at three discrete points located at the airfoil trailing edge, the separation point, and the airfoil trailing-edge station on the separation streamline. Such an approach, however, requires the solution of a non-linear system of equations within the framework of the distributed-singularity theory. The undesirability of an iterative-solution approach for multi-element systems led to the search for a simpler approach.

One alternate approach to the problem is to empirically define the separated-wake shape, i.e., the inviscid streamline emanating from the separation point, and assume that



the equivalent-body contour follows that streamline. The result is an open-base airfoil element defined by the displacement surface and this separation streamline. The analytical form of the separation streamline then must be established.

An attempt was made to determine the shape of the separated wake experimentally. Photographs of the approximate separation streamline were made during a 2-D wind tunnel test program (Reference 12). Typical photographs obtained for the separation streamline emanating from an NACA 64A210 (modified) airfoil section with 22-percent-chord leading-edge flap are shown in Figures 10 and 11 for angles of attack of 25.5 and 26.5 degrees, respectively. These photographs were taken by a remotely controlled wide-angle-lens

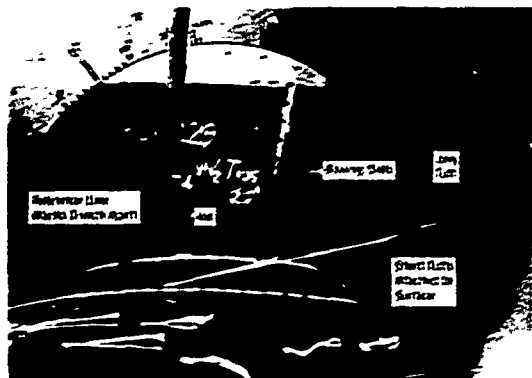


Figure 10. Separation Streamline Experiment - Plain Flap Deflected 20 Degrees,  $\alpha = 25.5$  Degrees

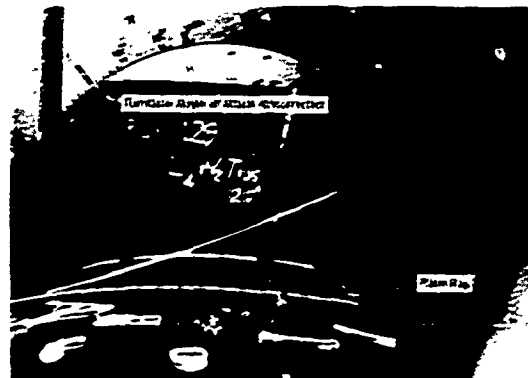


Figure 11. Separation Streamline Experiment - Plain Flap Deflected 20 Degrees,  $\alpha = 26.5$  Degrees

camera installed in the 2-D blowing-wall insert of the tunnel. An approximate chordwise position of the separation point was visually determined by tufts attached to the model. A long tuft (approximately 18 inches) attached to a tapered rod was inserted from the tunnel roof to this approximate separation point. It was observed that as the long tuft was moved downstream it was steady up to a certain point, after which it suddenly began to oscillate violently, presumably as it entered the separated wake region. Photographs were taken with the rod extremity adjusted to a point just upstream of the condition where the tuft entered the separated-wake region. A qualitative indication of the separation streamline shape may be noted in the figures. Unfortunately, the camera position selected was such that the separation streamline emanating from steeply deflected flaps and slats could not be photographed. Further, since this procedure was quite time consuming, photographs were not obtained for enough configurations to empirically define the separation streamline shape as a function of the separation-point location and incidence.

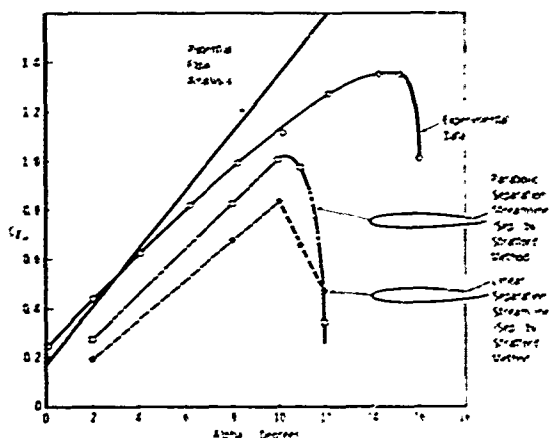


Figure 12. Separation Streamline Shape Effect

A brief analytical study was carried out to determine if the streamline emanating from the separation point could be approximated by an analytical function. An NACA 64A210 (modified) airfoil section was used in the analysis. The separation point used was predicted by applying Stratford's (Reference 13) separation criteria for predicting incipient separation based on the potential-flow pressure distributions. The predicted lift curves for a linear and parabolic streamline assumption are shown in Figure 12. The linear streamline was aligned with the freestream direction, while the parabolic streamline was oriented so that it was tangential to the local surface at the separation point and parallel to the freestream direction at the trailing edge. The agreement between the calculated and the experimental lift curves

is very poor, although the parabolic-streamline model shows some improvement over the linear-streamline model. Perhaps by a trial-and-error method a satisfactory analytical definition for the separation streamline could be obtained for the configuration under investigation, but it would have to be proved valid for a variety of multi-element airfoil configurations and locations of separation points.

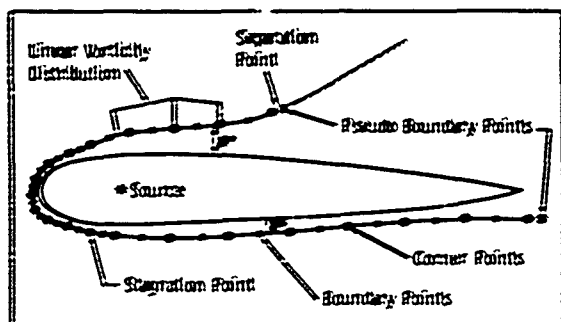


Figure 13. Equivalent-Airfoil Model - Separated Flow

airfoil element is considered as a finite-thickness base. The pseudo boundary point just downstream of the trailing edge on the upper surface in the blunt-trailing-edge airfoil analysis case is moved to a point just downstream of the separation point. The pressure distribution downstream of the separation is assumed to be constant and equal to that value of pressure obtained by linear extrapolation of the boundary point pressures to the separation point.

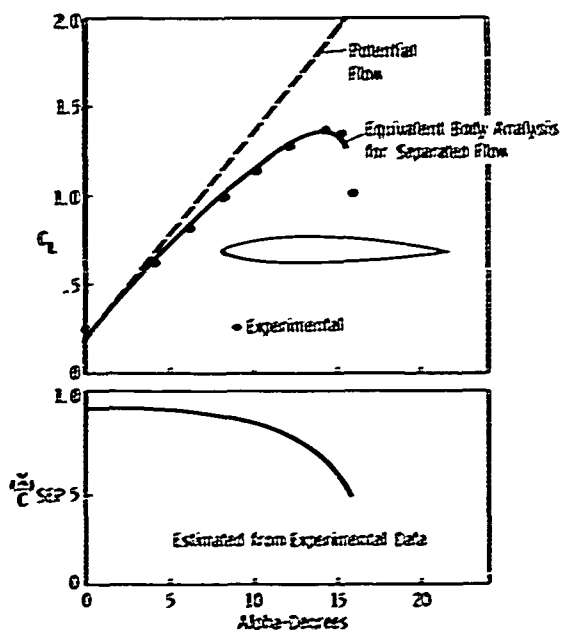


Figure 14. Lift Comparison - Free-Streamline Model

pressure gradients and large amounts of flow circulation that tend to cause premature separations near the walls due to the interference of model and wall boundary layers. Wall-interference effects on the experimental data used to substantiate the theoretical model were eliminated through use of the blowing-wall test technique first developed by Boeing Co. and later refined by Convair Aerospace Division and Canadair Ltd. (References 12, 14, and 15). When used correctly, this test technique eliminates the interference between wall, model, and boundary layer, and near-perfect two-dimensional flow is obtained in the test section. The data presented in this section were obtained at the 6-ft by 9-ft low-speed tunnel of the National Aeronautical Establishment of the National Research Council, Ottawa, Canada, with a 2-foot-chord model, a nominal Mach number of 0.2, and a Reynolds number of 2.5 million (Reference 12).

In the comparisons that follow, the equivalent-airfoil theoretical model is evaluated by calculating the pressure distributions with the separation-point location estimated from the experimental data. The specified separation point thus provides a true evaluation of the equivalent potential-flow model independently of the viscous-separation prediction method. It is not the intent of the present paper to evaluate boundary-layer separation methods or the iterative coupling of the potential- and viscous-flow methods.

### 5.1 Single-Element Airfoils

Results for two single-element airfoils are presented. One is an NACA 64A210 (modified) cruise airfoil; the second is the same airfoil with a 22-percent-chord leading-edge flap. The comparisons between experimental and theoretical pressure distributions for the

A free separation-streamline approach was investigated next. The model is shown schematically in Figure 13. This free separation-streamline model is defined by satisfying the boundary conditions of tangential flow on only that part of the airfoil having attached flow. The tangential flow conditions are also satisfied at the separation point and the trailing edge. Since no flow control is exercised at points downstream of the separation point, the separation streamline develops freely from the separation point. The resulting model is mathematically identical to the model used to analyze airfoils with finite-thickness trailing edges. In this case, the total separated region of the

The NACA 64A210 (modified) section was used to check the validity of this model. In order to assure the correct choice of the separation point, it was determined from experimental pressure distributions. Excellent correlation between theoretical and experimental lift curves was obtained for this configuration as shown in Figure 14. Comparisons between experimental and theoretical pressure distributions for this and several other configurations made to check the validity of the free-streamline model are discussed in the next section.

## 5. MATHEMATICAL MODEL SUBSTANTIATION

The validity of the free separation-streamline model was checked by comparing theoretically calculated pressure distributions with experimental data. Comparisons are presented first for single-element airfoils and then for multi-element airfoils.

Meaningful comparisons require that true two-dimensional data be obtained. High-lift systems in general generate steep adverse

17-9

first configuration are shown in Figures 15 through 18 for angles of attack of 8.3, 10.2, 14.3, and 15.2 degrees, respectively. The potential-flow pressure distributions are also shown on these figures to emphasize the improvement of the viscous-model solution over the potential-flow solution. The effect of boundary-layer displacement thickness was not taken into account in the definition of the equivalent body for these comparisons. The displacement effect is small, as will be shown in a following comparison. The separation-point locations were estimated from the experimental data.

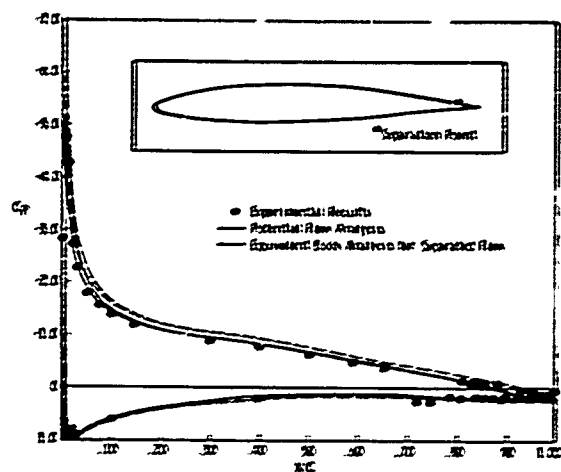


Figure 15. Cruise Airfoil Pressure Distributions,  $\alpha = 8.3$  Degrees

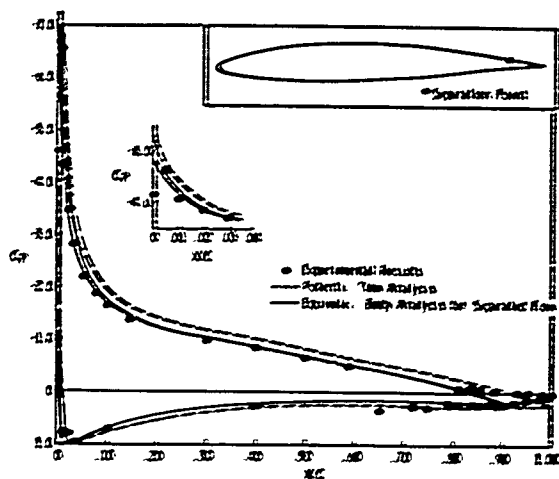


Figure 16. Cruise Airfoil Pressure Distributions,  $\alpha = 10.2$  Degrees

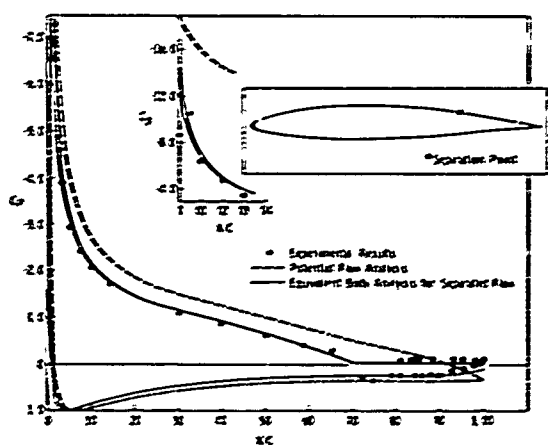


Figure 17. Cruise Airfoil Pressure Distributions,  $\alpha = 14.3$  Degrees

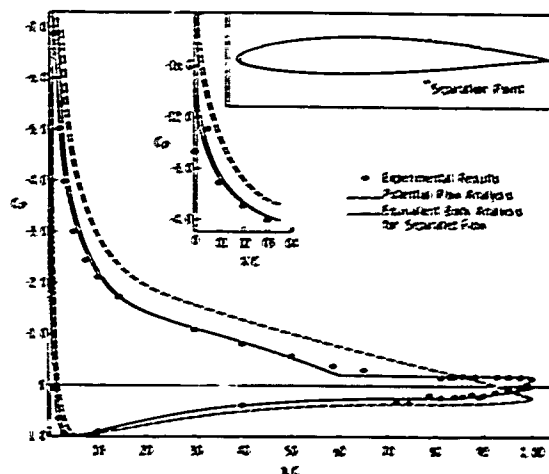


Figure 18. Cruise Airfoil Pressure Distributions,  $\alpha = 15.2$  Degrees

Excellent correlation between experimental and theoretical results are noted for all angles of attack except in the separated region at the lower angles of attack. The simplified model does not pose a condition of equal pressure on the upper and lower surface at the trailing-edge location. Such a condition would perhaps improve the pressure correlation at the airfoil trailing edge. It is noted from Figure 14 that  $C_{l_{max}}$  occurs at about the 14.5-degree angle of attack.

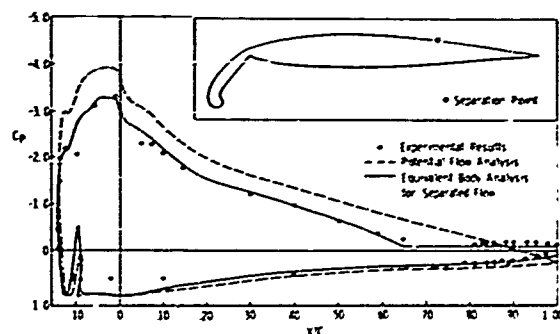


Figure 19. Flapped Airfoil Pressure Distributions,  $\alpha = 18.5$  Degrees

The comparisons between experimental and theoretical results for the NACA 64A210 (modified) airfoil with a 22-percent-chord leading-edge flap are shown in Figures 19, 20, and 21 for angles of attack of 18.5, 20.5, and 22.3 degrees, respectively. Potential-flow analysis results are also shown on these figures. Again the effect of boundary-layer displacement thickness is ignored in the definition of the equivalent body. The separation-point locations were estimated from experimental data. Excellent agreement is obtained between experimental and theoretical results for angles of attack of 18.46 and 20.46 degrees except on the lower surface of the flap.

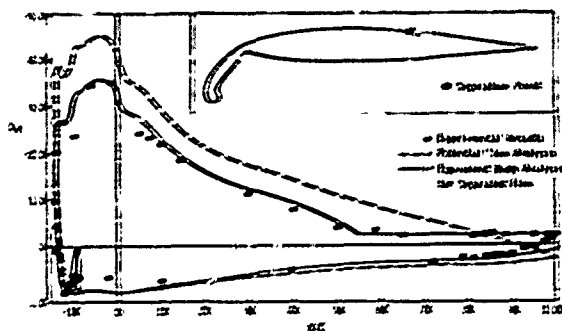


Figure 20. Flapped Airfoil Pressure Distributions,  $\alpha = 20.5$  Degrees

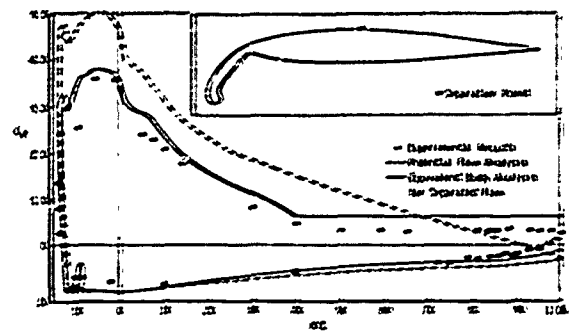


Figure 21. Flapped Airfoil Pressure Distributions,  $\alpha = 22.3$  Degrees

Here, experimental data seem to indicate a laminar-flow bubble, which was not considered in the theoretical analysis. For the angle of attack of 22.31 degrees, the agreement between experimental and theoretical pressure distributions is only fair. At this angle of attack, the separation point is at 40-percent chord and poor agreement can perhaps be attributed to the lack of pressure conditions on the separated wake in the simplified model.

## 5.2 Multi-Element Airfoils

Results for two multi-element airfoil configurations are presented. One configuration is an NACA 64A210 (modified section) with a 22-percent-chord slat; the second is the same but with a 35-percent-chord single-slotted flap deflected 30 degrees.

Comparisons between the computed and experimental pressure distributions for the first configuration (no trailing-edge flap) are shown in Figures 22, 23, and 24 for angles of attack of 14.3, 21.5, and 23.2 degrees, respectively. Theoretical results for the

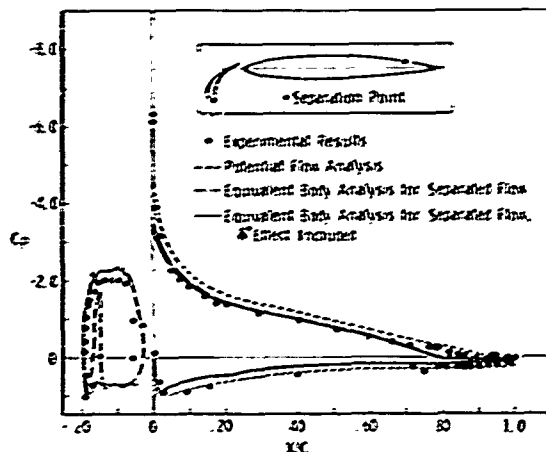


Figure 22. Two-Element Airfoil Pressure Distributions,  $\alpha = 14.3$  Degrees

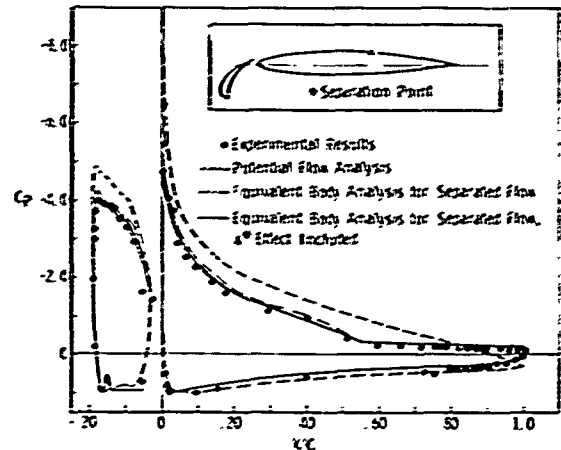


Figure 23. Two-Element Airfoil Pressure Distributions,  $\alpha = 21.5$  Degrees

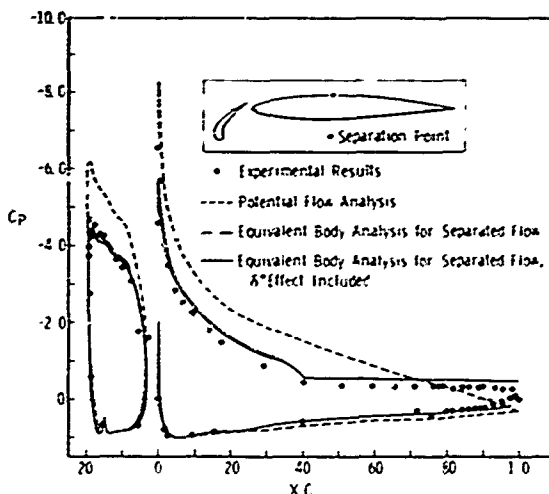


Figure 24. Two-Element Airfoil Pressure Distributions,  $\alpha = 23.2$  Degrees

equivalent system obtained by both neglecting and including the effects of boundary-layer displacement thickness are presented in these figures. The separation-point locations on each element are noted on the airfoil sketch in these figures. Also, potential-flow results are shown for comparison with the simulated viscous solution. These data show that the theoretical and experimental distributions are in very good agreement for angles of attack of 14.30 and 21.53. The effect of including the boundary-layer displacement thickness is seen to be small but tends to improve the agreement between experimental and theoretical pressure distributions. At the 23.17-degree angle of attack (experimental  $C_{l_{max}}$ ) agreement between experimental and theoretical results is only fair which, again, may perhaps be attributed to the absence of a wake pressure condition in the model.

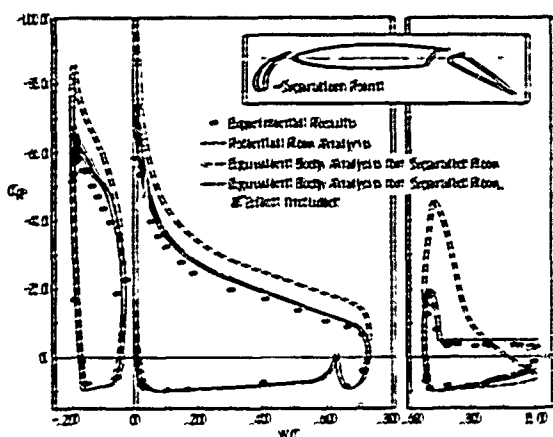


Figure 25. Three-Element Airfoil Pressure Distributions,  $\alpha = 18.7$  Degrees

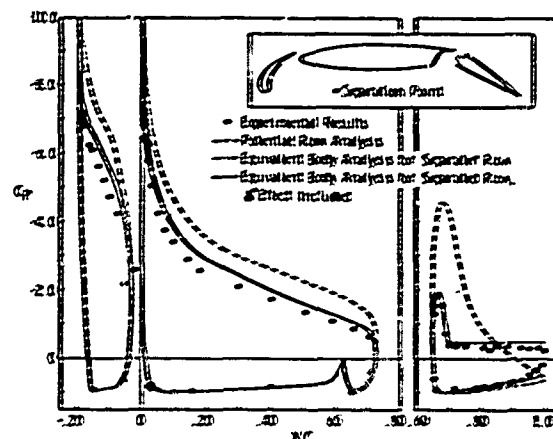


Figure 26. Three-Element Airfoil Pressure Distributions,  $\alpha = 20.7$  Degrees

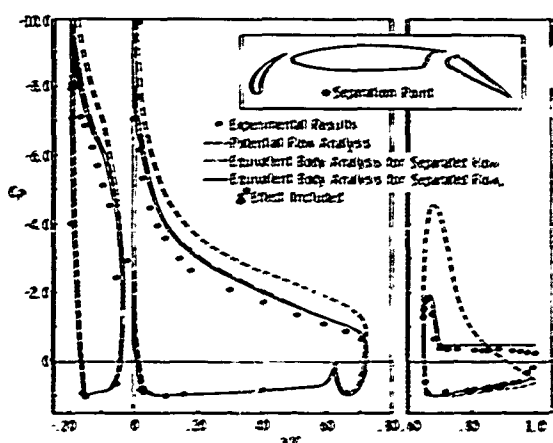


Figure 27. Three-Element Airfoil Pressure Distributions,  $\alpha = 22.9$  Degrees

Comparison of experimental and theoretical pressure distributions for the second multi-element configuration are shown in Figures 25, 26, and 27 for angles of attack of 18.7, 20.7, and 22.9 degrees, respectively. The potential-flow solution is shown for comparison, and the theoretical pressure distributions for the equivalent system with and without the effect of boundary-layer displacement thickness are presented. The experimental pressure distributions show a separation point on the flap which remains invariant over the angle-of-attack range analyzed. The effect of including the boundary-layer displacement thickness is again noted to be small. The experimental and theoretical pressure distributions over the flap are in good agreement, but the theoretical pressure distributions over the wing section and slat are only in fair agreement.

## 6. CONCLUDING REMARKS

A simplified mathematical model has been defined which permits the analysis of arbitrary multi-element airfoils in viscous flow, through the analysis of an equivalent system in inviscid flow. Comparisons of computed pressure distributions with experimental data verify that the model is reasonable, even near stall. Some discrepancies existing near the trailing edge of the airfoil elements point to a deficiency in the simple model. This deficiency may possibly be corrected by enforcing a constant-pressure condition in the separated wake. An approximation for such a pressure condition that does not unduly complicate the model (by adding non-linearities into the system, for example) is required.

Work on the complete iterative solution method is being continued under the sponsorship of the United States Air Force Flight Dynamics Laboratory (FXM), Mr. R. F. Osborn, program monitor. The ultimate objective of the study is to provide the capability to predict force and moment characteristics of multi-element airfoil systems over the complete angle-of-attack range.

## REFERENCES

1. Bhateley, I. C., "Investigation of Inviscid Incompressible Flow, Part IV: Potential Flow Analysis about Arbitrary Multiple Two-Dimensional Bodies by the Method of Distributed Singularities," General Dynamics, Convair Aerospace Division Report ERR-FW-669, March 1968.
2. Davenport, F. J., "Solution of Several Two-Dimensional Potential Flow Problems by the Multi-Vortex Lifting Line Method," Boeing Document D6-7202, March 1961.

3. Bennett, J. A., and Gordia, S. H., "Methods for Analysis of Two-Dimensional Airfoils with Subsonic and Transonic Applications," Lockheed-Georgia Company Report ER8591, July 21, 1966.
4. Hess, J. L., and Smith, A. M. O., "Calculation of Potential Flow about Arbitrary Bodies," Progress in the Aeronautical Sciences, Vol. 8 (D. Kucheman, Editor) Pergamon Press, New York, 1966.
5. Jacob, K., "Berechnung der abgelösten inkompressiblen Strömung um Traflügelprofile und Bestimmung des maximalen Auftriebs," Zeitschrift Für Flugwissenschaften, 17 Jahrgang, July 1969.
6. Stevens, W. A., Goradia, S. H., and Braden, J. A., "Mathematical Model for Two-Dimensional Multi-Component Airfoils in Viscous Flow," NASA Contractor Report, NASA CR-1843, July 1971.
7. Callaghan, J. G., and Beatty, T. D., "A Theoretical Method for the Analysis and Design of Multi-Element Airfoils," Douglas Paper 5967 presented to the AIAA 10th Aerospace Sciences Meeting, January 1972.
8. Harris, A., and Thomas, L. P., "Pressure Distribution Over an NACA 23012 Airfoil with a Fixed Slat and a Slotted Flap," NACA Report 732, 1942.
9. Cebeci, T., Smith, A. M. O., and Wang, L. C., "A Finite Difference Method for Calculating Compressible Laminar and Turbulent Boundary Layers, Part I: General Description," McDonnell Douglas Report DAC-67131, March 1969.
10. Ward, K. E., "Prediction of the Chordwise Position for Transition of the Boundary Layer on an Airfoil Section," General Dynamics, Convair Aerospace Division Report TN-69-AE-04, March 1969.
11. Gaster, M., "The Structure and Behavior of Laminar Separation Bubbles," Aeronautical Research Council R&M No. 3595, 1969.
12. Goodwin, L. C., "Wind Tunnel Test for Phase III of High-Lift Systems Research and Development Program," Canadair Report ERR-CL-RAA-228-103, February 1971.
13. Stratford, B. S., "The Prediction of Separation of the Turbulent Boundary Layer," Journal of Fluid Mechanics, Vol. 5, 1959.
14. Hebert, J., Jr., "High Lift Research", General Dynamics, Convair Aerospace Division Report GDC ERR-AN-1306, December 1967.
15. Goodwin, L. C., "Wind Tunnel Test on a 2-D Model of an NACA 64A210 (Modified) Section With Various Leading and Trailing-Edge Devices, Using the Canadair 2-D Blowing Walls, in the NAE 6x9-Ft Low-Speed Wind Tunnel, NAE Test 6x9/0140, DIR Project A11 - Phase II, Volumes 1, 2, and 3," Canadair Report No. ERR-CL-RAA-228-010, September 1969.

#### ACKNOWLEDGMENT

The authors would like to acknowledge the work of Mr. J. W. McWhirter who diligently programmed the method for digital computation and of Mr. P. D. Whitten who contributed significantly to the evaluation of the model.

## THE EFFECT OF LEADING-EDGE GEOMETRY ON HIGH-SPEED STALLING

by

G F Moss, Royal Aircraft Establishment, Farnborough, Hants, UK  
 A B Haines, Aircraft Research Association, Bedford, UK  
 R Jordan, Aircraft Research Association, Bedford, UK

## SUMMARY

In the first part of this paper it is shown by means of an example how small modifications to the leading-edge profile of a sweptwing can result in large effects on lift performance at the stall in the higher range of subsonic speeds. The basic types of leading-edge pressure distribution for any one fixed geometry over the whole range of subsonic speed are discussed and the difficulties in designing a profile shape which gives a satisfactory compromise in wing performance across this range is emphasized.

In the second part of the paper, two types of variable-geometry device at the leading edge are discussed, each of which allows some degree of optimization in the shape required for good aerodynamic performance across the range of Mach number. The first of these, the leading-edge slat, is shown to work in quite a different way at high speeds from that in its more conventional role at landing and take-off conditions. Recent UK research work is used to demonstrate some important aerodynamic features of slats when used at high speeds in near-optimum positions. The second type of variable-geometry device is a new one, recently developed within the UK. The essential feature is a linkage system, entirely contained within the nose of the profile, which can be used to change the shape of the leading-edge of the 'clean' wing in such a way to improve performance over a range of aerodynamic conditions. The aerodynamic possibilities of the use of this device in the higher subsonic speed range are demonstrated by reference to some recent UK wind-tunnel tests.

## 1 INTRODUCTION

In the design of sweptwings one of the choices which has to be made at an early stage is the selection of the wing-section profile shape (or shapes) to be used. This selection is made very often with the help of theoretical work and two-dimensional wind-tunnel tests, having due regard to the operational requirements of the project throughout the speed range and to the various constraints imposed by structural considerations. The design requirements are usually in conflict and as a result the final choice of profile to be used is generally a 'best compromise' which can have serious deficiencies at one or more important points in the flight envelope. Considering the design of the profile at the leading edge, variable-geometry in the form of slats, Kruger flaps or other such devices is generally found essential to meet the particular deficiency which arises at low-speed, high-lift conditions (for take-off and landing), and recently the use of these devices set at intermediate angles has been resorted to in order to improve stalling characteristics at high subsonic speeds (for high-speed manoeuvres). But a high price is paid for the use of leading-edge devices at high-speeds. The higher loading conditions imply extra weight to be carried and the need to specify precisely extra settings implies complications to the structure and control system. Also some of the aerodynamic effects can be adverse. Because of the extra drag involved for instance, performance at 'cruise' can be sacrificed in some important respects.

Two points therefore need to be stressed at the start of this discussion. Firstly, it is important to increase our understanding of the particular sensitivities of stalling characteristics at high speeds to small variations in leading-edge profile shape, and secondly it is necessary to be more aware of the aerodynamic situations which arise when devices such as leading-edge slats are used to improve maximum-usable-lift at high subsonic speeds. It is hoped that this paper will contribute a little on both these issues.

## 1.1 Basic Types of Pressure Distribution at the Leading Edge

In the higher-subsonic speed range, the stall of sweptwings is primarily associated with the development of flow separations due to the interaction of the shock wave system on the upper-surface of the wing with the boundary-layer. The situations which arise at flow separation can be extremely complex even in two-dimensional flow, particularly when there is interaction between these shock induced separations and separations near the trailing-edge<sup>1</sup>. On the complete swept wing the flow fields are affected by root and tip effects and the interference from the body, the nacelles and stores (if any). With increase of Mach number these three-dimensional effects are aggravated as the effective aspect ratio is reduced. However, provided the leading-edge sweep is not excessive and the leading-edge radius is not so small that leading-edge separations of the slender-wing type develop, a viable approach to the problems of separation can be made by considering the flows as quasi-two-dimensional in the first instance, taking account of the three-dimensional implications subsequently.

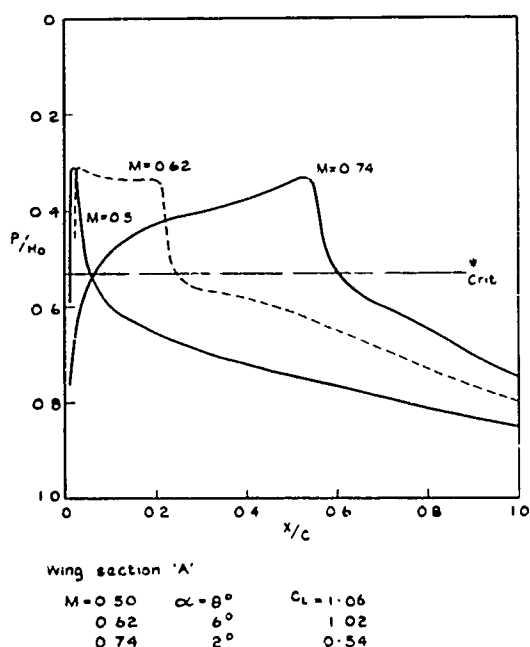


Fig 1 Basic types of upper-surface pressure distributions at super-critical conditions before flow breakdown

Thus we may start by considering three main types of upper-surface pressure distribution near the leading edge, which can occur at conditions just prior to flow breakdown on a particular aerofoil (Fig 1). Three examples are shown with approximately the same shock strength. At the lower end of the high subsonic range under discussion, say at speeds near  $M = 0.5$ , the flow usually separates at the shock which is very close to the leading edge and which increases in strength as lift is increased. At higher speeds, however, a nearly-constant velocity supercritical region tends to develop over the forward part of the wing upper-surface, terminating in a shock wave which moves further aft and increases in strength with increased lift until the separation of the flow from the surface is induced. At still higher speeds the supercritical region may extend as far back as 55%-65% of the wing chord and the shock, when strong enough to cause separation, is typically preceded by a progressive increase in local velocity. In all these phases of development, each culminating in the stall, the geometry of the leading edge plays a critical part, either directly because of local effects on the shock waves, or indirectly because of effects on the general state of the boundary-layer and thus on its tendency to separate further aft on the wing upper surface. Bearing these three main types of leading-edge pressure distribution in mind, three specific examples of leading-edge geometry changes will be presented and discussed in this paper.

## 1.2 Specific examples of Leading-Edge Geometry Changes

Using the first of these examples, described below in section 2, it is shown how a small modification to the leading-edge profile can cause large effects on lift performance which are only beneficial at one end of the high subsonic speed range. The need for a satisfactory compromise across the whole range is thus emphasized. In the second example given in section 3, the use of leading-edge slats at high subsonic speeds is discussed and by reference to some recent UK research studies these devices are shown to work in quite a different way from their more conventional use at low speeds. Finally, section 4 describes the use of a new type of variable-geometry device recently developed within the UK. The use of this device to improve lift performance across the whole of the high subsonic speed range will again be demonstrated by reference to some recent UK test data.

## 2 WING-SECTION PROFILE CHANGES

The first piece of work presented concerns a modification made to the leading-edge profile of a variable-sweep research model. Details of the complete model configuration used in the investigation are given in Fig 2. Two sweep angles for the wings were used in the investigation and the appropriate values of aspect-ratio and wing-twist ('wash-out') are noted on the Figure. One model was used for the measurement of forces (presented in Figs 7 and 8) and another rather larger version of the same configuration was used for the measurement of pressure data, (quoted in Figs 9 and 10). The wing-section employed is also shown in Fig 2, designated as 'basic wing-section A'. Two-dimensional tunnel data for this section and for the modified section 'B' is quoted in Figs 1 and 3-6.

### 2.1 Two-dimensional considerations

The basic section 'A' used on this model was a comparatively thick one (about 13% thick, perpendicular to the wing quarter-chord line) and had a reasonable degree of rear loading and a fairly small leading-edge radius.

Fig 3 shows the stall boundary obtained for this profile as obtained from two-dimensional tests and the criteria used to define this boundary are also indicated by means of inset sketches in the figure. The three types of pressure distribution shown in Fig 1 have been taken from this same set of test data. As will be seen the boundary is fairly flat from  $M = 0.4$  up to about  $M = 0.58$  and over this range of Mach number we have the first type of pressure distribution mentioned previously with a very sharp suction peak and a strong shock near the leading edge at conditions before flow breakdown. In the region  $0.6 < M < 0.65$ , however, the second type of pressure distribution applies, with a nearly-constant-velocity supercritical region developing over the forward part of the profile upper-surface terminating in a strong shock. At higher Mach numbers, the third type of distribution shown in Fig 1 is apparent, velocities building steadily from the leading edge to form a triangular type of supercritical distribution culminating in a strong shock much further back on the chord.

Fig 3 also includes a sketch showing in what manner the leading-edge profile was modified to form the second profile designated as wing section 'B'. The modifications of most significance were the increase in nose droop and the change to the local surface curvature round the leading-edge. The effect on the sectional stall boundary is given also in Fig 3 and shows that the maximum lift of the profile has been raised at the low end of the speed range without apparent harm to the performance at the higher Mach numbers. The marginal improvement at high speeds is possibly due in part to the small change in section thickness (about 0.3%) also included in the modification, so no credit can

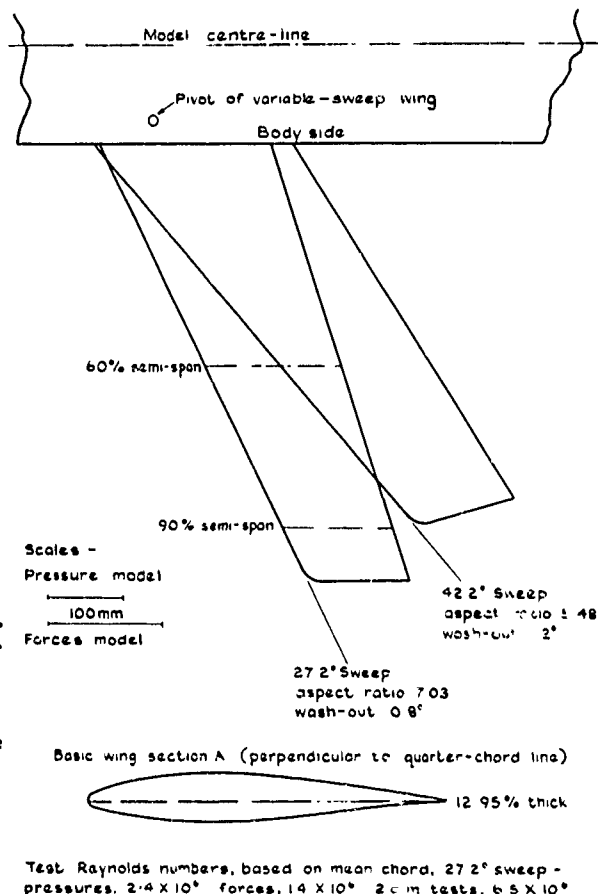


Fig 2 Details of the geometry of the variable-sweep wing used to obtain the data of figs 7 and 8



really be taken for this. It is of course all too easy to modify the leading-edge shape of a profile to improve the maximum lift developed at low speeds at the expense of performance at the high end of the range, so this particular modification very much represents a compromise solution. Also, as anyone acquainted with so-called 'supercritical' types of aerofoils will know, it is all too easy (but not necessarily inevitable) to devise sections with substantial improvements in maximum lift at high speeds at the expense of usable lift at low speeds. Before leaving this figure attention must be drawn to the scale of equivalent Mach number included for the wings of the complete model when set at  $27.2^\circ$  sweep. As will be seen the benefits of the sectional modification reduce with increasing Mach number becoming virtually zero at a Mach number of about 0.7 for the wing at this sweep setting. For the wing swept at  $42.2^\circ$ , this Mach number would be in the region of  $M = 0.85$ .

Before discussing the actual effects of this sectional modification on the measured lift coefficients for the complete swept wing, it is worth considering briefly how these benefits in lift coefficient have materialized. Fig 4 shows the lift-incidence curve for both the basic section 'A' and the modified section 'B' at  $M = 0.5$ . There is a change in the lift developed at constant incidence before the stall, mainly due to the change in overall chordwise camber, but of more significance is the increase in the maximum lift developed. From the measured pressure data there is evidence of a reduction in suction-peak height, and thus a reduction in shock strength, for the same lift at conditions prior to flow breakdown (a comparison at  $C_L = 1.14$  is shown to demonstrate this in the inset diagram.) Since the maximum lift attained is by and large governed by the strength of the shock reaching some critical value, the result is an overall increase in

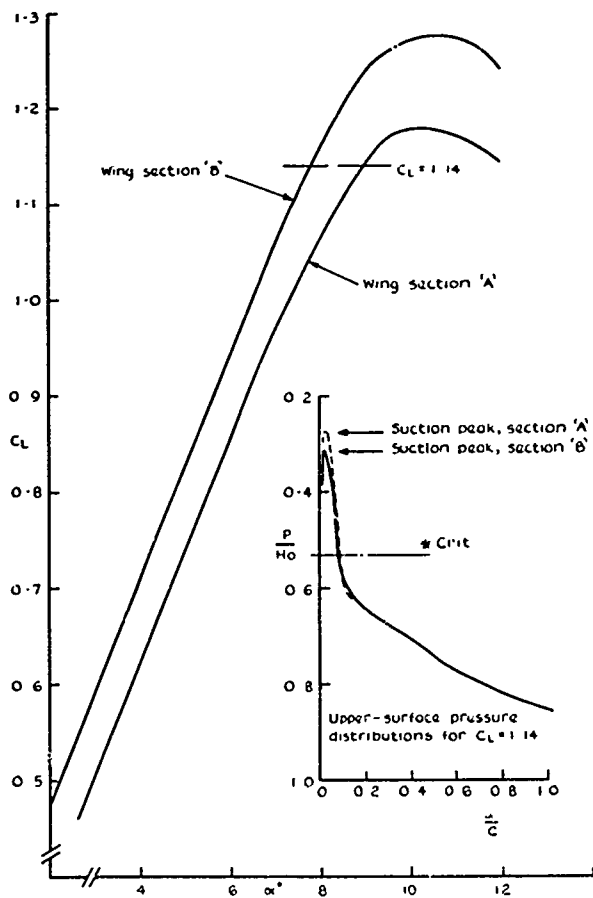


Fig.4 Characteristics of wing sections 'A' and 'B' at  $M = 0.50$

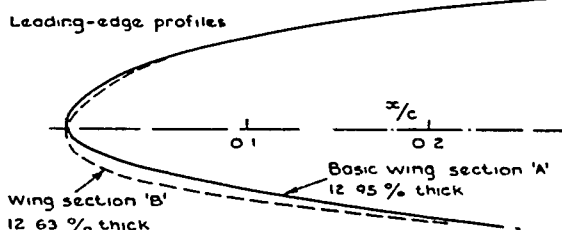
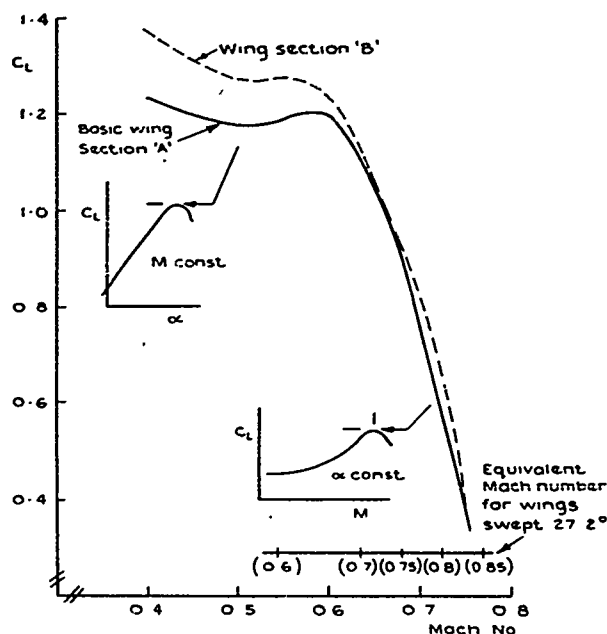


Fig.3 Stall boundaries from two-dimensional tunnel tests on wing section 'A' and on the modified section 'B'

maximum lift-coefficient in favour of the modified section (0.09 at this Mach number). At high Mach numbers a different flow situation arises and it is instructive to consider in this case the comparison of pressure distribution at high lift when the shock terminating the supercritical region on the two profiles is likely to have the same effect on the boundary-layer behaviour. Fig 5 shows what the comparison between the lift-incidence curves looks like for the two sections at  $M = 0.7$ , and the inset diagram shows the comparison of upper-surface pressure distribution at an incidence of about  $3.5^\circ$  when the shock has about the same strength and position on the chord. Marginal benefits to usable lift at this Mach number partly arise from the section modification due to increased suction being induced aft of the leading edge in the supercritical region.

Fig 6 demonstrates some extra important effects of this section modification in two-dimensional conditions. Firstly, there was a general tendency for the upper-surface shock on the modified section to be a little further aft when compared on a  $C_L$  basis except at  $M = 0.66$ . Secondly, the forward movement of the shock as flow separations developed tended to be more abrupt on the modified section. As may be seen from the typical pressure distribution in Fig 5, the more triangular form of the supercritical pressure distribution on the original section would tend to make the shock weaker as it moved forward. The resultant stabilizing effect on the stall development would not have been present on the modified section with its much flatter supercritical pressure distribution ahead of the shock. Thirdly, the shock strength compared on a  $C_L$  basis tended to be greater for the modified section, but before the stall the rate of increase of shock strength with lift decreased resulting in comparable conditions at the point of flow separation, (case for  $M = 0.6$  is shown). We shall refer to these points later in the discussion.

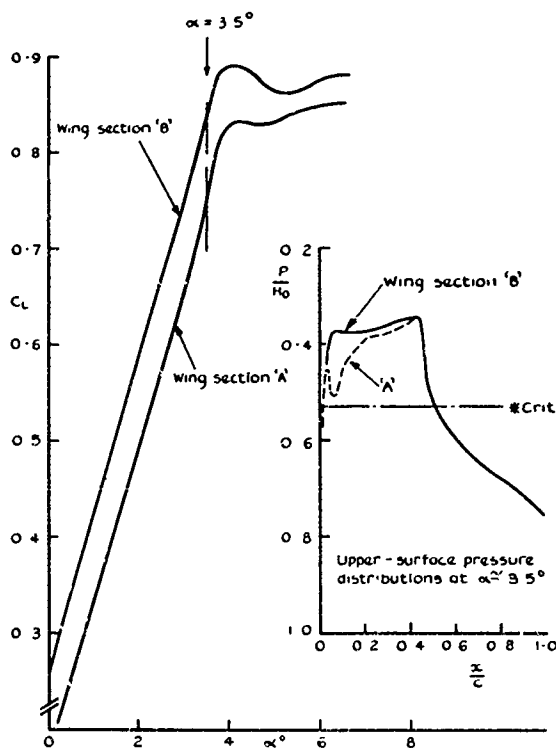
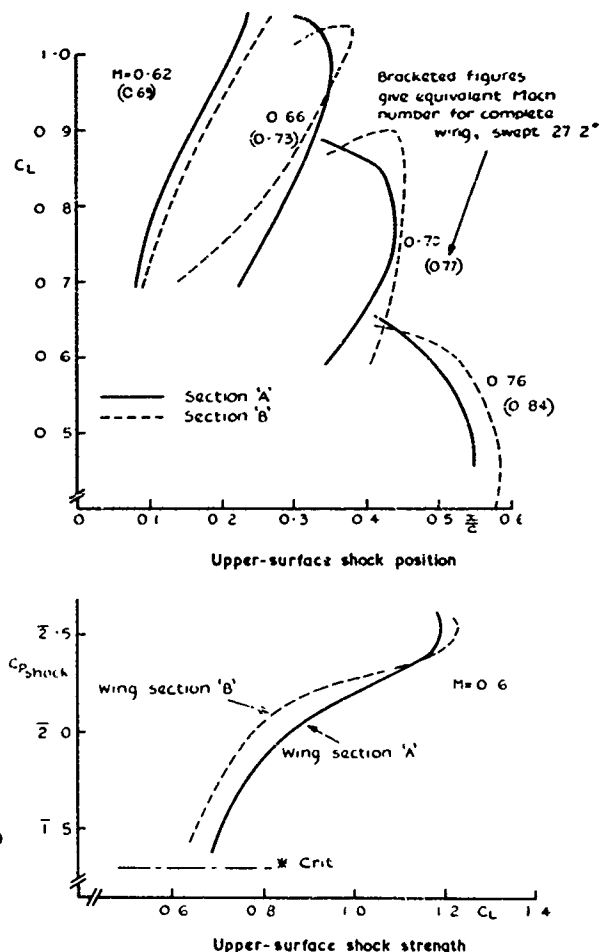
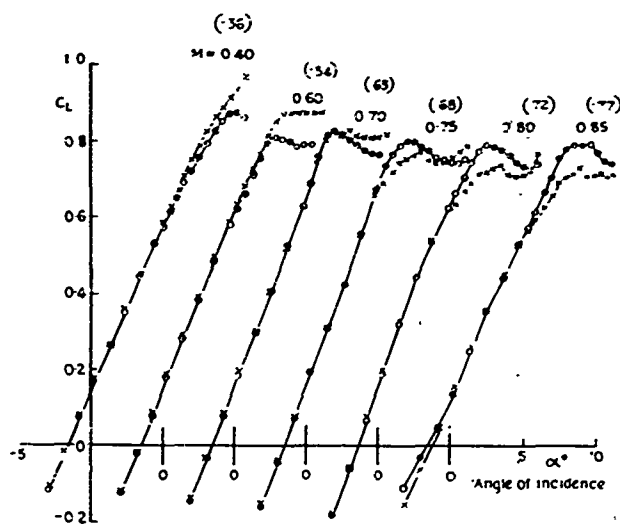
Fig 5 Characteristics of wing sections 'A' and 'B' at  $M=0.70$ 

Fig 6 Upper-surface shock position and strength from two-dimensional tests on wing sections 'A' and 'B'

## 2.2 Application to the complete model configuration

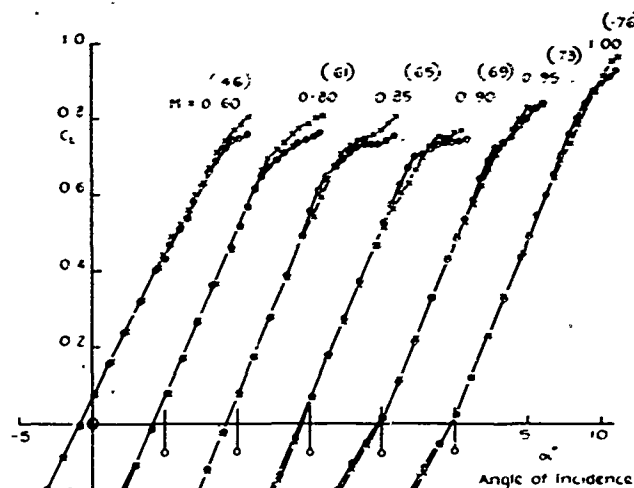
Turning now to the lift-coefficients measured on the complete model of Fig 2 before and after this leading-edge modification was incorporated, we see that the promise of improvement from the two-dimensional tests has not entirely been fulfilled. In Fig 7 the lift-incidence curves for the configuration with wings set at  $27.2^\circ$  sweep are shown. Whereas the leading-edge modification has improved the maximum lift at the lower Mach numbers, at the higher speeds positive harm is done, the  $C_{Lmax}$  being lower and early breaks appearing in the curves. The benefits at lower speeds reduce to zero by  $M = 0.70$  and it is interesting that this at least was predicted from the two-dimensional tests (equivalent  $M = 0.63$ ). Before discussing the reasons for the losses in maximum lift at the higher speeds, it is instructive to note some similarities with the lift-incidence characteristics measured at higher wing sweep of  $42.2^\circ$  (Fig 8). The benefits of the modification made to the wing leading-edge are not so marked at the lower Mach numbers even allowing for the normal sweep effect, and there are indications in the more gradual nature of the loss of lift at high incidence that the stall is altogether more three-dimensional in character than at the lower sweep. However, there is once more a tendency for these benefits at low speed to disappear at about  $M = 0.85$ , i.e. at virtually the same equivalent two-dimensional Mach number found at the lower wing sweep,  $M = 0.65$ . At the higher Mach numbers, i.e. above  $M = 0.70$  at the lower wing sweep and  $M = 0.85$  at the higher wing sweep, an early break develops in the lift curves when the modified section is used, due to premature flow separations outboard on the wing. Thus the value of usable lift has been made worse rather than left unchanged as demonstrated in the two-dimensional data (Fig 3). Taken as a whole we would say that the leading-edge modification made to the basic wing section, although restricted in the improvement achieved at low speeds in order to maintain performance at the higher speeds, has only shown benefits up to  $M = 0.70$  at the wing sweep of  $27.2^\circ$  and up to  $M = 0.85$  at the wing sweep of  $42.2^\circ$ . Above these points in the subsonic speed range positive harm has been done to the stall boundary.

The reasons for this state of affairs at the higher Mach numbers is explained by reference to some pressure measurements made on the complete model. Fig 9 shows for a Mach number of 0.80 with the wings swept  $27.2^\circ$  the development of the local chordwise lift-coefficient at two spanwise stations as incidence is increased. A comparison is shown with the equivalent two-dimensional data, due allowance having been made for induced incidence and body-upwash increments at each position. The figure shows how at 60% semi-span the development of local lift is at least as great as, if not greater than, the sectional characteristic, but at stations nearer the tip there is an early break, ( $\alpha = 2.5^\circ$ ), in the development of lift resulting in significant losses over this region of the wing at the final stall boundary ( $\alpha = 7^\circ$ , see Fig 7). At inboard spanwise stations (not shown) very much better lift-incidence characteristics than those found in two-dimensions are developed and the general picture which emerges at these higher subsonic speeds is of strong three-dimensional effects on the spanwise loading and on the character of the flow development up to the stall, biased against good performance at the tip. It is worth noting from this figure that the order of wing twist needed to postpone flow separation at the tip is large, even were this permissible from other (aero-dynamic) considerations.



Approximate equivalent 2-dimensional Mach number given in brackets  
 —○— : Wing section 'A' —x— : Wing section 'B'

Fig 7 Lift-curves for complete model  
 with wings swept  $27.2^\circ$

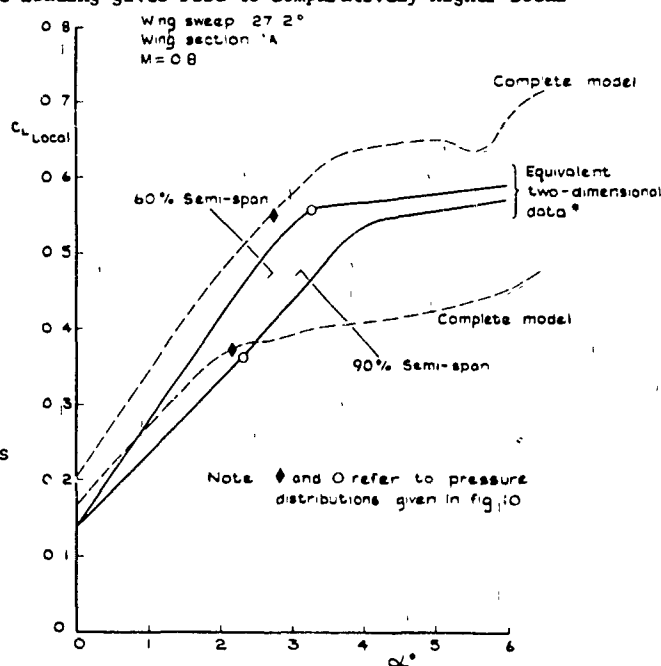


Approximate equivalent 2-dimensional Mach number given in brackets  
 —○— : Wing section 'A' —x— : Wing section 'B'

Fig 8 Lift-curves for complete model  
 with wings swept  $42.2^\circ$

It is useful to look at the chordwise pressure distribution at these two spanwise stations, and this has been done in Fig 10 for those points in the lift development indicated by the 'diamond' symbols marked in Fig 9. Comparison is made with the equivalent two-dimensional pressure distributions marked similarly by 'circle' symbols. For each spanwise station the comparison is made at about the same lift-coefficient and in each case the conditions taken are those just before the break in the local lift development with incidence (in either the two-dimensional or the three-dimensional data). This comparison shows that, although agreement in the pressure distribution at 60% semispan is fairly good, at 90% semispan the shock terminating the supercritical region is both stronger and further forward on the complete model and that there is a tendency for increased suction to develop over the forward portion of the supercritical region resulting in a higher, flatter roof-top type pressure distribution. These observations are entirely compatible with the classic situation which arises on straight-tapered swept wings of constant chordwise section<sup>2,3</sup>. At the tip, thickness effects cause local reductions in isobar sweep towards the leading-edge, and a little further inboard, (say at 2/3 to 3/4 semispan) a maximum in the spanwise loading gives rise to comparatively higher local lift-coefficients. Taken together these two factors induce a shock front at high subsonic speeds which is of reduced sweep over the whole outer portion of the wing upper-surface and shocks which are thus further forward and of higher strength than elsewhere on the wing. The result is that shock-induced separations generally occur first near the tip and progress inboard as incidence is increased.

Thus we may obtain some insight into why the leading-edge modification applied to the basic wing section did harm on the complete model in the higher range of speeds. At mid-span, at near-two-dimensional conditions, we can see that the expected increase in suction at the forward end of the supercritical region (see Fig 5), can easily be accommodated with some benefit and the tendency for a further aft shock (see Fig 6) with no significant change in strength will do little harm locally and even some good. However, this further aft position of the shock locally at mid-span indirectly has an adverse effect because it makes worse the basic tendency for the shock to become less swept over the outer portions of the wing. At the wing tip adverse effects are more obvious. The increase of suction forward on the profile will in this case cause adverse pressure gradients to appear in the supercritical region resulting in the shock moving forward more abruptly at an earlier incidence and becoming stronger as it does so. Thus the section modification will have aggravated the classic development of shock-induced flow separations usual on swept wings by a tendency to reduce shock sweep and increase shock strength over the whole of the outer wing. The features which bring this about are apparent in the sectional characteristics but do no harm in two-dimensional conditions. It should be noted that at low speeds in the range of Mach number under review, shocks inducing flow separations only occur at positions very close to the leading edge so none of this argument about shock movements applies. The wing in



Complete model with wings swept  $27.2^\circ$ ,  $M=0.8$   
 Two-dimensional data at  $M=0.72$  shown for comparison

\*Note: The two-dimensional data includes allowances for body-upwash and induced incidence

Fig 9 Comparison between local-lift curves at  $M=0.80$  for the complete model configuration and for the equivalent two-dimensional data at two spanwise positions

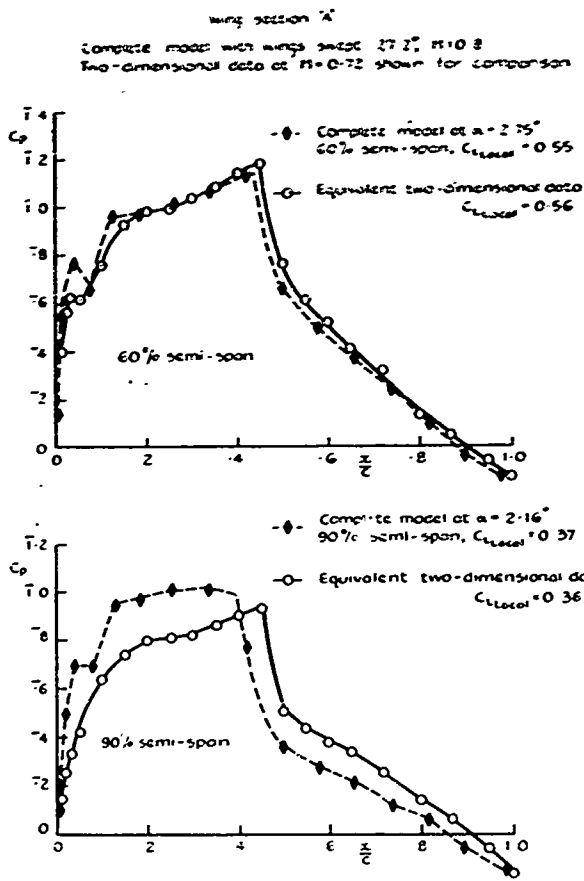


Fig. 10 Comparison between chordwise pressure distribution at  $M = 0.80$  for the complete model configuration and the equivalent two-dimensional distribution at the same local lift-coefficient

### 3 THE USE OF LEADING EDGE SLATS AT HIGH SUBSONIC SPEEDS

At moderate subsonic speeds such as  $M = 0.5$ , when the shockwave is near the leading edge, the mechanism by which a leading-edge slat can give an increase in usable  $C_L$  is essentially the same as at low speeds. Deflection and extension of the slat can reduce the peak suction near the leading edge and so delay the onset of a shock-induced separation. Typically, the optimum deflection is roughly half that used for landing. At higher subsonic speeds, however, eg  $M = 0.65$  for  $25^\circ$  sweep or  $M = 0.80$  for  $45^\circ$  sweep, a slat can still improve the stalling characteristics but the nature of the improvement and the mechanism by which it is achieved are not the same as at lower speeds. A fair amount of research has been undertaken within the UK during the past few years to show what factors can contribute to a good slat design for wings of similar thickness to those discussed earlier and how to retain the effectiveness up to as high a Mach number as possible.

Initially, tests were made on a high aspect ratio wing with  $27^\circ$  leading-edge sweepback (not the same wing as that discussed earlier but of similar thickness) with three slat designs A, B, C (Fig 11) and one droop design B, formed by fairing over the slot of slat B. The leading-edge devices extend over the full span of the nett wing but because the wing design includes three-dimensional treatment with the section shape varying across the span, the slot geometry also varies considerably as shown in fig 11. Overall  $C_L - \alpha$  curves are shown in fig 12 for  $M = 0.55$  and  $0.65$  and typical pressure distributions over the forward part of the wing at mid semi-span at  $M = 0.65$  are compared in figs 13 (a, b). It will be seen that at  $M = 0.55$ , slat A which is drooped  $12.5^\circ$  over most of the span improves the maximum lift by at least  $\Delta C_L = 0.2$  but it is the results for  $M = 0.65$  that are of more interest and which pose the greater challenge. The first point to note is that the high-lift performance of the clean wing is

three-dimensions can thus take advantage of the gains demonstrated in the sectional test data.

### 2.3 The need for variable geometry

The foregoing discussion centred round the measured effects of a particular modification to the leading edge shape of a profile used on a swept wing at high subsonic speeds leads to two conclusions. Firstly, the requirements at the low and high ends of the high-subsonic speed range are basically in conflict as regards the improvement of usable lift. At lower speeds the strong adverse gradient and/or shock strengths which develop at high incidences can be reduced by the use of leading-edge nose-down camber, although in excess this can lead to subsidiary problems at other flight conditions. However, at the high end of this speed range, application of this nose camber can increase velocity, and thus the local shock strengths, at critical conditions. Secondly, even when great care is taken not to compromise the performance of the wing section at high speeds by modifications made to improve the performance at the lower speeds, - and this can be first well established by two-dimensional tests, - basic three-dimensional effects on the complete wing at the higher speeds can result in strong adverse effects at the stall due to such modifications.

The case for variable geometry rests on the basic need to resolve the conflicting requirements of leading-edge geometry across the high-subsonic speed range. In the last section of this paper the possible use of variable leading-edge profiles is presented as a means to improve performance over a wide range of speed, but first the aerodynamics of leading-edge slats at high speeds is discussed below.

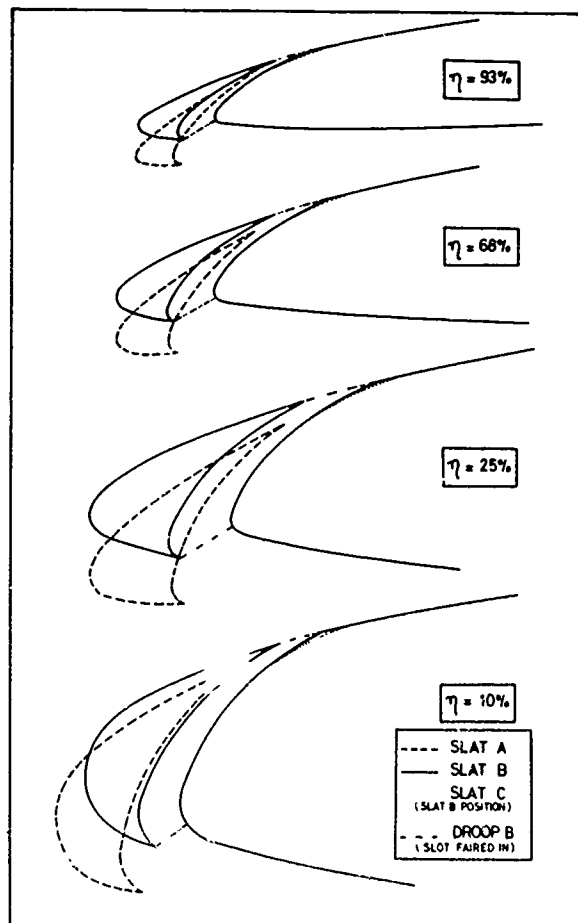


FIG 11

SLAT DESIGNS DIFFERENT STATIONS  
ACROSS SPAN OF 3D SWEEP WING

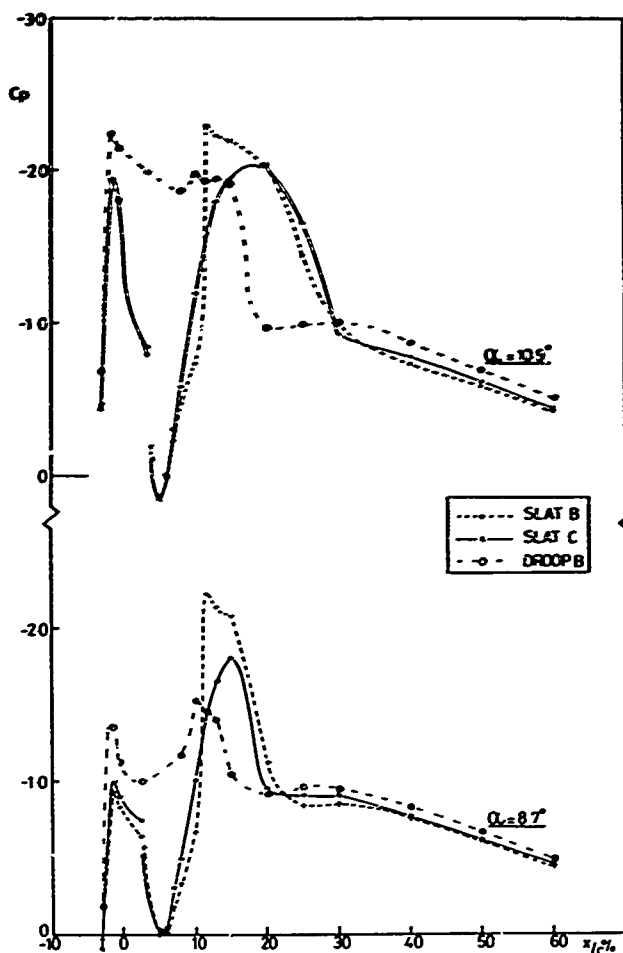


FIG. 13a FORWARD PRESSURE DISTRIBUTIONS:  
M = 0.65, 0.5 x SEMISPAN

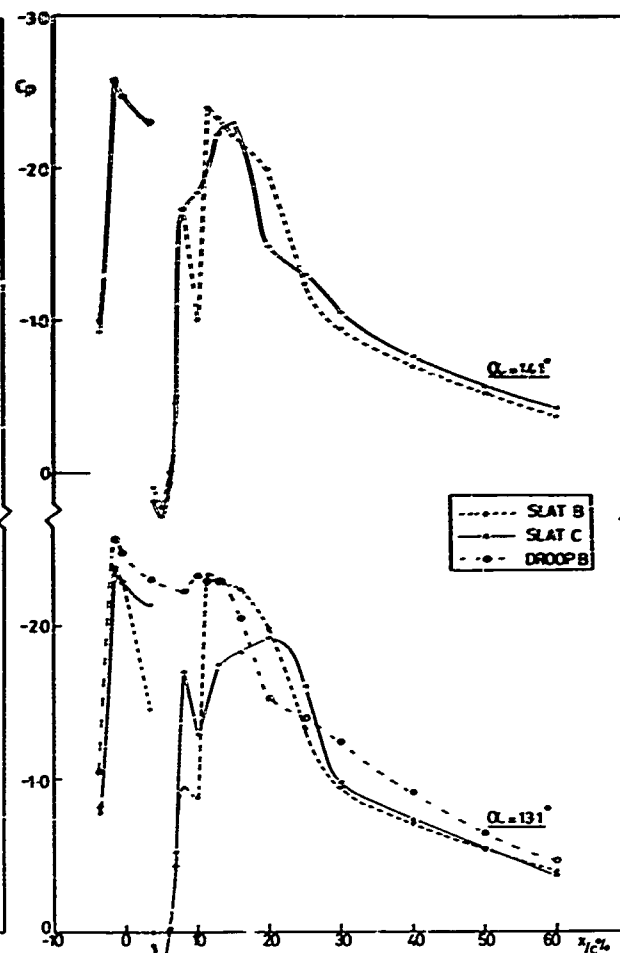


FIG. 13b FORWARD PRESSURE DISTRIBUTIONS:  
M = 0.65, 0.5 x SEMISPAN

leading-edge devices, when the incidence is increased beyond that for separation-onset, the shockwave moves forward towards the leading edge. Considering the wing as a whole, inboard of the separated area the shock front loses its sweepback, thus leading to an increase in shock strength and encouraging the separation to extend inboard. With a slat extended, however, as shown in fig 13, the shock tends to remain in a position about 0.10-0.15c behind the slot exit. At higher Mach numbers, when the shock prior to separation is further aft, it moves forward under the influence of a separation to about this position but then again remains stationary for a sizeable range of incidence. This is helpful in two senses: first, lift is maintained over the forward part of the main wing ahead of the shock and second, the shock retains its full sweepback. Also, as the incidence is increased, the lift on the slat itself continues to increase. A separate supersonic region forms and between  $\alpha = 10.9^\circ$  and  $13.1^\circ$ , this extends rearward towards the slat trailing edge. This rearward movement occurs first with slat C, ie, it is influenced by the shape of the main wing leading edge. By  $\alpha = 14.1^\circ$ , fig 13b, even with slat B, the flow is supersonic back to the slat trailing edge but there is still a two-shock system with a pressure-rise ahead of the step on the main wing surface. With slat C, on the other hand, the slat shock moves onto the main wing surface and coalesces with the second shock. To judge from the  $C_L - \alpha$  curves in fig 12, this is a favourable development and so in these respects also, the shape of the main wing surface for slat C represents a distinct improvement over slat B. It should perhaps be mentioned however, that even here one has to compromise between requirements for different Mach numbers. At M = 0.65, slat C is to be preferred for the reasons stated; at lower Mach numbers, this applies to a greater extent because the peak suction near 0.12c for slat B is even greater and there is a premature separation due to the adverse pressure gradient behind this peak suction; at higher Mach numbers, on the other hand, the strongly triangular nature of the pressure distribution with slat C leads to worse drag characteristics, the drag-rise Mach number at moderate  $C_L$  being typically about 0.02 lower with slat C than with slat B.

This brief discussion of the results for slats B and C in figs 12, 13 has shown that in any assessment of the effectiveness of a slat at high Mach number, two incidences are of particular importance:

- $\alpha_A$ : the incidence at which the shock-induced separation on the main wing extends to the trailing edge, and
- $\alpha_B$ : the incidence at which the supersonic flow over the slat upper surface extends to the slat trailing edge.

For a good slat design,  $\alpha_A$  should be as high as possible and  $\alpha_B$  obviously should be nearly the same value. Slats B and C are poor in both respects. Even with slat C,  $(\alpha_A - \alpha_B) = -3^\circ$  approximately and it is arguable that if supersonic flow at the slot exit has appeared by about  $\alpha_A$ , much better control would have been exercised over the subsequent development of the stall. Further, if the supersonic flow over the slat can be achieved before  $\alpha_A$ , the total lift carried at  $\alpha_A$  would be greater. On these arguments, therefore, one suspects that the optimum value for  $(\alpha_A - \alpha_B)$  should be slightly positive and this tentative conclusion has been borne out by an extensive, systematic research programme on different slat designs using the model illustrated in fig 14. This is a half-model wing-fuselage configuration where for engineering convenience,

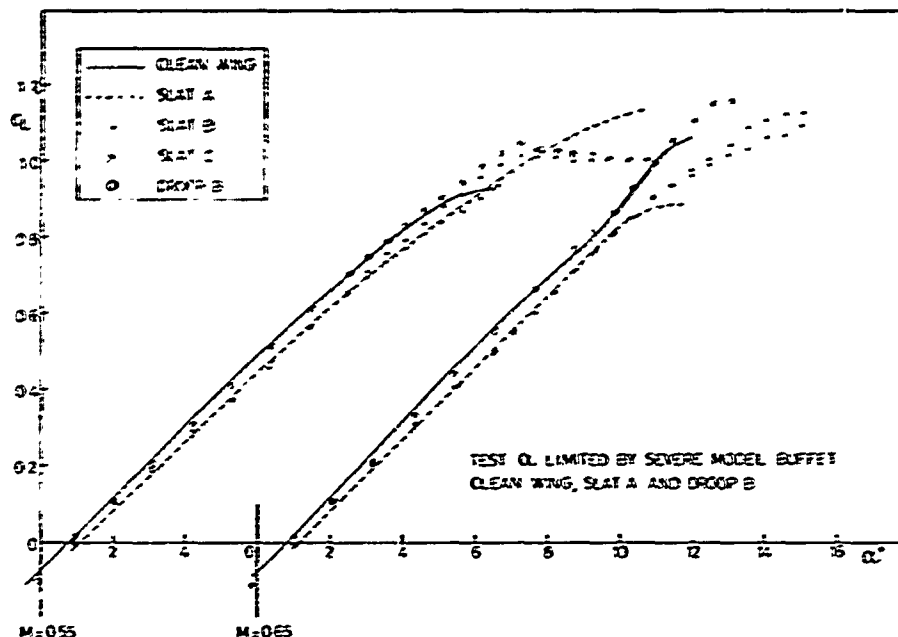


FIG. 12

EFFECT OF SLATS AND DROOPED NOSE ON OVERALL LIFT OF 3D WING

particularly good at  $M = 0.65$ , the maximum usable lift being assessed as  $C_L = 1.04$  as compared with  $C_L = 0.84$  at  $M = 0.55$  or  $C_L = 0.89$  at  $M = 0.71$ . Pressure-plotting tests showed that at high lift at  $M = 0.65$ , the local supersonic region over the forward upper-surface of the clean wing was well-conditioned with a peak suction near the leading edge followed by a largely isentropic recompression back to a relatively weak shock. It was therefore realised from the outset that it might be difficult to obtain sizeable improvements through the use of high-lift devices and at first sight the results in fig 12 do not appear too encouraging. Slat A is clearly deflected too much and gives a reduction of at least 0.15 in usable maximum lift-coefficient, irrespective of how this is defined. Slats B and C are more difficult to assess: pessimistically, the break in the  $C_L - \alpha$  curve again occurs at a lower  $C_L$  than for the clean wing but with slat C at least, the ultimate  $C_{Lmax}$  is higher. It is only droop B that gives a clear improvement, by about  $\Delta C_L = 0.09$  of which only 0.03 can be ascribed to the extra wing area. Referring to the pressure distributions in fig 13, it will be seen that at moderate incidences, eg  $\alpha = 8.7^\circ$  in fig 13a, droop B produces two local supersonic regions, the first near the leading edge and the second near  $0.10c$  but at higher incidences, eg  $\alpha = 10.9^\circ$  and  $13.1^\circ$ , these link to give an extensive peaky supersonic region with considerable isentropic recompression ahead of the shock. The results with droop B are therefore similar in character to those for the clean wing but higher values of  $C_L$  for separation-onset are achieved because the supersonic region as can be imagined, is more extensive. One should note however that the results are presented for droop B beyond  $\alpha = 13.1^\circ$ . This is because severe model bounce developed and it was impossible to obtain any steady readings. To judge from experience on other models, the likely explanation is that the shockwave moved forward rapidly and the supersonic region round the leading edge failed to develop over part of the span. This means that high values of  $C_L$  for separation-onset had been achieved at the expense of an abrupt stall development; to make this acceptable, one would possibly have had to introduce some variation in section shape across the span.

Turning now to slats B and C, neither of these proved to be an optimum configuration but nevertheless, the analysis of the results leads to some important general conclusions. The shape and position of the slat itself is the same in these two cases. It is merely the shape of the main wing upper surface near and downstream of the slot exit that is different (fig 11). With slat B, there is a rapid change in slope near  $0.12c$  and a forward facing step corresponding to the finite trailing edge thickness of the slat; with slat C, the change in slope is eased by a fairing undercutting the step. This change in geometry may appear to be small but the consequences are significant. Fig 13a shows that even at the moderate incidence condition of  $\alpha = 8.7^\circ$ ,  $C_L = 0.7$  ie more than 0.1 in  $C_L$  below the  $C_L$  for separation-onset for the clean wing, (Fig 12) a strong shock is already present on the main wing upper surface with both slats B and C but it has been weakened considerably by the change from B to C. With slat B, the suction reaches a maximum near the step and there is then some recompression ahead of the shock whereas with slat C, the fairing has eliminated the forward peak suction, and the local upstream Mach number (normal to the shock) ahead of the shock is about 1.26 as compared with 1.41 for slat B. Even with slat C however, a shock-induced separation is clearly imminent and so one must conclude that neither slat has been successful in postponing separation-onset relative to the clean wing. It is arguable that some improvement would have been obtained if the fairing of slat C had been gentler and had extended over more of a chord. This has immediately highlighted two features of a good slat design for high Mach numbers: the change in direction imposed on the flow out of the slot exit and the curvature of the main wing surface downstream of this exit should both be kept as small as possible. This is equivalent to saying that the rear of the slat should be thin and that the slat trailing edge should be positioned as far aft as possible, eg at about  $0.18c$  rather than  $0.12c$ . It is quite understandable that the optimum curvature of the surface between  $0.2$  and  $0.3c$  should ideally be less than for a good clean wing design; in the latter case, when the flow is supercritical, the effect of the expansion waves from this part of the surface tends to be offset by the incoming compression waves reflected from the forward sonic line but at moderate incidences with the slat extended, the forward sonic point is further aft and these reflected compression waves will largely be absent.

It is clear therefore that it is difficult but not impossible to improve separation-onset at high subsonic speeds by means of a slat. Slats B and C do not achieve this but they are effective in controlling the subsequent development of the separation. As described in Section 2 above, with a clean wing with no

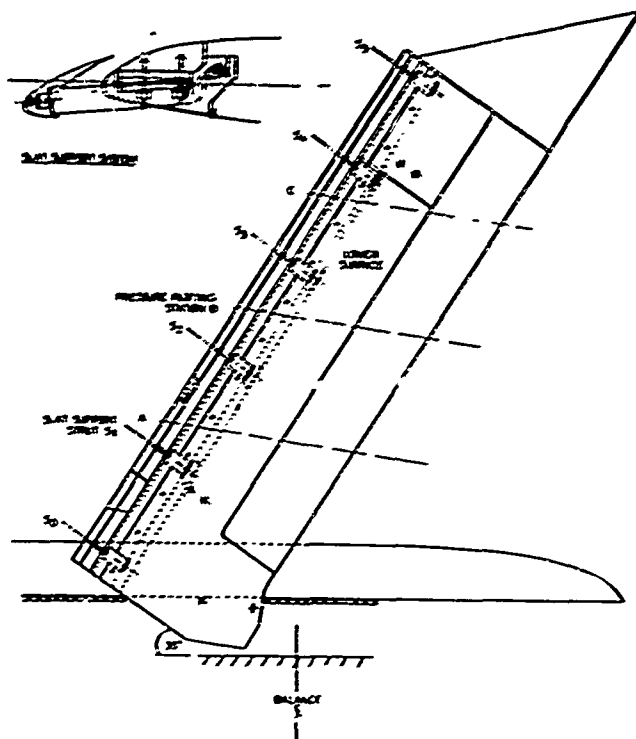


FIG. 14 VARIABLE SWEEP WING FOR SLAT/FLAP RESEARCH

apparently produced an improvement. Analysis of the pressure plotting data showed that this was because the only significant change as the gap was reduced, was in the pressures on the lower surface of the slat. These pressures increased thus giving more lift on the slat, but presumably, if the gap were decreased further, adverse effects would begin to appear. Thus once again, the lesson is that at the higher Mach numbers, the changes with any geometrical variable are no longer monotonic.

In the discussion in this section so far, the results have been analysed on a quasi-two-dimensional basis. With increasing Mach number and/or sweepback however, three-dimensional effects become important and this can be illustrated by presenting some results for the same model at  $35^\circ$  sweepback. Tests were made on the slat and droop (slat, slot closed) configurations shown in fig 16. Results for the mid-semi-span pressure-plotting station A are presented for slat 1 in fig 17 and in general terms although not in detail, this again illustrates the ability of the slat to control the development of the flow separation. A shock-induced separation bubble at the foot of the shock is first observed in condition 2; this extends back to the trailing edge by condition 3; the supersonic region on the slat extends back to the trailing edge of the slat by condition 4; the coalescence of the two shocks occurs near condition 5 and some lift is maintained on the main wing ahead of the shock up to beyond condition 6. The shockwave is held behind the slot exit and thus retains a sweep near  $35^\circ$ ; the shock-induced separation tends to roll up into a swept bubble or vortex-type flow and this leads to an improvement in the pressure recovery near  $\alpha = 14^\circ$  between conditions 5 and 6 and thus to the increase in lift-curve slope in this range. The important extra feature in these results for  $35^\circ$  sweep however is the spanwise variation in slat effectiveness as shown in fig 18. At the lower Mach numbers such as  $M = 0.5$ , it is not unexpected to find that the slat is successful in coping with the premature tip-stalling tendency of the clean wing but the more surprising results are those obtained at high

the basic wing is untapered. The wing can be mounted at varying angles of sweepback but is shown in fig 14 set at  $35^\circ$  sweep and fitted with the tip actually made for tests at  $45^\circ$  sweep. The slat supports are shown; through the use of different supports and wedge packing pieces, a wide range of slat deflections, extensions and gaps could be tested.

The results obtained at  $25^\circ$  sweep are summarised in fig 15. The increments in maximum usable normal force  $\Delta C_N$  (measured by the balance but assessed on the pressure plotting evidence) are plotted against the product  $(\alpha_{TE} - \alpha)$  and curves drawn through points for a given slat deflection  $\delta$ . The symbols are defined in the sketch in the figure. At  $M = 0.5$ , a reasonable correlation is obtained showing that within the range tested but not necessarily outside this range, increasing deflection, extension and gap tend to increase  $\Delta C_N$ . At  $M = 0.65$ , however, it is a more complicated story. The best results,  $\Delta C_N \approx 0.2$  are obtained as suggested above for configurations giving  $(\alpha_A - \alpha_B)$  in the range  $0^\circ$  to  $2^\circ$ . Increasing the slat deflection and extension are only helpful while  $(\alpha_A - \alpha_B)$  remains in this range; ultimately,  $(\alpha_A - \alpha_B)$  becomes negative and the slat effectiveness then decreases. This is shown particularly by the sequence of results for  $(\alpha_{TE} - \alpha) \approx 16$  showing a reduction in  $\Delta C_N$  as  $\delta$  is increased from  $5^\circ$  to  $15^\circ$ , this increase in  $\delta$  reducing the loading on the slat at a given incidence, thus increasing  $\alpha_B$  and reducing  $(\alpha_A - \alpha_B)$ . The best slat designs give improvements of about  $\Delta C_N = 0.2$ , a notable achievement relative to the results for slats B and C discussed earlier since we are still considering the same Mach number ( $0.65$ ), the same sweepback ( $25^\circ$ ) and a similar thickness/chord ratio. Another interesting point of detail about the results in fig 15 is that the reduction of the slat gap has

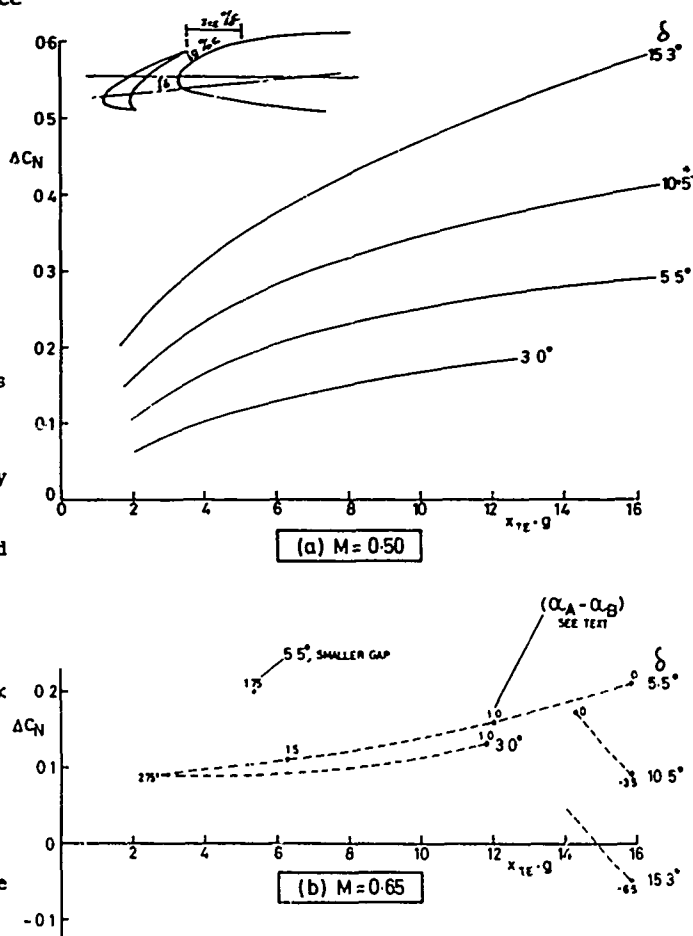


FIG 15 ESTIMATED INCREASE IN USEABLE  $C_N$  DUE TO SLATS UNTAPERED WING  $\Lambda = 25^\circ$

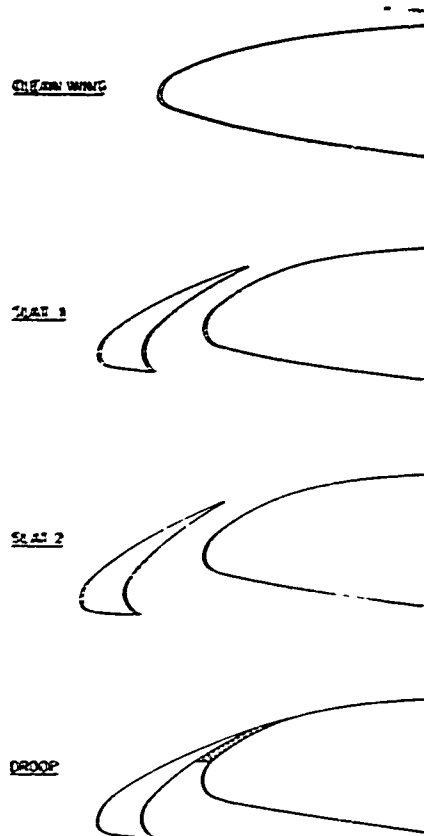


FIG 16 TYPICAL SLATS TESTED ON RESEARCH WING

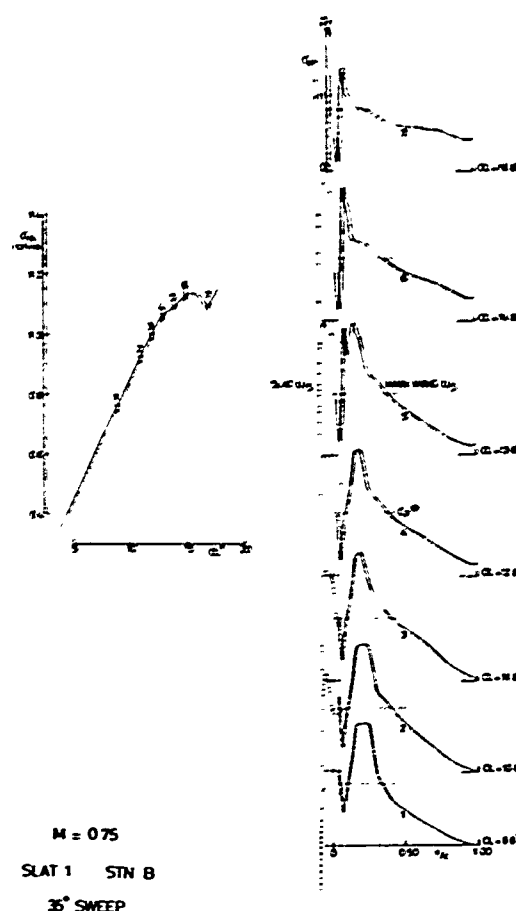


FIG.17 FLOW DEVELOPMENT NEAR MID-SEMISPAN WITH TYPICAL SLAT

Mach number where the slat is relatively ineffective near the tip but strongly effective near the root. Extending a slat can therefore be used to control not merely the forward but also the inward development of the area of flow separation.

The reasons for the variation in slat effectiveness across the span at high Mach number are not entirely clear but analysis of the pressure plotting results has shown that again, the trend can be interpreted in terms of the parameter  $(\alpha_A - \alpha_B)$ . As noted earlier,  $\alpha_A$  depends primarily on the suction generated in the supersonic region aft of the slot exit but typically, ahead of the wing maximum thickness. The suction in this region are likely to be higher and as a consequence,  $\alpha_A$  lower on the outer wing. Also, the results have shown that  $\alpha_B$  is lower on the inner wing; the impression seems to be that on the outer wing, the rearward movement of the slat shock towards the trailing edge is delayed by a local flow separation over the rear of the slat. It follows that on both counts,  $(\alpha_A - \alpha_B)$  tends to be positive on the inner wing and negative on the outer wing. Clearly, one would welcome a better result on the outer wing than that obtained with slat 1 because separation-onset for the wing as a whole will be at a lower  $C_L$  at high Mach number than for the clean wing, but on the other hand, even when this happens, the slat still retains its ability to control the development of the separation as shown graphically by the shape of the  $C_L - \alpha$  curves for  $M = 0.80$  in fig 18.

The overall results for all the configurations at  $35^\circ$  sweep are presented in fig 19. It will be seen that substantial improvements are achieved at  $M = 0.50$  and even more so, in the case of slat 1, at  $M = 0.65$  but there is then a deterioration at the higher Mach numbers. This figure has however been included not so much to show the actual increments in usable lift due to each configuration but to illustrate that with the slats particularly, because of the gradual development of the flow separations, it may be impossible to quantify these increments merely on the basis of the breaks in the overall  $C_L$  (or  $C_N$ ) curves. To take for example the results for slat 1 at  $M = 0.75$ , one would certainly not expect the maximum usable  $C_N$  to be better than about  $C_N = 1.18$  just past the major break in the  $C_N - \alpha$  curve but an analysis of the pressure plotting data and the unsteady output from wing root bending moment gauges suggest that moderate buffet, and hence possibly an operational limit, may be as low as  $C_N = 0.97$  or only 0.10 above the assessed value for the clean wing. Setting the limit at this point would imply reverting to condition 3 on fig 17. This may appear contradictory in that one is not taking advantage of the ability of the slat to maintain lift over the forward part of the wing up to condition 6 but this is not so because the performance of the wing as a whole is being degraded by what is happening outboard of station B. It is worth pointing out that the adverse effects on the outer wing may be particularly pronounced in this example because the results have been obtained for an untapered wing with a far from ideal tip shape. In practice, with a real aircraft, having a tapered wing, some twist and a properly designed planform and section shape near the tip, the adverse effects could be much less pronounced and then, one would be able to capitalise on the separation control evident at station B.

To summarise, a slat designed with careful attention to the shape of the main wing surface near and downstream of the slot exit can improve separation-onset except possibly near the tip up to quite high Mach



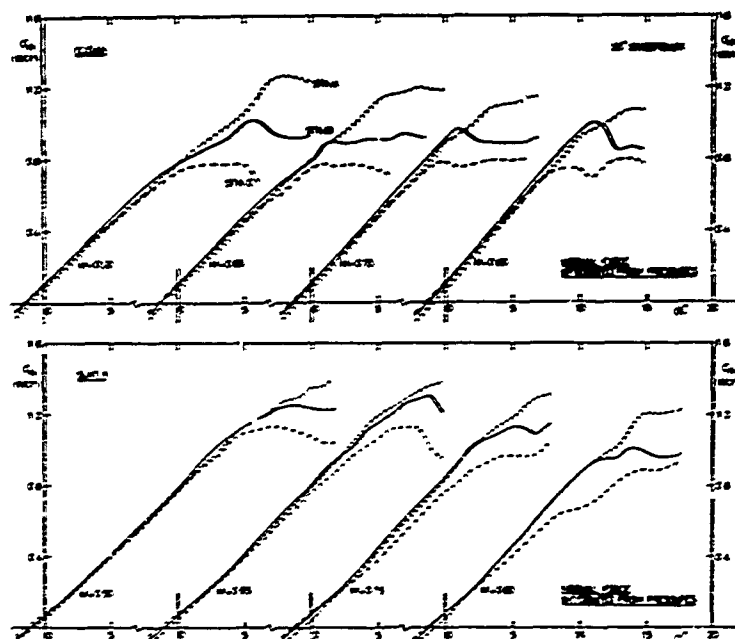


FIG 18 EFFECT OF SLAT ON SPANWISE DEVELOPMENT OF STALL 35° SWEEP

numbers but the main virtue of a slat at high Mach number is in controlling the forward and inward spread of the flow separation and thus, improving the buffet penetration qualities. The more it is successful in this aim, the more uncertain becomes the assessment of the true maximum usable lift. More research is needed on this point.

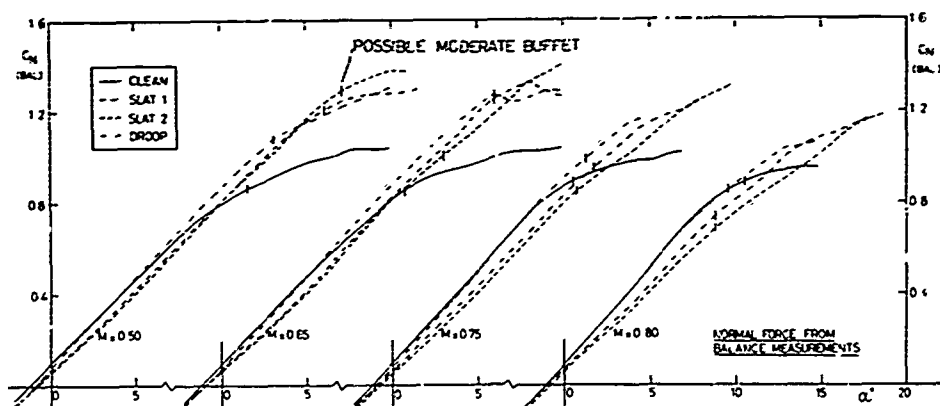


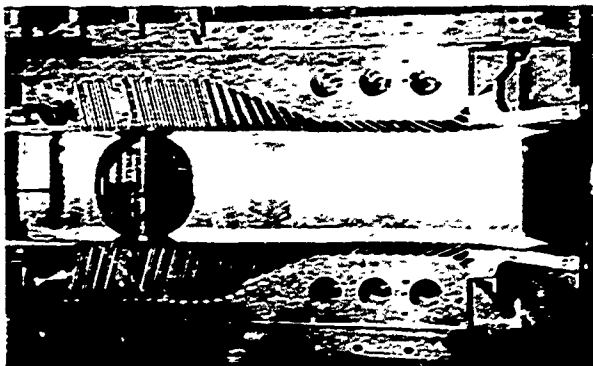
FIG 19 EFFECT OF SLATS (AND DROOP) ON USEABLE LIFT 35° SWEEP

#### 4 THE USE OF VARIABLE GEOMETRY WING PROFILES

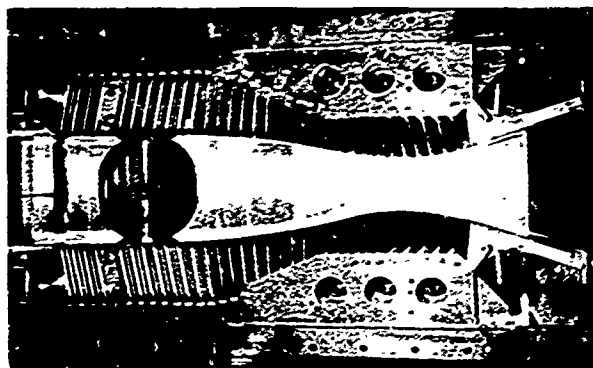
After all that has been said in the preceding sections the advantages of being able to change the actual profile shape at will to suit the various aerodynamic conditions as they arise at different points in the flight envelope are fairly obvious. We are a very long way off from this ideal situation, of course, but a small advance has been made by the recent development within the UK of a linkage system able to control surface shape locally from within the wing. This device has been called the 'Royal Aircraft Establishment Variable Aerofoil Mechanism' or 'RAEVAM' for short, (Patent rights have been filed under Patent Application No 27787/69).

##### 4.1 The RAEVAM Device

The starting point for this idea was the development of a new type of variable liner for the working section of a supersonic tunnel at RAE<sup>4</sup> to meet a requirement for a fast and accurate system to use in conjunction with a 'dynamic simulator'<sup>5</sup>. Fig 20 shows the finished system now in operation. The flexible walls of the working section are positioned by a large number of stiff links pivoted at one end at points along the walls and at the other on rigid earth-frames. The forward and rear ends of each flexible wall are free to slide fore and aft at the points where they blend with the fixed walls of the nozzle, and suitable sliding joints have been designed to avoid any disturbances locally. The lengths of the links and the position of the pivots on the earth-frame were chosen so that, as the flexible walls are moved fore and aft by means of a hydraulic jack, the required range of liner shapes is formed. The geometry of the linkage system is in fact completely determined by specifying the exact shape of the walls required at three specific points in the range, but choosing these points with care it was found in practice that the liner shape between these



Flexible walls set at shape for  $M \leq 1$



Flexible walls set at shape for  $M = 2-3$

Fig. 20. Mechanism used in R.A.E. 18ins x 18ins supersonic tunnel for the rapid and accurate variation of mach number (Based on the RAEVAM principle)

a mention here. It is perhaps worth noting that the system shown in Fig 21 always implies a shortening of the chord as profile nose-down camber is increased. The installation shown in Fig 22 however, shows how with the small extra complication of an extra motion controlled by a second jack, some forward extension of the leading-edge can be included in the variable geometry. Other subsidiary motions can include rotation of the whole leading edge about a second pivot as shown in Fig 23. In this case only one sliding joint is needed at the blend point between the flexible and fixed areas of the skin.

design points gave as good quality tunnel flow at intermediate Mach numbers as achieved normally with fixed liner blocks.

This principle has now been applied to the surface profiles of wings. In this paper we are concerned with changes of profile at the leading edge, and in particular with the need to vary the shape in this region through the high subsonic speed range to improve lift performance at the stall. A typical installation is shown in Fig 21. The leading edge is conveniently left solid and is constrained by the arm 'A' to rotate about some point 'P'. The rest of the skin is made flexible and is constrained in shape by means of a series of links pivoted at the underside of the skin at one end and at various points on an extension to the main spar at the other. The ends of the flexible skin slide in sealed joints where they blend with the main fixed parts of the wing profile. Variation of the profile shape is achieved by means of a single jack, 'J', rotating the leading edge frame, pivoted at 'P'. As with the wind-tunnel liner, the lengths and pivot positions of the links are determined by specifying three precise nose shapes required. In the studies we have made so far, we have generally taken one of these shapes as that extreme droop position needed for low-speed  $C_{Lmax}$  and the other two as those needed to meet two particular requirements of high-lift performance at high speeds. The variation of profile shape between these design points is, of course, always smooth and progressive and appears to raise no problems in practice. There are, however, some practical constraints to consider. For instance, the position of the pivots at the fixed ends of the links must lie within the profile, but the links can be allowed to cross each other so there is a surprising amount of design freedom to accommodate the types of profile change typically required.

Several variations to this first simple mechanism described above are possible, but need no more than

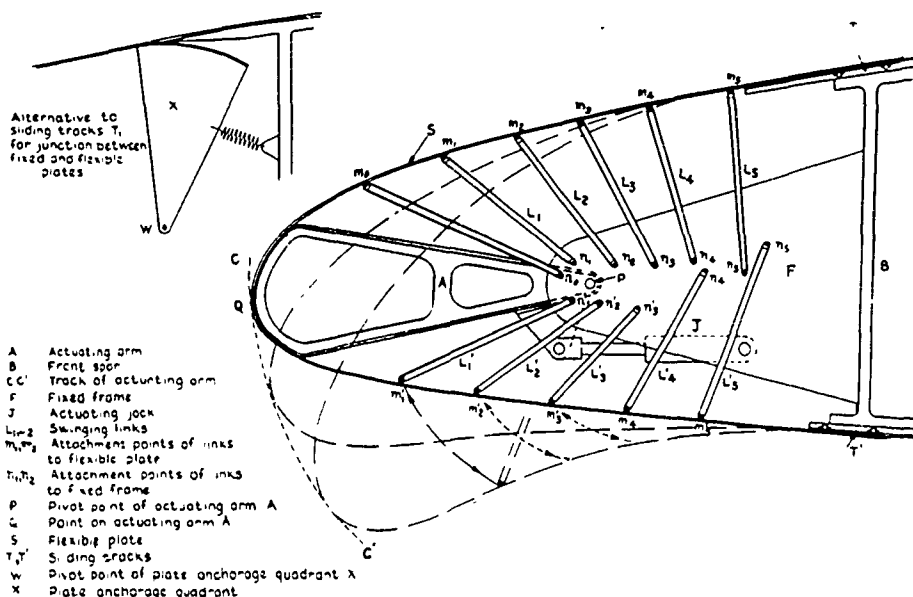


Fig 21 RAEVAM Mechanism for flexible leading-edge section of aerofoil

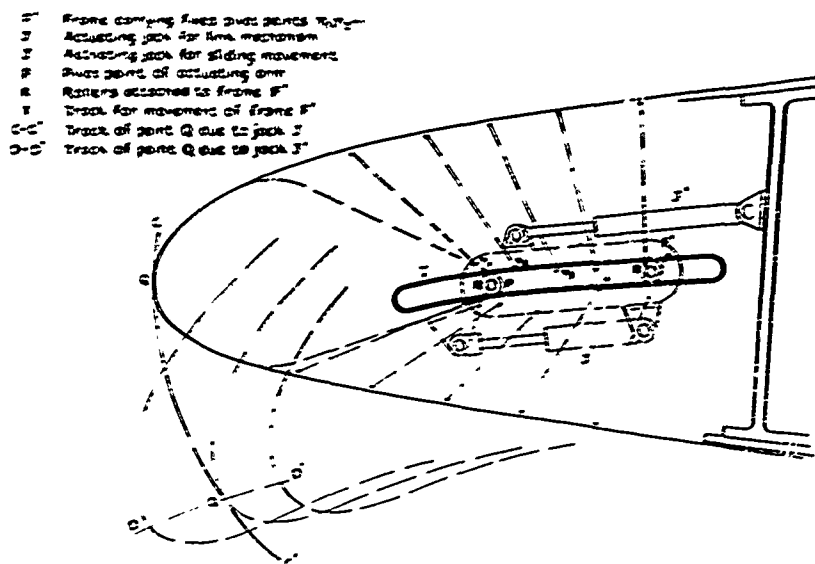


Fig.22 Combination of flexible nose section with sliding movement

#### 4.2 Aerodynamic Considerations

If we refer back for a moment to Fig 1 in this paper it is interesting to speculate on what variable-geometry device such as RAEVAM can do to improve performance at the stall over the high-subsonic speed range. The three typical pressure distributions quoted before are given again in Fig 24 and the diagrammatic effects of nose droop are sketched in with dotted lines. At the low end of the speed range, the height of the leading-edge suction peak and the strength of the associated shock wave can be effectively reduced by nose-down changes to the leading-edge profile. This, as we have seen previously is beneficial since the incidence for the stall is increased and hence the value of  $C_{Lmax}$  achieved. At the high end of this speed range the application of small nose-up changes in profile can counteract the basic tendency for triangular types of supercritical pressure distribution to arise. Not only can prescribed peaks at the start of the supercritical region be induced to appear to improve the local lift directly, but the whole of the development of the supercritical flow up to the shock can be manipulated by this means. For the same shock strength considerably more lift can thus be carried by the proper use of such profile modifications. At intermediate Mach numbers, however, provided the original profile design was a reasonably good one, there is probably little that can be done directly by the use of shapes generated by the RAEVAM device. Down-droop of the leading-edge will basically tend to strengthen the shock (at fixed incidence) and up-droop will tend to make the supercritical pressure distribution too 'peaky', the latter resulting perhaps in multi-shock systems and (at best) worse boundary-layer conditions at the main shock and further aft along the wing chord. In practice it has been found that the benefits of nose-down droop at the lower Mach numbers and of nose-up droop at the higher Mach numbers can overlap in the speed range, thus avoiding these difficulties at intermediate conditions.

On the complete wing, as we have seen in earlier parts of this paper, there is not only a need for a variation of leading-edge profile with Mach number, but variation is also desirable across the wing span to cope with the strong three-dimensional effects which can arise at near-stalling conditions. This raises

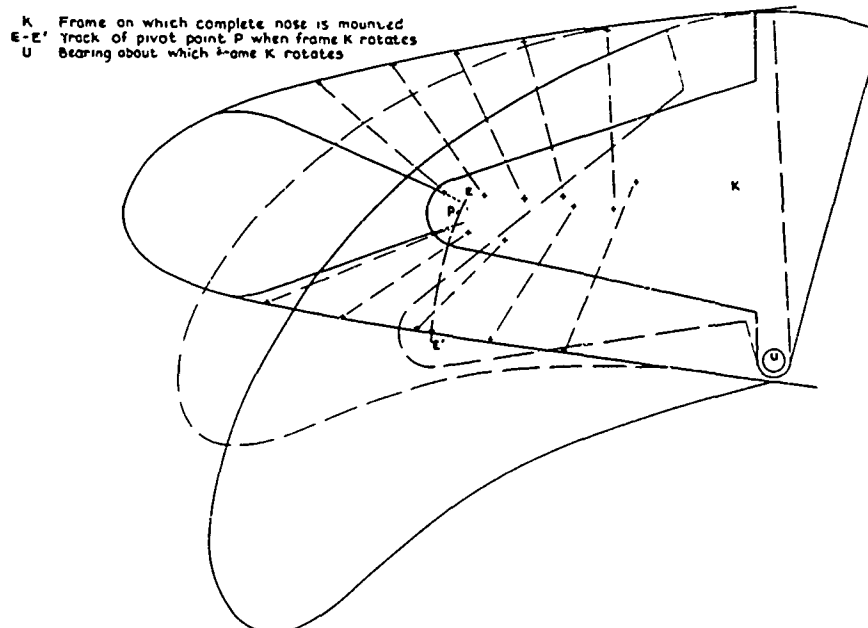


Fig 23 Combination of flexible nose section and rotary movement

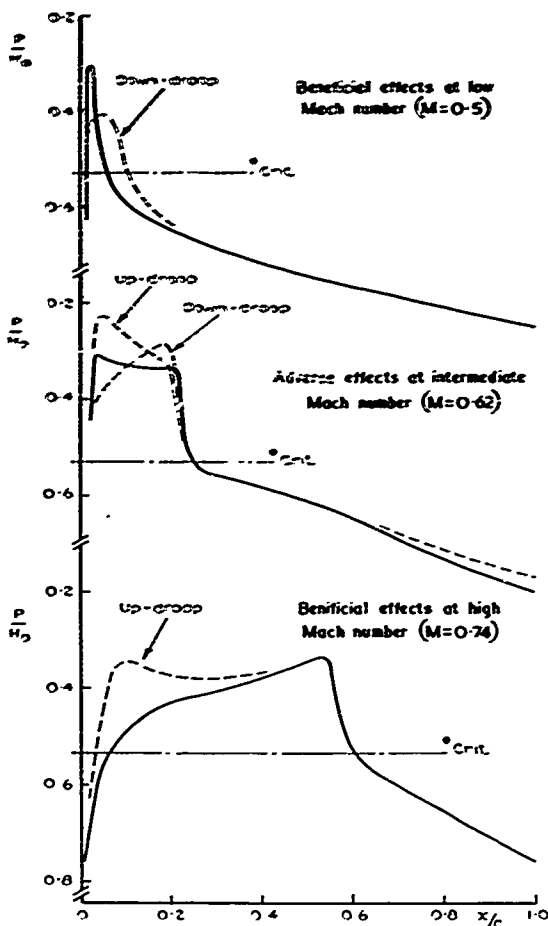


Fig.24 The diagrammatic effects of 'Raevam' down-droop and up-droop at the leading-edge on the basic types of pressure distribution shown in Fig 1

improved over all the range of high subsonic Mach number from  $M = 0.5$  to  $M = 0.75$ .

Figs 26 and 27 show some samples of the pressure distributions measured during these tests. In Fig 26, the small nose-up droop variation was adverse at  $M = 0.6$  as expected, the shock being strengthened and moved forward on the chord (note also the deterioration of the trailing-edge pressure). At  $M = 0.75$  this change in the profile geometry was beneficial, extra suction being developed before the shock which itself was virtually unaffected in strength. There was even a small improvement in trailing-edge pressure recovery. In Fig 27, the  $5^\circ$  down-droop variation in geometry both lowers and spreads the suction peak as expected at  $M = 0.5$  resulting in an increase in stalling incidence and  $C_{Lmax}$ . At  $M = 0.7$ , however, the effects are adverse since the main shock is considerably strengthened at constant incidence resulting in earlier flow separations as incidence is increased.

From this initial pilot set of measured data, it can be said that the use of this variable-geometry device shows great promise in the context of the aerodynamic problems discussed in this paper. Studies in connection with the use of this device to improve  $C_{Lmax}$  at low speeds are proceeding in parallel with further work at high speeds, and a review is being made of the structural problems likely to arise in the incorporation of the device on an actual aircraft wing.

## 5 CONCLUSIONS

This paper has emphasized by means of some recent examples of research work the critical importance of the geometry of the leading edge as regards the stalling characteristics of wings at high subsonic

engineering complications in the use of any moving leading-edge device, but it is comforting to note from the preceding discussion on the use of slats that leading-edge devices can change, and thus be used to control, the spanwise development of flow separation even when no spanwise grading of the geometry is employed. Perhaps the best approach to the problems of spanwise variation in stalling behaviour at high speeds lies initially in the spanwise variation of the shape and thickness of the basic profiles used in the wing design coupled with some incorporation of wing twist and a proper use of the inevitable effects of aeroelastic distortion. However, a limited degree of spanwise variation in the settings of variable-geometry devices may be desirable in addition to this. Continuous variation of such settings across the span should not be ruled out in the future as we become more and more able to cope with the engineering complications involved, but for the present we probably have to content ourselves with discontinuities across the span which bring with them their own problems.

## 4.3 Recent test results at high speeds

The data shown in Figs 25, 26 and 27 have been included to demonstrate the use of the RAEVAM device at high speeds to improve the stall boundary of a wing profile. The section used with the leading-edge modifications tried is shown at the bottom of Fig 25. The solid leading-edge piece was restricted to 2% chord in this case and a blend-point with the main profile shape was selected at 18% chord. The shapes, which were tested in the 2ft x 1½ft tunnel at RAE, were compatible for the pivot position shown with a practical linkage system of the type shown in Fig 21. The results of the  $5^\circ$  down and  $1½^\circ$  up modifications to the section are given in the top figure and show how the benefits achieved at low speed and high speed overlap in the speed range near  $M = 0.65$ . The inference from this figure is quite clear: the whole boundary has been

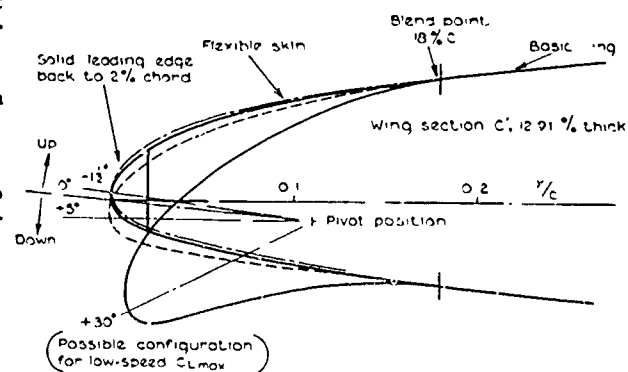
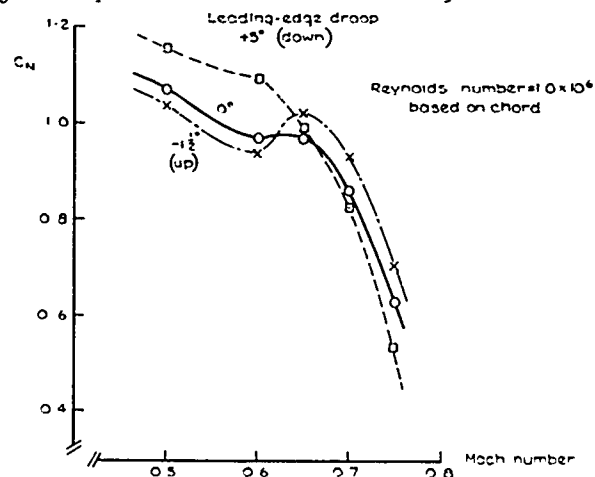


Fig 25 Stall boundary from tunnel tests on a family of nose shapes generated from basic section 'C' using the 'Raevam' device

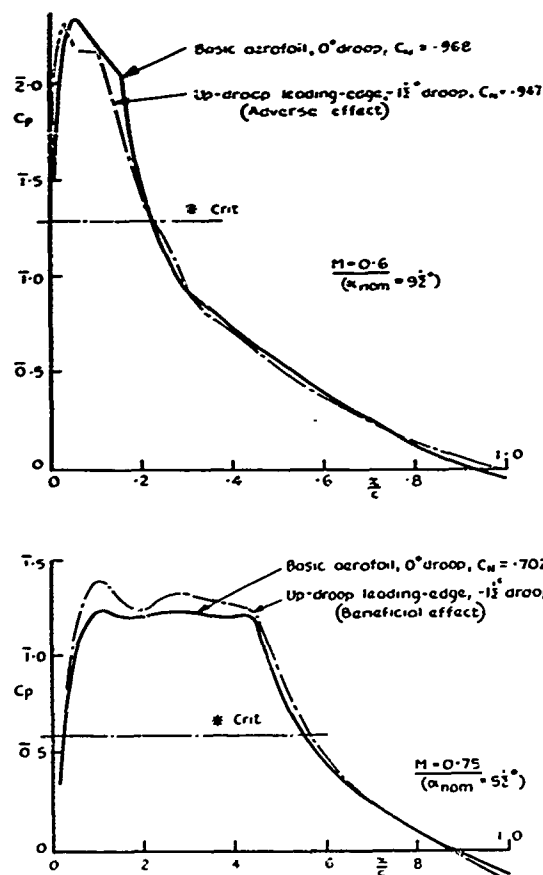


Fig.26 The effect of Raevam up-droop at the leading-edge on wing section 'C' at fixed incidence

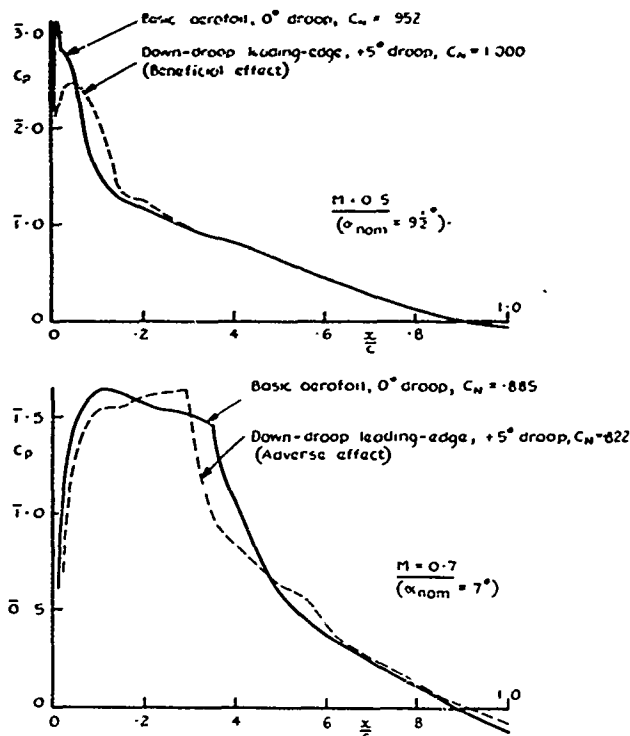


Fig.27 Effect of Raevam down-droop at the leading-edge on wing section 'C' at fixed incidence

speeds. To match performance over a range of these speeds some use of variable geometry is needed and the use of devices such as leading-edge slats raise their own problems of making compromises across the speed range. More work is wanted to enlarge our understanding of the particular supercritical aerodynamic flows associated with the use of such

devices in both two-dimensional and three-dimensional situations. In parallel with this is the need to develop better devices fundamentally more suited to the basic design processes of wings and more able to cope with the complexities of the flows which develop near leading edges at high incidence at these high speeds.

#### NOTATION

A	sweepback angle of wing
c	chord of wing section
$\bar{c}$	mean chord of wing
$C_N$	normal-force coefficient
$C_L$	lift coefficient
$C_p$	surface pressure coefficient
P	static pressure
$H_0$	total pressure, free stream
M	Mach number
$\alpha$	angle of incidence
x	distance along wing chord
$\eta$	proportion of wing semi-span
$\delta$	angular rotation of slat, deg
g	slat gap, at slat trailing edge, % chord
$x_{TE}$	forward extension of slat trailing-edge, % chord

## REFERENCES

- 1 H H Pearcey      The inter-action between local effects at the shock and rear separation - a source  
J Osborne      of significant scale effects in wind-tunnel tests on aerofoils and wings.  
A B Haines      AGARG CP 35, Paper 11, 1968.
- 2 E W E Rogers      An introduction to the flow about plane swept-back wings at transonic speeds.  
I M Hall      J Roy Aero Soc 64 449-464, 1960.
- 3 I M Hall      Part I The flow pattern on a tapered sweptback wing at Mach numbers between  
E W E Rogers      0.6 and 1.6. Part II Experiments with a tapered sweptback wing of Warren 12  
planform at Mach numbers between 0.6 and 1.6. ARC R & M 3271, 1960.
- 4 D Pierce      A simple flexible supersonic wind tunnel nozzle for the rapid and accurate  
variation of flow Mach number.  
ARC Current Paper 865 1965.
- 5 L J Beecham      Proposals for an integrated wind tunnel - flight dynamics simulator system.  
W L Walters      ARC Current Paper 789, 1962  
D W Partridge

# A PRACTICAL LOOK AT THE STALL AND HIGH LIFT OPERATION OF EXTERNALLY BLOWN FLAP STOL TRANSPORT CONFIGURATIONS

David J. Moorhouse  
Control Criteria Branch  
Air Force Flight Dynamics Laboratory  
Wright-Patterson AFB, Ohio 45433, USA

## SUMMARY

This paper considers some practical design aspects of the stall of powered-lift aircraft having externally blown flaps. Techniques are examined for predicting the increment in maximum lift coefficient due to power. Numerical results are presented for an existing theory based on the assumption of a leading-edge stall and the use of basic jet-flap theory. The accuracy of the theory is better than might be expected, and an empirical factor is added to produce good correlation with measured values. A completely empirical approach is shown to be effective as a simple technique to provide quick approximations to the increment in maximum lift coefficient.

An externally blown flap configuration is characterized by large asymmetric forces and moments as a result of an engine failure. The lateral control system is thus a critical factor in determining the usable lift. A comparison is made of the impact of various control concepts on stall and the usable lift. It is concluded that the most effective single control is boundary layer control ailerons with supercritical blowing.

Available NASA STOL flight test data indicate that a smaller stall margin is required than is common in conventional practice. The normal acceleration response of externally blown flap aircraft to a step gust is shown to be almost constant as airspeed is reduced. A basic stall margin of 0.3g load factor margin is suggested to replace the conventional speed margin.

A consequence of the discussion of the factors involved is to show that maximum lift coefficient and the stall of an externally blown flap system cannot be optimized independently, but must be considered as an integral part of the total vehicle design. Great emphasis must be placed on the design of the leading-edge device and the lateral control system in order to effectively use the capabilities of the externally blown flap system.

## LIST OF SYMBOLS

AR	Aspect Ratio
$C_j$	Jet momentum coefficient = $\frac{\text{jet momentum flux}}{qS}$ for jet flaps, or effective blowing coefficient = $\eta C_u$ for externally blown flaps
$C_L$	Lift coefficient = $\frac{\text{lift}}{qS}$
$C_{L_{\max}}$	Maximum lift coefficient
$C_u$	Gross thrust coefficient = $\frac{\text{thrust}}{qS}$
q	Freestream dynamic pressure
n	Normal acceleration, g's
S	Reference wing area
V	Velocity
$V_s$	Stall speed
$V_{\min}$	Minimum flight speed
$\alpha$	Angle of attack (radians)
$\alpha_c$	Power-off stall angle of attack (radians)
$\Delta$	Denotes an incremental quantity
$\delta$	Effective jet deflection angle (radians)
$\delta_f$	Flap deflection
$\eta$	Measured turning efficiency of externally blown flaps
Special:	
$\Delta C_L(C_u)$	Increment in $C_L$ due to $C_u$
$\Delta C_{L_{\max}}(C_u)$	Increment in $C_{L_{\max}}$ due to $C_u$
$C_{L_{\alpha}}(C_u=0)$	Power-off lift curve slope (per radian)

## 1. INTRODUCTION

For conventional aircraft, take-off or landing speeds can be set at some factor, such as 1.2 or 1.3, times the stall speed. Also, as a simplification, the flap system design can be optimized to give maximum lift for landing and high lift with low drag for take-off almost independent of the airplane design. For STOL aircraft powered-lift adds another dimension to be considered, and has been utilized for some time in the form of propeller slipstream effects. With the current trend in transport design being

almost exclusively towards turbofan engines (their amenability to noise treatment being no small consideration), a popular STOL concept is the externally blown flap configuration, as illustrated in Figure 1. This concept is not new but is only now approaching use in a flight vehicle and solutions are currently being sought to the detail design problems. There is strong dependence of the aerodynamic forces and moments on thrust, as well as cross-coupling of the forces and moments between axes. The apparent simplicity of the externally blown flap concept leads to a complex design problem, some aspects of which are considered herein.

During the past 15 years a number of reports on the externally blown flap concept have been published by NASA. These reports contain considerable test information but, until recently, there was no systematic variation of design variables during the experiments. The available data resulted from measurements on a variety of model configurations. Nevertheless, representative ranges of sweep angle, aspect ratio, etc., have been tested. A systematic investigation of the externally blown flap concept has been initiated by NASA and the Air Force, but few of these results are available, as yet. In addition, most major airframe companies are actively studying this concept but the majority of their results are proprietary and not generally available. Specific data used in this paper will be limited to those which are readily available.

The premise of this paper is that the actual achievement of a high lift coefficient is not the major design criterion. Rather the criterion of design performance for a safe, practical, operational STOL transport should be the amount of USABLE lift available considering engine failure, atmospheric turbulence, etc. This paper examines each of the following topics:

- 1) The mechanics of maximum lift for externally blown flap configurations
- 2) The control problems associated with powered-lift stall
- 3) The flight operational problems of high lift

The discussion will consider how these factors are related for externally blown flap configurations.

## 2. MAXIMUM LIFT COEFFICIENT OF EXTERNALLY BLOWN FLAP CONFIGURATIONS

Although the usable lift coefficient is considered to be the more important design parameter, a method for estimating the maximum lift coefficient is still required. Reference 1 presents a theory for estimating the maximum lift coefficient of wings with high lift devices. A leading-edge stall was assumed in order to fix the loading at one point on the wing in the region of the leading edge. The flapped wing was assumed to stall at the same local loading value as the unflapped wing, so that the maximum lift coefficient of the flapped wing could be related to the maximum lift coefficient of the unflapped wing. Reference 2 extended this theory to obtain an expression for the simultaneous effect of jet flap blowing and flap deflection on maximum lift coefficient. The current paper takes the approach that power-off flapped data are available and a method is required to estimate the effects of blowing. The increment in maximum lift coefficient due to blowing at a constant flap deflection can readily be extracted from Reference 2 (with a change in notation) to give:

$$\Delta C_{L_{\max}}(C_{\mu}) = \frac{3}{4} \Delta C_L(C_{\mu}) \quad (1)$$

This simple expression indicates that, at a constant flap deflection, the increment in maximum lift coefficient due to blowing is three-quarters of the increment in lift coefficient due to blowing. The lift increment to be used in Equation (1) is the value at the power-on stall angle of attack, as illustrated in Figure 2. This figure also indicates that there is a reduction in stall angle of attack given by:

$$\Delta \alpha_s = -\frac{1}{3} \frac{\Delta C_{L_{\max}}(C_{\mu})}{C_{L_{\alpha}}(C_{\mu} = 0)} \quad (2)$$

Substituting the theoretical expression for the two-dimensional lift increment developed by Spence (Reference 3) into Equation (1) and using Equation (2) to relate the result to the power-off stall angle of attack, an equation for the increment in maximum lift coefficient due to blowing results.

$$\Delta C_{L_{\max}}(C_{\mu}) = 3\pi \left[ \frac{B_0 \alpha_s + D_0 \delta}{1 + B_0/2} \right] \quad (3)$$

where  $\alpha_s$  is the power-off stall angle of attack and  $\delta$  is the effective jet deflection angle (a function of the flap deflection). For externally blown flaps,  $B_0$  is a function of the effective blowing coefficient,  $C_{\mu}$ , and  $D_0$  is a function of  $C_{\mu}$  and a developed flap chord ratio which takes into account any Fowler motion. Expressions for  $B_0$  and  $D_0$  are given by Spence in Reference 3. The change in stall angle of attack associated with the lift increment of Equation (3) is given by:

$$\Delta \alpha_s = -\frac{1}{2} \left[ \frac{B_0 \alpha_s + D_0 \delta}{1 + B_0/2} \right] \quad (4)$$

Leading-edge devices generally increase the power-off stall angle of attack and Equation (3) illustrates the resulting benefit in increased maximum lift capability. Equation (3) also demonstrates that there is an increment in maximum lift coefficient due to blowing even at zero flap deflection.

Equation (3) has been used to calculate the theoretical increment in maximum lift due to blowing for a number of externally blown flap configurations (References 4-9), with flap deflections from zero to 70° and blowing coefficients up to 3. The measured values of power-off stall angle of attack, static turning efficiency and effective jet deflection angle were used for each configuration. The



span loading of an externally blown flap configuration will differ considerably from an elliptical distribution, and it is suggested that maximum lift coefficient may correlate better with the three-dimensional lift increment. The results given by Equation (3) have, therefore, been corrected for finite aspect ratio effects using the correction factor developed by Maskell and Spence in Reference 10. Figure 3 shows that the aspect ratio correction worsens the agreement but reduces the data scatter slightly. This approach will be used.

It is easy to find reasons why the theory behind Equation (3) should not apply to a practical externally blown flap configuration. Again it is pointed out that the theory assumes a leading-edge stall, and Reference 1 suggests that "it may well be easier to predict maximum lift coefficient in the presence of a powerful trailing-edge flap than it is for clean aerofoils." This could be true for plain leading edges. In practice, however, the use of a powerful trailing-edge flap promotes the use of a powerful or very effective leading-edge device to delay leading-edge stall. In addition an externally blown flap configuration is characterized by highly localized blowing effects near inboard-located engines in a wing configuration that has highly loaded inboard sections. These factors tend to promote stall from the outboard trailing edge. This reasoning is supported by measurements of the effectiveness of conventional outboard ailerons on a typical externally blown flap configuration, for example Reference 7. These data show complete loss of aileron effectiveness at the stall angle of attack. Thus, the basic assumption of the theory, that a leading-edge stall is present, is often not true. Another consideration is that externally blown flap configurations are optimized for the power effects so that the flap gaps are larger than would be chosen for an unpowered flap system. The power-off maximum lift coefficient tends to be less than it could be if the gaps were optimized for the power-off conditions. The increment in maximum lift coefficient in going from non-optimum power-off conditions to more optimum power-on conditions is, therefore, larger than if both were optimized separately. This is a possible reason for the measured increments in maximum lift coefficient being greater than the theoretical values.

The results of Figure 3(b) all lie close to one straight line, indicating an empirical factor to improve the correlation. The final expression then becomes:

$$\Delta C_{L_{\max}}(C_{\mu}) = 5.5\pi \left[ \frac{B_o \alpha_s + D_o \delta}{1 + B_o/2} \right] \left[ \frac{AR + 0.637C_j}{AR + 2 + 0.604\sqrt{C_j} + 0.876C_j} \right] \quad (5)$$

This basic equation is not limited to externally blown flaps, of course, but it is not known whether the empirical factor will change for other powered-lift concepts.

A completely empirical approach can also be used as in Reference 11. The maximum lift coefficient is reasoned therein to be a function of the total camber of the wing; and blowing is considered to act as an effective camber increase. A measure of the increase in camber is taken to be the component of thrust normal to the airfoil,  $\eta C_{\mu} \sin \delta$ . Figure 4 presents the increment in maximum lift coefficient due to blowing versus the normal component of thrust, showing that the data all group around a single curve. A comparison with the theoretical form of Equation (5) indicates that this empirical approach can only be an approximation. The approximation is expected to improve as flap deflection increases, i.e., at typical landing and possibly take-off conditions, as supported by the data. Thus the curve of Figure 4 is suggested as a simple technique to obtain a rapid approximation to the increment in maximum lift coefficient for externally blown flap configurations.

One topic which appears to have received little attention to date is the pitching moment at the stall. The outboard trailing-edge stall, as previously discussed, promotes extreme pitch up tendencies as demonstrated by all the externally blown flap configurations tested by NASA. Although artificial devices such as stick pushers are common, it would be desirable to have natural pitch-down at stall. This requires that stall be initiated at the leading edge of the inboard portion of the wing. There is therefore a conflicting design problem, since the initial design effort is directed towards preventing premature separation at the leading edge of the wing. Some increment in maximum lift coefficient will have to be traded for control of the stall characteristics. All swept-wing aircraft require attention to this problem during the design phase. The magnitude of the problem, however, increases with increasing lift coefficient and is further compounded by the characteristics of the externally blown flap concept.

The angle of attack at which stall occurs is also a critical design parameter. Figure 5 illustrates the wide range of power effects on stall angle of attack which have been measured, indicating the importance of design details (References 4,8,9,12). This figure shows that even with a large (19% chord) leading-edge device, one configuration has a stall angle of attack as low as 2°. A typical STOL approach path angle of 7° would result in a nose-down pitch attitude of about 15°. Thus although this configuration has a maximum lift coefficient of about 6 the pitch attitude makes this lift unusable. Another configuration shows that a significant increase in stall angle of attack is also possible, but this is also undesirable because of engine-out characteristics. If power-on stall angles are larger than power-off stall angles, the wing with the failed engine stalls first so that extremely large rolling moments would be produced at stall. The resulting motion would be uncontrollable and is certainly to be avoided, if possible by minimizing the dependence of stall angle of attack on power.

Thus, although the externally blown flap concept is relatively simple, the practical design problem places great emphasis on the detail design. Ideally, the leading-edge devices should be optimized to:

- 1) Obtain the greatest possible benefit from the power effects
- 2) Minimize the dependence of stall angle on power
- 3) Promote initial stall inboard on the wing leading edge to promote nose-down pitching moments at stall

### 3. CONTROL PROBLEMS ASSOCIATED WITH POWERED-LIFT STALL

Control effectiveness is a major design consideration for STOL aircraft. Not only do the control power requirements for maneuvering become more severe as flight speed is reduced, but the requirement to trim asymmetric conditions resulting from an engine failure can be as important as the maneuver requirements. Some aircraft have eliminated the asymmetries due to engine failure by coupling the propulsive lift effects between right and left wing panels. Examples are the interconnected propellers of the Brequet 941 and the cross-ducted boundary layer control system of the Boeing model 367-80 (707 prototype). It would be extremely difficult, however, to effectively couple the engines of an externally blown flap configuration. The asymmetric forces and moments must be accepted, and the control system must then be designed to provide trim plus maneuver capability. Various lateral control system possibilities are available, and will be considered in turn.

The asymmetric moments are functions of both the configuration and operational procedures. This discussion considers only representative values, therefore. Values of rolling and yawing moments for each of the most promising control systems are presented in Figure 6 (References 7,8,13). Typical values of the required rolling moments and available yawing moment from the rudder after trimming the engine-out yawing moments are also presented.

To provide roll, a spoiler can be deployed on the opposite wing to the failed engine. Spoilers do have the advantage of generating favorable yawing moments, however the generation of sufficient rolling moment entails an appreciable lift loss. The data of Figure 6 involve a decrement in lift coefficient of approximately 1.0. This lift loss due to spoiler control adds to the reduction in lift due to loss of power. In addition, spoilers can also adversely affect the stall angle of attack. Thus trimming engine-out conditions with spoilers will give an appreciable penalty in usable lift.

Lift loss due to engine failure can be minimized by increasing the flap deflection on the wing with the failed engine and reducing flap deflection on the opposite wing. This arrangement can develop sufficient rolling moment for trim but the adverse yawing moments that it produces represent an impossible design condition for the rudder.

By themselves conventional ailerons of a practical size are not effective enough to trim the typical rolling moment values due to an engine-out for externally blown flap configurations. Depending on the configuration, the required rolling moment may be achieved using boundary layer control ailerons with supercritical blowing, i.e., more blowing must be provided than the amount required to just produce attached flow. Also, with sufficient blowing the ailerons can be drooped to minimize lift loss. The data of Figure 6 show that BLC ailerons produce little yawing moment compared with conventional ailerons or differential flap deflection. The reason for this may be conjectured by considering the spanwise loading distribution. The effect of power on an externally blown flap is to highly load the inboard sections of the wing. The effective aspect ratio, and hence the span efficiency, is quite low. Deflecting the blown aileron can be expected to improve the spanwise load distribution and hence the span efficiency. The expected increase in induced drag on the panel may then be balanced by the increase in span efficiency with correspondingly small induced yawing moments.

The preceding arguments indicate that BLC ailerons are generally the most efficient single lateral control device for externally blown flap configurations. The optimum control system will obviously depend on the total vehicle configuration, and could easily require a combination of control devices.

Engine failure is an important consideration in determining the proportion of the maximum lift capability that is usable. The lateral control concept has been shown to be a factor in determining the engine-out trimmed lift, and can also have a significant impact on the stall characteristics of the blown wing. As indicated in the previous section, a wing with an externally blown flap will tend to stall first in the region of the aileron panel. The use of BLC ailerons may reduce or eliminate this tendency.

### 4. FLIGHT OPERATIONAL PROBLEMS WITH HIGH LIFT (POWERED-LIFT)

Regular operation of STOL transport aircraft will require special consideration of stall margins, and STOL performance rules in general. The Federal Aviation Regulations for conventional aircraft have been modified to apply to powered-lift configurations (Reference 14). NASA has also suggested a set of requirements that are based on flight test experience (Reference 15). There is still much controversy about STOL performance rules, however, and some comments on stall margins are presented in this section.

Figure 7 illustrates the operational envelope of a typical STOL transport. Although operation within this entire envelope is possible, margins indicated by the cross-hatching are applied to the boundaries of the envelope for safety reasons. In particular, a margin is required on the maximum lift or  $V_{min}$  boundary to provide a margin for control of glide path angle by the pilot. A margin is also required to prevent excursions outside the operational envelope caused by inadvertent upsets due to gusts.

The maneuver aspect of the conventional speed margin is equivalent to a load factor margin. In addition, the initial aircraft response to gusts is mainly sensed as an increment in normal acceleration. Thus there is justification for using a load factor margin in place of the normal speed margin.

Conventionally, a speed margin is equivalent to providing normal acceleration or load factor margin, given by:

$$\Delta n = \frac{V^2}{V_s^2} - 1$$

Thus a conventional landing at  $V = 1.2 V_s$  would imply a load factor margin of 0.44g. The same basic relationship holds for powered-lift configurations, but the conventional stall speed is now replaced by a minimum speed,  $V_{min}$ , the value of which accounts for engine-out stall speed, power setting, minimum

control speed, etc. The results of the flight tests reported in Reference 15 indicate a mean approach speed of  $1.15 V_{\min}$  was selected as adequate by the pilots. This implies a lg load factor margin of

$$\frac{V^2}{V_{\min}^2} - 1 = 0.32$$

The reduction from 0.44g to 0.32g is a significant amount.

In addition, a lg stall implies reducing airspeed at constant power. As a result the non-dimensional thrust coefficient,  $C_{th}$ , increases with a corresponding increase in the maximum lift coefficient. On the other hand, small or rapid maneuvers are made at essentially constant airspeed and power, i.e., constant  $C_{th}$ , resulting in a lower maximum lift coefficient than the lg stall value. The maneuver load factor margin is therefore less than the lg load factor margin, if dynamic overshoot is ignored.

In the landing approach configuration of a powered-lift system changes in thrust provide a significant load factor capability which is a function of the actual power setting. This capability of STOL aircraft may be expected to offset a portion of the required load factor capability due to angle of attack, so that a smaller speed margin or load factor margin is acceptable. This trade-off is discussed fully in Reference 15, in justifying the  $1.15 V_{\min}$  or 15% speed margin.

This suggested speed margin should be qualified to apply to rates of sink less than 800 ft/min. The flight test data presented in Reference 15 show that a larger speed margin was chosen for rates of sink greater than 800 ft/min, except when a complete flare was not done during landing.

In order to complete the rationale for choosing a particular stall margin, it is also necessary to consider the susceptibility of the aircraft to inadvertent upsets such as gusts. As airspeed decreases, a constant gust velocity represents a larger change in angle of attack. For a powered-lift system, however, it may be assumed that equilibrium flight at reduced airspeed is achieved by using more power. Thus, at reduced airspeeds a smaller proportion of the total lift is "aerodynamic" (i.e., circulation lift as opposed to thrust component), making the aircraft less dependent on angle of attack changes. Figure 8 illustrates this reduction in aerodynamic lift for a range of externally blown flap configurations (References 4, 5, 7, 9, and 16).

To gain some insight into the susceptibility of powered-lift aircraft to gusts, values of the initial normal acceleration due to a step gust have been calculated for a number of externally blown flap configurations. In this calculation it was assumed that the thrust vector is unchanged while the aircraft experiences instantaneous changes in angle of attack and dynamic pressure, and an instantaneous rotation of the circulation-related force vector. These changes cause an increment in the force perpendicular to the initial flight path, which in turn yields a normal acceleration. In order to yield typical numbers, a wing loading of 80 psf. and a 10 knot gust perpendicular to the flight path were assumed. The results, presented in Figure 9, show that there are only small and inconsistent effects of power on the initial normal acceleration due to the gust. This means that that portion of the operational margin required to protect against upset by vertical gust can be taken to be the same as for conventional operation (zero thrust coefficient). The data of Figure 9 indicate that a load factor margin of approximately 0.2 to 0.25g is required to counteract a 10 knot gust.

A gust along the flight path causes only a change in dynamic pressure, with no change in angle of attack until the airplane has had time to respond. At the airspeeds consistent with a 2000 ft field length the initial normal acceleration due to such a gust is less than that caused by a vertical gust of the same magnitude.

The preceding analysis considered only the initial acceleration due to a step gust, whereas a full analysis would consider the complete response. As this is a function of individual airplane characteristics it is not easy to generalize and is beyond the scope of this paper. In addition flight in turbulence must also be considered with respect to stall margins. This is a more difficult problem, however analytical progress is being made towards defining the stall in unsteady flow. For oscillatory motion, Reference 19 calculates the reduction in adverse pressure gradient on the airfoil surface, which implies a delay of the stall. It is well known that small transient excursions beyond the static stall angle of attack will not cause a stall. This phenomenon needs further study to obtain an analytical solution to the unsteady stall problem, before the dynamic alleviation of stall can be considered in formulating required stall margins.

For a powered lift system additional load factor capability is available by increasing power. This capability offsets some of the required stall margin due to angle of attack, resulting in an acceptable stall margin which is lower than conventional practice, as supported by flight test results. The load factor margin should be based more on usable lift than absolute maximum lift. At any flight condition the relevant value of maximum lift is obtained at that particular power setting. Another consideration in determining maximum usable lift is the minimum control speed. Considering the flight test results plus a simple consideration of gust effects, a load factor margin of 0.3g is suggested.

## 5. CONCLUSIONS

A theoretical method predicts with reasonable accuracy the increment in maximum lift coefficient due to power for externally blown flap configurations. An empirical factor is used to provide good correlation with measured values. A completely empirical approach is also suggested as a simple technique to obtain quick and reasonably accurate approximations to the increment in maximum lift coefficient.

Engine failure causes large asymmetric forces and moments, producing a significant impact of the lateral control system on the total airplane design. The most effective lateral control system uses boundary layer control ailerons with supercritical blowing.

A load factor margin of 0.3g is suggested as the basic stall margin to replace the conventional speed margin of  $1.2 V_S$ .

With a powered-lift system, sufficient power can be used to generate almost any value of lift coefficient. In practice, however, a usable lift coefficient is desired. For an externally blown flap configuration maximizing this usable lift coefficient represents a complex design problem, which includes optimizing the lateral control system and leading edge devices as well as the trailing edge flaps.

## 6. REFERENCES

1. McRae, D. M., The Aerodynamics of High-Lift Devices on Conventional Aircraft, Part I, J. R. Ae. S., Vol. 73, No. 702, pp. 535-541 (1969).
2. Perry, D. H., A Review of Some Published Data on the External-Flow Jet-Augmented Flap, RAE TR 70240 (1970).
3. Spence, D. A., The Lift on a Thin Aerofoil with a Jet-Augmented Flap, The Aeronautical Quarterly, Vol. IX, pp. 227-299, August, 1958.
4. Fink, M. P., Aerodynamic Characteristics, Temperature, and Noise Measurements of a Large-Scale External-Flow Jet-Augmented-Flap Model with Turbojet Engines Operating, NASA TN D-943 (September 1961).
5. Parlett, L. P. and J. P. Shivers, Wind-Tunnel Investigation of a STOL Aircraft Configuration Equipped with an External-Flow Jet Flap, NASA TN D-5364 (August 1969).
6. Freeman, D. C., Jr.; S. B. Grafton and R. D'Amato, Static and Dynamic Stability Derivatives of a Model of a Jet Transport Equipped with External-Flow Jet-Augmented Flaps, NASA TN D-5408 (September 1969).
7. Parlett, L. P., D. C. Freeman, Jr., and C. C. Smith, Jr., Wind-Tunnel Investigation of a Jet Transport Airplane Configuration with High Thrust-Weight Ratio and an External-Flow Jet Flap, NASA TN D-6058 (November 1970).
8. Freeman, D. C. Jr., Wind-Tunnel Investigation of a Jet Transport Airplane Configuration with an External-Flow Jet Flap and Inboard Pod-Mounted Engines, NASA TN D-7004 (December 1970).
9. Vogler, R. D., Wind-Tunnel Investigation of a Four Engine Externally-Blowing Jet-Flap STOL Airplane Model, NASA TN D-7034 (December 1970).
10. Maskell, E. C. and D. A. Spence, A Theory of the Jet-Flap in Three Dimensions, Proc. Roy. Soc., A, Vol. 251, pp. 407-425 (1959).
11. May, F. and C. A. Widdison, STOL High-Lift Design Study, AFFDL-TR-71-26, Vol. I (1971).
12. Smith, C. C. Jr., Effect of Engine Position and High-Lift Devices on Aerodynamic Characteristics of an External-Flow Jet-Flap STOL Model. NASA TN D-6222 (March 1971).
13. Parlett, L. P., H. D. Greer, R. L. Henderson, and C. R. Carter, Wind-Tunnel Investigation of an External-Flow Jet-Flap Transport Configuration having Full-Span Triple-Slotted Flaps, NASA TN D-6391 (August 1971).
14. Federal Aviation Regulations, Part XX, Tentative Air Worthiness Standards for Powered Lift Transport Category Aircraft, (August 1970).
15. Innis, R. C., C. A. Holzhauser, and H. C. Quigley, Airworthiness Considerations for STOL Aircraft, NASA TN D-5594 (January 1970).
16. Johnson, J. L., Jr., Wind-Tunnel Investigation at Low Speeds of Flight Characteristics of a Sweptback-Wing Jet-Transport Airplane Model Equipped with an External-Flow Jet-Augmented Slotted Flap, NACA TN 4255 (July 1958).
17. Carta, F. O., Effect of Unsteady Pressure Gradient on Dynamic Stall Delay, Journal of Aircraft, Vol. 8, No. 10, pp. 839-840 (1971).

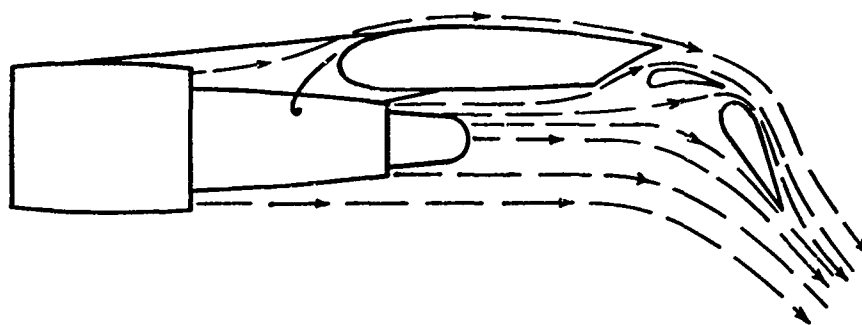


FIGURE 1 SKETCH OF EXTERNALLY BLOWN  
FLAP CONCEPT

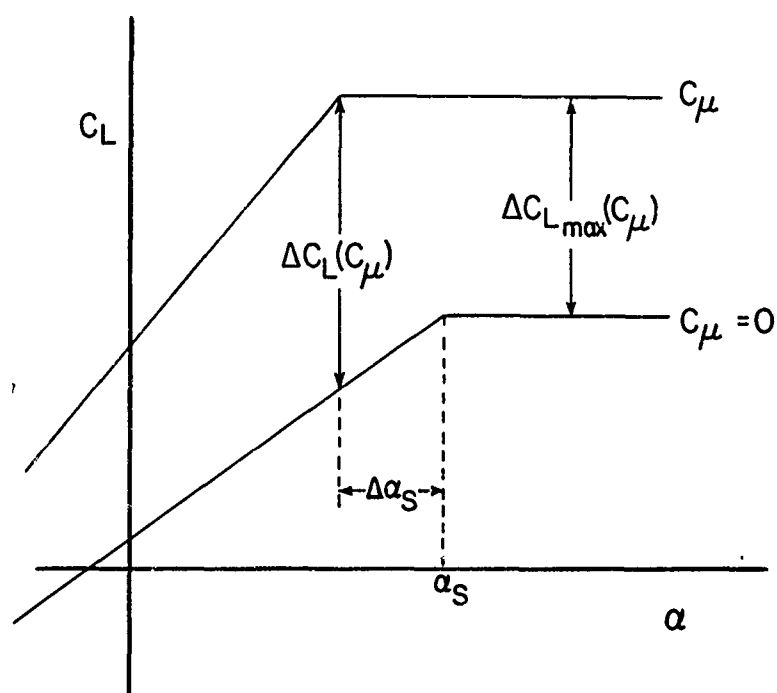
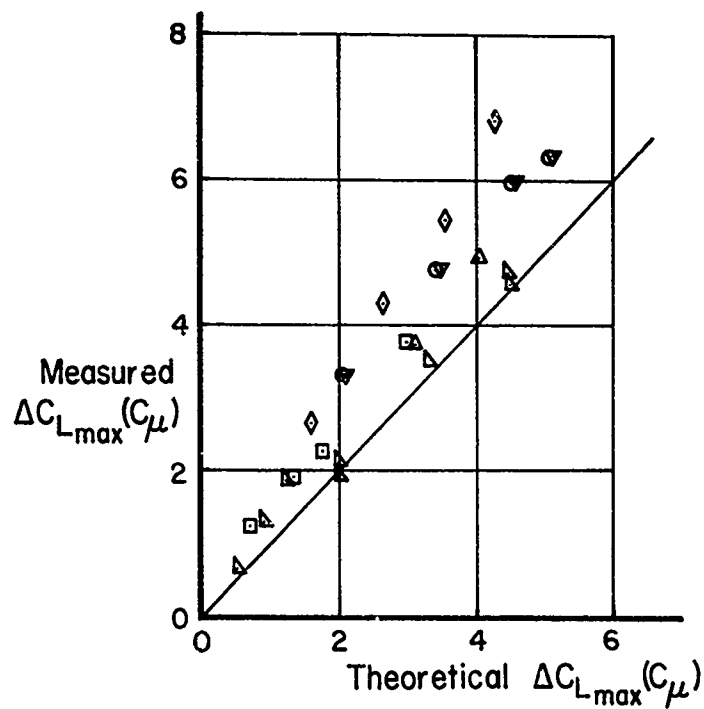
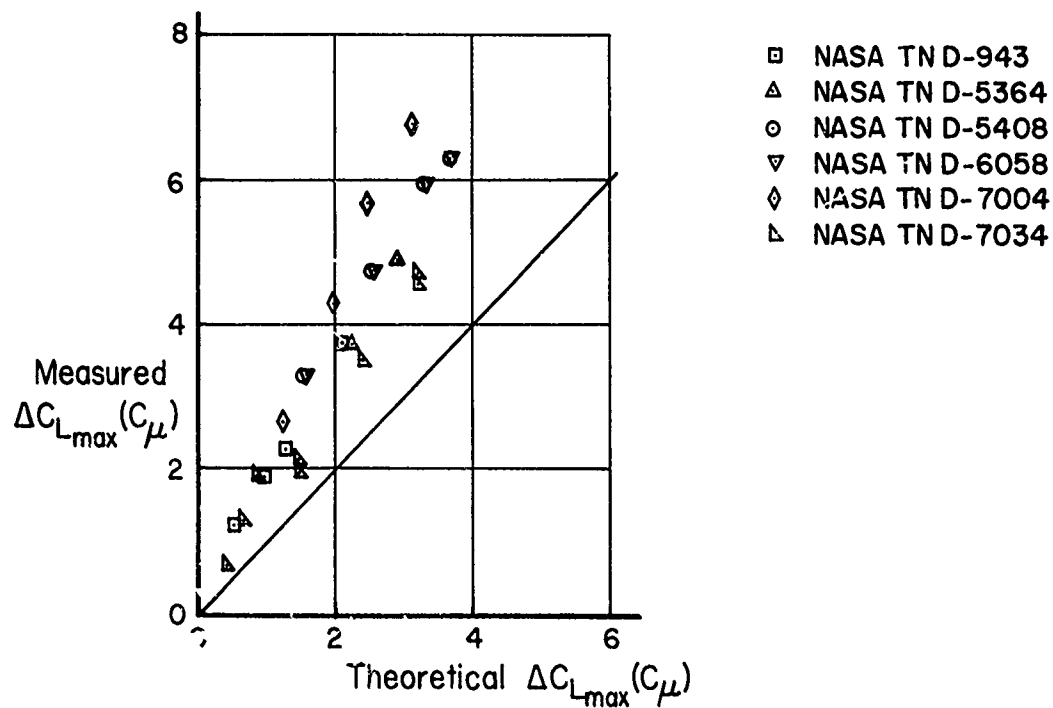


FIGURE 2 IDEALIZED SKETCH OF STALL  
CHARACTERISTICS



(a) Theory without aspect ratio correction



(b) Theory with aspect ratio correction

FIGURE 3 INCREMENT IN MAXIMUM LIFT  
COEFFICIENT DUE TO POWER

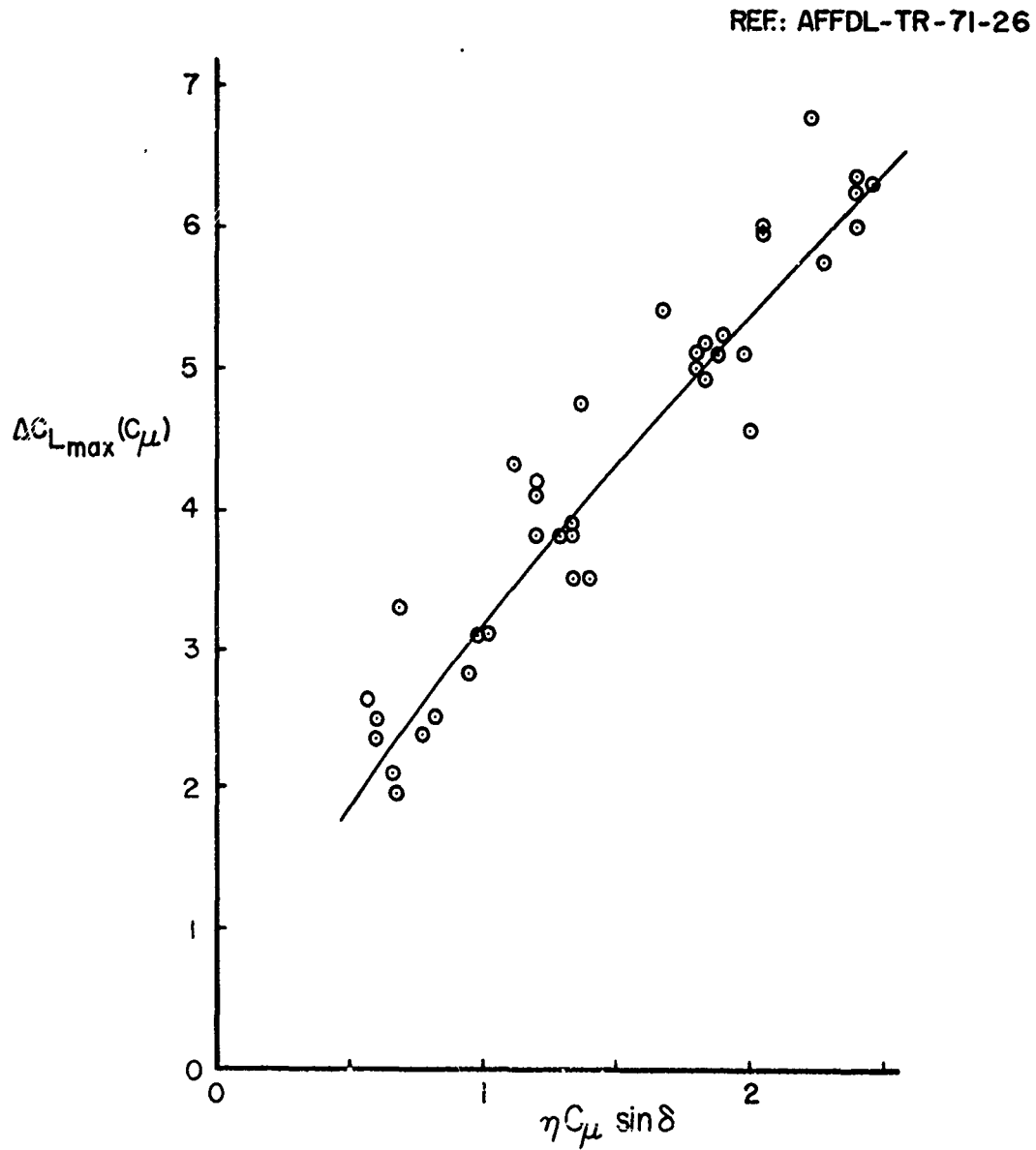


FIGURE 4 INCREMENT IN MAXIMUM LIFT  
COEFFICIENT DUE TO POWER

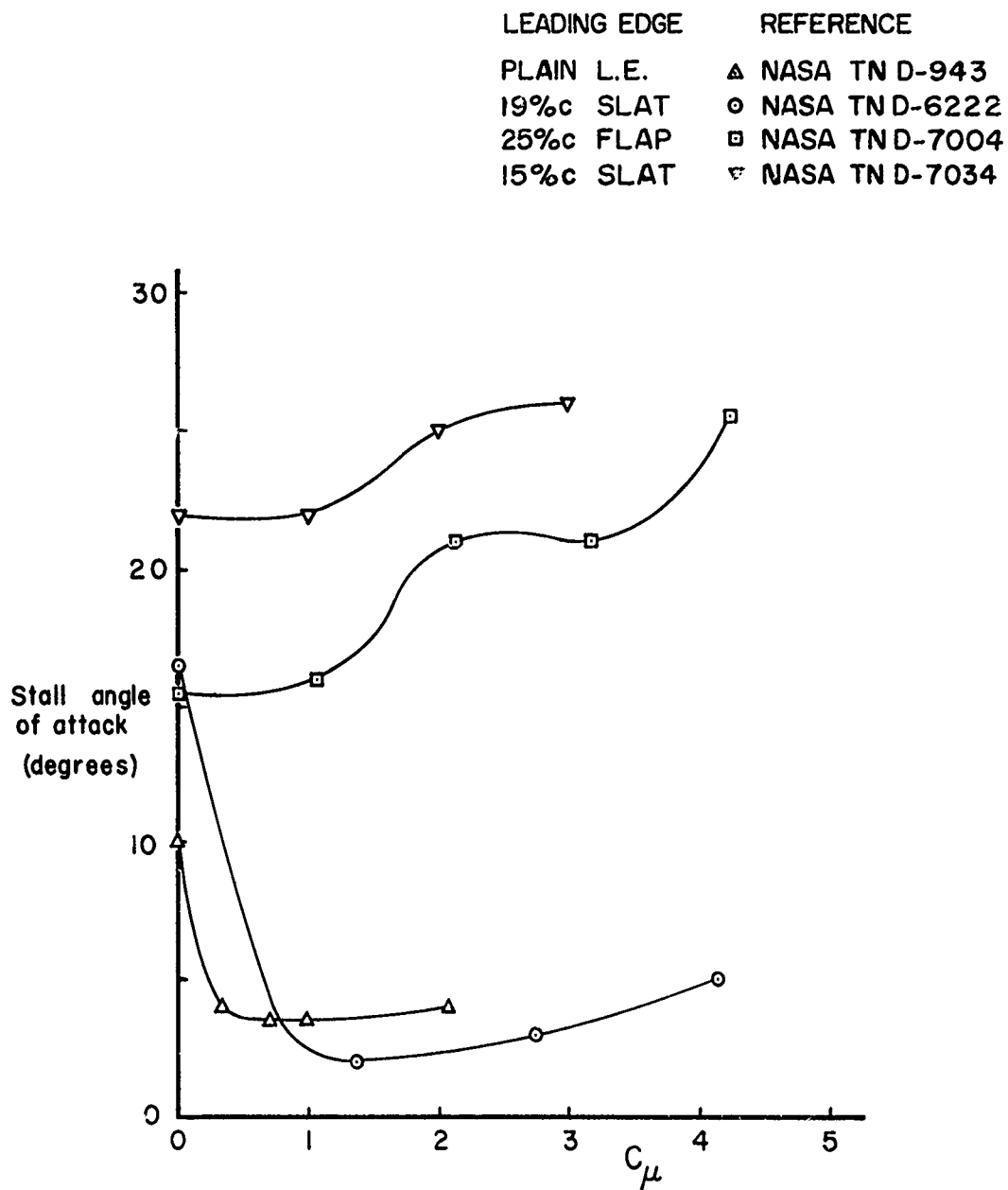


FIGURE 5 EFFECT OF POWER ON THE  
STALL ANGLE OF ATTACK



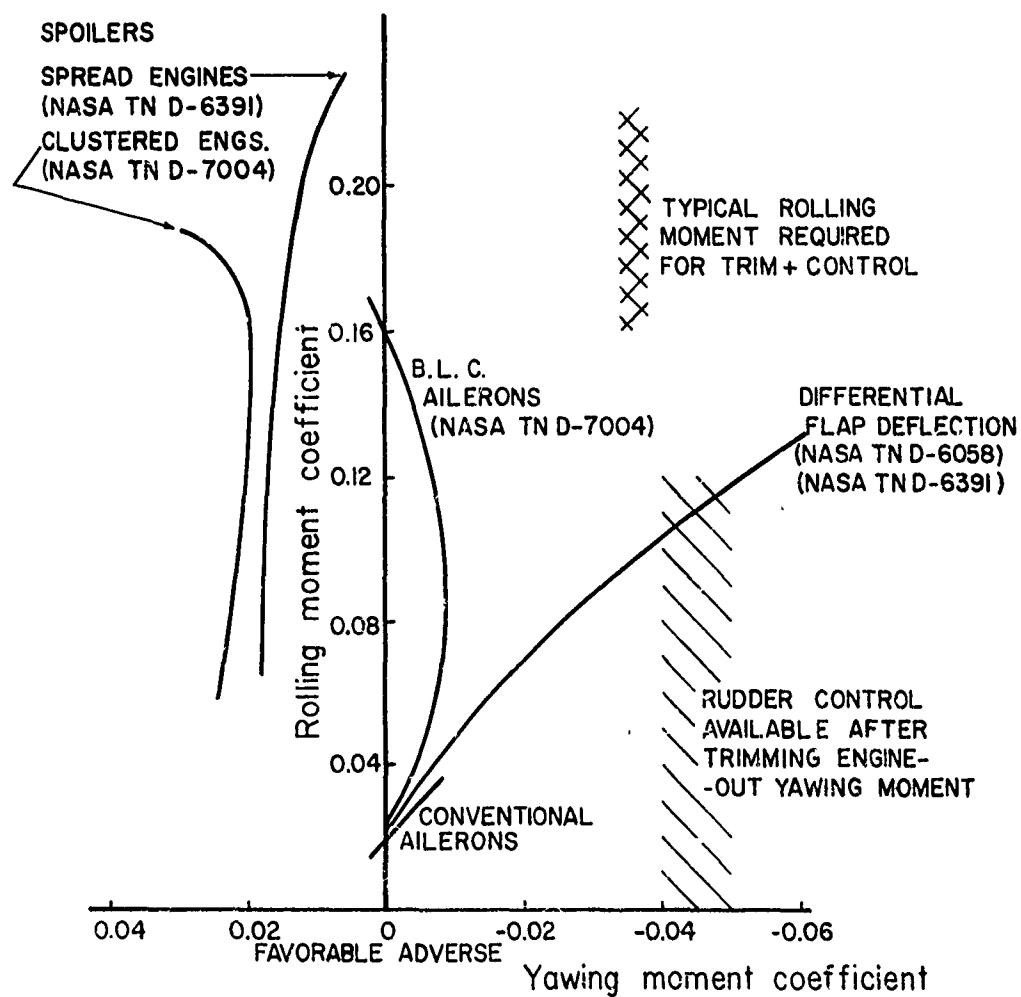


FIGURE 6 TYPICAL CONTROL TRENDS FOR  
EXTERNALLY BLOWN FLAPS

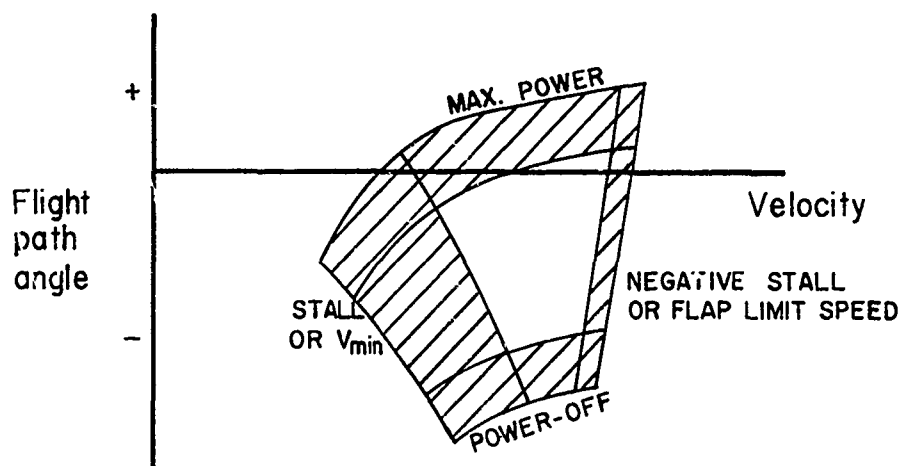


FIGURE 7 TYPICAL STOL OPERATIONAL  
ENVELOPE - LANDING CONFIGURATION

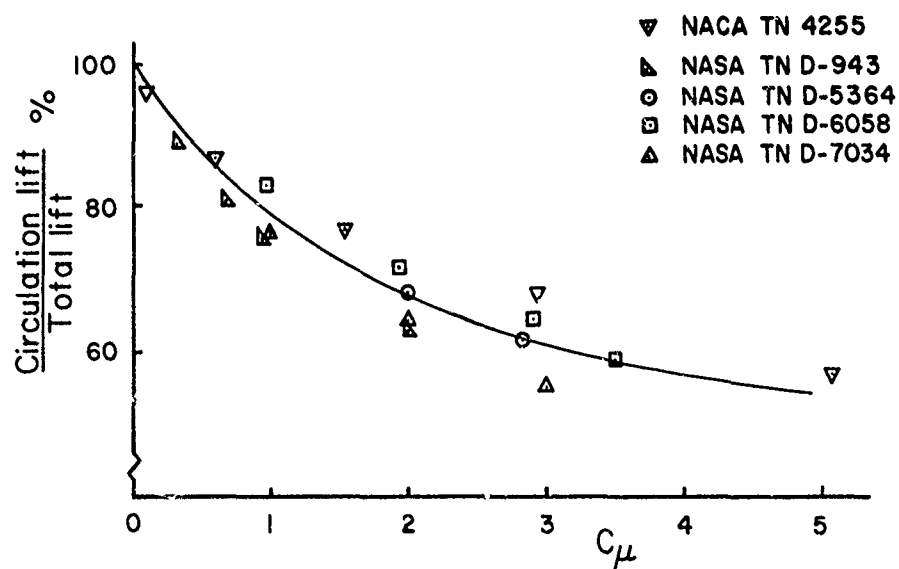
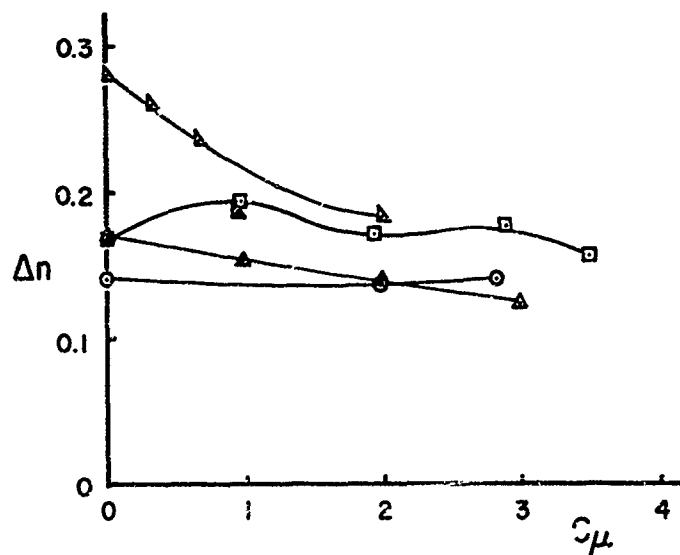
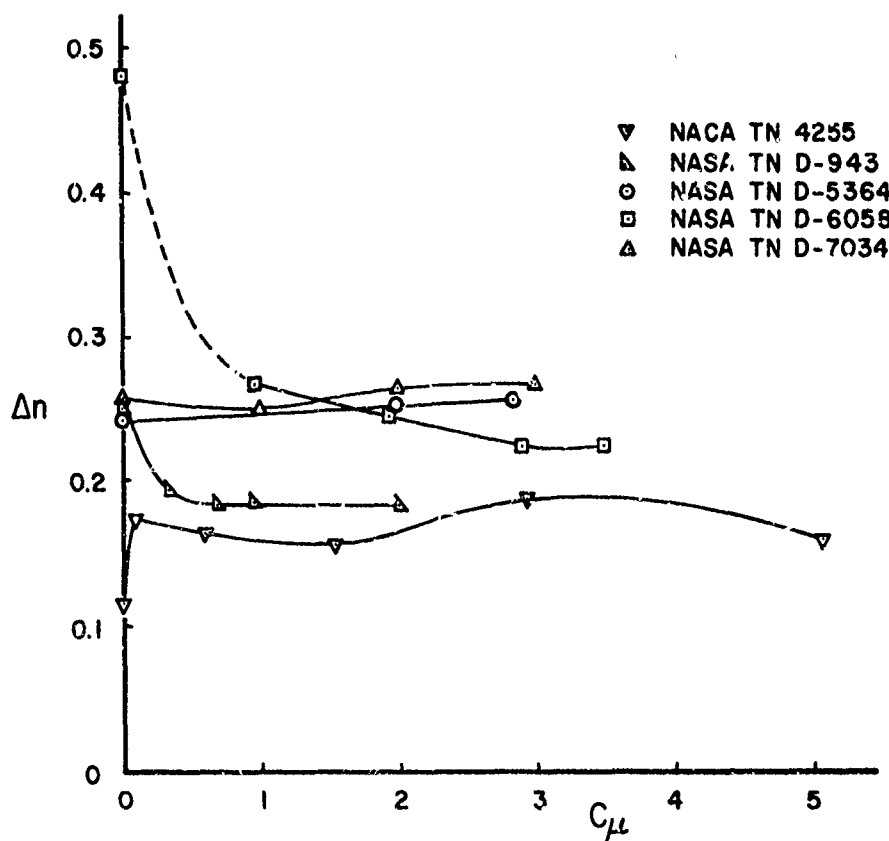


FIGURE 8 EFFECT OF POWER ON PROPORTION  
OF CIRCULATION LIFT

(a) Angle of attack  $10^\circ$  below stall

(b) Zero angle of attack

FIGURE 9 EFFECT OF POWER ON NORMAL ACCELERATION DUE TO GUSTS

FLIGHT DEVELOPMENT OF THE STALLING CHARACTERISTICS

OF A MILITARY TRAINER AIRCRAFT.

W.D.Horsfield  
Chief Aerodynamicist

G.P.Wilson  
Aerodynamics Department

British Aircraft Corporation Limited,  
Military Aircraft Division,  
Warton Aerodrome,  
WARTON, Nr. Preston,  
Lancashire

SUMMARY:

It is a primary design requirement of a military trainer aircraft that the stalling characteristics are such as to give warning of the approach of the stall as well as marking it by a clear drop of the aircraft nose without excessive wing drop. Lateral, directional, and pitch control must be available up to and above the stall. Flight experience on the B.A.C. Mk.5 Jet Provost is used to illustrate this, as the subject of this paper.

The B.A.C. Jet Provost Mk.5 and Strikemaster 167 aircraft are developments of earlier versions embodying a pressurised cabin, more thrust and greater armament. The shape changes involved on the intake and front fuselage caused a change in maximum lift and stalling characteristics, resulting in too mild a stall for training demonstration. Considerable flight development was necessary to achieve the desired characteristics of a clearly marked stall with adequate warning of approach without penalty on maximum lift and without involving large aircraft modifications.

The development is described and possible procedures for achieving stall warning on future aircraft of the type are suggested.

## 1. INTRODUCTION

The Mark 4 Jet Provost, in service with the Royal Air Force is a side by side two seat trainer with an unpressurised cabin (Figure 1). The Mark 5 (Figure 2) is a development with a pressurised cockpit to give better usage at high altitudes, which was first flown in 1967, and has been in service use since September 1969. The Strikemaster an even further development of the Mark 5 with a more powerful engine and substantial ground attack armaments, has been in production since August 1968 and is in service in nine countries.

The aerodynamic modifications involved in the change from Mark 4 to Mark 5 and Strikemaster were considered minimal (Figure 4). They were changed cockpit lines, a wider intake with diverter, and the necessary revision of fairings. In the event, they changed the stalling behaviour considerably and the spinning behaviour slightly, and a significant amount of flight development was involved to achieve satisfactory clearance.

Before describing this, it seems worth making two digressions - one on desirable stall characteristics and the other on the Mark 4 Provost history.

## 2. STALLING CHARACTERISTICS

Desirable stalling characteristics differ somewhat for different types of aircraft. An ideal characteristic for a combat aircraft might be thought to be a stall which occurred gradually without nose drop or wing drop, in which deep stall penetration was possible maintaining full control of attitude without loss of lift, with increasing buffet and touchiness in roll and pitch providing warning of penetration, and with straight-forward recovery possible at any time by moving the stick forward.

This was the stall behaviour we got on the Mark 5 Provost - by accident rather than design. It was not, however, what our Air Force required from a training aircraft, as several discussions with them made clear. What a training aircraft wants is a stall clearly defined by a sharp nose down pitch, with a minimum amount of wing drop, preceded by natural warning in the shape of buffet. This is clear and sensible.

The earlier Provosts had been developed by ad hoc flight testing to give just this characteristic, together with a spin which was regular, easily achieved and from which a clean recovery could be made. This resulted in wing and tail sections modified from their original form by various leading edge changes as follows:

Wing root	-	leading edge camber increased
Wing tip	-	leading edge sharpened and camber reduced.
Tailplane	-	leading edge sharpened in order to bring about stalled flow in the spin.

This gave us sections without any background of two dimensional testing, and which were not too amenable to theoretical treatment. (Figure 5).

In addition, a modification had been made early in the life of the Provost to reduce the tailplane height, by putting a bend in the fuselage just aft of the wing, in order to increase stall warning buffet by bringing the tail into the wing wake.

## 3. MARK V JET PROVOST

This brings us then to the Mark 5. The problems - maximum lift was low with flaps down ( $CL_{max} = 1.75$  compared with a require 1.85) with an associated small loss in airfield performance. The stall characteristics flaps up and down lacked the required sharp nose down pitch to define the stall (Figure 7). Stall warning existed in the form of buffet - not so much prior to the rather indefinite stall as occurring with increasing intensity as the stall was penetrated. We needed to improve maximum lift and stall definition, keeping or introducing stall warning, without of course, introducing any modification which would mean higher costs in manufacture or delays in production, or which would adversely affect spinning or high Mach number behaviour.

Our initial analysis was that all the critical features were a function of a premature stall in the wing root caused by changes more or less local to the root region. Improving  $CL_{max}$  could well automatically give a more defined stall and nose down pitch and the higher incidence would take the wing wake up onto the tailplane to give the standard prestall buffet. The first phase of flight testing therefore concentrated on  $CL_{max}$  improvement. The wing root fairing was extended and reshaped. The intake external line was altered and the wing leading edge modified in the root area (Figures 8, 9)

These changes were successful (see Figure 10) Max  $CL$  was increased from 1.75 to 1.95 (beyond the Mark 4 value) flaps down, and from about 1.0 to 1.40 clean. The stall was marked by a clear pitch down with flaps up and down, but stall warning disappeared both with flaps up and flaps down. This level of lift, however, gave us a margin to work on and our second phase of testing concentrated on achieving stall warning. The use of artificial stall warning was considered but left as a last resort.

FLIGHT DEVELOPMENT OF THE STALLING CHARACTERISTICS  
OF A MILITARY TRAINER AIRCRAFT.

W.D.Horsfield  
 Chief Aerodynamicist  
 G.P.Wilson  
 Aerodynamics Department  
 British Aircraft Corporation Limited,  
 Military Aircraft Division,  
 Warton Aerodrome,  
 WARTON, Nr. Preston,  
 Lancashire

SUMMARY:

It is a primary design requirement of a military trainer aircraft that the stalling characteristics are such as to give warning of the approach of the stall as well as marking it by a clear drop of the aircraft nose without excessive wing drop. Lateral, directional, and pitch control must be available up to and above the stall. Flight experience on the B.A.C. Mk.5 Jet Provost is used to illustrate this, as the subject of this paper.

The B.A.C. Jet Provost Mk.5 and Strikemaster 167 aircraft are developments of earlier versions embodying a pressurised cabin, more thrust and greater armament. The shape changes involved on the intake and front fuselage caused a change in maximum lift and stalling characteristics, resulting in too mild a stall for training demonstration. Considerable flight development was necessary to achieve the desired characteristics of a clearly marked stall with adequate warning of approach without penalty on maximum lift and without involving large aircraft modifications.

The development is described and possible procedures for achieving stall warning on future aircraft of the type are suggested.

#### 4. STALL WARNING

By this stage, it had become necessary to know more about the flow development, and, for instance, whether the standard Mark 4 warning came via the aileron to the stick, the elevator to the stick, or in the form of general airframe buffet from the wings or the impingement of the wing wake on the tailplane.

Vibration instrumentation was not readily available, so these issues had to be settled by experiment and argument. Overall, this pointed to wing wake impingement on the tailplane as the most important source of stall buffet. Some flights were done with depth tufts on the tailplane lower surface, and with streamers from the wing, which indicated that the wake only marginally reached the tailplane but that this mechanism did exist. The use of wing airbrakes was known to cause buffet of the same character as the Mark 4 prestall buffet and this was demonstrated by use of the depth tufts, to come from impingement on the tail.

Wind tunnel tests had previously been put in hand to see what sort of modifications would influence the root stall, though much latitude had to be allowed for interpretation in view of the low Reynolds Number of  $1.0 \times 10^6$  compared with  $6 \times 10^6$  in flight.

Flight tests were carried out with wing tufts to examine stall progressions on both Mark 4 and Mark 5 (Figures 12 and 13). These showed the difference in a quantitative form, tying up with the different behaviour - the Mark 4 developing slowly at first, then spreading to give pitch down, the Mark 5 having an immediate rapid spread. Three lines of geometric change were then followed in flight testing, on the philosophy of sacrificing some lift in order to develop warning.

First, since the fuselage/wing root fairing change had powerfully cleaned up the stall, it seemed possible to alter this to a shape which would allow a trailing edge stall to develop to give buffet, but to stage its progression to the leading edge so that a few knots warning occurred before major loss of lift and hence pitch down - on the lines of Figure 14.

A systematic series of root fairings were tested in flight (Figure 15) - built up by glueing balsa planks to the airframe and then cutting to the required shape. This could be done quite easily - a fairing could be completely changed in shape overnight in a way impossible for metal work - and the construction stood up to use at quite high speeds very well. The same technique with fabric doped over the finished shape, was also used successfully for the more highly loaded leading edge modifications.

These tests were unsuccessful. Taking away parts of the big fairing from the trailing edge we kept  $CL_{max}$  with no prestall buffet until reaching fairing C, when the aircraft reverted to low  $CL$ 's with buffet - its original behaviour. Building up from the front,  $CL$  stayed low with no nose down pitch until -bang- high  $CL$ 's no buffet. The fairing was the trigger mechanism between the two types of behaviour, and there was no compromise.

Secondly, following up the fact that airbrakes gave buffet, we found the necessary spanwise extent of obstacles necessary and tried a similar approach, of inducing a trailing edge stall but trying to arrest its extent to allow some buffet to develop, using section bumps, after carrying out hopeful calculations of boundary layer separation. These bumps made no difference whatsoever.

Having failed by these means to control forward movement of the stalled area, we were evidently not developing a sufficiently large area of separated flow before the stall proper, and were not getting it high enough to strike the tailplane. We therefore needed more incidence. Consequently we tried a further improved wing leading edge (Figure 17) plus vortex generators set to control outward stall progression and also to give vortex formation in a direction to lift the separated inboard wake. After some experimenting with vortex generator position, this was completely successful (Figure 18). An adequate value of  $CL_{max}$  was obtained, a satisfactory nose down pitch occurred without wing drop, and prestall buffet was obtained both flaps up and down. The modifications were relatively easy to apply to the production aircraft, and were cheap and light. The main disadvantage was a loss of a few knots in top speed, due to vortex generators.

Flight test and Aerodynamics congratulated themselves on solving the problem. Design Office and the work shops grumbled about how long they had taken.

As a last test, before setting out to clear the spinning and high speed behaviour, we decided to try a further modification we had in the pipe line - a small vane, half vortex generator and half a low aspect ratio slat, positioned in front of the wing leading edge at the root (Figure 19). This was added to the developed configuration. This gave even better results - higher  $CL$  and more pronounced buffet warning - due to both partial suppression of the stall and a stronger vortex to help lift up the wake.

We fitted this vane on its own to a Strikemaster with the original wing and intake, and found that it worked well when associated with a small fence under the intake to reduce the crossflow out over the wing root.

This fence existed on the Strikemaster as a gun housing. It had to be added to the Mark 5. We were then able to do away with the wing leading edge change, the fairing change, and the vortex generators and reach all our objectives, so that we had a very simple and elegant solution. We subsequently tried optimising the vane position, but any movement virtually nullified its effect, so we left well alone.

5. FINAL REMARKS

The buffet felt by a pilot, of course, depends on many features of the aircraft, even when it is narrowed down to airframe vibration rather than control surface/stick movement. The most important variables are :

1. Extent and position of the originating region of disturbed flow.
2. Any further impingement of disturbed flow on the airframe.
3. Dynamic pressure - i.e. aircraft speed, which scales the whole input to the system.
4. Position of the pilot in relation to the aircraft vibration modes.
5. In the case of prestall buffet, rate of approach to the stall.
6. Structural/aerodynamic damping.

Complicating features in any flight investigation are also structural response to turbulence, and pilot's threshold effects.

The first four of these effects can fairly readily be appreciated, but the importance of the rate of change in such tests as stall approaches can be over looked. In the case of the Provost, a 'fast' approach gave appreciably high lift coefficients, as in Figure 20, but less warning.

The effects of speed and pilot threshold effects were also clearly demonstrated in the flight investigations, when we found that with configurations such as in Figure 10, buffet prior to the 'g' stall at higher I.A.S. was noticeable to the pilot whereas it was inadequate at the low speed 1 'g' conditions.

6. APPLICATION TO OTHER AIRCRAFT

This work and experience with other aircraft suggested that an inboard stall with wake impingement on the tailplane would always give a positive pre-stall warning. This is in contrast to aircraft like the Lightning where we had plenty of buffet before the stall from vortex flow breakdown on the wing tips, but in general this covered too much of the incidence range to be usable in the context desired for training. In the proposed design of a new trainer for the Royal Air Force, therefore, we used a technique of measuring wing wake position in the tunnel in order to give some better guidance as to the vertical tail position needed. A pitot rake (Figure 20) has proved to be useful as well as tufts, and we have had some interesting results (Figure 21). Neglecting Reynolds number for a moment, the wake positions showed that we could expect difficulty in getting adequate pre-stall buffet with flaps up and down - if we had the tail low enough for the flaps down case we might well be too low with flaps up, giving premature buffet dying out just before the stall. We were, however, able to find a position which we regarded as just satisfactory, since the wake flaps down was quite extensive.

Whether it would have been satisfactory in flight we shall never know, as the contract for that aircraft has gone elsewhere. It would however, have been very interesting to see how useful low Reynolds number tests could be as a guide in this sort of problem.

To speculate a little :

1. One might well expect the prestall wake to be thinner at higher Reynold's number. Will this extend to a partially stalled wake ?
2. How far will disturbed flow exist outside the actual wake ? Some evidence suggests to twice the wake width.
3. Does a higher Reynold's number change the mean wake position at a given incidence before the stall ?
4. Does the spanwise pattern on the wing remain sufficiently the same, together with the wing stall characteristics. i.e. can one extrapolate the low Reynolds number result to a high Reynolds number stall incidence; will the rate of progression of the stall - which is what this is all about be sufficiently the same ?

We believe that low Reynolds number testing can be used as a guide, but that anyone trying to solve this problem of providing good stall warning should budget for a reasonable period of flight development on a prototype, with tail height an important variable.

This paper has been about stall warning. I hope it will be useful to anyone with similar interests.



FIG. 4 BAC JET PROVOST - EXTERNAL  
CHANGES BETWEEN MK. 4 AND MK. 5

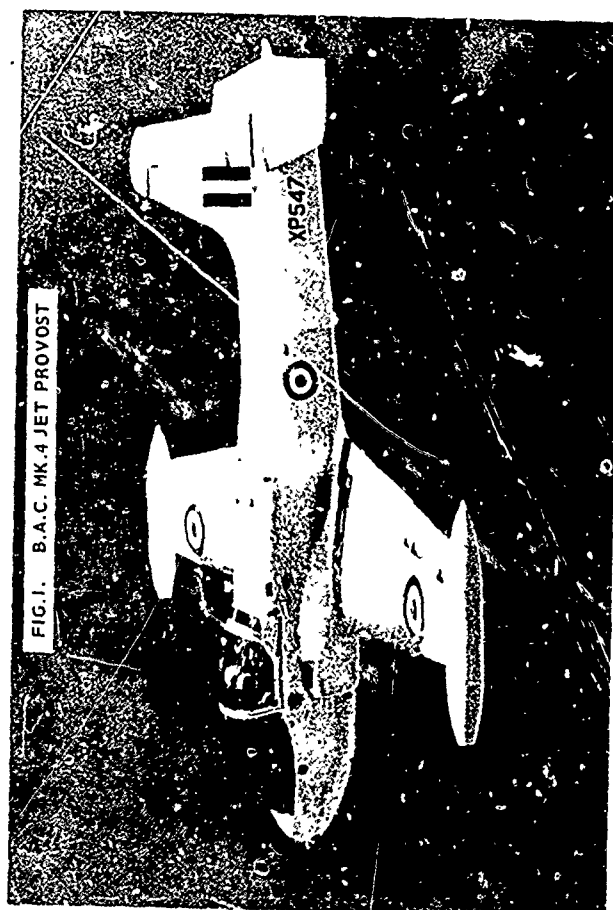
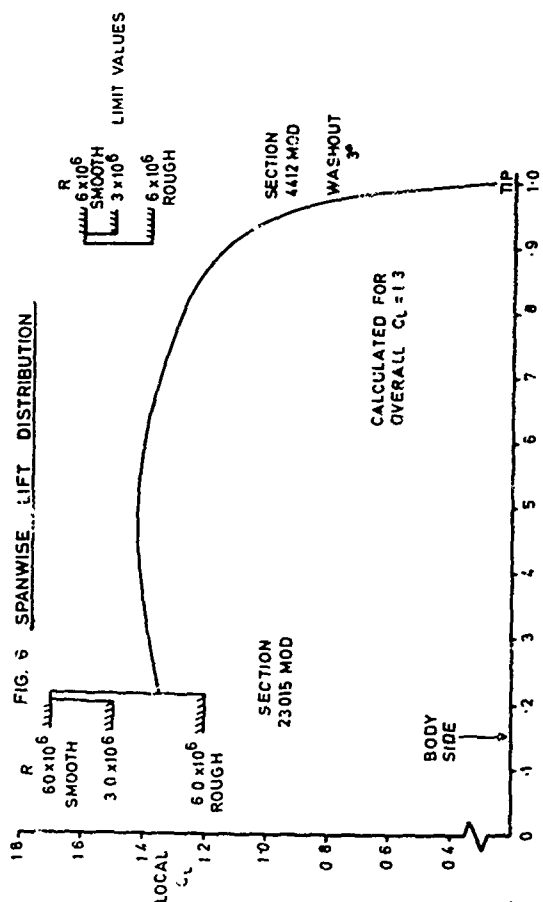
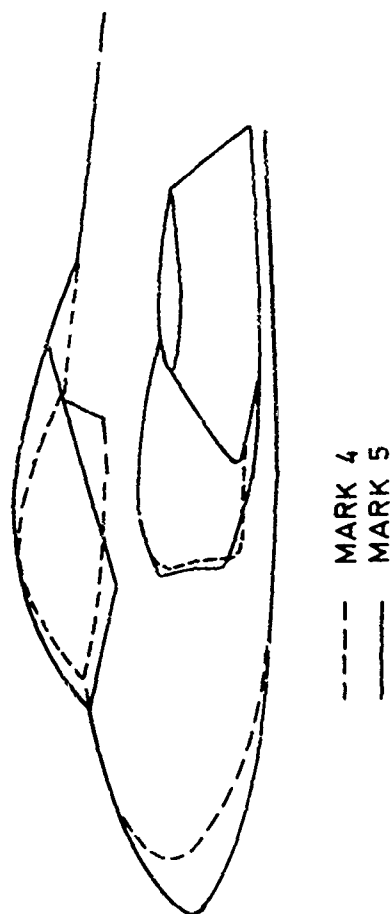


FIG. 1. B.A.C. MK. 4 JET PROVOST

FIG. 2. B.A.C. MK. 5 JET PROVOST



FIG. 7 JET PROVOST MARK 5  
EARLY STALL BEHAVIOUR, FLAPS UP

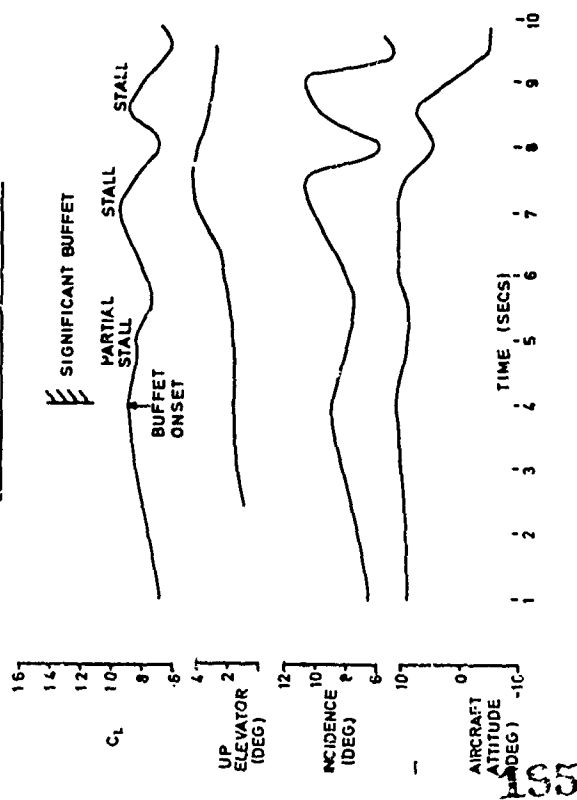


FIG. 9 MK 5 - MODIFIED WING ROOT SECTION

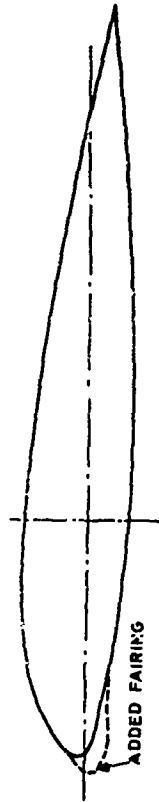


FIG. 8 MARK 5 - MODIFIED INTAKE  
FAIRING LINES

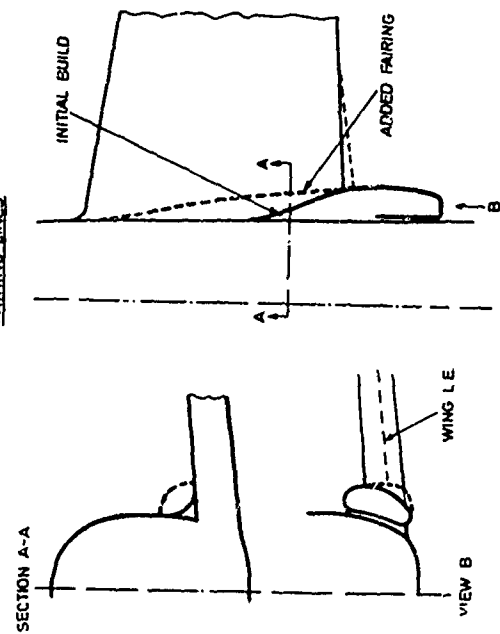


FIG. 10 JET PROVOST MARK 5  
INTERMEDIATE DEVELOPED STALL FLAPS UP

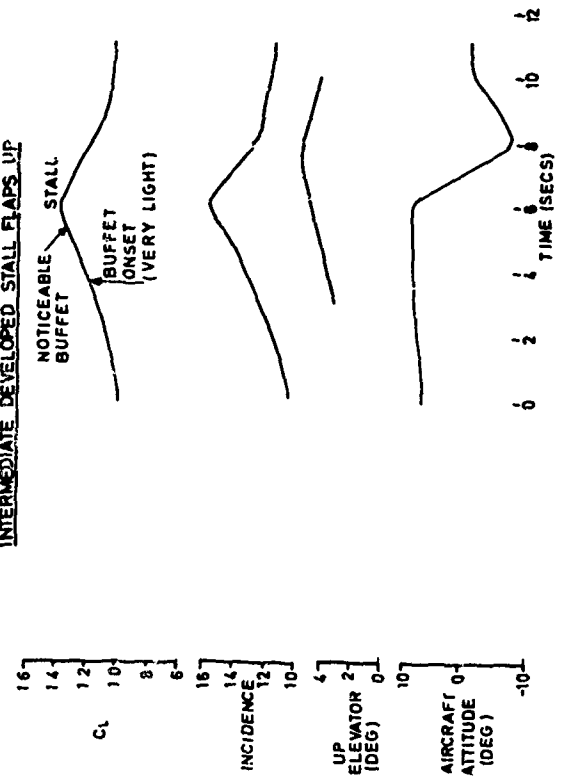


FIG. 12 FLAPS UP STALL PROGRESSION  
MARK 4 PROVOST

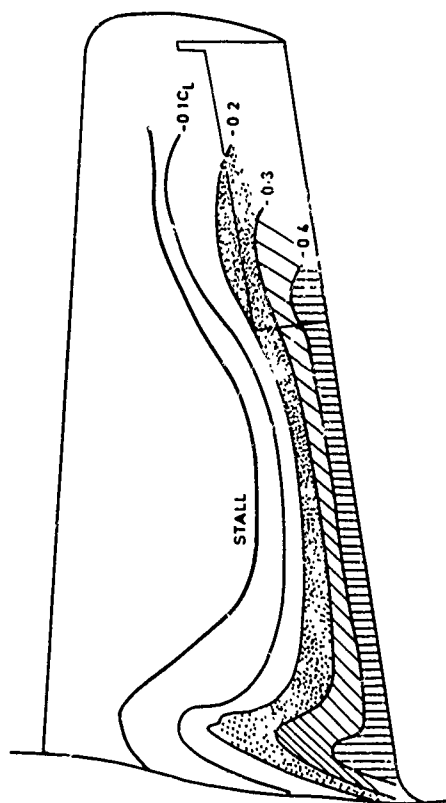


FIG. 14 DESIRED STALL PROGRESSION  
(DIAGRAMMATIC)

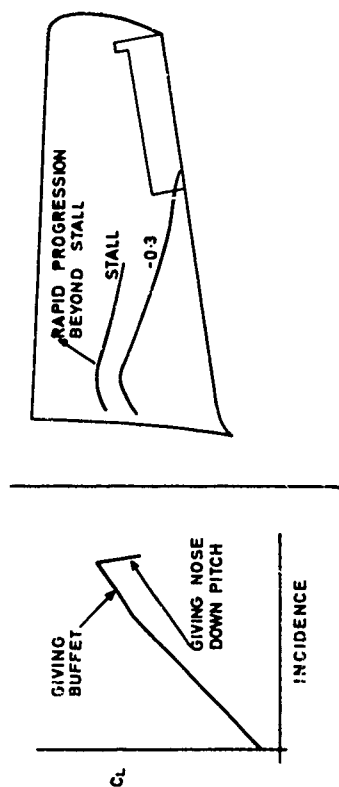


FIG. 13 FLAPS UP STALL PROGRESSION  
MARK 5 - INTERMEDIATE STANDARD

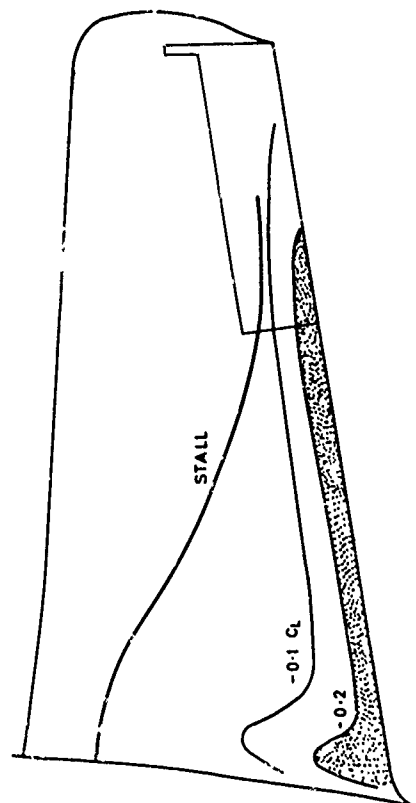


FIG. 15 SKETCH OF ROOT FAIRINGS

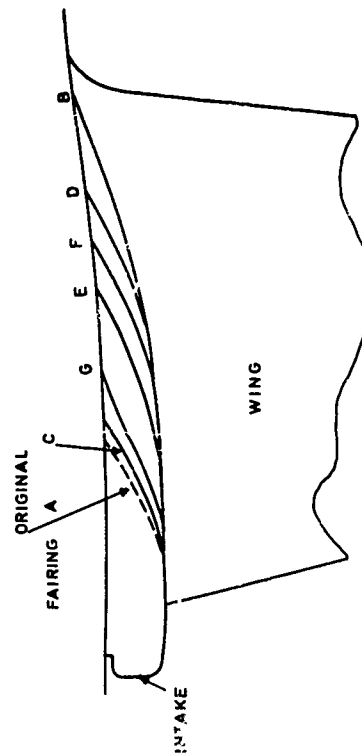


FIG. 19. MARK 5 FINAL CONFIGURATION FROM STALL DEVELOPMENT

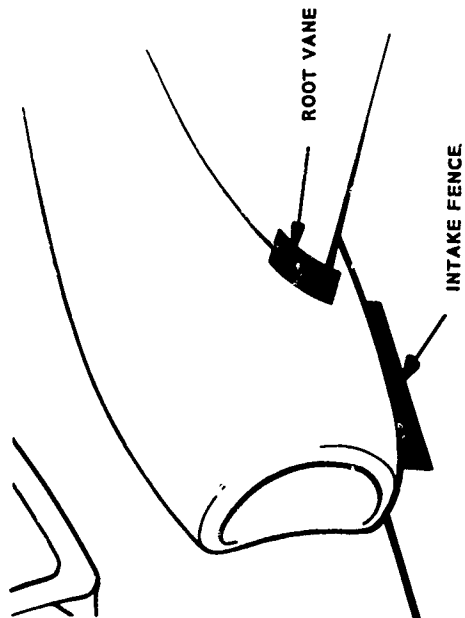


FIG 17 FURTHER WING DEVELOPMENT

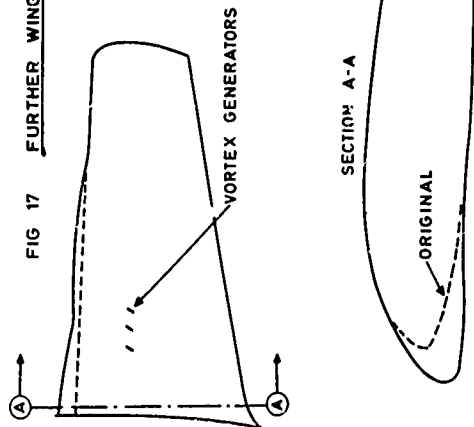


FIG 18 JET PROVOST Mk.5 DEVELOPED STALL, FLAPS UP GOOD PITCH DOWN, GOOD WARNING

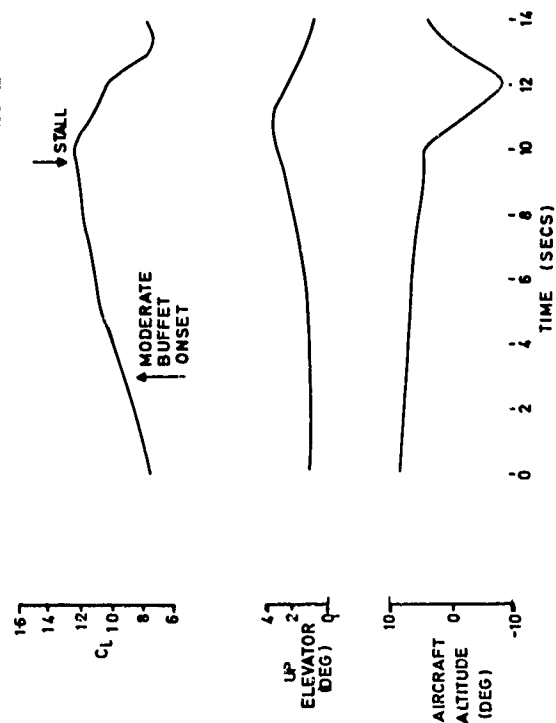
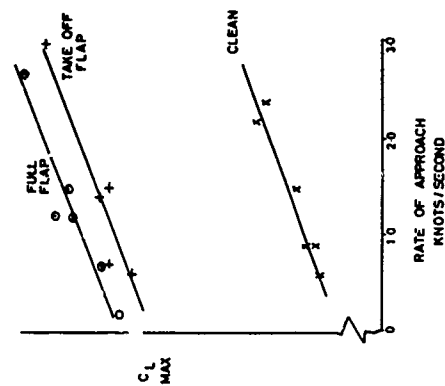
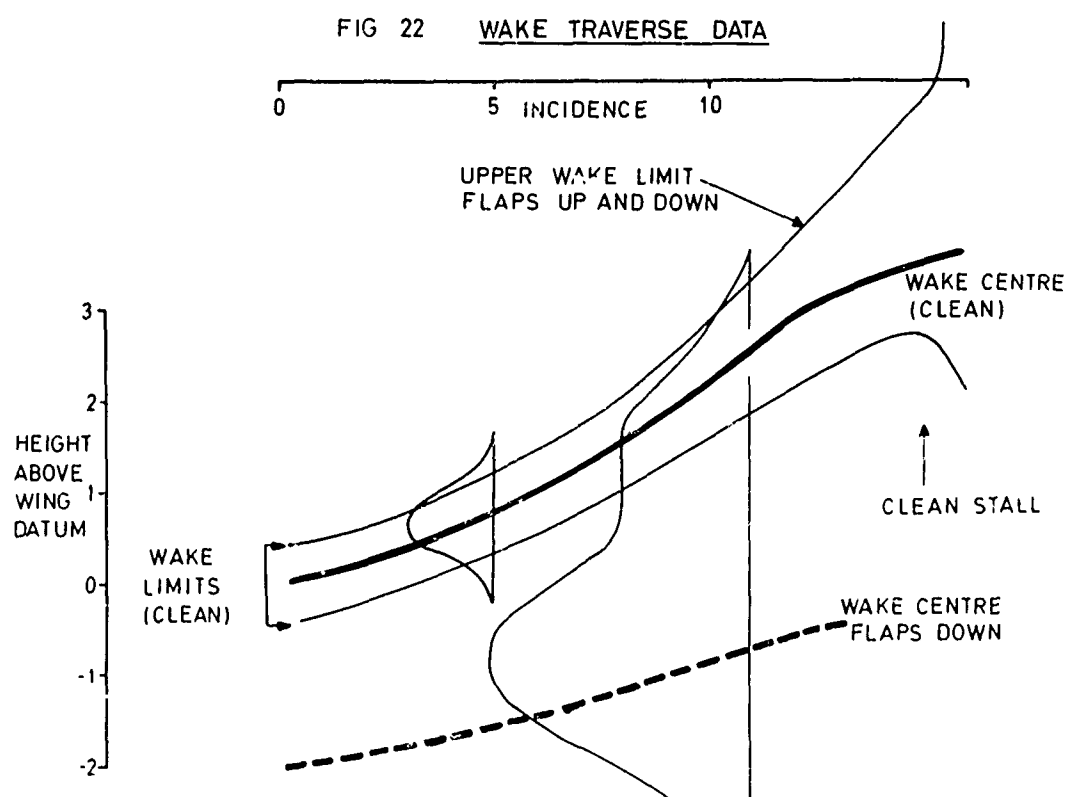
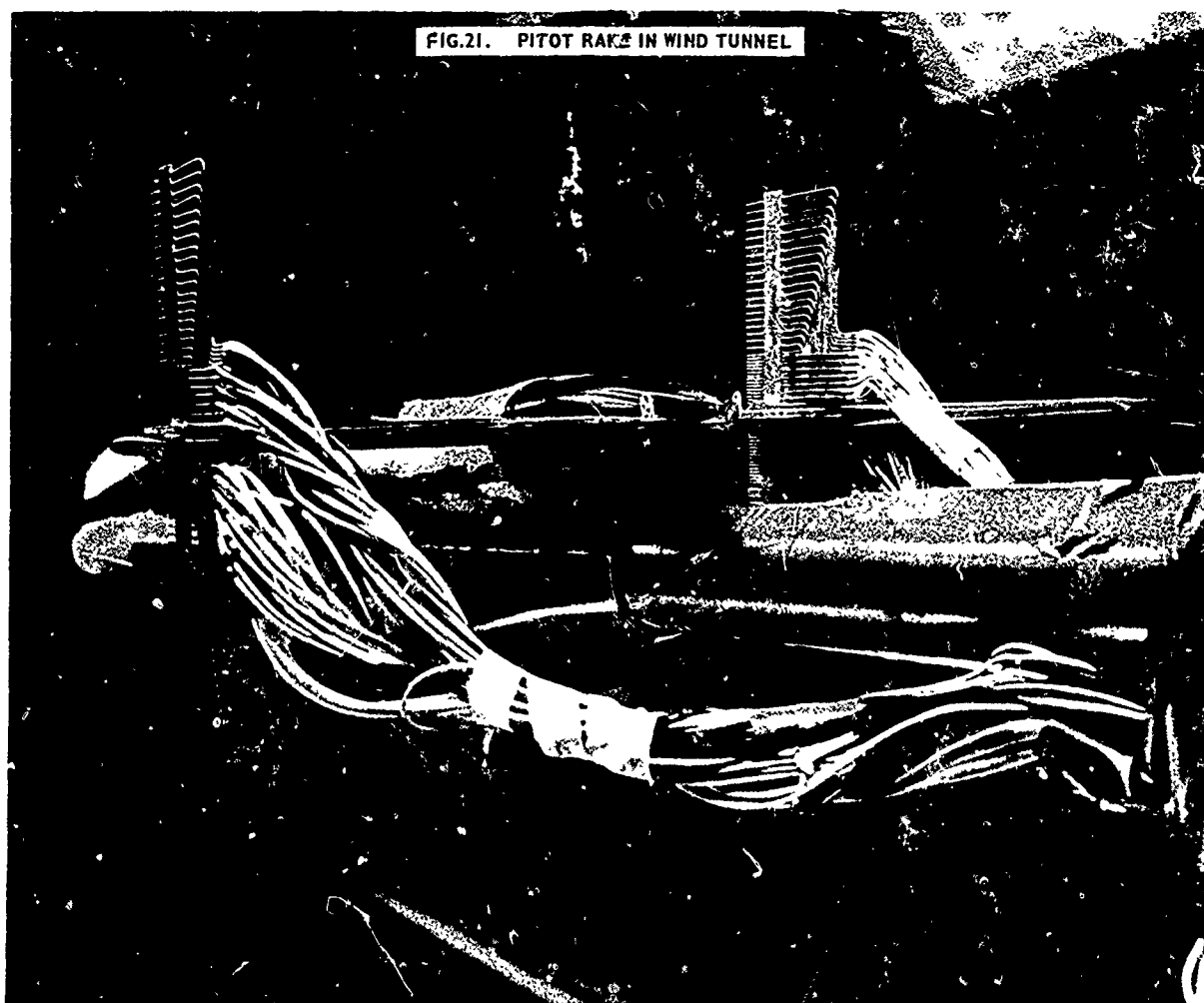


FIG 20 JET PROVOST MARK 5 EFFECT OF RATE OF APPROACH TO THE STALL





# STALL/POST-STALL CHARACTERISTICS OF THE F-111 AIRCRAFT

by

Charles A. Anderson  
Aerosystems Group Engineer  
Stability and Control  
General Dynamics  
Convair Aerospace Division  
Fort Worth, Texas

## SUMMARY

This paper contains a description of the stall/post-stall characteristics of the F-111 aircraft. These characteristics have been defined on the basis of wind tunnel tests, free-flight model tests, radio-controlled drop-model tests, analytical analysis, and flight tests. The extent of each type of testing will be discussed in detail and a brief summary of results will be presented. An attempt will also be made to compare the results obtained from the various model tests with flight test results where applicable.

A discussion of the regression techniques used to obtain aerodynamic derivatives in the Convair high-angle-of-attack simulator will be discussed and its usefulness assessed.

A summary of the conclusions drawn during the conduct of the program will be presented. An attempt will be made to establish the limitations and good points of each method used for predicting full scale results. Recommendations will also be made on the manner in which future stall/post-stall/spin prevention programs should be conducted.

## NOTATION

Symbol	Definition	Units	Symbol	Definition	Units
A/C, A/P	Aircraft or Airplane		$\delta_a$	Aileron Deflection	Deg
PRE-SWIP	Aircraft 1 - 30		$\delta_r$	Rudder Deflection	Deg
SWIP	Aircraft 31 and On		$\delta_{Sp}$	Spoiler Deflection	Deg
Re, RN	Reynolds Number	Per Ft	C <sub>l</sub>	Rolling Moment Coefficient	
V	Velocity	Ft/Sec	C <sub>n</sub>	Yaw Moment Coefficient	
$\alpha$	Angle of Attack	Deg	C <sub>y</sub>	Side Force Coefficient	
$\dot{\alpha}$	Rate of Change of Angle of Attack	Deg/Sec	C <sub>A</sub>	Axial Force Coefficient	
$\beta$	Angle of Sideslip	Deg	C <sub>N</sub>	Normal Force Coefficient	
$\dot{\beta}$	Rate of Change of Sideslip Angle	Deg/Sec	C <sub>m</sub>	Pitching Moment Coefficient	
$\delta_e$ $\delta_H$	Horizontal Tail Deflection	Deg	p	Body Roll Rate	Deg/Sec
			q	Body Pitch Rate	Deg/Sec
			r	Body Yaw Rate	Deg/Sec

## 1. INTRODUCTION

The F-111 is the first American production aircraft to incorporate a variable-sweep wing and a self-adaptive flight control system. Since the beginning of the F-111 program, a number of studies have been undertaken to determine the stall/post-stall/spin characteristics of the aircraft. In this paper, my objective is to review these studies, to summarize the advantages and disadvantages of the various investigative methods, and to present the more significant results.

Methods employed to date during F-111 stall/spin investigations have included vertical wind tunnel tests, free flight model tests, radio-controlled drop model tests, analytical studies, simulation, and full-scale flight tests. Results of these investigations show that the stall/post-stall/spin characteristics of the F-111 are similar to those of current high-speed, low-aspect-ratio, swept wing aircraft.

On the basis of experience gained during the F-111 program, it appears feasible to predict the stall/post-stall/spin characteristics of an aircraft by means of analytical programs in which use is made of a reduced amount of full-scale flight testing.

## 2. DISCUSSION

This paper is directed to a definition of stall, post-stall, and spin characteristics of F-111 aircraft along with a description of the testing conducted to determine these characteristics.

## 2.1 Stalls

During an approach to stall, control effectiveness about all axes is good. In the cruise configuration, buffet will be encountered before stall angle of attack is reached but may not be usable as a stall warning since it tends to reach a constant level at angles of attack well below stall. In the landing configuration, adequate stall warning in the form of buffet is not available either. Artificial stall warning, in the form of a rudder pedal shaker and an audio visual system, has been incorporated in the aircraft.

As the stall angle of attack is approached, a small amount of low-amplitude, low-frequency wing rock or wing drop may occur just before the aircraft departs, but this action may be masked by the action of the roll damper. Roll control effectiveness will be rapidly degraded as the departure angle of attack is reached, and the pilot's workload required to maintain the desired aircraft attitude will be noticeably increased. Aircraft directional stability will also be rapidly degraded as the departure angle of attack is approached; however, this degradation may not be readily apparent to the pilot. Elevator effectiveness will be good up to and slightly in excess of the departure angle of attack.

At departure, the aircraft will diverge in yaw and roll. The initial divergence will occur in yaw and may give the pilot the impression of sliding, as on ice, if appropriate cues are available, such as the horizon or another aircraft. Roll divergence will follow as a result of the roll-due-to-yaw characteristics of the aircraft, along with further yaw divergence. The yaw and roll divergence are generally smooth and gradual at first. No sudden loss of lift, "g" break, or sudden stick force changes are available to warn the pilot of impending departure.

In general, the aircraft flying qualities are such that, unless the pilot monitors angle of attack, he may not be aware of an impending departure and may be completely surprised to find that control has been lost. Rapid roll divergence is usually the first recognizable cue that the aircraft has departed from controlled flight.

## 2.2 Post-Stall Gyration

Post-stall gyrations are normally encountered during deep stall penetration (angles of attack in excess of 25 to 28 degrees) and after spin recovery. These motions may be mistaken as the incipient phase of a spin. Post-stall gyrations entered from unaccelerated stalls with flaps and slats extended or retracted are usually characterized by yaw divergence (yaw slice) at stall which, because of the roll-due-to-yaw characteristics of the aircraft will produce roll divergence. As the aircraft nose passes below the horizon, the aircraft may appear to be entering a spin since the combination of aircraft pitch, roll and yaw attitude may result in a tight nose-down spiral. In some instances, the aircraft may also enter a series of rolling maneuvers which can be mistaken for a spin because of the nose-down attitude of the aircraft. Post-stall gyrations entered from accelerated conditions are expected to exhibit the same characteristics as those entered from unaccelerated conditions except that possible roll reversals and/or yaw reversals may occur. These reversals are due to yaw divergence and will normally result in rolling over the top or under in a turn and yawing through approximately 180 to 270 degrees. During this yawing excursion, the aircraft nose will rise briefly and then fall below the horizon. After the initial yaw, roll, and pitch maneuver, the aircraft will exhibit post-stall gyration characteristics similar to those encountered after unaccelerated entries.

## 2.3 Developed Spins

Developed spin entries are usually a result of very deep stall penetration or improper application of spin recovery controls. The flight testing has not been completed on the aircraft; consequently, the spinning characteristics of all configurations have not been confirmed. Flight testing conducted to date has been limited to 26 degrees of wing sweep without external stores and with flaps and slats retracted. Spin investigations conducted during wind tunnel testing have indicated that the aircraft exhibits a tendency to enter a spin in any configuration and at all wing sweeps. However, limited flight test results to date have indicated a reluctance of the aircraft to enter a developed spin. Spin entry from a 1 "g" stall with symmetrical controls has been possible in some instances in the wind tunnel but has not been encountered during the limited flight testing conducted to date. During model testing, pro-spin rudder and/or lateral control at stall produced spin entries in all configurations tested. Pro-spin rudder was the only method by which a spin was induced during flight tests. Crossed controls at or before accelerated stalls could likewise produce abrupt entries into erect or inverted spins and should therefore be avoided. The aircraft is expected to enter spins from both upright and inverted conditions and is expected to exhibit both upright and inverted spin modes.

### 2.3.1 Upright Spins

Upright spins are expected to be primarily oscillatory in nature with excursions of up to  $\pm 35$  degrees in pitch and  $\pm 35$  degrees in roll. The spin rates can vary from 4 to 10 seconds per turn. The oscillatory mode appears to be the most predominant spin mode and is expected to exhibit the following characteristics. During the initial phase, up to completion of the first turn, the aircraft motions are expected to be very similar to those of a post-stall gyration. After completion of the first turn, the spin rate should stabilize, and definite pitch and roll oscillations should be apparent to the pilot. The pitch oscillation will usually result in movement of the nose from approximately 50 degrees below the horizon to 10 degrees above the horizon. Wind tunnel tests have also indicated that a flat spin mode may be encountered at wing sweeps aft of 35 degrees. This mode appears to be relatively free from oscillation about any axis, and the spin rates are

expected to vary from 2 to 4 seconds per turn. The spin rate encountered in a flat spin can produce pilot loads up to 5.0 g's transverse (forward). The flat spin mode should rarely be encountered, and it is believed that it would develop only after an oscillatory spin has been permitted to build up for several turns.

### 2.3.2 Inverted Spins

Inverted spins are expected to be very similar in nature to an upright oscillatory spin except that the crew will be subjected to a negative "g" condition.

### 2.4 Model Tests

The model testing conducted during the F-111 program has been extensive in some areas and lacking in others. Considerable testing has been conducted in the vertical and free flight tunnels, along with radio control drop model testing. Very minimal force and rotary derivative testing at high angle of attack has been conducted.

#### 2.4.1 Vertical Tunnel Tests

The vertical tunnel testing conducted on the F-111 is summarized in Figure 1. As can be seen in this figure, considerable testing has been conducted. This testing has consisted of determining basic aircraft spin modes, predicting recovery controls, and sizing the spin recovery parachute system. The testing was conducted with a 1/40th-scale model at a Reynolds number of approximately 80,000. As can be seen, the Reynolds number for this type of testing is very low; therefore, it is felt that test results from this type of testing should be used with caution.

NUMBER OF TESTS	~ 2000	F-111A SWIP
	~ 800	F-111B SWIP
WING SWEEPS	CLEAN A/P 26°, 50°, 72.5°	
	FLAPS DOWN 20° PRE-SWIP	
MODEL	1/40 SCALE	RE ~ 0.08 MILLION/FOOT

FIG. 1 VERTICAL SPIN TUNNEL TESTS

The results obtained from these tests have indicated that the aircraft can exhibit both oscillatory and flat spin modes and that it will spin readily. The tests have also shown that the aircraft may be slow in recovering from developed spins. The very limited flight tests conducted to date have neither confirmed nor denied these results but have indicated that the aircraft is reluctant to enter a spin.

On the basis of the flight test and analytical results obtained to date, it appears that the following conclusions can be drawn regarding the usefulness of the vertical spin tunnel data:

1. As a result of scaling and Reynolds number effects, the results tend to be pessimistic and the data obtained from this type of testing should only be used to examine possible spin modes, areas, general trends, and preliminary recommended recovery controls and to size a spin recovery parachute system.
2. As a result of the required testing techniques, no information can be obtained regarding entry and post-stall characteristics and no reliable technique is available for accurately extrapolating these results to full scale.

#### 2.4.2 Free Flight Tests

Extensive free flight model testing has been conducted on the F-111. The testing was conducted by using a 1/10-scale model in the Langley full-scale tunnel at a Mach number of approximately 0.10 and a Reynolds number of 375,000. Tests were conducted over a wing sweep range of 16 through 72.5 degrees and a lift coefficient range from approximately 0.5 to 2.2. The tests were accomplished by actually flying the model until stall or departure angle of attack was achieved.

In general, the results of the testing have shown that the aircraft stall will be defined by yaw or roll divergence. The angle of attack at which divergence was observed is presented in Figure 2 as a function of wing sweep. This data was used to set the angle of attack limits for the F-111 and these limits are shown in this figure. The limits were set to maintain at least 8 degrees of margin below stall at 26 degrees wing sweep and 10 degrees of margin at 72.5 degrees wing sweep. Also shown in Figure 2 is the angle of attack for which stability axis static directional stability ( $C_{N\beta}$ ) is calculated to be zero. The data used for this calculation was obtained from static force tests conducted on the free flight model and will be discussed in a later section. The difference between the model and predicted divergence angle of attack is probably due to obtaining some effect from  $C_{N\beta}$  dynamic on the model.

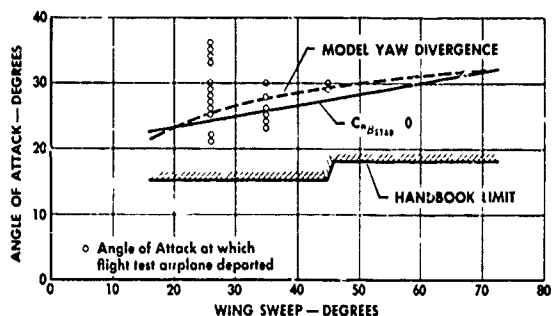


FIG. 2 PREDICTED YAW DIVERGENCE BOUNDARY

The departure angles of attack obtained from the flight testing conducted to date are also presented in Figure 2. As shown, good correlation is obtained between the model yaw divergence angle of attack and the flight test values except possibly at wing sweeps forward of 35



degrees. The low value of Reynolds number at which the free flight model tests were conducted could have resulted in more pronounced flow separation at wing sweeps forward of 35 degrees and thus more conservative values of yaw divergence.

On the basis of analysis and comparison with flight test results, the following conclusions about the usefulness of the free flight model can be drawn:

1. The free flight model is extremely useful in determining the stall or divergence angle of attack and in setting initial angle of attack limits for flight test, but as a result of the limitations of the testing techniques that must be used, information on aircraft characteristics after departure cannot be obtained.
2. As a result of the low Reynolds number at which the testing was conducted, the yaw divergence angle of attack determined from the model may be conservative for the case of the forward wing sweeps.

#### 2.4.3 Radio Control Model Tests

The radio control drop model testing conducted on the F-111 is summarized in Figure 3.

NUMBER OF TESTS	47	F-111A PRE-SWIP
WING SWEEPS	CLEAN A/P 26°, 41°, 50°, 72.5°	
MODEL	1/9 SCALE	RE - 1.0 MILLION/FOOT

FIG. 3 RADIO CONTROL DROP MODEL TESTS

As can be seen, a fairly comprehensive program has been conducted to determine basic aircraft entry, post-stall, and spin characteristics and to define acceptable recovery techniques.

The testing was accomplished by using a 1/9th-scale radio controlled model of the F-111 at a Reynolds number of approximately 1.0 million. The model was controlled from the ground and incorporated a complete duplication of the control surface sizes and authorities except for the

spoilers. It was determined that the spoilers were not required since earlier force model testing had shown them to be ineffective in any axis at or near the stall angle of attack. (The limited F-111 flight testing conducted to date has indicated that this assumption may not have been valid since it appears that the spoilers produce considerable yaw.) The tests were conducted by dropping the model from a hovering helicopter and pulling it into a stall and/or forcing it into a spin. After the model was stalled or spinning, the effect of control application was determined. Data was obtained from photo coverage and from an on-board data system. A sample of the data obtained is shown in Figure 4.

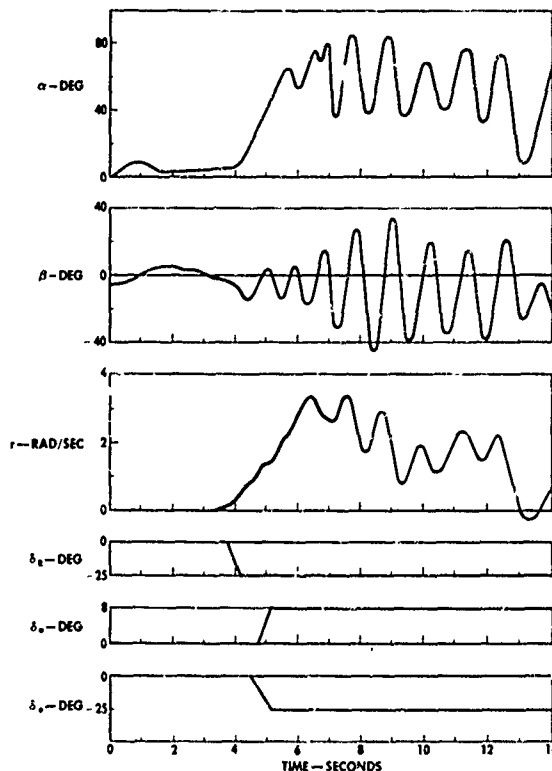


FIG. 4 TYPICAL DROP MODEL SPIN TIME HISTORY

In general, the results obtained from this model indicated that the aircraft is prone to enter spins at all wing sweeps. They also confirmed the fact that the aircraft can exhibit both oscillatory and flat spin modes. Examination of the control application studies indicate that neutral to forward elevator is pro-spin. The optimum recovery technique for all types of spins was found to be elevator full back, aileron full with the spin and rudder full against. The testing also indicated that satisfactory recovery from spins was questionable, especially from the flat mode.

Although this testing technique represents a definite advancement over vertical and free flight model testing, it is still subject to scaling effects and Reynolds number uncertainties that leave questions as to how to apply the data to full scale. On the basis of analysis and flight test results, the following conclusions can be drawn:

1. The results obtained from this type of testing should be more representative of full scale and allows examination of entry conditions, post-stall behavior, spin mode determination, and recovery techniques all in one model.
2. As a result of low Reynolds number and Mach number test conditions, the ability to extrapolate the results to full scale is questionable.
3. Limited flight test data and simulator analysis have indicated that forward or neutral elevator control is not pro-spin and that stick forward and aileron with the spin may be as effective a recovery control technique as stick back and aileron with spin.

#### 2.4.4 Static and Dynamic Force Model Tests

Very limited static force and dynamic testing at stall angle of attack and above has been conducted on the F-111. The majority of the testing conducted across the Mach range for documentation purposes has been obtained on the 1/15th-scale and 1/24th-scale models at approximately 2.5 million Reynolds number, and this testing was limited to approximately 20 degrees angle of attack because of model strength or balance capacity limits.

The limited amount of static force and dynamic testing conducted at high angle of attack is presented in Figure 5. As can be seen, the data has been limited to low Mach numbers. The maximum Reynolds number that could be obtained was limited by model strength or balance capacity limits.

MODEL	TUNNEL LISTED IN	TYPE OF DATA	MACH RANGE	RE RANGE	$\alpha$ RANGE	$\beta$ RANGE	$\delta$ RANGE	$\delta_1$ RANGE	$\delta_2$ RANGE	WIND SPEED	APPROX DATE RUN
1/24	AMES 12 FT	STATIC FORCE	0.2	0.2 - 1.6	45° - 90°	-10° - 30°	0	0	0	30'	JUNE 1964
1/24	AMES 12 FT	STATIC FORCE	0.1 - 0.2	0.2 - 1.6	7° - 30°	0° - 6°	0.8 - 10°	0.8 - 10°	30°	30'	JUNE 1964
1/15	AMES 12 FT	STATIC FORCE	0.2	2.0	0° - 90°	-10° - 35°	0.8 - 30°	0.8 - 10°	30°	30'	OCT 1963 TO
1/15	AMES 12 FT	STATIC FORCE	0.2	7.0	0° - 90°	-10° - 35°	0.8 - 30°	0.8 - 10°	30°	50'	FEB 1966
1/15	AMES 12 FT	STATIC FORCE	0.2	2.0	0° - 90°	-10° - 35°	0.8 - 30°	0.8 - 10°	30°	72.5'	
1/10	LANGLEY FULL-SCALE	STATIC FORCE	0.1	0.375	-10° - 45°	> 5°	0.8 - 10°	0.8 - 10°	30°	15', 30', 50', 72.5'	OCT 1964
1/10	LANGLEY FULL-SCALE	DYNAMIC DRIVABLE	0.1	0.375	-10° - 45°	0	0	0	0	15', 30', 50', 72.5'	OCT 1964
1/9	LANGLEY FULL-SCALE	STATIC & DYNAMIC	0.1	0.70	-10° - 45°	> 5°	0	0	0	24', 50', 72.5'	11-48 TO 1966

FIG. 5 SUMMARY OF WIND TUNNEL DATA AVAILABLE

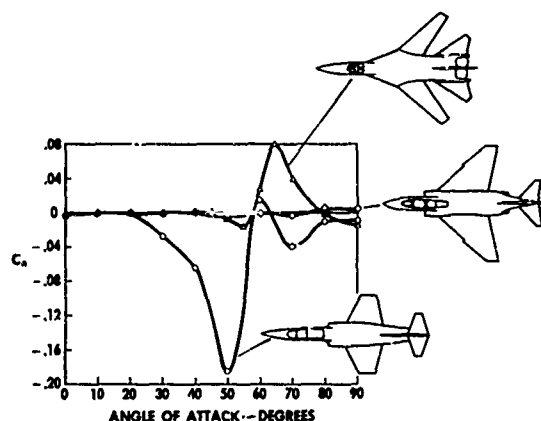


FIG. 6 VARIATION OF YAWING-MOMENT COEFFICIENT WITH ANGLE OF ATTACK FOR SEVERAL AIRPLANES

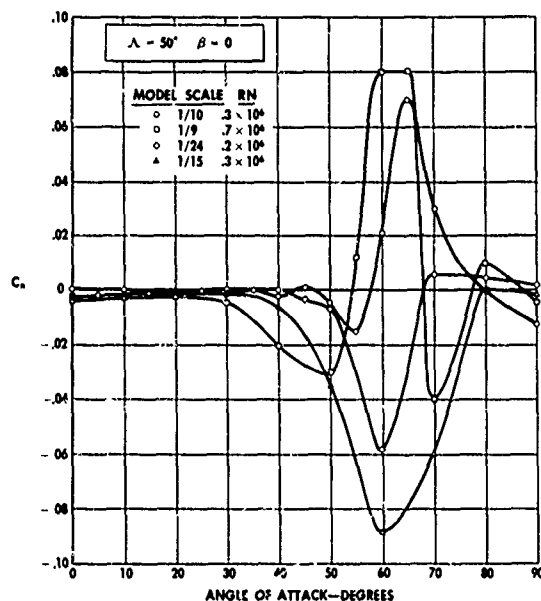


FIG. 7 VARIATION OF YAWING-MOMENT COEFFICIENT

Past experience has indicated that, in the case of an aircraft with a long pointed nose, it is very important to test at a Reynolds number in excess of the critical Reynolds number of the fuselage to prevent premature flow separation on the nose. An example of the effect of nose shape on the yawing moment coefficient ( $C_n$ ) versus angle of attack at zero sideslip is shown in Figure 6. It can be concluded from looking at the data in Figure 6 that the longer and more pointed the nose, the greater the tendency and the stronger the separation on the nose will be. Figure 7 contains a summary of the data obtained from various scaled models of the F-111 which were run in different tunnels. The data indicates that the nonlinearity in yawing moment shows no definite trend and is probably a function of model nose shape irregularities or tunnel flow conditions. Because of the lack of repeatability and the fact that using the nonlinear data in the Convair high angle of attack simulator will not duplicate flight test, it is our belief that the data was not obtained at sufficiently high Reynolds number. It is also our belief that, if the model had been capable of being tested at higher Reynolds numbers, the nonlinearities would not have been present. It is hoped that the new proposed 1/12th-scale, high-strength model will prove this contention one way or the other. An example of the variation with angle of attack of the static stability parameter  $C_{n\beta}$  obtained from model tests and that required to make the simulator fly like the aircraft are shown in Figure 8.

Although little has been said about the dynamic data obtained, the same nonlinearities exist in the data over the same angle-of-attack range. It has therefore been concluded that the nonlinearities obtained to date are questionable and are affected by the nose configuration and Reynolds number just as the static data is affected.

On the basis of the data analysis and testing conducted to date, the following conclusions can be drawn:

1. Use of the static and dynamic data obtained to date in our high-angle-of-attack simulator has failed to reproduce the aircraft motion obtained from the stall/post-stall flight test program.
2. Use of the static and dynamic data obtained to date by NASA in theoretical spin calculations could not reproduce the motions obtained from testing the free flight model.
3. The effect of Reynolds number on the nose flow separation characteristics has not been determined because of model strength or balance limits.
4. No testing has been conducted to determine the effect of both Mach and Reynolds number on the static and dynamic stability characteristics.

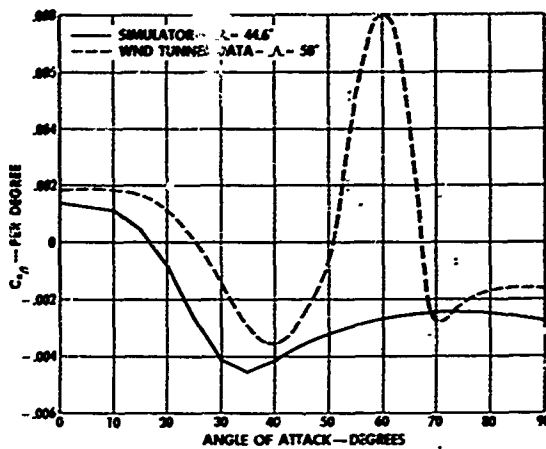


FIG. 8 F-111 BODY AXIS DIRECTIONAL STABILITY

program approved for the F-111 be changed to a program of stall/post-stall investigation and spin prevention. Since the F-4 had successfully completed such a program at this time and the desirability of doing a classic spin program was being questioned by both industry and government agencies, the committee recommended that the F-111 program be changed.

### 2.5.1 Early Testing

Early stall testing on the F-111 was mainly conducted in support of maximum lift. Demonstration testing was accomplished on boiler-plate, high-lift versions of the proposed production systems on F-111A Number 4 and 21. A summary of the amount of testing conducted in support of the high lift evaluations is presented in Figure 9. Very limited data on the post-stall characteristics of the aircraft were obtained during this testing since the testing was terminated as soon as the maximum lift coefficient was obtained.

CONFIGURATION	CONDUCTED		WING SWEEPS - DEGREES					
	FLIGHTS	MANEUVERS	16	26	35	45	50	72.5
FLAPS AND SLATS EXTENDED								
STALL APPROACHES	1/2	2	*	*				
STALL	56	212	*	*				
FLAPS AND SLATS RETRACTED								
STALL APPROACHES	1/2	4		*	*	*	*	*
STALLS	4			*	*	*	*	*
1 "g" ENTRIES CONDUCTED		7		*	*			
2 "g" ENTRIES CONDUCTED		10		*	*			
SPINS	3							
ENTRIES ATTEMPTED		4		*				
SPINS DEVELOPED		2		*				

FIG. 9 F-111 FLIGHT TEST SUMMARY

sweeps was not attempted because of the size of the recovery chute. NASA directed that we increase the size of the recovery chute from 35 to 45 feet in order to assure recovery from the fast flat spin mode that may be encountered at aft wing sweeps. This increased chute size requirement and the subsequent loss of F-111A Number 4 brought the early testing to a halt. In general, the results of the early test program showed the following:

1. Aircraft flying qualities are such that the pilot may not be aware of impending departure and will always depart in yaw, which will result in roll divergence.
2. It is very difficult for the pilot to distinguish between a post-stall gyration and a spin because of the nose-down attitude and the rolling motions.
3. The aircraft at 26 degrees of wing sweep was reluctant to enter a spin and recommended spin recovery controls must be removed very quickly or the aircraft will enter a spin in the opposite direction.

### 2.5.2 Current Testing

The current stall/post-stall gyration investigation and spin avoidance program being conducted on the F-111 is an outgrowth of recommendations from us and the Ad Hoc committee. As the title of the program suggests, the current program is oriented toward an understanding of the aircraft stall and post-stall characteristics and the prevention of spins. We have long contended that the ideal flight test program should be a blend of stall/post-stall investigations and spin testing. The exact ratio is a function of the aircraft mission. It is obvious that the ratio required for a fighter would be different from that required for a bomber. No intentional spins are currently programmed during Convair's Category I program. If an inadvertent spin is encountered, recommended spin recovery controls will be applied and evaluated.

A summary of the current program is presented in Figure 10. As shown in this figure, the program is being conducted in two phases or Block Flight Test Plans (BFTP). The first phase, BFTP-30, is designed to examine 1.0-g and 2.0-g entries at selected wing sweeps. This phase is designed to produce data for evaluating the aircraft characteristics under relatively controlled

## 2.5 Flight Test Results

The stall/spin flight test program for the F-111 is one which has undergone tremendous change. The original program was designed to satisfy the classic spin demonstration specification, MIL-S-25015. Consequently, plans were made to conduct some 495 spins. The program was projected to last two years, and cost was estimated to be approximately 10 million dollars.

As a result of a delay in the production airplane stall/spin program which was caused by reorientation of the flight test program, a two-phase stall/post-stall investigation program was initiated. Subsequent loss of an F-111A in a spin accident resulted in the formation of an F-111 Ad Hoc committee to evaluate the F-111 stall/spin program. During the course of the committee hearings, it was recommended that the classic spin demonstration pro-

As mentioned above, a short program was initiated on F-111A Number 4 to obtain an early look at the stall/post-stall/spin characteristics of the F-111. The program was limited to examination of 1.0-g and 2.0-g entries and recovery characteristics. A summary of the testing conducted during this program is also presented in Figure 9. As can be seen, the testing was limited and covered only 26 and 35 degrees of wing sweep. Testing aft of these

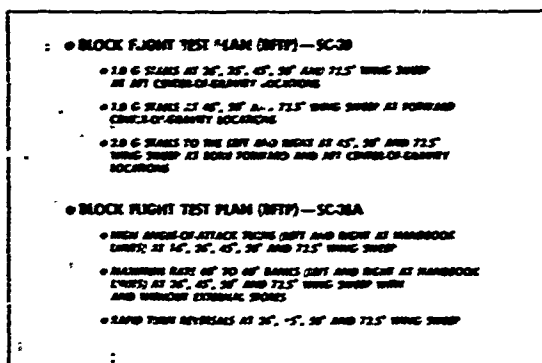


FIG. 10 CURRENT CATEGORY I FLIGHT TEST PROGRAM

conditions. The second phase, BFTP-38A, is designed to examine the aircraft stall characteristics during dynamic maneuvering conditions. The data from these tests will be used to determine the maximum recommended maneuvering angle of attack for the aircraft.

To date, very little of the current program has been accomplished. Initial testing during the first phase was terminated after three data flights because of encountering a post-stall mode which we did not understand and could not recover from by using the pre-briefed recovery controls. The spin recovery chute was used to recover the aircraft, but it failed because it was deployed at three times design "q". Later analysis of the flight test data and simulation on the Convair high-angle-

of-attack simulator revealed that the application of the selected recovery controls resulted in coupling at angles of attack below stall. Therefore, when the recovery controls were applied, the aircraft was not stalled and entered a pitch/roll coupling mode. This mode had never been encountered before, and since it is usually associated with higher speeds, it was not investigated in the regime of stall speeds. The data analysis methods used and a discussion of the Convair high-angle-of-attack simulator will be covered in Section 2.6. A discussion of the proposed Convair stall inhibitor system for the F-111 will also be provided in that section.

The current schedule calls for completion of our portion of the flight test program in July of this year. At that time, the aircraft will be turned over to the Air Force at Edwards Air Force Base for evaluation. It is estimated that the Air Force program will cover approximately one year and will be designed to be the first program to be run against the new spin demonstration Mil Specification (MIL-S-83691).

The results of the testing conducted to date on F-111A Number 21 have shown the following:

1. Application of lateral control with the roll or yawing motion combined with forward stick at angles of attack below stall can result in pitch/roll coupling. Simply neutralizing controls will produce recovery.
2. Application of forward stick in combination with aileron at angles of attack above stall appears to be a very effective recovery technique.

## 2.6 Analytical Program Results

The analytical program originally planned for the F-111 was one in which both static and dynamic testing were used in conjunction with catapult launched model data. The catapult launched model was later replaced by the radio-controlled model. The original plan was to obtain static and dynamic testing over the expected aircraft entry Mach range at high angles of attack and Reynolds number. This data would then be used in a six-degree-of-freedom digital or simulation program to predict stall/post-stall/spin characteristics. The predicted characteristics were to be compared to the drop model results at the same conditions and the data adjusted to match the drop model. Predictions were then to be made at actual flight test conditions and compared with flight test data. It was believed that the flight test program could be shortened considerably through the use of a checkout analytical program. It was also felt that the use of an analytical program would result in our obtaining considerably more detailed analysis of the stall/post-stall/spin mechanics at a cost considerably less than that of flight testing.

The original F-111 analytical program was terminated in early 1966. The basic reason for cancellation of the program was that the feasibility of an analytical program was doubted as a result of suspected uncertainties in interpretation and in the use of force and dynamic data. Since this basic doubt existed, there was reluctance to spend the necessary wind tunnel time to obtain sufficient data for an adequate data bank. We and the F-111 System Project Office (SPO) have always felt that the analytical program was obtainable. After the cancellation of the analytical program, it was decided to take the flight test data and wind tunnel data available and build a high-angle-of-attack simulation. The first step in the plan was to use all the available wind tunnel data in the simulation and attempt to match a flight test maneuver. It soon became obvious that the aerodynamic data available was not sufficient to reproduce the flight test maneuver chosen for this matching (Flight 92 of F-111A Number 21). It was then decided to try to obtain aerodynamic data from flight test by using regression techniques.

The selected regression technique uses flight test information to determine aircraft linear and angular accelerations at the center of gravity. Then, the six total aerodynamic coefficients were calculated by using the flight test rates and accelerations and known inertial and engine gyroscopic characteristics. Next, the flight test time histories of rates, velocities, and surface positions were fed into the simulator, and the six total aerodynamic coefficients were calculated. The total aerodynamics obtained from flight test and the simulator were then compared to determine how closely the simulator represented the aircraft. A sample flow diagram of the process is shown in Figure 11.

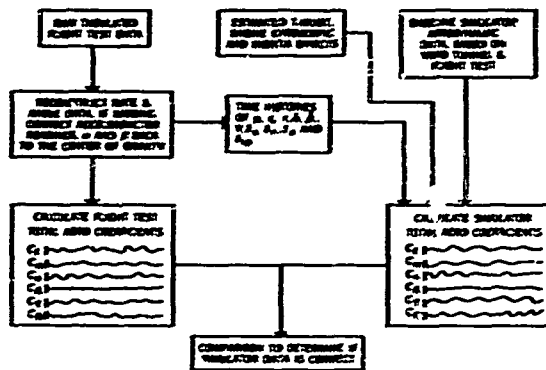


FIG. 11 SIMULATOR DATA VERIFICATION

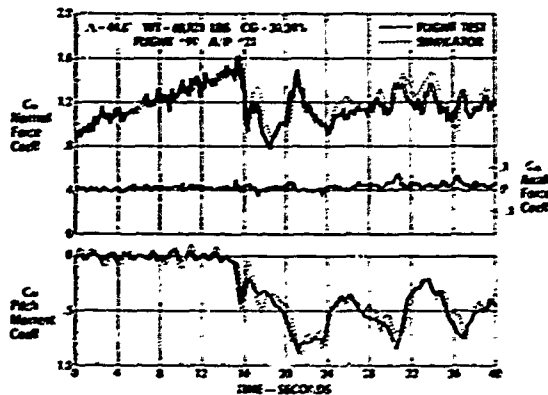


FIG. 12 LONGITUDINAL FLIGHT TEST AERODYNAMIC COEFFICIENTS PRELIMINARY DATA, 3 DEC 1971

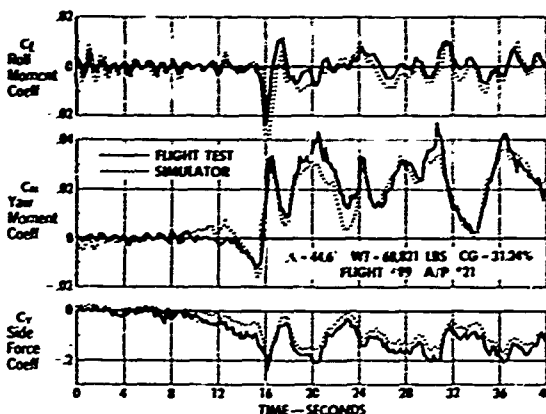


FIG. 13 LATERAL DIRECTIONAL FLIGHT TEST AERODYNAMIC COEFFICIENTS PRELIMINARY DATA, 3 DEC 1971

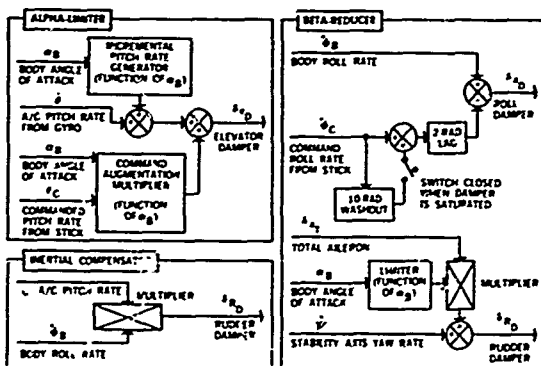


FIG. 14 STALL/POST-STALL GYRATION INHIBITOR SYSTEM

After a total coefficient comparison is completed, the individual aerodynamic derivatives are adjusted in the simulator data bank to make the simulator and flight test coefficients match. A sample of the comparisons obtained for the pitch/roll coupling maneuver experienced on Flight 99 of F-111A Number 21 is presented in Figures 12 and 13. It is currently planned to conduct this type of analysis on all the flights conducted during the testing of BFTP-30. By using the regression techniques described above and the data obtained from the current flight test program, it is our intention to develop a high-angle-of-attack simulator that will be truly representative of the F-111 aircraft.

As a result of the aircraft lost because of stall/post-stall related accidents and the development of the high-angle-of-attack simulator, Convair has proposed a stall inhibitor system (SIS) for the F-111. The F-111 SPO has authorized development of two sets of flight test hardware, and a proposal has been submitted for flight testing. In general, the system contains an angle of attack limiter, a beta reducer, and an inertial coupling reducer. A simplified block diagram of the proposed SIS is shown in Figure 14.

The angle of attack limiter is designed so that the maximum angle of attack which the aircraft can obtain with full back elevator control is approximately 25 degrees. Since divergence angle of attack is approximately 28 degrees, the SIS is not limiting the useful angle of attack of the aircraft. The beta reducer function of the SIS was added since both lateral control and directional stability are minimal at high angles of attack. The beta reducer function essentially stiffens the aircraft by use of a rudder aileron interconnect (ARI) and by feeding rudder to oppose stability axis yaw rate. The ARI also helps coordinate rolling maneuvers at high angles of attack. The inertial coupling reducer was added as a result of the coupling encountered on Flight 99 of F-111A Number 21. Essentially, the inertial coupling reducer feeds back rudder as a function of pitch and roll rate to reduce the sideslip which keeps the system coupled. Although the proposed SIS does not prevent the aircraft from being intentionally stalled, it provides protection from inadvertent entries. If the aircraft is stalled with the SIS operating, the pilot must want to stall the aircraft.

### 3. CONCLUSIONS

#### 3.1 Vertical Tunnel Tests

On the basis of the results obtained from the vertical tunnel, it is felt that use of this type of testing should be limited in scope. It appears that the usefulness of this data is limited to predicting possible spin modes, recovery controls and recovery parachute system sizing. Use of the data to determine the susceptibility of an aircraft to enter the spin modes is not within the current state-of-the-art.

#### 3.2 Free Flight Tests

This type of testing is an excellent method of determining the angle of attack at which yaw divergence can be expected. Although the data obtained from the free flight model may tend to be conservative, it is excellent information upon which to base flight test angle-of-attack

limits. The main drawback is the low Reynolds and Mach number of the tests and the inability to examine anything but departure characteristics.

### 3.3 Radio-Controlled Drop Model Tests

The advantages of this type of testing over the vertical and free flight testing techniques are obvious. Not only does it provide information on departure characteristics, but it also allows examination of the post-stall and spin susceptibility characteristics. The basic drawback is the low Mach and Reynolds number conditions at which the data is obtained. Use of the F-111 drop model data has been limited to determining trends since no attempt was made to obtain aerodynamic data from which to make full-scale predictions. Use of this type of model test to obtain aerodynamic data for application in a prediction technique would be of tremendous value.

### 3.4 Static Force Model Tests

Static force and dynamic derivative data is a very important part of any stall/post-stall/spin investigation program. Without this type of data it is almost impossible to examine the individual effect of each aerodynamic derivative on the stall/post-stall/spin characteristics of the aircraft. The static force and dynamic derivative data obtained on the F-111 were very minimal and were obtained at low Mach numbers. It is also believed that the data were obtained at Reynolds numbers below the critical fuselage value. The actual flight test time histories of maneuvers could not be duplicated by using the force and dynamic data available on the F-111 in the high-angle-of-attack simulator. To date, it is not known if this inability to match flight test data is due to Mach, Reynolds number, or other effects. It is felt that a program should be initiated to resolve this dilemma.

### 3.5 Flight Test

The flight test program for stall/post-stall/spin investigation of an aircraft should be one in which the emphasis is placed on stall/post-stall recovery procedures and spin susceptibility. If a spin susceptible area is found, the spin recovery characteristics should be evaluated. The extent to which this investigation should be pursued would depend on the mission requirements for the aircraft. It is believed that the new spin demonstration MIL Specification (MIL-S-83691) represents an attempt to provide the procedures necessary for identifying aircraft stall/post-stall/spin characteristics. The main drawback to the new specification is that the contractor must assume that he will have to perform all phases of the testing required and bid it accordingly. Consequently, the cost of the program is maximized.

### 3.6 Analytical Programs

As a result of the work done on both the B-58 and F-111 aircraft, it is our opinion that aircraft stall/post-stall/spin characteristics can be predicted by means of analytical programs. It is also our feeling that they should be used more and more to reduce the costs and hazards normally required to determine and demonstrate the stall/post-stall/spin characteristics of an aircraft. This opinion is based on the fact that aerodynamic data can be extracted from either flight or drop model tests.

### 3.7 Recommendations for Future Programs

In view of the experience gained during the B-58 and F-111 programs, it is our opinion that future programs directed to the determination of stall/post-stall/spin characteristics should be conducted as follows:

1. Obtain a baseline data bank for use in a six-degree-of-freedom simulation. Data should consist of high-angle-of-attack force and dynamic data obtained at high Reynolds number over the expected entry Mach range.
2. Conduct drop model tests with a model instrumented well enough to permit use of regression techniques to obtain total aerodynamic coefficients. If the model could be dropped at higher "q" conditions, the quality of the data would be improved. Compare total aerodynamic coefficients of model and simulation data and use the resulting data to update the aerodynamic data bank.
3. Conduct a limited flight test program to obtain sufficient data to update the simulation data bank. Aerodynamic data would be updated by using the same regression techniques as those used on model data.
4. Use simulation to determine areas where aircraft is most susceptible to stall/post-stall/spin entries and subsequently demonstrate the characteristics of interest by flight test in these areas.

## POST-STALL AERODYNAMICS OF THE "HARRIER" GR1

Cliff. L. Bore

Assistant Head of Research,  
Hawker Siddeley Aviation Limited,  
Kingston, Surrey, England

### SUMMARY

The wing of the HS. "Harrier" GR1 had to achieve high usable lift coefficients during manoeuvring at subsonic speeds, without incurring a weight penalty for leading edge devices. It was designed so that, after buffet onset, the areas of boundary layer separation spread steadily and symmetrically as incidence increases.

Planform sections and twist were designed with this objective, and arrays of B. L. C. devices (such as vortex generators) were intended from the start. Arrays of fences and vortex generators had important effects on maximum usable lift and post-buffet flight steadiness.

Since the developed configuration of this aircraft is free from post-buffet flying vices such as wing drop, wing rock or pitch-up, the maximum usable lift at moderate altitudes can be determined by the intensity of buffeting. The simple-minded method of buffet prediction outlined gives results which are consistent with flight measurements on several aircraft.

### PROBLEMES AERODYNAMIQUES CONSECUTIFS AU PHENOMENE DE DECROCHAGE SUR LE "HARRIER" GR1

### SOMMAIRE

Durant les manoeuvres aux vitesses subsoniques, la voilure du "Harrier" GR1 devait se caractériser par des coefficients de portance élevés sans faire appel à des dispositifs de bord d'attaque, lesquels entraîneraient une indésirable augmentation de poids. Elle était conçue de façon qu'après le début du buffeting, les zones de décollement de la couche limite se propagent d'une manière régulière et symétrique lorsque l'incidence augmente.

La forme en plan, les coupes et le vrillage étaient conçus dans ce but et les dispositifs de contrôle de la couche limite étaient envisagés dès le début. Cloisons et générateurs de tourbillons avaient une influence marquante sur la portance maximum disponible et la stabilité de vol consécutives au buffeting.

La configuration de l'avion qui fut mise au point ne se caractérise, après le buffeting, par aucun vice, tel que perte de portance, oscillation de la voilure ou cabrage. Aux moyennes altitudes, la portance maximum disponible peut être déterminée par l'intensité du buffeting. La simple méthode esquissée permet d'évaluer l'effet du buffeting et les résultats obtenus s'accordent avec les mesures faites sur plusieurs avions.

## 1. INTRODUCTION

In order to appreciate why the wing of the "Harrier" was designed that way it is necessary to understand the factors that determine the usefulness of the aircraft.

The essential function of the Harrier is to carry various external stores at high subsonic speed from a confined site, perform those manoeuvres necessary to deliver the load on target, and return to land on the confined site. Since the take-off and landing sites may be as small as a tennis court, the all-up weight of take-off is determined by the installed thrust. Then the total useful load of stores and fuel is given by the excess of the thrust over the basic weight of the aircraft. This was maximised by making the air intake efficiency very high and the basic weight of the aircraft very low.

We will see that the wing design was a very important factor in achieving high load and range capability. For example, if the total useful load were as much as one half of the basic weight, then a 1% reduction of basic weight would permit 2% increase of stores-plus-fuel. If this were used for extra fuel the range might be increased by about 3%, while if used for store load this would be worth perhaps 6% more load. Due to the cumulative effects of resizing an aircraft during the initial design stage, that final 1% weight saving could result from an initial reduction only one-third as large. In addition to the direct effects of weight, reducing wing area also reduces drag, fuel requirements and so on. Thus we see that the primary aim of the wing design was to reduce the weight and size as much as possible, consistent with providing the required flying qualities.

Now the fundamental advantage of the vectored-thrust aircraft is the fact that it is freed from the conventional aircraft's penalty of a heavy wing and flap system for take-off. Even if the aircraft is heavily over-loaded and has available a conventional runway, it is more efficient to vector the thrust at take-off so that only a small fraction of the weight has to be lifted by the wing. So the size of the wing can be reduced until it is just sufficient to provide the manoeuvrability required at combat conditions. This clearly indicates the design problem: how to achieve the required usable manoeuvrability from the lightest and smallest wing? The more important conditions involved Mach numbers from 0.6 to about 0.9, at high altitudes.

## 2. WING DESIGN

Obviously this aim calls for a combination of high structural efficiency and high usable lift coefficient. Now most of the wing weight is concentrated near the wing root: indeed, on aircraft with proportions similar to the Harrier, much of the weight is in the part that crosses the fuselage. Therefore, the wing was given a large root chord and fairly large thickness/chord ratio at the root. Both the chord and the thickness/chord ratio were reduced sharply towards the tips - where the aerodynamics is more crucial. Thus we had high structural efficiency where the weight was concentrated, and slim sections where the aerodynamics problems dominated.

The planform had been chosen to provide a high maximum usable lift coefficient for the chosen sweepback, according to the indications of ref. 1. These choices of thickness taper and basic planform had been worked out for the previous aircraft - the "Kestrel", but the Kestrel's wing was not good enough for the Harrier. There would be 10% more weight to be manoeuvred, and the extra external stores would reduce the pitching stability. More serious, the Kestrel indulged in "wing rocking" without warning at Mach numbers between about 0.7 and 0.9, at lift coefficients where otherwise light buffet might be expected. The pilots did not like being rocked suddenly by up to  $\pm 25^\circ$ , so in effect they restricted their manoeuvres well below the buffet boundary. Despite these deficiencies, the Kestrel's wing provided quite good usable lift coefficients in the combat speed range.

Now the Harrier had to be in service quickly and with minimum expense, so there was the usual designer's brief: improve it all without changing anything (as far as possible). However, it was considered that all the improvements needed could be provided without changing the front spar or any structure aft of that. To improve the stability an extended wingtip would be provided. To increase the usable lift coefficient and eliminate the unheralded wing rocking, the shape forward of the front spar would be redesigned in accordance with a new philosophy that already had been partly developed (for the P.1154 - which had just been cancelled). Fig. 1 shows the extent of the alterations that were made from the planform of the Kestrel.



The wingtip extension moved the aerodynamic centre the right amount aft, so that solved the pitching stability problem. In the process the section shapes were redesigned so that supercritical flow could develop over the curved tip without shocks. We will see later that these wingtips do not stall.

It was decided to base the redesigned leading portion of the wing on the supercritical aerofoil sections that had been developed earlier for the P.1154. These aerofoils were able to produce supercritical flow over the front half of the chord, terminated by shock waves of modest strength. These sections would provide more lift at combat speeds before the boundary layer started separating, - but the Harrier was to be flown without restrictions to incidences far beyond buffet onset - so the remaining problem was how to achieve the highest possible usable lift beyond buffet onset.

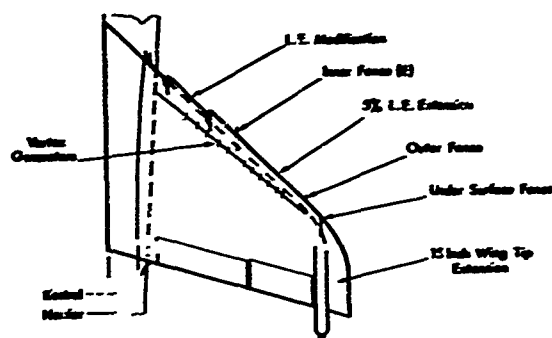


Fig. 1 Planform of Harrier Wing

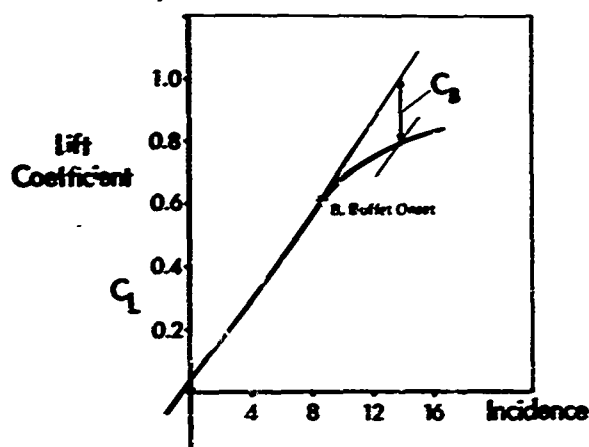


Fig. 2 Buffet Relationship

### 3. DESIGN FOR POST-STALL MANOEUVRABILITY

#### 3.1 Buffet

On the wings of this sort of planform, the lift curve may continue to rise with incidence beyond the point at which boundary layer separation starts (point B, in fig. 2). It has been shown (refs. 2, 3) at least for the five types of strike/fighter aircraft investigated so far that the coefficient of buffeting force can be taken as approximately proportional to the decrement  $C_B$  shown. If we postulate that buffet response is to be measured by the peak accelerations ( $B.g$ ) suffered by the mass of the aircraft responding to the unsteady aerodynamic force, we can estimate the expected intensity of "buffet" response from the simple formula:

$$B = KC_B / \left( \frac{W}{qS} \right) \quad \dots \dots \dots (1)$$

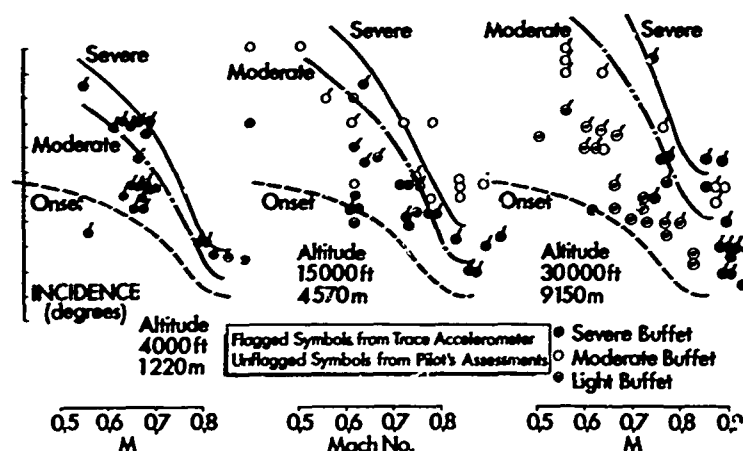


Fig. 3 Flight Buffet vs Predictions  
(Aircraft A, incidence)

where  $W$  is the aircraft weight,  $S$  is wing area,  $q$  is dynamic pressure and  $K = 1$  has been found satisfactory for the constant of proportionality.

Since given buffeting force requires larger buffeting coefficient at higher altitudes, it follows that there can be a substantial altitude effect, such that considerably higher normal force coefficients may be attained at high altitudes before given intensity of buffeting response is reached. Since the usual flying vices (such as wing drop, pitch-up and wing rocking) set in at particular incidences, whereas buffeting limits rise with altitude, it may happen that buffeting limits manoeuvrability at low altitude, but other vices may supervene at high altitudes.

Figs. 3, 4 and 5 illustrate typical comparisons of predicted buffet boundaries with flight test data. On fig. 3 can be seen data from analyses of the amplitude of normal vibration from trace accelerometers, together with pilots' assessments of buffet severity. It can be seen that the agreement is as satisfactory as can be expected at the present stage of flight buffet measurements. Perhaps the most notable feature of fig. 3 is that the measured altitude effect is greater than the considerable effect predicted. The measured vibration was greater than predicted at low altitude, but less at high altitude. Perhaps this may be connected with atmospheric turbulence, which varies in the right direction. Whatever else may be said, those flight data certainly do not contradict the theoretical concept of a substantial altitude effect.

The peak acceleration criteria used for various degrees of buffeting were as follows:-

onset: negligible, corresponds with point B of fig. 2.	
light (just perceptible):	$\pm 0.2g$
moderate:	$\pm 0.6g$
severe (tolerable for only a short time):	$\pm 1.0g$

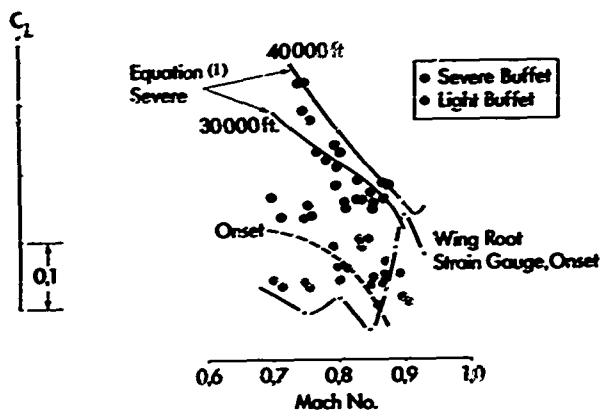


Fig. 4 Flight Buffet vs Predictions  
(Aircraft B)

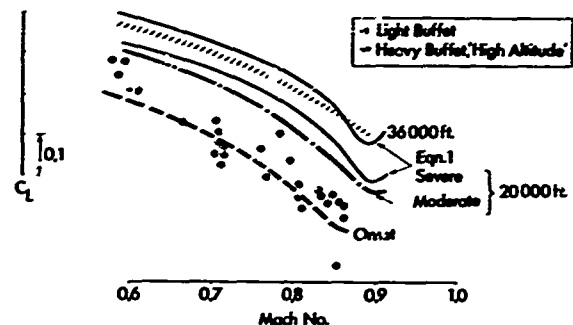


Fig. 5 Flight Buffet vs Predictions  
(Aircraft C)

### 3.2 Post-Stall Flying Characteristics

We have seen that aircraft with high wing loadings will not be limited by buffeting until the lift curve has bent substantially below the extrapolated linear portion of that curve. In other words, they can be flown to lift coefficients well above buffet onset, provided that the lift curve continues to rise with incidence, and provided all the usual post-stall flying vices are avoided. Raising the lift curve and eliminating the vices proved to be an interesting piece of applied research, - especially as it had to be completed quickly.

Now if the lift curve continues to rise steeply above the buffet - onset point, this implies that the stall spreads only slowly over the wing as incidence increases (here the word "stall" is a short term for "boundary layer separation"). Furthermore it was believed that the post-buffet flying vices are associated with sudden "chunks" of stall spread: if stall spreading could be made slow, smooth and symmetrical, there need be no flying vices other than a gradual increase of buffeting with lift.

It was chosen to design for stall to start near the tip and spread inboard. There are several factors that make the wing root more reluctant to stall - not least the lower local lift coefficients at the root of the tapered wing. This would make it easier to achieve progressive stall, and also permit more maximum lift. When lift is lost on the outer part of the swept wing, the pitching stability would be reduced, but eventually, as stall spreads towards the wing root, the stability would increase strongly - as in effect the centre of lift of each stalled section moves aft to around half chord. This was considered a better stability variation than given by the opposite progression of stall - which would give strong stability at the start of buffet penetration, falling off rapidly as the manoeuvre is tightened. So the inward spread of stall was preferred from three aspects: higher maximum lift, an easier technical task, and preferred stability variation. These expectations have been realised in flight.

As it was known that stall would start forward of mid-chord the front parts of the aerofoil profiles were varied so that the outer sections were more adverse than inner sections. At manoeuvring conditions, these sections were always working supercritically, so the experimental two-dimensional pressure distributions as applied to the tapered wing were used to guide the design. Wings with this type of section gradation had been tested earlier for the P.1154, and it was known that such variations alone could not provide the smoothness of stall progression required. An array of boundary layer control devices was intended from the outset. The experimental research was concerned largely with this array of devices.

### 3.3 Experimental Development

The wind tunnel tests were made on a 1/10th scale model of the Harrier GR1 in the Aircraft Research Association 9ft x 8 ft (2.75m x 2.45m) transonic tunnel. Flight development was started early, by modifying a Kestrel wing to the basic Harrier shape, and flying it on a Kestrel fuselage. Thus some of the crucial points were tested in the wind tunnel and in flight at the same time. All tests were performed with two 100 gallon (454 litre) drop tanks in place.

Rolling moments were monitored with on-line continuous pen recorders. This proved to be a very valuable technique, for it was found that flight behaviour correlated well with the rolling-moment records. For example, if the pen oscillated continuously (e.g. between the dotted curves in fig. 6) then the aircraft experienced wing rocking, - whereas a steady excursion of rolling moment corresponded with "wing low" in flight.

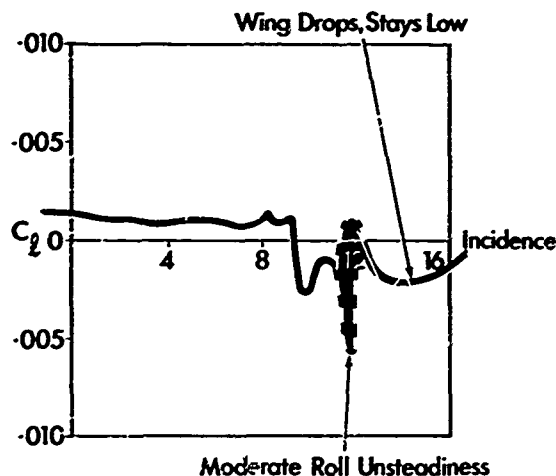


Fig. 6 Roll Unsteadiness

Oil flow investigations were used extensively to examine the stall patterns. These were observed continuously by closed-circuit TV and photographed by remote control.

Initial tests on a bare wing showed that the roll unsteadiness was far better than for the Kestrel wing, but below the standard aimed at - as there was a moderate wing drop at  $M = 0.88$ . Effects of sawtooth position were checked.

The vortex generator arrays were all of the type first proposed in ref. 4. They were scaled in size and spacing in proportion to the boundary layer thickness, so that effectiveness is maintained across the span. They were mounted almost along free stream direction so that at low aircraft lift there was little drag, but at high lift coefficients the local airflow turns inboard and approaches the vortex generators at a substantial local incidence. This causes stronger vortices as the aircraft lift increases. An innovation for the Harrier application was the scheme of increasing the local incidence of successive vortex generators, proceeding inboard. One such array succeeded in controlling the spread of shock-induced separation at  $M = 0.88$  (fig. 7). It can be seen that the separation spread over far less of the outer panel when the vortex generators were present.

A small leading edge fence alone on the outer panel raised the lift curve at Mach numbers from 0.4 to 0.7, but without improving the steadiness in roll (fig. 8). If the fence was moved far, this extra lift was lost.

A major step forward was combining vortex generators with a fence, for the combined effect was better than the sum of the individual effects. The lift increase at the lower Mach numbers was kept and the delay of roll unsteadiness, at the reduced levels already shown in fig. 6.

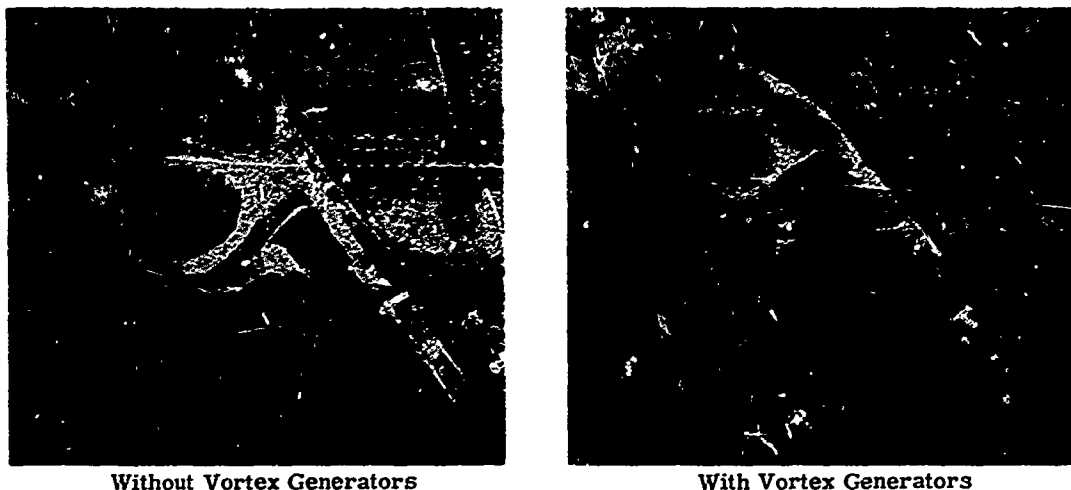


Fig. 7 Effect of Vortex Generators on spread of B. L. separation

A small fence below the wing tip eliminated a wing-low effect at  $M = 0.6$ , and prevented stalling of the curved tip at any conditions.

By this stage of the wind tunnel research, the flight tests had checked most of the important results and confirmed them, apart from an elusive difference of pitching stability - which was probably due to jet efflux interference in flight. Flight tests with a wide range of fence sizes showed a sharply-peaked optimum size, so far as maximum usable lift was concerned, and they suggested a substantial Reynolds number effect.

Important advances were made when two fences were tried. The wind tunnel showed a sharp deterioration of roll steadiness, but the flight tests showed a marked improvement! It was suspected that again there was a scale effect such that the inter-fence spacing should be related to the wing boundary layer thickness. Further testing showed that this inter-fence spacing had a critical effect on the post-stall roll steadiness. When the fences were too close, the wing rocking was unacceptable (A, fig. 9) but when they were well spaced the roll steadiness was excellent (B, fig. 9). The maximum lift also was improved (fig. 8). It was also found that fence positions influenced the maximum usable lift appreciably, for given inter-fence spacing (fig. 10).

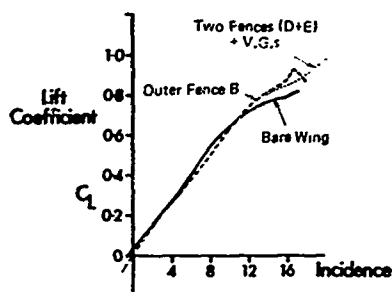


Fig. 8 Effects of Fences

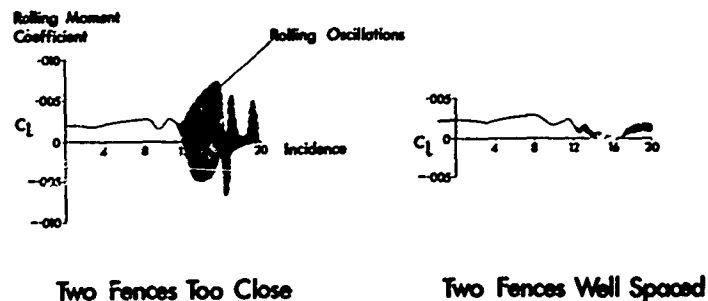


Fig. 9 Roll unsteadiness with Two Fences

By this stage, maximum usable lift was far above buffet onset, on a lift curve that was flattening off at high incidences. This was due to stall spreading rapidly over the inner wing at the highest incidences. The inner wing was therefore provided with a new graded leading edge, to raise the top end of the lift curve and improve roll steadiness at the highest incidences. This also permitted about  $10^\circ$  of flap deflection for high speed manoeuvring.

In the final configuration, the Harrier GR1 can be manoeuvred safely to 'stick hard back' or the structural limits with no fear at any conditions of losing control or entering any gyrations. Near maximum lift, directional stability reduces, of course, and a "wallowing" motion can develop if conditions are held. Buffet can be penetrated progressively without suffering pitch-up, wing drop or wing low - although moderate wing rocking can occur near "moderate buffet" conditions, which dies out before maximum lift.

The maximum usable manoeuvring acceleration per unit area of wing is compared with several other aircraft in fig. 11, which shows data for two U.S. fighters and four other British strike/fighters. It can be seen that the maximum usable lift coefficient exceeds all the others for which data were available at Mach numbers above 0.7.

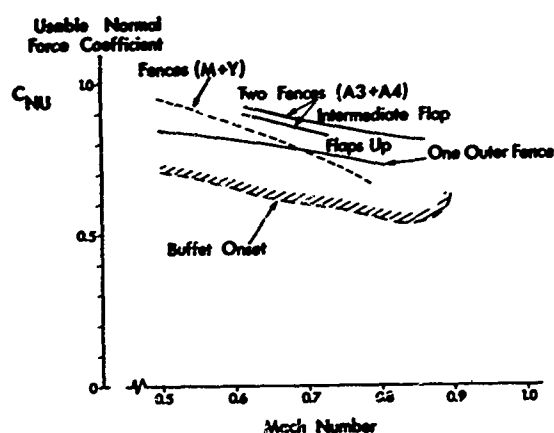


Fig. 10 Typical Usable Normal Force Coefficients

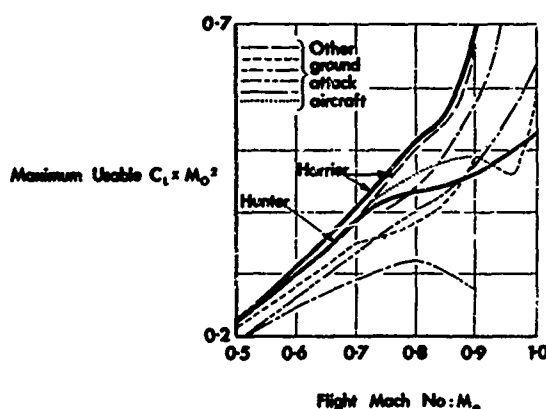


Fig. 11 Usable Manoeuvrability Coefficients

These developments resulted in achievement of a high - g wing that weighed only 6 lb/square foot (30 kg/m<sup>2</sup>). To put this into perspective, the Harrier and the Hunter have similar all-up weights, but the wing of the Harrier weighs roughly 1 ton (1 tonne) less than the wing of the Hunter. This represents about 17% reduction of basic weight, compared with the Hunter (see fig. 12).

In the course of this work, knowledge was gained on such topics as optimum arrays of fences and vortex generators, sawteeth, buffet prediction, and the application of supercritical aerofoils to swept wings - including curved tips. Most important, perhaps, was the demonstration of a design for safe and steady post-stall flying characteristics at all attainable conditions.

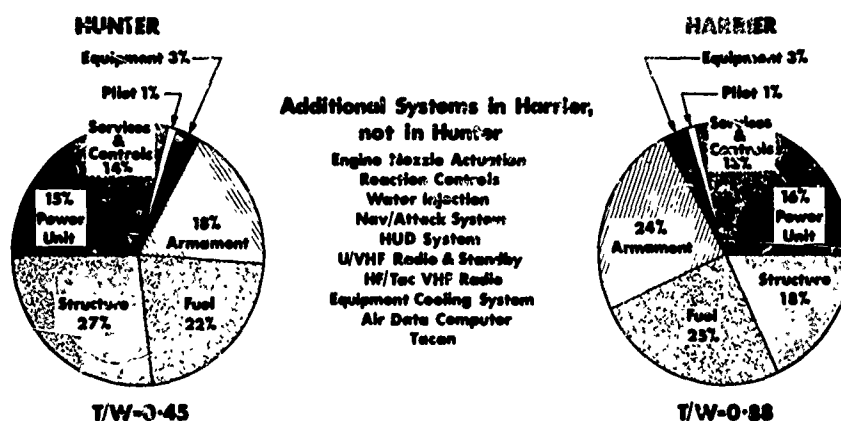


Fig. 12 Take-off Weight Breakdown

#### 4. REFERENCES

1. C. L. Bore & A. T. Boyd      Estimation of maximum lift of swept wings at low Mach numbers. J. R. Ae. S. April 1963.
2. C. L. Bore      A new method for estimating buffet boundaries from wind tunnel data. HSA KIN PON 981 January 1966.
3. C. L. Bore & R. F. Baker      Buffet prediction from wind tunnel data: flight checks on three aircraft. HSA KIN PON 1418 March 1969.
4. C. L. Bore      On the tapered array of vortex generators. HSA KIN PON 616 November 1962.

## AERODYNAMICS OF WING STALL OF THE FOKKER F28

by

Tj. Schuringa  
Aerodynamics Department  
"Fokker-VFW" NV  
Schiphol-Oost  
The Netherlands

## SUMMARY

Some topics of the aerodynamic development of the F28 wing with regard to the stall are described. First, the investigation in the wind tunnel is reported, dealing with the influence of boundary layer fences, secondly the correlation with flight tests is presented. It may be concluded that, apart from minor modifications, satisfactory agreement was found between wind tunnel and flight test results.

## NOTATION

$c$  - wing chord  
CG - centre of gravity, % mean aerodynamic chord  
 $C_L$  - lift coefficient  
 $C_{Lmax}$  - maximum  $C_L$   
 $C_m$  - pitching moment coefficient  
 $Re$  - Reynolds number  
 $V$  - speed  
 $V_s$  - stalling speed  
 $\alpha$  - angle of attack

## INTRODUCTION

The F28 Fellowship aircraft has been developed by Fokker for use over short to medium distances. It can accommodate up to 65 passengers in the standard configuration, while a stretched version will provide an additional 15 seats; the latter is at present in the process of certification. In figure 1 the features of the standard F28 are shown.

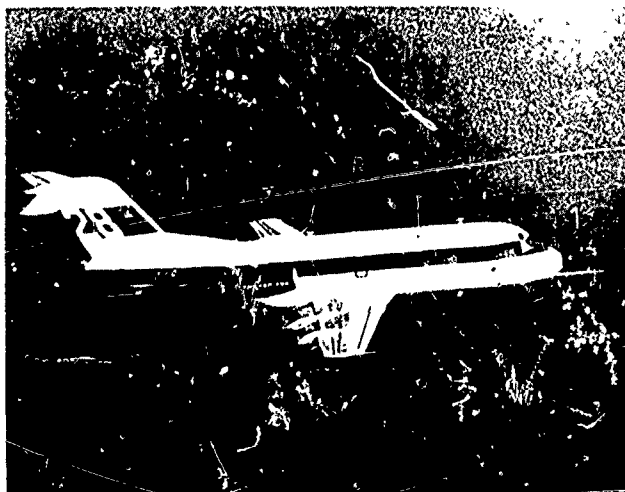


Fig. 1 F28 first prototype aircraft.

As a consequence of the short haul character much attention was paid during the design to attain optimum airfield performance and low speed handling qualities. On the other hand jet operations required the wing to be designed for acceptable transonic characteristics.

A major design goal was the achievement of relatively high values of  $C_{Lmax}$ . This required a compromise solution with limited sweep angle of the wing, in combination with a wing geometry suitable for the speed regime of cruise and dive.

The maximum operating Mach number being  $M_{MO} = 0.75$ , the dive Mach number  $M_D = 0.83$ .

The preliminary design phase was characterized by wind tunnel investigations to establish the optimum wing planform as determined by the two main design objectives just mentioned. In this process about 1000 hours were spent in the NLR tunnels in Amsterdam on testing models of the complete aircraft. Four different basic wing configurations, designed for the same

cruise Mach number and covering a range of thickness ratios and sweep angles, were tested. Each basic wing configuration then was tested with detail modifications in geometry. A picture of a model with the final wing configuration is shown in figure 2.

The F28 wing has a  $16^\circ$  sweep angle at the quarter chord line; its wing sections are modified NACA four digit series sections with rather large nose radii primarily to improve section maximum lift. The maximum lift capabilities of the wing are further increased by a Fowler type flap which is single slotted at settings up to 18 degrees and double slotted at the larger settings, when the vane becomes ineffective after the flap has expanded to form the second slot.

In view of the significance of single engine take-off performance of the two-engined civil aircraft, the flap design was optimised for low drag at all single slotted take-off positions. The increment in maximum lift is approximately 1.0 at the landing flap setting, for which 42 degrees deflection is used. Wing sections and the flap shape evolved from extensive two-dimensional wind tunnel testing.

In relation to stall behaviour of aircraft the correlation between final wind tunnel results and flight results is one of the most speculative and also intriguing elements of the initial flight test phase. Very limited degrees of freedom exist for the aircraft designer to change the characteristics in this phase of development. On the F28 wind tunnel results were available at  $2.8 \times 10^6$  Reynolds number for a complete aircraft model and at  $5 \times 10^6$  for a half wing model. This paper reports on the characteristics achieved, and on the correlation with full scale test results.

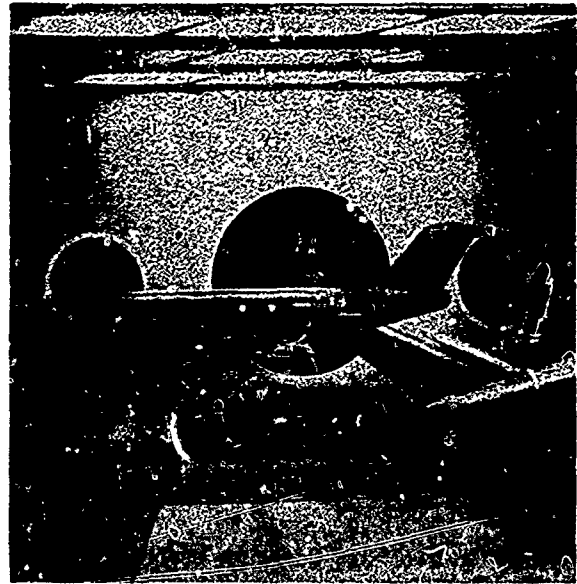


Fig. 2 Final F28 wind tunnel model

#### INVESTIGATION OF THE STALL IN THE WIND TUNNEL

As already mentioned earlier, attaining high values of  $C_{L_{max}}$  was an important design objective for the F28. The associated stall characteristics should however also satisfy the civil airworthiness requirements, which ask for easy recognition by the pilot of the developing stalled wing condition and for gentle behaviour of the aircraft in the stall to avoid large attitude changes and consequently great losses in height. In a flight simulator programme, which was used to convert wind tunnel characteristics into pilot assessed full scale behaviour, it was recognized that an unmistakable nose down pitching motion at or near the stall would provide satisfactory results. This was particularly the case because of the reduced longitudinal stability, which had to be expected for angles of incidence beyond the stall for T-tailed aircraft.

Figure 3 shows the relationship between pitching moment and angle of attack as obtained in the final stage of wind tunnel testing. It can be noticed, that immediately beyond the angle for maximum lift a sharp increase in nose down pitching moment appears.

The clean wing stall was characterized by a rapid spanwise spread of separation. The result on figure 3 was obtained by controlling the location of initial flow separation on the wing by use of a small boundary layer fence near the wing leading edge. Further details of this effect will be shown later.

Figure 3 also shows the characteristic variation of the pitching moment at extreme angles of attack for an aircraft equipped with a T-tail, which is caused by the immersion of the horizontal stabilizer into the wing wake. When the model size is small enough relative to the dimensions of the test section of the tunnel, scale effects are negligible in conditions of separated flow over the full wing span. Pitching moment data at these large angles of attack, as obtained in the wind tunnel, are therefore valid for the full scale aircraft. A typical picture of the investigation at extreme angles of incidence is shown in figure 4.

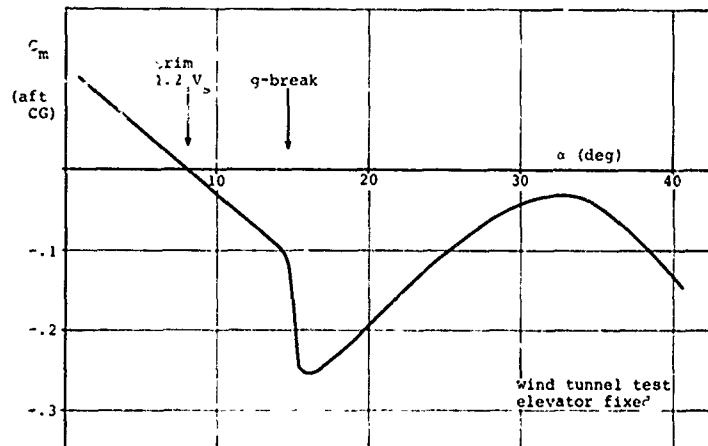


Fig. 3 F28 pitching moment characteristics

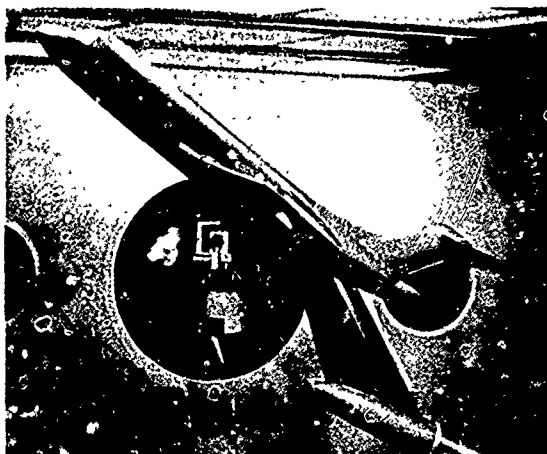


Fig. 4 F28 wind tunnel model at extreme angle of incidence

The desired increase of the nose down pitching moment near maximum lift can be obtained by initial flow separation on the inner wing, which causes a favourable change of the downwash field at the horizontal stabilizer. Apart from this effect flow separation on the inner wing also results in retention of full lateral control up to angles of attack at which the flow on the outer wing separates. There is however one restriction relative to early flow separation for the case of the F28 as distortion of the engine intake flow should be avoided up to stall onset. This implies that the wing sector immediately in front of the engines should preferably stall at an incidence angle beyond maximum lift.

In the wind tunnel phase many aerodynamic gadgets were tried out to probe possibly satisfactory configurations in full scale testing. The small boundary layer fence was the most promising in relation to high maximum lift in combination with the desired characteristics.

Figure 5 shows the model used for high Reynolds number stall flow visualization.

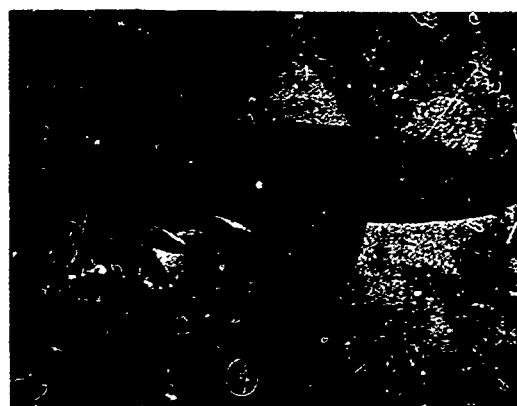


Fig. 5 Half wing wind tunnel model

A number of boundary layer fence sizes tried at one wing section (station 4700) is shown in figure 6. The intention of this survey was to obtain a minimum fence size for the desired characteristics. As it was realized that the effect of the fence, the local provocation of flow separation, was most pronounced at the leading edge. The short fence 3 in front of the suction area and fence 4 located aft of this area on the wing nose failed to produce any effect in stall behaviour. Fence 1 and 2 were almost equally effective.

The way in which the progression of flow separation is affected by the introduction of a boundary layer fence is depicted in figure 7. It can be observed that the small fence at the leading edge of station 4700 changes the stall progression of the F28 wing completely. Local separation is introduced at the inboard side of the fence at  $10^\circ$  angle of attack, the maximum lift is attained at approximately  $13^\circ$ , the aileron region stalls at  $19^\circ$ , while the wing without fence abruptly loses lift at  $15.7^\circ$  due to full span stall.

A very slight loss in lift accompanies the changed separation pattern.

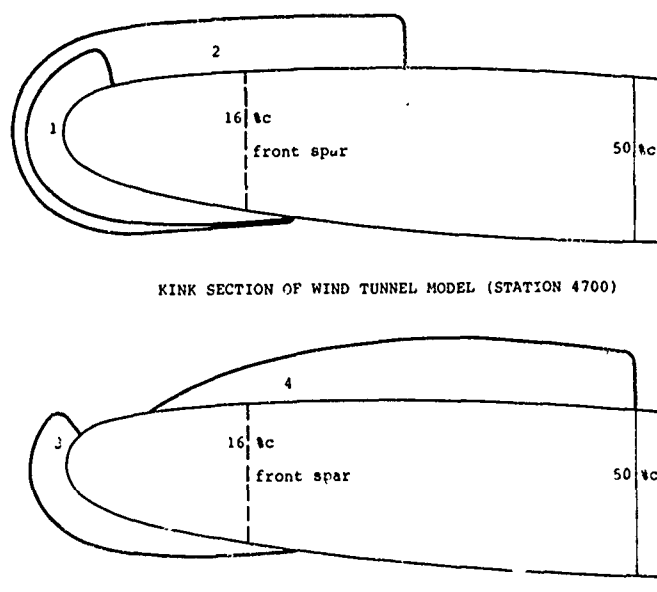


Fig. 6 Boundary layer fence sizes tested in wind tunnel

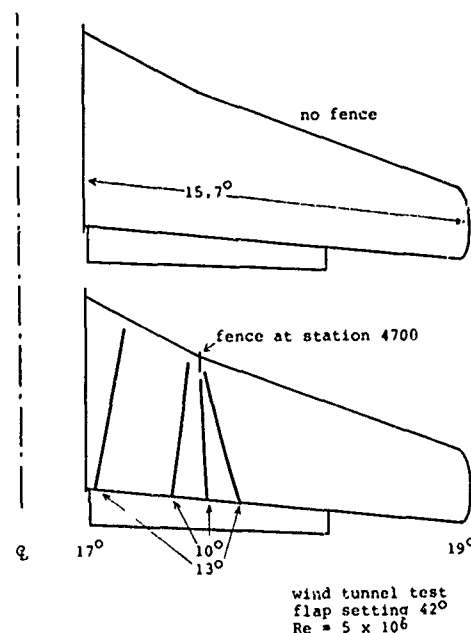


Fig. 7 Effect of fence on progression of flow separation

Figure 8 presents the influence of the spanwise location of one fence on the progression of flow separation. This progression is depicted by showing the angle of attack for onset of flow separation, for maximum lift and for separation in the aileron region. The identical characteristics at root and tip represent in fact the absence of the fence. The figure shows the result of tests on the wing with fully deflected flaps, being the most critical with respect to stalling behaviour. It can be concluded from the figure, that a small leading edge boundary layer fence in almost any position largely affects the progression of flow separation. The separation in the aileron region is thereby postponed to much larger angles of attack than without fence. This improvement is accompanied by a



slight loss in maximum lift as can be recognized from the smaller angle of attack for maximum lift. Pitching characteristics in the stall were only satisfactory for the inboard positions of the fence. The initial flight testing was therefore started with a fence at wing station 4700, the section at the kink in the leading edge of the wing.

Finally, it should be stated, that testing at extreme angles of attack in the wind tunnel revealed that a nose down pitching moment was obtained throughout the angle of attack range with the elevator deflected downward; this applies for all flap settings.

Fig. 8 Effect of spanwise fence location on progression of flow separation

#### FULL SCALE STALL INVESTIGATION

The stall tests with the fence at the 4700 wing station basically confirmed the characteristics observed in the wind tunnel. However, the initial buffeting which preceded the actual stall of the wing was quite strong, and affected adversely the obtainable maximum lift. Because of this observation it was decided to include in the flight test programme at least a number of alternative fence positions previously investigated in the wind tunnel.

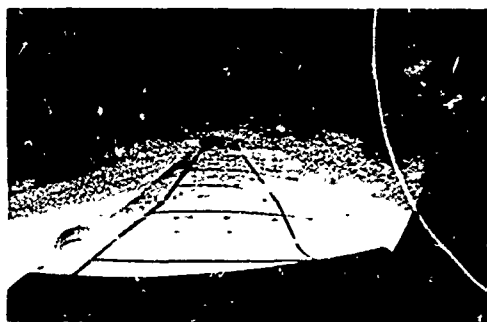


Fig. 9 Flow visualization on wing of prototype aircraft

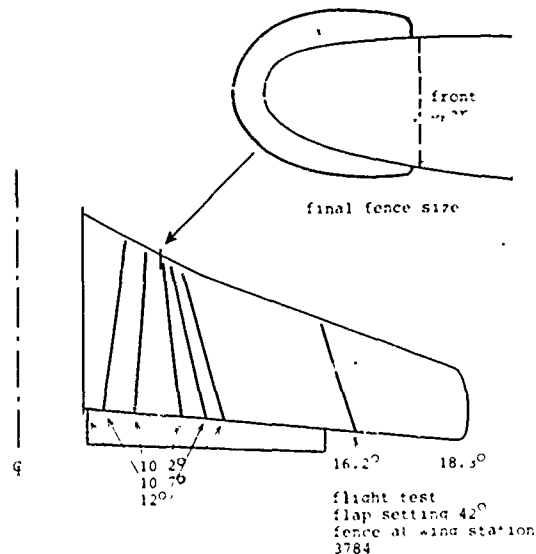
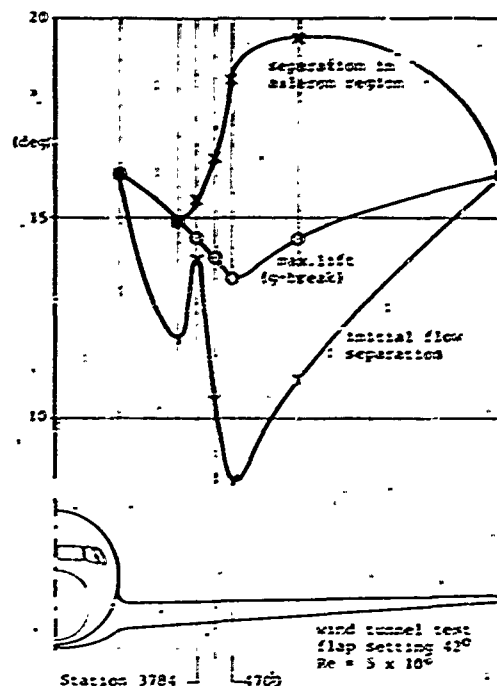


Fig. 10 Progression of flow separation on prototype aircraft



The qualities of the various arrangements were in the first instance judged by the testpilots; furthermore test recordings were available together with photographs of the tufted wing. The latter were obtained by a camera equipped with a 180° wide angle lens mounted in the escape hatch above the wing; a typical picture is shown in figure 9. From these pictures the progression of flow separation has been constructed, an example of which is given in figure 10, which also shows the shape of the fence.

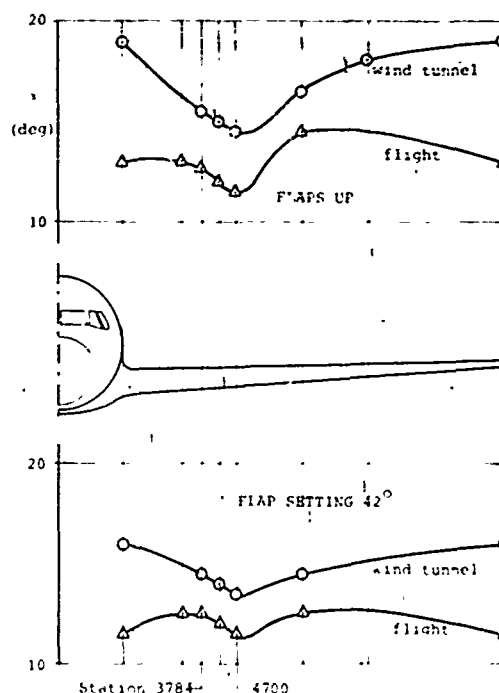


Fig. 11 Effect of spanwise fence location on angle of attack for maximum lift (g-break)

The lift capabilities are shown in figure 11, presenting the variation of angle of attack at maximum lift with fence position. The circles represent the maximum lift angle of attack of the wind tunnel model as already given in figure 8. It should be noted that the wind tunnel data stem from flow visualization tests on the half wing model; this implies that identical flow conditions on model and aircraft may occur at different indicated angles of attack. The effect of fence location is however quite comparable.

The flight tests showed that the optimum location of the fence is not wing station 4790 but 3 ft more inboard at station 3784, both from a point of view of obtainable maximum lift and overall stall characteristics.

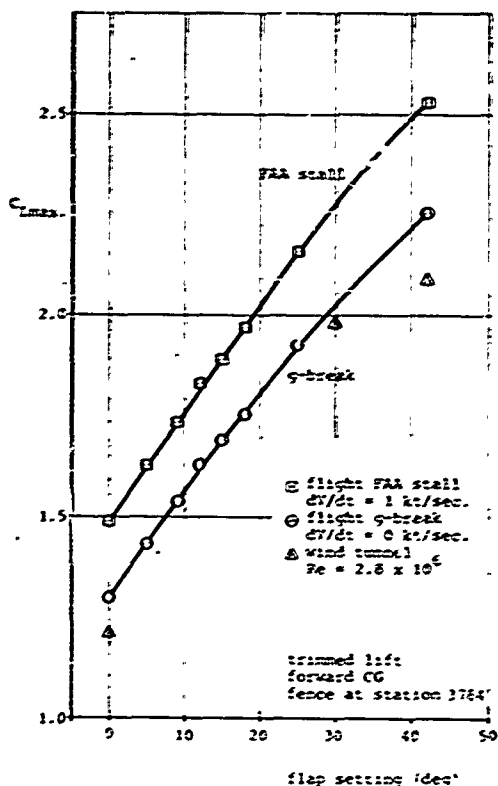


Fig. 12 Maximum lift capabilities of F28 wing

After the optimization of the fence location on the basis of comparative tests, the maximum lift values were determined. The results are presented in figure 12, compared to those of the wind tunnel model. The maximum lift is shown versus flap deflection for a forward centre of gravity position. The q-break lift values are those corrected to a speed bleed off rate of zero; the upper line represents the maximum lift calculated on the basis of the minimum speeds determined during certification trials, i.e. at a speed bleed off rate of 1 kt/sec.

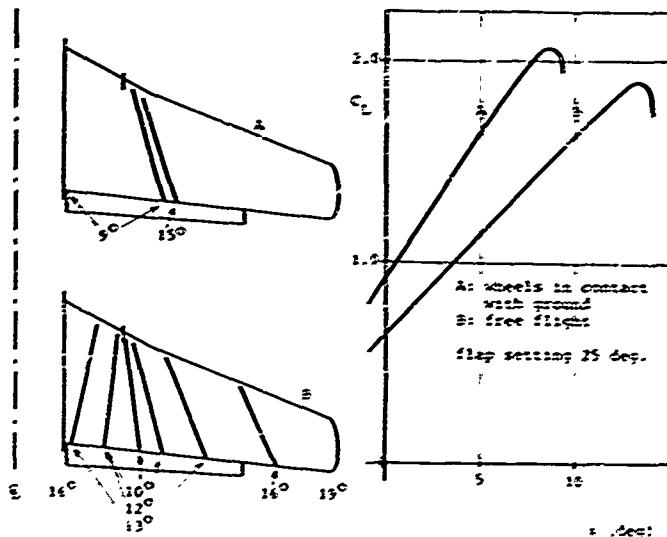


Fig. 13 Influence of ground proximity on wing stall

In addition to free flight stall conditions the effect of the vicinity of the ground on flow separation, especially in relation to the determination of the minimum unstick speed,  $V_{MU}$ , is important for civil aircraft.

In figure 13 free flight stall and the stall with wheels in contact with the ground are compared for a typical take-off flap setting. The stall progression in the ground proximity case is considerably different from free flight. On the F28 only the inboard wing can be stalled in ground effect. The maximum lift is unaffected and is reached at some 4 degrees smaller incidence angle. The F28 as a consequence is rather lift limited than drag limited in a  $V_{MU}$  condition.

#### CONCLUSION

Perfect correlation of wind tunnel and flight results could not be expected, however, by proper interpretation of results obtained in both areas satisfactory results could be achieved with limited amount of flight development testing. It may therefore be concluded, that the stall development on the F28 prototype aircraft, aimed at achievement of both high maximum lift values and satisfactory stall characteristics, was advanced to a high degree by extensive use of the wind tunnel.

#### ACKNOWLEDGMENTS

This paper came about thanks to the efforts of our test pilots who faithfully performed numerous stalls. Thanks are also due to colleagues, particularly professor Blom head of aerodynamics department, for their comments and assistance.

# PREDICTING THE LOW SPEED STALL CHARACTERISTICS OF THE BOEING 747

by

John K. Wimpers  
The Boeing Company

## SUMMARY

It is important to estimate accurately the stall speed of a modern high-speed transport since take-off and landing performance, which has a large impact on the airplane's economic success, is based on this parameter.

The pre-flight estimates for the Boeing 747 were based on wind tunnel data obtained at a Reynolds Number of approximately 1 million. These test results were adjusted to full scale flight values using correlation factors developed from other Boeing transport airplanes. As an independent check, high lift data were obtained in a pressurized wind tunnel up to a Reynolds Number of 7.5 million and extrapolated to the full scale value of 40 million.

Flight results show that the correlation factors were moderately successful in predicting stall speeds. Also, extrapolating the pressure tunnel data to full scale Reynolds Numbers predicted the flight value of maximum lift coefficient with reasonable accuracy.

The wind tunnel data at all Reynolds Numbers predicted satisfactory handling characteristics throughout the stall that were confirmed during flight testing.

## 1. INTRODUCTION

Modern jet transport airplanes normally fly at speeds well separated from their low speed stalls. There is no need for them to perform extreme maneuvers at low or moderate speeds or at high altitudes that might force them near their maximum lift coefficient. Only during take-off and landing, where the lowest possible speed is desired, does the stall become a matter of concern in the design. In these two critical phases of flight, the operational speeds must be such that adequate margin exists for atmospheric turbulence and piloting tolerance and that sufficient lift is available for necessary maneuvering. The magnitudes of these margins have been established through many years of experience and are defined, with but minor variations, by the various certifying agencies throughout the world, both military and civil. Usually, the operational speeds for take-off and landing are defined in terms of the stall speed of the airplane in the same configuration.

These operational speeds in turn define the useable take-off and landing field lengths of the airplane. The useable field lengths have a large impact on the economic usefulness of the transport, so much effort is exerted in making the operational speeds as low as possible. Thus, there is a desire to make the stall speed low and also to predict it accurately early in the design stages when the initial sales guarantees are being made. The initial predictions will be made several years before the airplane flies, and even the detail predictions for the final production configuration will be made some two years before the airplane is certified.

The importance of making the stall speed prediction accurately is demonstrated by considering the case where the airplane is designed to land with a full payload in exactly the field length available at its destination. In this case, an error of only 5 percent in predicting the stall speed will result in a 38 percent loss in payload capability and an even more dramatic 55 percent loss in the potential profit available to the operator on this particular mission.

The initial estimate of the stall speed of the 747 was made early in 1966 during negotiations with Pan American World Airways, the original buyer. These predictions were steadily refined during the design development of the airplane. Development of the low speed configuration involved some 4000 hours of wind tunnel testing over a period of 3-1/2 years. Many different detailed configurations were considered, but this paper will discuss only the final configuration selected for production and the methods used to predict its performance on the airplane.

The methods used to predict the full scale flight performance, starting from the wind tunnel data of the final configuration, were not particularly elegant from the standpoint of theoretical aerodynamics. They involved no detailed analysis of the boundary layer or effect of Reynolds Number on the various high-lift components. The approach used was one of practical engineering, limited in scope by the usual restrictions of time, people, and money. At the time the 747 was being developed, Boeing had already built and tested a series of jet transport having sweptback wings, different engine installations, and largely varying gross weights. This experience provided a great bank of flight data that could be correlated with the corresponding wind tunnel data as a function of configuration, center of gravity position, and wing

loading. These correlations served as the primary bridge between the wind tunnel data and the predicted full scale performance of the 747.

However, the 747 had a leading edge flap that was markedly different from those on other Boeing airplanes, and therefore, it was felt necessary to evaluate the effects of Reynolds Number on these leading-edge flaps. High Reynolds Number tests were made that extended the wind tunnel data from a Reynolds Number of approximately 1 million up to 7.5 million, based on the wing mean aerodynamic chord.

The flight test results shown in this paper are those obtained during the Federal Aviation Agency (FAA) certification of the 747. A total of 636 instrumented stalls were conducted to get stall speed data at all flap settings and gross weights and to completely evaluate the handling characteristics during the stall maneuver. A remote sensor of static pressure trailing behind the airplane was used for all air speed measurements. Accelerometers and rate and position gyros were used to establish the airplane motions, and a calibrated fuselage-mounted vane was used for measuring angle of attack.

This paper, in keeping with the subject of this meeting, emphasizes the prediction of only the stall speed portion of the low speed flight regime. It does not consider the equally important and more difficult task of predicting the low speed drag.

## 2. DESCRIPTION OF THE 747 HIGH LIFT SYSTEM

A diagram of the 747 high lift system is shown in Figure 1. The wing has an aspect ratio of 7 and is swept back  $37\frac{1}{2}$  degrees at the quarter chord. Both leading-edge and trailing-edge high lift devices are used. The leading-edge devices cover the entire span of the wing except for a small region next to the body. Inboard of the inboard nacelle is a flat Krueger flap with a rounded nose similar to that used on the 707. Between the nacelles, and outboard of the outboard nacelle, the Krueger flap is more sophisticated. As the flap is extended, a mechanical linkage bends the skin to form a continuous curve throughout its length. Also, the flap moves far enough forward to create a slot between it and the wing leading edge. This installation was the first time such a curved, slotted, Krueger flap had been used on a Boeing airplane.

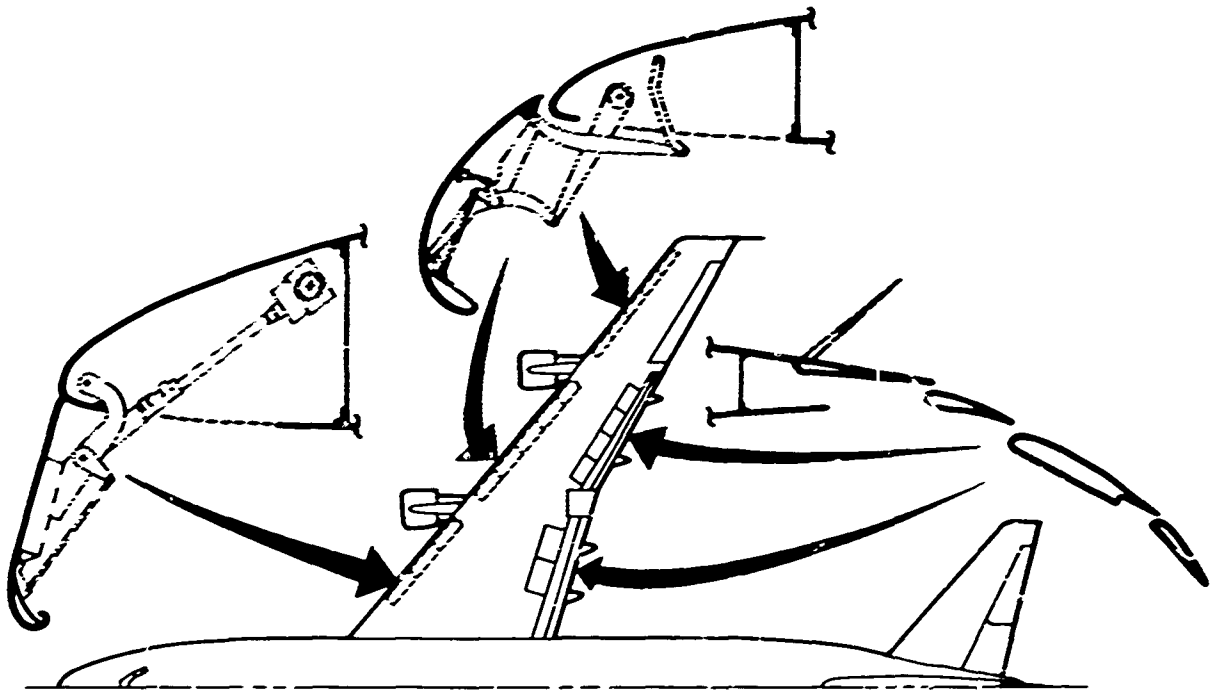


FIGURE 1: 747 HIGH LIFT SYSTEM

The trailing-edge flaps extend from the body to approximately 70 percent of the span. The flap is divided into two major components separated to allow clearances for the jet efflux of the inboard engine. This space on the trailing edge is used for the inboard high-speed aileron. The trailing-edge system is triple-slotted, similar to that used on the 727 and 737, but tailored to the long-range mission of the 747. For take-off, the flap setting, as measured by the angle of the mid-segment, varies between 10 and 20 degrees, depending on take-off weight. The motion includes a great deal of Fowler action before much angular deflection occurs. For landing, the flap is extended to its full 33 degree deflection.\* The various settings were selected after consideration of both the lift and drag, and the corresponding effects on field length performance, post-take-off climb, and go-around after a refused landing.

\*Called "position 30" in the flight handbook

### 3. THE BASIC WIND TUNNEL DATA

The basic low-speed wind tunnel data were obtained in the University of Washington Aeronautical Laboratory wind tunnel, which has an 8 foot by 12 foot closed test section vented to the atmosphere. The model, shown in Figure 2, was a .04 scale replica of the 747 having a wing span of approximately 8 feet. This model duplicated carefully all the flap supports and fairings as well as all the contours, gaps, and slots that exist on the actual production airplane. Particular care was taken, since our experience has shown that many of the discrepancies between wind tunnel and flight, often blamed on scale effects, are in fact caused by an inadequate representation of the details of the flight configuration by the wind tunnel model. The data for representing the airplane flying near to the ground were obtained using a fixed ground plane.

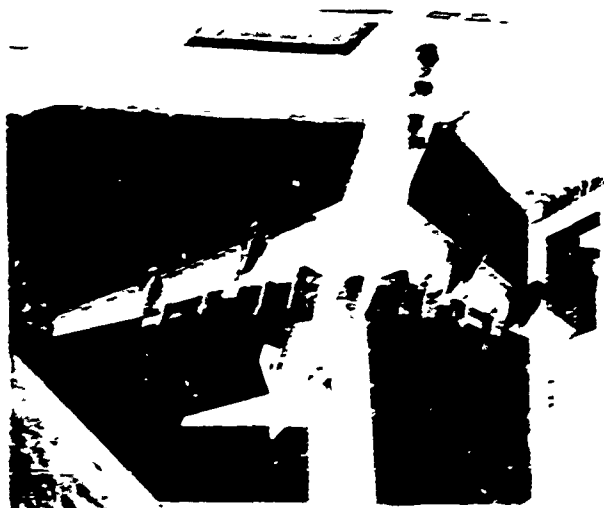


FIGURE 2: 747 HIGH LIFT WIND TUNNEL MODEL

An example of the data obtained from this model is shown in Figure 3. Normal wall and blockage corrections have been applied. Data is shown for a landing flap configuration of 33 degrees and a typical take-off position of 20 degrees.

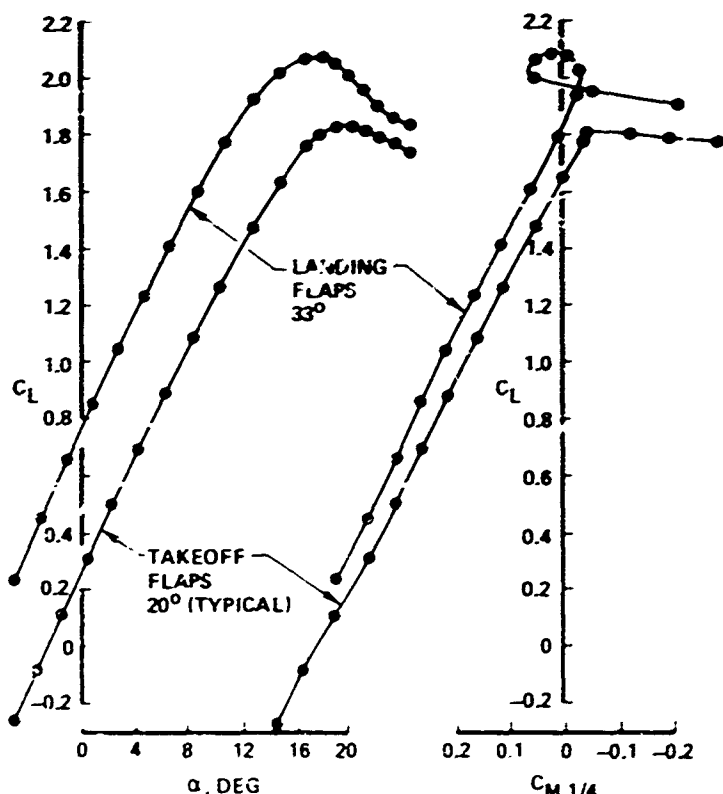


FIGURE 3 HIGH LIFT WIND TUNNEL DATA (LOW REYNOLDS NUMBER)

Several full scale parameters must be estimated from this lift and pitching moment data as indicated in Figure 4, which shows the flight records obtained during a typical flight test stall. The principle item to be estimated is the Federal Aviation Regulation (FAR) stall speed. This speed is defined as the minimum speed obtained during a full stall that is approached at the rate of 1 knot per second. This minimum speed occurs during a dynamic maneuver, and the airplane usually will be somewhere between .80 and .90 g's at the time this minimum speed is reached. This FAR stall speed is used by the FAA as one consideration in determining take-off and landing speeds for airplanes certified within the United States. The corresponding FAR  $C_{L_{Stall}}$  is defined as  $C_{L_{Stall}} = \frac{W}{\frac{1}{2} \rho V_{Stall}^2 S}$  without considering the reduced load

factor existing at the time  $V_{Stall}$  occurs. Another stall speed is the 1 g stall speed, which is defined as that speed which occurs just as the normal acceleration breaks to a reduced value. This speed also is measured during a dynamic maneuver and may not occur at exactly 1 g normal acceleration. This 1 g stall speed is used as the basis for setting the take-off and landing speeds by the U. S. Air Force. The

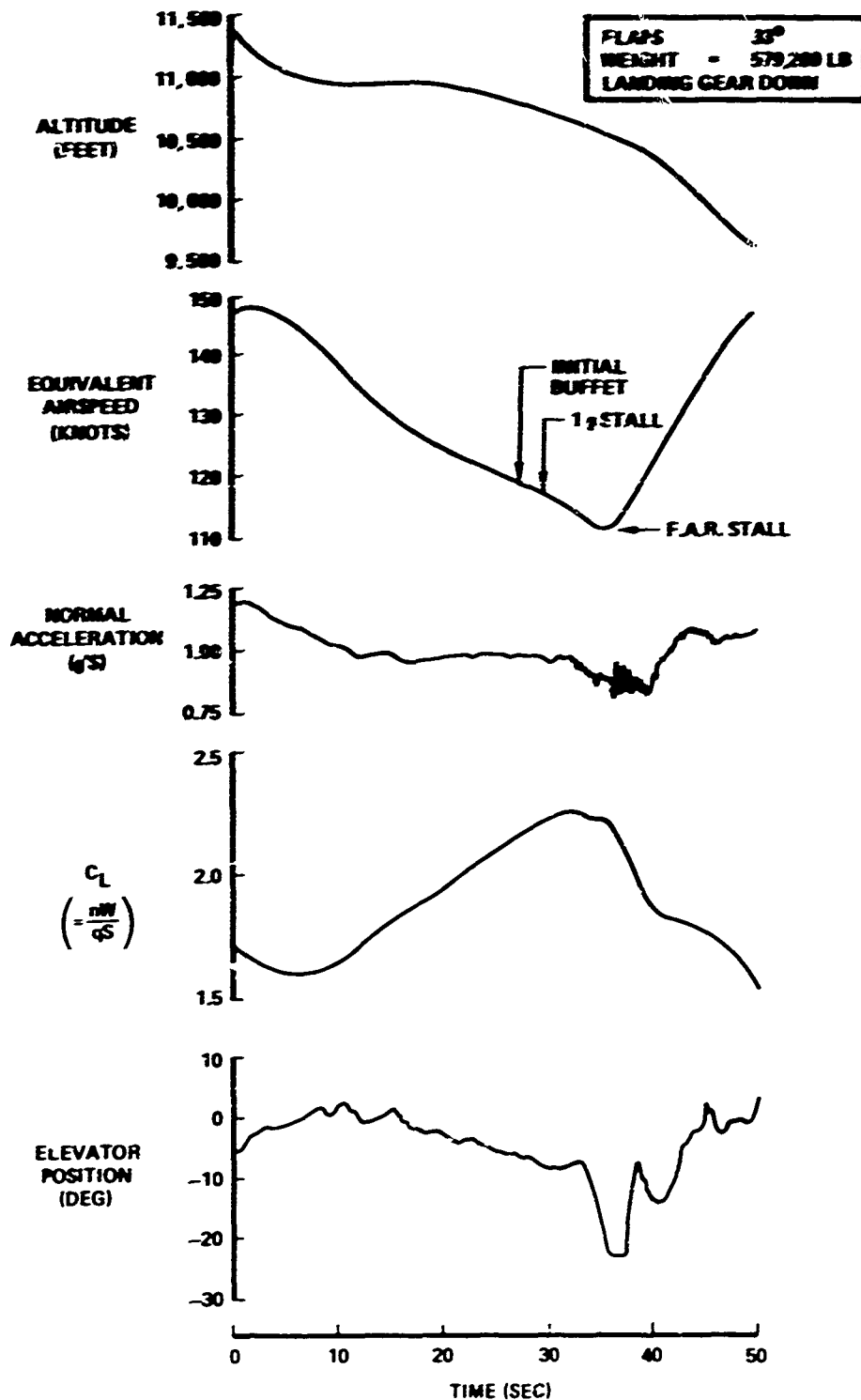


FIGURE 4: FLIGHT RECORD OF A STALL MANEUVER

corresponding  $C_{L_{\text{max}}}$  historically has been used as  $C_{L_{\text{max}}}$  in the structural analysis of the airplane. Also to be estimated, is the true  $C_{L_{\text{max}}}$  achieved during the stall maneuver, where  $C_{L_{\text{max}}}$  is defined as  $\frac{nW}{qS}$ . This maximum lift coefficient usually occurs at a speed below the 1 g stall speed and is the flight  $C_{L_{\text{max}}}$  most nearly corresponding to the one measured in a wind tunnel test.

#### 4. CORRELATION CURVES AND FLIGHT TEST RESULTS

##### 4.1 FAR $C_{L_{\text{Stall}}}$ and $C_{L_{\text{max}}}$

Figure 5 summarizes the high-lift flight and wind tunnel data from a series of Boeing airplanes by showing the ratio of the FAR  $C_{L_{\text{Stall}}}$  to the wind tunnel  $C_{L_{\text{max}}}$ . The data shows appreciable scatter between airplanes, and the solid line was chosen as the value of the parameter to be used in estimating the 747 performance. The 747 flight test results generally lie somewhat below this estimated value. The data points shown in the upper part of the chart are for the airplanes at the maximum weights tested. The lower plot presents the trend of the stall speeds as a function of airplane wing loading, and shows that increasing gross weight decreases slightly the stall lift coefficient. This wing loading effect has been consistent throughout the history of Boeing airplanes and seems far too large to be accounted for by zeroelastic distortions of the wing affecting the stall speed. It apparently is dependent on the dynamics

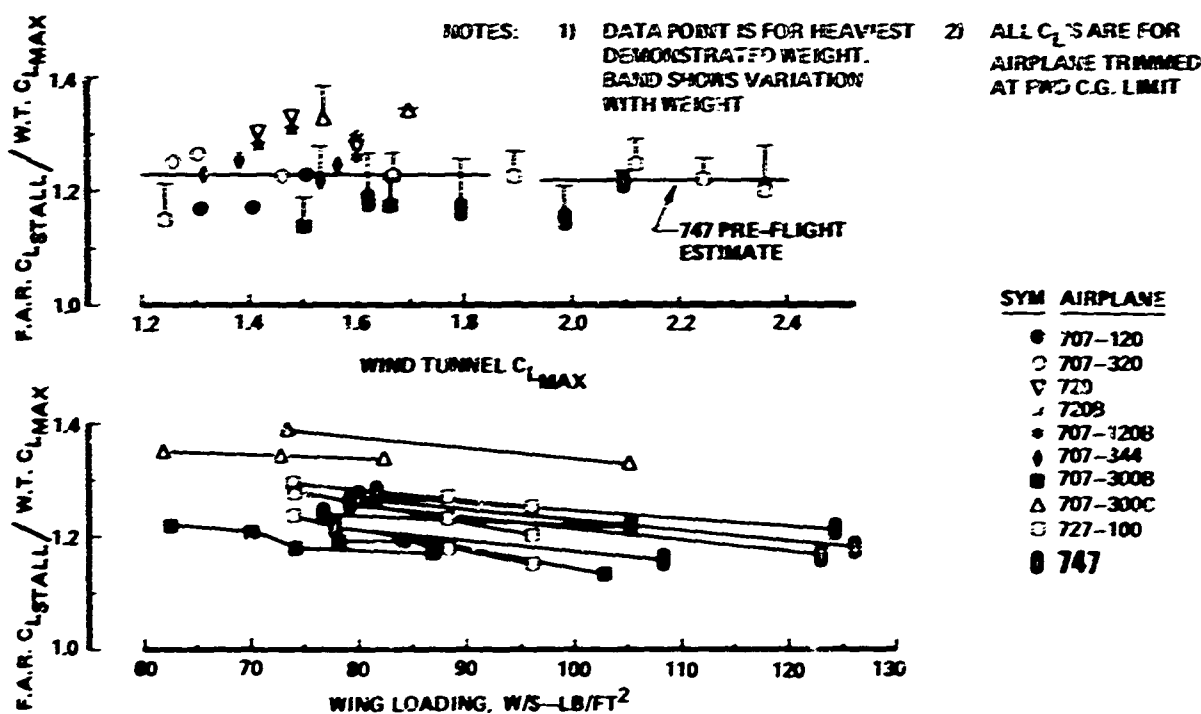


FIGURE 5: COMPARISON OF FLIGHT FAR  $C_{L_{\text{Stall}}}$  AND WIND TUNNEL  $C_{L_{\text{max}}}$

of the stall maneuver and its variation with gross weight. Since these dynamics are a very complicated function of the drag and pitching moments of the airplane as well as the lift, the actual value of this trend with weight is very difficult to predict accurately. The values of wind tunnel  $C_{L_{\text{max}}}$  used to develop these plots differs slightly from those shown in Figure 3. The reason is that there were no blockage corrections used in reducing the 747 wind tunnel data shown here. This was done in order to compare with the previous tests of the Boeing family, made before blockage corrections were a normal part of the wind tunnel data reduction procedure.

A similar summary of the 1 g  $C_{L_{\text{Stall}}}$  is shown in Figure 6. Again, there is appreciable scatter in the data, and the solid line represents the value used in making the 747 pre-flight estimate. The 747 flight test results gave 1 g  $C_{L_{\text{Stall}}}$  as much as 8 percent below the original estimate. This fact is particularly surprising since a test installation of the 747-type leading-edge flap on a 707 gave a correlation factor well above the other airplanes. The 1 g  $C_{L_{\text{Stall}}}$  showed the same trend with wing loading as was indicated for the FAR  $C_{L_{\text{Stall}}}$ .

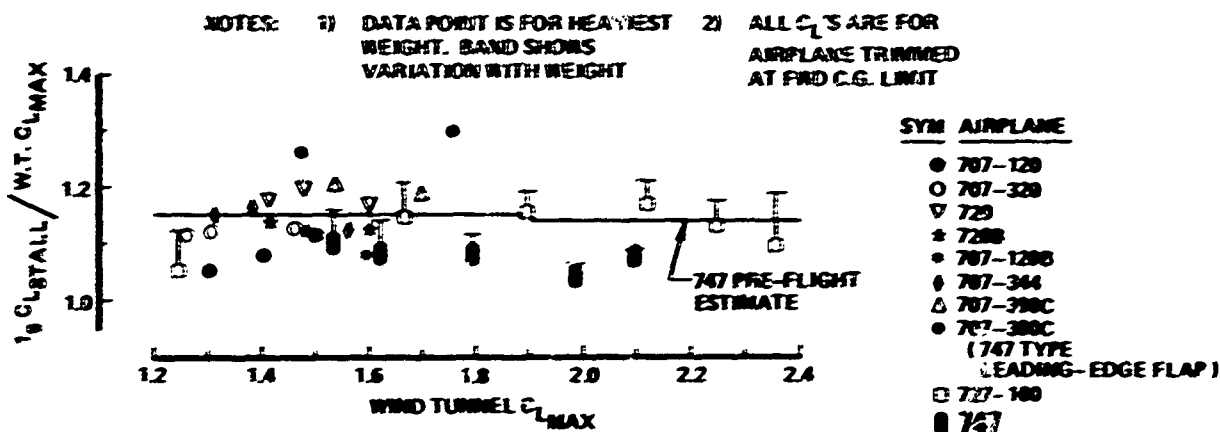


FIGURE 6: COMPARISON OF FLIGHT  $1/2 C_{L\text{STALL}}$  AND WIND TUNNEL  $C_{L\text{MAX}}$

At the time these estimates were being made, it was recognized that the 747 had a leading-edge device that might render past wind-tunnel-to-flight-test correlations inaccurate. Past Boeing airplanes had a leading-edge device, either Krueger flap or slot, that was relatively sharp, creating high pressure peaks and rapid pressure recoveries which would make the flow sensitive to Reynolds Number effects. The 747, on the other hand, had a leading edge device that was carefully designed using aerodynamic theory to produce a smooth pressure distribution having no severe gradients at high angles of attack. With the gradient selected to give no separations at low Reynolds Number, no appreciable increase in lift should be expected as Reynolds Number is increased.

In order to evaluate these considerations, a wind tunnel test was made in the 12 foot pressure tunnel at the Ames Aeronautical Laboratory of the NASA where the Reynolds Number could be varied from approximately 1.2 million up to 7.5 million. These data, shown in Figure 7, are in good agreement at low Reynolds Number with the data obtained in the University of Washington wind tunnel when corrected to the forward center of gravity position used in this figure. The increase in  $C_{L\text{MAX}}$  with Reynolds

Number was relatively modest, and the data showed enough linearity to allow extrapolation to the full scale Reynolds Number of 30 to 40 million. The flight test data shown are the maximum  $C_L$ 's achieved in the stall ( $C_{L\text{MAX}} = \frac{mW}{\rho S}$ ) and indicate an agreement within 2 percent or less of the extrapolated wind tunnel values.

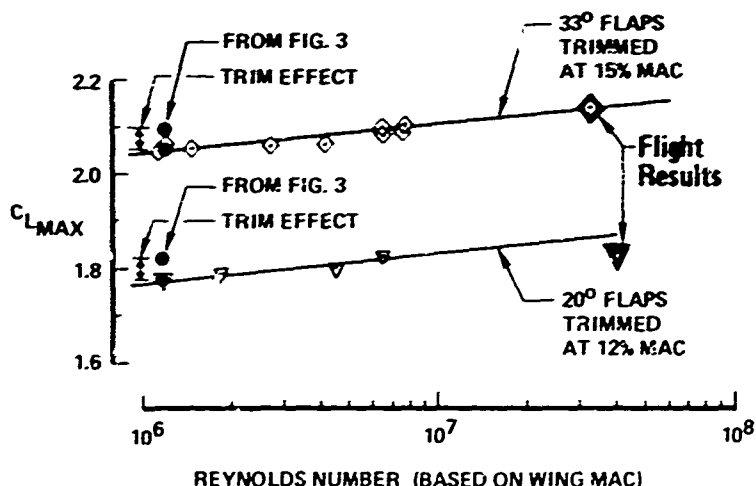


FIGURE 7: HIGH REYNOLDS NUMBER DATA

#### 4.2 $C_L$ 's for Minimum Un-Stick Speed

FAA certified lift-off speeds are related to the minimum speed that the airplane can demonstrate a complete take-off, called  $V_{MU}$ . The lift coefficient for this condition can be limited by either  $C_{L\text{MAX}}$  or by the angle of attack existing when the aft body contacts the ground. Therefore, it is necessary to estimate both the lift curve shape and the  $C_{L\text{MAX}}$  in ground effect. The basic data for making this estimate



mate were obtained in the wind tunnel using a fixed ground plane modified to allow unusually high pitch attitudes, as shown in Figure 8. The lift curve so established was checked at high Reynolds Number and

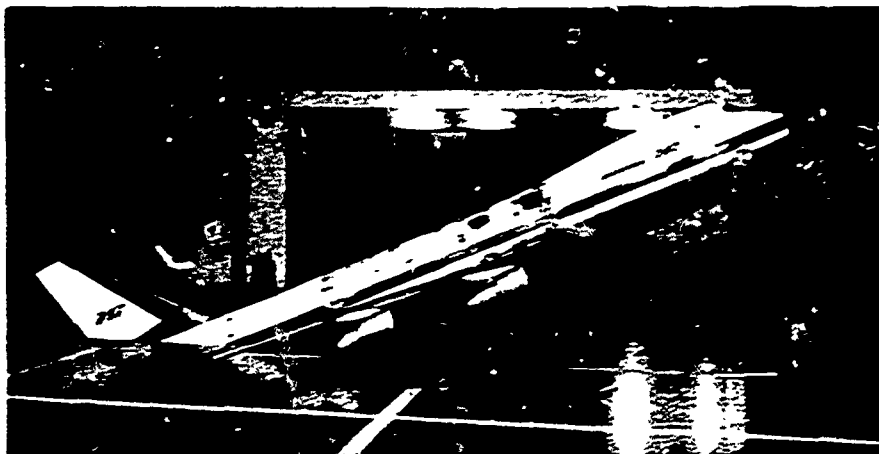


FIGURE 8: TEST FOR  $C_{L_{MAX}}$  IN GROUND EFFECT

found to be essentially unchanged. Since angle of attack is such an important parameter under these conditions, the model used for this test had the wing twisted to represent the zeroelastic distortion of the actual airplane during heavy weight, flaps down, flight. These wind tunnel data were then corrected by correlation factors obtained on previous Boeing aircraft similar to those shown for the free-air conditions. Resultant pre-flight estimates and subsequent flight data are shown in Figure 9. The data shows

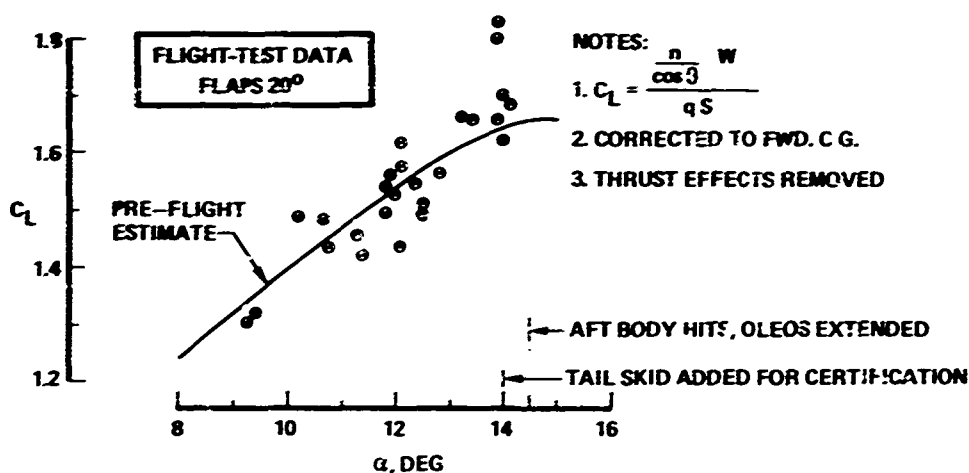


FIGURE 9: LIFT CURVE IN GROUND EFFECT

a scatter of  $\pm 5$  percent, typical of flight test information taken during the take-off phase. However, it does straddle very well the pre-flight estimate. A picture of this rather dramatic flight testing for  $C_{L_{max}}$  in ground effect is shown in Figure 10.

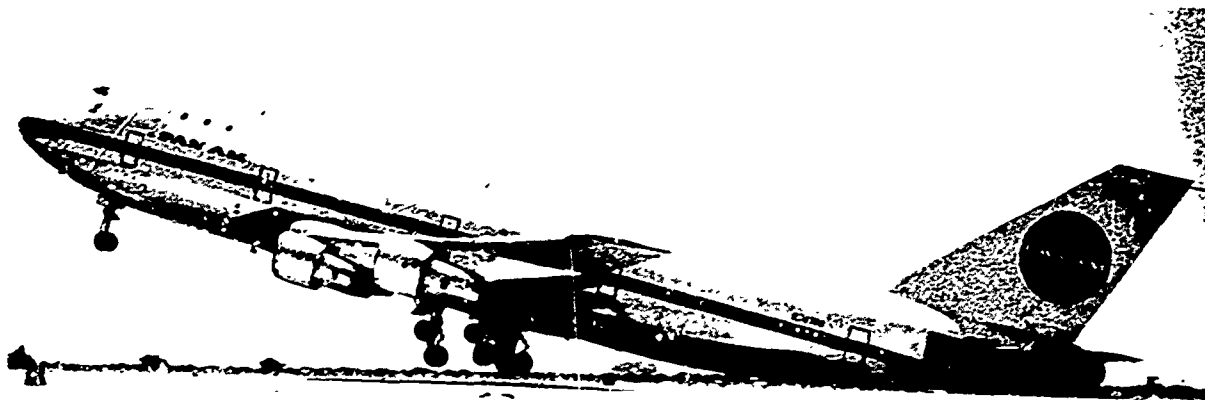


FIGURE 10:  $V_{LO}$  FLIGHT TEST

### 4.3 Pitching Moments

The static longitudinal pitching moments play a dominant role in determining the handling characteristics of the airplane during the stall maneuver. Local separations on a swept wing can have large effects on wing pitching moments. Separations on the wing, body, and nacelles can influence the tail contribution to stability. Since these separations can be sensitive to Reynolds Number effects, it is difficult to predict the airplane's full-scale behavior if the wind tunnel data indicate a situation that is marginal in any way. At Boeing our philosophy has been for many years to design for good pitching moment characteristics under low Reynolds Number conditions to assure good characteristics in flight. A small pitch-up in the stall is permissible and tends to hold the airplane to a slightly lower speed before it pitches down out of the stall. This permissible pitch-up must cause only a limited excursion in angle of attack, say 4 to 6 degrees, involve essentially no increase in  $C_L$  once the pitch-up begins, and must be followed by strong pitch-down to assure a good clean break away from the stall.

The wind tunnel pitching moment data at both low and high Reynolds Number and the corresponding flight data are compared in Figure 11. There is practically no change in wind tunnel pitching moment data with Reynolds Number, probably a result of the cambered leading-edge flap. The flight data show slightly superior stability at stall entry than the wind tunnel data indicate. They also show that the wind tunnel predicted quite accurately the flight values for the angle of incipient pitch-up and the angle of recovery. These pitching moment characteristics produced an airplane extremely easy to fly throughout the stall maneuver.

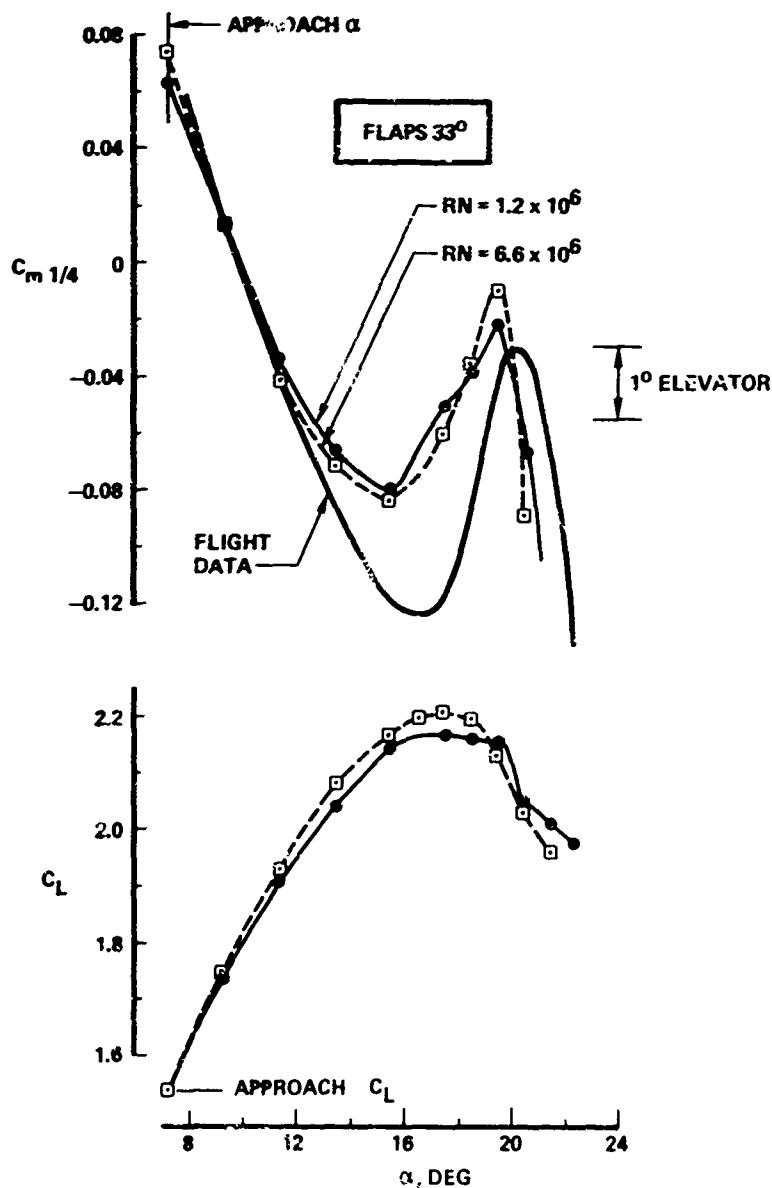


FIGURE 11: PITCHING MOMENTS IN THE STALL

## 5. CLOSING REMARKS

The methods used to predict the stall characteristics of the 747, based on previous experience of Boeing transport airplanes, predicted the FAR  $C_{L_{Stall}}$  within about 5 percent, well within the confidence band expected during the design phase. In this particular instance, a better estimate would have been achieved by extrapolating the  $C_{L_{max}}$  data taken at varying Reynolds Number to full scale Reynolds Number to get a full scale  $C_{L_{max}}$ . This  $C_{L_{max}}$ , when used with corresponding values for drag and pitching moments in a dynamic simulation of the stall maneuver on a computer, would have produced a better estimate of the flight  $C_{L_{Stall}}$ . However, applying the same techniques to other Boeing airplanes would not produce as accurate an estimate. One must conclude that predicting the  $C_{L_{Stall}}$  remains a difficult engineering problem in which judgment based on experience must continue to play a large part. Eventually, better understanding of the detailed aerodynamics of stalled flow, particularly as it is affected by Reynolds Number and the other full-scale items such as surface roughness and mechanical protuberances, may lead to a more scientific approach to the problem.

## ON AIRFLOW SEPARATION AND BUFFET ONSET DURING FIGHTER AIRCRAFT MANEUVERING

by

Maj. (Dr.) Peter J. Butkewicz

Air Force Flight Dynamics Laboratory (AFSC)  
 Aeromechanics Branch (FXM)  
 United States Air Force  
 Wright-Patterson Air Force Base, Ohio, USA

## SUMMARY

The occurrence of airflow separation on fighter aircraft wings during transonic combat maneuvering, buffet, wing-rock and adverse yaw, etc., severely degrade the combat potential of the aircraft. The need therefore exists to perform an in-depth, quantitative investigation of the airflow separation/buffet onset relationship, and determine means to delay this flow separation to higher values of lift coefficients. An experimental flight test program was sponsored by the Air Force Flight Dynamics Laboratory to determine the buffet characteristics of four high performance aircraft. The aircraft were flown in transonic maneuvers encountering conditions from buffet onset through heavy buffet. The aircraft were heavily instrumented, i.e. accelerometers (wing tips, c. g., pilot seat), wing root strain gages, wing static pressure taps, and also had one wing tufted for flow visualization photographs. The aircraft were flown in the baseline configuration as well as with various deflections of leading and trailing edge flaps. Some wind tunnel data were also correlated with the flight test results. The purpose of this paper is to discuss the results of the flight test program, examine the effects of mechanical high lift devices on buffet, and present some wind tunnel/flight test correlations.

## NOTATION

Symbols

$\alpha$	Angle of Attack
$b$	Wing Span
$c$	Wing Chord
c.g.	Center of Gravity
$C_D$	Drag Coefficient
$C_L$	Lift Coefficient
$C_N$	Normal Force Coefficient
$K$	Scaling Parameter
$\Lambda$	Wing Sweep Angle
L.E.	Leading Edge
$m$	Meters
$M$	Mach Number
T.E.	Trailing Edge

Subscripts

B.O.	Buffet Onset
.25c	Quarter Chord
$w$	Wing

## 1. INTRODUCTION

Throughout much of the history of heavier than air flight, the problems associated with airflow separation from wings were mainly analyzed from the standpoint of airplane stall and spin. Since many of these early aircraft were grossly underpowered, and possessed undesirable stability and control characteristics, the avoidance of the stall point became an essential requirement during flight. Classically, the stall point was defined as that point on the lift curve where the lift coefficient ceases to increase proportionally with angle of attack, and often turns sharply downward.

With the advent of modern propeller fighter aircraft during World War II, flight speeds had increased to the point where the critical Mach number was reached over the wings. Compressibility and buffet effects were encountered during high speed combat maneuvers and power dives. However, sustained, long term buffet was not yet encountered.

Finally, in the evolution of high performance aircraft, comes the modern jet fighter. Typically, these feature a high thrust to weight, thin, moderately to highly swept wings, small leading edge radius, and have the capability to operate in sustained supersonic flight. During combat however, while performing high "g" maneuvers and altitude/velocity trades, it is found that even these fighters operate over long periods in the transonic regime, and are limited in maneuvering capability by increasingly severe buffet, wing rock, and consequent adverse tracking and handling qualities.

In order to more thoroughly understand the buffet phenomenon, flight test programs were undertaken by the Air Force Flight Dynamics Laboratory. During these programs, four high performance fighter

aircraft, Fighters A, B, C, and D, were flight tested in the transonic regime at altitudes of 25,000 and 35,000 ft (7,620 m and 10,668 m) nominally, while performing wind-up turns, and encountering conditions from buffet onset through severe buffet. The purpose of this paper is to discuss the results of the flight test programs relating high speed flow separation to buffet, examine the effects of mechanical high lift devices on buffet, and present some wing tunnel/flight test buffet correlations.

## 2. TRANSONIC FIGHTER BUFFET

### 2.1 Airflow Separation - Incipient Buffet

The flow separation phenomenon as experienced on the wing of a fighter is a complex process. Leading edge separation, trailing edge separation, shock-boundary layer induced separation, and their various combinations can all be present while maneuvering, and depending on the airfoil shape, angle of attack, and Mach number, any of these may induce buffet. However, it may be generally stated that leading edge separation (low  $M$ ; high  $\alpha$ ) and shock-boundary layer induced separation (high  $M$ ;  $\alpha$ ) are the two primary forms of flow separation which induce buffet. The separation process is also progressive, generally beginning at the wing tip, and expanding inward to the wing root. This systematic progression was found to be similar on all the aircraft tested, including the delta wing Fighter D. Figure 1 shows the initial separated areas on Fighter A's wing at Mach Number .81 and with separation confined to the wing tip region. The criteria used to establish initial flow separation and buffet onset was the initial increase in oscillation of the wing tip accelerometer. Static pressure tap readings correlated this separation well with the accelerometers. The interesting point here arises that when these initial oscillating buffet loads are transmitted to the fuselage and superimposed on the engine, duct, etc., vibrations, the buffet intensity is attenuated, and the pilot does not feel the buffet onset. As higher lift coefficients are demanded, the separated area increases, and buffet intensity increases and is sensed by the accelerometer at the cockpit (See Fig. 2). Finally upon near total flow separation (Fig. 3) heavy buffet is in progress and lateral/directional oscillation onset and wing rock are experienced. It is generally at this point when the airplane dynamic stability and handling qualities are so degraded that gunsight tracking is deteriorated and further combat maneuvering is not attempted.

### 2.2 Buffet Flight Test Review

With the above qualitative idea of the airflow separation - buffet relationship in mind, some quantitative results of the flight test program will be presented. The first point to be examined is the relationship of buffet to the classical stalling point. On all aircraft tested, the initial flow separation (buffet onset) occurred at reasonably low values of lift coefficient as would be expected, without a break in the lift curve. Figure 4, showing lift curves for Fighter C, indicates that buffet onset occurs where the lift curves are still linear, and not until heavy buffet do the curves begin to bend over. This trend is also shown in Figure 5, for Fighter D. The high speed analogy to the stalling point, therefore, correlates with the heavy buffet point and is associated with near total flow separation and severely degraded dynamic stability and handling qualities.

Since for all the aircraft, initial airflow separation occurred at fairly low values of  $C_L$  and  $\alpha$ , the second point to be examined is the angle of attack for buffet onset. Figure 6 shows the buffet onset angle of attack for these aircraft. It is of interest to note that for the fighters with conventional, swept wings (Fighters A, B, C) the correlation across the entire mach number range is good, in spite of the rather large range of wing loading and differences in plan form. However, for the delta wing Fighter D, the correlation did not hold up. Two factors are considered probable to effect this situation. Basically, Fighter D's lift curve has a much lower value of  $C_L$  at  $\alpha = 0$ , and has a lower slope than the other aircraft (See Fig. 5). Therefore, to attain the same lift coefficient, a higher angle of attack is required. Secondly at high angles of attack, the leading edge vortex from the delta wing energizes the flow sufficiently to keep it attached lower. Hence higher angles of attack were possible for each of the buffet levels.

The shift in the angle of attack curves during the transition from light to heavy buffet was generally well behaved. Figure 7 compares the trend for both Fighters C and D. It is noted that changes in slope are small for a given Mach number, and it appears that the light buffet curves were merely translated upward. However, on Fighter A, the very nature of the angle of attack curve changes from (light) buffet onset to heavy buffet at the onset of lateral directional oscillation (See Fig. 8).

Of extreme interest was the analysis of the lift coefficient (or normal force coefficient in the case of Fighter D) occurring during buffet onset, and a correlation of these data. Figure 9 shows the variation of  $(C_L)_{BO}$  with Mach number. Although the lift coefficient for buffet onset is a function of the aircraft geometric characteristics (wing sweep, aspect ratio, leading edge radius, thickness to chord ratio, etc.), mass parameters, and flight condition, it is seen that the  $(C_L)_{BO}$  variation with altitude is small. This was especially true with Fighters A and D, and to a lesser degree with the Fighters B and C. Of special significance was the fact that the altitudes and speeds constituted the majority of combat conditions encountered.

As a further step in reducing the data shown in Fig. 9 in an attempt to compress the data field, the  $C_{LBO}$  was operated with a number of "scaling" parameters, i.e. altitude density ratio, sweep angle, wing loading, etc. Since this plot showed minimal altitude effects, the altitude density and pressure ratios were not of value as scaling parameters, and therefore the aircraft geometric and mass parameters were stressed. The best scaling parameter found was  $(1/K \cos \Lambda .25c)$  where

$$K = 4 \sqrt{\frac{\text{particular aircraft } (W/S)}{\text{average all aircraft } (W/S)}}$$

23

Other parameters (i.e. aspect ratio, taper ratio, critical Mach number) were investigated, however, inconsistencies developed, and consequently these parameters were dropped from consideration. The results of operating on  $CL_{80}$  with this scaling parameter are shown in Figure 10 with the dashed line showing the mean. Variations from this mean line range from 3% in the low transonic range, 10% in the mid transonic range to about 13% for Mach numbers at about 0.9.

Although this was relatively simple scaling parameter, the results obtained were quite encouraging, and were applied to other aircraft. Buffet onset  $C_N$ 's for Fighters E and F were obtained from NASA FRC, and also scaled. These scaled points for Fighter E fell within the bounds established by the other AFFDL flight test aircraft, as is shown in Figure 10. However, the Fighter F buffet onset did not correlate well, as shown in Figures 11 and 12. Figure 11 shows that the unscaled  $C_N$  for the buffet onset of Fighter F departed from the trends exhibited by the other fighters, for Mach numbers above 0.80. Since the general shape and slope of the Fighter F unscaled buffet onset curve was at variance with that of the other aircraft, the scaled curve also shows poor correlation, as shown in Figure 12.

As was stated earlier, the effect of the scaling parameter was to compress the buffet onset curves. The procedure was reasonably satisfactory for all aircraft examined, except for Fighter F. It should be noted that with this single exception, all other aircraft possessed moderate wing sweep ( $25^\circ$  to  $60^\circ$ ), conventional airfoils (NACA 0004-64, 65; NACA 65A005.5, types), and for the flight conditions, had wing loadings below 100. Fighter F had geometric/weight characteristics which differ from the above and furthermore possesses a sharp leading edge, thus the lack of correlation is not surprising. However, further work in the buffet onset correlation area is in progress, including incorporation of additional aircraft, as well as additional mass and geometry parameters.

### 3. MANEUVERING FLAP INVESTIGATION

As was mentioned earlier, the flight test programs included the use of mechanical flaps to investigate their effect on buffet and air-to-air tracking. It should be understood that the flaps were those originally designed for use during take-off and landings, and therefore had to be mechanically fixed to the desired deflection prior to flight. The single exception to this was in the use of fixed maneuvering slats on Fighter C, which were specifically designed for maneuvering conditions.

In classical, incompressible aerodynamics, the effect of flaps and slats on the lift curve are well known. The trailing edge flap deflection increases the  $CL_{MAX}$  of the wing, and shifts the curve to the left, decreasing the angle of attack for zero lift. The effect of slats, ideally, is to increase  $CL_{MAX}$  and the angle of attack at which it occurs, without shifting the lift curve.

During the AFFDL buffet flight test programs, both transonic wind tunnel data and flight test data assessing flap effects were obtained. Wind tunnel test results for Fighter B with various leading and trailing edge flap deflections are shown in Figure 13. It is seen that the effects of these devices transonically is generally consistent with the predicted incompressible results. Leading edge flap deflections generally increase the  $CL_{MAX}$  without shifting the lift curves, and trailing edge flap deflections both raise and shift the lift curves to the left. Flight test results show the same general trends, however, some deviations are shown. Figure 14 shows the effect of flaps and slats on the lift curve of Fighter C. It is seen that in the case of leading edge flaps  $0/8^\circ/8^\circ$ , with no trailing edge flap deflection, there is a slight degradation of the lift curve. Otherwise, the effect of flaps and slats is as expected.

The effects of maneuvering flaps and slats on buffet onset are clearly illustrated in Figures 15, 16, and 17. (Buffet onset is again defined as initial airflow separation.) Figure 15 shows  $CL_{80}$  for Fighter C from Mach .75 up to .95. Successive increases in  $CL_{80}$  are seen across the entire speed range for each of the flap/slat deflection combinations shown. The highest values of  $CL_{80}$  are obtained with maneuvering slats in combination with a trailing edge flap deflection of  $15^\circ$ . This increase over the baseline (no flap/slat) amount from 135% improvement at  $M = .75$  to 38% improvement at  $M = .925$ . Clearly, these gains are significant. A second point of interest seen on this figure is that the apparent degradation of the lift curve (for  $0/8/8, 0$ ) is not carried over to  $CL_{80}$ . This implies that during maneuvering, a leading edge flap deflection delays the initial airflow separation. A further point of interest is the effect of slats on the drag polar. This is shown in Figure 18 for Fighter C. It is seen that an increase in drag is indeed experienced at the lower lift coefficients, however for the higher lift coefficients ( $M > 0.5$ ) required during combat maneuvering, the drag level is reduced attesting to the improved wing flow field.

It is pointed out that the flap deflection combinations chosen were not necessarily those which were optimum. Furthermore, care should be taken with respect to generalizing and extending these results to other aircraft. For example, in the case of Fighter A, a leading edge flap deflection of  $9^\circ$  is excessive, and leads to degraded buffet characteristics. This is shown in Figure 17, where the highest  $CL_{80}$ 's were attained with trailing edge flaps only. The leading edge flap deflection does give slight gains up to Mach .87, however, a degradation of  $CL_{80}$  below that for the baseline aircraft occurs after that point. Implicit in the above discussion is the fact that the flap deflections are a sensitive parameter, and tests must be conducted to optimize these settings for maximum maneuvering efficiency. Ideally, such tests should be performed in a wind tunnel, with later inflight verification.

### 4. WIND TUNNEL - FLIGHT CORRELATION

The problems of obtaining credible transonic wind tunnel data are extremely complex, and have been the subject of numerous recent meetings. Typical of these problem areas are:

#### a. Tunnel to Tunnel Correlation

##### (1) Acoustic Noise

## (2) Test Section Mach Number/Static Pressure Gradient

## (3) Wall Porosity (Percent &amp; Distribution)

## (4) Sting Interference

## b. Reynolds Number Effects

## c. High Lift, Wall Interference, Buffet Conditions

## d. Extrapolation of data to full scale flight

Nonetheless, during the Fighter B and C flight test efforts, a limited amount of wind tunnel/flight test correlation was possible, which showed some significant trends, and from which some general conclusions could be drawn.

Since buffet onset was defined in this paper as the initial airflow separation, this parameter will be examined in more detail, with respect to wind tunnel versus flight predictions.

The detection of initial airflow separation as sensed by static pressure taps, is shown for Fighter C in Figure 19. It will be noted that the wind tunnel and flight test instrumentation spanwise locations are not identical. In spite of the differences in location, the agreement between flight and wind tunnel for initial airflow separation is quite good. A similar trend is shown in Figure 20 which shows initial airflow separation as sensed by the wing-tip accelerometer. Upon comparing Figures 19 and 20, a close agreement for angle of attack at initial airflow separation is shown between the wing tip accelerometer and static pressure instrumentation.

A final comparison between flight and wind tunnel indications of buffet onset is shown in Figure 21, for Fighter B. The agreement on the buffet onset point between flight and wind tunnel is again seen to be good. It should be remembered however, that the above plots were for the baseline aircraft (no flaps). With the deflection of leading edge and trailing edge flaps, the agreement even as to initial airflow separation varied widely and further study in this area is warranted.

## 5. CONCLUDING REMARKS

The material presented in this paper was intended to be a qualitative and quantitative investigation of the relationship of airflow separation to fighter aircraft buffet. However, there is a completely different aspect of the problem which is encountered when the pilot is introduced into the system. Simply stated, the pilot is usually able to perform accurate air-to-air gunsight tracking, even under moderate to heavy buffet, as long as wing rock and adverse yaw conditions do not occur. This point was shown through quantitative scoring of tracking films during the NASA FRC flight tests. Furthermore, some fighter pilots have expressed feelings that buffeting enables them to "know where they were" with respect to the aircraft's remaining maneuvering potential. Finally, comments have been made that the improvement of specific excess power is a more important consideration than buffet for combat maneuvering. These points are well taken, and in fact with the development of new advanced fighters with thrust-to-weight ratios on the order of one, the thrust limitation should be greatly diminished.

From the material presented in preceding sections, certain general conclusions can be made:

- a. The buffet phenomenon is initiated with initial airflow separation at the wing tips.
- b. The aircraft is in a buffet condition while still on the lower part of the lift curve, and without the pilot being aware of it.
- c. The use of maneuvering flaps/slats greatly increases the usable lift and combat potential of the aircraft, without a severe drag penalty.
- d. Wind tunnel indications of initial airflow separation (buffet onset) gives good agreement with flight test for the baseline aircraft.

Although buffet intensity alone does not appreciably degrade the pilot's tracking capability until moderate to heavy intensity levels are reached, the separated flow produces a significant performance degradation and leads ultimately to a serious handling qualities deficiency-wing rock. Thus work should be continued to delay buffet onset, and to reduce its intensities wherever possible. Some areas where work should be continued are:

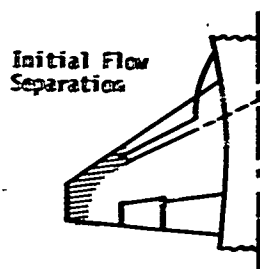
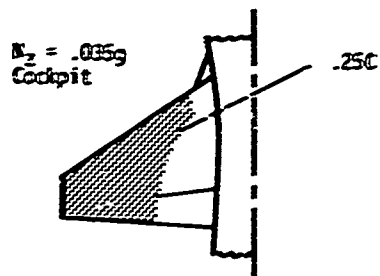
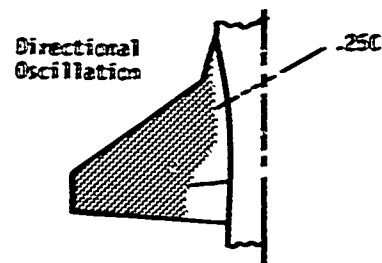
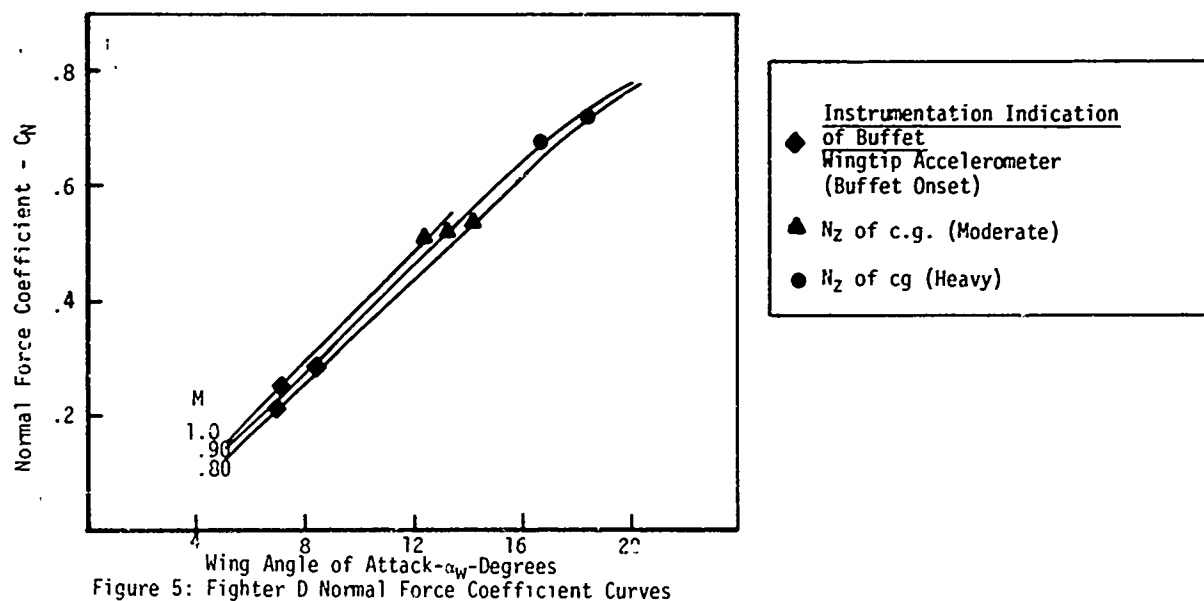
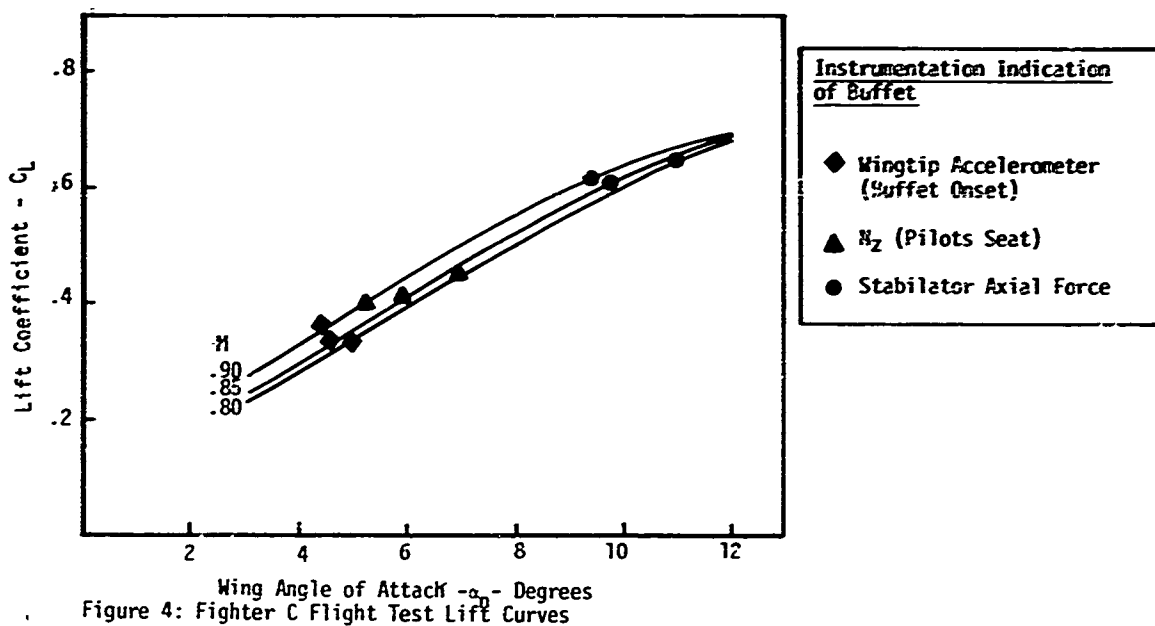
- a. Continued correlation of existing buffet data up through heavy buffet.
- b. Relationship of heavy buffet to loss of dynamic stability.
- c. Wind tunnel optimization of maneuvering flap/slat schedule for maneuvering.
- d. Wind tunnel techniques for improved correlation of buffet data with flight.

## 6. ACKNOWLEDGEMENT

This paper has been compiled from source material which resulted from several USAF contracts. Particular acknowledgement is given to Mr. Thomas R. Sisk, NASA Flight Research Center, for the suggestions which he provided. Finally, thanks are in order for the members of the Flight Mechanics Division, Air Force Flight Dynamics Laboratory, for their review and comments.

Mach Number = 0.81

(Note: Tuft Oscillation shown by shaded areas)

Figure 1  
Tuft Oscillation;  $C_L = 0.44$ Figure 2  
Tuft Oscillation;  $C_L = .56$ Figure 3  
Tuft Oscillation;  $C_L = .66$ 



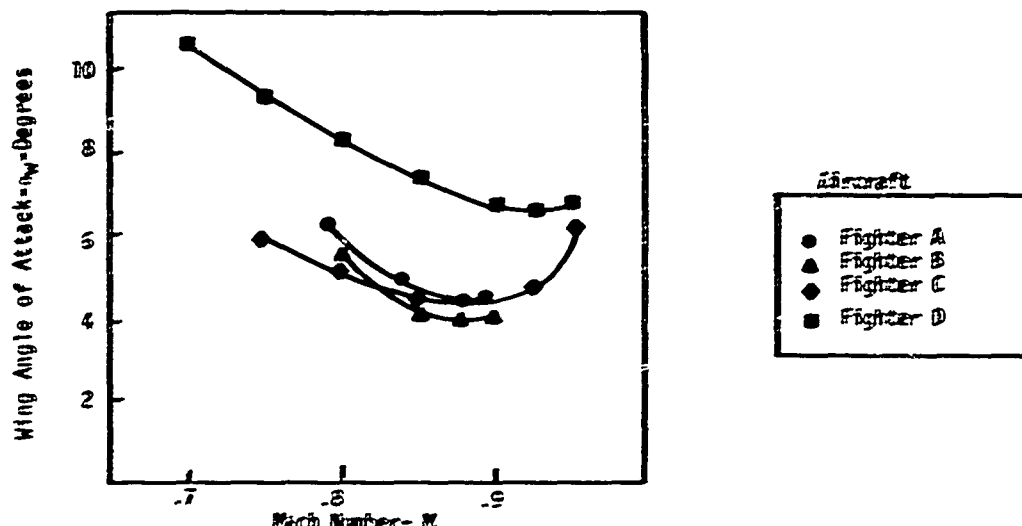


Figure 6: Wing Angle of Attack At Buffet Onset (Initial Flow Separation)

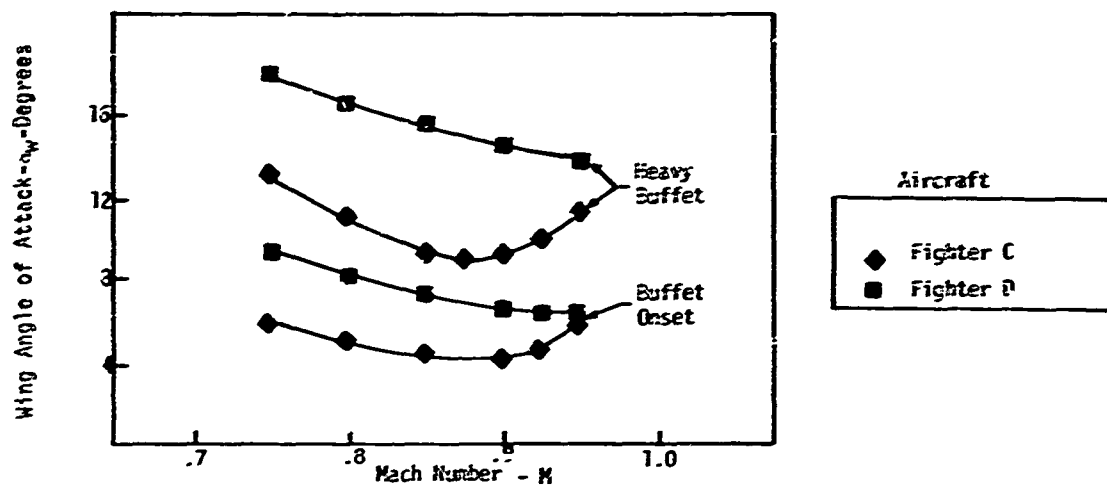


Figure 7: Angle of Attack Variation With Buffet Intensity

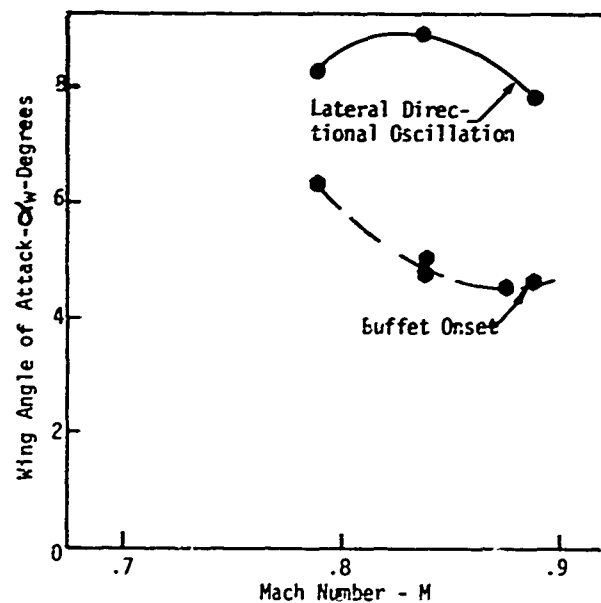


Figure 8: Fighter A Angle of Attack Variation with Buffet Intensity

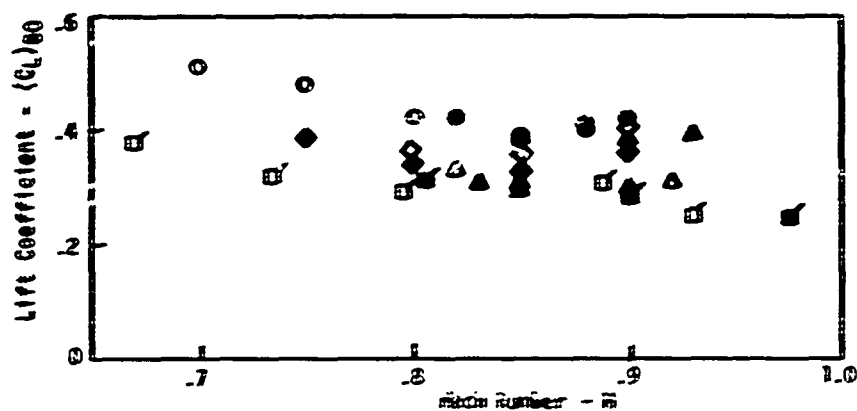


Figure 9: Lift Coefficient at Buffet Onset

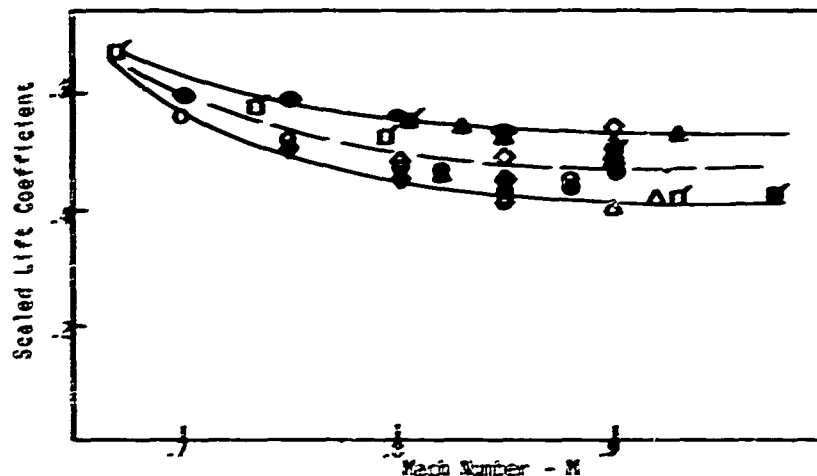
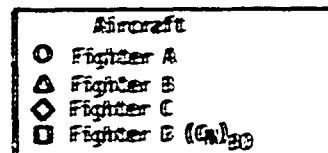


Figure 10: Scaled Lift Coefficients at Buffet Onset

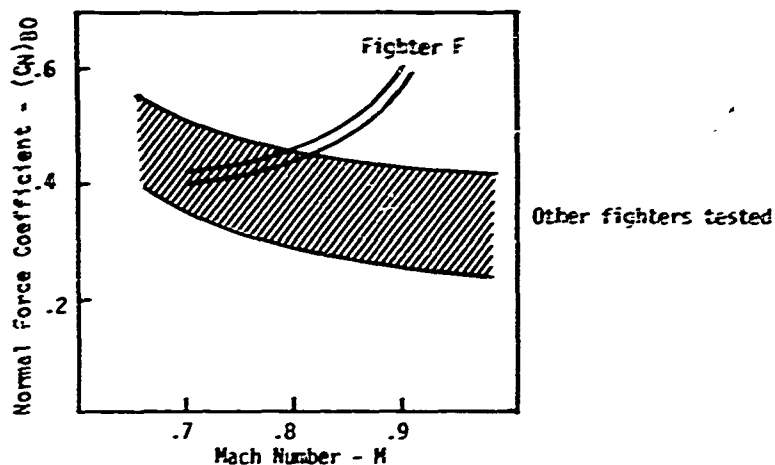
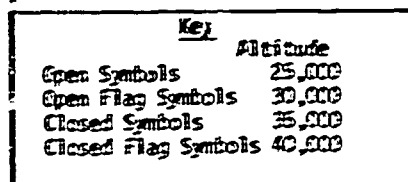


Figure 11: Fighter F Buffet Onset Normal Force Coefficient

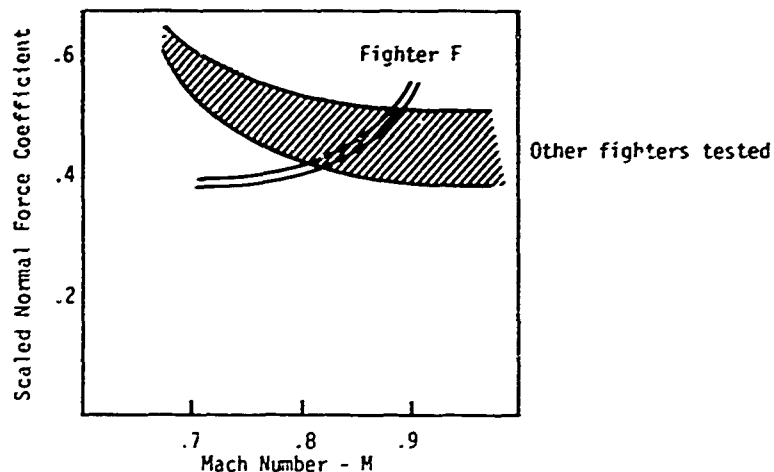


Figure 12: Fighter F Buffet Onset Scaled Normal Force Coefficient

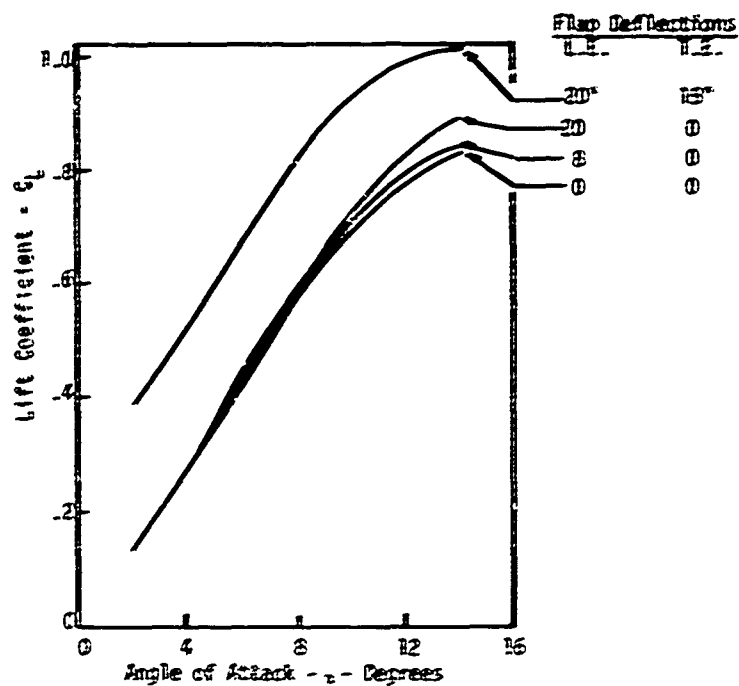


Figure 13:

Effect of Flaps on Fighter B Lift Curve (Wind Tunnel Test;  $M = 0.25$ )

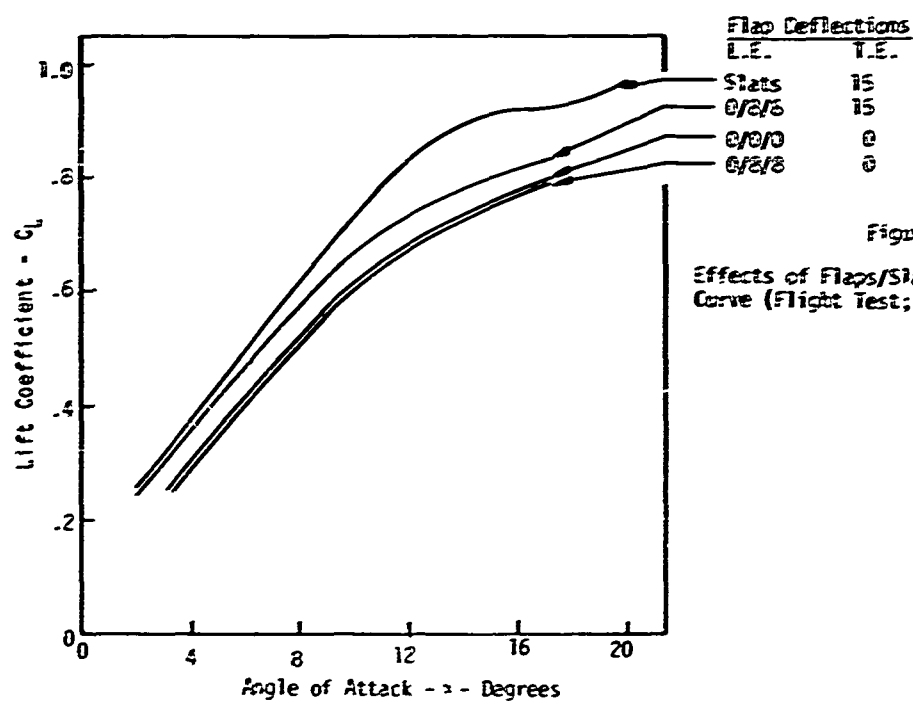


Figure 14:

Effects of Flaps/Slats on Fighter C Lift Curve (Flight Test;  $M = 0.25$ )

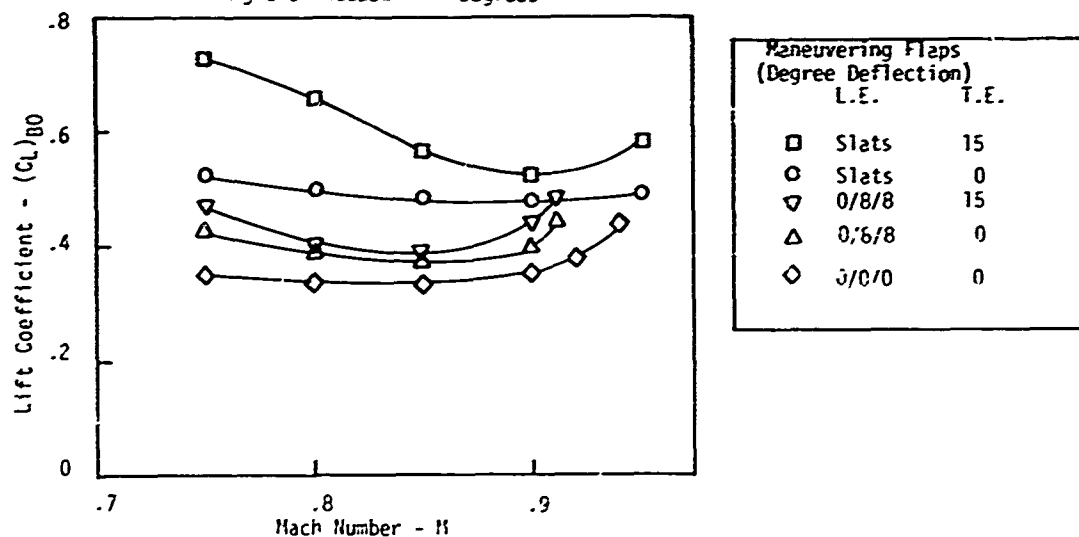


Figure 15: Maneuvering Flap Effects on Fighter C Buffet Onset Lift Coefficient

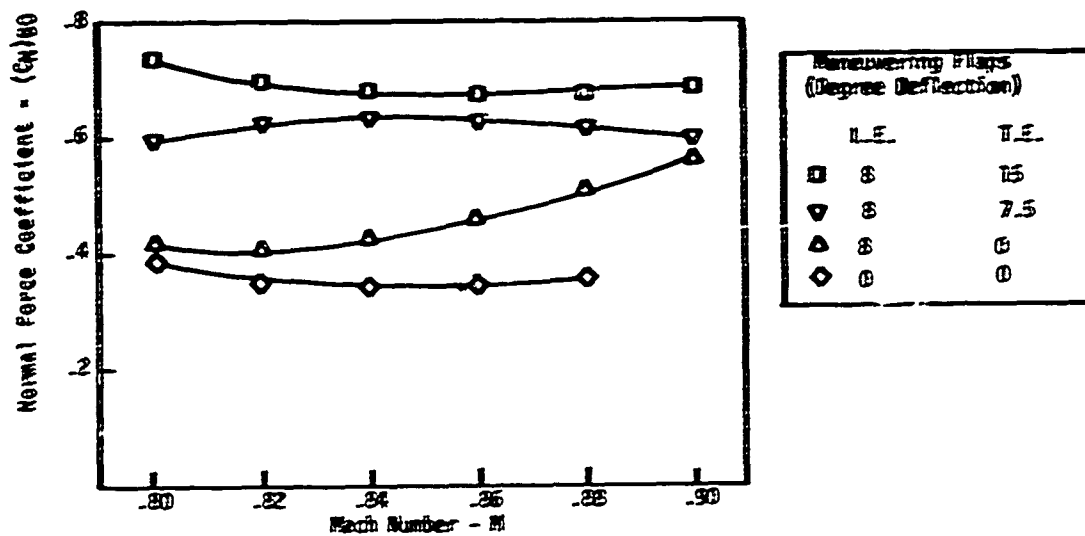


Figure 16: Maneuvering Flap Effects on Fighter B Buffet onset Normal Force Coefficient

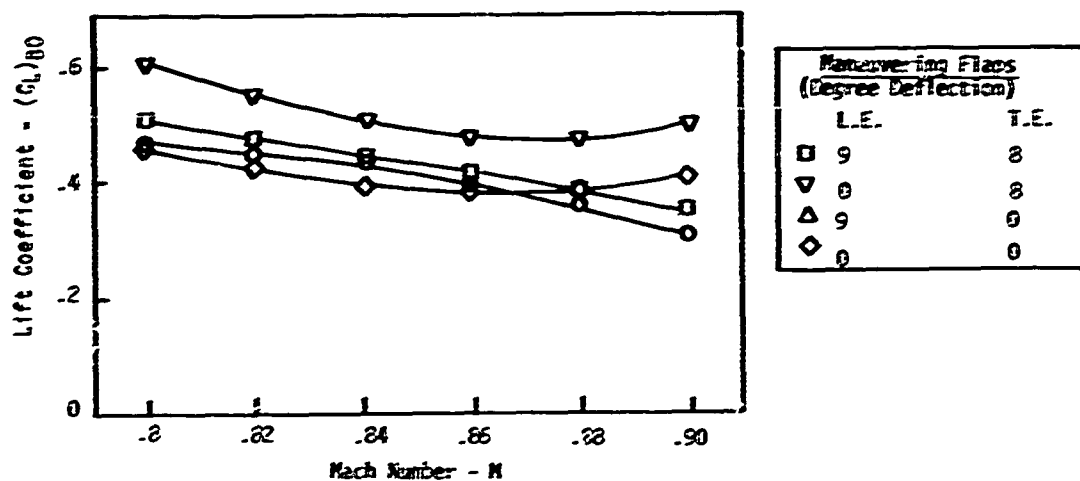


Figure 17: Maneuvering Flap Effects on Fighter A Buffet Onset Lift Coefficient

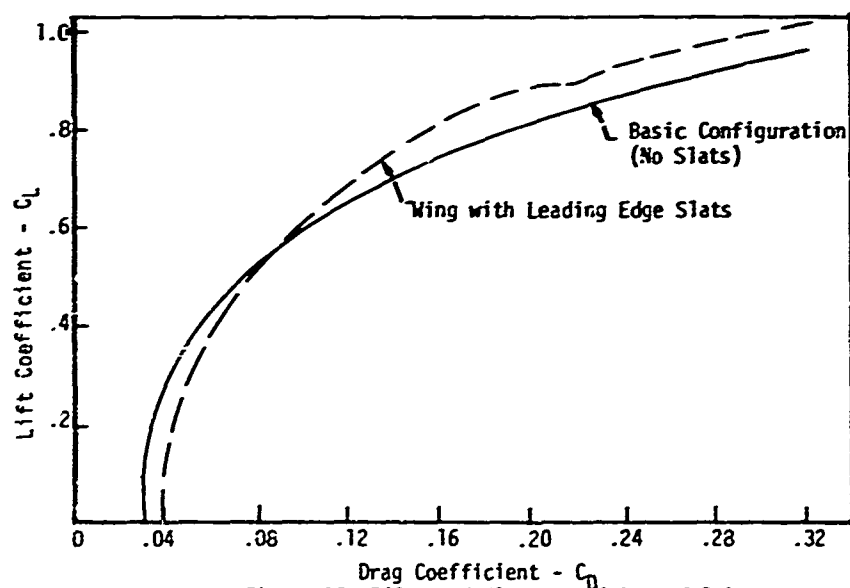
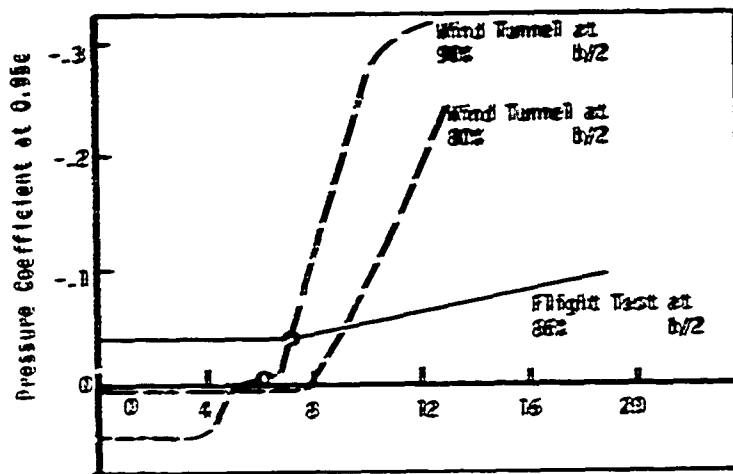


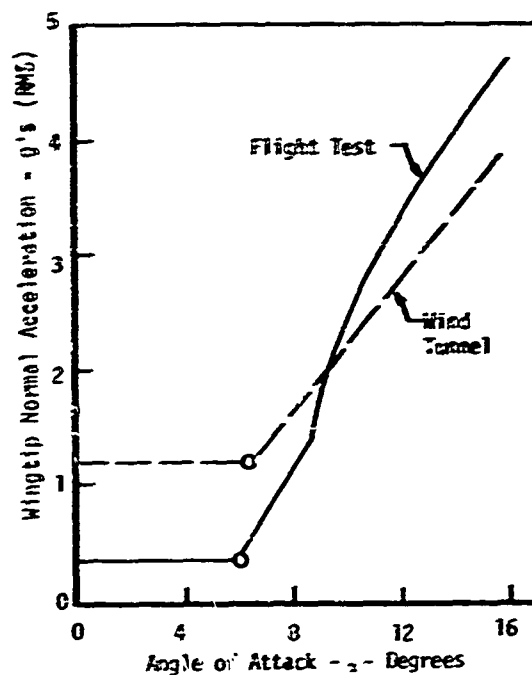
Figure 18: Effect of Slats on Fighter C Polar



Angle of Attack -  $\alpha$  - Degrees

Note: 0 Instrumentation Indication of Airflow Separation

Figure 19: Comparison of Flight Test and Wind Tunnel Static Pressure Coefficient at 0.95c. (Fighter C;  $M = 0.8$ )



Note: 0 Instrumentation Indication of Airflow Separation

Figure 20: Comparison of Wind Tunnel and Flight Test Wingtip Accelerometer Indication of Airflow Separation (Fighter C;  $M = 0.8$ )

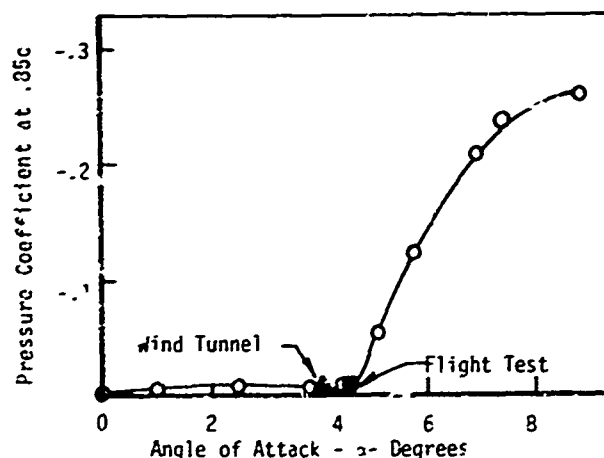


Figure 21: Comparison of Flight Test and Wind Tunnel Static Pressure Coefficient at 0.85c. (Fighter B;  $M = 0.85$ )

## THE DYNAMIC ANALYSIS OF BUFFETING AND RELATED PHENOMENA

by  
J G JONES  
Royal Aircraft Establishment  
Bedford, England

## SUMMARY

A basic feature of the dynamical analysis of wing structural buffeting is the closed-loop interaction between the fluid motion, involving separated flow, and the motion of the wing surface. The problem of formulating an appropriate theoretical model for buffeting is discussed. An analogous problem concerning the choice of appropriate analytical model occurs in connection with the oscillatory rigid-body motion known as wing-rocking. In illustration, buffeting measurements obtained from flight tests using a small combat trainer aircraft have been analysed.

## 1. INTRODUCTION

Over the past few years, aerodynamic problems of buffeting behaviour and handling characteristics at high lift have received increased attention, particularly in the context of manoeuvrability of combat aircraft in the transonic speed range. As a consequence of the occurrence of regions of separated flow on the wing at high incidence, the high-g performance of a combat aircraft may be limited either by vibration (buffeting), mainly associated with structural flexibility, or by degradation in handling characteristics. Phenomena in this latter category include 'wing-rocking', 'wing-drooping' and 'nose-dive'. For example, Fig 1 illustrates a typical penetration to high normal force coefficient  $C_N$  of a fighter aircraft, such as might occur during a 'high g' turn. Two types of oscillatory response are apparent. One is in the filtered wing-tip acceleration trace, predominantly at the frequency (of order 10Hz) of the first symmetric wing-bending mode and known as buffeting. The other is primarily in the roll-rate trace, at a frequency of about 1 Hz, in a rigid-body fluctuating motion usually referred to as wing-rocking. Both types of response, one in a structural and the other in a rigid-body mode, are associated with unsteady separated flow conditions above the wing. Since such forms of fluctuating motion clearly have a derogatory effect in the manoeuvre capability of high performance aircraft it is of great practical interest to be able to understand and predict such characteristics.

The behaviour of aircraft beyond the buffet-onset boundary has become increasingly important as a feature in the process of aircraft design and we need to put prediction techniques for aircraft characteristics in this regime on a firmer footing. One way to obtain information concerning buffeting behaviour at the design stage is to use wind-tunnel models with fully scaled flexibility. However, such models are expensive and not readily available. An alternative is to make measurements using relatively rigid models, but in this case a theoretical foundation for our understanding of buffeting is required, in order to provide a sound basis for the prediction of full-scale characteristics. The objective of the present paper is to outline the available theoretical methods for the dynamic analysis of buffeting and related phenomena such as wing-rocking, and to identify gaps in our understanding of the problems involved.

Historically, work on buffeting dates back to the investigation of an accident in 1930 which led to wind-tunnel testing of tail vibration at high angles of attack due to immersion in the separated stalled-wing flow. Originally the expression 'buffeting' was applied to such tail vibrations, and early work concentrated on what we now call 'tail buffeting'. Subsequently, interest shifted to the excitation of the wing itself by the fluctuating stalled flow above it, and this is what is currently meant by the term 'buffeting'. More recently, in the context of combat manoeuvres of fighter aircraft at high subsonic speeds, buffeting associated with shock-induced separations has become of primary importance. A related problem, mainly associated with work on high performance compressor and helicopter blades, is the oscillatory motion of a stalled wing in such a way that the nature of the flow separation differs at different instants in the cycle, possibly switching from attached to separated flow or from a leading-edge to a trailing-edge stall. This phenomenon, known as stall-flutter, is usually associated with a marked torsional (pitching) wing motion. The affinity between buffeting and stall-flutter has been discussed by Ring who pointed out that there may be situations where it is difficult to make the distinction. A basic feature of these problems is the closed-loop interaction between the fluid motion, involving separated flow, and the motion of the wing surface. Two types of mathematical model are available. One takes the form of non-autonomous equations representing a FORCED VIBRATION. The other consists of autonomous equations (ie not containing time explicitly) representing a non-linear LIMIT CYCLE. (This latter type of motion we will refer to as NON-LINEAR FLUTTER).

Whilst it is customary to regard structural buffeting as a forced vibration, in which the aerodynamic forcing term can in principle be obtained from measurements on a fixed wing, more basic research is required to determine the limits of applicability of this approach. In the distinction between forced vibration and non-linear flutter it is probable that the mean amplitude of wing motion is a relevant parameter, motion of small amplitude leaving the turbulent fluctuations in the separated flow essentially the same as in the fixed-wing case but leading to a small additive motion-dependent aerodynamic component (whose influence is primarily in damping). As the amplitude of motion increases, however, the possibility arises of the 'entrainment' of the larger scale irregular flow fluctuations, which influence circulation and wing lift, into a deterministic relationship with the wing motion. This type of resonance is of course most likely if the frequency of wing motion (Strouhal number) is close to some natural frequency of vorticity shedding in the separated flow. Thus, as the amplitude of motion increases, a changeover in the type of closed-loop interaction could occur.

An analogous problem concerning the choice of appropriate theoretical model also occurs in connection with wing-rocking. It is not yet clear whether wing-rocking should be regarded as the aerodynamically forced response of a stable system or in terms of limit-cycle oscillations of a system which is unstable at small amplitudes but whose motion is bounded by amplitude-dependent non-linear forces. An important area for future work is to determine the appropriate characteristics that may be identified on relatively rigid wind-tunnel models indicating the onset of wing-rocking at full scale. Corresponding to the two types of theoretical model (forced vibration or limit cycle) appropriate indications either take the form of measured fluctuating aerodynamic forces (such as rolling moments) or of the breakdown of some linear stability criterion for rigid-body motion (Dutch Roll stability for instance). The basic distinction is that the former method is based on the FLUCTUATING part of measured aerodynamic forces under separated flow conditions whilst the latter is based on the MEAN aerodynamic forces which determine stability derivatives.

## 2 GENERAL OUTLINE OF THEORETICAL MODELS

A common element of the problems discussed in this paper is the closed-loop interaction between the unsteady fluid motion, involving separated flow, and the motion of a wing. In this section we outline the ways in which a mathematical formulation of such problems may be made.

We begin by considering the influence of (in general) time-varying boundary conditions, applied at the surface of a wing, upon a rotational flow field. Two cases can be distinguished:

**a RANDOM FLOW FIELD** In this case substantially different flow time histories follow from nominally identical realisations of the boundary conditions. Thus, corresponding to given boundary conditions, there exists a whole family of compatible flow fields. Quantitative analysis is concerned with statistical properties, such as mean and correlations, of such a family.

**b DETERMINISTIC FLOW FIELD** Vorticity sheds in a regular manner from the boundary, and the flow field at any instant depends uniquely on the past history of boundary conditions.

An instructive example is that of a fixed cylinder shedding a regular vortex street. Despite the high degree of order in the vorticity distribution, the phase of the flow fluctuations is not determined by the boundary conditions and we have a special example of a random flow field. However, if the boundary conditions are changed by forcing the cylinder to perform sinusoidal oscillations of sufficient amplitude and appropriate frequency, in the neighbourhood of the natural shedding frequency, the phase of the flow fluctuations may become controlled by the cylinder motion, and the flow field becomes deterministic. This is an extreme example of the important result that, when the vorticity distribution contains a high degree of order, there is a tendency for the appropriate choice of theoretical model to depend on the mean amplitude of structural motion.

In the above distinction between random and deterministic flow fields the time-varying boundary conditions may either be externally imposed, by forcing the wing to follow some prescribed time history, or may arise through the structural response of the wing to aerodynamic forces. In the latter case the wing motion becomes one of the unknowns in the dynamic equations and we have a 'closed-loop' interaction.

The interaction between fluid motion and wing motion may be described in 'systems analysis' terms. The simplest system representation (Fig 2a) consists of a fluctuating aerodynamic force applied to a structure (which we take to represent either flexible or rigid-body response). Provided all aerodynamic force components are included, this model is a valid description of all the problems considered. In general, however, there are aerodynamic forces which depend on the motion of the structure, and these are not known a priori. Consequently, the open-loop formulation illustrated in Fig 2a, whilst valid in principle, is not generally the most useful.

The simplest 'closed-loop' system representation arises when the flow field is deterministic, depending uniquely on the past history of structural motion. As illustrated in Fig 2b there are in this case TWO independent deterministic relationships between the structural motion and the aerodynamic force (a generalised force, appropriate to the mode of response in question, taking the form of a weighted integral of pressures over the structure). One relationship is obtained from the equations of motion of the structure; and since the flow field is uniquely dependent upon the past history of structural motion we can, in principle, deduce a second relationship between structural motion and aerodynamic force from the equations of motion for the fluid. The joint time variation of structural motion and aerodynamic force may then be deduced as that compatible with these two independent relationships. The closed-loop system may be referred to as 'autonomous' or 'self-excited' and the motion takes the form of a limit cycle. Whilst the structural response can usually be adequately defined using linear equations, the fact that two INDEPENDENT functional relationships exist between aerodynamic force and structural motion requires that the aerodynamic feedback loop be nonlinear (we exclude the trivial case where the closed-loop fluctuations take the form of sinusoidal oscillations of an overall linear system in neutral equilibrium). We will refer to all such types of motion as **NONLINEAR FLUTTER**.

Finally, we consider the closed-loop system representation in the case where the flow field is random, differing flow time-histories following from identical realisation of structural motion. The appropriate system formulation then takes the form illustrated in Fig 2c, where two components of aerodynamic force are shown separated, one determined by, and one independent of, structural motion. Two particular cases of this formulation may be distinguished. In the first case the combination (indicated in Fig 2c by a dashed line) of structural motion and motion-dependent aerodynamic force forms a stable system which, left to itself, would settle down to a state of equilibrium. This is the **FORCED VIBRATION** model for the closed-loop system. In the second case the feedback loop itself produces self-excited oscillations and we have the situation of an essentially autonomous system disturbed by external noise. Whilst this latter theoretical model is little used in practice it is required conceptually if we wish to consider a continuous transition between forced vibration and nonlinear flutter.

In practical applications of the forced vibration model (Fig 2c) several further assumptions are often made which require careful investigation. In the first place it is usually assumed that the aerodynamic excitation, or 'motion independent aerodynamic force', is relatively wide band and can be obtained from measurements on a fixed wing. This assumption may be justifiable for low amplitudes of structural motion but requires validation in the general case. For, whilst the aerodynamic excitation of the system illustrated in Fig 2c is motion independent in the sense that it may be regarded as an 'external noise generator', the **STATISTICAL PROPERTIES** (such as power spectral density) of this force may in fact depend on the mean amplitude of structural motion. This possibility appears to have been first discussed in Ref 2, where it was invoked as a possible explanation of a trend in the experimental results. Since we cannot necessarily relate the aerodynamic forces illustrated in Fig 2c to forces measured on a fixed wing, the question arises as to how the separation into 'motion-dependent' and 'motion-independent' components of aerodynamic force may be made conceptually. It is shown in Ref 6 that this decomposition requires the introduction of an external test signal (such as an additional force).

If we make the assumption that the aerodynamic excitation may be obtained from measurements on a fixed wing, and also are able to obtain numerical estimates for the motion dependent aerodynamic force (of which the significant component is usually aerodynamic damping) the forced vibration model provides the basis of a method for predicting the amplitude of closed-loop response. It is therefore important to know whether the existence of separated flow significantly affects the linearity or magnitude of aerodynamic damping. Existing published information indicates a significant increase of damping under these conditions. In the case of

buffeting at high subsonic speeds some relevant results from recent flight tests are described in section 9.

Whilst the preceding discussion has been quite general, and applicable to an arbitrary mode of structural response, in the case of wing structural buffeting we take the view (in common with most previous workers) that a linear forced vibration model is generally appropriate. In the following section we consider in more detail such a model for buffeting response in the first wing-bending mode.

### 3 STRUCTURAL BUFFETING AND WING-ROCKING

In the case of structural buffeting of a wing it is usual to assume that a forced vibration theoretical model with linear aerodynamic damping, and aerodynamic excitation obtainable from fixed-wing measurements, is applicable. The response in the mode with displacement defined by the generalised co-ordinate  $z(t)$  is then represented by the linear differential equation

$$M \frac{d^2 z}{dt^2} + 2M \xi_a \omega_0 \frac{dz}{dt} + M \omega_0^2 z = x(t). \quad (1)$$

$x(t)$  is the aerodynamic excitation, having no feedback from wing motion, obtained as an integral over the wing involving the associated fluctuating pressure distribution and the mode shape. Statistical response calculations, on the basis of equation (1) involve the power spectrum of  $x(t)$ , obtainable in principle from cross-correlation measurements of fluctuating pressures. This analytical model (Fig 3), applied to the first symmetric wing-bending mode, has been the usual way to treat structural buffeting in the past<sup>1,2</sup>. In equation (1),  $M$  is an 'equivalent mass' and  $\omega_0$  is the undamped natural frequency. It is assumed that the significant component of motion dependent aerodynamic force takes the form of a linear viscous damping term, with damping ratio  $\xi_a$ , the effect of aerodynamic forces on the stiffness and inertia being negligible. In general, aerodynamic damping will depend on frequency, but since we are considering the response in a single relatively lightly-damped structural mode, the approximation with  $\xi_a$  taken as a constant will be adequate provided we use a value appropriate to the bending frequency. The contribution of structural damping has been purposely omitted from equation (1), as its contribution appears to be significantly smaller than that of aerodynamic damping in the buffeting situation on a full-scale aircraft and, moreover, its correct representation is still subject to uncertainty. The simplest assumption would be to assume a viscous damping proportional to the rate  $dz/dt$ , in which case the energy dissipated per cycle would be proportional to frequency. However, there is evidence that both the slipping effects of a riveted structure and the internal damping of many engineering materials exhibit a type of damping in which the energy loss per cycle is proportional to the square of the strain amplitude, independent of the frequency. This is the assumption made in the theoretical analysis in Ref 2. It should be noted that equation (1) neglects possible aerodynamic coupling between the mode under consideration and other structural modes. As discussed in section 2 the principle questions raised by the forced vibration model, equation (1), and which require further experimental investigation, are whether the statistical properties of  $x(t)$  are in fact independent of the mean amplitude of wing motion and whether the aerodynamic damping is both linear and predictable.

The dynamic analysis of rigid-body motions in the presence of separated flow follows the general pattern outlined in section 2 and will only be discussed here in general terms. The principle rigid-body mode of interest is the lateral roll-yaw oscillation, or Dutch Roll. In the case of wing-rocking, two possible types of analytical model exist, analogous to the systems illustrated in Figs 2b and 2c, one representing an autonomous oscillation and the other a forced vibration. On the basis of existing information it is not yet clear which is the appropriate formulation. However, a flight-test investigation of this question is in progress (see section 9). If wing-rocking proves to be an autonomous oscillation with the motion unstable at small amplitudes but confined to finite amplitudes by nonlinear forces, its onset may be preceded by a detectable decrease in Dutch Roll stability. This would link wing-rocking with those phenomena involving a divergent instability (wing-drooping, nose-slice) whose onset has previously been associated with linear stability boundaries. In all such cases, the aerodynamic derivatives required are those relevant to the separated flow condition, including effects of wing separated flow on the rear fuselage or tail and in the case of damping derivatives should be evaluated at small amplitudes of motion. The other possibility is that wing-rocking be interpreted as a forced vibration, excited by fluctuating aerodynamic forces which are independent of wing motion. Fluctuating rolling moments have been observed on fixed models at high lift, but it is not known to what extent coupling arises when rolling motion occurs.

### 4 CONTRAST BETWEEN EXTERNALLY FORCED AND STRUCTURALLY RESPONDING WING

Whilst the mutual interaction between the separated flow field and the motion of the wing surface is an essential part of the buffeting phenomenon, significant information can be obtained by breaking into the loop and considering the fluid motion, and associated pressure fluctuations, in response to an externally imposed time history of wing motion. We will refer to such open-loop response as 'externally forced' in contrast to the closed-loop, mutually interacting, case when we will say the wing is 'structurally responding' (Fig 4). The distinction is that in the case of a structurally-responding wing the aerodynamic force is related to wing motion through the equations for structural response. In the case of externally-forced motion however, the existence of additional externally imposed forces destroys the influence of pressure fluctuations (and the associated aerodynamic force) upon wing motion.

Using the terminology introduced in section 2, if the motion of the structurally responding wing takes the form of non-linear flutter, the fluid motion is related to wing motion in a completely deterministic manner. In this case the flow field and associated pressure fluctuations depend only on the time history of motion of the wing and are independent of whether it is externally forced or is structurally responding. However, if the structurally responding wing motion takes the form of an aerodynamically 'forced vibration' (section 2), the flow field is random and the statistical properties of pressure fluctuations will, in general, differ from those occurring on an externally forced wing, even for identical time histories of wing motion. For, in the case of externally forced motion, the ensemble (family) of fluid motions corresponding to a given time history of wing motion consists of all those flow fields compatible with the boundary conditions imposed by the wing surface velocities. In the case of a structurally responding wing, however, there is a smaller ensemble of compatible fluid motions consisting of the subset of flow-fields which satisfy IN ADDITION the relation between aerodynamic force and wing motion imposed by the equations for structural response (Fig 4). Since the aerodynamic force is obtained as an integral over the wing involving pressure fluctuations and mode shape, in the case of a structurally responding wing there is an additional integral constraint enforced on the ensemble of possible flow fields. A particular consequence is that the fluctuating aerodynamic forces on externally-forced and structurally-responding wings have differing statistical properties, which we will illustrate by means of a numerical example.



Consider the structurally-responding wing whose motion is defined by the differential equation

$$\frac{d^2 z}{dt^2} + 2(\xi_a + \xi_s) \frac{dz}{dt} + z = x(t). \quad (2)$$

This is a simple extension of equation (1) to include the effect of viscous structural damping  $\xi_s$ . Without loss of generality we have chosen units such that the undamped natural frequency is unity. The overall damping ratio  $\xi_t$  of the system has been taken as 0.1, 20% of which is contributed by structural damping. Thus

$$\xi_a = 0.08, \xi_s = 0.02, \xi_t = 0.1.$$

The power spectrum of aerodynamic excitation  $x(t)$  is taken to be flat in the vicinity of the resonant frequency, and to have unit power per unit bandwidth. The power spectra  $\Phi_z$  of wing motion and  $\Phi_y$  of total aerodynamic force (Fig 3) are then as illustrated in Fig 5. It can be seen that whilst  $\Phi_z$  has a peak for frequency  $\omega = 1$ ,  $\Phi_y$  has a corresponding region of low spectral density (a 'hole' in the spectrum.)

Suppose now that an experiment be performed in which the wing is externally forced (Fig 4) to follow an identical time history of motion. That is to say, the wing is constrained by additional external forces to move in such a way that  $z(t)$  follows the solution of equation (2), but is now completely uncorrelated with the motion-independent component of aerodynamic force  $x(t)$ . In this situation, although the spectra of  $z(t)$  and  $x(t)$  are unaltered, the spectrum of total aerodynamic force  $\Phi_y$  differs from  $\Phi_y$  as illustrated in Fig 5,  $\Phi_y$  having a peak related to that in  $\Phi_z$ . It is clear from a comparison of  $\Phi_y$  and  $\Phi_z$  that, in the case of a structurally-responding wing, the phase-relation existing between  $z(t)$  and  $x(t)$  has a dominating effect on the spectral density of the total aerodynamic force in the neighbourhood of the resonant frequency. The correlation existing between  $z(t)$  and  $x(t)$  is an essential element of the way in which aerodynamic damping operates: by partial cancellation of the motion-independent component of aerodynamic force. Some implications of this result for the interpretation of measured pressure fluctuations from flight-tests are discussed in section 6.2.

## 5 INTERPRETATION OF STRUCTURAL RESPONSE MEASUREMENTS

The consequences of the 'forced vibration' theoretical model, for the interpretation of structural response measurements of a buffeting wing, have been extensively discussed elsewhere (see, for example, Ref 2). Here we briefly review those results applicable to full-scale flight tests.

Measurements of structural response may be made using strain gauges or accelerometers. The former technique has been extensively used in the past for predicting full-scale buffeting intensity on the basis of wind-tunnel tests, for instance in the technique of Mabey in which relatively rigid models are used and tunnel noise employed as a reference excitation. However, if the objective is to measure the fluctuating motion of the wing, accelerometers may be preferable.

On the basis of the forced vibration model (Fig 3), applied to buffeting response in the first wing-bending mode (for instance), the effects of varying air density may be deduced. If we make the assumption that the damping is predominantly aerodynamic, then since aerodynamic forces are proportional to air density, we have

$$\xi = \text{constant} \times \rho. \quad (3)$$

Making the additional assumption that the aerodynamic excitation  $x(t)$  has a relatively flat spectrum in the vicinity of the resonant frequency,  $\xi$  may be deduced from the rate of decay of the autocorrelation function of a band-pass filtered accelerometer (or strain gauge) signal. In conjunction with equation (1), equation (3) implies that

$$\sigma = \text{constant} \times \rho^{1/2}, \quad (4)$$

where  $\sigma$  is the root-mean-square value of fluctuating normal acceleration (for instance) over the bandwidth of the mode considered. Equations (3) and (4) refer to conditions in which dynamic pressure is varied whilst non-dimensional aerodynamic parameters are held constant. In particular, it is assumed that the separated flow 'pattern' is insensitive to associated changes in Reynolds number. It should be noted that this restriction almost certainly excludes conditions near buffet onset, when separated flow is first developing on the wing.

Measurements of the structural response of a buffeting wing, obtained from full-scale flight tests in which variable air density was obtained by testing over a range of altitudes, are described in section 9. In the case of wind-tunnel experiments it is in principle possible to subject theories for buffeting to a more critical test by comparing models with differing stiffness. For example, Rainey and Byrds tested models having identical geometry but constructed of steel, aluminium, and magnesium alloys, and compared results with theoretical predictions (including effects of structural damping). In Ref 2 the possibility of a significant variation of the statistical properties of aerodynamic excitation  $x(t)$  (Fig 3) with the mean amplitude of wing motion is suggested and the linearity of aerodynamic damping in buffet queried. Twelve years later, answers to such questions are still only speculative and the need for further wind-tunnel experiments is apparent. Moreover there is now a requirement to extend our understanding to higher transonic speeds where shock-induced separations play a crucial role. An experimental programme to investigate these problems further is currently being developed at the Royal Aircraft Establishment.

## 6 SOME APPLICATIONS OF FLUCTUATING PRESSURE MEASUREMENTS

There is an increasing trend towards the use of fluctuating pressure measurements for the study of buffeting. We now consider some possible applications of such measurements on the basis of the forced vibration model of buffeting.

### 6.1 Measured fluctuating pressures on rigid wing

By taking measurements at a sufficient number of points, and integrating pressures to obtain overall forces, it is in principle possible to use fluctuating pressures on a scaled-model rigid wing in a wind-tunnel as the basis of a statistical calculation of buffeting response. The basic quantity required for such a calculation is the power spectrum of  $x(t)$  (Fig 3), which arises as an integrated product of the structural mode shape and the cross-spectrum of pressure fluctuations. As a result, only those fluctuating pressures which are correlated over distances of the order of a 'wavelength' of the structural mode will significantly contribute to the excitation. In the case of the first symmetric wing-bending mode, only those pressure fluctuations contributing to fluctuations in circulation, and lift on associated chordwise wing sections, will be relevant. In contrast to the excitation of wing panels by a region of separated flow,

when the associated relatively high frequency pressure fluctuations are generated primarily in the shear layer and appear almost exclusively directly beneath the region of separated flow, the effects of separation on circulation and associated lift arise in a way that is not fully understood. One possibility is that a significant component of fluctuating circulation may arise as an indirect effect of the separated flow, through the breakdown of the Kutta condition which normally determines the circulation. We cannot necessarily assume that the relevant pressure fluctuations are located only beneath the separated flow region. It is quite possible that the whole flow field around the wing is inherently unsteady and thus pressure fluctuations which contribute to fluctuating lift may be significantly large at all points where there are large spatial mean-pressure gradients.

On the assumption that the aerodynamic excitation  $x(t)$  is statistically independent of the mean amplitude of wing motion, and that some means of estimating the damping is available (see section 7), an estimate of the power spectrum of  $x(t)$  based on rigid-wing measurements may be employed in a calculation of buffeting response using equation (1). This method has previously been employed for a slender wing with a leading-edge vortex. However, in the case of a swept wing at high subsonic speeds, the possibility of using fixed-wing pressure fluctuations as a basis for the prediction of buffeting amplitudes requires critical investigation. The aerodynamic damping ratio  $\xi_a$  in general contains components from both attached flow and separated flow regions on the wing, and should of course take the value appropriate to the mode frequency. In section 9, flight-test results are described which indicate large variations with  $C_N$  of aerodynamic damping on a buffeting wing. This may imply a significant limitation on the quantitative use of pressure fluctuations measured on rigid wings.

## 6.2 Measured fluctuating pressures on structurally responding wings

We turn now to the case where fluctuating pressures are measured on a buffeting wing which is structurally responding in a flexible mode. This includes both full-scale flight experiments and measurements in wind-tunnels using models with scaled elastic properties. The interpretation of such measurements, if taken in isolation, is complicated by the fact that the fluctuating pressure distribution is in general the sum of superposed aerodynamic excitation and response fields (including aerodynamic damping). As we shall indicate, considerably more information may be obtained from wind-tunnel tests if fluctuating pressures on structurally-responding wings and on rigid wings with similar geometry are compared.

We suppose that the wing buffeting is approximately modelled as a forced vibration, in which case the fluctuating pressure  $p(t)$  at an arbitrary point on the wing may be expressed as the sum of two components: a 'motion dependent' component  $p_d(t)$  and a 'motion independent', or aerodynamic-excitation, component  $p_x(t)$ . The power spectrum of  $p_d(t)$  will consist of a narrow-band peak at the resonant frequency of response and the spectrum of  $p_x(t)$  is assumed to be relatively wide band. At points on the wing where the primary component of  $p(t)$  is  $p_d(t)$  (this probably includes most points on the lower surface) the spectrum of  $p(t)$  will consist of a narrow band peak (see Fig 12b). In general, however,  $p_x(t)$  and  $p_d(t)$  will both contribute significantly and the shape of the spectrum of  $p(t)$  will depend critically on the degree of correlation, and the phase-relationship, between these two components. It is argued in Ref 6 that the power spectrum of  $p(t)$  could in principle take any form between a wide-band spectrum with a superposed narrow-band peak and a wide-band spectrum with a 'hole' similar to that in  $\Phi_y$ , Fig 5. However, the latter phenomenon would require almost perfect correlation between  $p_d(t)$  and  $x(t)$  and between  $p_d(t)$  and the 'motion-dependent' aerodynamic force, and it is doubtful whether the spatial correlation of  $p_x(t)$  is ever sufficiently strong for this condition to be realised on a three-dimensional wing.

We may conclude from the above discussion that measured pressure fluctuations on a structurally responding wing, as in flight test, are difficult to interpret on a quantitative basis. In contrast, by comparing power spectra of fluctuating pressures on a structurally-responding wing and on a rigid wing with similar geometry in a wind-tunnel experiment, it should be possible to obtain a relatively direct test of the appropriate analytical model for buffeting. Whilst the interpretation of spectra at resonant frequencies is subject to the uncertainties described in the previous paragraph, the conclusions to be drawn by comparing spectra from structurally-responding and rigid wings at off-resonance frequencies are relatively straightforward. A basic assumption required in most practical applications of the forced vibration analytical model of buffeting is that the statistical properties of aerodynamic excitation are independent of the mean amplitude of motion. This result implies that spectra of fluctuating pressures measured on structurally-responding and rigid wings should be identical except in the immediate neighbourhood of resonant frequencies. If, due to wing motion, the spectra are modified over a wide frequency band, but a significant amount of energy remains at off-resonance frequencies, the forced vibration hypothesis may still be valid but the statistical properties of excitation cannot be deduced from rigid-model tests and the analytical model loses much of its practical value. If, as a result of wing motion, a negligible amount of energy remains in the pressure fluctuation spectra, except in the neighbourhood of the resonant frequency and its harmonics, the flow field on the structurally-responding wing has become essentially deterministic and the concept of a forced vibration is no longer appropriate.

The essential characteristics of the above type of experiment remain unaltered if, instead of using a structurally responding wing, we use one which is externally forced to oscillate sinusoidally at the appropriate frequency and amplitude. As discussed in section 4, pressure fluctuations measured at the frequency of oscillation may differ significantly in this case from those on the structurally-responding wing. However, the interpretation of the effect of wing motion at frequencies other than that of the forced oscillation is essentially as discussed in the previous paragraph.

Whilst experiments of the above general type have been previously performed, none is directly relevant to wing buffeting at high subsonic speeds. It would appear that some basic research of this type is necessary in support of the experimental investigation of wings at high lift currently being planned on the basis of wind-tunnel tests of relatively rigid models.

## 7 THE MEASUREMENT OF AERODYNAMIC DAMPING

In order to make use of measured pressure fluctuations on a rigid wing, as described in section 6.1, in a dynamic calculation of buffeting intensity it is necessary to estimate the aerodynamic damping. A general review of experimental techniques for this purpose is given in Ref 11, where a wide variety of methods is discussed in detail. Here we indicate the novel features that can arise through the existence of random pressure fluctuations associated with regions of separated flow. Particular attention is paid to wing flexible response, but the general ideas are equally applicable to the case of rigid-body motions.

To recapitulate, on the basis of the linear forced vibration model for buffeting, it is assumed that the time-varying forces on the wing may be separated into two components, one providing stabilising forces (particularly damping) linearly dependent on the motion, and the other providing the driving mechanism. In contrast to the case of attached flow, motion-dependent forces such as damping must be measured statistically, ideally averaged over many cycles of wing motion.

Three main types of damping measurements are possible in the present context:

- (a) Those which are based on analysis of the natural buffeting response, assumed to be due to the fluctuating force component  $x(t)$ .
- (b) Those which make use of external influence to set up initial conditions, the analysis being based on the subsequent transient response.
- (c) Those which make use of a continuously-applied external fluctuating force.

We discuss each of these in turn.

(a) On the assumption that the fluctuating input  $x(t)$  is not only unaffected by wing motion but also has a flat spectrum in the neighbourhood of the structural response frequency, the shape of the power spectrum of wing motion  $Z(t)$ , or alternatively the autocorrelation function of  $Z(t)$ , may be used to estimate the total damping. In the case of a power spectrum measurement the damping may, in principle, be determined from the bandwidth of the spectrum peak between the half-amplitude points, and in the case of the autocorrelation function from the logarithmic decrement of successive peaks. In practice, because of the smoothing effect of the 'windows' employed in spectral analysis, the latter method generally proves more satisfactory. Assuming that the structural damping is either known (say from ground-resonance tests), or negligible, we can thus infer the magnitude of the aerodynamic damping ratio  $\xi_a$ .

(b) Under conditions of attached flow, a standard method for the measurement of damping ratio involves perturbing the system with an initial transient excitation and measuring the subsequent rate of decay of response. For instance, in flight tests, 'bonkers' at the wing tip are sometimes used in flutter investigations, and in a wind tunnel, initial perturbed conditions may be set up and the model subsequently freed. An analogous test method may also be used in the presence of separated flow provided the results are analysed appropriately. In this situation the transient response does not decay to zero but to an 'equilibrium' level of fluctuation dependent on the amplitude of excitation  $x(t)$ . Indeed, it is this residual response fluctuation which is used to measure damping in method (a) above. The method under discussion makes use of response amplitudes raised above the residual fluctuation level by the externally imposed initial conditions. This increase in response amplitude will lead to improved accuracy in damping estimates in the sense that the amplitude of motion can be measured to a higher percentage accuracy. However, the choice of method is not entirely arbitrary, and depends on the proposed application of the damping measurements. Since, particularly under separated flow conditions, the aerodynamic damping may in fact be amplitude dependent (non-linear), estimates for use in an (approximate) linear model should be based wherever possible on measurements at the response amplitudes of interest. If it is desired simply to estimate the parameters in the dynamic model of buffeting response illustrated in Fig 3, the response level of interest is that of the residual fluctuation after any transient disturbance has decayed and method (a) above is appropriate. However, if it is desired to predict the response of the system in the presence of external disturbances (such as atmospheric turbulence), or to investigate possible non-linear (amplitude dependent) effects, or if the residual fluctuation level is so low that accurate amplitude measurements cannot be made, the use of an externally imposed initial disturbance is called for.

The evaluation of damping ratio from the decay of response subsequent to prescribed initial conditions must take account of the existence of the continuing fluctuating force  $x(t)$  (here assumed to be of non-negligible amplitude). The standard method, appropriate in the attached-flow situation, of taking the log-decrement of successive response peaks, leads to an estimate of damping biased to low values, as the effect of  $x(t)$  is to reduce the average rate of decay of successive peak amplitudes. It can be shown<sup>6</sup>, however, that an unbiased damping estimate can be based not on two peak values but on the response amplitudes at two successive instants, the first of which corresponds to a peak and the second occurs a time later equal to one mean period (owing to the disturbing effect of  $x(t)$  the time interval between successive peaks will vary in a random manner). Furthermore, such estimates should be combined<sup>6</sup> using a weighting factor equal to the square of the initial peak amplitude (as the effect of  $x(t)$  is relatively less at large amplitudes of response). It can also be shown that if, as a special case, this technique using weighted estimates is applied to the free response of the system to the continuous aerodynamic excitation  $x(t)$ , the result obtained for damping ratio is exactly the same as the autocorrelation estimate described in method (a).

(c) A third approach to damping measurement makes use of an externally applied continuous fluctuating force, or 'test-signal'  $u(t)$  (see Fig 6). It can in fact be subdivided into two distinct methods, one of which makes use of cross-correlation techniques and the other of the measured rate of working of an external force. As in case (b), above, it is relevant that the aerodynamic damping in the presence of separated flow may be amplitude dependent, and so the test signal must not raise the average response level above that relevant to the particular application for which a damping estimate is required. If the required amplitude is that corresponding to structural response to the aerodynamic excitation  $x(t)$ , we have the problem that the test signal  $u(t)$  should be of an intensity which is measureable and yet small enough to leave the overall amplitude of response essentially unaltered.

Using cross-correlation techniques, the test signal  $u(t)$  should be a random function with bandwidth significantly larger than that of the buffeting wing motion. The aerodynamic transfer function, and in particular the aerodynamic damping ratio at the structural response frequency, may then, in principle, be obtained as the ratio of cross-spectra  $\Phi_{uy}/\Phi_{ux}$  (Fig 6). This method has the disadvantage that measurement of the fluctuating aerodynamic force  $y(t)$  is required, involving integration of measured pressures over the wing, and to the author's knowledge has not yet had a practical test.

A simpler method of analysis is that described in Ref 3. This makes use of the fact that the total damping in the closed-loop is related to the average rate of working of an external force. Moreover, this quantity is relatively simple to evaluate for a sinusoidal forcing function at the undamped natural frequency of the wing. It is shown in Ref 3 that, using the terminology of equation (1) and taking time averages:

$$2M\xi\omega_n \overline{u(t) dz/dt} = \overline{u^2(t)}.$$

Ref 3 describes an electromagnetic shaker system whereby  $\overline{u^2(t)}$  is determined from the current and  $\overline{u(t) dz/dt}$  from the power consumed. Thus the total damping  $\xi$  may be measured and, assuming that the structural damping is known (eg from a wind-off wind-tunnel test), then  $\xi_a$  can be deduced.

The above method is not the only one possible involving external excitation: a variety of similar techniques are described in Ref 11. It has been singled out for attention here because it has been practically tested with apparent success in the context of unsteady separated flow.

A fundamental difficulty in all techniques involving the application of externally forced excitation is that motion must take place in the mode of interest. In the case of rigid-body modes there may be relatively little problem, but in the case of structural response in a flexible mode it is generally difficult to excite motion purely in a particular chosen mode - a fact that is well known in the context of aircraft ground resonance testing.

## 8 RESPONSE TO TRANSIENT BUFFET EXCITATION

We end this outline of theoretical methods for the dynamic analysis of buffeting by mentioning that the 'forced vibration' model (Fig 3) has been used as a basis for the investigation of buffeting response occurring during a transient incursion into the buffet regime, due to either a gust or a manoeuvre. Using the theory of non-stationary random processes, observed lags in buffeting build-up and decay can be shown to be of similar size to the predicted delays in the response of wing structure. These delays in structural response are in addition to lags associated with unsteady aerodynamics. A particular application discussed in Ref 12 concerns the buffeting induced on a subsonic transport aircraft by a vertical gust. Such an aircraft often cruises quite close to its buffet onset boundary and, in severe turbulence, may be expected to intermittently penetrate beyond its buffet boundary due to fluctuations in incidence.

The dynamic analysis of this situation may be based on the model illustrated in Fig 3, in conjunction with the theory for the transient response of a linear system excited by a random input. This theory may be used to evaluate the response of the system, in statistical terms, when an input signal such as  $x(t)$  (Fig 3) is either suddenly switched on, or grows smoothly from zero amplitude in some prescribed manner.

For instance, suppose that  $x(t)$ , equation (1), takes the form

$$x(t) = \alpha(t)N(t),$$

where  $N(t)$  is 'white noise' of uniform spectral density  $\Phi$  (per rad sec<sup>-1</sup>) and  $\alpha(t)$  is a prescribed function, related to the incidence penetration beyond buffet onset, satisfying

$$\alpha(t) = 0, t < 0.$$

Then it can be shown that the equation for the (ensemble) mean square response  $\sigma_z^2$  at time  $t$  is given by

$$\sigma_z^2(t) = (\pi \Phi / M) \int_0^t \alpha'(\tau) h^2(t-\tau) d\tau,$$

where  $h(t)$  is the response of the system to a unit impulse. Practical applications of this result are described in Ref 2, and include, for instance, the effect of the length of a gust on the alleviation of maximum buffeting response.

## 9 FLIGHT TESTS TO INVESTIGATE BUFFETING

During 1971 flight tests on wing buffeting and handling characteristics of a small combat trainer aircraft during high 'g' manoeuvres have been carried out at the Royal Aircraft Establishment, Bedford. The general objective of this flight programme, which it is intended to continue in 1972, has been a clarification of the handling limitations, associated with wing flow separations, particularly in the range  $M=0.7$  to  $0.9$ . Whilst the emphasis in the quantitative results obtained so far has been on wing structural buffeting, particularly in the first symmetrical bending mode, it has become increasingly apparent that the primary limitation on the performance of this aircraft at high 'g' levels is the degradation in handling qualities associated with wing-rocking (see section 1). The aircraft, which has a 7% thick swept wing, carries on-board recording equipment for pressure altitude, airspeed, normal acceleration, wing incidence (obtained using a nose probe) and aileron angle. Telemetry is employed to obtain ground-based records of fluctuating wing-tip and cockpit acceleration, and fluctuating pressures at three points on the wing upper surface and one on the lower. Quasi-steady buffeting conditions have been obtained for periods of approximately 10 sec during diving turns in which Mach number and normal acceleration are held approximately constant. A typical measured power spectrum of the fluctuating output of a wing-tip accelerometer is illustrated in Fig 7. A variety of modes, indicated by spikes in the spectrum, are present, the one of lowest frequency corresponding to symmetric wing bending. The response in this mode appears to play a significant role in the pilot's perception of buffeting, and was selected to provide a measure of buffeting intensity for quantitative analysis. For this purpose the output from the wing-tip accelerometer was filtered so as to remove most of the contribution from other modes. Fig 8 is typical of results obtained in this manner. Buffeting intensity, as measured by the root-mean-square intensity of the filtered signal, steadily increases as normal force coefficient is increased above a level corresponding to 'buffet onset'.

A typical sequence of events, as wing incidence is increased, is for a local region of separated flow first to appear over a small region of the wing in the vicinity of the tip. The fluctuations associated with such a separation are of relatively high frequency and excite only high order structural modes. As incidence is further increased the area of separated flow grows and the structural response extends to lower frequencies. (The relationship between the spatial extent of a separation bubble and the associated frequencies of fluctuation has recently been discussed by Mabey<sup>10</sup>). Only when the separated flow covers a considerable area does the first wing-bending mode become significantly excited and it is at this point that a pilot appears to first become aware of structural buffeting. It was established that pilot perception of buffet onset corresponded approximately to an rms output of  $\sigma = 0.75g$  from the filtered wing-tip accelerometer (Fig 8). This quantitative value was subsequently used to identify the buffet-onset boundary, Fig 9. The general trend of this boundary is consistent with results obtained using wind-tunnel models, the upturn at  $M > 0.85$  being associated with the change from a leading-edge bubble-type separation to an outboard shock-induced separation at the higher Mach numbers.

The opportunity has been taken to measure the damping of the first wing-bending mode during buffeting. On the assumption of the forced vibration model for buffeting, involving wide-band excitation, the damping may be obtained from the autocorrelation function of the wing-tip accelerometer signal. Typical results are illustrated in Figs 10 and 11. As the interpretation of the auto-correlation function in terms of damping is subject to the theoretical model assumed, we have called  $\xi$  the 'apparent damping'. Values of  $\xi$  before buffet onset are obtained from dynamic tests using excitation by small tip rockets (bonkers) or flights through turbulence. It can be seen from Fig 10 that  $\xi$  increases markedly as the buffet onset level is approached, and subsequently decreases again. This result indicates that practical problems occur as to the choice of damping values to be employed if calculations covering the whole range of buffeting intensities are to be made on the basis of a forced vibration theoretical model. The variation of  $\xi$  with altitude illustrated

in Fig 11, corresponding to a fairly high level of buffeting intensity at  $M=0.88$ , is compatible with the theoretical result, equation (3). In addition, the associated measured values of root-mean-square buffeting intensity  $\sigma$  at this Mach number are compatible with equation (4).

Sample results from measured pressure fluctuations are presented in Figs 12 and 13. Fig 12 illustrates power spectra of typical upper and lower surface measurements, the former being influenced by both excitation and damping fields and the latter predominantly by damping (see discussion in section 6.2). Fig 13 illustrates the variation with  $C_N$  of the intensity of pressure fluctuations at two stations on the upper surface. It should be noted that the outboard transducer shows a higher level of fluctuation around buffet onset, rises to a maximum value, and subsequently decreases again when the separated flow is well established.

It is planned to make detailed investigations of the wing-rocking motion of the aircraft during 1972. The aircraft has been fitted with additional instrumentation to record roll-rate, yaw-rate and lateral acceleration. It should thus be possible to define the motion in detail by means of model-matching techniques. In addition it is intended to measure aerodynamic derivatives within the range of lift coefficients beyond buffet onset but prior to wing-rocking. The objective is to investigate the properties of the Dutch Roll mode to see if any significant trends occur as the wing-rocking condition is approached. It is already apparent from pilot comments that there is a marked increase in Dutch Roll damping as the aircraft penetrates beyond buffet onset. This part of the programme is being backed-up by theoretical stability studies incorporating estimates of aerodynamic derivatives at high lift obtained from wind-tunnel data.

#### REFERENCES

- 1 Y C Fung An introduction to the theory of aeroelasticity - John Wiley, 1955
- 2 A G Rainey An examination of methods of buffeting analysis based on experiments with wings of varying stiffness - NASA TND-3, 1959
- 3 T A Byrdsong  
A G Rainey Measurement of aerodynamic forces for various mean angles of attack on an airfoil oscillating in pitch and on two finite-span wings oscillating in bending with emphasis on damping in the stall - NACA Rep 1305, 1957
- 4 H W Liepmann Parameters for use in buffeting flight tests - Rep No SM-14631, Douglas Aircraft Co, 1953
- 5 W R Burris Effect of wing leading edge geometry on manoeuvring boundaries and stall departure  
D E Hutchins AIAA Paper No 70-904, 1970
- 6 J G Jones A survey of the dynamic analysis of buffeting and related phenomena  
RAE Tech Rep (to be published)
- 7 C G B Mitchell Calculations of buffeting of slender wing aircraft at low speed - Unpublished MOD Report
- 8 D G Mabey An hypothesis for the prediction of flight penetration of wing buffeting from dynamic tests on wind tunnel models. - ARC CP 1171, RAE Tech Rep 70189, 1970
- 9 L F East Proposals for research into the aerodynamics of wing buffet  
Unpublished RAE memorandum
- 10 D G Mabey Pressure fluctuations caused by separated bubble flows at subsonic speeds  
RAE Tech Rep 71160, 1971
- 11 J B Bratt Wind tunnel techniques for the measurement of oscillatory derivatives.  
AGARD Manual of Aeroelasticity, Part IV. Chap. 5.
- 12 J K Zbrozek Transient buffet loads on wings.  
J Sound Vib. 5(2), 1967
- 13 J G Jones Evaluation of the transient response of a linear system excited by a random input.  
RAE Tech Rep TR 69092, 1969.

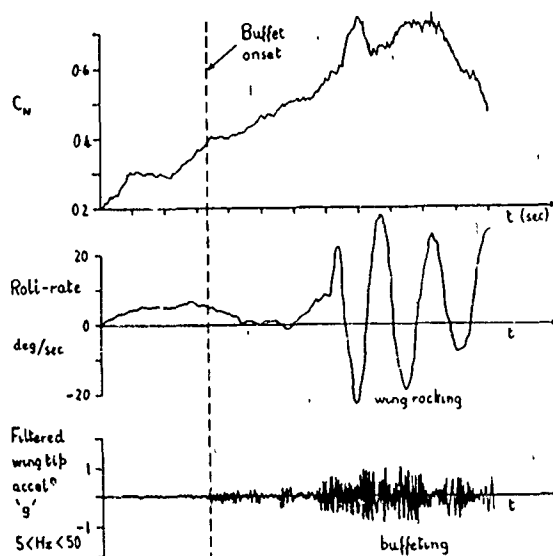


Fig 1 Typical penetration to high  $C_N$  of fighter-type aircraft (schematic)

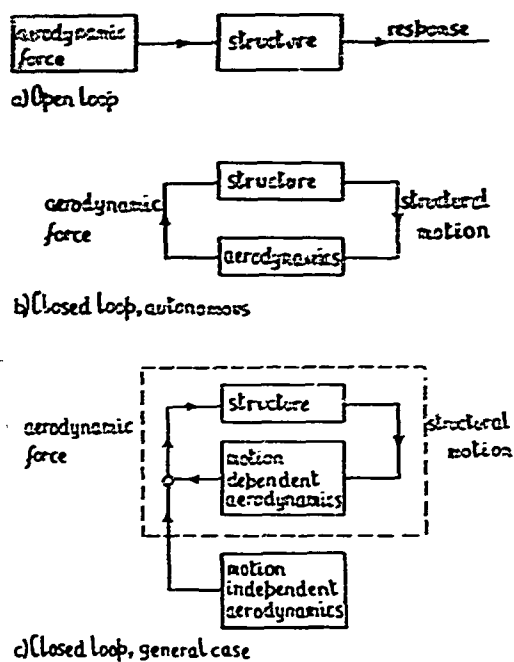


Fig 2 Models of dynamics

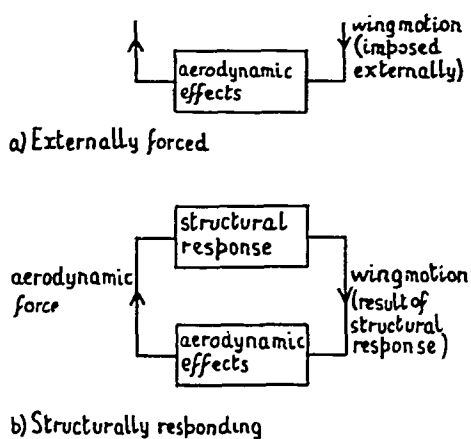


Fig 4 Externally-forced and structurally-responding wing

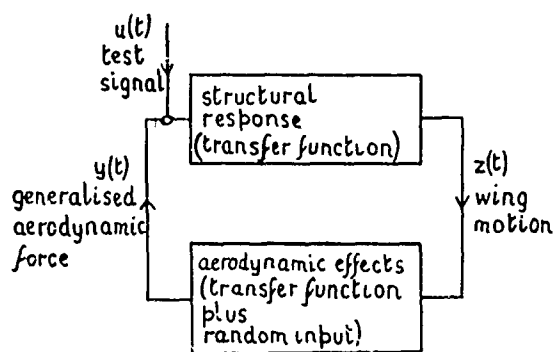


Fig 6 Use of test signal in damping measurement

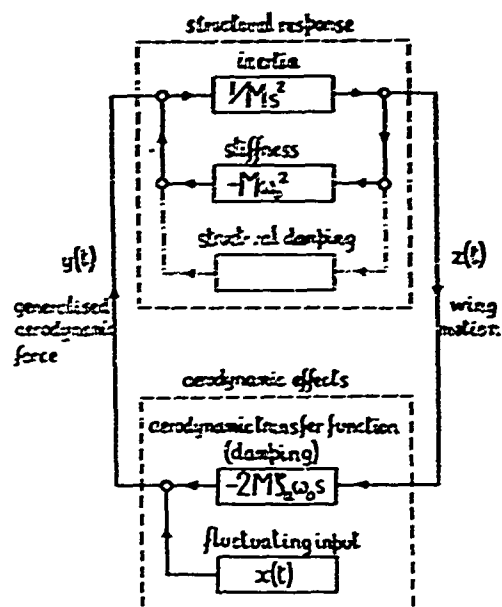


Fig 3 Block diagram for structural buffeting

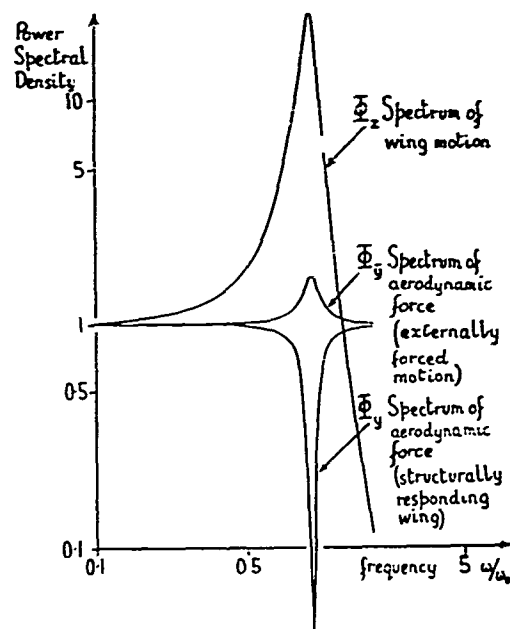


Fig 5 Power spectra of aerodynamic forces on externally-forced and structurally-responding wing

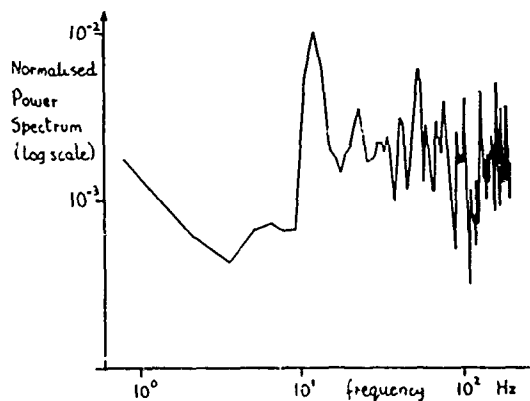


Fig 7 Power Spectrum of normal acceleration at wing tip

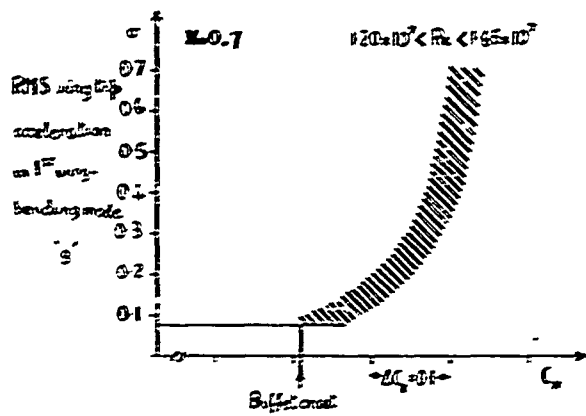


Fig 8 Variation of buffeting intensity with  $C_N$

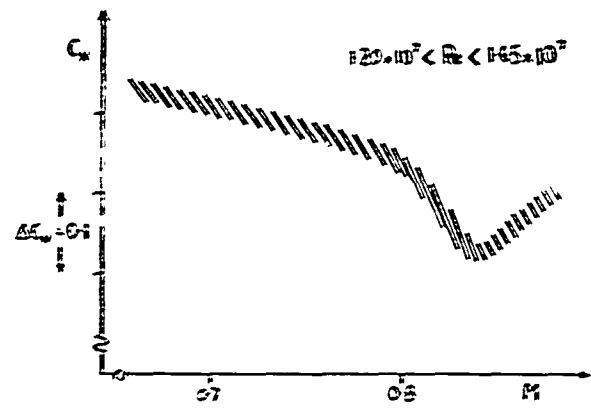


Fig 9 Measured buffet onset boundary

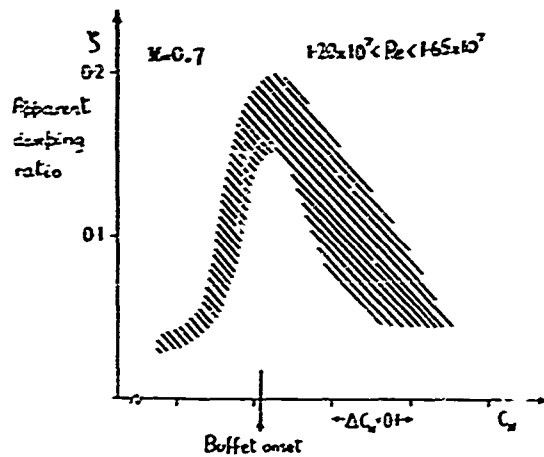


Fig 10 Measured variation with  $C_N$  of apparent damping of 1st wing-bending mode

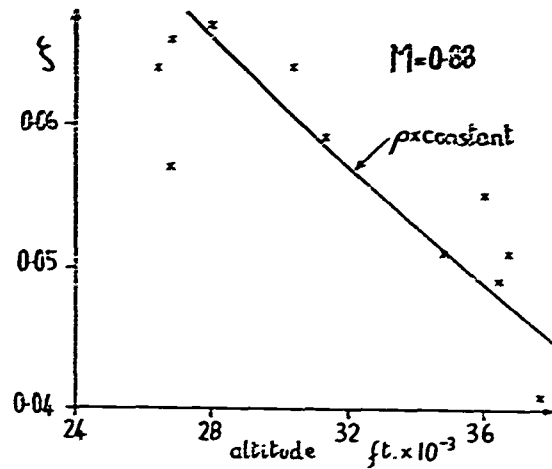


Fig 11 Measured variation with altitude of apparent damping ratio

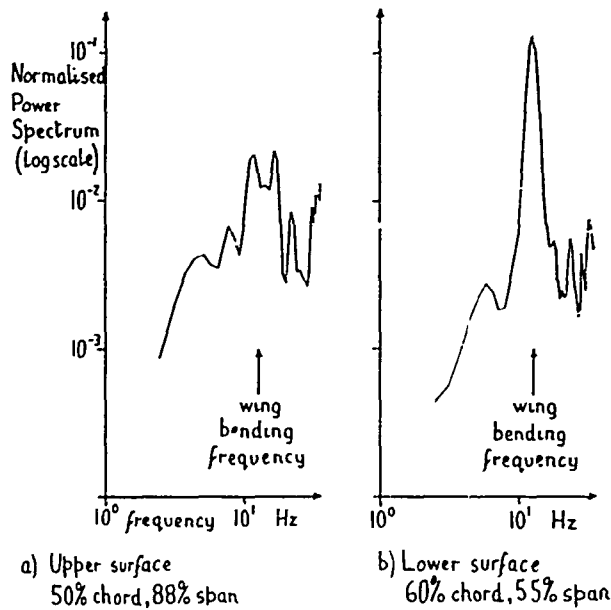


Fig 12 Power spectra of wing pressure fluctuations

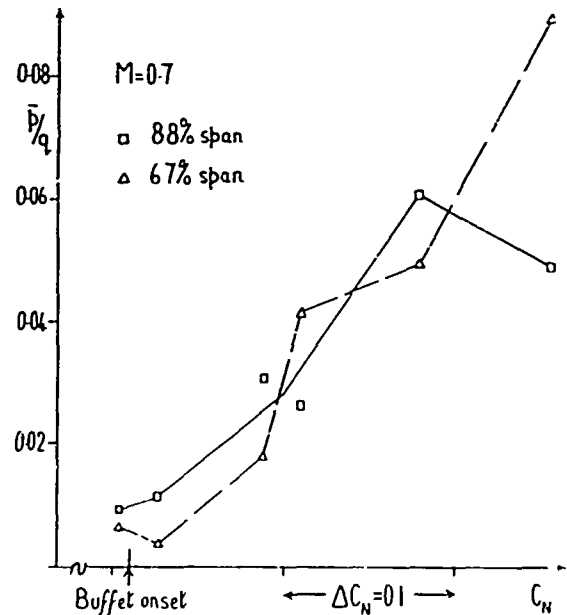


Fig 13 Measured rms intensity of pressure fluctuations at 50% chord on upper surface of buffeting wing

## MANUEVER AND BUFFET CHARACTERISTICS OF FIGHTER AIRCRAFT

Edward J. Ray\* and Linwood W. McKinney\*

NASA Langley Research Center

Hampton, Virginia, U.S.A.

and

Julian G. Carmichael†

McDonnell Aircraft Company

St. Louis, Missouri, U.S.A.

## SUMMARY

The emphasis of the present studies was placed on the high subsonic and transonic characteristics of fighter aircraft and the factors affecting aerodynamic boundaries, such as maximum obtainable lift, buffet onset, pitching, "wing rock," and "nose slice." Investigations were made using a general research configuration which encompassed a systematic matrix of wing design parameters. These results emphasized the sensitivity to section and planform geometry at the selected design point. The incorporation of variable-wing-geometry devices in the form of leading-edge slats or flaps was shown in a number of flight and wind-tunnel studies to provide controlled flow over a wide range of flight conditions and substantial improvements in maneuver capabilities. Additional studies indicated that the blending of a highly swept maneuver strake with an efficient moderately swept wing offers a promising approach for improving maneuver characteristics at high angles of attack without excessive penalties in structural weight.

## NOTATION

AR	aspect ratio, $b^2/S$	EXP.	experimental results
b	wing span	$I_X$	rolling moment of inertia
c	wing chord	$I_Z$	yawing moment of inertia
$C_D$	drag coefficient	L.E.	leading edge
$\Delta C_D$	change in drag coefficient	M	Mach number
$C_L$	lift coefficient	S	wing reference area
$C_{L_{BUF}}$	lift coefficient for buffet onset	t/c	thickness-chord ratio
$C_{L_{MAX}}$	maximum usable lift coefficient	T.E.	trailing edge
$\Delta C_L$	change in lift coefficient	WSG	wing strain gage
$\Delta C_{L_{BUF}}$	change in buffet-onset lift coefficient	W.T.	wind tunnel
$C_l$	rolling-moment coefficient	$\alpha$	angle of attack
$C_{l_\beta}$	rolling moment due to sideslip	$\beta$	angle of sideslip
$C_n$	yawing-moment coefficient	$\delta_F$	trailing-edge flap deflection
$C_{n_\beta}$	yawing moment due to sideslip	$\delta_{LE}$	leading-edge flap deflection
$C_{n_\beta DYN}$	dynamic directional-stability parameter,	$\delta_S$	leading-edge slat deflection
	$\frac{\partial C_n}{\partial \beta} - \frac{I_Z}{I_X} \frac{\partial C_l}{\partial \beta} \sin \alpha$	$\Lambda_C/4$	wing quarter-chord sweep
		$\Lambda_{LE}$	wing leading-edge sweep

## 1. INTRODUCTION

The maneuver and performance capability of aircraft engaged in air-to-air combat is often limited by flow separation which can be manifested in a variety of adverse factors such as buffeting, increases in drag, and losses in lift and stability. Figure 1 illustrates the impact that these limiting factors could have on the maneuver characteristics of a fighter aircraft. This presentation illustrates the sensitivity of turn rate to typical aircraft boundaries at subsonic, transonic, and supersonic speeds. The fighter configuration selected for this illustration represents a moderately swept, thin-wing

\* Aerospace Technologists, High-Speed Aircraft Division.

† Engineer - Aerodynamics, McDonnell Aircraft Company, St. Louis, Missouri.



aircraft with a supersonic capability of about Mach 2. The boundaries shown illustrate the relationship between the maximum lift capability of the aircraft, the structural and thrust limits, and the steady turn boundary. The shaded area shown in the high subsonic range represents a region in which the maneuver capability of the aircraft is impaired as a result of buffeting and degradations in performance and stability.

The present trend toward designing one aircraft to accomplish a variety of missions over wide velocity and altitude spectra often leads to aerodynamic compromises, particularly in this high subsonic and transonic range. It will be noted here that the maximum maneuver capability of this aircraft is restricted by aerodynamic considerations before reaching the limits dictated by available thrust and structures. There is a potential, therefore, to achieve significant increases in the maneuver characteristics of this and many other aircraft through aerodynamic improvements.

Because of continuing interest in the high subsonic and transonic combat arena, a considerable amount of research has been directed toward improvement of fighter maneuverability in this speed range. The purpose of this paper is to review some of these research efforts, with emphasis on factors which affect the aerodynamic boundaries illustrated in figure 1 and on methods which have been found to broaden and increase the high-subsonic operating corridor.

## 2. TYPES OF WING AIRFLOW

### 2.1 Stall Separation

Before discussing the dependency of the aerodynamic boundaries on specific design variables, let us examine briefly the aerodynamic behavior of a fighter configuration in the environment of several different airflow conditions over the wing. Figure 2 illustrates the variation of lift with angle of attack for a variable-sweep configuration at a high subsonic Mach number with the wings in a low-sweep position and in a highly swept position. A variable-sweep configuration was selected for this discussion since it illustrates several classic types of wing flow behavior.

The low-sweep results (solid line) are characterized by a rather high lift-curve slope and an almost linear variation of lift in the low to moderate attitude range. In this region of attached flow, aircraft usually exhibit relatively low drag, good stability characteristics, and in general, a high degree of aerodynamic efficiency. However, for this class of conventional, moderately swept wings, the linear variation is inevitably followed by an abrupt reduction in lift which is normally accompanied by large increases in drag, rapid increases in buffet intensity, and losses in stability. Even though the lift is increasing at the higher angles of attack, this type of leading-edge separation generally produces such a profound degradation in aerodynamics that the aircraft's maneuver capability is restricted to angles of attack below the stall.

### 2.2 Early Leading-Edge Separation

Unlike the low-sweep case, the highly swept configuration exhibits a relatively low lift-curve slope at low angles of attack with gradual increase in the lift-curve slope throughout the  $\alpha$  range. This supersonic sweep condition naturally is not optimum for subsonic performance, but the example illustrates that the leading-edge separation occurs early on highly swept wings and produces a highly stable spiral vortex system with flow reattachment and large vortex-lift increments. This type of behavior usually produces an early onset of buffet corresponding to the occurrence of leading-edge separation, with a very gradual progression in the buffet intensity. There is also an absence of other abrupt divergences such as those associated with a stall separation. It is interesting to note that for the vortex-flow case, buffet onset accompanies an increase in lift slope rather than a decrease. This phenomenon must be kept in mind when attempting to use lift inflections to predict buffet onset. The remainder of this presentation will be concerned primarily with factors which affect the range of linear aerodynamics and secondly with techniques which might be utilized to stabilize flow separation at angles of attack exceeding the point of initial separation.

## 3. SENSITIVITY OF BUFFET TO WING GEOMETRY

### 3.1 Planform and Airfoil Characteristics

The NASA has recently completed an extensive wind-tunnel study to assess the sensitivity of buffet onset and other aerodynamic boundaries to wing planform and section design. Figure 3 represents a brief summary of some of the results. The basic configuration, as shown at the top of figure 3(a), featured an untwisted 63A wing with aspect ratio of 6, thickness ratio of 8 percent, and quarter-chord sweep of 35°.

The only parameter selected for this summary is the lift coefficient for buffet onset. The studies have indicated, however, that for this particular matrix the wings displaying the highest buffet-free lift coefficients generally exhibited superior aerodynamic efficiency characteristics. The onset points were determined primarily by the wing bending gage method.<sup>1</sup> The results indicate the variations of buffet-onset lift coefficient with systematic wing changes in the design lift coefficient, twist, aspect ratio, thickness-chord ratio, airfoil section, and quarter-chord sweep angle.

It will be noted from the Mach 0.5 results shown in figure 3(a) that the point of initial separation, as reflected in the buffet-onset conditions, is favorably affected by increases in camber, twist, aspect ratio, and thickness. In addition, a forward movement in the position of maximum thickness and reductions in sweep angle provided beneficial increments.

The high subsonic Mach number results shown in figure 3(b) indicate a pronounced change in the trends discussed for the Mach 0.5 case. Although the conventional camber is still shown to be effective in postponing separation, there is a definite reduction in the influence of the higher camber. Increases in twist and sweep and a rearward movement in the position of maximum thickness provided favorable effects. There was also a definite tendency toward additional improvements as the aspect ratio and thickness-chord ratio were reduced. This systematic matrix of wing variables vividly illustrates the sensitivity of section and planform geometry at the selected design point.

### 3.2 Plain Leading- and Trailing-Edge Flaps

In addition to the conventional wing modifications, the basic wing was investigated with a plain 20-percent-chord leading-edge flap and 30-percent-chord trailing-edge flap. The Mach 0.5 results (see fig. 3(a)) indicate that with a leading-edge deflection of  $20^\circ$  and a trailing-edge deflection of  $60^\circ$ , sizable improvements were achieved in the lift coefficient for buffet onset. At the higher Mach number (fig. 3(b)) substantial benefits were again achieved with modest deflections of the wing flaps. The reduction in the optimum flap deflection with increases in Mach number is analogous to the trend toward reducing camber at the higher subsonic Mach numbers. The investigation of these relatively simple maneuver devices resulted in a postponement in the stall angle of attack and provided an aerodynamic flexibility not afforded by any one airfoil selection from low subsonic speeds to Mach numbers exceeding 0.9.

## 4. MANEUVER DEVICES

### 4.1 Maneuver Slats and Flaps

The use of wing maneuver devices has been studied on a sizable number of scaled wind-tunnel models of current fighter aircraft. Several comparisons have been made between wind-tunnel results obtained from conventional sting-mounted models and flight results, with particular emphasis upon buffet and maneuver characteristics. In most cases, the interpretive and test techniques which have been developed have led to good correlations between wind-tunnel and flight characteristics.

One of the most extensive studies of this type was conducted jointly by the NASA Langley Research Center and the McDonnell Aircraft Company in a program directed toward improving the high-subsonic maneuverability of the F-4 aircraft.<sup>2</sup> A brief summary of some of the findings from this study is shown in figure 4. The sketch of the aircraft indicates that the maneuver devices consisted of leading-edge slats on the mid and outboard portions of the wing and the existing inboard trailing-edge flap system. This configuration represents only one of a large number that were studied in the wind tunnel. The selection was made from wind-tunnel results which indicated that this particular arrangement would provide significant improvements in buffet onset, drag, and lift characteristics without seriously compromising the longitudinal handling qualities at high subsonic speeds.

The results shown in figure 4 represent wind-tunnel and flight buffet-onset lift coefficients as a function of Mach number. Again the primary source of buffet information was the outputs of wing bending gages. The curves represent wind-tunnel results and the symbols represent buffet-onset points determined in flight. Flight results were obtained over a wider range of Mach numbers,<sup>3</sup> however, the Mach 0.90 results illustrate the degree of agreement between the trends determined in the wind tunnel and in flight.

A comparison of the results for the basic configuration and the configuration with wing slats indicates that the slats provided a very substantial improvement in the buffet-onset lift coefficients throughout the Mach number range. Additional improvements were derived by deflecting the trailing-edge flap system. Only buffet characteristics are shown here; however, the flight evaluations indicated an overall improvement in the maneuver capability due to significant increases in both the lift-limited and thrust-limited turning performance. Excess-thrust characteristics were enhanced and there was an apparent reduction in the buffet intensity at high angles of attack.

### 4.2 Lateral-Directional Characteristics With Maneuver Slats

The subject of lateral and directional stability has not been addressed directly in the preceding discussions. It has been found, however, that the tracking performance and overall maneuver capability of current fighter configurations is often impaired and restricted by undesirable lateral-directional characteristics such as "wing rock" and "nose slice." In many cases, divergences such as these have been shown to be associated with loss of lift on the outboard part of the wing, which results in a degradation of the effective-dihedral characteristics.<sup>4</sup> A major portion of the F-4 studies was directed toward a determination of the effects of wing maneuver devices on the lateral and directional characteristics.

Figure 5 shows wind-tunnel results which were obtained with the F-EE model over an angle-of-attack range which extended from about  $5^\circ$  to  $45^\circ$ . The curves represent the variations of the static directional-stability parameter  $C_{m\dot{\alpha}}$ , the effective-chordal parameter  $C_{l\dot{\alpha}}$ , and the dynamic directional-stability parameter  $C_{m\dot{\alpha}}^{DYN}$  with angle of attack. The parameter  $C_{m\dot{\alpha}}^{DYN}$  is used here as a function of the static derivatives  $C_{m\dot{\alpha}}$  and  $C_{l\dot{\alpha}}$  and the inertial characteristics of the aircraft and accounts for the roll freedom in the real motion. Experience has indicated that the parameter  $C_{m\dot{\alpha}}^{DYN}$  provides a good indication of directional divergences at high angles of attack.<sup>5</sup>

The solid curves in figure 5 indicate results for the basic configuration and the dashed curves pertain to the slatted-wing model. These wind-tunnel results indicate that at the high angles of attack the slats provide an improvement in the static directional stability and a large favorable increase in the effective-chordal characteristics. The  $C_{m\dot{\alpha}}^{DYN}$  results indicate that the basic model "diverges" at an angle of attack near  $21^\circ$ , whereas the configuration incorporating the maneuver slats exhibits positive values of  $C_{m\dot{\alpha}}^{DYN}$  throughout the entire angle-of-attack range. The improvements suggested here were confirmed in flight by qualitative reports which indicated postponements in the onset of wing rock, reduction in wing rock intensity, and an apparent improvement in directional stability at high angles of attack.

### 4.3 Krueger Flaps

It was recognized that because of structural considerations and physical size, adapting maneuver slats to many thin-wing configurations might represent an impractical solution. This particular study, therefore, included tests of the basic wing modified by the addition of simple Krueger devices which could be readily stowed beneath the leading edge of a wing.

Figure 6 presents Mach 0.90 results which were obtained for the basic wind-tunnel model and the basic model with the addition of the maneuver slats and of Krueger devices. The span coverage of the two types of wing devices was almost identical. Lift and drag characteristics are shown for the three different configurations. It can be seen that there is a definite improvement in lift at the high angles of attack when the Kruegers are employed. The buffet-onset lift coefficient for the Krueger configuration approached the value predicted for the slatted configuration, which indicates that significant improvements could be achieved by utilizing Krueger flaps. The incorporation of the Krueger devices also leads to large reductions in the high-lift drag levels. Although the improvements indicated with the Kruegers were not as profound as those with the slats, these simple devices were shown to provide very beneficial effects on the static lateral-directional trends as well as on the lift and drag characteristics.

## 5. VORTEX-LIFT MANEUVER STRAKES

### 5.1 Effect of Strake on Lift and Drag Characteristics

The preceding discussions have been concerned with various methods which have been demonstrated to be effective in postponing the stall to higher angles of attack. Another promising approach which appears to be effective in allowing maneuvers well beyond the normal aerodynamic boundaries of fighter aircraft with a low weight increment is the use of a highly swept maneuver strake that blends with a moderately swept main wing planform. The strake provides vortex lift to high angles of attack and stabilizes the flow on the main wing panel.

A sketch of a general research model with a maneuver strake is shown in figure 7. Experimental and theoretical lift and drag results are presented to illustrate the aerodynamic characteristics of the model with and without the strake. The results in the upper portion of the figure indicate the variations of lift coefficient with angle of attack. The experimental lift results for the strake-off configuration (circular symbol) indicate a pronounced reduction in the lift-curve slope at the high angles of attack. The experimental lift results for the strake-on model (square symbol) show a nonlinear variation in lift with a gradual increase in the lift-curve slope. A comparison of the experimental results indicates the large increase in lift provided by the strake at the high angles of attack. The dashed curves indicate theoretical estimates of the lift characteristics for the model with the strake on. The short-dash curve represents the potential-flow estimates<sup>6</sup> and the long-dash curve illustrates the nonpotential-flow estimates<sup>7</sup> based on the assumption that a vortex system develops on the strake. The difference between the two theoretical lift curves then represents an estimate of the vortex increment which would be provided by the strake. It will be noted by comparing the experimental with the theoretical strake-on results that the experimental curve falls slightly below the nonpotential-flow (or vortex) estimate but is considerably higher than the potential-flow estimate. This suggests that even though the full nonpotential-flow values are not reached because of stall of the outer wing panel, a substantial vortex-lift effect is produced by the strake.

The drag results shown in the lower portion of the figure indicate that at the low lifts the addition of the strake produces slightly higher drag values. At a lift coefficient of about 0.5, leading-edge thrust is completely lost on the basic wing, resulting in a rapid progression in the drag rise. Because of the

nonlinear increase in lift produced by the highly swept strake, the addition of the strake results in large reductions in the high-lift drag coefficient. It can be seen from these results that the benefit of the strake approach is that higher lift (or load factors) can be provided without the weight penalty which would be associated with the lower wing loadings required to accomplish the same improvement.

### 5.2 Airflow Characteristics With Vortex-1 Lift Strakes

In order to gain some insight into the aerodynamic behavior of the straked configuration, studies were conducted with buffet gages, wing duffs, and an additional six-component balance installed in the forebody of the model. The model sketch at the top of figure 8 indicates the general locations of the balances and the wing-buffet buffet gage. It will be noted from this drawing that the internal strain-gage balances were mounted in such a way that the rear balance would measure the forces and moments of the integrated model and the forward balance would indicate the aerodynamic load on the strake-forebody combination.

Figure 8 shows the variations of lift with angle of attack for the strake-off configuration (solid line) and the strake-on configuration (dashed line). The composite sketches included with the total-lift curves illustrate the lift behavior on the strake-on model (the top portion of each sketch) and the strake-off configuration (shown in lower half of the sketch). The lift displays were traced from video-type recordings. The lower figure illustrates the variation with angle of attack of the direct lift contribution of the strake (solid line) and the lift induced on the wing by the strake (dashed line).

Addressing first the total-lift figure, the lift sketch for low angles of attack shows that the airflow on the basic planform is fully attached. The strake-on part of the sketch illustrates that a narrow spanwise flow system is generated on the basic planform by the strake. The total-lift curves indicate that at low angles of attack the strake reduces the lift only slightly and maintains a relatively high lift-curve slope. Unlike the highly swept planform discussed earlier in the paper (fig. 2), there is a vortex system on the wing, but because of the moderately swept outer panel the efficiency of the integrated strake-wing combination remains relatively high. It will be noted that, as in the case of highly swept wings, there was an indication of a mild onset of buffet at a relatively low angle of attack. The incremental-lift results at 40° angle of attack indicate that because of the spanwise flow behavior on the main wing, the small adverse lift increment induced on the wing is slightly larger than the direct lift contribution of the strake. The lift sketches show that at the higher angles of attack the airflow over the basic wing panel with the strake off is almost completely separated. This is reflected in the drastic reduction in the lift-curve slope of the basic configuration. The sketch of the straked wing indicates an extensive spanwise flow system which apparently confines the separated area to small portions of the wing tip. It was observed from the visual studies that as the angle of attack is increased the spanwise flow system moves progressively outboard and reduces the area of separation. The progression of the vortex system is reflected in the constant increase in the lift of the straked-wing configuration. It can be seen from the incremental-lift curves that at the high angles of attack there is a profound increase in the favorable lift induced on the wing. At an angle of attack of about 20°, the lift induced on the wing is equivalent to the direct lift of the strake.

With regard to the buffet characteristics at high angles of attack, there was a pronounced absence of increase in the apparent buffet intensity of the straked configuration. The basic configuration, however, exhibited a relatively high buffet-onset lift coefficient which was followed by a progressive rise in the apparent intensity characteristics.

### 5.3 Effect of Wing Efficiency on Strake Contribution

The design lift coefficient of the basic wing panel utilized in this phase of the straked-wing investigation was zero. Studies were made with cambered wings and with wings incorporating leading-edge flaps to determine the effectiveness of the strake in combination with a more efficient wing. Some of the results from these studies are presented in figure 9. The sketch at the top of the figure depicts the model with the maneuver strake and a symmetrical wing with segmented leading-edge flaps. These leading-edge devices were made up of a constant-chord flap and when deflected they in effect twisted and cambered the wing, thereby increasing the high-lift efficiency of the basic planform. The flap deflections which were used to obtain the results shown in this comparison are indicated in the model sketch. The deflection angles were, from the outboard segment inward, 20°, 16°, 12°, and 8°. These deflections do not necessarily represent an optimum condition; however, this arrangement provided the most promising results of the several combinations which were studied. The data which are shown represent the increments in lift and drag due to the addition of the strake. The strake effects are shown by the solid curves for the plain wing and by the dashed curves for the flapped wing.

It will be noted from these results that when the flaps are deflected the favorable lift increment due to the strake is significantly reduced. This reduction in lift is directly reflected in a reduction in the favorable drag benefits due to the strake. As might be expected, the camber and flap studies have indicated that as the wing design is improved to delay separation on the main wing panel, the beneficial effects of the strake are delayed to increasingly higher angles of attack. The drag results also point out that at the lower angles of attack there are small penalties associated with the addition of the strake. It is believed, however, that proper cambering and twisting of the integrated strake-wing combination can alleviate the low-lift penalties while maintaining the strake benefits of stabilized flow and improved buffet and maneuver characteristics at higher angles of attack.

## 6. CONCLUSION

The series of studies has illustrated the sensitivity of section and planform geometry to the selected design point. A number of flight and wind-tunnel studies have shown that variable-wing-geometry devices in the form of leading-edge slats and flaps can provide controlled flow over a wide range of flight conditions and substantial improvements in maneuver capabilities. The incorporation of a highly swept maneuver slat with an efficient moderately swept wing appears to offer a promising approach for improved maneuver characteristics at high angles of attack for a low cost in structural weight.

## REFERENCES

1. Ray, Edward J.  
Taylor, Robert T.      Buffet and Static Aerodynamic Characteristics of a Systematic Series of Wings Determined From a Subsonic Wind-Tunnel Study. NASA TN D-5205, 1970.
2. Hollingsworth, E. G.  
Cohen, M.      Determination of F-4 Aircraft Transonic Buffet Characteristics. J. of Aircraft. Vol. 8, No. 10, Oct. 1971, pp. 757-763.
3. Cohen, Marshall      Buffet Characteristics of the Model F-4 Airplane in the Transonic Flight Regime. AFFDL-TR-70-56, U.S. Air Force, Apr. 1970.
4. Chambers, Joseph R.  
Bowman, James S., Jr.  
Anglin, Ernie L.      Analysis of the Flt-Spin Characteristics of a Twin-Jet Swept-Wing Fighter Airplane. NASA TN D-5409, 1969.
5. Chambers, Joseph R.  
Anglin, Ernie L.      Analysis of Lateral-Directional Stability Characteristics of a Twin-Jet Fighter Airplane at High Angles of Attack. NASA TN D-5361, 1969.
6. Margason, Richard J.  
Lamar, John E.      Vortex-Lattice FORTRAN Program for Estimating Subsonic Aerodynamic Characteristics of Complex Planforms. NASA TN D-6142, 1971.
7. Polhamus, Edward C.      A Concept of the Vortex Lift of Sharp-Edge Delta Wings Based on a Leading-Edge-Suction Analogy. NASA TN D-3767, 1966.

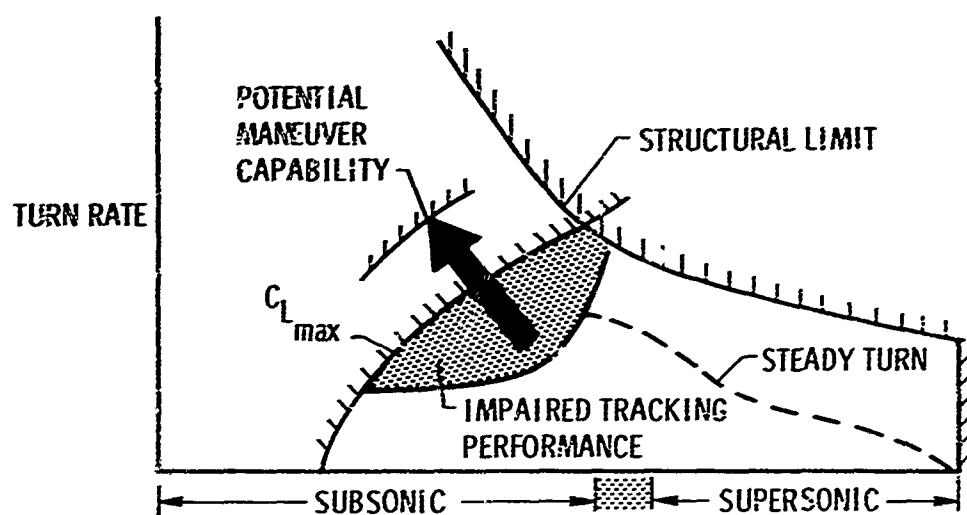


Figure 1.- Maneuver boundaries of a typical fighter aircraft.

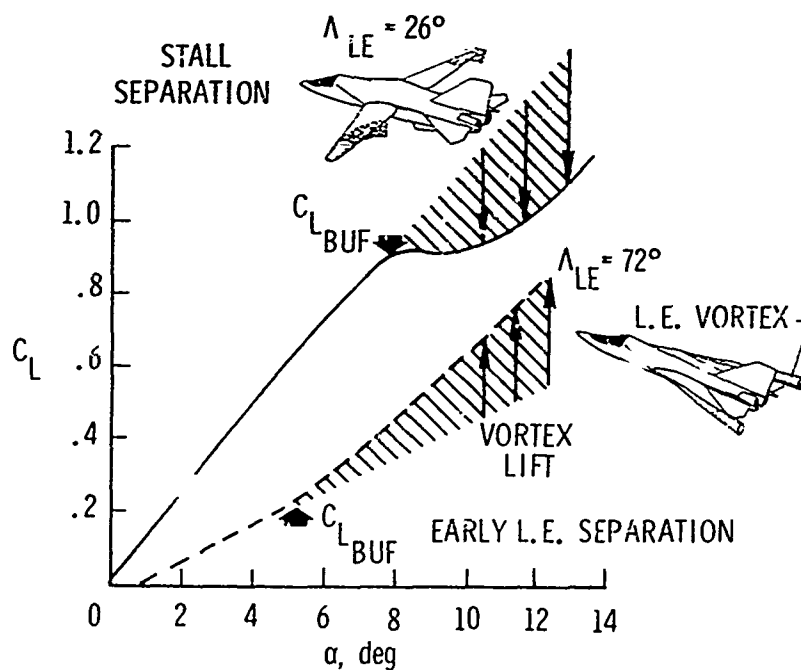


Figure 2.- Effect of aerodynamics on the maneuverability of a variable-sweep aircraft.

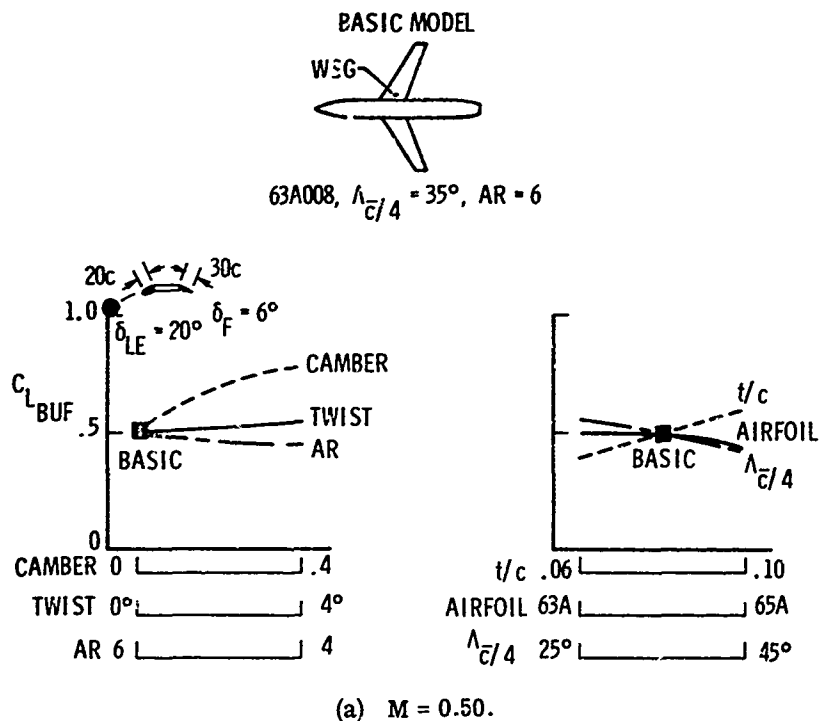


Figure 3.- Effect of wing geometry on buffet characteristics.

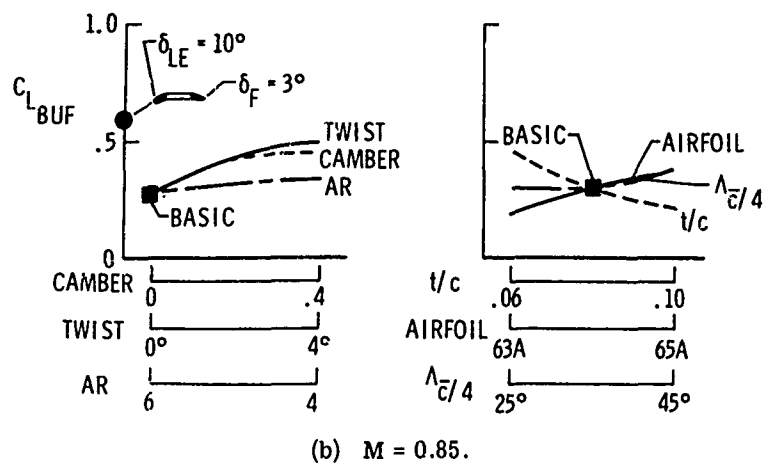
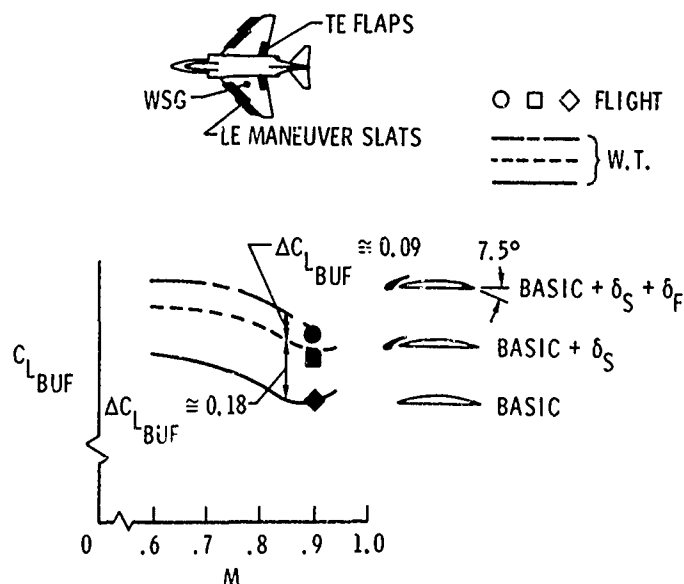


Figure 3.- Concluded.



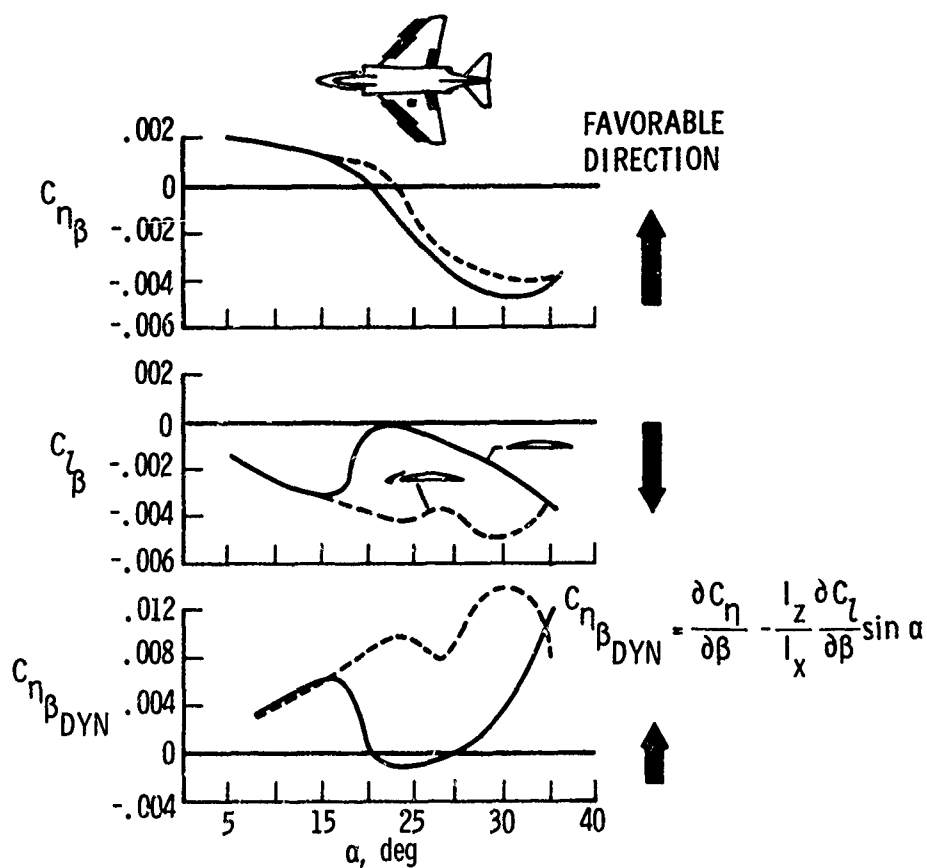


Figure 5.- Effect of maneuver slats on lateral-directional characteristics.

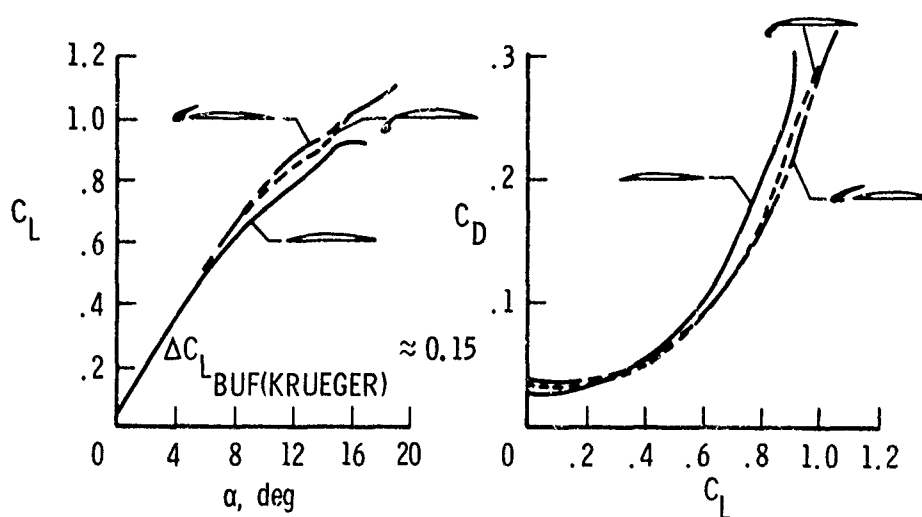


Figure 6.- Effect of maneuver slats and Krueger flaps on lift and drag characteristics.  $M = 0.90$ .



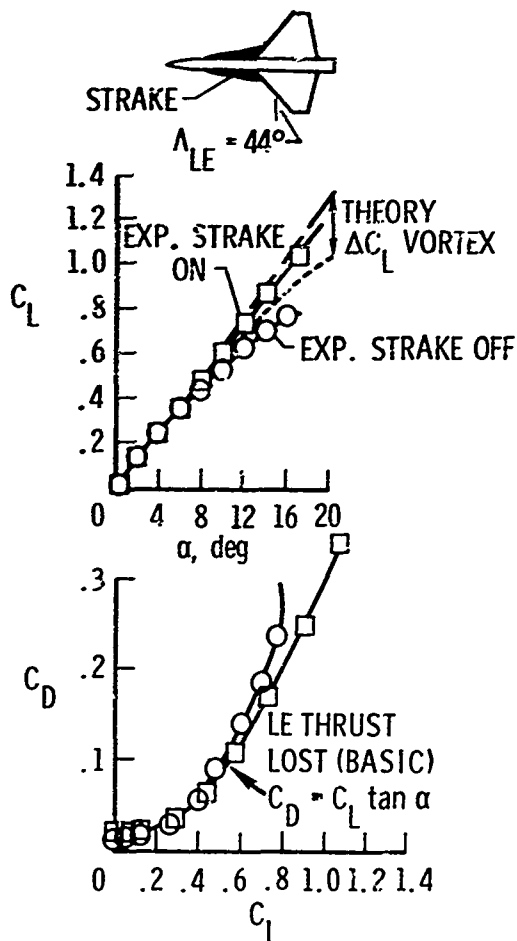


Figure 7.- Effect of maneuver strake on lift and drag characteristics.  $M = 0.85$ .

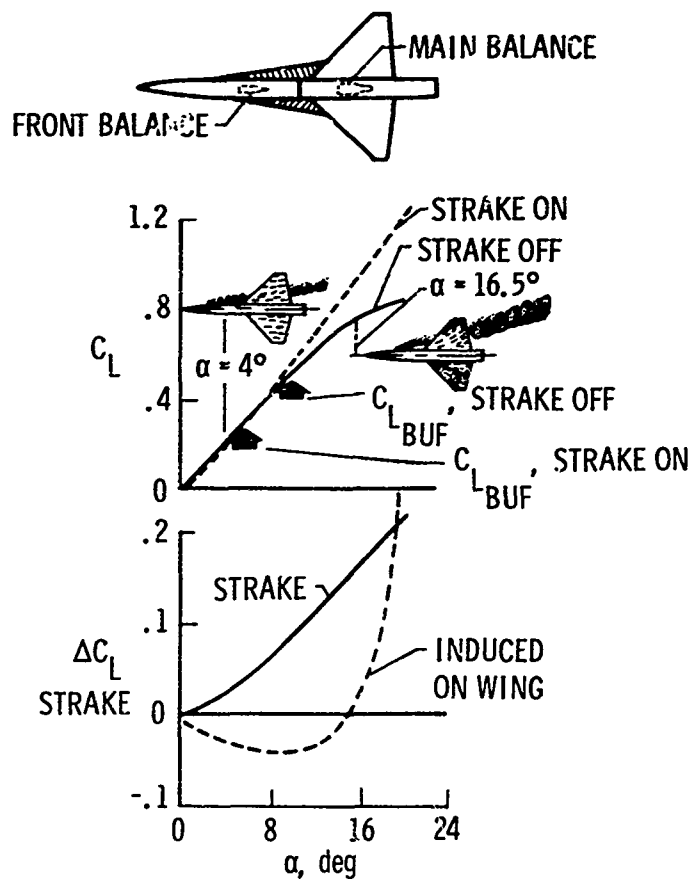


Figure 8.- Influence of maneuver strakes on wing airflow characteristics.

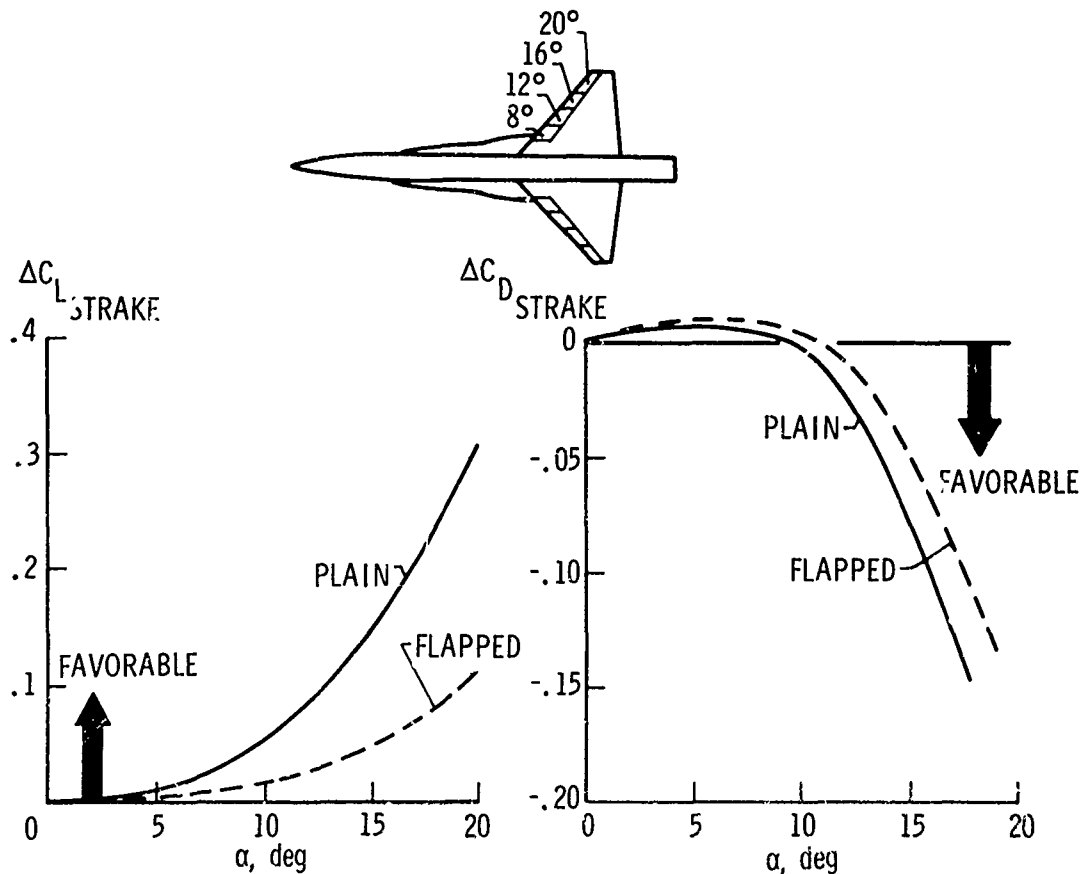


Figure 9.- Comparison of maneuver strake on plain and flapped wing.  $M = 0.40$ .

AERODYNAMIC DESIGN AND FLIGHT TEST  
OF  
U. S. NAVY AIRCRAFT AT HIGH ANGLES OF ATTACK

by  
W. R. Burris and J. T. Lawrence

Naval Air Systems Command  
Department of the Navy  
Washington, D.C. 20360

SUMMARY

Aerodynamics of U. S. Navy aircraft at high angles of attack in the region beginning with buffet onset and continuing through maximum maneuvering boundaries, stall, departure from controlled flight, post-stall gyrations and the spin are given considerable emphasis during design and flight test for each aircraft development program. This paper discusses the application of current methods and the philosophy employed by the Naval Air Systems Command to design and develop Navy aircraft in the high angle of attack region, along with results obtained in specific cases.

LIST OF SYMBOLS

$\alpha$  angle of attack

$I_x$  moment of inertia about longitudinal body axis

$I_z$  moment of inertia about normal body axis

$C_{l\beta}$  dihedral effect in body axes

$C_{n\beta}$  static directional stability in body axes

$C_{n\beta} \text{ dyn} = \frac{I_z}{I_x} C_{l\beta} \sin \alpha$

dyn dynamic

AERODYNAMIC DESIGN AND FLIGHT TEST  
OF  
U. S. NAVY AIRCRAFT AT HIGH ANGLES OF ATTACK

By W. R. Burris and J. T. Lawrence

Naval Air Systems Command  
Washington, D.C. 20360

## 1. INTRODUCTION

For many years engineers in the Aerodynamics and Hydrodynamics Branch, NAVAIR (Naval Air Systems Command) have been involved in a series of real world "laboratory experiments" in the high angle of attack characteristics of U. S. Navy aircraft. Being concerned with all phases of the aircraft's design and operation, these "experiments" have begun with establishing design requirements, conducting design evaluations and predicting high angle of attack characteristics and then followed through model tests, analyses and flight tests to the final observation and analysis of service experience. Included has been experience with all aircraft now in the Navy inventory, as well as the initial phases of those still to come. Types of aircraft include most models currently in U. S. Navy use, from light piston engine trainers, large and small turboprop, patrol, cargo, and counter insurgency type aircraft, to high performance jet combat aircraft. The application of the design and flight test of Navy aircraft requires genuine teamwork between NASA (National Aeronautics and Space Administration), Navy field activities such as NATC (Naval Air Test Center), NSRDC (Naval Ship Research and Development Center) and NADC (Naval Air Development Center), the contractor and NAVAIR engineers and program management.

This paper is concerned with the aerodynamic design, engineering development, and flight testing of Naval aircraft at high angles of attack. For this paper the discussion will deal primarily with the flight regime beginning with buffet onset and proceeding up through departure from controlled flight. It must be kept in mind, however, that the flight regime beyond departure, namely post-stall gyrations, the various spin modes, and recovery from any of the high angle of attack flight conditions are also of vital importance. Contractor and Navy design, development, and flight testing thoroughly investigate this entire flight regime. However, a considerable research and development effort is still required to advance the current state-of-the-art in high angle of attack aerodynamics in order to permit accurate analysis of the flight characteristics in this regime during the early design phase so that future aircraft will have satisfactory high angle of attack flight characteristics.

Historically, the aircraft manufacturer's design proposals have included only a minimal amount of aerodynamic data for definition of the high angle of attack flight characteristics other than buffet onset, maximum aerodynamic lift coefficient, and pitching moment data. Up through the latest Navy design evaluations the design criteria considered most feasible for achieving good maneuvering capability was to require an appropriate level of buffet onset lift coefficient. Based on state-of-the-art aerodynamics, the maximum useable lift could be expected to be at a reasonable level above buffet onset. The prime reason for this approach was that buffet onset could be predicted, both for preliminary design and proposal evaluation, with an ever increasing degree of confidence over the years. It could also be measured during flight tests for specification compliance with a reasonable degree of accuracy. It is fully realized that this method of attempting to achieve satisfactory maneuvering boundaries is highly imperfect, but lack of other more satisfactory criteria has necessitated its application.

## 2. THE DESIGN CHALLENGE

Over the past years, with the resurgence of close-in air-to-air combat, a considerable amount of interest and effort has been placed on obtaining information through both model and flight tests in the flight regime beyond buffet onset. The primary areas of concern are discussed in the following subparagraphs.

### Buffet Onset

Buffet is defined as unstable boundary layer flow on the wing where the boundary layer intermittently separates and attaches in a somewhat random manner. This occurrence is caused basically by high angle of attack pre-stall flow breakdown at subsonic speeds, and by local shock wave and boundary layer interaction in the transonic speed range. The degree to which one or the other of the above flow characteristics causes buffet on a particular aircraft is primarily a function of airfoil section, thickness, and camber, as well as wing aspect ratio, sweep angle and taper ratio. Buffet onset is defined as oscillations in normal acceleration of  $\pm 0.05g$  at the aircraft center of gravity. This value has been found to correlate well with pilot opinion, though the fuselage elastic characteristics will obviously effect these results.

Analytical means are currently available for prediction of buffet onset with a reasonable degree of accuracy. The methods are presented in Ref [1] and are based on the airfoil and wing characteristics mentioned above. Wind tunnel test techniques have also been developed which allow a more accurate assessment. Wind tunnel prediction methods utilize lift coefficient, axial force coefficient, wing root bending moment, wing trailing edge pressure, wing tip accelerometer, and oil flow photograph data, all as a function of angle of attack. These methods have been refined to the point where acceptable accuracy can usually be achieved in buffet onset prediction. More detailed discussions of experimental techniques are contained in Refs [2] and [3].

#### Build-up in Buffet Intensity

At present there are no known reliable means of predicting buffet intensity build-up analytically or in the wind tunnel. Only educated guesses can be made from wind tunnel tests of buffet onset parameters such as tip accelerometer, wing root bending moment, and trailing edge pressure data. A consistent, repeatable build-up in buffet intensity is, however, a desirable parameter in giving the pilot a positive indication of impending stall/departure. This is a difficult characteristic to achieve, and some aircraft, such as the A-7 and F-4, have an angle of attack range between buffet onset and stall/departure which is so large as to preclude the use of buffet build-up as reliable stall/departure warning. Methods of delaying buffet onset and achieving a satisfactory build-up in buffet intensity, while maintaining a high degree of maneuverability, need to be developed.

#### Definition of Moderate and Heavy Buffet Levels

Pilot definition of moderate and heavy buffet levels has been found to be a highly nebulous item. While most pilots are in relatively close agreement on the buffet level for onset, there is a wide range of opinion to define levels beyond onset. Experience has shown that both the frequency and amplitude of the buffet can influence pilot opinion. This variability demonstrates the need for considerable research in this area.

Buffet intensity level has a direct effect on the maximum angle(s) of attack for the tracking tasks involved in utilizing the various weapons available, particularly in air combat maneuvering. Depending on the weapon to be used, the maximum buffet level tolerable to the pilot will vary since each weapon requires a different degree of tracking accuracy. For example, a heat seeking missile does not require the same tracking accuracy as a gun.

#### Maneuvering Boundaries

For tactical aircraft various maneuvering boundaries are of interest such as the optimum maneuvering angle of attack and the maximum usable angle of attack for offensive and defensive maneuvering. These boundaries are primarily based on pilot opinion as determined from flight tests and correlated with various measured parameters. The optimum maneuvering angle of attack is usually a compromise among parameters such as sustained turning performance, instantaneous normal acceleration capability, buffet intensity, and overall flying qualities. Offensive and defensive boundaries are determined by the tasks required for air combat maneuvering. Differences can occur in these angles because offensive maneuvers require the pilot to, first, maneuver his aircraft to within the range and angular offset limits for use of the selected weapon, and, second, to then be able to accurately track the target and fire the weapon. However, defensive maneuvers may very well be executed at angles of attack closer to stall/departure than offensive maneuvers due to the urgency of the pilot's situation. For offensive maneuvers, if a particular airplane has not yet reached a tracking buffet limit, its usable maneuvering capability will be determined by aerodynamic characteristics close to stall/departure. An airplane's characteristics may well be such that the buffet intensity and/or flying qualities at the angle of attack for obtaining a tracking position are not acceptable for actual tracking, and the pilot will have to reduce his angle of attack to utilize the selected weapon. As stated previously, this angle may vary depending on the weapon to be used. Defensive maneuvers are normally flown close to the stall/departure angles and, unless the particular aircraft has a high degree of stall/departure resistance, the aircraft will probably be flown into the stall/departure conditions frequently during both training and actual air combat maneuvering. It is imperative, therefore, that the maximum usable angles of attack, and the stall/departure susceptibility and characteristics be well defined in order to raise pilot confidence to such a level that the full maneuvering capability of the aircraft can be effectively utilized.

#### Stall Angle of Attack

The three basic definitions for stall angle of attack normally referred to are:

- Angle of attack for the highest load factor, normal to the flight path, that can be attained at a given speed or Mach number.
- Angle of attack for a given airspeed or Mach number at which intolerable, uncommanded motions occur (i.e., excessive wing rock, nose wander, or nose rise tendencies).
- Angle of attack for a given airspeed or Mach number at which intolerable buffeting is encountered.

The lowest angle of attack based on the above is defined as the stall angle for a given aircraft at that speed or Mach number. The first of the above is initially determined from wind tunnel test data for maximum lift coefficient properly corrected for such effects as Reynolds number. However, determining whether or not one or both of the latter two definitions will supersede the aerodynamic maximum lift cannot be accurately predicted from model testing or analysis.

## Departure

Departure is defined as the event in the post-stall flight regime which precipitates entry into a post-stall gyration and/or spin. It is characterized by divergent, large amplitude, uncommanded aircraft motions such as pitch up, nose slice, or snap roll. Stall and departure on modern fighter and attack aircraft configurations normally occur at nearly the same angle of attack and are therefore considered jointly throughout this discussion.

## Post-Stall Gyration, Spin and Recovery

Post-stall gyrations are the uncontrollable oscillatory motions about any or all axes following departure from controlled flight and before the airplane reaches a spin condition. Spins are basically characterized by sustained rotation in yaw at angles of attack above the stall that may have oscillations about any or all axes superimposed on it. The incipient spin is the initial transitory phase of the motion during which it may not be possible to identify that the airplane is spinning. When the spin progresses to the point where it is fully developed, it should be readily recognized: no significant changes will occur from turn to turn and the trajectory will approach the vertical. The recovery transition from out-of-control to controlled flight encompasses the period between pilot actuation of recovery control and the reduction of the angle of attack to below stall with no significant uncommanded motions remaining. As with most of the high angle of attack pre-stall characteristics, the post-stall behavior of an aircraft is not amenable to analysis. Consequently, a considerable amount of wind tunnel and flight test results are required to adequately define the post-stall characteristics.

## 3. DESIGN PROCESS

During the design and engineering development phases a wide variety of wind tunnel facilities are used to define the aerodynamic characteristics of the aircraft. Basic static force and moment tests are conducted in contractor tunnels, NASA (National Aeronautics and Space Administration) Research Center facilities, as well as privately operated facilities such as those at the Cornell Aeronautical Laboratory. These tests normally cover angles of attack to about 25 degrees and sideslip angles up to about 5 degrees. These data are limited to the lower angle ranges by considerations such as balance accuracy and strength requirements, model scale, and tunnel blockage. These are particularly limiting as Mach and Reynolds numbers are increased.

Dynamic wind tunnel test data are also collected as the design phase progresses, utilizing essentially the same angle of attack and sideslip ranges. The model scale, Reynolds number, and Mach number capability vary greatly among the various tunnels available. These facilities yield a wide variety of data which must be properly analyzed and correlated to obtain a consistent set of aerodynamic characteristics. This is a difficult task and considerable time and knowledge are required to arrive at satisfactory results. These tests and data are oriented primarily toward an accurate definition of aircraft characteristics in the lower angle of attack flight regime. This is where the majority of flying will be accomplished and where performance characteristics must be accurately determined.

In order to obtain the required data for definition of high angle of attack characteristics, a series of tests are conducted at NASA facilities specifically utilized for this purpose. A typical program would be pursued as follows:

- Low Mach number (0.2M), high Reynolds number ( $6 \times 10^6$  per foot) tests are performed at angles of attack to 90 degrees and sideslip angles to 40 degrees.

- Static force and moment tests for similar Mach number and pitch and yaw angle ranges are conducted, but at a much lower Reynolds number usually below  $1 \times 10^6$  per foot. These results are compared with the high Reynolds number results and the differences are taken into account in further tests and analyses.

- Dynamic stability derivatives are also obtained utilizing forced oscillation and rotary balance test techniques. These data are combined with the previously obtained static force and moment data and utilized in six degrees of freedom computer studies to predict probable flight characteristics and recovery techniques up to stall/departure. Predictions in the post-stall and spin regimes are also made; however, little confidence is currently placed in these results, due to lack of sufficient correlation with flight test.

- Free flight tests are then conducted utilizing the same model as for the static tests, however, the model is now actually being "flown" in the tunnel. This "flight" is accomplished by attaching a cable to the model. Electrical power lines are routed through the cable to actuate control surfaces. Compressed air lines are also routed through the cable for thrust simulation as well as a steel cable to catch the model upon termination of the test, or if uncontrollable motions occur. Using this technique, the model is "flown" up to the stall/departure in order to investigate the flight characteristics using various types and combinations of control surface inputs. Aerodynamic characteristics such as wing rock, nose wander, pitch up, lateral-directional divergence, and stall/departure may be identified. Even though these tests are conducted at low Mach and Reynolds numbers, the results in terms of overall characteristics as well as the approximate angles of attack and types of stall/departure, have generally correlated reasonably well with actual flight experience.

- Concurrent with the free flight model tests, spin tunnel test results are utilized to define the spin and recovery characteristics for all combinations of control surface deflections in both right and left spins. The various spin modes such as upright, inverted, flat, steep, oscillatory and non-oscillatory are determined. The recovery techniques from each are also determined. Variables investigated include the effects of external store loadings (including asymmetric loadings), center of gravity and moments of inertia, and the use of devices such as

speed brakes, slats, and flaps. The spin tunnel, Ref [4], is a vertical tunnel into which the model is head launched at about 90 degrees angle of attack with induced rotation into the rising airstream. Control surfaces are activated remotely by a magnetic field in order to investigate recovery control positions.

In addition to determining the basic spin and recovery characteristics, the emergency out-of-control recovery system to be used on the flight test aircraft is also demonstrated. This system often consists of a parachute mounted on the back end of the aircraft to provide recovery. The parachute diameter and riser length is sized in the spin tunnel to recover the aircraft from the most critical spin condition predicted for the aircraft while holding full pro-spin controls.

● The free flight tests in NASA's 30 x 60 foot tunnel yield the aircraft flight characteristics up to the stall/departure, while the spin tunnel tests define the developed spin and recovery characteristics. The main questions that now must be answered are (1) how does the aircraft depart from controlled flight into post-stall gyrations, (2) will it enter any or all of the developed spin modes identified in the spin tunnel, and (3), if it does spin, will it recover. To obtain these answers the NASA/Langley Research Center conducts free flight tests of a radio controlled model. These tests consist of dropping from a helicopter a model which is controlled by radio signals from the ground. The unpowered model is dropped from a nominal attitude of 5,000 feet and is allowed to stabilize in a dive with essentially neutral longitudinal control deflection. Longitudinal control is then applied to increase the angle of attack up to the stall/departure. This permits an investigation of the flight characteristics and departure tendencies in free air. Lateral-directional control inputs are then radioed to the appropriate control surfaces in order to induce or aggravate departure. Using this technique the characteristics and recovery procedures from stall/departure through the fully developed spin can also be investigated. As opposed to the 1-g stall/departures "flown" in the free flight tunnel, accelerated stall/departures are normally investigated with the radio controlled drop model. These techniques are discussed in Ref [5].

The data obtained from the above described test program covers the full angle of attack range. These data in conjunction with the computer analyses and simulator studies are used as a guide in designing the full scale high angle of attack flight test program.

The entire test program is conducted with close coordination among Navy, NASA, and contractor engineers. As problem areas are identified they are given immediate attention. Contractor engineering and flight test personnel continually revise and update high angle of attack predictions. Maximum use is made of these predictions to minimize the flight test program. It must be emphasized, however, that the results of the model test program, while providing a valuable guide in the flight regime leading to stall/departure and up through the fully developed spin, do not provide sufficient information on the various important parameters between buffet onset and stall departure. In addition, they are all obtained at very low Mach number and, with the exception of the static force and moment tests in the NASA/Ames Research Center 12 foot Pressure Tunnel, are all at very low Reynolds number. If we are to achieve a satisfactory collection of aerodynamic data to adequately define the high angle of attack characteristics of aircraft that can be used with sufficient confidence in computer analysis and simulation programs during design and engineering development, it is imperative that the analytical and experimental capability to obtain sufficiently accurate data be developed on a high priority basis.

#### 4. Flight Tests

Flight tests in the high angle of attack region begin soon after first flight of a new Navy design. Because of the limitations of accurately predicting flight characteristics in this area and heavy reliance on pilot opinion to define such things as maneuvering boundaries and to establish the acceptability of stall warning, stall and post-stall characteristics, considerable emphasis is placed on high angle of attack testing. The basic philosophy of the Navy's flight test program is for the contractor pilots to demonstrate the flight characteristics under the most critical conditions anticipated during the operational use of the airplane. This is accomplished by making maximum use of the analysis and experimental data discussed earlier and through flight test build-ups to the critical conditions. Determination of critical conditions are based on gross weight, center of gravity location, power settings and external store loadings (symmetrical and asymmetrical) for the various configurations, i.e., cruise, landing, combat, etc. Navy pilots evaluate these characteristics periodically to determine their acceptability and to determine the capability of the airplane, as well as to establish procedures for fleet pilots to safely use the full potential of the airplane. The demonstrations by contractor pilots and evaluations by Navy pilots are performed separately in order to concentrate on the objectives of the testing which experience has shown leads to the most efficient use of flight testing.

Initially the contractor's tests investigate the stall warning, approach to stall and stall characteristics. As the program progresses, for highly maneuverable aircraft such as trainers, attack and fighters, full post-stall and spin tests are performed. For aircraft not designed for extensive high angle of attack maneuvering such as patrol, ASW and cargo designs, testing is terminated after full post-stall motions have developed from 1g and accelerated entries. No attempt is made to spin these aircraft. During both the stall and spin testing of the highly maneuverable aircraft the effects of various store loadings, fuel loadings, and centers of gravity are investigated in order to determine their most critical conditions for each individual demonstration.

The contractor's entire flight program in this area should be preceded by the appropriate phases of the analytical and model experimental tests described previously, in order to achieve maximum safety. All stall/spin test aircraft are contractually required to have a back-up emergency out-of-control recovery device installed in order to provide an alternate means of recovery should the maneuver become so disorienting that the pilot applies improper recovery

controls or does not properly interpret the motions being experienced. As part of the final high angle of attack demonstration of the aircraft, the contractor is required to demonstrate this emergency recovery system in the most critical post-stall condition to the satisfaction of the Navy. For aircraft not required to spin the use of an emergency recovery device for high angle of attack testing is left to the contractor's discretion. If used by the contractor, only functional demonstrations are required in flight. A demonstration to determine its effectiveness to recover the airplane from a spin is not required. The contractor has chosen to equip the S-3 high angle of attack test airplane with a spin chute to permit a thorough investigation of the post-stall motions. The size of the spin chute was determined in the spin tunnel using the same test procedures as discussed previously.

Once the contractor has demonstrated the normal, accelerated, and inverted stall characteristics, as well as the most critical spin and recovery conditions, the airplane is turned over to the Naval Air Test Center test pilots for a Navy evaluation of the entire high angle of attack flight regime. This Navy program is conducted with the knowledge that the contractor has already demonstrated the characteristics of and recovery from the most critical conditions that may occur, as well as the satisfactory operation of the emergency out-of-control recovery device, if employed. This program is designed to investigate flight characteristics under the most adverse conditions anticipated during fleet use. By having the contractor concentrate primarily on demonstrating critical conditions, and having Navy pilots investigate the overall high angle of attack flying qualities, two basic objectives are achieved. First, the airplane can be evaluated from an operational as well as an engineering viewpoint, yielding more meaningful results in terms of determining the mission capability of the aircraft, and resulting in an operational pilot oriented definition of high angle of attack characteristics and procedures for the flight manual. This situation is achieved through the Navy system of selecting pilots with recent operational fleet experience, having them serve a three year tour as test pilots and then returning them to the fleet, often to fly the same type of aircraft they have evaluated. The Navy test pilots are, therefore, familiar with the current tactics employed in the fleet, the problem of the fleet pilot/airplane "team", and are usually proficient in most Navy aircraft of the type being evaluated. The second objective is the cost savings incurred by having the contractor demonstrate only the critical conditions, or, in other words, the extremes of the flight envelope. Most of the flight testing within these extremes is then conducted solely by Navy pilots. Certainly, the contractor pilots conduct a significant amount of testing inside the extremes as part of their build-up program, and do make a gross assessment of the maneuvering potential of the aircraft. However, it is the Navy test pilots who obtain the fleet oriented definition of characteristics and determination of mission suitability.

The Navy high angle of attack evaluation defines most of the areas of concern previously detailed. The definition of these various characteristics are the product of a sufficient number of test pilots to obtain as objective a determination as possible. This evaluation places heavy emphasis on both avoidance of and recovery from the various flight characteristics to be encountered between buffet onset and departure from controlled flight. This emphasis is of greatest importance for fighter, attack, and trainer type aircraft, where the full maneuvering envelope must be utilized by the pilot in order to achieve the maximum capability of his airplane. This being the case, stalls and departures will occur with some frequency and must be fully tested, fully understood, and completely defined in the flight manual. An extensive description of the Naval Air Test Center's stall/post-stall/spin program is contained in Ref [6].

To illustrate the many factors involved in the high angle of attack maneuvering range trimmed lift curves for two Navy designs, the A-7 and F-4 (Figs 1 and 2), are shown in Figs 3 and 4 showing a progression of events that occur from buffet onset to post-stall gyrations. The A-7 (Fig 3) has a lift curve which exhibits a well defined maximum aerodynamic lift coefficient. Its flight characteristics show buffet onset in the vicinity of 10 to 12 degrees. The rudder pedal shaker, which is set at an angle of attack to provide artificial stall warning in the landing approach configuration, is activated at 17 degrees, which happens to coincide with the lower portion of the 17 to 19 degrees band where heavy buffet is encountered. At 18.5 degrees the roll augmentation system is automatically turned off to preclude pro-spin aileron inputs in the stall/departure region. Above 18.5 degrees exclusive use of the rudder should be made for roll control. Stall occurs at 20 degrees and is characterized by very heavy buffet and weak lateral-directional stability which results in a nose wander in yaw. Departure from controlled flight will occur between 20 and 24 degrees depending on the rate of change of angle of attack and on any lateral control inputs that may be inadvertently applied by the pilot. The departure will usually occur in the form of a rapid nose slice accompanied by snap rolls in the direction of the slice. The A-7 departure is very disorienting to the pilot and the recovery technique as determined by Navy tests is to release the stick to avoid inadvertent lateral control inputs and to wait until the post-stall gyrations have ceased. At this point the aircraft will be in an unstalled condition and can be flown back to level flight by proper use of controls to avoid a second stall/departure. If the post-stall recovery procedures are not properly followed, it is likely that the airplane will enter a spin.

In contrast to the A-7, the F-4 has a local maximum lift point at 18 degrees angle of attack (Fig 4) and a later maximum aerodynamic lift at 26 degrees. The F-4's flight characteristics show buffet onset occurring in the 9 to 11 degrees angle of attack region. Above 11 degrees lateral control should not be used. Roll control should be achieved by judicious use of the rudder only. Lateral control is pro-spin and could induce an early departure from controlled flight. The rudder pedal shaker is activated at 17 degrees to supply artificial stall warning for landing approaches. At 18 to 19 degrees wing rock is first encountered. Heavy buffet begins at 20 degrees along with a build-up in wing rock. Stall occurs between 22 and 25 degrees and is characterized by excessive buffet and wing rock, and nose rise tendencies. Departure will occur above 25 degrees primarily in the form of a nose slice with roll in the direction of the yaw. As is the case with the A-7, inadvertent lateral control inputs and rate of change of angle of attack may cause an earlier and more aggravated departure. Recovery is achieved by smoothly moving the stick forward

to reduce the angle of attack, while simultaneously neutralizing lateral-directional controls. The drag chute can also be utilized in departure recovery attempts. Failure to recover promptly will most likely result in entry into either a steep oscillatory spin or, on very rare occasions, a fast flat spin. An item of particular interest is that the F-4 is capable of flight well beyond the first local maximum in the lift curve and even though drag is so high that a level flight constant speed condition cannot be maintained, angles of attack well beyond the local maximum are still usable. These angles are often experienced in the real world of air combat maneuvering.

It is interesting to note that the term  $C_{n\beta \text{ dyn}}$ , which is described in Refs [7] and [8] as one cycle of a highly unstable Dutch roll oscillation, correlates reasonably well with the departure angle of attack for both of these aircraft. The first departure motion of each aircraft begins with a nose slice. Figs. 5 and 6 show the values of  $C_{n\beta \text{ dyn}}$  as a function of angle of attack for the A-7 and F-4 aircraft, respectively. The A-7, while having a positive value of this parameter up through the stall/departure angle of attack range, has a minimal value in the 20 to 24 degree region which is indicative of very weak lateral-directional stability. The F-4 values for  $C_{n\beta \text{ dyn}}$  actually go unstable in the vicinity of 25 degrees angle of attack. Also shown on these figures are the effects of leading edge devices on the  $C_{n\beta \text{ dyn}}$  parameter. Fig. 5 for the A-7 shows that significant improvement in  $C_{n\beta \text{ dyn}}$  can be achieved by utilizing either a wing leading edge flap or by increasing the radius of the wing leading edge. Fig. 6 shows the improved  $C_{n\beta \text{ dyn}}$  obtained by using wing leading edge slats on the F-4. Both of these aircraft have been flight tested with the wing leading edge modifications and have exhibited improved lateral-directional flying qualities at high angle of attack. The slats on the F-4 have resulted in the achievement of increased maneuvering boundaries. Ref [8] contains a considerably more detailed discussion of the use of wing leading edge devices on high angle of attack characteristics.

While the  $C_{n\beta \text{ dyn}}$  parameter is considered a good guideline for design and evaluation, many investigators in the field of high angle of attack phenomena feel that it is by no means the whole story and continued research is required in this area to define additional important parameters, as well as the interrelationships that exist among them.

Fig. 7 shows the F-4's trimmed lift curve with the wing leading edge slats extended. Significant improvements in the high angle of attack characteristics can be seen by comparing Figs. 4 and 7. Referring to these figures it can be seen that the angles of attack for buffet onset, rudder only roll control, wing rock onset, optimum maneuvering, stall, and departure have all been substantially increased over those of the basic F-4. The lift coefficient beyond approximately 10 degrees has been significantly increased, and the dip following the first local maximum lift has been considerably diminished. The wing rock onset for the slatted airplane is much more mild and gradual in build-up than that of the basic aircraft, and heavy buffet has not been identified with the slat. Two ramifications of these characteristics are that the slatted F-4 stall is defined primarily by nose wander and nose rise tendencies, vice the basic F-4's nose rise tendencies, and excessive buffet and wing rock.

Since only limited flight tests have been conducted on this configuration, the optimum maneuvering angle of attack is not yet defined. Simulator study, however, has shown a 24 degree angle for optimum maneuvering as opposed to the 15 degrees on the basic airplane. Also, a limited number of departures have indicated that they are milder for the slatted F-4 than for the basic airplane. The characteristics of the departure also are somewhat different in that the basic F-4 exhibits more yaw than roll, while the slatted F-4 shows more roll than the basic airplane. This is attributed to the increased dihedral effect with slats. Comparison of Figs. 6 and 7 shows good correlation between the minimum level of  $C_{n\beta \text{ dyn}}$  and the departure angle of the slatted F-4.

##### 5. DEPARTURE/SPIN PREVENTION

An additional consideration for high angle of attack maneuvering which is gaining widespread popularity is to prevent the airplane from entering a spin, or even to prevent a departure from controlled flight. Since little is known on how to design these characteristics into an aircraft in a practical fashion, the current emphasis is on use of the basic flight control and/or stability augmentation systems. Various efforts are being made in this area and the results to date are promising. A prime object of this work is to accomplish the prevention task without detracting from the full maneuvering envelope of the aircraft. For this reason longitudinal stick pushers of all but the most complex types have been deemphasized due to the reliability and maintainability problems that would result from their use. The first practical demonstration of this concept was a post-stall gyration prevention system developed by Cornell Aeronautical Laboratory under U. S. Navy sponsorship. The system was installed in an F7U-3 "Cutlass" and flight tests in 1959 demonstrated that it did prevent the airplane from entering its characteristic post-stall gyration when stalled in combat type maneuvers (Ref [9]).

NASA/Langley is currently involved in an analytical and experimental investigation of automatic spin prevention through use of the basic aircraft control systems, including stability and control augmentation systems. Some of the results of this continuing program are presented in Ref [10]. In addition, the Navy has funded a contractor study of F-14 stall/spin avoidance/prevention which has yielded two promising techniques, one for departure prevention, and one for spin prevention. Both techniques will be flight tested during the development program. The spin prevention system could also be referred to as a departure recovery system. The prime reasoning behind such efforts is that the spin has no practical value and so long as the ground rule of not affecting the basic combat maneuvering envelope of the aircraft is not compromised, there is no reason to have an aircraft capable of proceeding into the flight regime beyond departure from controlled flight.



Currently, there are two problem areas in the development of satisfactory spin prevention systems. The first, formulation of sufficient demonstration requirements to insure that the design is adequate to perform its task, is a new concept which must be thoroughly explored. Until now, demonstrations of critical spins and recovery capability have been specified and appropriate entry maneuvers, loading conditions, and configurations were defined. The task of defining demonstration requirements for a departure avoidance system is indeed formidable, and considerable effort by both government and industry is required in this area. The second problem area is the design of the system such that it is totally reliable, easy to check out and maintain, and free of failure modes which compromise pilot/airplane safety.

#### 6. FUTURE HIGH ANGLE OF ATTACK EFFORT

At this time the state of the art in the prediction and measurement of high angle of attack aerodynamic characteristics is severely limited. The test facilities currently available, while performing an invaluable service, are inadequate for the future need to provide sufficient and accurate data in the high Reynolds and Mach number ranges. This includes both static and dynamic aerodynamic derivative data. In addition, high angle of attack maneuvering guidelines and criteria now in existence are totally inadequate for future aircraft design. Considerable research and testing, both ground and flight, are required to provide the necessary qualitative and quantitative information necessary, not only for the designer, but also for the Navy personnel who must evaluate and flight test the designs. The Naval Air Systems Command is currently in the process of embarking on a program to provide specific aerodynamic design guidance to aid in insuring that future high performance airplanes will possess satisfactory high angle of attack characteristics throughout the flight envelope. Whereas most past and current investigations have been concerned primarily with spins and spin recovery, this program is oriented directly to the regime between buffet onset and departure from controlled flight. It is in this area where the primary air combat maneuvers of the airplane will be performed.

#### REFERENCES

<u>No.</u>	<u>Author</u>	<u>Title</u>
1	LCDR Thomas L. Lindsay	"A Procedure for Estimating Buffet Onset Normal Force as Effected by Wing Geometry," NSRDC Technical Note AL-70, dtd June 1968
2	J. F. Mayes, M. E. Lores, and H. R. Barnard	"Transonic Buffet Characteristics of a 60 Degree Swept Wing with Design Variations," AIAA Paper No. 69-793, dtd July 1969
3	Mark Siegal	"Analysis of Wind Tunnel Test Results on Wing-Body Configurations Designed to Delay High Speed Buffet Onset," GAC Rpt. No. ADR 01-01-69.1, dtd Sept 1969
4	Anshal I. Neihouse, Walter J. Klinar, and Stanley H. Scher	"Status of Spin Research for Recent Airplane Designs," NASA Technical Report R-57 dtd 1960
5	Joseph R. Chambers	"Status of Model Testing Techniques" NASA/Langley Research Center Paper presented at the U. S. Air Force Stall/Post-Stall/Spin Symposium in Dec 1971
6	LTCOL E. B. Russel, USMC, J. A. Nial, and LT E. R. Curtis, USN	"The U. S. Navy Stall/Post-Stall/Spin Program," paper presented at the U. S. Air Force Stall/Post-Stall/Spin Symposium in Dec 1971
7	Joseph R. Chambers and Ernie L. Anglin	"Analysis of Lateral-Directional Stability Characteristics of a Twin-Jet Fighter Airplane at High Angles of Attack," NASA TN D-5361, dtd Aug 1969
8	William R. Burris, and Dale E. Hutchins	"Effect of Wing Leading Edge Geometry on Maneuvering Boundaries and Stall Departure", AIAA Paper No. 70-904, dtd July 1970
9	John M. Schuler	"Flight Evaluation of an Automatic Control System for Stabilizing the Large Uncontrolled Motions of Airplanes in Stalled Flight" Cornell Aero Lab Report No. TB-1132-F-2, dtd Oct 1959
10	William P. Gilbert	"Automatic Spin Prevention," NASA/Langley Research Center paper presented at the U. S. Air Force Stall/Post-Stall/Spin Symposium in Dec 1971

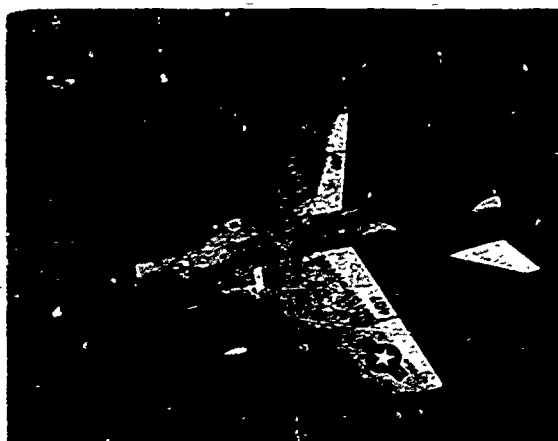


Fig.1 Model A-7 airplane

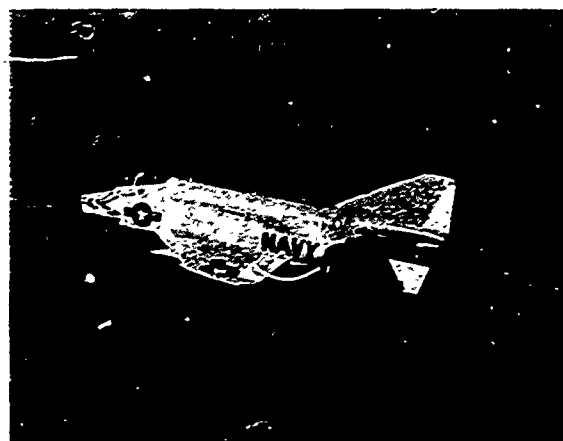


Fig.2 Model F-4 airplane

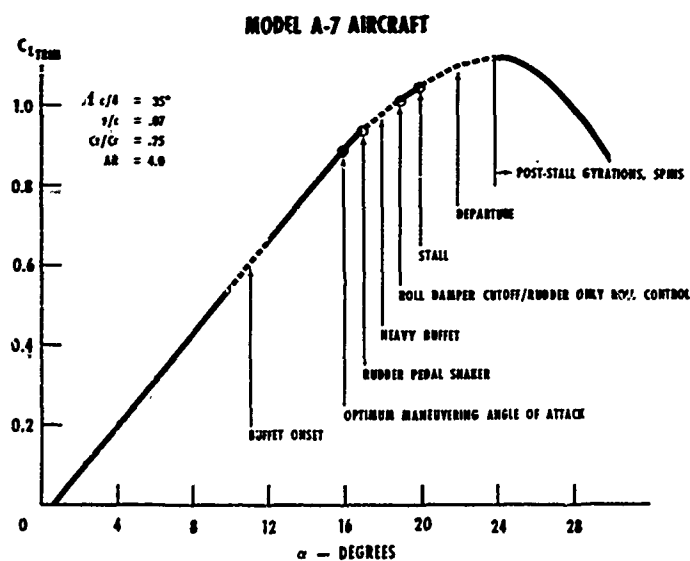


Fig.3 A-7 trimmed lift curve

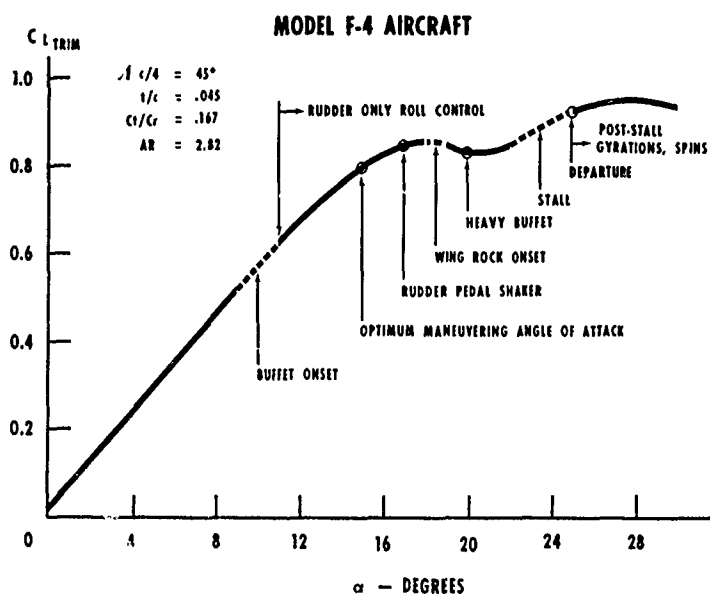


Fig.4 Basic F-4 trimmed lift curve

## MODEL A-7 AIRCRAFT

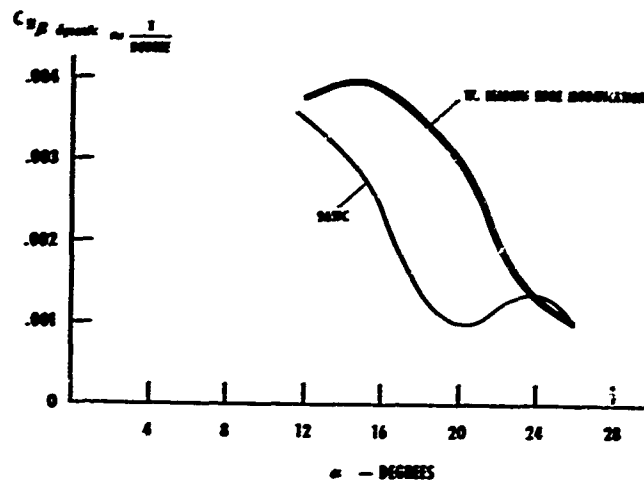


Fig.5 Effect of wing leading edge modification on A-7 lateral-directional characteristics

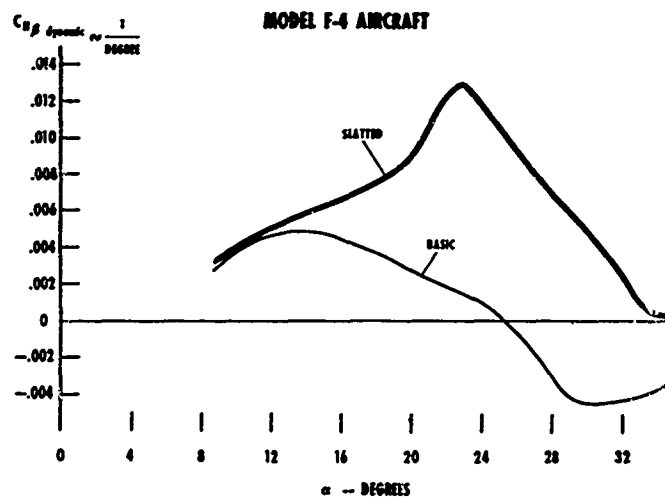


Fig.6 Effect of wing leading edge slats on F-4 lateral-directional stability

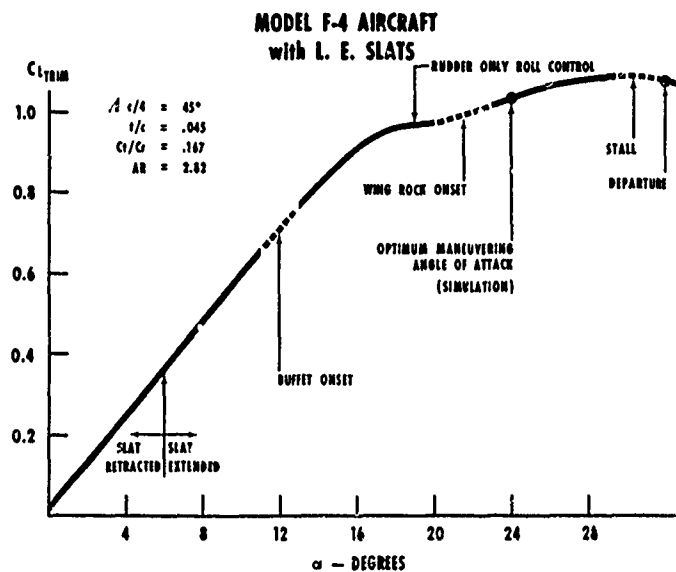


Fig.7 F-4 trimmed lift curve with wing leading edge slats

**PREPARED COMMENT ON PAPER 25**

It has not been possible to prepare the text of this contribution for inclusion in these proceedings. However, the salient points have been embodied in Section 4.1 of the Technical Evaluation Report, printed at the front of this volume.

## APPENDIX A

### DISCUSSIONS

following the presentation of papers at the  
AGARD Fluid Dynamics Panel Specialists' Meeting on

### FLUID DYNAMICS OF AIRCRAFT STALLING

April 1972

Lisbon, Portugal

Compiled by Madame J. Genet, Secretary to the Panel

This Appendix contains the discussions which followed presentation of the papers at the Specialists' Meeting on "Fluid dynamics of aircraft stalling" held at the Laboratorio Nacional de Engenharia Civil, Lisbon on 26-28 April 1972.

These discussions are transcribed from forms completed by the authors and questioners during the meeting and are keyed (by reference number) to the papers contained in this Conference Proceedings.

Le présent Appendice est un recueil des discussions qui ont suivi la présentation des exposés à l'occasion de la Réunion des Experts tenue à la Laboratorio Nacional de Engenharia Civil, Lisbonne du 26 au 28 Avril 1972 et consacrée au thème "La dynamique des fluides du décrochage des avions".

Le texte de ces discussions a été transcrit à partir de fiches remplies à cet effet par les auteurs et par ceux ayant désiré leur poser des questions. Les discussions sont numérotées suivant les numéros de références des exposés.

**Discussion of Paper 1**  
**"Review of the Field (Based on AGARDograph 136)"**  
 presented by G.J.Hancock, UK

**E.L.Ericson, US (Comments only):** In regard to Prof. Hancock's call for more attention to lateral flow effects on stall, the straight wing space shuttle configuration experienced (during drop tests of transition maneuver) reattachment on one wing (half) before the other, causing snap roll that cannot be controlled. On the delta planform space shuttle, use of the lateral controls also cause asymmetric flow breakdown with similar control problems.

**J.Seddon, UK:** Commenting on the accident statistics shown by Mr T.C.Muse in his prepared comment, I emphasize the importance which is attached to the need to cover the stalling problem as exhaustively as possible in the wind tunnel before going into flight development. In the UK we are currently building a new low speed wind tunnel, the case for which is based largely on the need to achieve a Reynolds number of about 6 million in order to work effectively and reliably in this area. This leads to a question, since I understand that NASA had some years ago a wind tunnel of about the same size and capability, the use of which has however been discontinued. Does this fact indicate a belief that still higher Reynolds numbers are required for wind tunnel work at high lift and stall, or that perhaps the concentration should be on other kinds of development work, e.g. flight testing?

**A.Gessow, US (Comments only):** I would like to comment in answer to Dr Seddon's question about NASA's spin research program. NASA's effort in this area emphasizes the use of radio-controlled aircraft models dropped from helicopters to study spin entry, spin characteristics and the effectiveness of various recovery systems. In addition, static and dynamic stability derivatives having a bearing on the stall are measured in tunnels with special balances and support systems. Plans are underway to install such balances in a transonic tunnel to study scale and Mach number effects.

**F.W.Riegels, Germany:** Mr Hancock showed an example by K.Jacob who calculated pressure distributions considering the displacement effect of a separated region. In this case the separated region has been approximated by a source distribution on the contour of the profile within the separated region. This example from 1963 works with an assumed separation point. About four years later K.Jacob combined this method with additional boundary layer calculations for the changed pressure distribution between the stagnation point and a new separation point. Then he repeated the potential flow calculation and so on. With this rapidly converging method he then calculated the pressure distributions for some profiles at several angles of incidence and Reynolds numbers. By integrating the pressure distributions he could show the stalling qualities of the lift curve in dependence of the Reynolds number. This work - which could not be continued on behalf of other duties of K.Jacob - has been published as: - Theoretische Berechnung von Druckverteilung und Kraftbeiwerten für beliebige Profile bei inkompressibler Strömung mit Ablösung. A.V.A. Bericht 67A62, 1967. Translated as: Theoretical calculations of pressure distribution and force coefficients for any profile in incompressible flow with separation. ARC 31936, 1970.

**Discussion of Paper 2**  
**"Some Research on Two-Dimensional Laminar Separation Bubbles"**  
 presented by E.Dobbinga, J.L.van Ingen and J.W.Kooi, The Netherlands

**A.D.Young, UK:** I would first like to congratulate Prof. van Ingen and his colleagues on this excellent method for visualising regions of separated flow and the beautiful pictures that they have obtained.

The authors indicate that they propose to apply Prof. van Ingen's method for calculating the position of transition in the separated shear layer. We have tried to do this for comparison with our measurements on laminar separation bubbles but the results we have obtained have not been encouraging. It is possible that we have not applied the method properly and I shall be glad to know if Prof. van Ingen has taken his own calculations far enough to feel confident about the likely accuracy of his method.

**J.L.van Ingen, The Netherlands:** I would like to start by saying that full credit for the design and construction of the experimental equipment should go to the first author of our paper, Mr Dobbinga.

Indeed we intend to try and extend our transition prediction method for attached flow also to the case of separated flows.

About 3 years ago I did some rough calculations for the large cylinder. I think I showed them at the Euromech Colloquium in 1969 in Sweden. The calculations had to be very rough because we did not have available the proper stability diagrams. The results were promising to some extent. However, we have not yet worked this out so far that we can be confident about final success.

It is very important however, that one applies the right stability diagrams. From recent results obtained by Wazzan, Smith et al., it follows that the stability diagram for the Hartree separation profile differs considerably from that calculated earlier by Pretsch. So, it would be important to know which stability diagrams have been used in your investigation.

**A.D. Young, UK:** We used calculated stability characteristics derived in the standard manner for profiles approximating the measured ones. As I said earlier, we got poor agreement at the measured transition positions for the van Ingen amplification factor as compared with the value derived for attached boundary layers. However, it is possible that our calculations of the stability characteristics were too crude.

**G.F. Mess, UK:** I wonder whether we could try to link these studies with boundary layer conditions at the point of the stall on a wing. In model experiments we often have to accept that transition occurs at a laminar-separation bubble near the leading edge. On the other hand, at full-scale conditions, transition will occur at a point nearer to the stagnation point, if indeed any laminar flow occurs at all. The experiments described in this paper all use artificially induced separations in the laminar layer, except for the cylinder where large-scale separations occur making this also a special case. I would like to ask whether in the speaker's experience there is any difference between the boundary layer characteristics further aft of the separation point between the cases where separation is induced artificially and those where it occurs naturally.

**J.L. van Ingen, The Netherlands:** In the experiments we dealt with natural separation on the one hand and artificially induced separation on the other.

Both cases can best be compared using the results for configurations (e) and (f). Here we have separation at the same streamwise position on the same flat plate. For configuration (e) separation was induced in a more or less natural way by means of auxiliary airfoils. For configuration (f) a whole series of steps with different heights  $h$  was used. It was found that the separation angle  $\gamma$  was independent of  $h$ , so long as  $h$  is sufficiently large compared to the boundary layer thickness.

The separation angle  $\gamma$  for configurations (e) and (f) is sufficiently in agreement to state that  $\gamma$  does not seem to depend on the way in which separation is induced.

Of course this agreement only concerns the first part of the separation bubble; as soon as we start talking about transition and reattachment it is obvious that we can only consider the case of natural separation.

**J.J.D. Domingos, Portugal:** I think that your theoretical considerations have questionable basis apparently due to a generalized mis-statement of the mathematical and physical problem:

1. The singularity at the wall referred to in §2 seems to be due to the expansion method of Goldstein and others, and not to the basic boundary layer equations themselves.
2. After separation the boundary-layer equations are no longer valid as a physical approximation; also from a mathematical point of view, they have no solution in the usual sense.
3. Similar solutions and the "second branch" of the solution of the Falkner-Skan equation have no real physical meaning because a similar solution is always a very peculiar one because it only exists for special initial/boundary conditions. In particular for the case under discussion, if we started from a similar profile just behind separation, introduced a small perturbation and proceeded with a formal solution it would be seen that the solution will be unstable in a mathematical sense. This means that the similar solution on the verge of separation corresponds in fact to an unstable solution.

We mean unstable in a mathematical sense. Physically this instability can mean transition or not. If not, the flow would be well discussed by the "laminar solution" of elliptic problems which arise when full account is taken of the two momentum equations.

4. Numerical methods, as long as you are in laminar flow, if properly understood and used can do very well both in accuracy and generality. My comments should be taken in the sense that your experimental results deserve a wider scope of interpretation and generalization.

**J.L. van Ingen, The Netherlands:**

1. I do not agree with your remark. I think that the essentials of Goldstein's results are confirmed by the accurate numerical calculations of Leigh, Terril and others.
2. Of course there is an upstream effect in the separation region so that parabolic equations cannot be used. This however is true for the attached flow as well. The "elliptic" aspects for foil calculations get in because the boundary layer characteristics at the trailing edge determine the upstream pressure distribution. Hence for airfoil calculations the parabolic system of boundary layer equations can only produce good results by an iterative process where in turn pressure distribution and boundary layer calculations are made. Moreover it should be understood that our work does not intend to give more than engineering accuracy.

3. Of course I know the difference between similar and non-similar solutions of the boundary-layer equations. In approximate solutions of the boundary-layer equations we use "interpolating functions" to represent the velocity profiles. That these functions are sometimes taken from a series of similar solutions does not imply that these could only be applied to similar boundary layers.
4. No comment is required.

**H.Schlichting, Germany:** I would like to make a very short remark. For calculating the position of the point of transition from laminar to turbulent flow from the velocity profile in the boundary layer of the bubble, the degree of turbulence of the outer flow is a very important parameter.

This has not yet been mentioned up-to-now. The distance of the transition point from the instability point depends very strongly on this parameter, decreasing very considerably with increasing degree of turbulence. There is a diagram about this subject in the latest English Edition of my book.

**J.L.van Ingen, The Netherlands:** Yes, I agree with you that the turbulence level in the outer flow has an important influence on the distance between the points of instability and transition. It should be understood that in our paper we assumed a very low degree of turbulence in the outer flow as is the case in flight and in a good low speed wind tunnel. I think that we could take into account the influence of turbulence level on the amplification factor at transition using the figure in your book which you mentioned.

Ref. Book: "Boundary Layer Theory" (1968), H.H.Schlichting.

**J.Seddon, UK:** Mention was made by Prof. van Ingen (only in passing) that the pressure at reattachment might be expected to be close to the value corresponding to full recovery without separation. If the boundary layer at reattachment is turbulent, I think such a statement is untenable. By definition, the reattachment profile will have zero slope at the surface, denoting zero skin friction, and it follows that substantial pressure recovery will take place downstream of this point before a normal turbulent profile is restored. Perhaps Prof. van Ingen would like to comment on this but my question is a general one to the meeting, namely to ask whether workers in any area are studying, or intending to study such reattachment aspects of separated flow, particularly at subsonic speeds.

**J.L.van Ingen, The Netherlands:** I think I said "that people like to think" that the pressure comes back to the curve for unseparated flow. I think that for not too extensive bubbles this might be a reasonable engineering approximation. However, I agree that much more research should be done in this field.

We do not intend to do this type of research in the near future. We will concentrate first on separation and transition prediction.

**H.Schlichting, Germany (Comments only):** Dr Seddon has raised the question of the pressure distribution on a profile in the vicinity of a separation bubble. I agree that this pressure distribution cannot be calculated by theoretical methods only. This problem is very important in the Reynolds number range (based on profile chord)  $Re = 10^5$  to  $10^6$ . This Reynolds number range is practically very important for cascade blades of turbomachines. In Braunschweig in recent years we have carried out a research programme which deals with the aerodynamic coefficients of cascades (especially loss coefficients) where separation bubbles and their dependence on Reynolds number, Mach number and turbulence level are involved. The experimental part of this programme was carried out in the Variable Density High Speed Cascade Wind Tunnel, in which the Reynolds number and the Mach number can be varied independently.

This field has been discussed at some length at the Joint Meeting of the Fluid Dynamics Panel and the Propulsion and Energetics Panel on "Boundary Layers in Turbomachines" which was held last week at ONERA, Paris.

**K.Gersten, Germany:** Did you take into account the displacement effect of the boundary layer in your calculation of the pressure distribution? Especially for the determination of the separation point the higher order effects, here mainly due to displacement, are supposed to be quite important.

**J.L.van Ingen, The Netherlands:** The pressure distribution was only calculated for the separated region. The boundary layer upstream of the separation point was calculated from the measured pressure distribution which of course contains the displacement effect.

The calculation of the separated flow was based on

1. the value of  $(R_\theta)_{sep}$
2. the empirical correlation between  $\gamma$  and  $(R_\theta)_{sep}$
3. the physical observation that the separation streamline appears to be straight over a considerable distance.

All these three factors contain the displacement effect implicitly, I think.

I agree with you that for a calculation which starts from, for example air foil coordinates, the displacement effect should be included.



Written comments received from Prof. J.J.D.Domingos, Portugal, relating to Papers No. 2 (and 5).

1. In a session devoted to Basic Fluid Dynamics I think it is a disturbing fact that loosely defined concepts have been used and abused, and what should be a scientific discussion risks becoming an untractable problem in semantics! So to lay down a common basis, let us try to clarify ideas thinking first of purely laminar flow in two dimensions.

If we accept the Navier-Stokes equations, the flow is described by two momentum equations and a conservation of mass equation. These equations, if time dependent form a parabolic set in time (time appears only in a first order derivative). If steady state (time independent) the set of equations is elliptic. Elliptic equations need for their solution the specification of velocities over *all* the boundaries (upstream, downstream, wall, inviscid stream . . .). Prandtl simplified these elliptic set to the boundary layer form neglecting second order derivatives in the main streamwise direction. Physical justification implied small crossflow. The mathematical consequence is that the equations become parabolic in the x-coordinate and as such, downstream boundary conditions are not needed.

When we approach separation the physical justification breaks down . . . and, it seems, the first confusing point appeared because people started thinking that, if the crossflow is taken into account and the pressure gradient "adjusted", all the predictive value of boundary layer theory could be recovered. What has been forgotten is the fact that when separation appears,  $U$  becomes negative and with or without crossflow of any magnitude, the boundary layer equations from a strictly mathematical point of view become a completely different problem. This change in the mathematical behaviour is similar to a heat conduction problem in which, at a certain time, the thermal conductivity becomes negative. The conclusion is that no parabolic set can describe a velocity field with  $U < 0$ . So *all* methods including integral methods (which are approximate . . .) which start from the parabolic set (which are the boundary layer equations) are basically wrong, and would never be able to predict with generality. And if some authors claim success with some form of integral method, the reason is to be found elsewhere (the empirical input implicitly through the profile, or explicitly in adjustable constraints which compensate for particular cases and in a devious way compensate for the basic errors involved in the starting equations).

2. If we take this mathematical background I think that we should take as a definition of separation that region where  $U \leq 0$ , in which both physically and mathematically, the boundary-layer equations break down (we can also call these regions bubbles, recirculation regions, etc.).

How can we predict these effects?

- (a) Inside the bubble or separated region there is no way out – the elliptic problem must be solved and boundary conditions shall be given all around its boundary;
- (b) Outside, the boundary layer equations can be used but a boundary condition shall be given all around the bubble (this creates a matching problem . . .).

Practically, because the boundary layer equations are no more than a simplification of the elliptic problem, we can solve the whole flow as an elliptic set. This can be done (and has been done) by purely numerical methods. If computer capacity or time is a problem (a) and (b) are combined and the matching found by iteration. A more simplified approach can also be suggested in which the elliptic set is tackled by an approximate method of the weighted residuals variety (of which the von Kármán-Polhausen method is a particular case) which will constitute the natural way of implementing the integral methods used by the authors on a firm foundation.

3. If our proposal is clear, we can go to the second troublesome point which comes from the fact that separation is usually associated with transition from laminar to turbulent flow which seems to induce the tendency to confuse one problem with the other.

In fact, if we use time mean averages for the description of turbulent flow, what we already said regarding the definition of separation (i.e.  $U \leq 0$ ) applies equally well for laminar and turbulent boundary layer theory.

So, let us separate the concepts of separation and transition. If we agree in doing so we will cease blaming turbulence models (mixing length, etc.) within the boundary layer scope as responsible for failure of prediction methods in bubbles.

A reason to blame only comes when we have a method (and indeed we already have) to solve accurately the elliptic problem. We have taken a long time and have still not avoided being sketchy. We hope however that all of us recognize that clearing the connection between the physics and the mathematics of the problem can only help towards a further understanding.

### Discussion of Paper 3

"Recherches Théoriques et Expérimentales sur les Décollements  
Liés à une Déformation Locale de Surface"  
présenté par S.Burnel, G.B.Diep, P.Gougat et B.Prunet-Foch, France

**K.Gersten, Germany:** Have you taken into account any displacement effect of the boundary layer on the outer flow velocity distribution?

**S.Burnel, France:** Le travail que nous avons présenté ici avait pour but de mettre en évidence la présence de micro-décollements dans les creux de sinusoïdes présentant un rapport amplitude sur longueur d'onde très faible. Les résultats obtenus par le calcul étant déjà en bon accord avec ce que nous a montré l'expérience, nous n'avons pas jugé utile d'ajouter une correction due à l'épaisseur de couche limite.

### Discussion of Paper 5

"Prévision du Decrochage d'un Profile d'Aile  
en Ecoulement Subcritique"  
présenté par M.Vincent de Paul, France

**M.Lazareff, France:** L'auteur nous a montré de bonnes confrontations concernant le  $C_{zmax}$ , entre les éléments théoriques proposés et l'expérience. Il est suggéré que le coefficient de moment de tangage sont aussi soumis à des confrontations; en effet ce dernier paramètre est certainement beaucoup plus sensible que le  $C_z$ , tant en présentant un intérêt majeur pour l'ingénieur.

**M.Vincent de Paul, France:** Le coefficient du moment de tangage  $C_m$  est plus délicat à calculer. Il faut en effet pouvoir prévoir avec suffisamment de précision l'écoulement dans la région du bord de fuite. Nous étudions actuellement ce problème.

**A.D.Yeung, UK:** What were the assumptions made regarding the reattachment of the turbulent shear layer at the rear of the bubble which enabled you to determine the reattachment point?

**M.Vincent de Paul, France:** Il y a deux hypothèses principales en ce qui concerne le point de recollement R :

1. Le profil de vitesse est supposé connu (cf Annexe II § 1b);
2. La vitesse en ce point R est supposée être sur la courbe des vitesses en fluide parfait.

### Discussion of Paper 6

"Parametric Studies of Separating Turbulent Boundary  
Layer Flows"  
presented by A.Wortman and W.J.Franks, US

**K.Gersten, Germany:** You changed your turbulence model in the neighbourhood of the separation point. Therefore you have another free parameter in your calculation, namely the position of the change of the model. How did you determine this position and what is the effect of this position on the location of the separation point?

**A.Wortman, US:** We used several turbulence models to convince ourselves, that we do not have a generally satisfactory eddy viscosity relation. In our study we showed that the Lees-Alber model developed specifically for computing separation does not give correct trends with Mach number cooling etc., but used it only because of lack of anything better. It is not possible to get a smooth match when crossing over from one eddy viscosity model to another, and the location of separation is a rather strong function of the location of the cross-over point on the wing. Realizing that the boundary layer approach to prediction of separation is at best a rather crude engineering approximation we wanted to show that we don't even have a satisfactory eddy viscosity model and thus all the current calculations represent neither an engineering nor a theoretical contribution of any significant value. With our presentation we hope to stimulate the development of more satisfactory eddy viscosity models.

**Discussion of Paper 8**  
**"Comments on the Methods Developed at the NLR for Conducting**  
**Two-Dimensional Research on High-Lift Devices"**  
 presented by O. de Vries, The Netherlands

**D.N.Foster, UK:** I would like to explain why RAE adopted the wall boundary layer control (BLC) by suction technique. Our first real attempt to produce two-dimensional flow was for a wing with BLC over a flap by blowing. We had installed a wall BLC system using blowing, but found that the wall BLC interfered with the wing BLC to cause detachment of the flow over the flap. We have therefore adopted a suction system, which we feel gives a smooth control of the wall separations.

I would also like to ask about the two-dimensionality of the flow downstream of the trailing edge. Some two years ago NLR published results for the drag of the wing sections, as obtained by the wake survey method, and showed large variations across the span for a wing without wall BLC. Can you say if these results are repeated when wall BLC is used?

**O. de Vries, The Netherlands:** The variations of the wake drag across the span of a two-dimensional wing at high-lift, originates probably from irregularities in the boundary layer of the wing, or from three-dimensional effects introduced in the wake by the flap and slat brackets, which are necessary at several spanwise stations of the model and leads to clustering of the wake at definite spanwise stations by secondary flow.

There is no indication that these three-dimensional wake effects originate from the wing-wall junctions, because wall BLC did not diminish this effect.

**P.Carriere, France:** Le paramètre  $\lambda$  utilisé par l'auteur n'est qu'un repère pour un montage expérimental déterminé. L'auteur pourrait-il indiquer le rapport des surfaces de fente et de la surface de l'aile, de manière à permettre de généraliser l'influence de  $\lambda$  dans d'autres situations?

**O. de Vries, The Netherlands:** The slot width is about 2 mm, the leading edge slot is about 0.2 m long and the slot at the shroud extends about 0.2 m above the upper surface and about 0.1 m below the lower surface. The wing surface (flaps retracted) is  $0.6 \times 2.1 = 1.26 \text{ m}^2$ . The lengths of the blowing slots are not critical. It was not our purpose to develop an optimal wall blowing system. We were satisfied with a rather crude system, which could be applied to different configurations, without extensive supplementary tests.

**V. de Brederode, Portugal:** According to our findings on the behaviour of the flow down a two-dimensional backward-facing step, a quite undetectable convergence or divergence of the flow on the centre part of the separation bubble was associated with appreciably large changes in entrainment rate near the corners in such a way that, although we could assume the flow on the centre region was very nearly two-dimensional from a geometrical point of view, the measured values of base pressure coefficient and reattachment distance did not correspond to the aerodynamically two-dimensional case, i.e. to the infinitely long case, the small convergence or divergence of the flow altering the supply of fluid to the recirculating region and thus greatly affecting its size. So I wonder what would be, in your opinion, the degree of reliability if the two-dimensional data – such as  $C_{L \max}$  – obtained when using your tunnel wall boundary layer control set-up in the more demanding situation of an aerofoil exhibiting, for example, a long bubble burst type of stall.

**O. de Vries, The Netherlands:** I agree that wall blowing might affect the flow inside a separation bubble, especially when considering a long bubble. However, quite a number of the wing sections, which we have tested with the wall blowing set-up, showed a leading edge stall. Flow visualisation tests did not show any cross-flow before the stall, so we believe, the influence cannot be large. We have, however, no experience with a long bubble on the wing upper surface. In addition, it must be pointed out, that beyond the stall, the flow is no longer two-dimensional with wall-blowing.

**A.D.Young, UK:** Are you proposing to include viscous effects in your calculation methods in due course?

I note that in your diagrams the theoretical pressure distributions do not show pressure coefficients of unity at the trailing edge as expected for inviscid flow, but instead show coefficients more nearly those of experiment. Can you explain this?

**O. de Vries, The Netherlands:** We will certainly include viscous effects in our calculations in due course. In effect, some of us are working in this field already (displacement effects, turbulent boundary layers). The complete calculation of the BL flow around a multiple aerofoil has to include a lot of empirical data. The big difficulty is to evaluate the range of applicability of the empirical relations and it will take much time to gather the experience.

There are lively discussions at our laboratory on the question of the most efficient way to proceed, in view of the limited capacity available at our laboratory.

Your second question can be answered by pointing out, that with a panel method, the pressure is calculated at the mid-points of the panels.

To approximate the pressure at the trailing edge sufficiently accurately, one has to use a very fine panel distribution at the trailing edge.

Because we know a priori, that the pressure coefficient at the trailing edge is unity, we did not calculate this pressure and omitted it in the figures.

#### Discussion of Paper 9

"Corrections de Blocage dans les Essais en Souffleries –  
Effets dus aux Décollements"  
présenté par J.C.Vayssaire, France

J.Manee, The Netherlands: The separation drag is related in the paper to the difference between the theoretical drag (from the theoretical polar) and the measured drag. However, when separation starts on part of the wing, does not the change in lift distribution on the wing change the induced drag, thus making this way of estimating the separation drag inaccurate (especially at very high values of the lift coefficient)?

J.C.Vayssaire, France: Votre intervention est très intéressante car elle me permet de développer pour le cas des  $C_z$  élevés (c'est-à-dire supérieurs à 3) l'une des applications pratiques du principe énoncé dans le paragraphe 4.3 et résumé par la figure 11. Il est toujours possible de faire passer une parabole théorique parmi les points expérimentaux d'une polaire limités par un  $C_{z_u}$  supérieur et un  $C_{z_u}$  inférieur sans pour cela connaître les valeurs des  $C_{x_m}$  et  $C_{z_m}$ . On peut également déterminer cette parabole en l'absence de la connaissance du  $C_{z_u}$  inférieur, lorsque le montage expérimental ou la balance ne le permet pas. Ce fut le cas pour les demi-maquettes dans la soufflerie basse vitesse N°1 de l'Institut Aérotechnique de Saint-Cyr.

Ce fut aussi le cas pour la soufflerie Σ4 de ce même Institut.

L'estimation du  $C_{x_d}$  par ce procédé et les résultats ainsi obtenus, comparés à d'autres résultats, sont très satisfaisants.

En résumé, on confond la parabole avec la partie supérieure de la polaire éventuellement déjà influencée par de légers décollements. Ces décollements ne modifient que la valeur de l'allongement équivalent mais n'ont rien de commun avec les décollements du type d'eau morte qui aplatissent très rapidement la polaire expérimentale.

Ce procédé est en expérimentation comparée dans plusieurs souffleries en vue de la généralisation de son utilisation pour les très hauts  $C_z$ .

On doit préciser qu'il s'agit de hauts  $C_z$  obtenus par "voie aérodynamique pure" et non par soufflage ou tout autre apport d'énergie extérieure.

#### Discussion of Paper 10

Aerodynamics of High-Lift Airfoil Systems  
presented by A.M.O.Smith, US

J.Seddon, UK: The description of the multiple effects of gaps is highly interesting and informative but it leaves a residual question. In the process of extending a slat or flap, both the chord length and camber shape of the overall system are thereby altered significantly. Is it possible to say to what extent the improved lift characteristics are due to these changes and to what extent the air gaps themselves are responsible?

A.M.O.Smith, US: An airfoil is normally designed for cruise, so that maximum lift is low. To get high lift the shape must be changed. How should it be changed? That is the question underlying my paper. In the full paper I show that slots are advantageous. The limiting lift coefficient is not known (with fully attached flow) for a 2, 3 or 4 element air foil but  $C_{l_{max}} = 4$  is often reached, based on the extended chord (and at least 3.5 with fully attached flow). It is near 5 based on the original chord. The best possible section lift with fully attached flow on a single element airfoil is about 3.06 at  $R_c = 5$  million. With a reasonable thickness as in Figure 17 it is only 2.31. Wind tunnel tests found the maximum lift to be about 0.4 higher than this design lift. This value is still far below what a slotted airfoil can do, and it is some kind of upper limit. Hence I think we have shown that slots are advantageous, even though we have no similar theoretical limits. We are just beginning an ONR contract on the two-element problem and with luck we may be able to establish an upper limit for a two-element airfoil along the same lines as Dr Liebeck has done for a single element airfoil.

W.D.Horsfield, UK: In the correlation of calculated and experimental separations did the calculated separations use experimental upstream boundary layer data such as measured transition point?

A.M.O.Smith, US: The correlation curve represents a variety of data. In some cases transition was known experimentally. Then that knowledge was used. In most cases it was not and then Michel's method of predicting transition was used. Separation is less sensitive to errors in predicting transition points than in the prediction of drag. Otherwise the boundary layer calculations were a conventional calculation of laminar flow, then turbulent flow subject to the impressed pressure distribution, at the proper Reynolds number right to the separation point. All the data shown is at  $M = 0$ , in Figure 5.

D.M.McRae, UK: Can Mr Smith comment on how pessimistic the Stratford optimum rise data is? Perhaps I may quote the Stratford linear rise data for comparison? Consider an aerofoil 12% thick with a 60% roof top and a trailing edge  $C_p$  of about +0.25. Stratford's linear rise data state that such an aerofoil would be in separation troubles at all Reynolds numbers less than  $1.00 \times 10^6$  whereas in fact such aerofoils are certainly satisfactory at  $6 \times 10^6$  and possibly at  $1.0 \times 10^6$ . Thus there is a margin of at least 30 fold in Reynolds number in the linear case. What indications of margin are there for the optimum rise case?

A.M.O.Smith, US: I am surprised that you find separation. The airfoil in Figures 21 and 22 of my paper does not quite show separation according to our own partial differential equation method, and I would not expect the Stratford method to differ greatly. Notice its pressure at the trailing edge is  $C_p = +0.25$  just like you mentioned, but the rooftop is far different. Our experience is that the Stratford limiting pressure rise is conservative. For the airfoil similar to that in Figure 17, we designed it for a laminar rooftop and a Reynolds number of 2 million. In tests it worked well at 1 million. But when we tripped the boundary layer at 1 million it did not work. This is some kind of a measure of conservatism. More is shown by Figures 1, 2, 3, 4 and Reference 3.

A.D.Young, UK: In connection with the point raised by Dr Seddon I would like to refer to some pre-historic analysis of mine made many years ago on various forms of flaps and slats. From that analysis it was clear that one could simplify the process of predicting the aerodynamic characteristics of such devices by using the concept of effective chord which allowed for the associated changes of chord and area when the devices were extended. However, having said that there remained clear advantage arising from the slots and the effectively gentle camber changes, if these were well designed, and these advantages could be quantified on the basis of empirical data as well as theory.

Mr Smith has demonstrated that from the point of view of efficiency of pressure recovery, aerofoils with a concave form of pressure distribution over the rear were better than aerofoils with a convex form of pressure distribution. However, many years ago Squire and I produced a paper which showed on the basis of a plausible argument backed by experimental data that, with the former type of pressure distribution we can expect a much more rapid forward movement of separation with increase of incidence than with the latter, and hence the former aerofoils show much more vicious stall than do the latter. Indeed, I suspect that a major cause of the serious incidence of stalling accidents shown in the statistics of general aviation small unswept aircraft, referred to by Mr Muse yesterday, is the continued use of wing sections for such aircraft which show pressure distributions near the stall that are concave over the rear and are in consequence bad from the stalling point of view. I shall be glad to have Mr Smith's comments on this point.

A.M.O.Smith, US: In my analysis I have implicitly accounted for the effect of chord extensions. A lift coefficient should always be based on the chord of the configuration that is producing the lift. I think Prof. Young is correct for a concave pressure distribution, rear separation does indeed move forward more rapidly. A straight line pressure distribution (my  $m = 1$  case) may be a good compromise. On most aircraft other than clean single engine private types, the stall characteristics are a function of many more things than just the airfoil  $C_L$  v.  $\alpha$  curve. Nacelles, sweep, twist, slats, stores, a taper and wing-fuselage geometry are a few examples. In some cases as on simple clean single engine private type airplanes I would think the airfoil properties do become more important. But I was involved in a design of an airplane having a clean unswept wing and an airfoil whose lift stall was very sharp. The wind tunnel model showed a drastic drop in  $C_L$  at the stall. We were worried, but in flight there was no vicious wing dropping tendency at all. We still have a lot to learn.

Discussion of Paper 11  
"The Low Speed Stalling of Wings with High Lift Devices"  
presented by D.N.Foster, UK

J.Seddon, UK: Mr Foster showed a stall development in the presence of slot supports. From the evidence given I would think there was some doubt as to whether the supports had any ultimate adverse effect on the stalling level and general characteristic, or whether the supports merely acted as initial localisers of the development of separated flow. Is this situation clear?

**D.N.Foster, UK:** The situation is that from these tests it cannot be stated categorically that the supports had an adverse effect on the stall, but it is certain that they acted as a trigger for the initial separations. Nevertheless it is possible that had the supports been at different spanwise locations, the occurrence of the initial separations might have been delayed to a higher lift coefficient, and this in turn might lead to a higher maximum lift.

**C.A.Anderson, US:** Have you been able to separate the effects of Mach number and flexibility on the  $C_{L_{max}}$  in the wind tunnel and flight test? Do you intend to test both a rigid and flex wing in your new 5 metre tunnel to attempt to separate flexibility effects from Mach numbers?

**D.N.Foster, UK:** The test made to date in the wind tunnel for the effects of Reynolds number and Mach number have been on a single model representing the 1 g shape of the wing, and no attempt has been made to determine if it has distorted during these tests. It would obviously be sensible to consider how far the 5 metre tunnel could be used to determine the effect of wing flexibility.

**T.Schuringa, The Netherlands:** The agreement between flight and wind tunnel with regard to flow separation depends largely on the Reynolds number of the wind tunnel test. A picture is shown of the flow separation at  $Re = 1 \times 10^6$  in the wind tunnel and  $15 \times 10^6$  in flight which differs agreeably. At which Reynolds number in the wind tunnel is agreement obtained?

**D.N.Foster, UK:** Tests on another model of this aircraft in a pressurised wind tunnel suggested that the relationship between pitching moment and lift coefficient measured in flight could be reproduced at a Reynolds number of  $4.3 \times 10^6$ .

**A.Wortman, US:** In the calculation of the wake-boundary layer interaction a higher order boundary layer theory must be employed. Since turbulent boundary layers are not mathematically well defined, how can such a calculation be performed?

**D.N.Foster, UK:** The calculation method was in fact a simple integral method developed by Irwin (Reference 10 of paper). It is in some ways similar to a method published by Gartshore and Newman for wall jets in streaming flow. The velocity profile for the boundary layer is assumed to be a power law and the inner and outer wakes have Gaussian velocity profile. The momentum equation is then integrated over various parts of the viscous layer and initially assumptions were made about the variation of shear stress through the layer. More recently experimental measurements have been made of the variation of shear stress through the layer.

**C.J.Lievens, France:** L'auteur a écrit que l'optimum pour une configuration aile plus volet est obtenu avec une interaction faible et une absence de mélange entre le sillage de l'aile et la couche limite du volet. Au contraire pour une configuration bec plus aile plus volet, l'optimum correspondrait à un mélange complet entre le sillage de l'aile et la couche limite du volet.

Quelle est l'origine de cette différence? Cette assertion a-t-elle une valeur générale?

L'auteur a-t-il effectué une analyse fine de la structure de la couche limite de l'aile dans la zone où cette couche limite serait "contaminée" (rendue "plus turbulente") par le sillage du bec?

**D.N.Foster, UK:** Although the slot and flap are both used to enable the main wing to carry more lift, the means by which they do this is different. The slat reduces the magnitude of the suction peak on the leading edge of the wing, and the adverse pressure gradients in this region. It will continue to do this as the slat is brought closer to the wing, but at the same time the wake from the slat interferes with the boundary layer on the wing, and the optimum slat position occurs when the benefits of reducing the loading on the wing, and so making things easier for the boundary layer on the wing, is offset by the interference from the slat wake on the wing boundary layer. The flap enables the wing to carry more load by increasing the velocity at the wing trailing edge, and so reducing the adverse pressure gradients over the rear of the wing. Its optimum position is determined by the fact that the boundary layer on the lower surface of the wing and that on the upper surface of the flap, should not meet, and when this happens there is found to be weak interference between the total wake from the wing and the boundary layer on the flap.

We have made detailed measurements of the velocity distribution through the boundary layer on the wing and the wake from the slat, when they are in the merged condition. We have also measured the velocity distribution and the shear stress distribution for the flow above a flap, for a configuration for which the flap was very close to the wing so that the wake and the boundary layer were again merged.

**Discussion of Paper 12**  
**"A Simplified Mathematical Model for the Analysis of**  
**Multielement Airfoils Near Stall"**  
 presented by I.C.Bhateley and R.G.Bradley, US

**J.Mannee, The Netherlands:** It is frequently stated in reports concerning these calculations that one can save the expenditure of expensive wind tunnel testing by these calculations. However you exchange the wind tunnel costs for ever more expensive computer costs. At NLR it is estimated that the cost of a polar run in the wind tunnel and the calculation with only a potential flow method is about equal. Could the author give an indication about the computer time involved for his calculation on a multiple airfoil, including viscous effects, for one angle of incidence?

**I.C.Bhateley, US:** A typical cruise configuration analysis requires approximately 3 minutes while a high lift system analysis takes approximately 5 minutes of CDC 6600 central processor time.

**R.Epler, Germany:** Am I right, that you don't introduce any flow condition along the free streamline? Increase your source strength if you introduce separation?

**I.C.Bhateley, US:** No flow control is exercised downstream of the separation point. The source strength is determined by condition of continued tangential flow at a point very close to the separation point.

**R.J.Templin, Canada:** How do you decide upon the location of the "pseudo boundary points" near the trailing edges of finite-thickness trailing edge aerofoils, and do you have any idea of the sensitivity of the results to the location of these points?

**I.C.Bhateley, US:** The pressure distributions in the immediate vicinity of the trailing edge and separation points are sensitive to the location of the "pseudo boundary points". These points should be taken as close to the trailing edge as possible and depend on the accuracy of the computer being used for the analysis. Currently we are using  $10^{-5}$  of the reference chord.

**K.Gersten, Germany:** In real flow there is obviously a jump in the total head along the separating streamline. Isn't it necessary to put also vortices on the separating streamline in your model, in order to simulate the total head jump as well as the condition of constant pressure at that line?

**I.C.Bhateley, US:** The flow conditions internal to the wake are not correctly simulated by this simplified model at the present time.

**A.M.O.Smith, US:** In our flow calculation method we use sources to describe the shape and vortices to obtain the circulation. When we placed a point vortex within an airfoil we found it created a bump in the pressure distribution. You place a source within the airfoil to create open ended airfoils. Do you too get a bump?

About a year and a half ago we too tried simulating partially separated flow by just terminating the airfoil contour at the calculated separation point. Sometimes the method gave good results, other times poor. We had the same experience with Jacob's method. I believe we must represent the true physical flow process more accurately if we are ever to obtain satisfactory answers.

**Discussion of Paper 13**  
**"The Effect of Leading Edge Geometry on High Speed Stalling"**  
 presented by G.F.Moss, A.B.Haines and R.Jordan, UK

**D.Zonars, US:** As in the case of low speed characteristics, the Reynolds number of the test conditions play a dominant role on the variable geometry effects displayed here at transonic speeds. Of course, the existence of a shockwave interacting with the boundary layer adds another dimension to the complexity of the test results. The test conditions shown here are particularly sensitive to Reynolds number variation. What confidence do you have in the change over characteristics of the maximum lift coefficient as a function of varying airfoil nose geometry for the range of Mach numbers displayed? Also, was the Reynolds number for the two-dimensional data the same for the three-dimensional characteristics?

**G.F.Moss, UK:** I think we need to be careful in discussing scale effects at high subsonic speeds. Some types of shock induced boundary layer interaction are fairly insensitive to scale and permit useful work to be done at model Reynolds numbers and used successfully at full-scale conditions, provided a careful transition fixing technique is

used. The important thing is to understand the nature of the flow situations and to tackle on the model the same fluid-dynamics problem which obtains at full-scale Reynolds numbers. In our experience, values of maximum usable lift coefficient are not very scale dependent when the separation in question is primarily a function of shock-strength, and when the complications of interactions with other flow separations aft on the chord are not dominant. This is because the strength of the shock is closely tied to the value of the lift being generated. Care was taken in the work described here to use only moderate degrees of rear-loading and complete models with only moderate amounts of sweepback. In this way we avoided the more complex scale-sensitive situations which are dominated at model Reynolds numbers (only) by interactions between rear and shock induced separations. I would thus argue that the findings of this research given in this paper are valid for many full scale situations of current interest.

As the Mach numbers are reduced and different flow situations develop the whole picture changes, of course, and I would not be so confident.

The Reynolds numbers of the test work described in this paper are given in some of the figures (see Figure 2 for Section 2 and Figure 25 for Section 4). The Reynolds number of the tests described in Section 3 was in the band  $5$  to  $6.5 \times 10^6$  based on chord. For the reasons given above, I do not consider that the difference between the Reynolds number of the two-dimensional tests ( $6.5 \times 10^6$ ) and the three-dimensional tests ( $1.4 - 2.4 \times 10^6$ ) in the work described in Section 2 is an important factor in the context of the arguments presented.

**U.Sacerdote, Italy:** asked a question concerning the effect of various high lift devices, and in particular the "RAEVAM", on  $C_m$ .

**G.F.Moss, UK:** Most of this paper is concerned with sectional characteristics of the wing profile where pitching-moments are only of secondary importance. On the complete swept wing, however, overall pitching-moments are of great importance and are directly affected by modification to sectional characteristics across the span. A main purpose, of leading-edge high-lift devices at high speeds, as we have seen, is to reduce the strong three-dimensional effects associated with shock-induced separations which reduce drastically the value of usable lift. In doing this, pitching-moment characteristics are also greatly improved in most cases.

#### Discussion of Paper 16

"A Practical Look at the Stall and High Lift Operation of Externally  
Blown Flap\* STOL Transport Configurations"  
presented by D.J.Moorhouse, US

**J.K.Wimpress, US:** Recent Boeing data is in conflict with that shown in Figure 5. If the leading edge is properly protected to prevent a leading-edge stall, the EBF flow prevents a stall at the wing trailing edge and the entire wing can be carried to  $35^\circ$  to  $40^\circ$  angle of attack before the stall occurs.

**D.J.Moorhouse, US:** The figure actually shows a wide range of power effects, both increasing and decreasing stall angle. I agree that if the leading edge is designed properly then large increases are seen. The theory actually predicts a decrease in stall angle, and some configurations indicate an initial decrease followed by increasing stall angle with increasing power, indicating a change in stall characteristics. The particular data was presented to show that even with a large leading-edge, bad stall angles were achieved. The point was made in the presentation that design of the leading-edge device is critical to the total aircraft design.

**K.Gersten, Germany:** What are typical values of the measured turning efficiency  $\eta$ ? Does  $\eta$  change drastically with geometry and do you see any possibility for calculating  $\eta$  by theory without using any empirical data?

**D.J.Moorhouse, US:** Typical values of turning efficiency are 100% at zero flap deflection to 70 or 90% at high flap deflections ( $60^\circ$ ). At present I only know of the empirical correlations in Reference 11 of my paper, but work is being done to calculate  $\eta$  theoretically.

**D.J.Foster, UK:** I am wondering if the difficulties you experience with the application of an aspect ratio correction factor arise from the datum you used to evaluate the lift increment. As the theory is derived from a potential flow ... the conditions at the power-off stall may differ considerably from this model due to separation from highly deflected flaps. Have you ascertained if any other datum could improve the correlation?

**D.J.Moorhouse, US:** This is possibly true. My concern was to correlate the available EBF data with the deficiencies therein. The data includes a configuration with plain leading edge which may be expected to have a leading edge stall. Another configuration definitely did not have leading edge stall. Thus different configurations are contained within the scatter band.



**W.D.Horsfield, UK:** Are stall margins for landing adequate? Normally we use 30–40% of which 25% is used by a 10 Ft/Sec gust. Structure was to be designed against 50–70 Ft/Sec gusts. Stall accidents occur more frequently than structural accidents. Are these facts perhaps connected?

**D.J.Moorhouse, US:** I used 10 kt rather than the higher values because I was talking about terminal operations. I agree that stall margins require further study. We must not use STOL airplanes with the old conventional thinking. This study should be done before we fly STOL aircraft. My concern was not to dismiss the problem but to raise it.

**Discussion of Paper 17**  
**"Flight Development of a Military Trainer Aircraft**  
**with Particular Reference to Stall Warning"**  
 presented by G.P.Wilson and W.D.Horsfield, UK

**D.J.Moorhouse, US:** I do not think Mr Horsfield mentioned any wind tunnel tests before the earlier Marks of Provost. Were the actual stall characteristics predicted, or were they different to what was predicted?

**W.D.Horsfield, UK:** The Provost Series was developed by flight testing without significant wind tunnel testing. Tunnel tests on stall were carried out, and gave some similarities with flight stalling, but the differences at the Reynolds numbers tested were considered too great to pursue extensive tunnel work on the MK 4/MK 5 differences.

**J.Seddon, UK:** I should like to follow up on the previous question. Would Mr Horsfield say, retrospectively, that a modification such as that which was made to the leading edge, had it been tested in the tunnel beforehand, would have shown up the improvement in pitching-moment characteristics etc. which was actually found in flight?

**W.D.Horsfield, UK:** I think that tests at a sufficient Reynolds number may well have given an adequate match on the stall behaviour, but the stall warning aspects may be more dubious.

**B.Laschka, Germany:** You have pointed out, Mr Horsfield, that complete success of the desired stall progression has been finally achieved by vortex generators. One may observe from your Figure 17 that the vortex generators you have selected are of co-rotating type. Sometimes it has been stated that counter-rotating vortex generators supply more energy to the boundary layer and consequently are more efficient than co-rotating ones. Do you have some experience on this subject, and can you recommend which type to use for different separated flow patterns? Would you like to comment on this point?

**W.D.Horsfield, UK:** I have no experience with counter-rotating vortex generators. In the case of the Jet Provost, we wished to reinforce the general vortex field in one direction, and therefore used the appropriate direction of co-rotating generators. I would imagine most corner flows would also be of this type.

**G.F.Moss, UK:** First, I would like to suggest that the term "buffet" be restricted to the vibration of the airframe under the influence of unsteady aerodynamic excitation. The airframe responds to this excitation in the only way it can – at one or more of the natural deformation modes. It is best to distinguish carefully between this motion and the motion of the whole airframe, as in instability phenomena such as wing-rock etc. In my experience, in discussions of the type we are to have today, it is easy to confuse these matters. This is not connected in any way with anything that Mr Horsfield has said.

My question for Mr Horsfield is: has scale-effect on the stall been measured in flight? It is necessary to be careful about Mach number changes of course. We do tend to be mesmerized by flight-tunnel comparisons in the context of scale-effects and to forget that scale-effects can occur at flight Reynolds numbers.

**W.D.Horsfield, UK:** First, I agree that buffet is an airframe vibration at "structural" frequencies, and that is the context in which I have used it.

To the best of my recollection, we did not find any flight scale-effect. The "g" stall, at higher IAS than the 1 g stall was better marked by buffet warning because of this higher IAS amplifying the input, and was therefore an easier case. We did find substantial effects on maximum lift from different rates of approach (knots/sec) to the stall, and standardised our 1 g stall conditions to ensure comparable data.

**A.D.Young, UK:** I think that I can understand why the fence helped to improve the stalling properties of your aircraft, but I am not clear about the function of the small fence below the intake and why it helped. Could you explain its effect?

**W.D.Horsfield, UK:** I think it suppresses crossflow out from the fuselage intake over the leading edge of the wing but beyond that I leave the explanation to the theorists.

**G.J.Hancock, UK:** The author describes a series of ad hoc modifications to obtain acceptable buffet and stall characteristics. Does the author think that there are fundamental aspects which deserve research attention to obtain basic information which could reduce the amount of ad hoc testing?

**W.D.Horsfield, UK:** Although fundamental research could be done — for instance on stall “departure” in pitch — I doubt whether this special case would justify any work other than project-oriented. The stall characteristic was fairly easily achieved. Increase in buffet was required, not decrease, and this was more difficult.

**Discussion of Paper 18**  
**“Stall and Post-Stall Characteristics of the F.111 Aircraft”**  
 by J.E.Goode and presented by C.Anderson, US

**J.K.Wimpress, US:** Regarding the regression technique for getting derivatives from flight test. The aerodynamic derivatives usually occur in groups in the equations. How do you break down these groups into the individual derivatives?

**C.Anderson, US:** The group of derivatives that make up each total coefficient are looked at individually. That is, all the derivatives which make up the rolling moment coefficient are adjusted until the flight test and simulator total coefficient agree. The wind tunnel data is used as a guide to assume that the derivatives modified are not out of the ballpark.

**D.Zonars, US:** If you follow the wind tunnel data religiously, then why did you choose not to conform to the change over characteristic of  $C_{n\dot{\beta}}$  as a function of angle of attack around  $50^\circ$  since the flow is fully separated on both the wind tunnel and flight test article?

**C.Anderson, US:** The wind tunnel data is used as a guide only and is not religiously adhered to in either value and trends with angle of attack.

**G.F.Moss, UK:** In Figure 8 in your paper a gross discrepancy between the wind tunnel values of  $C_{n\dot{\beta}}$  and those necessary to simulate the full-scale behaviour are shown. However, at the high incidences where this discrepancy occurs ( $50^\circ$  to  $70^\circ$ ) there will be two pronounced wakes from the two wings which could be very much a feature of this derivative. I see the sweep of the wings is quoted as  $50^\circ$  in the wind tunnel experiment and  $4.6^\circ$  in the flight case. Can Mr Anderson assure us that this difference in wing sweep was not a factor in the discrepancy?

**C.Anderson, US:** Yes, since the same trend is there at wing sweeps of  $26^\circ$  and  $35^\circ$ .

**E.L.Ericson, US:** It has been shown that the anomalous  $C_{n\dot{\beta}}$  behaviour at high  $\alpha$  is caused by the shedding of asymmetric vortices off a pointed/slender nose. In the wind tunnel test the vortices are generated by roll-up of laminar separation sheets, in full scale they are probably generated by turbulent separation. The “oscillatory” behaviour of  $C_{n\dot{\beta}}(\alpha)$  in wind tunnel testing might be caused by additional vortices being added as  $\alpha$  is increased further. I think you or one of your colleagues has shown that by putting a pair of small strakes on the nose, thereby forcing the shedding to be symmetric — the  $C_{n\dot{\beta}}$  anomalies disappear.

**C.Anderson, US:** Yes, this was done by Jim Bowman at NASA Langley. I personally believe that putting the strakes on the nose simulate full scale Reynolds number.

**C.J.Lievens, France:** Quels essais avez-vous faits sur l'utilisation de parachutes:

- soit “parachutes de vrille” au sens strict, utilisables aussi lorsque la vrille est établie.
- soit “parachutes de perte de contrôle”, utilisables *seulement* dans les premières secondes qui suivent la perte de contrôle? D'une manière générale, quelle est la position de General Dynamics sur l'emploi de tels parachutes? Notamment:
- un parachute - frein peut-il servir aussi (en opération) de “parachute de perte de contrôle”?
- l'utilisation par le pilote moyen d'un “parachute de perte de contrôle” est-elle réaliste compte tenu du faible délai dont il dispose pour réagir?
- Avez-vous connaissance de cas où un pilote ait utilisé des parachutes anti vrille ou de perte de contrôle en opération?

**C.Anderson, US:** Yes. We think that recovery parachute is mandatory for flight test. If you are sure that you will never encounter a spin from which you will not recover, then a device such as a parachute the size of a drag chute could be used to recover from out of control situations.

I do not know why one would think they could recover from a spin and not a post-stall gyration or out of control situations.

**Discussion of Paper 19**  
**"Post-Stall Aerodynamics of the Harrier"**  
 presented by C.L.Bore, UK

**C.Anderson, US:**

1. What sizes the wing during design? Take-off or clean maneuverability?
2. Were all the curves shown on Figure 11 based on a common reference area?

**C.L.Bore, UK:**

1. For the Harrier, combat maneuverability sized the wing. The vertical take-off range was so important that the best flap system would be one that had zero weight. For an earlier aircraft (the Hunter) only a simple flap system was fitted, so the wing area was larger than the minimum essential for combat.
2. All the curves of Figure 11 are non-dimensional; so they could be regarded as comparing the relative "g"-pulling capabilities of aircraft all having the same wing loading.

**E.L.Ericson, US:**

1. Do you use the difference between extrapolated linear lift and actual measured static lift (at high  $\alpha$ ) as a measure of the forcing function for buffet?
2. It is important to recognize that there is also an additional effect involved which also is proportional (more or less) to this difference. That is the aerodynamic damping as affected by the separated flow. I believe this might be the dominant effect as in stall flutter of helicopter blades for instance. In this case one cannot alleviate the buffet by getting off a critical frequency. It is important, therefore, to make a distinction between the two effects.

**C.L.Bore, UK:**

1. Yes, or more strictly, the "lift curve" would be the tail-off normal force curve. If there is a slight kink in the curve before the beginning of boundary layer separation, it is the higher-incidence portion that is extrapolated.
2. The frequency of buffet vibration tends to be very low, where frequency effects are small. Also the aerodynamic amplitude of vibration is very small, so I suspect that damping cannot make much difference. I agree that it is most unlikely that buffet could be avoided by changing a response frequency, as the aerodynamic forcing frequency will, I think, tie itself to whatever wing response frequency that occurs.

**A.Wortman, US:** In your presentation you pointed out that the Harrier wing is so much lighter than a conventional wing with slats, flaps, etc. How do the weights compare when you account for the weight of nozzles, plumbing etc. which permit the Harrier wing to dispense with the conventional devices?

**C.L.Bore, UK:** It is difficult to make a fair comparison with the form of aircraft that one would have designed without vectored thrust. What is the required sortie for the conventional aircraft to do the same job? To operate into a given combat area, the VTOL aircraft can fly from airfields perhaps 100 feet square, near the combat zone — whereas a CTOL aircraft would have to use large fields much further from the combat area. In such a comparison the VTOL aircraft is lighter — much lighter at small ranges, less so at larger ranges, perhaps heavier at very long ranges. If I may guess some answers from uncontrolled examples of rather comparable aircraft, I think Figure 12 of the written paper suggests that rotating nozzles and so on total up to similar weights to the long fixed jet pipes that might otherwise be used.

Discussion of Paper 20  
"Aerodynamics of Wing Stall of the Fokker F.28"  
presented by T.Schuringa, The Netherlands

**M.Lazareff, France:** La figure 3 montre que l'avion complet comporte, au voisinage du décrochage, un accroissement très favorable du moment piqueur. Ce *changement de pente* de la stabilité est-il imputable en totalité à une variation de déflection\* au droit de l'empennage (qui augmente son gradient de portance en fonction de l'incidence de l'avion); ou bien une partie du *changement de pente* dans le sens favorable est-elle présente dès la configuration sans empennage, étant bien entendu que cette dernière configuration est instable.

**TRANSLATION:** In Figure 3 of your paper, it appears that near the stall, a strong favourable nose-down pitching-moment takes place near  $15^\circ$  angle of attack.

Is this stability slope change due only to a change in the deflection (downwash) at the tail, or partly due to a nose-down tendency on the configuration without tail (in this case the configuration is of course longitudinally unstable, but a special behaviour of the wing flow at this angle of attack can contribute to this nose-down tendency)?

**T.Schuringa, The Netherlands:** During the final stage of the F.28 wind tunnel testing, the complete model was generally used to investigate the overall effect of the various measures to affect the stall characteristics. The separate contribution of the tail surface and of the wing-body combination in the increment in nose-down pitching-moment at the stall is not available for the final configuration. From earlier tests on the model without horizontal stabilizer it is known that the main contribution in pitch-down is due to a changed downwash\* resulting from flow separation and loss of lift on the inboard part of the wing and in addition the wing itself contributes to nose-down pitching-moments under these conditions.

**E.J.Ray, US:** Did you notice any misleading characteristics as a result of the support device at high angles of attack? My experience has indicated that there could be a strong "splitter plate" effect.

**T.Schuringa, The Netherlands:** We did not test with another support in the NLR HST tunnel. However, comparative tests in the LST with different support struts, showed similar results with regard to  $C_m$  versus  $\alpha$  at high angles of attack.

**B.Laschka, Germany:**

1. Mr Schuringa has mentioned that for the evaluation of high lift characteristics two models have been used, one complete model and one half model. I presume that all the testing for these two models has been performed in the NLR pressurized wind tunnel in which Mach numbers and Reynolds numbers may be varied independently. Consequently an immediate comparison between the results of the two models should be available. Because of the controversial question of whether a half model gives acceptable information about the stall characteristics, I would appreciate it if Mr Schuringa could give indication of how the results from the two models compared.
  - (a) Has the stall flow pattern been in good agreement for both models?
  - (b) How did the  $C_{A_{max}}$  compare at the same Reynolds and Mach numbers?
  - (c) Is Mr Schuringa in a position to supplement Professor Hancock's listing of the minimum Reynolds numbers needed for correct representation of the stall flow pattern by F.28 results?
2. In Figure 11 the g-break for the F.28 is shown based on half model wind tunnel tests and flight tests. The difference ( $6^\circ$ ) in maximum angle of attack, especially for the case without a fence, is surprisingly high though the tunnel Reynolds number was five million. In many cases not only maximum lift but also maximum angle of attack is of interest. Do you indicate in your Figure that the maximum angle of attack cannot be well estimated from half model wind tunnel tests?

**T.Schuringa, The Netherlands:**

1.
  - (a) The progression of flow separation on both models was quite identical. However, there was a discrepancy in "indicated" angle of attack of  $2^\circ$  and  $3^\circ$  for the same flow pattern, this difference was partly attributed to the difference in Reynolds number.
  - (b) At the time of the tests no forces could be measured at the half wing mounting, so unfortunately no answer can be given on this question.
  - (c) On the half wing model some tests were performed with different Reynolds numbers, i.e. 1.2, 3.05 and  $4.85 \times 10^6$ . Quite identical flow patterns were observed for the two higher Reynolds numbers, however, at slightly smaller angles of attack for the lower Reynolds number (see also the above reply to your question 1(a)). At  $1.2 \times 10^6$  the differences in observed flow patterns become rather large. Regarding the

\*Note by T.Schuringa Another translation of "Deflexion" is downwash.

fair agreement in flow patterns and stall progression observed on the aircraft wing; and on the model, it might be concluded that for the case of the F.28 representative flow separation progression on the model is obtained at a Reynolds number of about  $3 \times 10^6$ , at angles of attack somewhat different from full scale. (See also the reply to your question 2.)

2. The discrepancy in indicated angle of attack as revealed by this figure, also puzzles us. However, it should be realised that at large angles of attack the prediction of the angle of attack from test information is a relatively inaccurate process, both for wind tunnel half models and for the free flight case.

We therefore tend to give not too much weight to the observed differences.

With regard to maximum lift, we are of the opinion that the same flow patterns and conditions in fact represent identical lift characteristics.

**P.P. Antonatos, US:** Figure 4 seems to indicate that, at high  $\alpha$  in the tunnel test, the model was close to the wall of the tunnel. This can have a decided effect due to wall interference on the high  $C_L$  values.

**T. Schuringa, The Netherlands:** If the nose was really near the tunnel wall the effect would be favourable. However, the photograph shows some distortion; furthermore it was taken at the maximum incidence angle of the test, this being  $38^\circ$ . In this condition there is still ample spacing between the model extremities and the tunnel wall.

#### Discussion of Paper 21

"Predicting the Low-Speed Stall Characteristics of the Boeing 747"  
presented by J.K. Wimpres, US

**C. Anderson, US:**

1. Why do you have different nacelles on the models in Figures 1 and 2? Did you find that flow-through was required?
2. On Figure 5 could the wing loading effect on stall speed really be a Mach number effect?

**J.K. Wimpres, US:**

1. Most low speed wind tunnel testing was done with flow-through nacelles. Figure 1 shows a special installation of nacelles powered by compressed air to check power effects on flaps-down performance.
2. Mach number effects may be partially responsible, but it is felt that it is more likely related to the effects of changing inertia on the stall dynamics.

**M. Roederer, Germany:**

1. Is the margin between the lift-off speed and  $V_{MU}$  of the B.747 8% or 10%? Is there not a need for a tail bumper for the aircraft in service?
2. What are the criteria for the required maximum negative lift and angle of attack for the tail to prevent a tail stall in strong recovery maneuvers (landing configuration, forward C.G.)?

**J.K. Wimpres, US:**

1. Flight tests were made on the 747 to demonstrate its take-off capability under abused conditions in anticipation of certifying it for lift-off at  $1.08 V_{MU}$ . However, the condition of reaching  $1.2 V_{STALL}$  at 35 feet, as required for FAA certification, ended up being the design parameter defining the airplane's take-off performance. So, the  $1.08 V_{MU}$  capability was not used. The airplane has no tail bumper. It does have an attitude warning system, but proper operation of this system is not required for dispatch on a commercial flight.
2. Prior to beginning a stall, the stabilizer is trimmed for flight at 1.3 times stall speed. As the airplane is pulled into the stall, the elevators move up to compensate for the change in local angle of attack as the airplane moves nose-up. However, the down load on the stabilizer actually decreases due to the shape of the tail-off  $C_L - C_m$  curve. The recovery maneuver of pushing the control column forward, and moving the elevator's trailing edge down, further reduces the down load on the stabilizer. Wind tunnel testing has shown that the maximum lift coefficient of the horizontal tail is approximately 1.0, with about 0.8 being usable before buffet occurs. The 747 horizontal tail operates at values well below this level.

**Ingelman-Sundberg, Sweden:** Mr Wimpres, you showed an extrapolation of wind tunnel  $C_{Lmax}$  over a factor of 10 in Reynolds number from  $8$  to  $80 \times 10^6$  and it gave a very accurate result. You said also that the reason was that 747 leading edge devices prevent any high pressure peaks at the leading edge which means that all leading edge separation will be prevented.

Do you think that would mean that in a wind tunnel test it would be sufficient or acceptable if, at this low tunnel Reynolds number, one could produce the correct type of separation even if then of course the boundary layer further back will be relatively too thick?

**J.K.Wimpress, US:** I think that most large non-linear Reynolds number effects on high lift occur when the flow around the leading edge changes from a laminar separation to a turbulent attachment. The whole pattern of the stall changes at this time and the maximum lift coefficient can be increased sharply. As Mr Ingelman-Sundberg points out, even if the flow at the leading edge is made turbulent on the model to give the right flow pattern, the boundary layer on the model will be proportionately too thick at the trailing edge. The stall, therefore, may commence at a slightly lower angle of attack. However, it is of the proper type, that is, beginning at the trailing edge; and the influence of the thickened boundary layer is relatively minor producing the small effects with increasing Reynolds number that was shown in my paper about the 747.

**B.Laschka, Germany:**

1. When comparing your Figures 3 and 9 where lift versus angle of attack has been plotted with and without ground effect one may realize a decrease in maximum lift as well as lift curve slope for the curves with ground effect. This is in contrast to the results shown for the F.28 by Mr Schuringa in the preceding lecture. Would you like to explain this decrease in slope, which is not predicted usually by linear potential theory. Is it due to the blockage effect of the extended flaps which reduce stagnation pressure near the ground or is there any other reason?
2. Mr Wimpress didn't mention any special tests for determining the  $C_{L_{max}}$  of the horizontal tail. Tail stall may have occurred at the B.747 during  $V_S$ -tests when the pilot makes a strong recovery (push over) instead of a stick-free recovery. Would you like to comment whether manoeuvres of this kind have been incorporated in the flight test program, and whether you have reached tail stall? If yes, what were the effects on the aircraft?
3. As far as I know B.747 horizontal and vertical tail are not equipped with any de-icing or anti-icing system. Ice accretion may reduce the aerodynamic properties of the tail appreciably. Have there been any problems with the loss in minimum tail lift? What manoeuvres have been performed to demonstrate sufficient stability and control with ice accretion?

**J.K.Wimpress, US:**

1. The effect of ground proximity on lift curve slope shown by comparing Figures 3 and 9 in my paper do agree with a theoretical analysis. The change in lift due to ground effect is caused by two components of the potential flow pattern. The image of the trailing vortex causes a decrease in downwash at the lifting line which tends to increase the lift at a fixed geometric angle of attack in proportion to  $C_L$  to the first power. The image of the bound vortex, on the other hand, decreases the local  $q$  felt by the lifting line, thereby reducing the lift at a constant geometric angle of attack. This effect is proportional to  $C_L^2$  and, therefore, becomes dominant at high lift coefficients. Our experience has been that ground proximity effects can be evaluated quite accurately by potential flow theory. The characteristics indicated for the F.28 by Mr Schuringa, may be caused by the wing being higher off the ground relative to the magnitude of the circulation created where the influence of the trailing image can be more important than that of the bound image.
2. The answer to this question is the same as that asked by Mr Roedere.
3. The 747, like other Boeing commercial jet transports, does not have anti-icing on the horizontal or vertical tail. To establish the effects of ice accretion, icing shapes were established from theoretical analysis and parametric tests in icing tunnels. These shapes were then put on the wind tunnel model to establish that the stability and control of the airplane would be satisfactory. The same shapes then were put on the flight test airplane and evaluated under all critical c.g. and flight conditions to establish that the stability and control was not affected adversely. In the case of the 747, the wind tunnel data showed essentially no effect due to ice accretions and the flight test confirmed this characteristic. There are two reasons for this situation. First, the horizontal tail is relatively lightly loaded, and unusually large lift coefficients are not demanded anywhere in the flight regime. Second, the airfoil section used on the horizontal tail has quite a sharp leading edge. Thus, the amount of ice that builds on it is small relative to the size of the surface.

**D.Zonars, US:** What criteria do you use in establishing the position of the leading edge of the ground effect plate since the angle of attack characteristics of the wing must have some influence on the flowfield ahead of the model?

**J.K.Wimpress, US:** The leading edge of the ground plane is at the leading edge of the test section. A flap at the trailing edge of the ground plane is used to match the blockage above and below the ground plane to get the incoming stagnation streamline to come straight at the ground plane. In addition, the leading edge of the ground plane is rounded to prevent any separation bubble at the leading edge of the ground plane.

**D.N.Foster, UK:** I have a question on the outboard leading edge device. You said that there was a small gap between the trailing edge of the device and the wing. Is this a result of the mechanism deploying the device, or is the device working as a slat?

**J.K.Wimpress, US:** The leading edge Krueger flap does act like a slotted slat.

**E.L.Ericson, US:** In Figure 6 the trends shown would be explained by elastic effects, but the magnitude is apparently not large enough. The reason I ask is that we recently found at Lockheed that a missile wing, without pods and with higher sweep than  $37^\circ$  was very severely affected by the elastic bending. As much as 40% loss of tip loading was predicted.

**J.K.Wimpress, US:** Although aeroelastic effects do have the proper trend to reduce the  $C_{L_{max}}$  with increasing wing loading, calculations have shown that they are too small to account for the values indicated by flight test.

**G.F.Moss, UK:** Stalling tests at full-scale usually have to be made at high altitude for safety reasons and I am sure the Boeing 747 is no exception. This means that Mach number is significantly higher than at the low levels where the operational problem is most acute. Remembering the figure in Mr Foster's paper which showed that Mach number effects can be comparable in size to scale-effects on  $C_{L_{max}}$ , can Mr Wimpress tell us whether the stalling tests in the tunnel were made at Mach numbers matched to the flight values? In particular, was the Mach number controlled during the scale-effect tests made in the Ames 12 ft tunnel?

The data given in Figure 7 is of great interest. It would also be of interest to see what the variation of  $C_{L_{max}}$  was like with Mach number (at constant Reynolds' number), if this has been investigated.

**J.K.Wimpress, US:** The high Reynolds number tests at the 12-foot tunnel of the NASA Ames Laboratory were run at essentially constant Mach number. Below a Reynolds number of about  $1.5 \times 10^6$ , the tunnel was operated at constant atmospheric total pressure with a Mach number varying between approximately 0.16 to 0.25. At higher Reynolds numbers, the total pressure in the tunnel was increased so as to retain a constant Mach number of 0.25 into the high Reynolds number region.

The airplane stall tests were made at altitudes varying between 8,000 and 15,000 feet. A constant airspeed of 110 knots results in a Mach number of 0.22 at 15,000 feet, 0.19 at 8,000 feet, and 0.17 at sea level. These are relatively small variations in Mach number, and no consideration was given in the certification to possible lift improvements that might occur at the lower Mach number at sea level. This procedure is realistic since the curve in Mr Foster's paper indicates only about 3 percent difference in lift between the highest test altitude and sea level conditions.

#### Discussion of Paper 22 "Airflow Separation and Buffet Onset During Fighter Aircraft Maneuvering" presented by P.J.Butkewicz, US

**A.M.O.Smith, US:** I was interested in your definition of buffet onset as being the first observable separation. Prof. Fred Thomas has a theory that buffet onset does not begin with the first separation but rather when the separation moves forward to and becomes coincident with the shock. These appear to be slightly different criteria and phenomena. Do you have any comments?

**P.J.Butkewicz, US:** It was noted in all of the Flight Dynamics Laboratory sponsored flight test programs, that there was a definite buffet felt at the wing tip which was directly correlatable with the initial airflow separation at that location. Since the purpose of the research effort was to investigate buffet onset for various fighter aircraft, this particular criterion for buffet onset was selected as a logical starting point to relate initial airflow separation and buffet onset.

**F.Thomas, Germany:** The theoretical method for calculating the buffet onset, which was just mentioned by A.M.O. Smith, was developed a few years ago and is published in the Jahrbuch der WGLR 1966. A more advanced version was described at the AGARD Specialists' Meeting held in Göttingen, Germany, in April 1971 (see AGARD Conference Proceedings CP 83). It was shown that the onset of buffeting was predicted very satisfactorily for quite a number of wings. Good agreement between calculation and flight or wind tunnel tests can, however, only be expected for wings with medium or large aspect ratios ( $A > 4$ ), medium wing thicknesses (10-14%) and sweep angles from  $0^\circ$  up to  $45^\circ$ . For this kind of wing, the wing section shapes play a predominant part in the separation pattern of the wing. It is, however, not possible to calculate the buffet onset with this method for the highly swept, small aspect ratio wings with very small thicknesses, which are typical for many modern high speed fighters. The separation pattern of these wings is predominated by three-dimensional effects, and it seems extremely difficult to find a mathematical model for the fluid dynamics of such wings in the region where buffeting occurs.

**P.J.Butkewicz, US:** I agree with you fully. As I mentioned in my introductory remarks, typical modern high speed aircraft with low aspect ratio, short swept wings are highly three-dimensional, close coupled air vehicles. Consequently, three-dimensional effects dominate the separation phenomena, and no mathematical models are available to predict the fluid dynamics.

**A.D.Young, UK:** You showed a slide showing a polar for an extended slat which indicated a reduction of drag due to the slat for lift coefficients greater than that at which you would otherwise expect buffet onset. What happens with a trailing edge flap?

**P.J.Butkewicz, US:** The drag polar which was shown resulted from data acquired from a separate research effort. No drag polars were obtained for any other wing configurations.

**C.L.Bore, UK:** May I give a warning about the use of trailing edge pressure points as universal correlators with wing buffet onset? Trailing edge pressure points indicate when boundary layer separation has reached the trailing edge. They may correlate quite well with buffet on a group of wings all of which have been designed in a similar manner. However, if a wing were designed differently, there need not be correlation. For example, on the Harrier, the flow on the wing tip does not separate at any incidence, so a static pressure hole there would not indicate buffet onset at all.

**J.P.Butkewicz, US:** Your point is well taken. The specific aircraft configuration and design conditions must be taken into consideration in any analysis. Also, sole reliance on wing tips or trailing edge instrumentation alone is not recommended in an overall buffet investigation. Wing root strain gauges and accelerometers, as well as accelerometers at the aircraft center of gravity and pilot's seat are essential for an understanding of the full spectrum of the problem.

**R.M.Bowman, US:** Although I came here as a scientist, I am also an ex-F.4 pilot and I would like to express my agreement with Major Butkewicz on the acceptability of buffet to the pilot. Buffet, though it reduces aerodynamic efficiency, does have some beneficial side-effects as a stall warning (as has already been brought out) and also as an indication of angle of attack. In a combat situation, the pilot cannot watch an instrument and must judge his optimum maneuvering angle of attack by aircraft "feel". In the F.4 this is marked by a particular level of buffet which the pilot learns to judge quite accurately.

For this and other reasons, I don't think a definition of "onset of buffet" which cannot be felt in the cockpit would or should gain widespread acceptance. Major Butkewicz's point that separation at the tips should receive design attention even though it cannot be felt is well taken. Still, I think another word (such as onset of separation) should be found so that "buffet" can remain a phenomena on which pilots and engineers can understand and agree with one another.

**J.P.Butkewicz, US:** As to your first comment, the concluding remarks section of my paper are in complete agreement with you. However, speaking from the standpoint of one who must develop efficient, maneuverable combat machines, I maintain that buffet onset has already occurred long before it is felt by the pilot, and it is in the early stages where the engineer can best take remedial action to delay the buffet progression and reduce its intensity.

**Discussion of Paper 23**  
**"The Dynamic Analysis of Buffetting and Related Phenomena"**  
 presented by J.G.Jones, UK

**M.Lotz, Germany:** I think it is not a meaningful question to ask whether the aerodynamic excitation is the same on a rigid wing and on a flexible wing. The aerodynamic excitation is by definition the force which would act on a rigid wing. The difference between this force and the force on the flexible wing is by definition the aerodynamic damping and, if it has a component in phase with the displacement, the aerodynamic stiffness.

**J.G.Jones, UK:** The possibility must be allowed that the motion of a flexible wing may influence the statistical properties of the aerodynamic excitation. A valid measurement of the motion-dependent aerodynamic force on a flexible wing may be made in principle by the introduction of an external test signal, as described in Section 7. The aerodynamic excitation may be deduced by subtraction of the motion-dependent component from the total aerodynamic force. It is then meaningful to ask if the aerodynamic excitation of the flexible wing, measured in this way, is the same as the aerodynamic force on a rigid wing.

**E.L.Ericson, US (Comments only):** A simple substitution of  $U^{-1}(\partial z/\partial t) = \dot{z}/U$  for  $\theta$  in the analysis presented in "Unsteady Airfoil Stall and Stall Flutter", NASA CR-111906, June 1970, by L.E.Ericson and J.P.Reding, should produce the apparent damping trends shown in Figure 10 for shock induced separation (provided that needed static experimental data is available).



**Discussion of Paper 24**  
**"Maneuver and Buffet Characteristics of Fighter Aircraft"**  
 presented by E.J.Ray and L.W.McKinney, US

**A.M.O.Smith, US:** The strake is a very effective device. It is interesting to remark that it was discovered and applied in a different form about 1936 to increase the vertical tail effectiveness of the DC 3. It was called a dorsal fin in this case.

**E.J.Ray, US:** Yes, vortex lift strakes indicate a potential for a variety of interesting applications.

**G.F.Mess, UK:** With a highly swept strake which has a sharp leading edge, a vortex of considerable energy will be shed. Has Mr Ray considered the effect on buffet-limited usable lift of possible vortex bursting?

**E.J.Ray, US:** The highly swept strake did have a sharp leading edge and it was evidenced in the results presented that there was a substantial vortex lift increment as a result of the strake addition. With regard to buffet characteristics, the study indicated that the onset of a mild buffet occurred at a comparatively low lift coefficient when the strake was incorporated; however there was a definite reduction in the rise of the apparent intensity levels.

**L.C.Bore, UK:** May I comment on the use of buffet onset as the criterion for judging the usefulness of devices, such as trailing-edge flaps? In our experience, it is possible to have conditions where a device (say, a flap) increases the  $C_L$  for buffet onset, but reduces the maximum usable  $C_L$  (which is the more important criterion). Would you comment on this?

**E.J.Ray, US:** The comments which were presented regarding buffet characteristics were concerned with the conditions at which the onset of buffet might occur, or more specifically the initial point of separated flow. In so far as the assessment of factors affecting maximum usable  $C_L$  are concerned, the determination of restrictive buffet intensity levels was not within the scope of the present studies.

**Discussion of Paper 25**  
**"Aerodynamic Design and Flight Test of US Navy Aircraft**  
**at High Angles of Attack"**  
 presented by W.R.Burris and J.T.Lawrence, US  
 including comments concerned with the contribution made by M. Ph.Poisson-Quinton

**E.L.Ericson, US:** In regard to the dynamic stall data shown by M. Poisson-Quinton, here is one case where static and dynamic considerations do not warrant a compromise. The higher one drives static  $C_{L_{max}}$ , through nose droop for example, the less the dynamic overshoot of static stall will be, and, as a consequence, the negative damping generated at stall penetration will be less (with associated decreased tendency towards stall flutter).

**D.J.Moorhouse, UK:** Stall in gusts was given as an area which requires further study, with which I agree. Also it was stated that helicopter people have given us an understanding of dynamic stall. Helicopter studies are concerned with sinusoidal disturbances which are not applicable to fixed wing aircraft, or to gusts. Do you agree that further work is required to define dynamic stall in an arbitrary motion?

**Ph.Poisson-Quinton, France:** I agree completely.

**J.G.Jones, UK:** I would like to compliment Mr Lawrence on his thorough review of the problems involved in aircraft manoeuvres at high angles of attack. As we shall be returning to these general problems tomorrow I limit myself here to three questions of detail.

1. With reference to the 0.05 g criterion for buffet onset, should not some specification of the bandwidth of the acceleration signal be provided to allow meaningful comparison of buffet intensities?
2. Does Mr Lawrence know of any applications of the  $C_{n\beta}$  criterion for loss of stability at high subsonic Mach numbers, say greater than 0.7? Does he agree that other criteria, such as the  $\omega_\phi/\omega_d$  adverse-yaw criterion may prove to be equally useful?
3. I was surprised to see flying qualities rated so low in importance in the pilots' list of adverse properties of an aircraft at high lift. Could Mr Lawrence clarify what he includes in "flying qualities" in this context. Surely phenomena such as nose-slice must be at the top of the list?

J.T. Lawrence, US:

1. US Navy experience has been that opinion obtained during flight test from a number of pilots on each aircraft agrees very well with the  $\pm 0.05$  g at the airplane center of gravity. These measurements are normally made during wind-up turn maneuver so that there is a near constant build up in normal acceleration, and it has been a relatively simple task to pick out the  $\pm 0.05$  g value from flight test data.
2. Application of the  $C_{n\beta_{dyn}}$  parameter has been limited to the subsonic flight regime for the most part. I am not aware of any good correlation which has been made in the transonic region. Concerning additional parameters, the paper discusses the need for research to determine additional parameters for determining high angle of attack characteristics. Although the A.7 and F.4 examples used in our paper displayed good correlation between  $C_{n\beta_{dyn}}$  and flight test, we feel that other parameters must be found to augment  $C_{n\beta_{dyn}}$  to obtain the total story.
3. The list referred to was for pilot determination of the so-called "optimum" maneuvering angle of attack. In this regard the pilot is primarily interested in the maneuvering performance of his aircraft and is therefore willing to accept degraded flying qualities in this regime. It will be noted, however, that the optimum maneuvering angles of attack shown occurred at angles well below heavy buffet and stall/departure. The pilot, therefore, does not fly anywhere near such characteristics as nose-slice when operating at his optimum maneuvering angle of attack.

G.J. Hancock, UK:

1. Is an indication of incidence given to a pilot?
2. No mention of rotary balance tests, or of model dynamic tests was made in the lecture. Are such tests performed?
3. Curves of  $C_n \sim \alpha$  are given in the text in which the various points of buffet onset, stall, etc. are identified.  $C_{n\beta}$  is also shown. Are similar curves for  $C_M \sim \alpha$ ,  $C_D \sim \alpha$ ,  $C_l \sim \alpha$ ,  $\beta$  available?

J.T. Lawrence, US:

1. Yes. Navy aircraft have an angle of attack indicator for the pilot which is calibrated in "units". For each type of aircraft the "units" correspond to different "degrees", however, and for my paper I have corrected the "units" to "degrees" for the three examples used.
2. The paper does cover the so-called dynamic derivative tests. Yes, rotary balance as well as forced oscillation balance techniques are used to obtain the dynamic stability derivatives. There are in addition to the free "flight" tests conducted in the NASA Langley Research Center 30 x 60 ft tunnel.
3. Yes, these additional data are available although I do not have them with me here. The curves I have shown are trimmed lift curves and I have indicated pitching moment characteristics by stating, for instance, that the stall on both the basic and slatted leading edge F.4 configurations is partially defined by nose rise tendencies which is indicative of a reduction of  $C_m - \alpha$ .

J. Seddon, UK: I hope I may be allowed to express the appreciation of the meeting to Mr Lawrence for a most stimulating and highly significant presentation. As M. Poisson-Quinton remarked, this brought the meeting to the "moment of truth" and I imagine that all the classical aerodynamicists among us are asking ourselves whether the things we are doing are contributing effectively to the real problem.

I have two questions. Firstly, in describing the design process, Mr Lawrence, you mentioned the drawback that all the tests were at low Mach number. How far are you really committed to that situation and not able to make tests at the appropriate Mach numbers.

J.T. Lawrence, US: With current facilities it is not possible to obtain high Mach and Reynolds numbers simultaneously, particularly at the high angles of attack. Also, we are interested in obtaining a consistent set of data up through the spin regime which means testing to  $90^\circ$  angle of attack. Current facilities limit testing to a Mach number of about 0.2, which high Reynolds number can only be achieved at NASA Ames Research Center in the 12 ft pressure tunnel.

J. Seddon, UK: So this is an important part of the case for a high Reynolds number transonic tunnel?

J.T. Lawrence, US: Very definitely.

J. Seddon, UK: My second question is this. In your final vugraph you emphasized the importance of research. Would you care to express a view as to where the emphasis should be placed in research?

J.T. Lawrence, US: Most research to date has been concerned with post-stall and spins. We feel that the prime areas for future research are in the usable angle of attack range up to stall/departure, and in the area of stall/spin avoidance/prevention.

**D.Zonars, US:** Did we understand you correctly that an analytical method exists to predict the onset of buffet? Is it for an arbitrary three-dimensional configuration or a two-dimensional shape, and for what Mach number range? That is, does it include transonic speed characteristics?

**J.T.Lawrence, US:** The method used to predict buffet onset is empirical in that the buffet onset characteristics of many different aircraft were combined to arrive at the prediction method. The work was accomplished a few years ago by Lindsay of the Naval Air System Command, and has been published as a Naval Ships Research and Development Center Report. Basically, the method yields the lift coefficients for buffet onset at  $M = 0.6$  and  $M = 0.7$ , as well as the Mach number for zero lift buffet for aircraft which display this characteristic, or the lift coefficient and Mach number for minimum buffet onset lift coefficient.

**A.D.Young, UK:**

1. Could you say something about the effects of stores that you carry on the stalling characteristics of the aircraft?
2. In view of what you say would you agree that the aircraft design should be developed from the first with the stores in mind?

**J.T.Lawrence, US:**

1. Stores do have an effect on the stall/departure characteristics, more on some aircraft than on others. Even on a given aircraft the location of the stores can make a difference. The F.4 is a good example. Stores carried on the fuselage centerline, including a 600 gallon fuel tank, have a negligible effect on the flying qualities. Wing mounted stores, however, and especially asymmetric store loadings can have a very significant effect on the high angle of attack for stall/departure, as well as affecting the character of the stall/departure.
2. Very definitely. For the types of aircraft which I have been discussing, that is highly maneuverable fighter and attack aircraft, their primary mission is to carry and deliver stores. Therefore, store loadings must be taken into account from the very conception of a design. This is, in fact, the case with current US Navy designs, including both engineering development and flight test.

**J.Lievens, France:** L'influence des charges extérieures dissymétriques se fait sentir par l'intermédiaire:

- d'un déplacement du centre de gravité de l'avion,
- d'une dissymétrisation des formes externes.

Avez-vous pu juger de l'importance respective de ces deux effets?

**J.T.Lawrence, US:** Although we have not separated the effects of center of gravity shift and aerodynamic characteristics on the overall behaviour of an aircraft with asymmetric stores at high angles of attack, I feel that the primary effect in the stall/departure and post-stall regimes comes from the changes in inertia properties of the aircraft.

**APPENDIX B**

**SUMMARY OF ROUND-TABLE DISCUSSION**

## SUMMARY OF ROUND-TABLE DISCUSSION\*

Chaired by Dr J.Seddon (UK), the Round-Table Discussion took the form of summaries of the main fields (Basic Fluid Dynamics, by Prof. K.Gersten, Germany; Theory and Experiment on Wings, by A.M.O.Smith, US; and Flight Experience, by Mr. J.K.Wimpress, US), which were followed by general discussion and by reviews made by Mons. C.J.Lievens (France), Mr W.D.Horsfield (UK) and Mr M.Ingelman-Sundberg (Sweden), together with closing remarks by the Chairman.

### 1. Basic Fluid Dynamics

Prof. Gersten commented first that, whilst Prof. Hancock's opening paper had put forward careful distinctions between stalling, "departure", flow separation, buffet onset, etc., the meeting had shown no general agreement on matters of definition. It appeared to be generally accepted, however, that whilst separation is a necessary condition for stalling, stalling is not necessarily a concomitant of separation. In the simplest case of separation in two-dimensional flow, the need for further theoretical and experimental research remains evident: experiments need to be made at higher Reynolds numbers, with parallel theoretical analyses. The flow situation comprises, typically, laminar separation followed by transition in the free shear layer, and then turbulent reattachment followed by turbulent separation towards the trailing edge; in these circumstances it is no longer possible to calculate the external flow separately from the separated region. One of the papers presented at the meeting (Paper 5) makes a first attack on the problem; mention was also made of Jacob's approach, and there is also the possibility of extending A.M.O.Smith's method to this strong-interaction problem. As regards laminar separation there is also available the paper, published in 1969 by Miss S.N.Brown and Prof. K.Stewartson in Vol. 1 of Annual Reviews of Fluid Mechanics (ed. W.R.Sears) pp.45-72.

The problem of the free shear layer has not yet been properly posed and solved, and represents an important area needing further study. The reattachment region needs a great deal more investigation, and the properties of the shear layer at reattachment constitute the initial conditions for calculating the subsequent (turbulent) boundary-layer development.

Prof. Domingos stressed first the importance of clear terminology: in particular, separation refers to the region where the mainstream velocity  $u$  is less than zero: mathematically, the boundary-layer equations then have no classical solution, whilst physically the approximations based on order-of-magnitude arguments are no longer valid. Usually, separation is accompanied by transition from laminar to turbulent flow and there is a tendency to regard transition and separation as synonymous: this must be avoided. The above definition of separation applies equally to laminar or turbulent flow (in the latter case with  $u$  understood to be  $\bar{u}$ ).

Because different phenomena enter at separation, both mathematically and physically, it is no longer possible to use classical boundary-layer theory in any fundamental way, for the flow can only be described by elliptic equations: in physical terms, downstream effects can no longer be neglected within the separated-flow region. The complete problem can be treated numerically. For an approximate treatment, if the separated region is small its effects on the outside region (where  $u > 0$  and boundary-layer theory can be used) can be taken into account empirically in several ways including profile methods, weighted-residual methods or their equivalent. This type of approach can have great practical value, but its basic inadequacies should be clearly understood, together with the limited scope of predictions based on them.

The above brief remarks relate to the mathematical treatment, which is the only problem in laminar flow. When transition occurs after separation we have as yet no adequate physical model for taking turbulence into account in the basic equations. This is also true of turbulent separation, even when a turbulence model of the eddy-viscosity (or a more refined) type can correctly predict the flow up to separation and downstream of reattachment. Only exceptionally will the whole flow be laminar; and the problem of turbulence is still far from solved. For these reasons it is understandable that there is a strong tendency to ignore what can be accomplished using existing methods for solving the basic elliptic equations, and to resort to empirical approaches covering both mathematical and physical aspects of the problem. This, however, provides no justification for confusion over concepts, nor for expecting boundary-layer theory to undertake tasks that it is inherently not contrived to fulfil.

\* It has not been possible to include a verbatim account, owing to a technical fault in the recording of the session, discovered afterwards. This Summary has therefore been prepared instead, by Dr R.C.Pankhurst, from notes taken at the meeting, together with written statements kindly provided by several of the speakers. Since not every contribution had been noted, apologies are due to those whose remarks have been inadvertently omitted.

The Chairman agreed about the impropriety of continuing to use boundary-layer theory in regions where the flow was separated, and about the need to use different methods of solution: in practice this would probably imply going over to numerical analysis. Prof. van Ingen added that the classical approach to solving the elliptic problem of the viscous flow around an airfoil section is a repeated application of parabolic boundary layer calculation methods. In most of these methods the boundary layer conditions at the trailing-edge of the airfoil determine the circulation and hence the upstream pressure distribution. After correcting the pressure distribution the boundary layer is recalculated etc. Hence the ellipticity of the problem is (at least approximately) taken into account by repeated applications of a parabolic method. Apart from mathematical considerations, Mr Dobbinga stressed the great complication of the engineering problems discussed at the meeting.

The Chairman asked if the general line of advance in three-dimensional flow would be by way of gaining a basic understanding or by a more direct attack. Dr Korkegi considered that the line of advance in three-dimensional flows will be through basic understanding of the physics. As regards turbulent boundary-layers, the transport properties are not known adequately, so that use is still made of concepts such as eddy-viscosity or mixing lengths. We are conscious that turbulent transport properties are dependent on flow history, unlike laminar properties which are dependent only on local conditions. Further progress should follow with improved mathematical models.

Also, in respect to a previous comment, he would not be inclined to discard boundary-layer theory whenever flow separation arises. While he agrees in principle that such flows ought strictly to be tackled by means of the Navier-Stokes equations, considerable useful progress is being made by extending boundary-layer theory, particularly in cases where the scale of separation is much larger than the boundary layer (or shear layer) thickness.

## 2. Wing Theory and Experiment

Mr A.M.O. Smith observed generally that we are getting to the point where we can make a fairly good job of analysing fully attached, two-dimensional flows. Good progress is being made and several of the papers at this meeting represent significant steps ahead. Therefore it seems that emphasis on the problems of flows with partial separation should increase. Two-dimensional flows, especially fully attached flows, are attractive to analyse and much still needs to be done; but it must be remembered that the flows of importance are three-dimensional. If we, as research engineers, are to be really useful we should work on problems that help the designer, not just ones for which we can easily find answers and produce papers.

Flows with partial separation should be attacked with both careful wind tunnel tests and theory. Van Ingen's work is a good example of the kind of work needed. By 1980 we should see very useful three-dimensional solutions in the low Mach number region. The '60's saw us fairly well clean up the two-dimensional problem and the '70's will probably see us do the same on the three-dimensional problem. But the three-dimensional will still be simple flows. It will cover wings alone and bodies of nearly any cross section, but definitely not wing-fuselage combinations, nor wings with nacelles or stores on them. It is worth noting, however, that for the inviscid flow aspect we essentially can analyse any geometry that may arise, including those just mentioned, providing bodies are streamlined so that gross areas of separation do not exist.

The hangup is in the part where neither boundary-layer nor inviscid theory applies, as at corners, or for vortex generators, fences, etc. It is worth noting that one book is already available on the subject of three-dimensional turbulent boundary-layers — by Nash and Patel.

The aerodynamics of design can be broken down into two categories:—

1. Those charged with final design must work along in any way they can. Often they must cure a problem without understanding the illness at all. They often must depend on cut and try methods using both wind tunnel and flight tests. For this kind of problem, theory is inadequate and wind tunnels are essential. This is ad hoc testing and it is rare that any general knowledge is gained that can be carried forward to the next design.
2. Somewhat in the background, more often following than leading, is the science of fluid dynamics. Sometimes it leads by pointing out something new. But more often its role is to analyse an existing device more accurately and give understanding to basic flow phenomena. The design aerodynamicist can then take this knowledge and do a better job, perhaps by eliminating butches, or reducing the number of tries in developing a "fix". Foster's and F.X. Wortmann's papers are examples that help point out proper directions in design. Mr Smith said he would expect this same relative role to continue far into the future.

It might be helpful for the Panel to identify important problem areas and by so doing encourage research in those areas. As already indicated, some of the major areas are flows with partial separation at both low speed and transonic. Another area is three-dimensional flows. We have advanced to the point where work in this area should yield results. Ten years ago it would have been somewhat premature, other than doing foundation work, such as the basic equations.

In simple problems, wind tunnel tests at chord Reynolds numbers of 6 million are sufficient. But at high Mach numbers where new effects come in, that may not be enough. Often, components are much smaller than the mean aerodynamic chord so their own Reynolds numbers would still be quite low. A wing tip on a highly tapered wing is an example. Hence Mr Smith would favour some higher Reynolds number facility. However, he warns that important discrepancies between wind tunnel and flight will still exist, even though Mach number and Reynolds number were matched exactly. Some reasons are: 1. General measuring accuracy. 2. A model is never an exact reproduction of an airplane. 3. The support and its corrections. 4. Wall-effects. These are still a considerable mystery. As far as he knows, for really correct testing the walls should have different porosities for drag measurement than they do for lift measurement.

But we continue to run into troubles requiring very costly flight tests. Hence further improvement in accuracy of wind tunnel tests certainly seems warranted.

The Chairman observed that whilst it was not going to be possible to get away from development work completely, research workers should surely take their work forward as far as they could. He invited comments on the proposition that, in wind tunnel investigations, greater emphasis needs to be placed on the task of distinguishing and quantifying the respective effects of Reynolds number and Mach number on high-lift systems. Major Bowman suggested that theory and experiment would eventually become effectively integrated in an "electronic wind tunnel" in which experiments would be made (on a computer) that would simulate a required situation better than is possible in the conventional wind tunnel as we know it today. Meanwhile, methods are now available for calculating three-dimensional flows with shock waves; other work is in hand on viscous problems, and the two advances will later have to be tied together. However, Mr Foster felt that we are not likely to be able to calculate the complex flow around a finite-aspect-ratio wing with high-lift devices, and so we shall need to continue to resort to wind tunnel testing. The requirement of extrapolating to full-scale Reynolds numbers, combined with the large effects of Mach number, makes it essential to be able to measure the effects of these two variables separately by means of a pressurised wind tunnel.

### 3. Flight Experience

As an applied aerodynamicist interested in aircraft design, Mr Wimpres was impressed by the capability of the theoretical aerodynamicist to describe analytically the flow pattern under conditions of separated flow. The large capacity computer with its ability to handle readily large matrix equations has enabled the theoretician to make appreciable advances in the last several years. On the other hand, he was somewhat disturbed by a large amount of effort being put into the precise analytical description of the separated flows. To the design aerodynamicist, a separated flow, generally, is an undesirable condition. It is a bound or limitation to the performance of an aerodynamic surface. More effort should be expended in learning about the conditions that cause separation so they can be eliminated and this bound pushed back with a resulting improvement in aerodynamic performance.

Theoretical aerodynamicists need to appreciate the tremendous pressures of time and money under which the design aerodynamicist operates. If an analytical procedure is to be used during an aircraft design, it must be readily understood and readily applied to the real situation. Too often, good theoretical work is left in so complicated a form that the design aerodynamicist must cast it aside and use a simpler, more empirical approach. Also, the theoretical aerodynamicist can contribute to the development process by describing the basic physics of fundamental flow patterns so that the applied aerodynamicist can recognize them when they are encountered in airplane design.

Airplanes using power to sustain an appreciable portion of their weight are being developed all over the world. These airplanes will not have a stall as we normally interpret it for conventional airplanes. The industry has little experience in this type of aircraft. With the exception of the Harrier, there appears to be no production airplane routinely flying below its power-off stall speed. Certification rules for proper margins for this type of aircraft have not yet been defined, although much thought has been given to it about the world. In the past, design certification rules were developed only after an airplane representative of the type had been flown, tested and thoroughly evaluated. That is, operational and certification rules developed after a successful design was developed, not before. Powered-lift airplanes will be no exception, and it is time to develop such an aircraft so that its operational limitations can be investigated.

In Mr Wimpres's view, wind tunnels and other experimental laboratories will always be necessary to handle the many non-linear problems encountered in aircraft design that are not susceptible to theoretical analysis: he did not share the feeling of many that if high Reynolds number facilities were available for wind tunnel testing, most of our flight test/wind tunnel data anomalies would disappear. There are other factors that are probably more important, such as proper model representation of the airplane, support system interference, and tunnel wall constraints, particularly very close to Mach 1. Some of the effects of these factors are even more difficult to extrapolate from the model data to the full scale quantities than are those changes associated with Reynolds number differences. Better design data might well be obtained by concentrating on these areas than through equivalent effort towards obtaining full-scale Reynolds number representation.

Mr Antonatos agreed about the continuing need for wind tunnel investigations; an experimental approach is essential to the evaluation of any new aircraft type.

#### 4. Review Statements

Mons Lievens began by discussing Reynolds number effects. Whether in comparing theories or in extrapolating results, it is essential to distinguish major effects (changes in type of flow) from minor effects, and to take cognisance of corrections needed in the case of particular wind tunnels: these various aspects must be carefully separated. The first requirement, rather than simply to achieve a high Reynolds number, is to ensure the right type of flow: if the type of flow is correctly reproduced, then extrapolating the results to full-scale conditions is fairly easy. Thus we must have adequate prediction methods: Paper 6 is particularly relevant here, and other work is in progress elsewhere. On the other hand, wind tunnel corrections appear to be receiving insufficient attention. High Reynolds numbers are certainly highly desirable, but there is no given value above which full-scale conditions always exist. Again, many mistakes have been made in the past by paying inadequate attention to information obtained at lower Reynolds number and ascribing to the low Reynolds number a failure to foresee phenomena encountered subsequently: all situations must be analysed completely. It is essential to devote large amounts of effort to evaluating tunnel corrections, to developing powerful theoretical tools for identifying the situations to be studied in the wind tunnel, and to exploiting fully the results.

Mr Horsfield felt that there is too often a tendency to conduct "backward-looking research" to improve aircraft retrospectively: there is a pressing need for forward-looking project research that gets all too easily suppressed under everyday pressures. It would be invaluable to experiment in the wind tunnel on aircraft projects, extending the range of the stalling investigations right up to the conditions of "departure", which he agreed to be of greater importance than the spin.

After recalling that the Chairman had asked what help the theoretician could give in solving the problem of predicting separation on aircraft, and that one of the things that Prof. Gersten suggested for analysis was the transition development above laminar separation bubbles, Mr Ingelman-Sundberg pointed out that one of the real problems facing the aircraft designer is the prediction, from low Reynolds number wind tunnel tests, of full-scale high Reynolds number maximum lift coefficients. The errors in the model test are of two different types: model separation at the leading edges can be of the laminar type when the corresponding full-scale aircraft will experience turbulent separation, and the turbulent boundary layer over the rear of the wing will also be relatively thicker and less resistant to adverse pressure gradients in the model than in the full-scale case. The separation kind of errors are very large and probably dominate the errors due to effects of the too thick turbulent boundary layer rearward.

If it were possible to predict theoretically the transition point for the full-scale case this would be of great importance because it would then be possible to know if one should use transition trips on the model forward of the laminar separation point or possibly not.

It is all the more important as there is no mean chord model Reynolds number which can be said to be sufficient, except the full-scale value, which however does not seem to be an economic optimum either, for a complete aircraft configuration. If a change in separation type over a slat or leading edge occurs at 70% of full-scale Reynolds number, a test at 60% is not at all good even if this is a very high Reynolds number. On the other hand if the separation type is already correct at 10% full-scale Reynolds number the test at that value is a good one.

The economic value of finding a theoretical method for predicting the relative locations of the transition and laminar separation points would really be very large.

One example of what can be done with transition trips for high angle of attack testing of a model modified with a peaky profile is shown in Figure 1. The aircraft has a moderately swept wing and the model Reynolds number is 2 million based on mean chord.

The maximum lift was limited by a long bubble-type of laminar leading edge separation. The modification from the ordinary profile to the peaky type caused a loss in model  $C_{L_{max}}$  of more than 0.2 for both clean and landing configurations.

Preventing the laminar separation with transition trips one row of tape bulbs  $1/4000$  chord high, also prevented the drop in maximum  $C_L$ . Later the flight tests at  $Re = 10$  million with the full-scale aircraft showed that the peaky modification had not influenced the stall speed. The factor 4.5 in Reynolds number in this case caused a complete change in stall type and even with that relatively typical model Reynolds number, the tests would have been misleading without the transition technique and surface flow studies.

Regarding the Chairman's question if something could have been overlooked in the program and discussions, possibly surface roughness effects (especially at leading edges) could have deserved a little more attention. It was mentioned briefly earlier by one speaker who called "tarmac on leading edges a very local problem".



On fast military aircraft in service, however, rain erosion effects on leading edges can be a rather common problem influencing, at least on certain aircraft types, the stall behaviour. The swept wing attack aircraft in Figure 2 with a 64A010 section is an example of this.

After ten years in service an increasing number of individual aircraft have developed a disturbing yaw tendency at roughly "over the fence speed" of 250-270 km/hour indicated. A slight disturbance existed also on normal aircraft but on certain specimens it had grown to an unacceptable level needing full rudder for control. The yaw is caused by a slightly unsymmetrical onset of leading edge separation outside the leading edge fences. With symmetrical separation the yaw disappears and the plane is fully controllable down to much lower speed.

Inspection of one of the problem aircraft selected for tests showed visible rain erosion marks which, however, when measured with a roughness meter were not more than 0.006 mm top to bottom compared with 0.0006 mm on new aircraft. The leading edges are normally left without paint.

It was assumed that the only possible way the roughness could influence the flow would be by triggering transition and changing separation from possibly laminar type to a turbulent type. In the case when, due to unsymmetrical roughness, this occurred only on one wing, separation would be postponed to a lower speed and thus the yaw developed.

On this aircraft, which was so bad that it was unacceptable for service, tests have been made to trip the boundary layer symmetrically with a 32 mm wide and 0.2 mm thick tape which was put over the leading edge outside the fences. The top edge of the tape is located where the transition trips in wind tunnel models have been shown to be effective.

The yaw disturbance before the landing almost disappeared and it was even less clear for normal aircraft.

Although the tests are not yet completed it seems possible that the use of transition trips can be a means not only to compensate for too low model Reynolds numbers in wind tunnels but also as a tool for modifying the stall characteristics of certain full-scale aircraft.

## 5. Conclusion

The Chairman said that it was scarcely possible to sum up the conclusions of the Round Table in a few words. Indeed, the Round Table had itself stimulated further thoughts, around which discussion should be continued. As regards fundamental research, however, he urged that greater attention might be paid to flow reattachment and downstream development, to balance the emphasis currently being placed on the separation phenomenon. Also, due account should be taken of what could be achieved by numerical analysis.

Coming to the applied research, in the case of transport aircraft it seemed that the important place of wind-tunnel work was generally accepted - the wind tunnel can contribute a great deal of exploratory information and thus effect economies in the subsequent development task. More needs to be done, however, on separating out the effects of Reynolds number from those of Mach number, and this may well require an increase in tunnel capability over that currently available, at least in Europe.

For combat aircraft, the respective roles of wind tunnel research and flight testing of particular types are less clear. Thus for example, according to Paper 25 the stall angle of attack at a given speed and Mach number should be defined as the lowest of the angles for (a) the highest attainable load factor (normal to the flight path), (b) the occurrence of uncommanded pitching, rolling or yawing motion, and (c) unacceptably high buffet level. There remains the question of whether or not the wind tunnel should be used to study all three areas and, if so, how. Paper 18 suggests problems in the case of a long, thin fuselage nose, which might persist to full-scale Reynolds numbers because they are due to shedding of a von Kármán vortex trail, in this context, French experiments on cones at high angles of attack are highly relevant. More work of this kind should be undertaken, to study the effect of body shape on the flow pattern created, and of the extent to which a full-scale pattern can be simulated in wind-tunnel experiments at lower Reynolds number. As for buffet prediction methods, that given by Mr. Bore, for example, has been shown to work very well - there remains the question of generality, however, and of the confidence with which such methods could be used in other cases.

Whilst a complete summary of the results of the meeting was not possible at this stage, the preparation of the Technical Evaluation Report would explore the possibility of drawing out specific recommendations for future work. As a concluding thought from the meeting the Chairman recalled a slide shown in Paper 25 depicting the A7 aircraft "on the point of departure" and the accompanying comment that here the pilot was about to get into real trouble, the way out of which, for that particular aircraft, was to release the stick and allow the aircraft to right itself. No pilot, the Chairman suggested, should be required to find that out for himself so long as there was anything more that could be done by wind tunnel and other investigations to understand and prepare for such a situation in advance. With these remarks the Chairman brought the proceedings to a close with thanks to authors of papers, contributors of prepared comments, members of the Programme Committee, to the hosts of the meeting with their many and varied helpers, and to the excellent simultaneous translation service.

**APPENDIX C**

**A SELECTION OF  
AGARD PUBLICATIONS IN RECENT YEARS**

**299**

A SELECTION OF  
AGARD PUBLICATIONS IN RECENT YEARS

CATEGORY I - PUBLISHED BY TECHNIVISION SERVICES AND  
PURCHASABLE FROM BOOKSELLERS OR FROM:-

Technical Press Ltd  
112 Westbourne Grove  
London W.2  
England

Hans Heinrich Petersen  
Postfach 265  
Borsteler Chausee 85  
2000 Hamburg 61  
West Germany

Circa Publications Inc.  
415 Fifth Avenue  
Pelham  
New York 10803, USA

Diffusione Edizioni Anglo-Americaine  
Via Lima  
00198 Rome  
Italy

1969

AGARDograph 120      Supersonic turbo-jet propulsion systems and components  
Edited by J.Chauvin, August 1969.

1970

AGARDograph 115      Wind effects on launch vehicles  
By E.D.Geissler, February 1970.

AGARDograph 130      Measurement techniques in heat transfer  
By E.R.G.Eckert and R.J.Goldstein, November 1970.

Conference              New experimental techniques in propulsion and energetics research  
Proceedings 38          Edited by D.Andrews and J.Surugue, October 1970.

---

CATEGORY II - NOT ON COMMERCIAL SALE - FOR  
AVAILABILITY SEE BACK COVER

1965

Report 514              The production of intense shear layers by vortex stretching and convection  
By J.T.Stuart, May 1965. (Report prepared for the AGARD Specialists' Meeting on  
"Recent developments in boundary layer research", May 1965.)

AGARDograph 91      The theory of high speed guns  
By A.E.Seigel, May 1965.

AGARDograph 97      Recent developments in boundary layer research  
(in four parts)          AGARD Specialists' Meeting, Naples, May 1965.

- AGARDograph 102      Supersonic inlets  
By Ione D.V.Faro, May 1965.
- AGARDograph 103      Aerodynamics of power plant installation  
AGARD Specialists' Meeting, Tullahoma, October 1965.
- 1966
- Report 525              The pitot probe in low-density hypersonic flow  
By S.A.Schaaf, January 1966.
- Report 526              Laminar incompressible leading and trailing edge flows and the near wake rear stagnation point  
By Sheldon Weinbaum, May 1966.
- Report 539              Changes in the flow at the base of a bluff body due to a disturbance in its wake  
By R.Hawkins and E.G.Trevett, May 1966.
- Report 542              Transonic stability of fin and drag stabilized projectiles  
By B.Cheers, May 1966.
- Report 548              Separated flows  
(Round Table Discussion), Edited by J.J.Ginoux, May 1966.
- Report 550              A new special solution to the complete problem of the internal ballistics of guns  
By C.K.Thornhill, 1966.
- Report 551              A review of some recent progress in understanding catastrophic yaw  
By J.D.Nicolaides, 1966.
- AGARDograph 109      Subsonic wind tunnel wall corrections  
By Gardner, Acum and Maskell, 1966.
- AGARDograph 112      Molecular beams for rarefied gasdynamic research  
By J.B.French, 1966.
- AGARDograph 113      Freeflight testing in high speed wind tunnels  
By B.Dayman, Jr, 1966.
- Conference  
Proceedings 4  
(two parts and one supplement)      Separated flows  
Specialists' Meeting, Rhode-Saint-Genèse (VKI), May 1966.
- Conference  
Proceedings 10          The fluid dynamic aspects of ballistics  
Specialists' Meeting, Mulhouse, September 1966.
- Conference  
Proceedings 12  
(in two parts)          Recent advances in aerothermochemistry  
7th AGARD Colloquium sponsored by PEP and FDP, Oslo, May 1966.
- 1967
- Report 558              Experimental methods in wind tunnels and water tunnels, with special emphasis on the hot-wire anemometer  
By K.Wieghardt and J.Kux, 1967.
- Advisory Report 13      Aspects of V/STOL aircraft development  
(This report consists of three papers presented during the joint session of the AGARD FDP and FMP held in Göttingen, September 1967.)
- AGARDograph 98        Graphical methods in aerothermodynamics  
By O.Lutz and G.Stoffers, November 1967.
- AGARDograph 117       Behaviour of supercritical nozzles under three-dimensional oscillatory conditions  
By L.Crocco and W.A.Sirignano, 1967.

- AGARDograph 119 Thermo-molecular pressure effects in tubes and at orifices  
By M.Kinslow and G.D.Arney, Jr, 1967.
- AGARDograph 121 Techniques for measurement of dynamic stability derivatives in ground test facilities  
By C.J.Schueler, L.K.Ward and A.E.Hodapp, Jr, 1967.
- AGARDograph 124 Nonequilibrium effects in supersonic-nozzle flows  
By J.Gordon Hall and C.E.Treanor, 1967.
- Conference  
Proceedings 19  
(in two parts) Fluid physics of hypersonic wakes  
Specialists' Meeting, Fort Collins, Colorado, May 1967.
- Conference  
Proceedings 22 Fluid dynamics of rotor and fan supported aircraft at subsonic speeds  
Specialists' Meeting, Göttingen, September 1967.
- Conference  
Proceedings 22 - S 4 As above - with supplement
- 1968
- AGARDograph 132 The electron beam fluorescence technique  
By E.P.Muntz, 1968.
- Conference  
Proceedings 30 Hypersonic boundary layers and flow fields  
Specialists' Meeting, London, May 1968.
- Conference  
Proceedings 30 Suppl. Supplement to the above.
- Conference  
Proceedings 35 Transonic aerodynamics  
Specialists' Meeting, Paris, September 1968.
- Conference  
Proceedings 35 Suppl. Supplement to the above.
- 1969
- Advisory Report 17 Technical Evaluation Report on AGARD Specialists' Meeting on Transonic aerodynamics  
By D.Küchemann, April 1969.
- AGARDograph 134 A portfolio of stability characteristics of incompressible boundary layers  
By H.J.Obremski, M.V.Morkovin and M.Landahl, 1969.
- AGARDograph 135 Fluidic controls systems for aerospace propulsion  
Edited by R.J.Reilly, September 1969.
- AGARDograph 137  
(in two parts) Tables of inviscid supersonic flow about circular cones at incidence  $\gamma = 1.4$   
By D.J.Jones, November 1969.
- Conference  
Proceedings 42 Aircraft engine noise and sonic boom  
Joint Meeting of the Fluid Dynamics and Propulsion and Energetics Panels, held in Saint-Louis, France, May 1969.
- Conference  
Proceedings 48 The aerodynamics of atmospheric shear flow  
Specialists' Meeting, Munich, September 1969.
- 1970
- Report 575 Test cases for numerical methods in transonic flows  
By R.C.Lock, 1970.
- Advisory Report 22 Aircraft engine noise and sonic boom\*  
By W.R.Sears. (Technical Evaluation Report on AGARD FDP and PEP Joint Meeting on "Aircraft engine noise and sonic boom".) January 1970.

\*See also Advisory Report 26 by J.O.Powers and M.Panko, June 1970. AR26 has the same title as AR22 but was produced by the Propulsion and Energetics Panel of AGARD and deals primarily with engine noise.

- Advisory Report 24      The aerodynamics of atmospheric shear flows  
By J.E.Cermak and B.W.Marschner, May 1970. (Technical Evaluation Report on AGARD Specialists' Meeting on "The aerodynamics of atmospheric shear flows".)
- Advisory Report 30      Blood circulation and respiratory flow  
By J.F.Gross and K.Gersten, December 1970. (Technical Evaluation Report on AGARD Specialists' Meeting on the above subject.)
- AGARDograph 133      Ballistic range technology  
By T.N.Canning, November 1970.
- AGARDograph 144      Engineering analysis of non-Newtonian fluids  
By D.C.Bogue and J.L.White, July 1970.
- AGARDograph 145      Wind tunnel pressure measurement techniques  
By D.S.Bynum, R.L.Ledford and W.E.Smotherman, December 1970.
- AGARDograph 146      The numerical solution of partial differential equations governing convection  
By H.Lomax, P.Kutler and F.B.Fuiler, November 1970.
- AGARDograph 147      Non-reacting and chemically reacting viscous flows over a hyperboloid at hypersonic condition  
Edited by C.H.Lewis. (M.Van Dyke, J.C.Adams, F.G.Blottner, A.M.O.Smith, R.T Davis and G.L.Keltner were contributors.) November 1970.
- Conference Proceedings 60      Numerical methods for viscous flows  
By R.C.Lock, November 1970. (Abstracts of papers presented at a Seminar held by the FDP of AGARD at the NPL, Teddington, UK, 18-21 September 1967.)
- Conference Proceedings 62      Preliminary design aspects of military aircraft  
March 1970. AGARD Flight Mechanics Panel Meeting held in The Hague, The Netherlands, September 1969.
- Conference Proceedings 65      Fluid dynamics of blood circulation and respiratory flow  
Specialists' Meeting, Naples, May 1970.
- Conference Proceedings 71      Aerodynamic interference  
Specialists' Meeting, Silver Spring, Maryland, USA, September 1970.
- 1971
- Report 588      Aerodynamic testing at high Reynolds numbers and transonic speeds  
By D.Küchemann, 1971.
- Advisory Report 34      Aerodynamic interference  
By D.J.Peake, May 1971. (Technical Evaluation Report of the Specialists' Meeting on "Aerodynamic interference", September 1970.)
- Advisory Report 25      Report of the high Reynolds number wind tunnel study group of the Fluid Dynamics Panel  
April 1971
- Advisory Report 36      Report of the AGARD Ad Hoc Committee on Engine-airplane interference and wall corrections in transonic wind tunnel tests  
Edited by A.Ferri, F.Jaarsma and R.Monti, August 1971.
- Advisory Report 37      Facilities and techniques for aerodynamic testing at transonic speeds and high Reynolds number  
By R.C.Pankhurst, October 1971. (Technical Evaluation Report on Specialists' Meeting held in Göttingen, Germany, April 1971.)
- AGARDograph 137 (third volume)      Tables of inviscid supersonic flow about circular cones at incidence,  $\gamma = 1.4$   
Part III, by D.J.Jones, December 1971.

- AGARDograph 148      Heat transfer in rocket engines  
By H.Ziebland and R.C.Parkinson, September 1971.
- Conference  
Proceedings 83      Facilities and techniques for aerodynamic testing at transonic speeds and high Reynolds  
number  
August 1971. Specialists' Meeting held in Göttingen, Germany, April 1971.
- Conference  
Proceedings 91      Inlets and nozzles for aerospace engines  
December 1971. Meeting held in Sandefjord, Norway, September 1971.
- 1972
- Report 598      Experiments on management of free-stream turbulence.  
By R.I.Lochrke and N.M.Nagib, September 1972.
- AGARDograph 156      Planar inviscid transonic airfoil theory  
By H.Yoshihara, February 1972.
- AGARDograph 161      Ablation  
by H.Hurwicz, K.M.Katsch and J.E.Rogan, March 1972.
- Conference  
Proceedings 93      Turbulent shear flows  
January 1972. Specialists' Meeting held in London, England, September 1971.
- Advisory Report 46      Turbulent shear flows  
By R.Michel, July 1972 (Technical Evaluation Report of the Specialists Meeting on  
"Turbulent Shear Flows", September 1971).
- Lecture Series LS42      Aerodynamic problems of hypersonic vehicles. (Two volumes)  
Ed. R.C.Pankhurst, July 1972
- Lecture Series LS49      Laser technology in aerodynamic measurements  
Ed. R.C.Pankhurst, March 1972.
- Lecture Series LS53      Airframe/engine interpretation.  
May 1972.

## FORTHCOMING PUBLICATIONS

- AGARDograph      Supersonic ejectors  
Ed. J.J.Ginoux